Vol.: XV
ISSN : 09726330
2022

Peer Reviewed and Refereed Journal

Rashtrasant Tukadoji Maharaj Nagpur University

SCIENCE JOURNAL

2022

An official journal of Rashtrasant Tukadoji Maharaj Nagpur University (Formerly Nagpur University)

ISSN-0972-6330 VOL. XV

RASHTRASANT TUKADOJI MAHARAJ
NAGPUR UNIVERSITY

SCIENCE JOURNAL - 2022

VOL. XV

Published by :

Dr. Raju Hiwase
Registrar
Rashtrasant Tukadoji Maharaj
Nagpur University, Nagpur

Printed by :

Mukul Barhanpure
Proprietor
Sarthak Creations
36, Kotwal Nagar, Ring Road, Nagpur - 440022

Price Rs. 475.00

Address for Correspondence :

Publication Officer
(Printing & Publication Department)
Dr. V. B. alias Bhausaheb Kolte Library,
University Library Building, Ramdaspeth,
Nagpur - 440 010

Editorial Board of RTM Nagpur University Science Journal

Dr. Sanjay J. Dhoble
Editor-in-Chief
Department of Physics, RTM Nagpur University, Nagpur

Dr. Kirtikumar Randive
Associate Editor-in Chief
Department of Geology, RTM Nagpur University, Nagpur

Editorial Board

Dr. P. B. Maheshwari
RTM Nagpur University, Nagpur

Dr. Prakash R. Itankar
Department of Pharmaceutical Sciences, RTM Nagpur University, Nagpur

Dr. Pramod B. Khedekar
Department of Pharmaceutical Sciences, RTM Nagpur University, Nagpur

Dr. Bharat A. Bhanvase
Department of Chemical Engineering, Laxminarayan Institute of Technology, RTM Nagpur University, Nagpur

Dr. Nishikant A. Raut
Department of Pharmaceutical Sciences, RTM Nagpur University, Nagpur

Dr. Dadasaheb M. Kokare
Department of Pharmaceutical Sciences, RTM Nagpur University, Nagpur

Dr. Santosh Jaju
G. H. Raisoni College of Engineering, Digdoh, Hingna Road, Nagpur

Dr. S. A. Dhale
Priyadarshini Engineering College, Hingna Road, Nagpur

Dr. C. C. Handa
Dadasaheb Kannamwar Engineering College, Great Nag Road, Nandanwan, Nagpur

Dr. Kailash Nemade
Indira Mahavidyalaya, Kalamb, Ralegaon Road, Yavatmal - 445401

PREFACE

Dear Colleagues,

We are happy to deliver the latest issue of the Rashtrasant Tukadoji Maharaj Nagpur University Science Journal (NUSJ) after taking over the responsibility of completing this coveted job. It hasn't been an easy journey, and took several twists and turns before the issue could be finally completed. The journal actually started in year 2021, when Hon'ble Vice Chancellor decided to revive the journal. So, he constituted new editorial committee. The new editorial team was quick to begin, and within lesser time the number of manuscripts required for the journal were obtained. Editorial handling was distributed to corresponding editors from respective disciplines. However, getting the manuscripts reviewed was not an easy task. Double blinded review of all the received manuscripts was carried out by the editors. Equally important was to redesign the journal, its pattern, look, and style. To justify all, professional typesetters were required, which also took some time. And finally in the first quarter of 2023, the volume is ready, almost after a long span of one and half years.

Since after taking over the publication responsibility, we also started our campaign to get our journal UGC listed. The formal proposal has already been submitted and the decision is awaited. The present and the subsequent issues of the NUSJ will also be communicated to UGC for the recognition, which we are hopeful to get sooner. One of the challenges in handling the responsibility of a multidisciplinary journal is to maintain a parity, continuity and consistency, which we all try to maintain. However, mistakes are inevitable. We appeal to all the readers to take some time and go through this new issue of the journal. We welcome all your comments, criticism and suggestions, so that we would make the subsequent issues free of errors.

The present issue of NUSJ comprises of 24 number of articles from different disciplines, written by the eminent authors who are experts in their respective fields. This volume promises to be an important reading material for the professionals and graduate students. We are confident that the readers would enjoy reading these articles and get benefitted.

At the end, we take this opportunity to thank our Hon'ble Vice-Chancellor Dr. Subhash Chaudhari for his initiative, constant support and guidance, Hon'ble Pro-Vice-Chancellor Dr. Sanjay Dudhe for his time to time help and support, Registrar Dr. Raju Hiwase, Finance and Accounts Officer CA Harish Paliwal, Dean of Science and Technology Faculty Dr. Prashant Maheshwari and Associate Dean Dr. Prakash Itankar for their necessary help and support. We also thank staff members of the Publication Division Mr. Gotmare, Mr. Sadiq Sheikh (Retd.), Composer and Printer M/S. Sarthak Creations, Nagpur. Last, but not the least, we thank all the reviewers, contributing authors and fellow Editorial Board members for their continuous help and support.

The Editorial Team,
RTM Nagpur University Science Journal

FORM - IV

1. Place of Publication	:	Rashtrasant Tukadoji Maharaj Nagpur University, Nagpur.
2. Periodicity of its Publication	:	Annual
3. Printer's Name	:	Mukul Barhanpure Sarthak Creations
Nationality	:	Indian
Address	:	36, Kotwal Nagar, Ring Road, Nagpur - 440022.
4. Publisher's Name	:	Dr. Raju Hiwase, Registrar
Nationality	:	Indian
Address	:	Rashtrasant Tukadoji Maharaj Nagpur University, Nagpur - 440 001
5. Editor's Name	:	Dr. S.J. Dhoble
Nationality	:	Indian
Address	:	Editor in Chief Professor, Department of Physics, Mahatma Jotiba Phule Educational Campus, Rashtrasant Tukadoji Maharaj Nagpur University, Amravati Road, Nagpur - 440 033.
6. Name & Address of Individuals who own the Journal and Partners of Share-holders, holding more than one percent of the total capitals.	:	The journal is owned by the Rashtrasant Tukadoji Maharaj Nagpur University, Nagpur.

I Dr. Raju Hiwase, hereby declare that the particulars given above are true to the best of my knowledge and belief.

The University assumes no responsibility for the statements expressed by the contributions.

Sd/-
Signature of Publisher
Dr. Raju Hiwase
Registrar
Rashtrasant Tukadoji Maharaj
Nagpur University, Nagpur

INSTRUCTIONS FOR AUTHORS

1. General Information :

The Science Journal is a State level, peer-reviewed, journal published and financed by the Rashtrasant Tukadoji Maharaj Nagpur University, Nagpur. The Journal features topics in all areas of Science including Life Science, Physics, Chemistry, Mathematics, Statistics, Computer Science, Pharmaceutical Science, Environmental Science etc. The main purpose is to provide a platform to regional researchers to publish the high-quality articles of outstanding scientific significance.

When submitting an article to the Science Journal authors are not changed any publication fee. All publication costs for the journal authors are covred completely by the Rashtrasant Tukadoji Maharaj Nagpur University, Nagpur. To support rapid publication authors re required to submit new manuscripts electronically by email on publicationrtm@gmail.com.

A Submission Checklist is available to help authors to provide all relevant data and information. Authors can interrupt the submission process at any time.

Manuscripts which fall within the scope of the journal and are of potential interest to its readership are subject to a peer review process. Based on the referees' recommendation, the editor-in-chief or the associate editors make a decision on the manuscript regarding publication, revision or rejection. On case of acceptance, a;; papers are subject to copyediting and layout to ensure that they conform to the journal style. Once the submitting author returns a corrected proof of the manuscript new articles are published in the journal.

2. Manuscript Preparation :

2.1 Word processing formats :

The following word processor file formats are acceptable for the main manuscript document for Science Journal :

a. Microsoft word (DOC,DOCX)

b. Note that figures, schemes and tables, equations should be included in the manuscript after the paragraph where they are first referenced. Chemical structures should preferably be embedded in their original chemical structure drawing file format (e.g. CDX for Chem. Draw)

c. TIFF (for photographs and screen dumps, 300 dpi if possible).

d. Text within figures should usually be either Arial or Times New Roman fonts: Courier may be used if a monospaced font is required. Text should be designed to be legible when illustration is scaled to a width of 600 pixels.

2.2 Style and Language :

a. The Science Journal accepts only manuscripts written in English.

b. Abbreviations should be used consistently throughout the whole manuscript. Non-standard abbreviations must be defined the first time they are used in the text.

c. Even though articles in the Science Journal have no page limit or restrictions on length and in the number of graphics, tables or supporting information they should adhere to scientific conciseness. Authors should provide enough background information to support the aim of study and the main claims of the paper, but unimportant or trivial information should not be included.

d. Authors are advised to write clearly, concise and simpy, and their article should be checked by colleagues before submission. The significance of the research should be objectively discussed. Nomnative speakers of English may choose to make use of a copyediting service since a manuscript may be rejected if it. Contains too many grammatical arrors or typing mistakes. Alternatively, authours may seek the advice from expert in English language.

2.3 Typography and Formatting :

a. Please format the manuscript as single-column text using double line spacing.

b. Common font (Arial) should be used to reduce problems during conversion of the manuscript to a PDF file.

c. Type the text without manual hyphenating words at line breaks.

d. Use line breaks only to end headings and paragraphs, and not to rearrange lines.

e. All pages should be numbered.

f. Footnotes must not be used in any section of the paper.

g. Greek and other special characters should preferably be included using the font type “sympol”. If you are unable to

reproduce a particular special character, please type out the name of the symbol in full.

2.4 Article Types :

Every manuscript submitted to the Science Journal has to be assigned by the authors to one of the following types of article:

a. Full Research Paper b. Letter c. Review

2.5 Organization of full Research Papers : 2500 words :

Manuscripts for full Research Paper articles submitted to the Science Journal should be divided into the following sections :

a. Title Font : Arial, Font Size: 12 pts, Bold

b. Authors' Names and affiliations: Font: Arial, Font Size: 11pts.

Where possible, supply given names, middle initials, and family names for complete identification. Use superscript lowercase letters to indicate different addresses. The corresponding author should be indicate with an asterisk, and contact details lfax, e-mail) should be placed in a footnote. Information relating to other authors (e.g., present addresses) should be placed in footnotes indicated by the appropriate symbols.

c. Abstract : 250 words Font : Arial (Italic), Font Size : 11pts

d. Keywords : 6 words separated by semicolon, Font : Arial, Font Size : 10pts

e. Introduction : Font : Arial Font Size : 11pts

f. Results and Discussion : Arial Font Size :11pts

g. Materials and Methods : Arial Font Size : 11pts

h. Conclusion : Arial Font Size : 12 pts

i. Supporting Information (if any) : Arial Font Size :11pts

j. Acknowledgements (Optional) : Arial Font Size :11pts

k. References : Arial Font Size :11pts

a. Scientific articles :

1. Mishra, S.; Karmodiya, K,; Suroliab, N.; Suroliaa, A. Bioorg. Med. Chem. 2008, 16, 2894.

b. Books :

2. Doe, J. S.; Smith, J. In Medicinal Chemistry ; Roe, P., Ed,; Pergamon : Oxford, 1990; Vol. 1, pp 301-383.

c. Patent/Chem. abstract :

3. Lyle, F. R. U.S. Patent 6,973,257, 1995;

d. Chem, Abstr. 1995, 123, 2870.

e. Conference Proceedings/Meeting abstract :

4. Prasad, A; Jackson, P. Abstracts of Papers, Part 2, 212th National Meeting of the American Chemical Society, Orlando, FL, Aug 25-29, 1996; American Chemical Society: Washington, DC, 1996; PMSE 189.

f. Citing and listing of Web references :

As a Minimum, the full URL should be given. Any further information, if known (author names, dates, reference to a source publication, etc.) should also be given. Web references can be listed separately (e.g. after the reference list) under a different heading if desired, or can be included in the references list. The digital object identifier (DOI) may be used to cite and link to electronic documents.

Figures, Schemes and Tables:

The Figures, Schemes and Tables should be illustrated in the manuscript as a Figures, Schemes and Table respectively. The designation scheme should be used primarily for reaction schemes.

1. Figures and schemes are consecutively numbered with Arabic numerals in the order they are first cited in the manuscript text (i.e. Figure 1, Figure2, etc.)

2. The legends of figures and schemes should be positioned directly below the corresponding graphic in the main manuscript rather than as part of the graphic file. They should comprise the bold typed figure.

3. Figures and schemes should be cropped as closely as possible to minimize whire space surrounding the graphic.

All tables must be inserted in the manuscript text after the paragraph where they are first mentioned. The following guidelines must be considered when preparing tables:

4. Tables are consecutively numbered with Arabic numerals in the order they are first cited in the manuscript text (i.e. Table 1, Table 2,etc.)

INDEX

S. No.	CHAPTER	PAGE NO.
1.	Low-cost Lithium Carbonate-Silica Gel Electrolyte System for Electrochemical Device Applications **Jasmirkaur Randhawa, Prashant Ambekar**	
2.	Security and Interoperability of Federated Clouds Using Single Sign-On : A Review **S.M. Barhate, M.P. Dhore, Satish J. Sharma**	
3.	Thermoluminescence and Photoluminescence properties of Europium doped Ba_2SiO_4 phosphor **P.P. Bhure, S.P. Puppalwar, S.J. Dhoble**	
4.	Role of Fluids in the Genesis of Green Mica Quartzites of Palasgaon-Saigaon Area, Western Baster Craton, India **Randive K.R., Shende S.S., Ramteke B.P., Sanjeevani Jawadand, Pratik Godbole, Dora M.L.**	
5.	Spectral Characterization of Various 8-Hydroxyquinoline Derivative Metal Complexes **Chitra S. Khade, N. Thejo Kalyani, S.J. Dhoble**	
6.	Thermoluminescence and Photoluminescence Study of Eu and Dy Activated $KSrSO_4Cl$ Phosphor **Archana Deshpande, S.C. Gedam, N.S. Dhoble, S.J. Dhoble**	
7.	Graphene-SiO_2 Nanocomposite-Based Nanofluid : Ultrasonic-Assisted Synthesis, Characterization and Thermal Conductivity **Arihant M. Patil, Divya P. Barai, Bharat A. Bhanvase**	
8.	Tourmaline Dumortierite and Borosilicates of India - A Review **Sneha Dandekar, Kavita Pande, Dilip Peshwe, Kirtikumar Randive**	
9.	Chlorite Geothermometry from a Quartz Xenocryst-laden Basaltic Dyke at Rorda, Chhota Udaipur Alkaline–Carbonatite Sub-province, Deccan Large Igneous Province, India **Sanjeevani Jawadand, Kirtikumar Randive**	
10.	Cryo-Electron Microscopy for Structural Analysis of Macromolecules **Mayuri S. Prasad, Pramod B. Khedekar**	
11.	REE Carbonate- Galgenbergite [$CaREE_2(CO_3)_4.H2O$] in Biotite Gneiss of Assam Meghalaya Gneissic Complex (AMGC), Chagligaon Area, Kamrup (Metro) District, Assam, North East, India **M. Alam Siddiqui, Rajkumar R. Meshram, Shatrughan Majhi, S.N. Bhagat, Hrushikesh Hari, Niketan Khedkar**	
12.	Design, Synthesis and Biological Screening of Novel 3-[2-(9*H*-carbazole-9-*yl*)-2-oxoethylamino]-2-arylthiazolidine-4-one as Antimicrobial Agent **Prafulla M. Sabale, Lata C. Potey, Nusrat B. Sayyad, Vidya Sabale**	
13.	Neutraceutical Value of Flavonoids : A Short review **Prafulla M. Sabale, Lata C. Potey, Priya Rahangdale, Vidya Sabale**	

S. No.	CHAPTER	PAGE NO.
14.	In Silico Designing of biologically Active 3-acetyl-2-oxo-2H-Chromen-7-yl Benzoate Derivatives **Prafulla Sabale, Nusrat Sayyad, Vaibhav Sawale, Vidya Sabale**	
15.	Enhancement of Solubility of Lurasidone Hydrochloride by Pastillation Method **Rohit Mudliar, Nilesh Mahajan, Purushottam Gangane, Amol Warokar**	
16.	Corona Pandemic **Akash G. Jadhav, Pramod B. Khedekar**	
17.	A Review on Carbon Nanotubes **Mangesh A. Mapari, Pramod B. Khedekar**	
18.	Antidiabetics Poteutial of Isolated Compound from the Stem Bark of Bauhinia Purpurea Linn. **Meshram Satish, Itankar Prakash**	
19.	An Overview on 3D Printing Technology and Biomedical Application **Ranjana S. Kumbhalkar, Pramod B. Khedekar**	
20.	Physicochemical Evaluation and Formulation of Microemulgel of Gaultheria **Kamlesh Machewar, Rajendra Kakde, Prafulla Sabale, Manish Kamble, Roshni Kunte**	
21.	An Overview on Synthetic Study and Biological Screening of Benzimidazole Derivatives **Kawade D.P., Bhadke M.Y., Asnani A.J., Chaple D.R.**	
22.	Combination Therapy against Breast Cancer (Overview of effective combination therapies for breast cancer) **Monu Shahu, Pramod B. Khedekar**	
23.	Design and Synthesis of Novel Chalcone Derivative from 5-Nitrosalicylaldehyde **Dhabarde Disha, Kamble Manish, Gupta Nandini, Baheti Jagdish, Sabale Prafulla**	
24.	Occurrence of Hydrothermal PGM in the Calcareosiliceous dyke of the Chhota Udaipur Carbonatite-Alkaline-Mafic Province, Deccan LIP, India **Tejashree Raut, Kirtikumar Randive, Sanjeevani Jawadand, M.M. Korakoppa, M.L. Dora, Tushar Meshram, Rajkumar Meshram, Manoj Sahu, J. Vijaya Kumar**	

Peer Reviewed and Refereed Journal 2022 **(ISSN : 09726330)**

Rashtrasant Tukadoji Maharaj Nagpur University

SCIENCE JOURNAL 2022

Vol. : XV

LOW-COST LITHIUM CARBONATE-SILICA GEL ELECTROLYTE SYSTEM FOR ELECTROCHEMICAL DEVICE APPLICATIONS

JASMIRKAUR RANDHAWA[1] & PRASHANT AMBEKAR[2]*

[1] Government College of Engineering, Nagpur, INDIA- 440018.

[2] Dharampeth M P Deo Memorial Science College, Nagpur, INDIA- 440033.

Corresponding author email : jbrandhawa2@gmail.com
*pacific0701@gmail.com
Mob. No. 7776899668

ABSTRACT

The pure lithium carbonate being hygroscopic nature, gives cross sensitivity to water molecules when used in electrochemical CO_2 gas sensors. Therefore, in the present study, composites of Silica-gel (SiO_2:xH_2O) dispersed Lithium carbonate with up to 5% in weight fractions of the dispersoid (viz. 1%, 3% and 5 %) were prepared and studied for its validity in electrochemical utility using Impedance analysis and ionic/electronic transport studies under different atmospheric conditions.Interesting results have been obtained while characterizing with ac conductivity measurements in the frequency domain of 5Hz to 13MHz in the temperature range 573 to 773K. Ac conductivity is also found affected by the CO_2 partial pressure variation in the atmosphere. An estimate of electronic contribution in the conductivity has been made with transport number measurements using Wagner's method. The investigation recommends potential applicability of this composite for electrochemical device applications operating below 573K of temperature.

Keywords : Composite; Electrochemical Devices; Electrolyte, Impedance analysis, Ionic Transport; Lithium Carbonate; Silica gel.

INTRODUCTION

The electrochemical CO_2 gas sensor is an electrode concentration cell using carbonate-based compounds for sensing electrode and/or electrolyte (figure-1) (Liu and Worrell, 1982). Carbonate based electrochemical devices suffer deviation from their performance due to its hygroscopic nature. Attempts have been made to overcome this limitation by preparing doped systems, binaries and composites (Singh et al, 1999). For preparing composite of carbonates, different inert phases such as Al_2O_3, SiO_2, Ferroelectric phases such as $LiNbO_3$

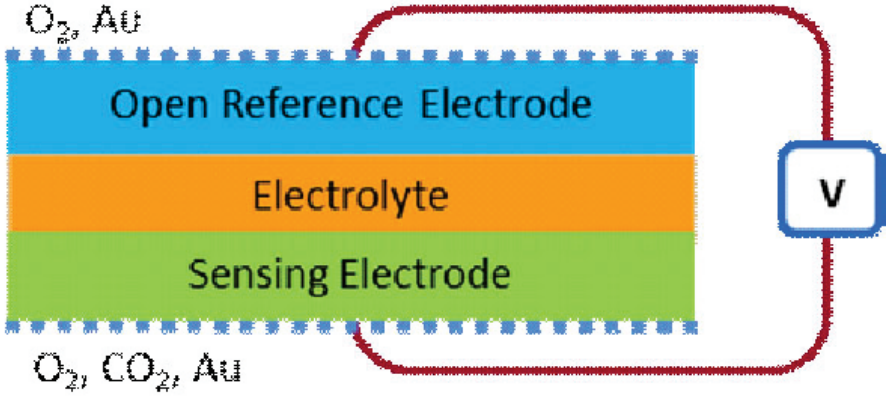

Fig.1: Schematic of an electrochemical potentiometric type-III sensor

and $KNbO_3$ etc. are dispersed in host (Ambekar et al, 2014). These composites possess large ionic conductivity at relatively lower temperatures and better thermal stability. Moreover, non-porous and improved mechanical interface with the reference electrode and sensing electrodes have attracted attentions of researchers since decades (Liang, 1973).

In order to achieve stability against water molecules, Silica gel (SiO_2:xH_2O) is used for preparing composites in the present study. It is an inert phase with amorphous form of Silicon dioxide which is able to adsorb moisture in varied amount and also releases moisture on heating. This particular characteristic was utilized in the present study. Moreover, its low cost and abundant availability in INDIA is an additional advantage. Composites of Lithium Carbonate were prepared with addition of different amount of Silica Gel. All compositions were subjected to *in-situ* impedance studies in different CO_2 gas partial pressures and humidity conditions at different temperatures for identification of highest conducting composition in different CO_2 gas concentrations(Shang et al, 2020; Anzai et al, 2019; Kamecki et al, 2019; Byl et al, 2012). The samples were further investigated by transport number determination at different temperatures.

EXPERIMENTAL

Composite electrolytes were prepared by adding different weight fractions of commercially available Silica Gel (SG) into Lithium Carbonate (LC) (E Merk) in the compositions 99LC+01SG, 97LC+03SG and 95LC+05SG in weight fractions using conventional melt quenching method. The LC component is deliberately kept 95% and above to maintain its sensitivity at higher side. Small pellets of size approximately 1-3 mm thickness and ~ 10 mm in diameter were prepared using hydraulic press applying a pressure of 10 tons per square centimeters. The so obtained pellets then sintered at a temperature of 823K for 8 hours. Pellets of all compositions were characterized for electrical characterization by forming platinum electrodes at both the surfaces. Ac conductivity was measured by impedance spectroscopy using HP4192A in the frequency range 5 Hz to 13MHz, temperature range 573 K to 773K and different CO_2 gas partial pressures ranging from zero to 100%. AC conductivity in dry and humid atmosphere was also measured for all temperatures. Transport number measurement was carried out on Keithley 2100 6.5 digit multimeter by Wagner's dc polarization method using both blocking electrodes (figure-2).

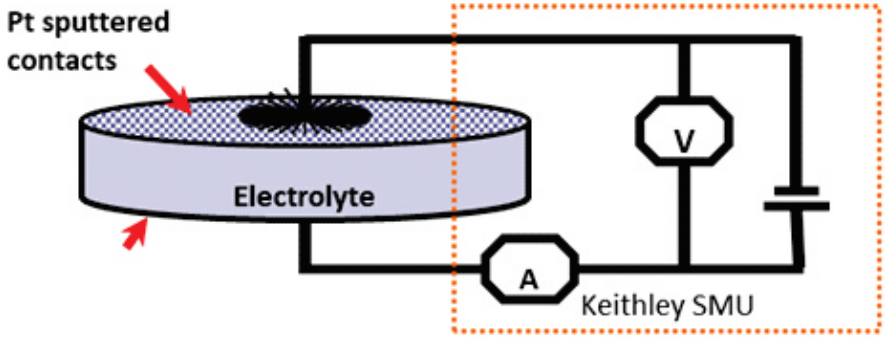

Fig. 2 : Schematic of experimental arrangement for Wagner's dc polarization method using both blocking electrodes.

RESULTS & DISCUSSION

Impedance plots for pure Lithium carbonate are found to be depressed semicircular in nature for all temperatures ranging from 573 to 773K, signifying one conduction mechanism, mostly due to ion migration through the bulk of grains and along the grain boundaries figure (3-A). The values of bulk resistance are found to be significantly affected by the CO_2 gas partial pressure. With increase in CO_2 gas concentration in the atmosphere, the bulk resistance was found is found increasing. Also, bulk resistance has higher value in humidified air than dry air. Figure 3-B,3-C&3-D shows the impedance plots for composite electrolyte wherein it is seen than with increased concentration of the dispersoid SG, two probable distinct semicircles are seen developing. These two distinguishable semicircles are due to two distinct conduction mechanisms. At high frequencies conduction due migration of ion through bulk of grains and parallel to grain boundaries are seen. At lower frequencies conduction due to ion migration perpendicular to grain boundaries are seen. These two

semicircles are indicated schematically in figure 3(C). Impedance plots for pure LC are seen terminating at zero whereas in the composite made with SG shows presence of an additional series resistance seems possible.

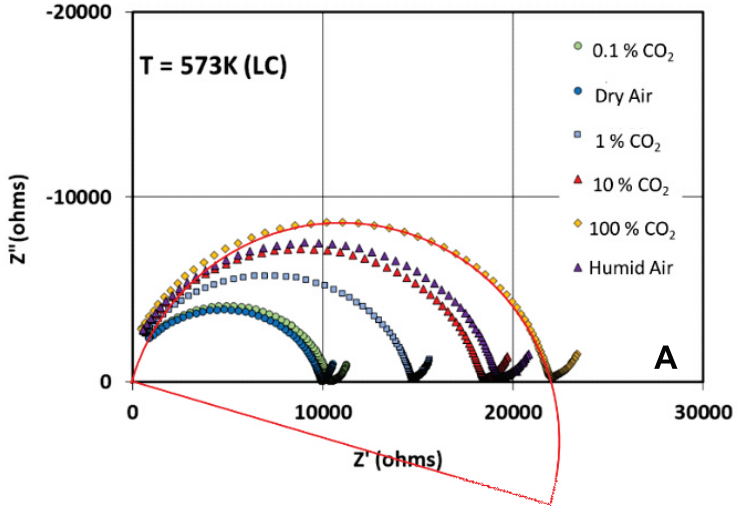

Fig. 3 (A) : Impedance plots for (A) Pure Lithium Carbonate

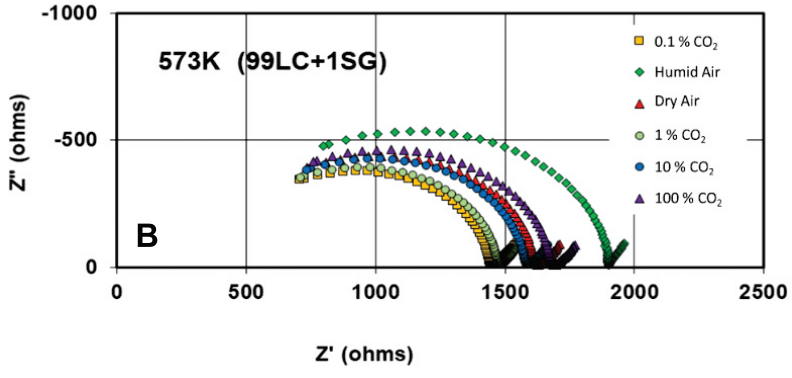

Fig. 3 (B) : 99LC+01SG, (C) 97LC+03SG and (D) 95LC+05SG at different atmospheric conditions.

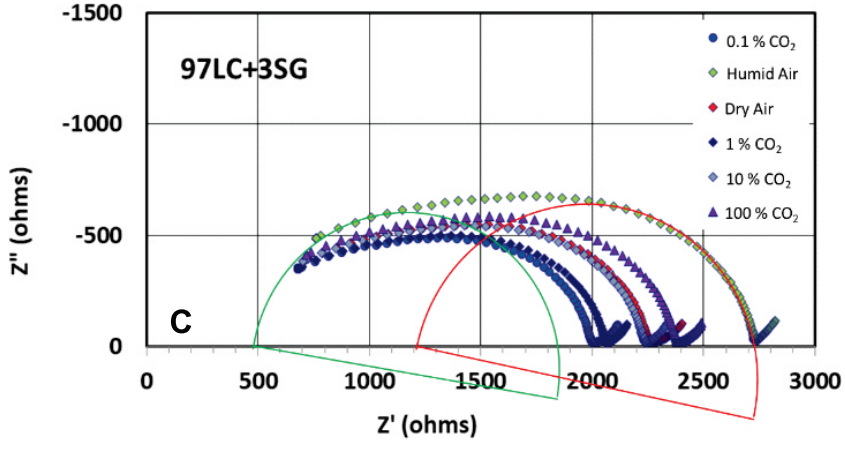

Fig. 3 (C) : 97LC+03SG

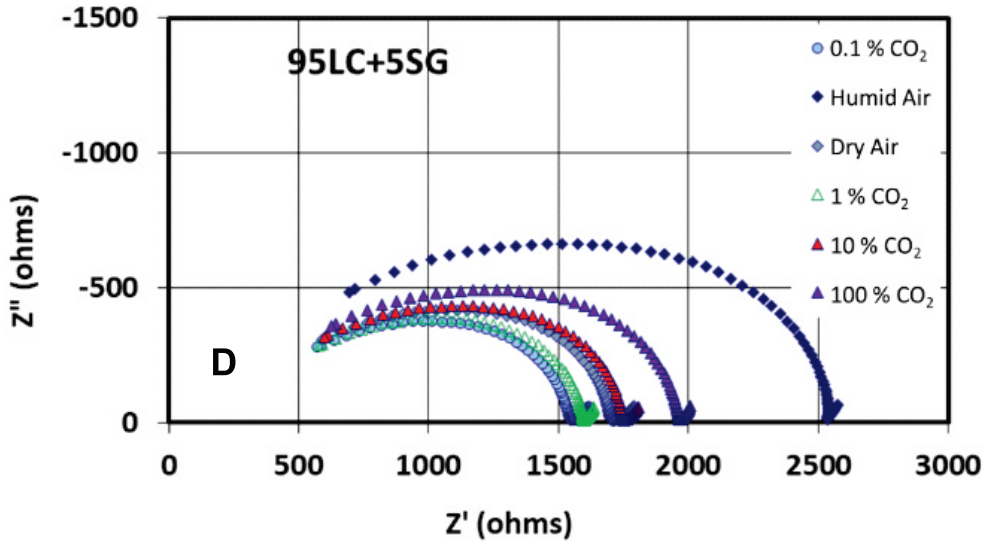

Fig. 3 (D) : 95LC+05SG at different atmospheric conditions.

Arrehenius plots shown in figure 4 depicts enhancement of two orders of magnitude in conductivity between the pure system and the composites. Slope difference signifies the lowering of activation enthalpy in composite phase as E_a for pure LC and the LC+SG are found to be 0.902 and 0.73 eV respectively. Effect of CO_2 or Humidity is obviated in the composite, making it an apt material as electrolyte for sensor application. CO_2 partial pressure variation or Humidity is found affecting the conductivity significantly in pure LC at lower temperatures.

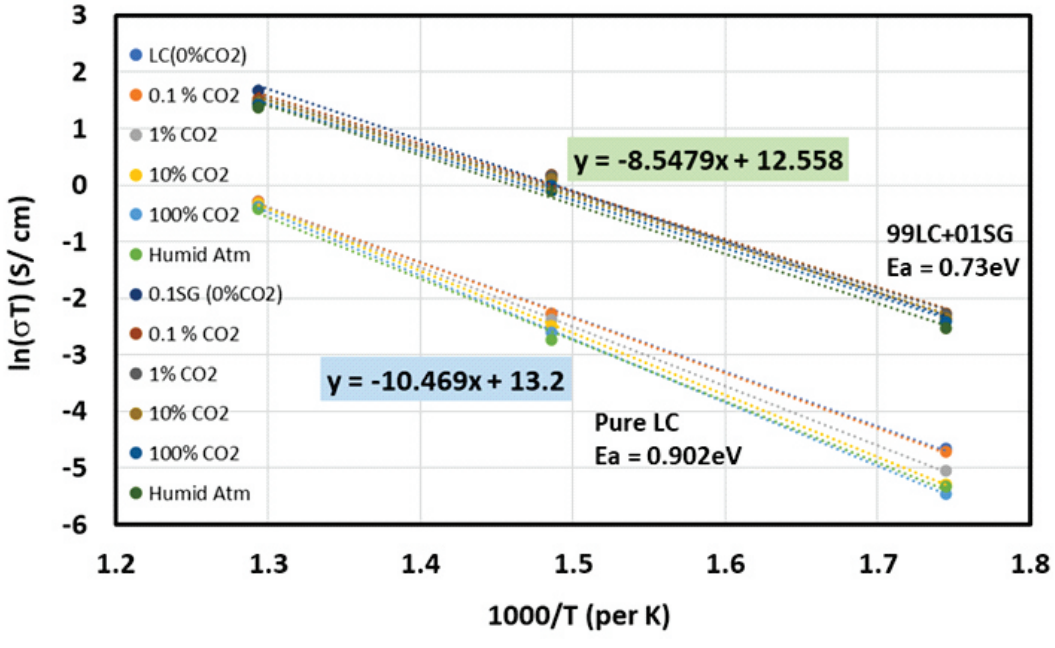

Fig. 4: Arrhenius plots for pure LC and 99LC+01SG composites.

Similar to that of pure LC, the bulk resistance is found increasing with increase in CO_2 partial pressures for all three composites. Which is due to obvious reason that increased CO_2 molecules in the atmosphere increases the number of

adsorbed CO_3^{2-} ions at elevated temperatures in presence of Pt. These ions bind the mobile L_i^+ ions from the bulk, and results into decrease in ionic conductivity. Effect of water molecule (humidified air) on conductivity of composite is found changed with that of LC.

Figure-5 shows the time response of the charges to small dc potential applied through inert electrode at different temperatures. Initially large current is observed to due migration of ions as well as electronic charge carriers. After some time, total polarization of ions sets in and we get steady current due to electronic charge carriers. Inset of the figure shows very fast polarization setting in even at high temperatures, suggesting fast migration of ions through the electrolyte even at elevated temperatures.

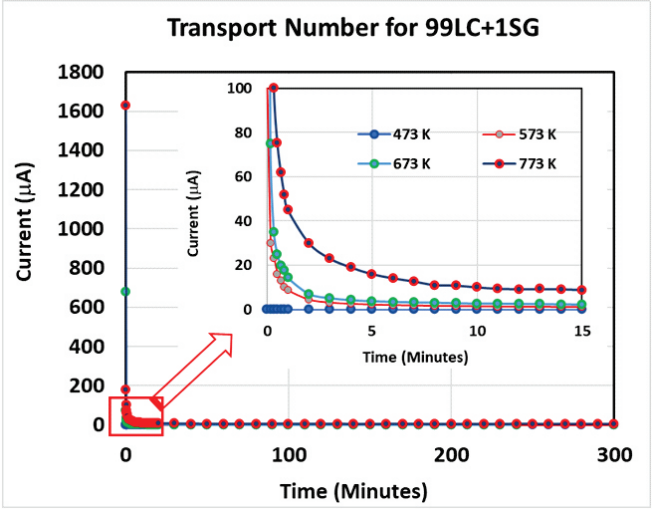

Fig. 5: Time response of 99LC+01SG composites to small constant DC potential of 500mV.

Figure (6A) shows comparison of total conductivity (S_o) and electronic conductivity (S_{oo}), showing more enhancement in total conductivity than electronic with rise in temperature. This is very clearly seen in figure (6B) showing significant rise in ionic transport number (t_i) with respect to electronic transport number (t_e) with increase in temperature. The ionic and electronic transport numbers are determined as the fraction of ionic and electronic conductivities to the total conductivity. Numerical values of the transport numbers of the composite electrolyte of composition 99LC+01SG are found to be t_i=0.99 and t_e =0.01 for temperatures more than 473K.

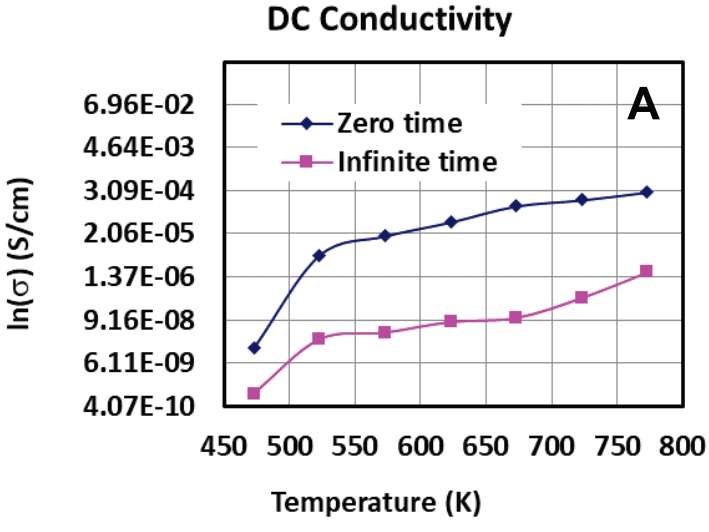

Fig. 6 (A) : DC conductivity measurement as a function of temperature;

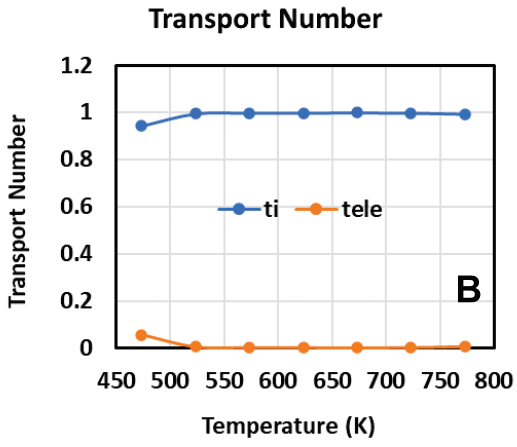

Fig. 6 (B) : Transport number comparison with temperature.

CONCLUSION

Addition of small amount Silica Gel into Lithium Carbonate enhances the ionic conductivity by two orders of magnitude due to composite nature as revealed from the impedance plots. The effect of CO_2 gas partial pressure variation and presence of water molecules on ionic conductivity is found significantly reduced for composites.Thus, the LC+SG composite makes a potential candidate for electrolyte application in electrochemical devices.

ACKNOWLEDGEMENTS

PA is thankful to CSIR, New Delhi; UGC-WRO, Pune; NCL, Pune and NPL, New Delhi for providing financial support/ work platform to carry out the work.

REFERENCES

1. Liu Q. G., Worrell W. L., (1982),Methods of manufacturing metal from a melt, determination of sulphur and carbon therein, sensors therefor and solid electrolyte compositions for said sensors, US Patentnumber- US4428770A.

2. Singh K, P Ambekar, SS Bhoga, (1999), An investigation of Na_2CO_3–ABO_3 (A = Li/K/Ba and B = Nb/Ti) heterogeneous solid electrolyte systems for electrochemical CO_2 gas sensor application,Solid State Ion., 122 (1-4), 191-196. https://doi.org/10.1016/S0167-2738(99)00033-8

3. Ambekar P, Randhawa J,Singh K, (2014),Modified transport properties of $LiNbO_3$ dispersed Li_2CO_3 composite system for electrochemical CO_2 sensor,Adv Matt Lett 5 (2) 75-79. DOI: 10.5185/amlett.2013.fdm.20

4. Liang C. C., (1973), Conduction Characteristics of the Lithium Iodide Aluminum Oxide Solid Electrolytes, J. Electrochem. Soc. 120 pp 1289. https://doi.org/10.1149/1.2403248

5. Shang Ju Ying et al, (2020), In Situ Transport Measurements Reveal Source of Mobility Enhancement of MoS_2 and $MoTe_2$ during Dielectric Deposition, ACS Appl. Electron. Mater. 2, 1273"1279. https://doi.org/10.1021/acsaelm.0c00085

6. Anzai Hiroshi et al, (2019),Unusual Oxygen Partial Pressure Dependence of Electrical Transport of Single-Crystalline Metal Oxide Nanowires Grown by the Vapor–Liquid–Solid Process, Nano Lett., 19 1675"1681. https://doi.org/10.1021/acs.nanolett.8b04668

7. Kamecki B., Miruszewski T. and Karczewski J., (2019), Structural and electrical transport properties of Pr-doped $SrTi_{0,93}Co_{0,07}$ $O_{3-\delta}$ a novel SOEC fuel electrode materials, J. Electroceram, 42:31–40 https://doi.org/10.1007/s10832-018-0143-0

8. Byl Celine, Berardan David and Dragoe Nita, (2012),Experimental setup for measurements of transport properties at high temperature and under controlled atmosphere, Meas. Sci. Technol. 23, 035603 (8pp) http://iopscience.iop.org/0957-0233/23/3/035603

Peer Reviewed and Refereed Journal 2022 **(ISSN : 09726330)**

Rashtrasant Tukadoji Maharaj Nagpur University

SCIENCE JOURNAL 2022

Vol. : XV

Security and Interoperability of Federated Clouds Using Single Sign-On: A Review

S.M. Barhate[1], M.P. Dhore[2], Satish J. Sharma[3]

[1,3] Department Of Electronics & Computer Science, RTM Nagpur University Nagpur-440033 (MS)

[2] Shri. Shivaji Science College, RTM Nagpur University Nagpur-440012 (MS)

ABSTRACT

Cloud Computing provides excellent services to its customers by setting up various data centres at different geographical locations. It takes care of serving each and every need of its customers right from infrastructure, Platforms, Software etc at any geographical location. The service providers often make use of proprietary management services or virtualization techniques to render the services. This creates a problem of interoperability and introduces migration as well as security issues. Along with this privacy and security are peeping out as a big challenge for providers as well as cloud users. There has to be multilevel security to the while entering in clouds in terms of cloud service providers, data centres etc. Security problems can be addressed if the users who access the resources are allowed to enter only if they are authenticated users. Access control can be implemented by restricting the users to enter the cloud. This paper is a review that deals with the user authentication issue of interoperability by using single sign-on for security of federated clouds and provides better bird's eye view for the researchers in this field.

I. INTRODUCTION :

Research in cloud computing is going on with tremendous efforts in the academic as well as in industries. Cloud computing has excellent growth in technologies with the modules such as IAAS (Infrastructure as a service), SAAS(Software as a service), PAAS(Platform as a service). But these services have their related security issues. In this growing era of cloud computing, security must be provided with all the services and that too with least complications.

Cloud Computing is an approach of using computing as a utility. The resources involved are dynamically scalable. The basic idea behind cloud computing is "Pay per use". In recent years cloud computing has a big impact on the way the cloud providers are getting augmented services. The cloud providers often present their data using proprietary services i.e through software or virtualization technologies. This definitely suppresses the interoperability and data migration among the different cloud providers (Dikaiakos et al., 2009) (Kuyoro et al., 2011). A way to respond to the interoperability problem is to make use of federated clouds. In the present work, we are addressing the security issues while considering interoperable federated cloud. Using Single Sign-On federated clouds provides a higher degree of security and control.

Keywords : Cloud computing; virtualization; data centres; single sign-on; federated clouds.

Literature Review :

Justice Opara Martins, et. al. in their work on "Critical Analysis of Vendor Lock-in and its impact on cloud computing migration: A Business Perspective", provided a critical analysis of vendor lock-in with business perspective. The paper surveys qualitative and quantitative study that has come up with various situations to give rise to vendor lock-in. The paper stresses the importance of interoperability and portability while migrating to and out from clouds. The analysis of the survey carried out in the paper also shows that the problem of vendor lock-in increases when the computer resources migrate from on-premise to the clouds. There are various solutions proposed in this work as how to avoid and mitigate lock-in risks when migrating to cloud computing. (Justice Opara Martins 2016)

Ilango Sriram et. al. focused on creating standards for allowing interoperability, and describes ways of designing and building clouds. A deep technical aspects of advances in cloud computing has been presented. Technical aspects which contribute to the advent of new technologies in cloud are reviewed. Advances in introduction of protocols, interfaces and standards along with the techniques of modelling clouds along with the use cases of cloud computing are discussed briefly in their work. Various definitions of cloud computing have been discussed and the working definition of National Institure of Standards & Technology (NIST) by Mell and Grance was found to be the most appropriate as it described cloud computing using a number of characteristics, service models and deployment models. (Ilango Sriram 2010)

Menatalla Ashraf Fawzy Kamel in his thesis "Vendor Lock-in the transition to cloud computing platform" focuses on vulnerability issue of vendor lock-in while transition in cloud computing platform. The researcher considers a company SCANIA IT which faces problem of vendor lock-in in cloud computing. The results are based on a case study of a similar company that moved to another cloud provider, specifically Microsoft Azure and an interview of Microsoft Azure of its view of risks involved in vendor lock-in. The results show that there are various risks involved in vendor lock-in while migrating in clouds. The thesis also provides recommendations to the various problems involved in vendor lock-in. (Kamel 2015)

Amlan Chaudhary, et. al. in their work on "A strong User Authentication Framework For Cloud Computing" stressed on the need for user authentication as the most important aspect of cloud computing. The paper has proposed a strong user authentication framework where a user has to prove his authenticity before entering the cloud. The proposed research work provides identity management, user authentication and session key establishment among the users. (Amlan Chaudhary 2011)

S. M. Barhate and M. P. Dhore in their work on "User Authentication Issues in Cloud Computing" have focused mainly on the user authentication issue as a security aspect in cloud computing. The paper mainly has stressed upon the important and understudied issue i.e. interoperability in cloud computing. The work focuses on the important point that interoperability has four main use cases as per the study of NIST. User authentication is the first and foremost important issue of cloud security aspect. The paper analyses the first interoperability use case which is user authentication. All the user authentication issues, the algorithms and the protocols used for securing user authentication are analysed in details, (S.M.Barhate, User Authetication Issues In Cloud Computing 2016).

S.Lee et al have proposed public key infrastructure and mobile-out-of band based authentication for cloud computing. However, the scheme transmits data (e.g. *ID, PW,* and *PKI*) in a plaintext form which can be easily intercepted by the adversaries. Moreover, their scheme does not care about data confidentiality, data integrity, user privacy and users are not allowed to change their password. As a result, their scheme is not fit for real time cloud computing. (S. Lee 2010)

Rajkumar Buyya, et.al., in their work on, "Intercloud: Utility Federation of Cloud computing Environments For Scaling Application Services", have presented vision, challenges, and architectural elements of InterCloud for utility-oriented federation of Cloud computing environments. The proposed InterCloud environment supports scaling of applications across multiple vendor clouds. The approach has been validated by conducting a set of rigorous performance evaluation study using the CloudSim toolkit. The results demonstrate that federated Cloud computing model has immense potential as it offers significant performance gains as regards to response time and cost saving under dynamic workload scenarios. (R. R. Rajkumar Buyya 2010).

Jamie Loret, et. al. in their work on "Architecture and Protocol For Intercloud Communication" propose that clouds should interrelate through networking protocols in order to provide scalability, efficiency and flexibility using services computational and storage resources infrastructures of the other clouds. They have proposed an architectural and

protocol model that allows exchanging information, data services, storage and resources among interconnected clouds. The architecture is highly scalable and permits to add new clouds easily. The protocol designed provides node discovery and fault tolerance. The testing and analysis have been done in controlled test bench. (Jamie Lloret 2013)

Grace A. Lewis in his report "Role of Standards In Cloud Computing Interoperability" has focused on the interoperability issue in cloud computing. The report has proposed various solutions to interoperability problem like standardization. The research report also proposes various interoperability use cases and their solutions as effort towards solving interoperability issue. It has focused on the four use cases of interoperability as follows: 1) User Authentication 2) Data Migration 3) Workload Migration and Management 4) Load Balancing. The paper also proposes various recommendations as a part of solution towards interoperability. (A.Lewis 2012)

Piyush Harsh, et. al. in their work "Using Open Standards For Interoperability: Issues, Solutions and Challenges facing Cloud Computing", have attempted to describe the problem, issues, possible solutions and challenges in achieving cloud interoperability. The research work is carried out with respect to European project Contrail that is trying to adopt open standards with available virtualization solutions to enhance users' trust in the clouds by attempting to prevent vendor lock-in, supporting and enforcing SLA's together with adequate data protection for sensitive data. Here, the research work has tried to identify some of the challenges faced by cloud computing. (Piyush Harsh July 2012)

S.M.Ranbhise et. al. in their work on, "Simulation and Analysis of Cloud Environment" have focused on the advantages of cloud environment. There are different resources in cloud environment like Virtual Machine, CPU, resource, Memory, Hard disk space of server machines located in data centre. The server machines are consuming energy to provide services to users in cloud computing. For analysing the resource allocation in cloud computing environment scalable to n servers will require Cloud simulation and modelling tool to create the cloud as per requirement. The work analyses simulation of cloud on CloudSim and Cloud report for better analysis of cloud environment. (S.M.Ranbhise 2014)

II. INTEROPERABILITY ISSUES

Cloud service users should be able to avoid the problem of vendor lock-in wherein the customer gets locked into a specific cloud provider and due to the lack of common protocol/standards or high cost of switching to a similar cloud gets difficult. Precisely one can say that the cloud customers lack interoperability while accessing various services from different clouds (Buyya et al., 2009). Interoperability can be defined as a measure of a degree to which diverse systems or organizations can work together successfully (Machado et al.2004).

A way to address interoperability is to implement open standards at all levels in the cloud. There are many cloud standardization initiatives being pursued in cloud computing industry. These standardization efforts concentrate on some of the issues like workload management, data migration user authentication etc. (Parmeswaran, 2009). From the various use cases, proposed and discussed by NIST, OMG and DMTF following are the use cases of interoperabilityin getting benefited by standardization:

1. **User Authentication** : A user who has established identity of one cloud provider can access the other cloud provider resources with same identity.
2. **Load Balancing** : A workload executing on one cloud provider can be uploaded with another cloud provider.
3. **Data Migration** : Data which resides on one cloud provider can be moved to another cloud provider.
4. **Work Load Management** : The tools for workload management of one cloud can be used to manage the resources from other cloud also. (Lewis et al., 2012)

In the present work, we have highlighted the first interoperability issue of user authentication as a security aspect of interoperability in clouds. Authentication is the process of identifying the user before allowing him to access the resources. This process involves identifying user through a username and then validating his identity by a user provided data(password).

III. CLOUD FEDERATION :

The need of the hour is the technology that would provide security to the customer and ease to migrate while providing interoperability. Hence, after detailing the interoperability use cases we would switch over to the technology for providing interoperability cloud federation. Federation addresses following basic interoperability features:

i) Resource Migration

ii) Resource Redundancy

iii) Combination of complementary resources & services.

The key elements of Federated Clouds are :

1. Cloud Coordinators : To provide cloud services and their management considering best possible QOS at low energy and cost.
2. Brokers: Act as a mediator among users and cloud coordinator.
3. Exchange: Allows sharing of capability across various cloud domains.

Cloud federation is the union of different cloud service providers (CSP's) which mutually consent to use standard approach to provide interoperability to the customers while switching from one CSP to another. A CSP has some resources available to the clients. In cloud federation, a client request is sent to a specific CSP or data centre. If the CSP cannot answer to the request of the client then it may affect many other clients waiting to get service from. This in turn has a substantial effect on the QOS to the client. This means an unavailability of resources in turn looses the important client of the CSP which is an undesirable case. Hence to solve this problem various CSP's with mutual understanding get ready for resource sharing with standard communication protocol.

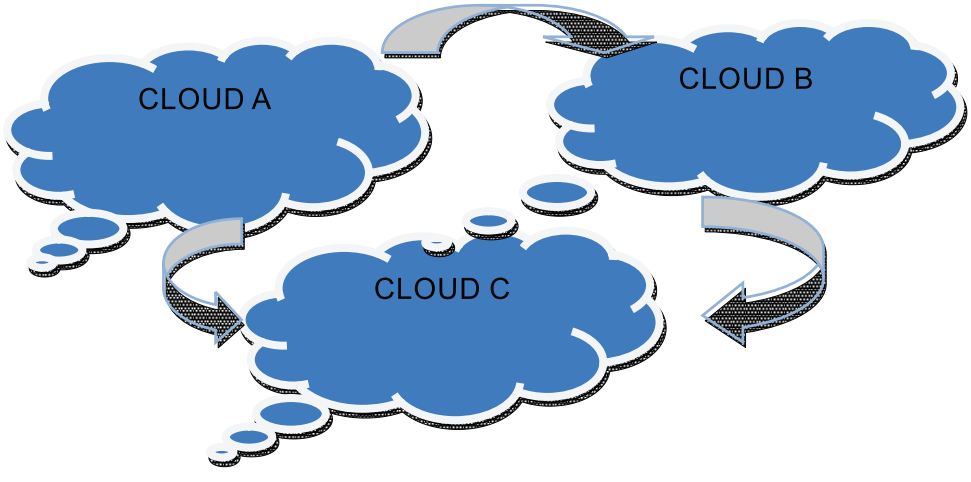

Fig 1. Schematic of a Cloud Federation

This in turn is the concept of cloud federation. Thus, cloud federation in short shares infrastructure for better resource utilization and QOS. The cloud federation comes in two flavours i.e. vertical as well as horizontal. Horizontal federation means collection of resources at specific service model such as IAAS, PAAS and SAAS. Whereas vertical federation means one type of service model uses the other type of service model from other CSP's. Thus cloud federation not only provides better resource utilization but also good QOS to the clients. The QOS can be measured in terms of various availability, interoperability, uptime, response time etc.

IV. SSO FOR IDENTITY MANAGEMENT :

Federation is a type of Web SSO using standardized approach such as SAML thereby creating a trusted relationship among the heterogeneous systems. The federated SSO provides us with a service provider which provides

token or the permission to log in. There is also a role of Identity provider which checks the identity of the one logging in.

SSO is a subset of Federated Identity Management as it speaks about authentication and has a great impact on technical interoperability.

We propose to use single sign-on technology which can be used as security and interoperability in federated clouds. This technology is a part of user authentication service where the user is allowed to use single set of credentials to access various applications. Single sign on is the facility wherein a user can log in once and can access resources through other service provider without the need to re-enter his username or password again. This service gives authentication to the end users to access all the applications for which the user has been given rights for and hence this eliminates the need for further prompting when the user is hopping to different applications during the same session. The SSO service is very helpful to backend users to maintain user activity log as well as user account monitoring.

The working of SSO service is handled by an agent module which takes the security credentials of the user through a dedicated SSO policy Server along with authentication of the user against a user repository for example LDAP (Light Weight Access Protocol Directory). Various users uses different protocols such as Kerberos and the SAML (Security Assertion Markup language).

V. PROPOSED EXPERIMENTAL WORK :

As we have a blue print prepared for a secure and interoperable framework of federated clouds the implementation is proposed to be tested using Cloudsim Framework. Cloudsim is a generalized framework which is used to simulate large cloud infrastructure on one computing node. Its features can be explored to design the cloud federation framework. Cloudsim provides various facilities for the researchers to design scheduling or resource provisioning clouds. But it does not provide any feature to study user authentication or authorization issues. This has motivated us to pursue work on the Cloudsim for simulating the user authentication process.

Fig 2. shows the flow chart depicting the SSO implementation in federated clouds. A cloud user sends a request for resource allocation to a CSP after proving his user identity through entering proper credentials that are considered are “Tokens”. As the user gets the permission he avails the required resources. If at all the resources are not available with the current CSP, he is redirected to other CSP’s after authenticating with the same credentials. As the federated CSP authenticates the user, it then provides the available services to the user. In this full workflow the Cloudsim does not provide any feature for cloud authentication. (Ranbhise et al., 2014)

In the present work we have divided the framework of SSO in Federated clouds in three parts i.e.

1) Cloud User
2) Cloud Service Providers
3) Identity Providers

Simulation of the first two group of cloud users are being supported by Cloudsim but the last part has to be added to make Cloudsim extend to support user identity issue.

SSO technology in federated clouds shows that the Cloud Users has to undergo three phases i.e. registering for the authentication process with identity provider, registration for resources access with a Cloud Service Provider and Requesting Services from other cloud service providers.

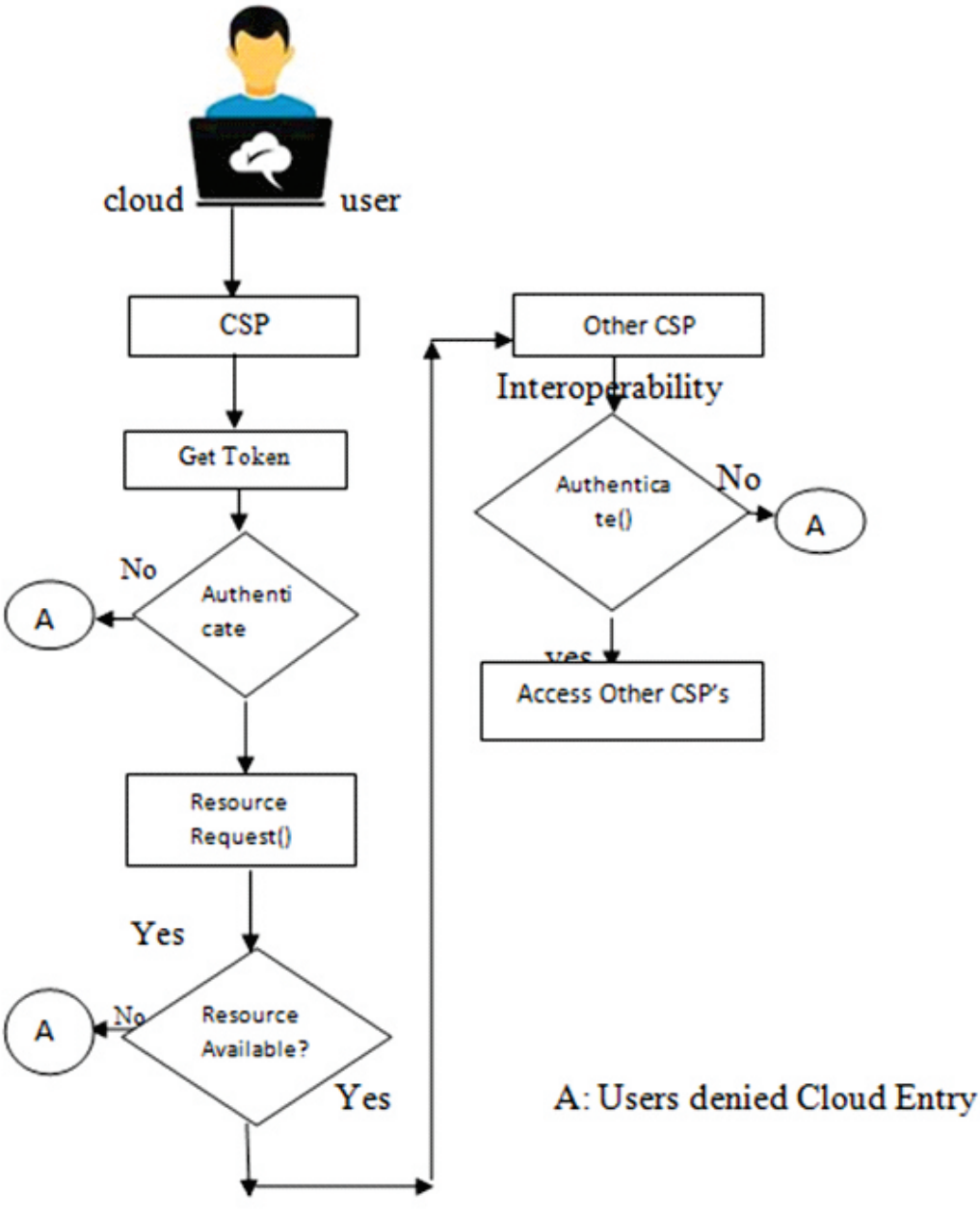

Fig 2: SSO In Federated Clouds

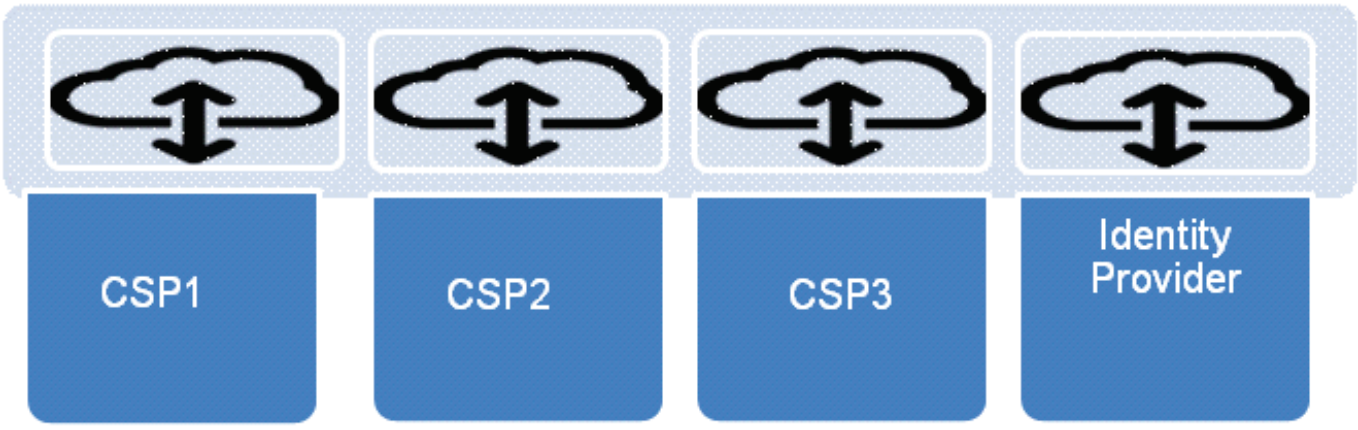

Fig 3: SSO Authentication & Interoperability In Clouds

The implementation process proposes to involve Cloudsim as a software to create Cloud Service Providers and cloud users. The idea is to extend Cloudsim to create the packages for identity provider cloud. The program is in Java to create functions for token allocation and token passing for the friend Cloud Service Providers. Cloudsim is also providing facilities to create federated clouds. While implementation we have to use an encryption technique for data security during passage of data from CSP's or during token passing to or from Identity Providers. Among the various encryption techniques available, we propose to the Symmetric Key Encryption technique through Advanced Encryption Standard(AES-128). We propose to use Oracle 11g as a backend to store data. The database would have the tables for storing data of the CSP users. The user's data table has the access rights associated with it which can be accessed during the authentication phase.

VI. Results and Conclusions

Interoperability issue in cloud environment is very well addressed by using federated cloud framework. The security aspects involved during the user switching is successfully satisfied with the use of single sign-on technology. The complexity involved during the switching of user from one cloud service provider has a significant reduction due to the use of single credentials only once. Also the users are not overwhelmed of the use of keeping track of multiple credentials every time for switching from one cloud service provider to another. There is significant rise in the response time by the usage of single sign-on technology. Also the execution time is realised to be reduced significantly with the use of SSO technology in federated clouds.

Refrences :

A.Lewis, Grace. *Role of Standards in Cloud Computing Interoperability.* CMU-SEI 2012, 2012.

A.V.Parmeswaran, Asheesh Chaddha. "Cloud Interoperability And Standardization." *SET Lab Briefings* 7 No.7 (2009).

Manoj V Thomas et.al. "Single Sign-on In cloud Federation Using cloudsim." *I.J.Computer Network and Information Security(Online Journal)* 6, no. DOI: 10.5815/ijcnis.2015.06.06 (May 2015): 50-58.

Alirezi Ghobadi, Koozbeh Karimi, Farnaz Heideri, Masoud Samadi. "Cloud Computing Reliability And Security Issue." *16 th Internatinal Conference In Advanced Communication Technology.* 2014.

Amlan Chaudhary, Pradeep Kumar, Mangal Sain,, Hoonjae Lee. "A Strong User Authentication Framework For Cloud Computing." *IEEE Asia -Pacific Services Computing Conference.* 2011.

Behnam Bagheri Ghavam Abadi, Mostafa Ghobaei Arani. "Resource Management of IaaS Providers in Cloud Federation." *International Journal of Grid Distribution Computing* Vol. 8, No.5 (2015): .327-336.

Best Practices For Data Migration. IBM Report, 2007.

"Bhupendra Panchal, Prof R.K.Kapoor." *International Journal of Advanced Research in Computer Science and Software Engineering* 3, no. 9 (September 2013): 143-150.

Burt Kaliski. *The Mathematics of the RSA Public-Key Cryptosystem.* RSA Laboratories.

Calheiros, R. B. Rodrigo N. "Cloudsim A toolkit for modeling and simulation of cloud computing environments and evaluation of resource provisioning al-gorithms." *Software-Practice & Experience*, 2010: 23-50.

Celesti, F. Tusa, M. Villari and A. Puliafito. "How to enhance Cloud architectures to enable cross federation Cloud Computing (Cloud)." *IEEE 3rd International Conference on.* 2010.

Choksi, Shikha. ""Comparative Study on Authentication Schemes for Cloud Computing." *IJDER* 2, no. 2.

"Cloud Analyst: An Insight of Service Broker Policy." *International Journal of Advanced Research in Computer and Communication Engineering* 4, no. 1 (2015): 122-127.

CSCC Interoperability and portability for cloud computing A guide. www.cloud-council.org.

Darsahan Agrawal, Dinesh Goyal. "A new Framework for Improving Security for Data Migration in Cloud Computing." *International Journal of Innovative Computer Science & Engineering* 3, no. 4 (July-August-2016): 04-08.

Dawei Sun, Guiran Chang, Lina Sun, and Xingwei Wang,. "Surveying and Analyzing Security, Privacy and Trust Issues in Cloud Computing Environments." *Scienceverse Science Direct , Elsevier,* , 2011.

Dr. Chander Kant, Yogesh Sharma. "Enhanced Security Architecture For Cloud Data Security." *International Journal OF Advanced Research In Computer Science And Software Engineering* 3, no. 5 (2013): 571-575.

Enol Fernandez-del-Castillo, Diego Scardacia, Alvaro L ´ ope Garcýab. "The EGI Federated Cloud e-Infrastructure." *Procedia Computer Science, Elsevier Journal* , 2015: 196-205.

Gaetano Anastasi, Emauele Carlini, Patrizio Dazzi. "Smart Cloud Federation Simulations with Cloudsim." *IEEE International conference On Cloud Engineering-Usage Control In cloud Federations.* USA, 2014.

Gagandeep Kaur, Er. Sushil Kamboj. "A Review Of Balancing The Load On Cloud By Using ACCLB Hybrid Load Balancing Technique." *International Journal of Technology and Computing (IJTC)* 2, no. 7 (2016): 347-354.

Garima Joshi, S.K. Verma. "A review Of Load Balancing Approach in cloud computing." *International Journal of Computer Applications (0975 – 8887)* 119 No.20 (June 2015): 36-39.

Hakobyan, Davit. *Authentication And Authorization Systems In Cloud Environment.* Sweden: Master Of Science Thesis, 2012.

Hetal Patel, Ritesh Patel. "Cloud Analyst: An Insight Of Service Broker Policy." *Internation Journal Of Advanced Research In Computer And communication EngineeringIJARCCE* 4, no. 1 (2015): 122-127.

Hussain AlJahdali, Abdulaziz Albatli, Peter Garraghan, Paul Townend, Lydia Lau, Jie Xu. "Multi-Tenancy in Cloud Computing ." *IEEE 8th International Symposium on Service Oriented System Engineering*, 2014: 344-351.

Ilango Sriram, K Hosseini. "Research Agends In Cloud Technologies." *1st ACM symposium On Cloud Computing.* 2010.

Iqbal, Nasreen. "Cloud Computing And E-Business Migration." August 2015.

Jamie Lloret, Miguel Garcia, Jesus Tomas, Joel Rodrigues. "Architecture and Protocol for Intercloud Communication ." *Journal Of Information Sciences, Elsevier*, 2013.

Jing Tai Piao, Jun Yang. "A Network-aware Virtual Machine Placement And Migration Approach In Cloud Computing." *Ninth International Conference on Grid and Cloud Computing.* USA, 2010.

Joan Daemen, Vincent Rijmen. "AES Proposal: Rijndael." 1999.

Joan Daemen, Vincent Rijmen. *Announcing the ADVANCED ENCRYPTION STANDARD (AES).* Federal Information.

Joshua Holden, Mohammad Musa, Edward Schaefer, and Stephen Wedig,. "A Simplified AES Algorithm." January 2010.

Justice Opara Martins, Reza Sahandi, Feng Tian. "Ciritical Analysis Of Vendor Lock-in On Cloud Computing Migration: A Business

Perspective." *Springer Journal Of Cloud Computing*, 2016.

Kamel, Mentalla Ashrasf Fawzy. "Vendor Lock-in in the transistion to a Cloud Computing Platform." Sweden, 2015.

Lawrence Chung, Tom Hill, Owolabi Legunsen, Zhenzhou Sun, Adip Dsouza,. "A goal Oriented Simulation approach for obtaining good private cloud based system architectures." *Journal Of Systems and Software* Volume 86 , no. Issue 9 (September 2013): 2242-2262.

M.Uthaya Banu, M.Subha. "A Survey of Resource Provisioning in clouds." *Internation Journal Of Engineering Research and Applications* 4, no. 2 (February 2014): 30-35.

Makhdoom Muhammad Naeem, *Hidayatullah Mahar Furqan Memon, Muhammad Siddique, Abdul Rauf. "An Overview Of Virtualizaion and Cloud Computing." *SINTE 8* 28(4) (2016): 3799-3803.

Manasarah, Ahmad. "A Variable Service Broker Routing Policy For Data Centre Selection in Cloud Analyst." *Journal Of King Saud University-Computer And Information Sciences* 29, no. 3 (2017).

Marios D. Dikaiakos, George Pallis, Dimitrios. "Cloud Computing: Distributed Internet Computing for IT and scientific Research ." *IEEE Internet Computing* 1089-7801/09 (2009).

Mazadi, Nazia. "Cloud Computing Security Issues And Challenges." *International Journal of Scientific & Engineering Research July-2013* 4, no. 7 (2013).

Mihaela-Andreea Vaile, Florin Pop, Radu-Loan Tutueanu, Valentin Cristea, Joanna Kolodziej. "Resource Aware Hybrid Scheduling Algorithm in Heterogeneous Distributed Computing." *Future Generation Computer Systems* 51 (2015): 61-71.

Mishra, S.K., Sahoo, B., Parida Priti. " Load Balancing In Cloud Computing: A Big Picture." *Journal of King Saud University – Computer and Information Sciences* , 2018: 1-10.

Mohammad Rezah Meshbahi, Amir Masoud Rahmani, Mehdi Hosseinzadeh. "Reliability And High Availability In Cloud Computing Environment : A Refernce Road Map." *Human Centric Computing And Information Sciences, Springer Journal* , 2018: 2 -31.

S.M.Barhate, M.P.Dhore. "Data Migration issues in Cloud Computing: A Survey." *Special Issue of International Journal of Electronics, Communication & Soft Computing Science and Engineering, ISSN: 2277-9477*, 2015: 360-363.

S.M.Barhate, M.P.Dhore. "Hybrid Cloud: A Solution To Cloud Interoperability." *IEEE Journal, Proceedings of the 2nd International Conference on Inventive Communication and Computational Technologies (ICICCT 2018),*, 2018: 1242-1247.

Nadeem, auhammad Amir. "Cloud Computing: Security Issues And Challenges." *Journal of Wireless Communications 1 (1)*, 2016: 10-15.

Piyush Harsh, Florian Dudoet, Roberto Cascella, Yvon Jegou And Christine Morin. "Using Open Standards For Interoperability : Issues, Solutions, and Challenges Facing Cloud Computing." *IEEE Journal* , July 2012.

Priyanka Nema, Sapna Chaudhary, Tripti Nema. "VM Consolidation Technique For Green Cloud Computing." *Internation Journal Of Computer Science And Information Technology* 6, no. 5 (2015): 4620-4624.

S.M.Ranbhise, K.K. Joshi. "Simulation And Analysis of Cloud Environment." *International Journal of Advanced Research in Computer Science & Technology* 2 no.4 (December 2014): 206-209.

Qiao, Hang Wei and Pei-Li. "Reliability Assessment of Cloud Computing Platform Based on Semiquantitative and evidentiall reasoning." *Journal of Control Science and Engineering*, 2016: 1-10.

R. Buyya, C.S. Yeo, S. Venugopal, J. Broberg,. "Cloud Computing and Emerging IT Platfoms: Vision Hype and Reality." *Future Generation of Compter Systems* 25 No.6, no. doi:10.1016/j.future.2008.12.001. (June 2009): 599-616.

R. Rajeshkannan, M.Aramudhan. "Comparitive Study OF Load Balancing Algorithms In Cloud Computing." *International Journal Of Science And Technology* 9, no. 20 (2016): 1-7.

R.Kanniga Devi, S.Sujan. "A Survey on Application of Cloudsim Toolkit In Cloud Computing." *International Journal Of Innovative Research in Engineering, Science & Technology* Vol 3, no. Issue 6 (June 2014): 13146-13153.

Rabia Khan, Amjad Mehmood. "Realization of Interoperability And Portability Among Open Clouds Using Agents Mobility And Intelligence." *International Journal Of Advanced Computer Science* 3, no. 11 (2013): 544-549.

Raghuwanshi, V. Bagwaiya and S. K. " "Hybrid approach using throttled and ESCE load balancing Algorithm in Cloud compuing ." *nt.*

Conf. Green Comput. Commun. Electr. Eng., pp. 1–6. 2014.

Rajani, Mrs. Parekh Madhuri and Mr. Ishan. "Improve Performance Of Clustering On Data Sets With Improved Agglomerative CURE Algorithm." *Internation Journal Of Science Engineering And Technology Research (IJSETR)* 4, no. 6 (2015): 2026-2029.

Rajkumar Buyya, Chee Shin yeo, Shrikumar Venugopal, James Broberg, Ivona Brandic. "Cloud Computing and emerging IT Platforms: Vision, hype and reality for delivering computing as 5th Utility." *Future Generation Computer Systems, Elsevier*, 2008: 1-18.

Rajkumar Buyya, Rajiv Ranjan, Rodrigo Calheros. "Intercloud: Utility Federation of Cloud Computing Environment for Scaling Of Application Services." *C.-H. Hsu et al. (Eds.): ICA3PP 2010, Part I, LNCS 6081.* 2010. 13-31.

Ronald Rivest, . ""MD5 Message-Digest Algorithm rfc 1321." 1992.

S. Lee, I. Ong, H.T. Lim, H.J. Lee. "Two Factor Authentication For Cloud Computing." *International Journal Of Cloud Computing KIMICS* 8 (2010): 427-432.

S.M.Barhate, M.P.Dhore. "Intercloud Architecture For Interoperability In Cloud Computing: A Review." *International Journal OF Advanced Computational Engineering And Networking* 3, no. 12 (2015): 78-82.

S.M.Barhate, M.P.Dhore. "User Authetication Issues In Cloud Computing." *IOSR Journals of Computer Engineering*, 2016: 30-35.

Seyyed Mansur Hosseini, Mostafa Ghobaei Arnani. "Fault-Tolerence Tecniques In Cloud Storage : A Survey." *International Journal Of Database Theory And Application* 8, no. 4 (2015): 183-190.

Shen, Qigni et al. " Sec DM: Securing Data Migration Between Cloud Storage Systems." *IEEE conference on Dependable Autonomic And Secure Computing.* 2011.

Shweta Barhate, M.P.Dhore. "Data Migration Issues In Cloud Computing." *International Journal Of Electronics, Communication &Soft Computing Science And Engineering, IJCSCSE*, no. Special Issue (2015): 360-363.

Stelios Sotiriadis, Nik Bessis, Pierre Kuonen, Nick Antonopoulos. "The Inter-Cloud Meta-Scheduling (ICMS) Framework." *IEEE Conference On Advanced Information Networking and Applications.* 2013.

Stelioss Sotiriadis, Nik Bessis, Euripides Petrakis. "An Inter-Cloud Architecture For Future Internet Infrastructures." European Countries , Future Internet Social Technological Alignment Research(Fi-STAR) project, !st April 2013.

Suma V, Chintureena Thingom. " Improving Reliability in Cloud Computing Systems, ." *International Journal of Computer Applications (ICACCTHPA-2014)*, 2014: 10-13.

Thoke Virendra Dilip, D. O. Shamkuwar, Dr.Amol Dakhane. "A Survey on Privacy Preserving in Authentication Protocol for Shared Authority Based Cloud Computing." *International Journal for Research in Applied Science & Engineering Technology* 5, no. 3 (March 2017): 523-527.

Tina Matthew, K.Chandra Sekaran, John Jose. "Study And Analysis Of Various Task Scheduling Algorithms." *International Conference On Advances in Computing, Communications, Informatics(ICACCI).* 2014.

Umamakeswari, P. Padmakumari and A. "Methodical Review on Various Fault Tolerant and Monitoring Mechanisms to improve Reliability on Cloud Environment." *Indian Journal of Science and Technology, IJRST* 8, no. 35 (2015): 1-6.

Uthriaraj, D.Chitra Devi and V. Rhymend. "Load Balancing in Cloud Computing Environment Using Improved Weighted Round Robin Algorithm For Non Premptive Dependant Tasks." *Scietific World Journal* 2016 (2016): 1-16.

V.A.Jane, , B.J. Hubert Shanthan, L.Arokiam. "A Survey of Algorithms for Scheduling in the Cloud: In a metric Perspective." *International Journal of Computer Sciences and Engineering Open Access* 6, no. Special Issue 2 (2018).

Virendra Singh Kushwah, Aradhana Saxena. "A Security approach for Data Migration in Cloud Computing." *International Journal of Scientific and Research Publications* 3, no. 5 (May 2013): 1-8.

Y .Demchenko, JAG Aspin, S.Figeurola, N.Ciulli. "Intercloud Architecture Framework for Heterogeneous Clouds Based Infrastructure Service Provisioning On Demand." *Research Gate*, January 2013.

Peer Reviewed and Refereed Journal 2022 **(ISSN : 09726330)**

Rashtrasant Tukadoji Maharaj Nagpur University

SCIENCE JOURNAL 2022

Vol. : XV

Thermoluminescence and Photoluminescence properties of Europium doped Ba_2SiO_4 phosphor

P. P. Bhure[1], S.P. Puppalwar[1*], S. J. Dhoble[2]

[1]Department of Physics, Kamla Nehru Mahavidyalaya, Nagpur 440024, India
[2]Department of Physics, RTM Nagpur University, Nagpur 440024, India

Corresponding author email :
suresh.puppalwar@gmail.com

ABSTRACT

An orange-red emitting phosphor Ba_2SiO_4 doped with europium ion with variable concentrations (0.2 – 1.5mol%) was synthesized by modified solid state reaction method. The phosphor $Ba_2SiO_4:Eu^{3+}$ was characterized by X-ray diffraction technique for structural analysis and scanning electron microscopy (SEM) for morphological studies. A single prominent glow peak was found at 146 ^{0}C which indicates that only one trap centre is formed in the sample.Sample show good TL glow curves for variableă-ray exposure time. The peak shape method was used to calculate kinetic parameters (activation energy and frequency factor).The resultsconfirm that $Ba_2SiO_4:Eu^{3+}$phosphor may be useful inradiation dosimetry.PL emission spectra consists prominent peaks ataround 594 and 614 nm in orange-red region when excited by 394nm wavelength.

Keywords : $Ba_2SiO_4:Eu^{3+}$; XRD; SEM; Thermoluminescence; Photoluminescence.

1. Introduction

Due to suitable energy band structure, high chemical stability, easy preparation and low-cost properties, silicates are the good hosts for the development of phosphors.Ca_2SiO_4 and Ba_2SiO_4 activated with Eu^{2+} were studied at different temperature which show green, orange emission band [1, 2].The long-lasting phosphor $Ba_2SiO_4:Eu^{2+}$ show a great application for X-ray technique and cathode ray tube [3].Eu^{2+} activated Li_2SrSiO_4 phosphor used as solid-state lighting [4, 5]. Light-emitting diodes (LEDs) for solid state lighting have significant potential in terms of energy savings and environmental advantages, and are expected to replace most gas discharge fluorescent lamps in the near future [6, 7]. The trivalent rare-earth ion plays a role of efficient emitter in various types of host materials having wide application in lighting world. Among the different RE species, Eu is the special rare earth element as an activator for the hosts, because it exists in divalent and as well as in trivalent also, and hence due to different valance it shows different optical properties [8].

There are few reports found on Ba_2SiO_4phosphor only on photolu-minescence, However the prepared material was studied another important luminescence study is thermoluminescence (TL).Thermoluminescence is a common method used for the measurement of doses of ionizing radiations.The position, shape and intensities of the glow peaks are related to the properties of the trapping states accountable for the TL. The

luminescent properties of dosimetric materials are enhanced by doping different rare earths [9-13].Many researchers studied the TL kinetic parameters of rare earth doped phosphors[14].

The present paper describes synthesisof trivalent rare earth Eu^{3+} doped Ba_2SiO_4 phosphor and examine photoluminescence and thermoluminescence properties characterized by XRD, SEM, TL and PL. To the best of our knowledge there is no report on TL properties of Ba_2SiO_4: Eu^{3+} phosphor. In this study, we have prepared Ba_2SiO_4: Eu^{3+} with changing concentration of Eu^{3+} (0.5, 1, 1.5, 2mol%) using conventional solid-state reaction technique. Thermoluminescence parameters were also calculated to check the suitability of prepared phosphors as an orange light source. The luminescence intensities of the prepared Ba_2SiO_4: Eu^{3+} phosphors can be improved by UV excitation at 392 nm and used as the potential UV-LED orange phosphor. Also, kinetic parameters of TL glow curve of Ba_2SiO_4: Eu^{3+}phosphor are determined.

2. Experimental

The sample investigated in this paper was prepared by high temperature solid state reaction method.For the preparation of Eu^{3+}doped Ba_2SiO_4 phosphor all starting materials used were of analytical grade. All the materials Ba_2CO_3, SiO_2 (A.R.), Eu_2O_3 (99.99%) were taken in stoichiometric ratio. The raw materials and dopant were mixed well by grinding using mortar-pestle.The ground powder wascalcined at 500^0C for 3 hrs in asilica crucible. The obtained mixture was again ground for 1 hr and was annealed at 900 ^{0}C for 5 hrs. The product on coolingagaincrushed andsuch fine powder sample was used for XRD, SEM, PL and TL characterization.

The chemical reaction used for stoichiometric calculation is :

$2BaCO_3 + SiO_2 + xEu_2O_3$'! Ba_2SiO_4:$xEu^{3+} + 2CO_2$'!

The structural characterization of as prepared phosphor was carried out by X-ray diffractionusing a PAN-analytical diffractometer with Cu Ká radiation (ë=1.5405 A0) operating at 40kV, 30mA. The data was collected at the angular rangefrom 10 to 80°, with the continuous scan mode.The morphology was characterized with JEOL, JSM-6360LV SEM scanning electron microscope.Excitation and emission spectra were measured by fluorescence spectrometer (RF-5301PC Spectrofluorophotometer) with a 150 W xenon lamp as excitation source, while the spectral slit width was 1.5 nm. For TL studies, samples were exposed to ă-rays from a ^{60}Co source at the rate 0.98 kGy/hr. The TL glow curves were recorded with the help of Nucleonix 1009 TL reader.All the measurements were carried out at room temperature.

3. Results and discussion

3.1. Structural analysis and morphology

Figure 1 represents the XRD pattern of the prepared Eu^{3+} doped Ba_2SiO_4phosphor.It shows that phosphor is well progressive and crystallized.Doping of Eu^{3+} ions does not affect the host material with significant changes.No other phase was identified indicating that the doping $Eu^{3+}$was incorporated into the matrix lattice, rather than forming new phases beside the host material in the synthesis process.The diffraction pattern obtained well matched with the standard JCPDS file (ICSD No. 26 - 1403). It is clear that Ba_2SiO_4:Eu^{3+} powderhas orthorhombic structure with the space group P*nam*having two crystallographic distinct of Cs symmetry phase with lattice constants are a = 7.508 A°, b = 10.214 A°, c = 5.809 A°, V=465.754A°^{3}.It suggests that the Eu^{3+} ions probably are occupying Ba^{2+} sites inBa_2SiO_4 network.The Ba_2SiO_4lattice structure and the Ba^{2+} and Si^{4+} sites areillustrated in Fig. 2(a).K. A. Denault et al. [15] described the Ba_2SiO_4structure as shown in Fig. 2(b).SEM image of Ba_2SiO_4phosphor is represented in Fig. 3 for the synthesized phosphor. It indicates that in solid state reaction synthesized phosphor, the particles are quiteagglomerated and show irregular shaped morphology.From the SEM image itwas also confirmed that the particles are in submicron range.

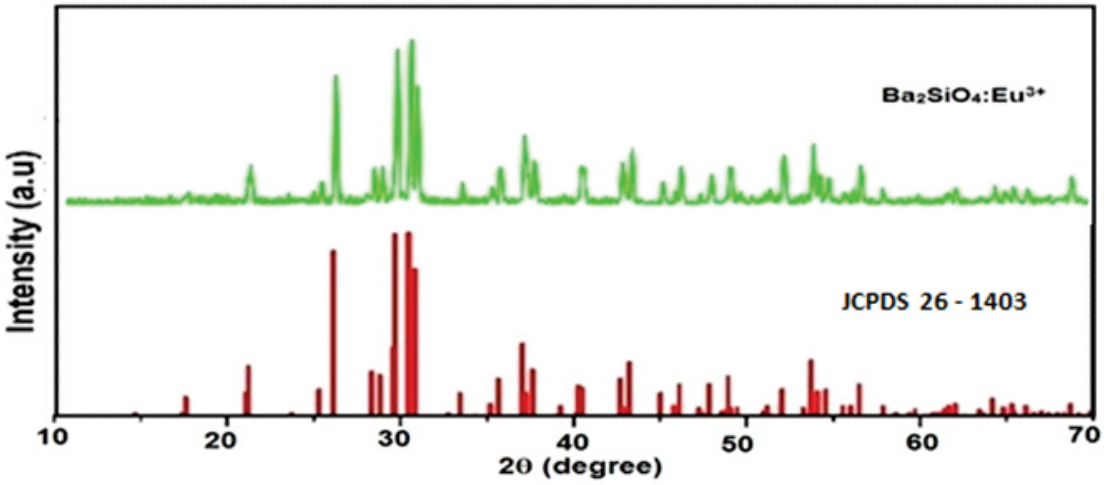

Fig.1. XRD pattern of Eu^{3+} doped Ba_2SiO_4 phosphor with standard pattern (JCPDS 26-1403).

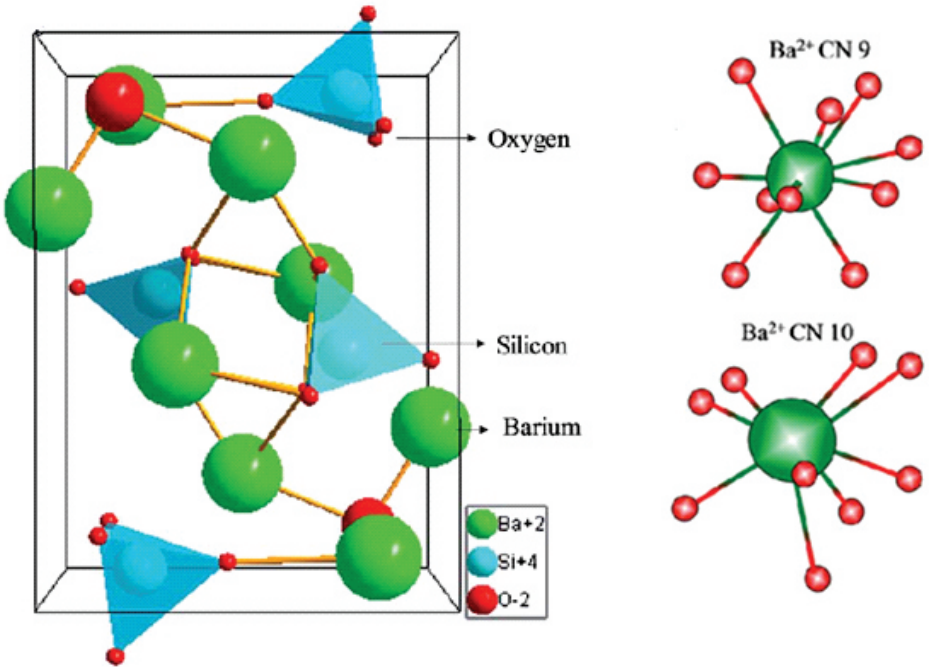

Fig. 2. (a) Crystal structure of Ba_2SiO_4, based on the CIF file available on Inorganic crystal structure database (ICSD); (b) representation of the two Ba^{2+} ion sites, with coordination number of 9 and 10 [15].

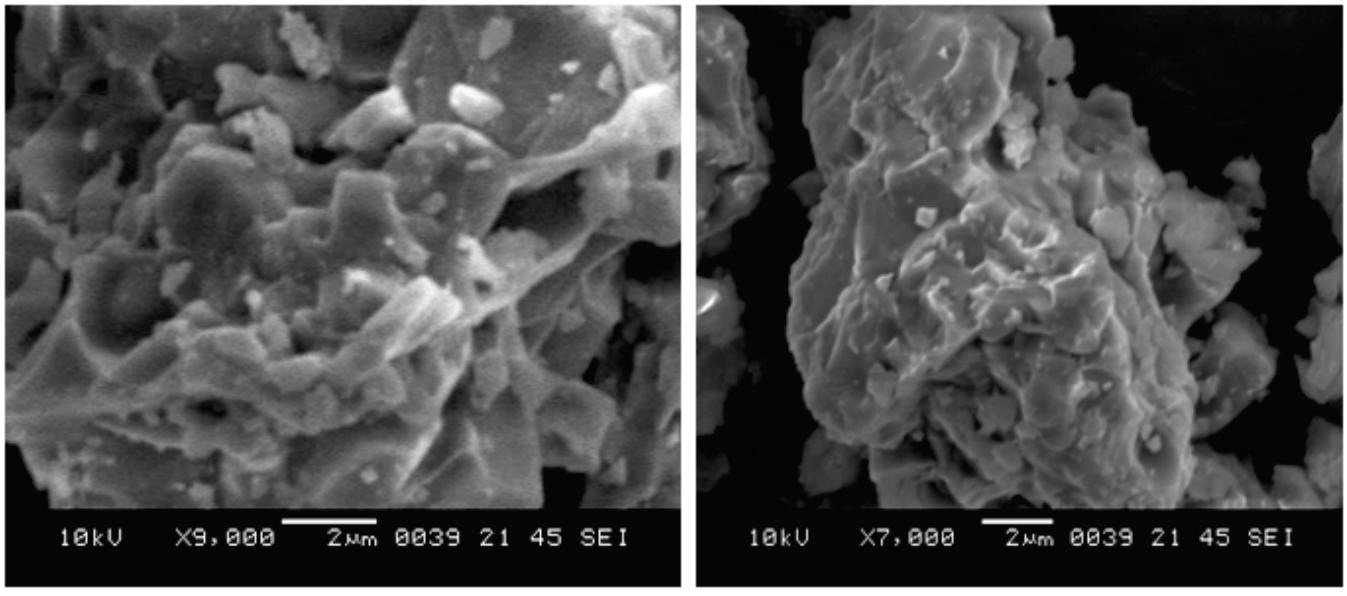

Fig.3. Scanning electron microscopy images of Eu^{3+} doped Ba_2SiO_4.

3.2 Thermoluminescence study

The TL glow curves of Ba_2SiO_4: Eu(0.5 mol %) phosphor exposed to ^{60}Co ă-irradiation at a heating rate of 5°C/s for different ă-rayexposure recorded in 50-400 °C temperature range are displayed in Fig 4. A prominent single peak of Ba_2SiO_4: Euphosphor at 146 °Cis recordedwhich is a good peak for thermoluminescence dosimeterpeak. It indicates that only one type of luminescent/trapping centre is created in the sample.

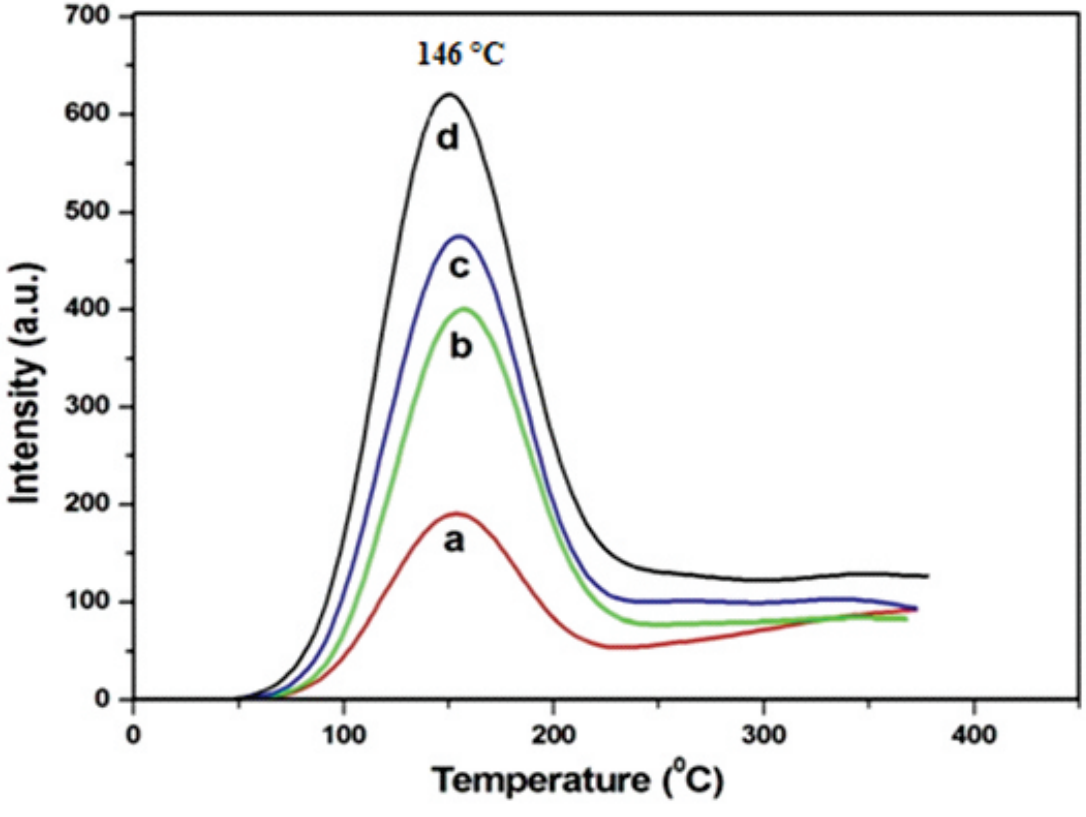

Fig.4.TL glow curve of Ba_2SiO_4: Eu (1mol %) for different doses of ã-ray exposure (a) 1min, (b) 2 min, (c) 3 min and (d) 5 min.

The peak centred at 146 °Cis due to formation of shallower trap.However, with increase in ă-rayexposuretime, the TL intensity goes on increases and becomes maximum for 5 min exposuretime after that it decreases. The trapping of electronsand recombinationefficiency depending on the exposure time is mainly responsible forvariation in glow peak intensity[16, 17]. From the figure, it can be seen that the shape and position of glow curve is constant for all different doses.Figure 5 shows the variation in TL intensity as a function of the exposure time, in the range from 1 to 5min exposure of ă-rays.The TL-dose dependence curve was observed to be almost linear in the studied dose range.

The analysis of TL glow curve leads to the estimation of kinetic parameters, namely activation energy E, frequency factor s, order of kinetics b. All the parameters are calculated by using the easiest and most popular peak shape method by usingChen's equations [18].

$E = C_\gamma (kT^2_m / \gamma) - b_\gamma (2kT_m)$ ----- (1)

where γ stands for τ, δ and ω respectively. The value of the C_γ and b_γ are calculated using

$C_\tau = [1.15+3(\mu_g - 0.42)]$; $b_\tau = [1.58+4.2(\mu_g - 0.42)]$

$C_\delta = [0.976+7.3(\mu_g - 0.42)]$; $b_\delta = 0$

$C_\omega = [2.52+10.2(\mu_g - 0.42)]$; $b_\omega = 1$

Once orders of kinetics and activation energy were determined, the frequency factor (s) was calculated by the equation,

$\beta E / kT^2m = s [1+ (b-1) 2kT_m / E] \exp (-E / kT_m)$ ----- (2)

where β is the heating rate.

The estimated kinetic parameters (E, ěg and b) are summarized in the Table 1.This shows that the experimental and theoreticalcurves are in good agreement.Activation energy is found to be 0.69 eV which shows very less energy required to release electron from the trap.

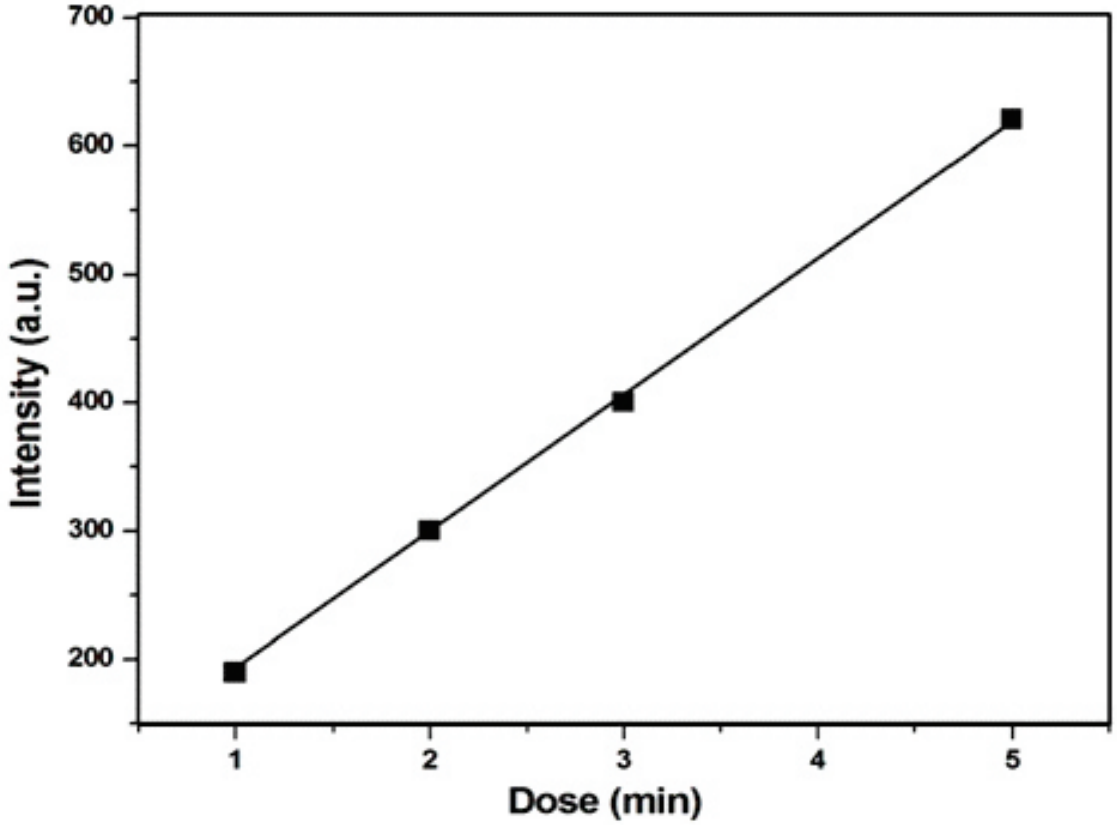

Fig.5. Dose response curve of Ba_2SiO_4: Eu phosphor

The frequency factor is found to be 5.236 x10^8 s^{-1}. It can be concluded that Ba_2SiO_4: Eu^{3+}phosphor is a good thermoluminesent material.

Table 1

The kinetic parameter of 146 °C glow peak of Ba_2SiO_4: Eu^{3+} phosphor.

Trap parameters	Mean values
T_1 (°C)	112
T_m (°C)	146
T_2 (°C)	196
E_τ(eV)	0.7338
E_δ(eV)	0.6714
E_ω(eV)	0.6945
Mean Activation energy 'E' (eV)	0.69
Symmetry factor 'μ_g'	0.51
Order of kinetics 'b'	2
Frequency factor 's' (s^{-1})	5.236×10^8 s^{-1}

3.3 Photoluminescence Properties

Figure 6 and 7 shows the excitation and emission spectra of Ba_2SiO_4: Eu, respectively. The excitation spectrum of the prepared sample monitored at 594 nm of emission is shown in Fig.6. In excitation spectrum the strong sharp peak is observed at 394 nmwhich is attributed to

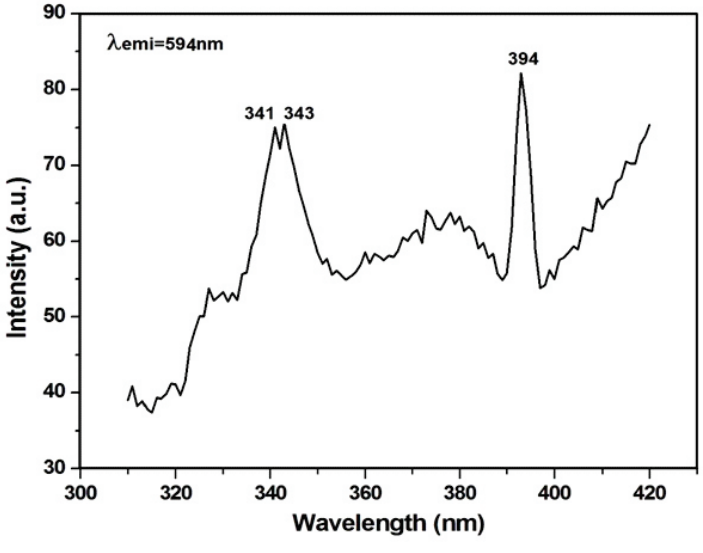

Fig.6. PLE spectrum of Ba_2SiO_4: 0.01Eu^{3+} phosphor at λ_{emi} = 594 nm

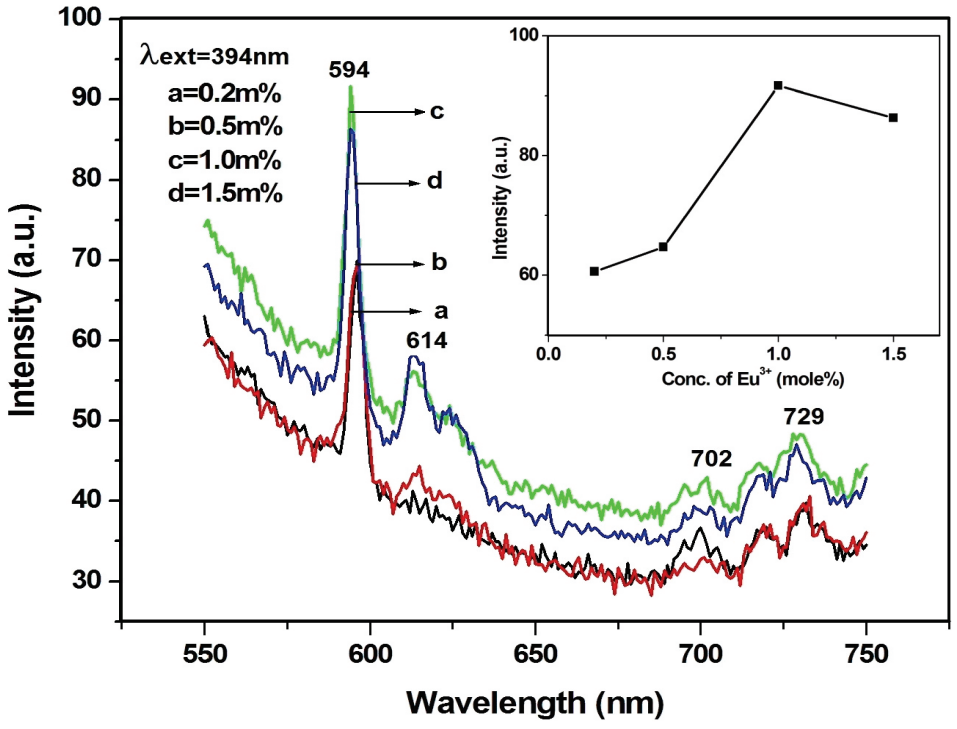

Fig.7 PL emission spectra of Ba_2SiO_4:xEu³⁺ phosphor at different concentrations at ë$_{ext}$ = 394 nm. Inset shows the relationship between emission intensity and concentrations.

the $^7F_0$'!$^5L_6$ transition of Eu^{3+}. In addition to this characteristic peak, the lessintense excitation peaks located at 341 nm, and 376 nm are ascribed to intra-configurational 4f-4f transitions of Eu^{3+} ion. The emission spectrum of Ba_2SiO_4:Eu^{3+}phosphor is displayed in Fig. 7, for the excitation of 394 nm.Eu^{3+} gives characteristic emission in the orange-red region of the spectrum corresponding to thetransitions $^5D_0$ '! ^7F_j(where j = 1, 2, 3, 4).All the spectra show prominent peaks at 594 and 614 nm corresponding to magnetic dipole transition ($^5D_0$–$^7F_1$) and electric dipole transition ($^5D_0$'!$^7F_2$), respectively. Apart from these prominent peaks, we could also observe other weak emission peaks centred at 702 and 729 nm corresponding to $^5D_0$'!$^7F_4$ transitions.As it is seen from Fig. 7, the orange emission of $^5D_0$–$^7F_1$at 594 nm is dominant, which reveals that Eu^{3+} is located in symmetrical site in Ba_2SiO_4.The excitation and emission spectra of Ba_2SiO_4:xEu^{3+} (0.2d"xd"1.5, x is in mol%) are similar in profile. Inset showstheconcentrationdependent orange-red emissionintensityofEu^{3+}ion in Ba_2SiO_4due to the $^5D_0$–$^7F_1$transition at594 nm, withexcitationat394 nm.Theemissionintensityincreases initially with the increase ofEu^{3+} concentration andreachesto the maximum at 1 mol%, thengraduallydecreasesduetothe internal concentrationquenching.

4. Conclusion

The phosphors Ba_2SiO_4:Eu^{3+} are synthesized by high temperature solid state reaction technique which is suitable for large scale production of phosphors. There is fair matching of XRD pattern of the prepared sample with the standard XRD patterns.The prepared sample has orthorhombic structure and no impurity phase was found in XRD.SEM micrographs of the phosphor shows agglomerated and irregular shaped particles.TL properties of ă-rayirradiated phosphor was investigated which shows a single peak at146 °Cindicates only one trap centre is formed in the sample.The TL glow curve analysis, shows that the TL glow curve peaks of Ba_2SiO_4:Eu^{3+}obey second order kinetics.Trap depth and frequency factor are found to be 0.69 eV and 5.236 x 10^8 s^{-1}, respectively.It is also observed that the intensity of glow peak increases linearly with the exposure time (dose) which indicates that theBa_2SiO_4: Eu^{3+} is suitable for radiation dosimetry application.For the excitation at 394 nm, the phosphor Ba_2SiO_4:Eu^{3+}emitsin the orange-red region.From the luminescence studythe optimum concentration of luminescence is found to be 1 mol%. It is concluded that Eu^{3+} acts as luminescent centre in Ba_2SiO_4:Euphosphor.

Acknowledgement

Author SPP is thankful to management of the Institution KNM, Nagpur for providing useful facilities of the instrumentation, SHIMADZU Spectrofluorophotometer (RF-5301 PC).

References

[1] Kim J.S., Park Y.H., Kim S.M., Choi J.C., Park H.L. 2005. Temperature-dependent emission spectra ofM_2SiO_4: Eu^{2+} (M = Ca, Sr, Ba) phosphors for green and greenish white LEDs. Solid StateCommun.133, 445-448.

[2] Grinberg M, Barzowska J. 2011. Characterisation of various Eu^{2+} sites in Ca_2SiO_4: Eu^{2+}. MaterialSci. 29, 272-277.

[3] Streit HC, Kramer J, Suta M, and Wickleder C. Red, Green, and Blue Photoluminescence ofBa_2SiO_4:M (M = Eu^{3+}, Eu^{2+}, Sr^{2+}) Nanophosphors.

[4] Yu X, Wang Y, 2010. Synthesis and photoluminescence improvement of mono dispersed Zn_2SiO_4: Mn^{2+}nanophosphors. J Alloy Compd. 497, 290-294.

[5] Saradhi MP,Varadaraju UV, 2006. Photoluminescence studies on Eu^{2+} activated Li_2SrSiO_4 a potential orange yellow phosphor for solid state lighting. J Chem Mater.18, 5267-5272.

[6] Nakamura S, 1994. Candela class high brightness in GaN/AlGaN double hetero structure blue lightemitting diodes. Appl. PhysLett.64, 1687.

[7] Shubert EF, Kim JU. 2005. Solid state light sources getting smart: Review. Science; 308, 1274-1278.

[8] Yong J., Yong L., Liu W., Zang Y., Fan H., Wang Y., Liu H., Lang J., Wang D. 2008. Luminescencebehaviour of Eu^{3+} in $CaSiO_3$: Eu^{3+} (Bi^{3+}) and Sr_2SiO_4: Eu^{3+} (Bi^{3+}), J. Alloys Compd. 454 (1–2), 506.

[9] Premkumar HB, Nagabhushana H, Sharma SC. 2014. Structural, photo and thermoluminescence studies of Eu^{3+} doped orthorhombic $YAlO_3$nanophosphors. Alloy Comp. 601, 75.

[10] KoreBP, Dhoble SJ,Park K, Dhoble NS. 2013. Photoluminescence and thermoluminescence properties of Dy^{3+}/Eu^{2+} activated $Na_{21}Mg(SO_4)_{10}Cl_3$ phosphors. J Lumin. 143, 337-342.

[11] Dhoble SJ, Moharil SV. Preparation and characterisation of Eu^{2+} activated $Sr_2B_5O_9Cl$ TLD phosphor J. Nucl. Instrum. Methods B 2000; 160; 274.

[12] S. P. Puppalwar and S.J. Dhoble, Development of high sensitive $LiNaSO_4$: Cu, Mg phosphor for TL dosimetry. J. Lumin. 137 (2013) 245–251.

[13] Horowitz YS, Moscovitch M.2013. Highlights and pitfall of 20 years of application of computerized glow curve analysis to thermoluminescence research and dosimetry. Radiatdosimetry. 153,1-22.

[14] Reddy AJ, Kokila M.K., Nagabhushana H., Sharma S.C., Rao J.L., Shivakumara C., Nagabhushana B.M., Chakradar R.P.S. 2012. Structural, EPR, photo and thermoluminescence properties of ZnO:Fe nanoparticles. Materials chemistry and Physics.133, 876-865.

[15] Denault K. A., Brgoch J., Klob S. D., Gaultois M. W., Siewenie J., Page K.andSeshadri R. 2015. Average and Local Structure, Debye Temperature, and Structural Rigidity in Some Oxide Compounds Related to Phosphor Hosts. ACS Appl. Mater. Interfaces. 7, 7264-7272.

[16] Chung K.S., Choe H.S., Lee J.I., Kim J.L. 2007. A new method for the numerical analysis of thermoluminescence glow curve. Radiation measurements. 42, 731-734.

[17] Chandrasekhar M., V.Sunitha D., Dhananjaya N., Nagabhushana H., Sharma S.C., Nagabhushana B.M., Shivakumara C., Chakradhar R.P.S. 2012. Thermoluminescenceresponse ingamma and UV irradiated Dy_2O_3. 132, 1798-1806.

[18] Chen R, 1983. Determination of the kinetic order of thermoluminescence in the presence of a distribution of electron trap activation energies J.Phys D. Appl. Phys. 16, 107-114.

Peer Reviewed and Refereed Journal 2022 **(ISSN : 09726330)**

Rashtrasant Tukadoji Maharaj Nagpur University

SCIENCE JOURNAL 2022

Vol. : XV

Role of Fluids in the Genesis of Green Mica Quartzites of Palasgaon-Saigaon Area, Western Bastar Craton, India

Randive K. R.[1*], Shende S. S.[1], Ramteke B. P.[1] Sanjeevani Jawadand[1], Pratik Godbole[1], Dora M. L.[2]

[1]Department of Geology, R.T.M. Nagpur University, Nagpur - 440001, India.

[2]Geological Survey of India, Central Region, Nagpur – 440006, India.

Corresponding author email : randive101@yahoo.co.in

ABSTRACT

The fluid inclusions occurring in the Cr-rich green-mica quartzites of Palasgaon-Saigaon area have been studies using Linkam THMS-600 Heating-Freezing stage. Two types of inclusions, viz. carbonic and aqueous-carbonic have yielded variable ranges of temperature (115°C to 218°C) and salinity (1.15 to 26.59 wt% of NaCl equivalent). Among the possibilities the sources of such fluids could either be Cr- rich hydrothermal fluids or the fluids formed during metamorphism of Cr- rich sediments under hydrous conditions. In this paper, former view is preferred.

INTRODUCTION

Green mica quartzites, which are often referred to as 'fuchsite' quartzites occur profusely in the Archaen metasedimentary terrains. The green micas are either chromium-muscovites or fuchsites in composition. Their peculiar color is commonly attributed to the concentration of chromium or iron in the micas. Two types of origins are commonly envisaged for the formation of green mica quartzites, namely, hydrothermal alteration, in which, mica is formed either due to replacement of pre-existing rocks or due to hydrothermal solutions emanating from magmatic intrusions (Whitemore et al., 1946; Gieger, 1963; Morata et al., 2001; Arif and Moon, 2007); or formed by metamorphism of chrome-rich minerals in the source rock (Leo et al., 1965; Argast, 1995).

In this paper we are presenting the data on fluid inclusions in quartz occurring within green-mica quartzites. An attempt has been made to investigate the source of chromium through the entrapped fluids.

Geology of the Area: The Bastar Craton is a square shaped (~500 Km^2) crustal block in south-central India (Fig. 1) bounded to the north by the Central Indian Tectonic Zone, south by Eastern Ghat Mobile Belt, east by Mahanadi Rift and west by Godavari Rift (Ramakrishnan and Vaidyanadhan, 2008; Meert et al., 2011). The high-grade gneissic terrain forms the basement for supracrustals represented by phyllite, schist, quartzite and meta-carbonate inter-bedded with metabasalts. The gneissic complex of the Bastar Craton consists of TTG (Tonalite-Trondjhemite-Granodiorite) suite of rocks that are extensively exposed in south and west of the Craton. The TTG gneisses enclose rafts of 'continental' sediments of quartzite-

carbonate-pelite (QCP) facies, together with minor BIF and mafic-ultramafic rocks (e.g. Sukma Group of Bastar and Amgaon Group of Bhandara).

The study area is bounded between latitudes 20º16' to 20º30' and longitudes 79º35' to 79º55' covering an area of about ~200 sq. kms (Fig. 1). Several lenticular ridges of quartzites are formed in the area, however, only few of these outcrops have green mica associated with them. Two such localities namely, Palasgaon and Saigaon were selected for study.

Microthermometric Measurements: The Microthermometric measurements were made using a Linkam THMS-600 Heating-Freezing stage; a silver block (THMSB) was used for heating. The unit operates in the temperature range of -195º to 600ºC. The stage is periodically calibrated by using demineralized water (H_2O melting point = 0ºC) and pure CO_2 inclusions (synthetic CO_2 standard, with triple point = -56.6ºC). The final melting temperature of ice (Tm_{ice}) was used to determine the salinity of aqueous phase. Homogenisation temperatures of the CO_2 (Th_{CO2}) were measured to determine the density of CO_2 and the total homogenisation temperature (Th_{Total}). Calculation of density, salinity and plotting the isochores of temperature and pressure were carried out by using Linksys software (version 1.8).

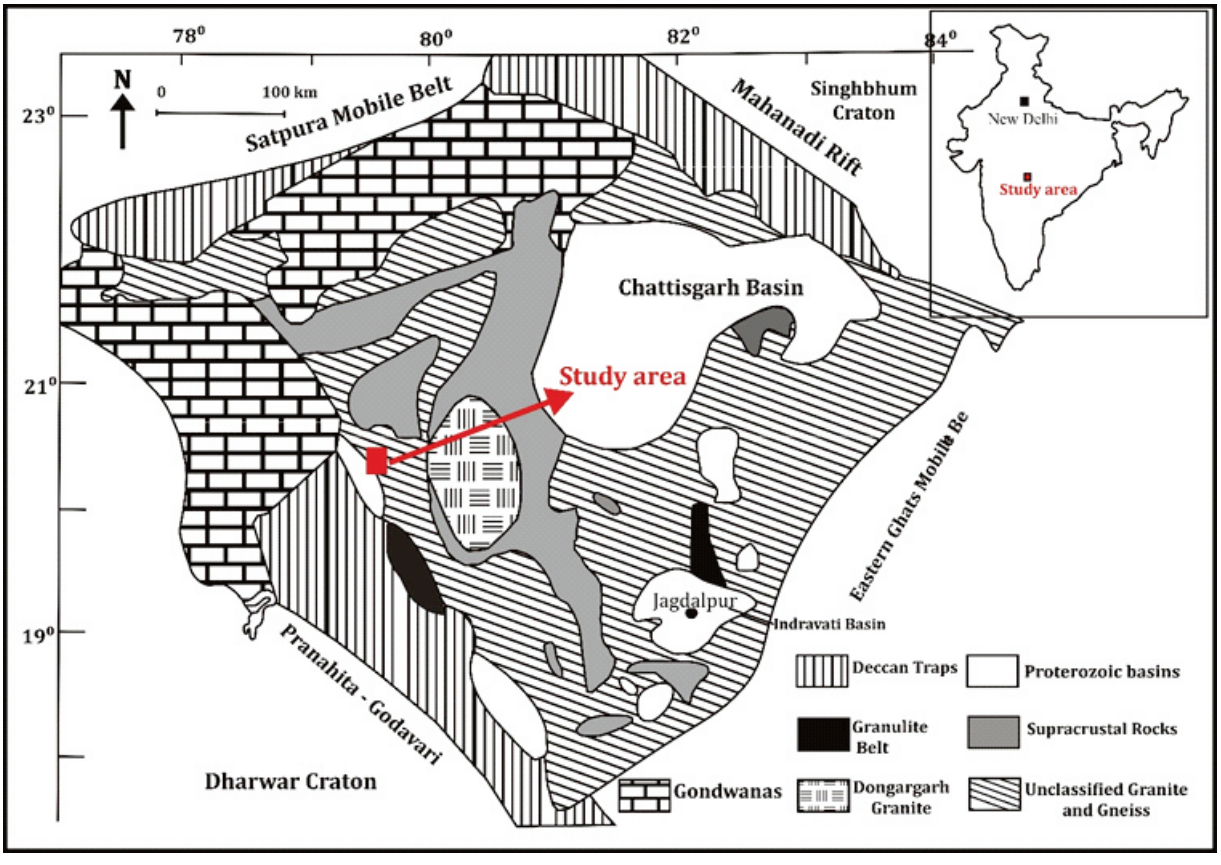

Figure 1: Geological map showing study area.

RESULTS:

Carbonic Inclusions: Carbonic fluid inclusions are less abundant than aqueous fluid inclusions in these samples. Primary carbonic fluid inclusions are scattered, and mono-phase at room temperature (Fig 2). During cooling experiments, a vapour bubble nucleates and homogenizes within the liquid phase. The melting temperature of CO_2 ranges from -56.8°C to -58.1°C indicating that the fluid is dominated by CO_2 and the maximum depression of melting temperature of CO_2 The isochors of carbonic inclusions are approximated by a CO_2 system, revealing that there was a change in fluid pressures; which varies from 1000 to 1600 bars. The carbonic inclusions probably formed from homogeneous trapping of the vapor phase only, so the temperature of total homogenization cannot be measured. The

density of the CO_2 varies from 0.67 to 0.82 g/cm^3.

Aqueous and aqueous carbonic inclusions: The observed temperature and calculated data of melting of ice (initial & final), temperature of homogenisation of CO_2 (Th_{CO2}) and total homogenisation temperature (Th_{Total}) of inclusions was determined. The Th_{Total} varies from 115°C to 218°C (average = 169°C) that corresponds to a salinity range of 1.15 to 26.59 wt.% NaCl equivalent (average 18.07 wt.% NaCl equivalent) following the equations of Bodnar (1983); Zhang and Frantz (1987); and Brown and Lamb (1988). The initial ice melting temperatures (TFM) range from - 55°C to - 35°C with an average of - 46.11°C. This suggests that the major component in aqueous phase is NaCl ± $CaCl_2$ in the fluid system. The maximum of first ice melting temperature of - 55°C may indicate the presence of $CaCl_2$ with NaCl and H_2O (Shepherd et al., 1985). The final melting temperature of ice ranges from -0.7°C to -27°C (average -14.88°C) corresponding with salinities of 1.15 to 26.59 wt.% NaCl equivalent.

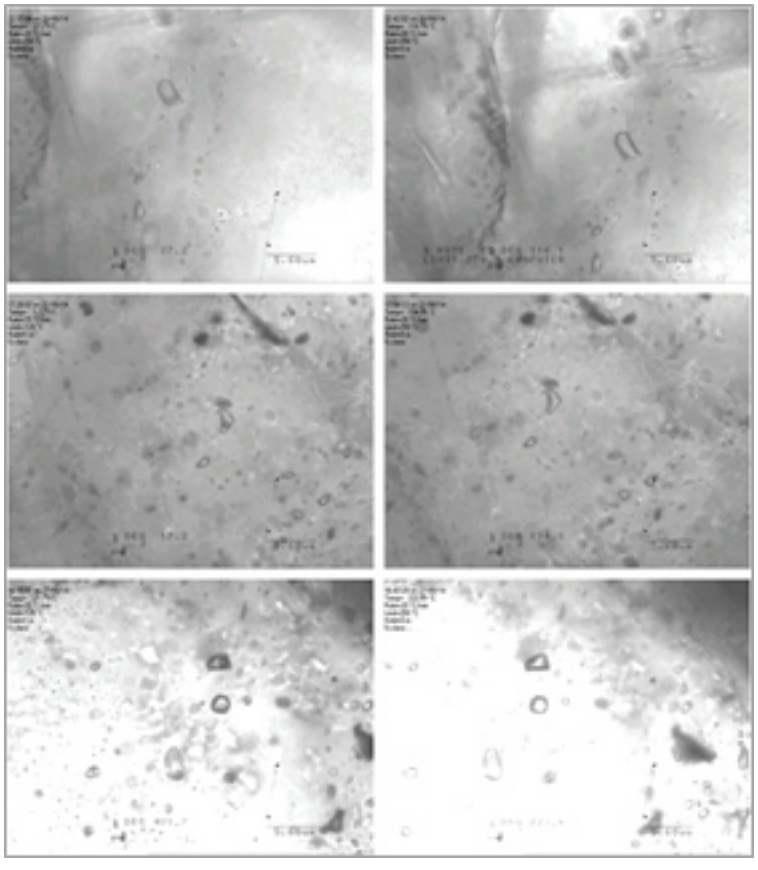

Figure 2: Photomicrographs showing initial state of inclusions (left side) and after attaining homogenization (right side).

The Temperature of homogenisation versus Salinity plot using the PVTX modeling software for fluid inclusions (version 2.01) is given in Fig. 3. The P-T estimates made from the total homogenisation of the aqueous-carbonic inclusions define a P-T path of evolution. The intersecting isochores are designed for inclusions, which record the trapping of immiscible fluids (Shepherd et al. 1985) and in the present case the isochores for mixed H_2O-CO_2 fluids are considered. The P-T curves of the inclusions studied are reported in Fig. 3. The isochores are representing individual fluid inclusions studied and are widely distributed from 115°C to 218°C of temperature of homogenisation (average = 169°C). The plot of co-existing aqueous and aqueous-carbonic inclusions shows intersecting isochores. The population of isochors measured ranges between 130°C - 175°C and 195°C - 215°C respectively.

The temperature of homogenization versus salinity plots for these inclusions are plotted in Fig. 4. The most characteristic feature is the clustering of data in the diagram. The trends of inclusion plots indicate the following

possibilities: (i) Simple cooling and (ii) Mixing with cooler and less saline fluid (Shepherd et al., 1985).

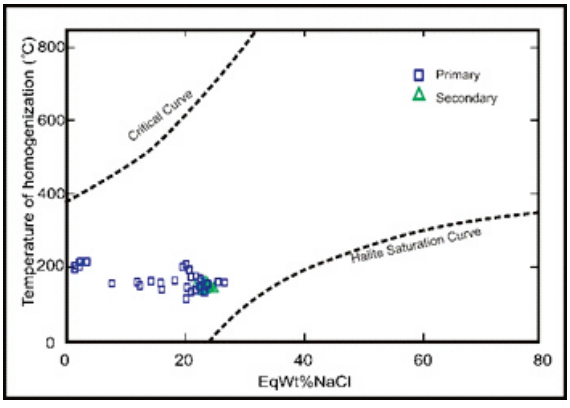

Figure 3: Plot of temperature of homogenization versus salinity.

Discussion and Conclusions: Majority of the Archaean fuchsite/chrome muscovite quartzites reported world-over were shown to be of metamorphic origin e.g. Acworth Township, New Hampshire; several deposits in Montana, U.S.A. (Heinrich, 1965); Dharwar craton, India (Argast, 1995); Outokumpu Finland (Treloar, 1987); although with some exceptions such as a Ghatti Hosa Halli and Belvadi, Dharwar craton (Raase et.al, 1983) where, hydrothermal leaching of the mafic-ultramafic rocks and subsequent fixing of Cr in clay fraction of sediment was proposed. On the other hand, there are localities such as Almaden mercury mining district of Spain (Morata et al., 2001) and Indus–Suture ophiolites, NW of Pakistan (Arif and Moon, 2007) where, hydrothermal alteration of primary Cr-rich spinels or extraction of Cr, Ni and Mg by hydrothermal solutions through wall rock alterations is proposed.

The Cr-muscovites are formed either within or along-side quartz crystals. The protuberances emanating out of mica join the micro- fractures within rock, even in schistose quartzite such inclusions are present within quartz crystals. The trapped inclusions form linear traces parallel to one another scavenging throughout the rock and continue occasionally through mica crystals, although many times truncated by bigger crystals of mica. There are two possibilities, either the Cr-rich hydrothermal solutions played a major role in formation of such fluids; or Cr-rich fluids were formed during metamorphism of Cr-rich sediments under hydrous conditions. Probable P-T conditions of crystallization of quartz estimated from the present study are much less than those of green-schist facies metamorphic conditions to which these rocks were subjected (Randive et al., 2015); therefore, role of Cr-rich hydrothermal fluids cannot be ruled out. However, whether the trapped fluids are chromium rich or not remains a moot point.

REFERENCES

Argast, Scott, 1995. Detrital origin of fuchsite-bearing quartzites in the western Dharwar craton, Karnataka, India. Journal Geological Society of India v. 45, 559-575.

Arif, M., Moon, C.J., 2007. Nickel-rich chromian muscovite from the Indus suture ophiolite, NW Pakistan: Implications for emerald genesis and exploration. Geochemical Journal 41, 475-482.

Bodnar, R.J. 1983 A method of calculating fluid-inclusion volumes based on vapor bubble diameters and P-V-T-X properties of inclusion fluids. Economic Geology, v. 78, 535-542.

Brown, P.E., Lamb, W.M. 1988 P-V-T properties of fluids in the system H2O-CO2-NaCl: New graphical presentation and implications for fluid inclusion studies. Geochimica et Cosmochimica Acta, v. 53, 1209-21.

Geijer, P., 1963. On the source of chromium micas. Arkiv. Mineral. Geol. v. 3, 415-422.

Heinrich, E. W., 1965. Further information on the geology of chromian muscovites. The American Mineralogist v. 50, 758-762.

Leo, G.W., Rose, Jr., Warr, J.J., 1965. Chromian muscovite from the Serra de Jacobina, Bahia, Brazil. The American Mineralogist v. 50, 392-402.

Meert, J.G., Pandit, M.K., Pradhan, V.R., Kamenov, G., 2011. Preliminary report on the paleomagnetism of 1.88 Ga dykes from the Bastar and Dharwar cratons, peninsular India. Gondwana Research v. 20, 335-343.

Morata, D., Higueras, P., Dominguez-Bella, S., Parras, J., Velasco, F., Aparicio, P., 2001. Fuchsite and other Cr-rich phyllosilicates in ultramafic enclaves from Almaden mercury district, Spain. Clay Minerals v. 36, 345-354.

Ramkrishnan, M., Vaidynadhan, R., 2008. Geology of India. Geological Society of India, Bangalore.

Randive, K. R.; Korakoppa, M. M.; Muley, S. V.; Varade, A. M.; Khandare, H. W.; Lanjewar, S. G.; Tiwari, R. R. and Aradhi, K. K. 2015. Paragenesis of Cr-rich muscovite and chlorite in green-mica Quartzites of Saigaon–Palasgaon area, Western Bastar Craton, India. Journal of Earth System Sciences; v. 124 (1), pp. 213 – 225.

Shepherd, T.J., Rankin, A.H. and Alderton, D.H.M. 1985. Practical Guide to Fluid Inclusion studies, Blackie, Glasgow and London, 239p.

Raase, P., Raith, M., Ackermand, D., Viswanatha, M.n., Lal, R.K., 1983. Mineralogy of chromiferous quartzites from south India. Journal Geological Society of India v. 24, 502-521.

Treloar, P.J., 1987. Chromian muscovites and epidotes from Outokumpu, Finland. Mineralogical Magazine v. 51, 593-599.

Whitemore, D.R.E., Berry, L.G., Hawley, J.E., 1946. Chrome micas. The American Mineralogist v. 31 (1 & 2), 1-21.

Zhang, Y.G., Frantz, J.D. 1987 Determination of the homogenisation temperatures and densities of superficial fluids in the system NaCl-KCl-CaCl2-H2O using synthetic fluid inclusions. Chemical Geology, v. 64, 335-350.

Peer Reviewed and Refereed Journal 2022 **(ISSN : 09726330)**

Rashtrasant Tukadoji Maharaj Nagpur University

SCIENCE JOURNAL 2022

Vol. : XV

Spectral Characterization of Various 8-Hydroxyquinoline Derivative Metal Complexes

Chitra S. Khade[1*], N. Thejo Kalyani[2], S. J. Dhoble[3]

[1] Department of Physics, G H Raisoni Academy of Engineering & Technology, Nagpur, India,

[2] Department of Applied Physics,Laxminarayan Institute of Technology, Rashtrasant Tukadoji Maharaj Nagpur University, Nagpur, India. thejokalyani@rediffmail.com

[3] Department of Physics, Rashtrasant Tukadoji Maharaj Nagpur University, Nagpur, India. sjdhoble@rediffmail.com

Corresponding author email: thejokalyaninallapareddy@gmail.com

ABSTRACT

Organic Light Emitting Diodes (OLEDs)have gained momentum due to their versatile applications as a light source, flat panel displays and solid-state lighting. In view of this, 8- hydroxyquinoline derivatives namely Mgq_2, Baq_2 and $MgBaq_4$have been synthesized by precipitation method at room temperature. These metal complexes were characterized by FTIR, TGA/DTA,UV/Vis absorption and photoluminescence (PL) spectroscopy. FTIR spectra confirm the molecular structure of the metal complexes.Thermo Gravimetric Analysis (TGA) probed the thermal stability of metal derivative to be in between 20^0C to 180^0C, while Differential Thermal Analysis (DTA) confirms the glass transition temperature to be around 150^0C.Absorption spectrum of 8-hydroxyquinoline metal complexes reported two absorption bands around 270 and 360 nm, attributed to the ^1B_b and ^1L_a electronic transition bands respectively. The synthesized 8-hydroquinoline derivative metal complex exhibit a bright emission in the range of 470-520 nm, which falls in bluish- green region of visible spectrum. This data was further used to study the optical transition parameters and stokes shift of the synthesized complexes. These results prove their potential as bluish green light emitters, mainly used for solid state lighting, OLED sand flat panel displays.

Keywords :
(1) 8-hydroquinoline
(3) OLEDs
(4) Hot panel displays
(8) Solid state lighting
(2) Photoluminescence

1. Introduction

OLEDs have diverse applications in divergent areas due to manufacturing simplicity; hence represent an important research line in the progress of opto electronic devices [1-3]. OLED is solid state semiconductor which consists of organic thin films in between anode and cathode. When electrical current is provided to OLED, it emits light of different color and intensities depending on the nature of the material [4]. In last two decades CRT and LCD were replaced by LEDs and OLED displays due to the fact that these devices don't require any back light , also they are more flexible, lighter, and thinner satisfying the basic requirement of micro display market [5]. However, there still exit a number of barriers that have to be prevail over, many of which may require innovation in material of OLED devices. The progress of OLED technology depends on the success in designing and synthesis of novel high performance, efficient and stable materials to replace those that are still deficient [6].In this regard 8-Hydroxyquinoline Aluminum (Alq_3) has been revealed to be the most potentialorganic materials which emits green light for the fabrication of flat panel display and OLEDs[7].Alq_3 have some unique distinguishing properties such as high thermal stability, easy synthesis route, good electron transforming features [8-11] and proved itself to be in the pioneer in this field. Other 8-hydroyquinoline derivative metal / complexes were found to generate photoluminescence in various spectral regions which have various applications in

displaydevices. [12-17]. Based on these facts, an attempt has been made to synthesize and investigate some of the spectroscopic aspects of various 8-hydroxy quinoline derivative metal complexes, namely Mgq_2, Baq_2 and MgBaqby cost effective and less time-consuming precipitation method at room temperature [18].

2. Experimental

2.1 Chemicals

The purity and make of the chemicals used for the preparation of 8-hydroyquinoline derivative are as follows: 8-hydroxyquinoline, [$C_{27}H_{18}AlN_3O_3$] (Aldrich Chemicals), Magnesium nitrate, [$Mg(NO_3)_2.6H_2O$] (Aldrich Chemicals), Barium dinitrate, [$Ba(NO_3)_2$] (Aldrich Chemicals), Acetic acid, [CH_3COOH] (Alfa Asar Chemicals), Ammonia solution, [NH_4OH] (Aldrich Chemicals), and double distilled water.

2.1.Synthesis of 8-hydroxyquinoline derivative

8-hydroxyquinoline derivative $Mgq_2$was prepared by simple precipitation method, which is well illustrated in the fine state of art [19, 20]. For preparing Mgq_2,25 ml Double Distilled Water and 25 ml Acetic acid were taken in beaker. In mixture of Double Distilled Water and Acetic acid,5 gm of 8-hydroxyquinoline was added and then stirred till the solution turn orange (solution I). Later 4.30 g of $Mg(NO_3)_2.6H_2O$ was dissolved in Double Distilled Water and stirred till clear solution was formed(solution II). Solution I is mixed with solution II and stirred for 15-20 minutes.Thereafter NH_4OH was added to the mixture drop by drop to enhance the process of precipitation. The precipitate was then filtered and washed for 8 to 10 times with double distilled water.The precipitate was dried in oven at 40-50 °C. Similarly, $Baq_2$was synthesized just by replacing $Mg(NO_3)_2.6H_2O$ by $Ba(NO_3)_2$. For the preparation of $MgBaq_4$, $Mg(NO_3)$,$Ba(NO_3)_2$ and 8-hydroxyquinoline are taken in 1:1:4 proportion. $Ba(NO_3)_2$ and $Mg(NO_3)$ dissolved in double distilled water and same procedure of simple precipitation was employed.

The prior state of art strongly recommends the incorporation of luminescent complexes in polymers due to the fact that the intensity of these complexes was found to augment in polymer matrices due to the phenomenon of co-fluorescence. Poly (methylmetacrylate) (PMMA) and Polystyrene(PS) were preferred as polymeric material for the preparation of blended films.These polymers have good film forming properties and at the same time they are optically and electrically inert.Blended films of Baq_2 in PS and PMMA at 1, 5, 10 weight % have been synthesized according to the literature methods [21] as it was found to be the best one among all the synthesized complexes. The chemical structure of Mgq_2, Baq_2 and $MgBaq_4$, are depicted in Fig.1 (a-c), respectively.

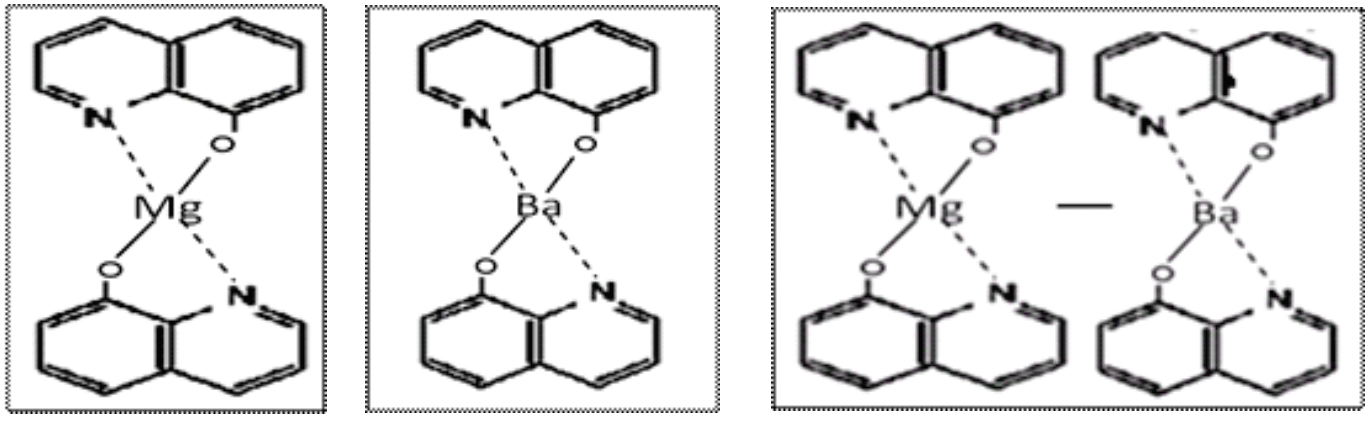

(a) (b) (c)

Fig. 1 : Chemical structures of (a) Mgq_2 (b) Baq_2 (c) $MgBaq_4$

3. Results and Discussion

Structural characterization of the synthesized complexes was explored by FT-IR spectra, carried out on SHIMADZU Model 8101A infrared spectrophotometer. Optical absorption spectra and PL spectra of the synthesized metal complexes and blended thin films have been carried out at room temperature on an Anlytik Specrod-50 spectrophotometer and HITACHI F-4000 spectrofluorometer, respectively. The thermal analysis (TGA and DTA) was carried out to investigate the thermal stability and glass transition temperature of these complexes on PerkinElmer Diamond TGA/DTA analyzer.

3.1 Structural characterization

3.1.1 Fourier Transform Infrared Spectroscopy (FTIR)

FTIR spectra of material reveal different functional groups as well as empirical structure in the so formed organic complex FTIR spectra of Mgq_2 reveals OH- stretching vibration at 3414 cm^{-1}, aromatic Amine resonances (C–N–C, 1370–1250 cm^{-1}) and aromatic stretching (C=C, 1600–1450 cm^{-1}) as potrayed in Fig.2. Carbonyl stretching vibrational bands appeared at 1695 cm^{-1}[22]. Sharp peaks in-between 600 to 800 cm^{-1}reveals the presence of quinoline ring and hence the desired complex. FTIR spectra of Baq_2 also shows the existence of OH- stretching vibration, aromatic stretching and quinoline ring as shown in Fig.3.

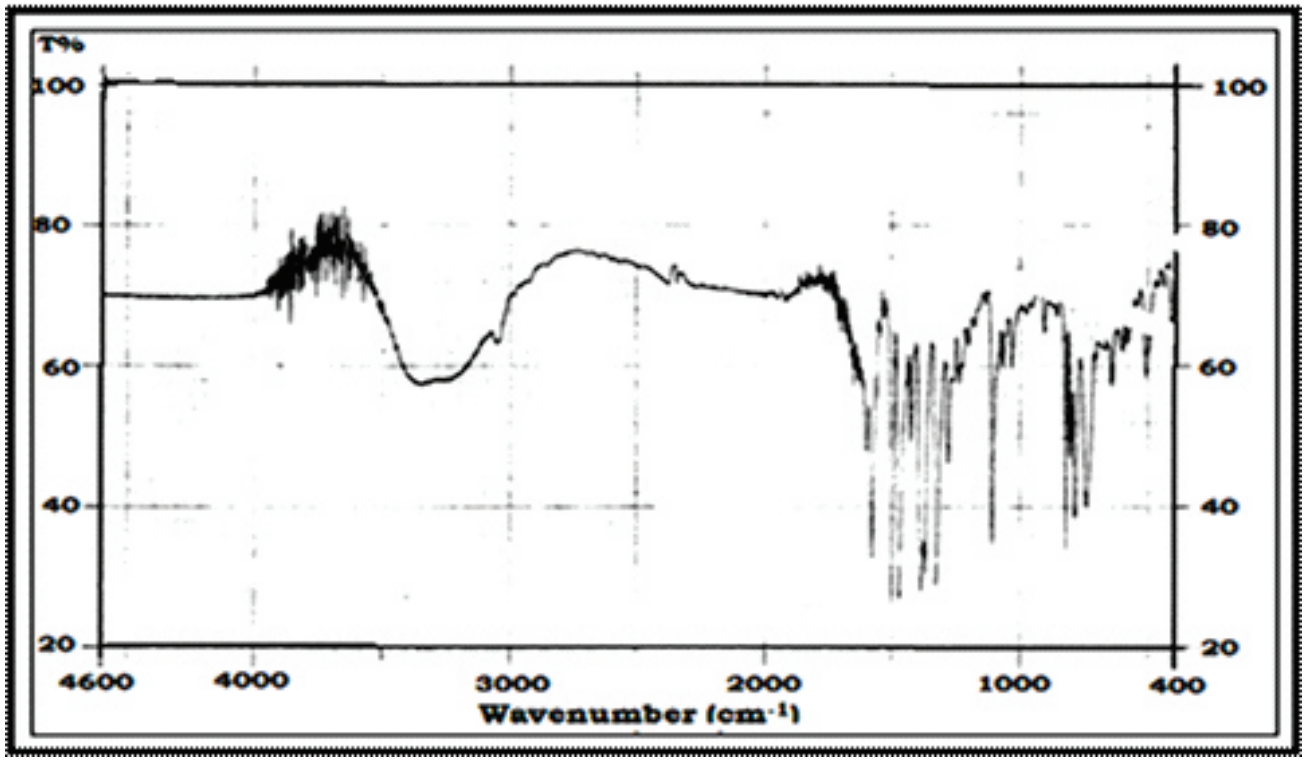

Fig. 2 : FTIR Spectrum of Mgq_2.

FTIR spectra of $MgBaq_4$ potray some characteristic peaks in-between 600 to 800 cm^{-1} shows the presence of quinoline ring [23]. Vibrational absorption peaks at 1277 and 1261 cm^{-1}shows the presence of –C-O bond. The prominent peaks at 1572, 1560, 1504 and 1464 cm^{-1} are corresponding to the aromatic ring skeleton. Vibration mode at 1686 and1655 cm^{-1} is judged to the stretching vibration of C-C- bondpresent in aromatic ring. The peak which is centred at 3050

cm^{-1} can be attributed to C-H bond in aromatic ring and at 3414 cm^{-1} OHŻ stretching vibration was also noticed. These results confirms the formation of the desired complex.

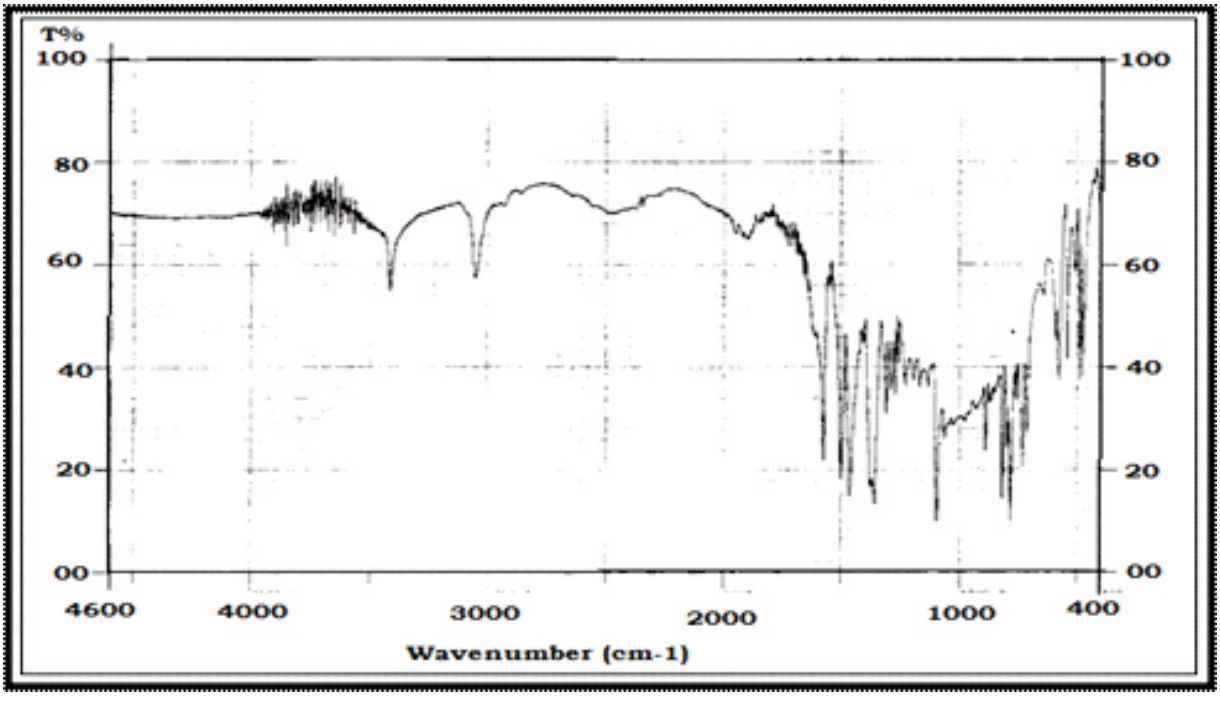

Fig. 3: FTIR Spectrum of Baq_2.

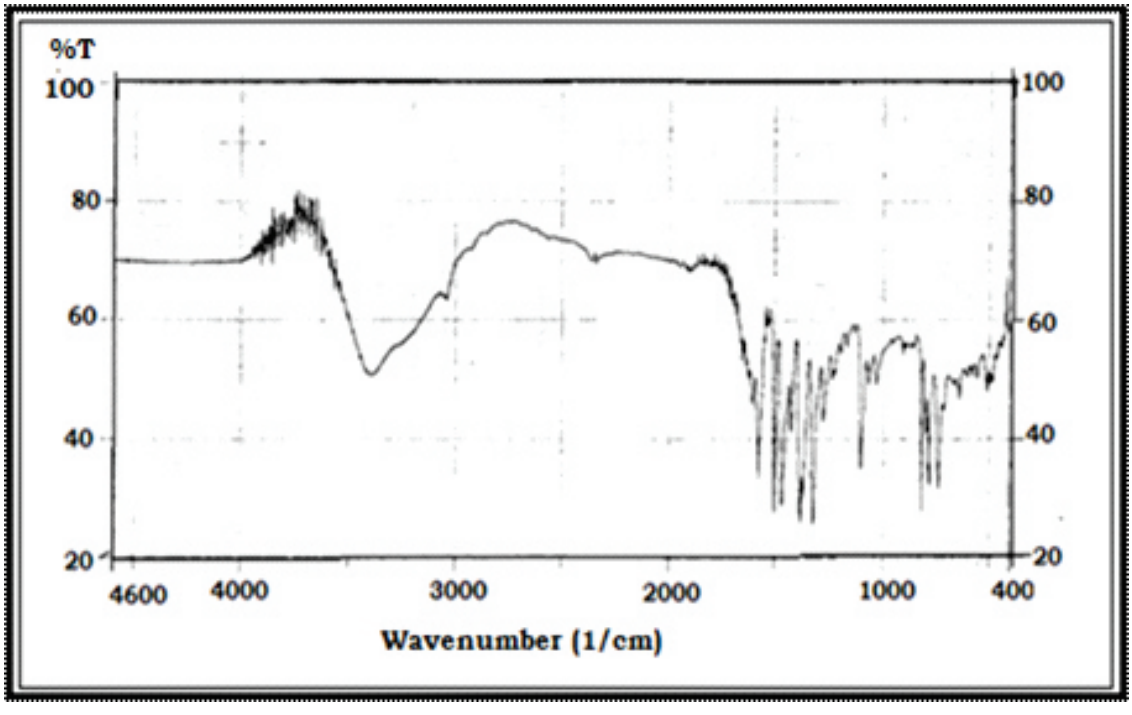

Fig. 4 : FTIR Spectrum of $MgBaq_4$.

3.2. Optical Characterization

3.2.1. Absorption spectra

The absorption spectrum of all 8-hydroxyquinoline derivatives show characteristic wavelength in the range of 250 to 450 nm, attributed to the overlapping of the ^1L_a (385nm) and ^1B_b (270 nm) transition bands. Two prominent peaks at 360 nm and 270 nm were observed in the absorption spectrum of $MgBaq_4$, Baq_2, Mgq_2 due to downward Itransitions among ^1L_a and ^1B_b.

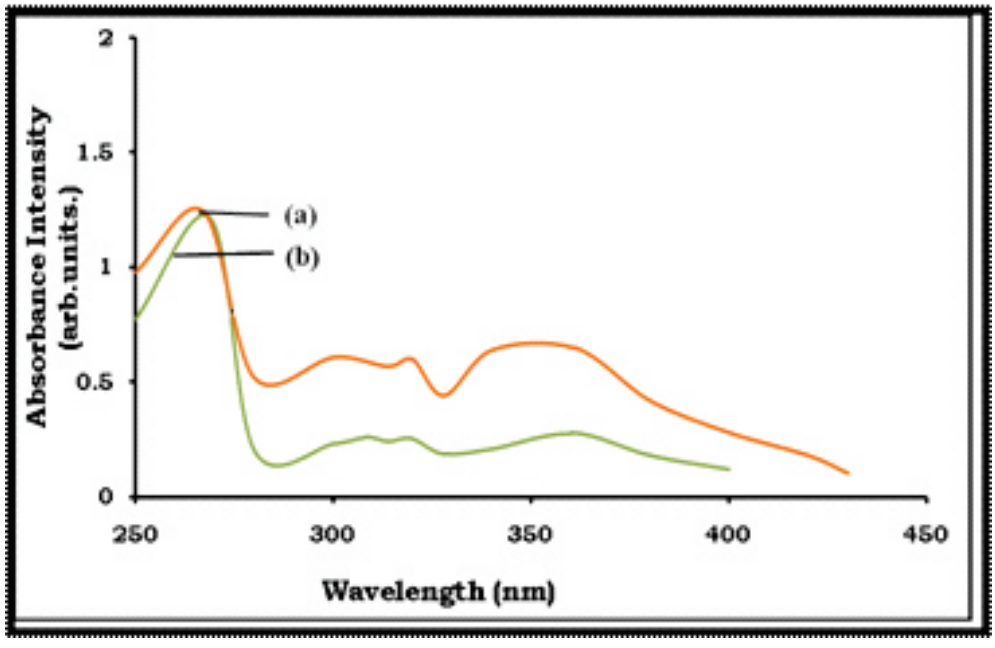

Fig. 5: Absorption Spectra of (a) Baq_2 (b) Mgq_2

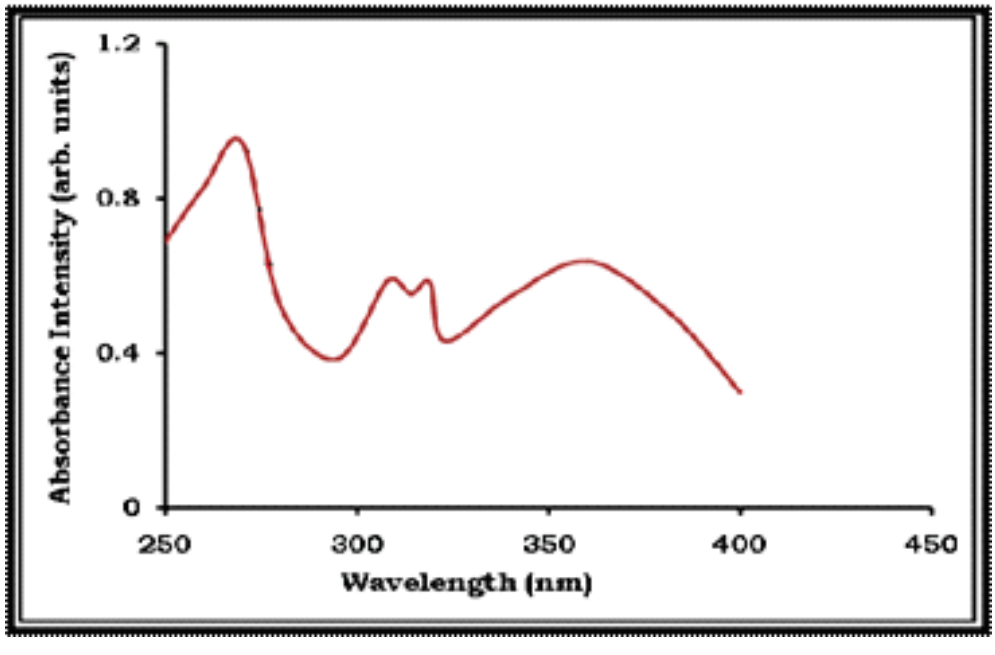

Fig. 6: Absorption Spectra of $MgBaq_4$

3.2.2. Optical Transition parameter

Absorbance A(l) dictates the ability of the material to absorb light of a particular wavelength [24], given by

$$\log\left(\frac{I_l^0}{I_l}\right)$$

Where, andare the intensities of the beams entering and leaving the absorbing medium, respectively.

As per Beer Lambert law [25] of absorbance of the sample,

$$A(\lambda) = \log\frac{I_\lambda^0}{I_\lambda} = \varepsilon(\lambda)\, lc$$

Where, l(e) is the molar absorption coefficient[26] which is a measures of the ability of chemical species or substance to absorb light at particular wavelength ; *c* is themolar concentration of those species; is generally known as path length. Absorption coefficient $\alpha(\lambda)$, is given by-

$$a(\lambda) = \frac{A(\lambda)}{l}$$

Naperian absorption coefficient is given by $\alpha(\lambda)$

$$\alpha(\lambda) = a(\lambda)\, ln\ 10$$

Molecular absorption cross section[27] is a measure for the probability of an absorption process [28,29] given by-

$$\sigma(\lambda) = \frac{2.303\varepsilon}{N_A} = 3.825\times10^{-19}\,\varepsilon\ (\text{in cm})$$

Number density (N) is given by

$$N = \frac{\alpha(\lambda)}{\sigma(\lambda)}$$

Table 1 : Optical Transition parameters of derivatives of 8 hydroxyquinoline

Metal Complex	λ_{max}	A(λ)	ε (λ)	α(λ)	ε	σ(λ)	N
Baq_2	270	1	1	2.30	1000	3.82×10^{-21}	
Mgq_2	270	1.25	1.25	2.87	1250	4.775×10^{-21}	2.61×10^{20}
$MgBaq_4$	270	0.97	0.97	2.33	970	3.7×10^{-21}	

Fig. 7 and 8 shows the optical energy band of Baq_2, Mgq_2 and $MgBaq_4$, calculated using the procedure described by Morita et al. [30]. 2.93eV and 3.17eV are energy band gaps of Baq_2 and Mgq_2 respectively and $MgBaq_4$ has 3.01eV.

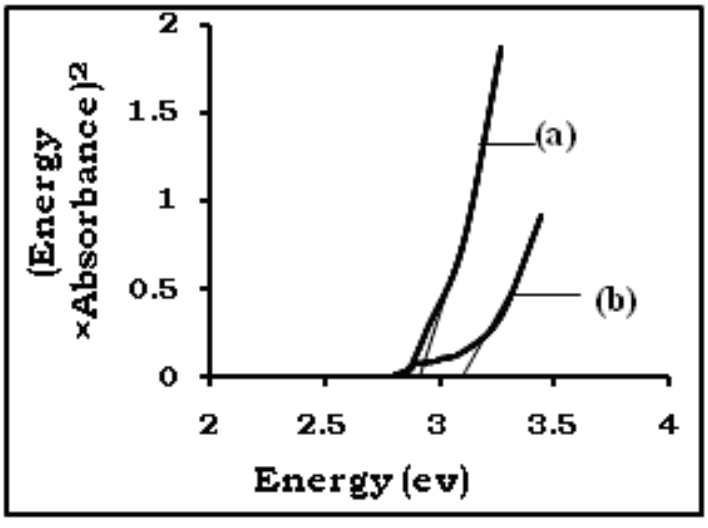

Fig. 7: Energy gap for (a) Baq_2 (b) Mgq_2.

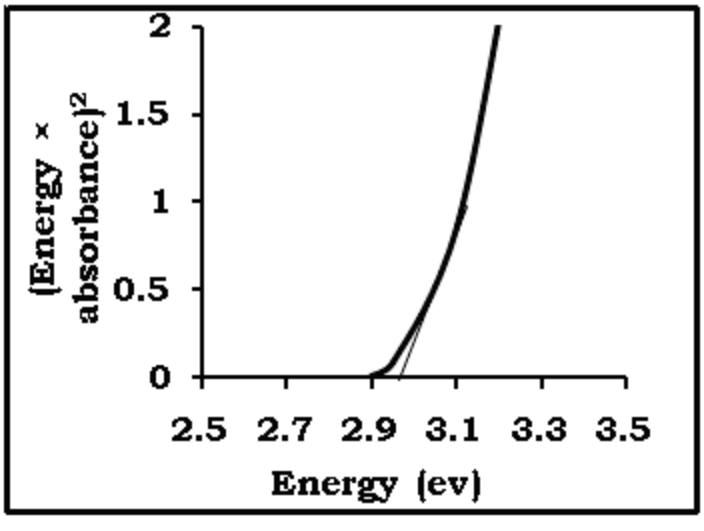

Fig. 8: Energy gap for $MgBaq_4$.

3.2.2: Photoluminescence Spectra

Photoluminescence is the processes of emission of light by the light emitting phosphor; when it absorbs photon and goes to an excited state, it re-radiates a photon during downward transition after its life time on the excited state.This energy is comparable with the energy difference between highest occupied molecular orbit (HOMO) and lowest unoccupied olecular orbit (LUMO). Amalgamations of electron donating and withdrawing substituent's on the 8 hydroxyquinoline ligand of the complexes allows the control of the HOMO and LUMO energies as well as the HOMO–LUMO gap,responsible for light emission from the complexes [31]. The PL spectrum of metal complex Mgq_2 and Baq_2 are given in Fig.9.

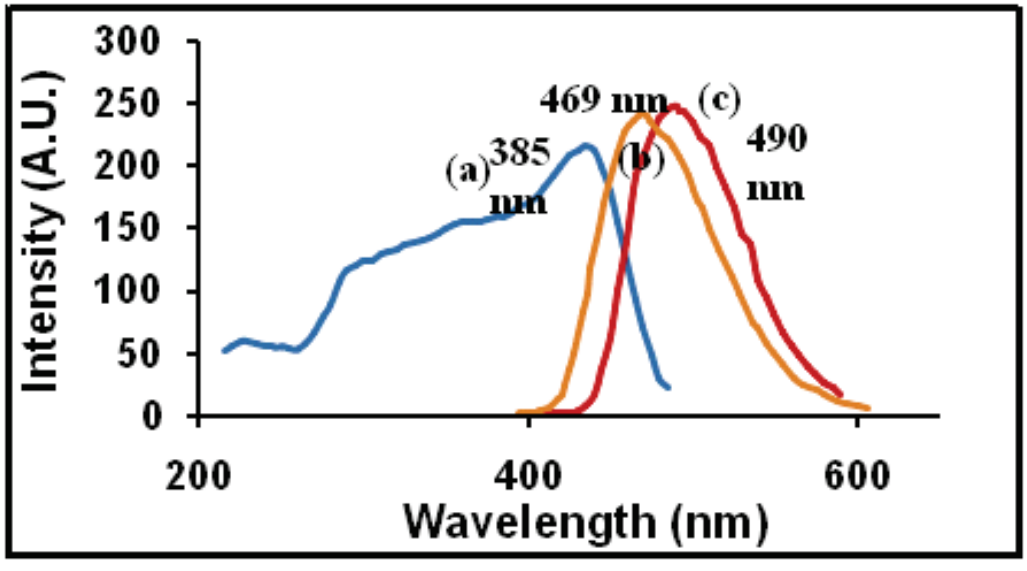

Fig. 9: (a) Excitation Spectra of Baq_2 and Mgq_2 (b) Emission Spectrum of Baq_2(c) PLSpectrum of Mgq_2.

Synthesized quinoline complexes $Mgq_2$and Baq_2 when excited in the range of 250 to 450 nm, a peak at 385 nm with weak adjacent shoulders were noticed. At this excitation wavelength, blue light emission was harnessed from Mgq_2 andBaq_2 with emission peak registeringat490 nm and 469 nm respectively. The light emission from organic material is generated by the ligand's electronic đ– đ * transition from HOMO and LUMO generally known as highest occupied molecular orbital and lowest unoccupied molecular orbital [32].

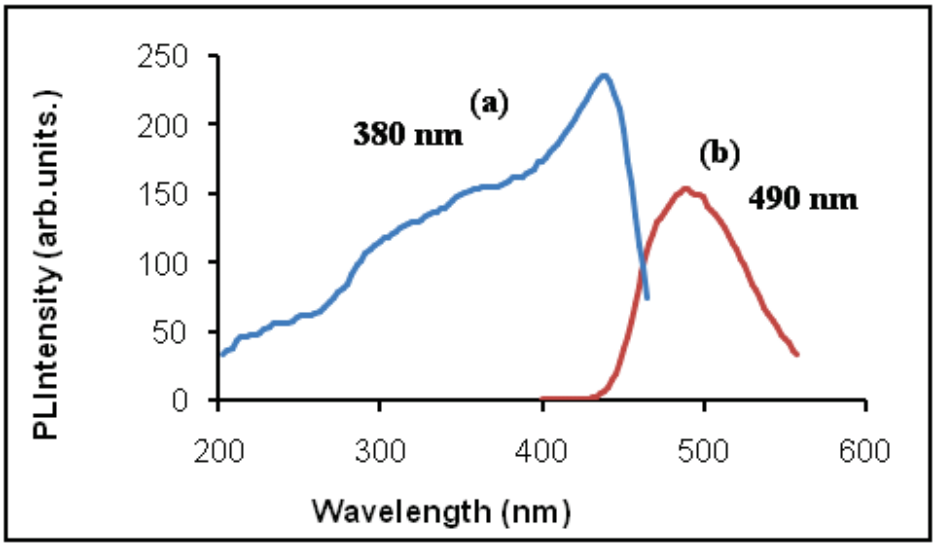

Fig.10 : (a) Excitation and (b) PL Spectra of $MgBaq_4$

Fig.10 reveals that upon exciting $MgBaq_4$ at 380 nm, emission was found to register at 490 nm. From luminescence computational studies and electro-absorption, it was observed that the lowest electronic transition derived from đ– đ * excitations. [33-35].

Full widths at half maxima of the PL spectrum in organic material were found to be in-between 70–80 nm. It is observed that, as atomic radii of quinolates increases, the blue shift can be observed in the photoluminescence excitation and emission wavelength of the synthesized complexes.Color emission from material shifted from green to blue, dictating color tunability. Table 2 composes the photo physical properties of 8 hydroxyquinoline derivatives.

Table 2: Photo physical properties of materialsof derivative of 8 hydroxyquinoline

Material	λ_{max} nm	λ_{ext} nm	λ_{em} nm	FWHM (PL)	Energy gap
Mgq_2	308,360	385	490	77	3
Baq_2	308,361	385	469	75	2.93
$MgBaq_4$	270,360	385	490	73	3.03

Stoke's shiftis the difference between the maxima of absorption spectraand PL emission spectrum. Fig. 11-13 shows that the Stoke's shift of organic complexes (Baq_2, Mgq_2, and $MgBaq_4$) lie in-between 105-150 nm.

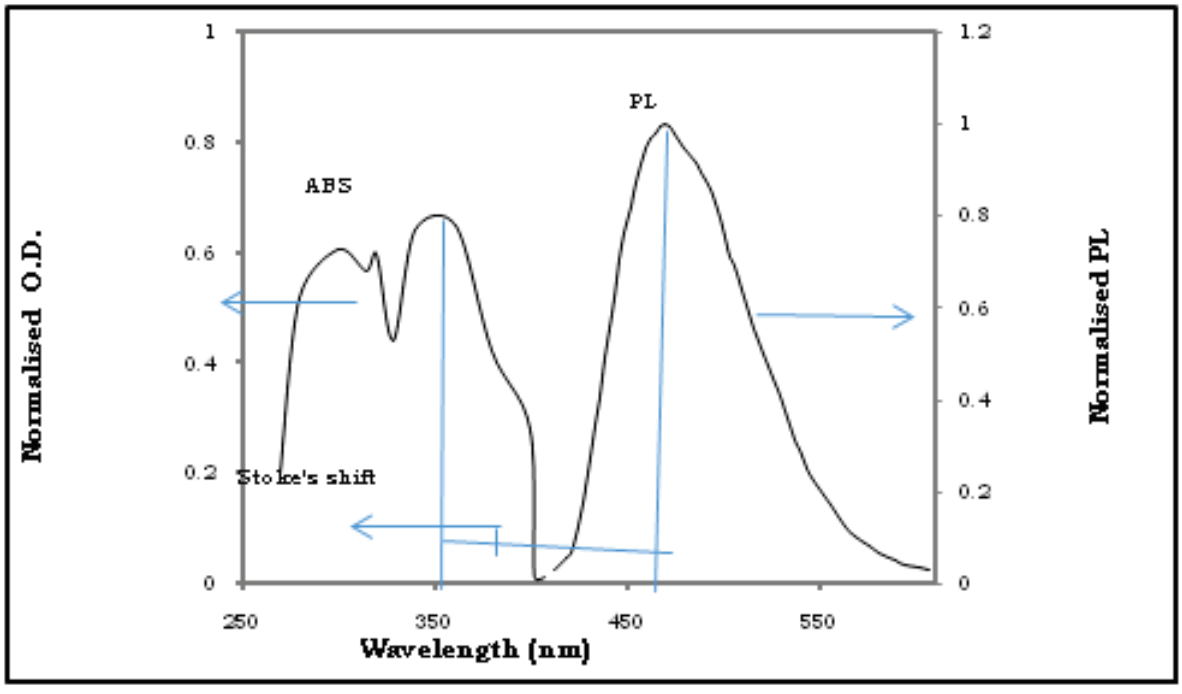

Fig. 11: Stoke's shift of Baq_2.

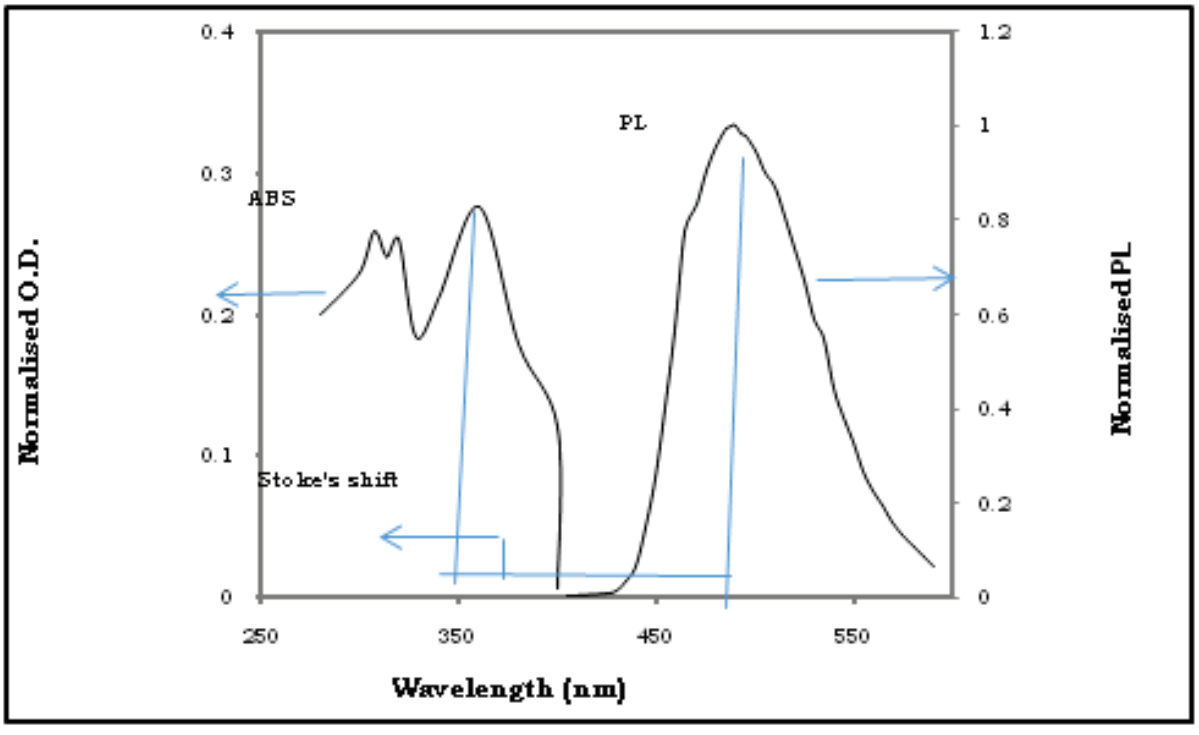

Fig. 12 : Stoke's shift of Mgq_2

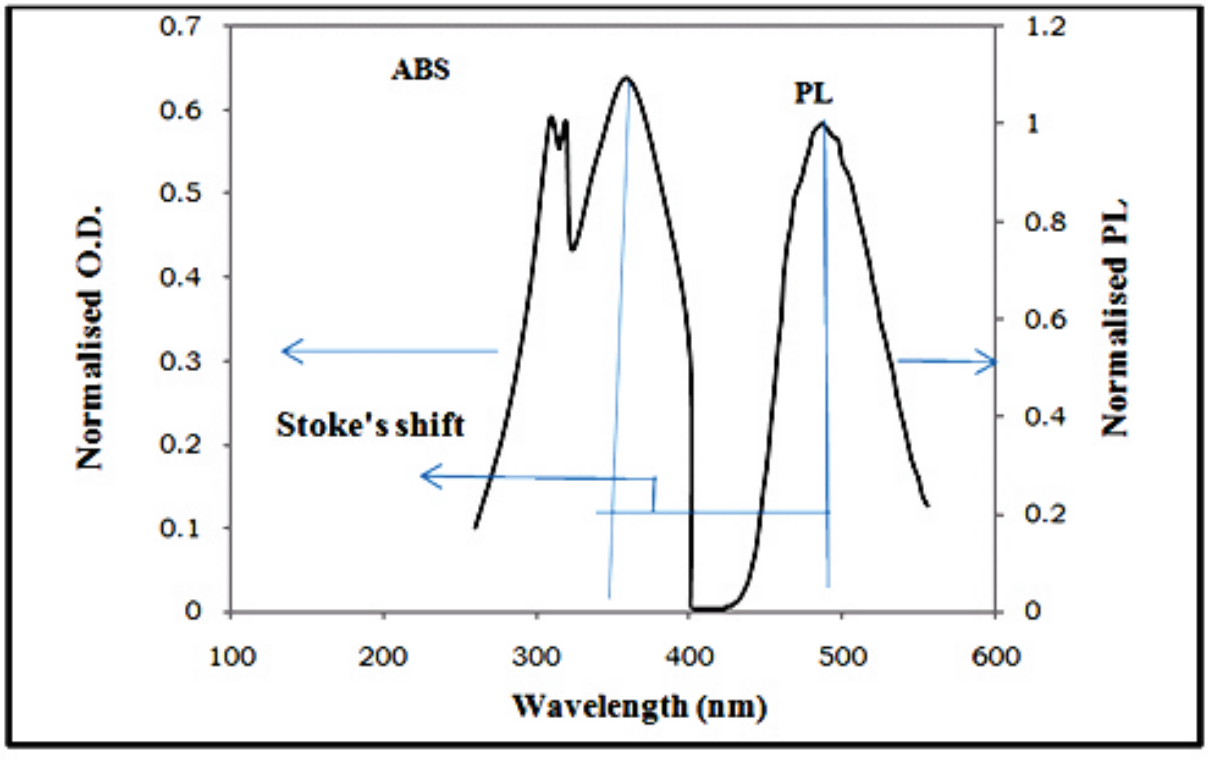

Fig. 13 : Stoke's shift of $MgBaq_4$

4. Optical investigations on blended thinfilms

Thin films of Baq_2, Mgq_2 and $MgBaq_2$ doped in polymeric PMMA and PS matrices were prepared at 10, 5, and 1 wt% in chloroform and the same were probed for excitation and emissionspectraas shown in Fig. 14 and 15, respectively.

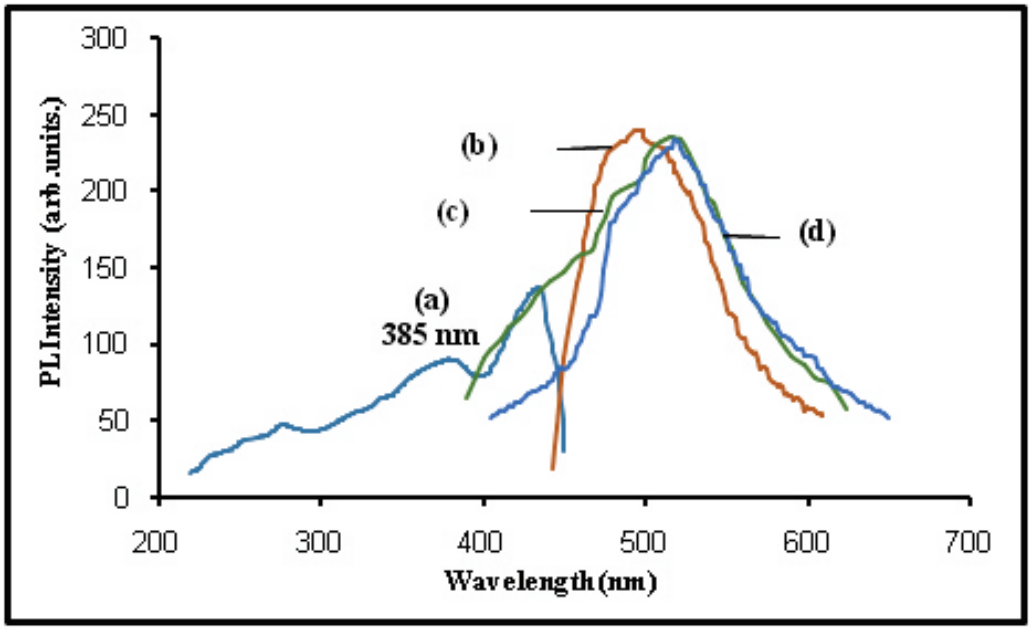

Fig. 14: (a) Excitation Spectrum of blended films and PL Spectram of (b) Baq_2+PMMA (5wt%)(c) Baq_2+PMMA (1wt%) (d) Baq_2+PMMA (10wt%).

Thin films of Baq_2 with PMMA in chloroform solution when excited between 270 to 425 nm portrays a broad peak centred at 385 nm. This wavelength was taken as reference and all the thin films of Baq_2(1, 5 and 10 wt%) were excited at 385 nm and the emission for the same was observed at 517, 516 and 500 nm respectively.

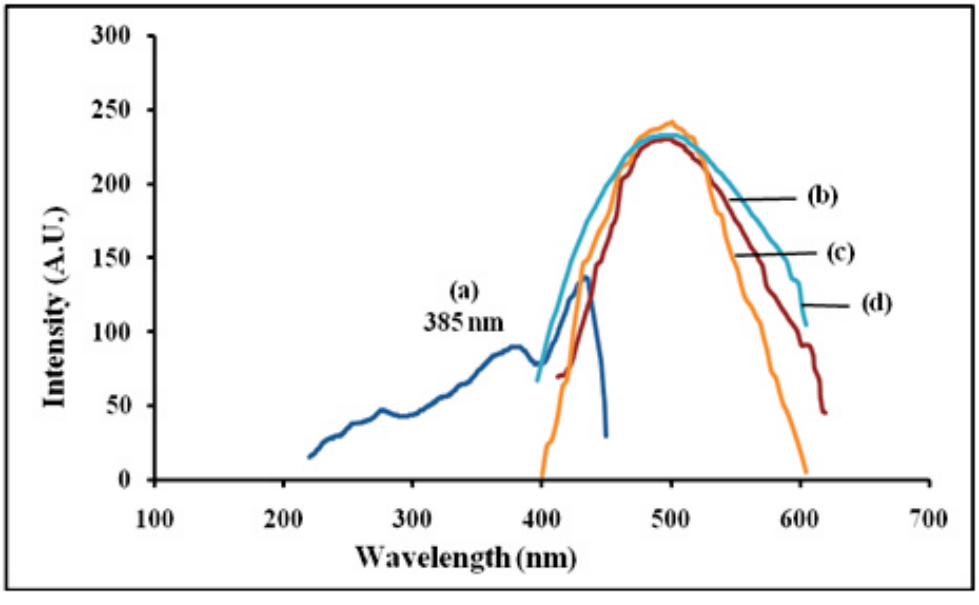

Fig. 15:(a) Excitation Spectrum of blended films and PL Spectra of (b) Baq_2+PS (5wt%) © Baq_2+PS (1wt%) (d) Baq_2+PS (10wt%).

When the films of Baq_2 and PS at different weight % are excited in between 270 nm to 425 nm, it shows a shar\ peak at 385 nm. The PL spectra of these films show green light emission at 501 nm, 501 nm, and 502 nm at 1, 5 and 10 wt% respectively.

3.2.3 Thermal Characterization

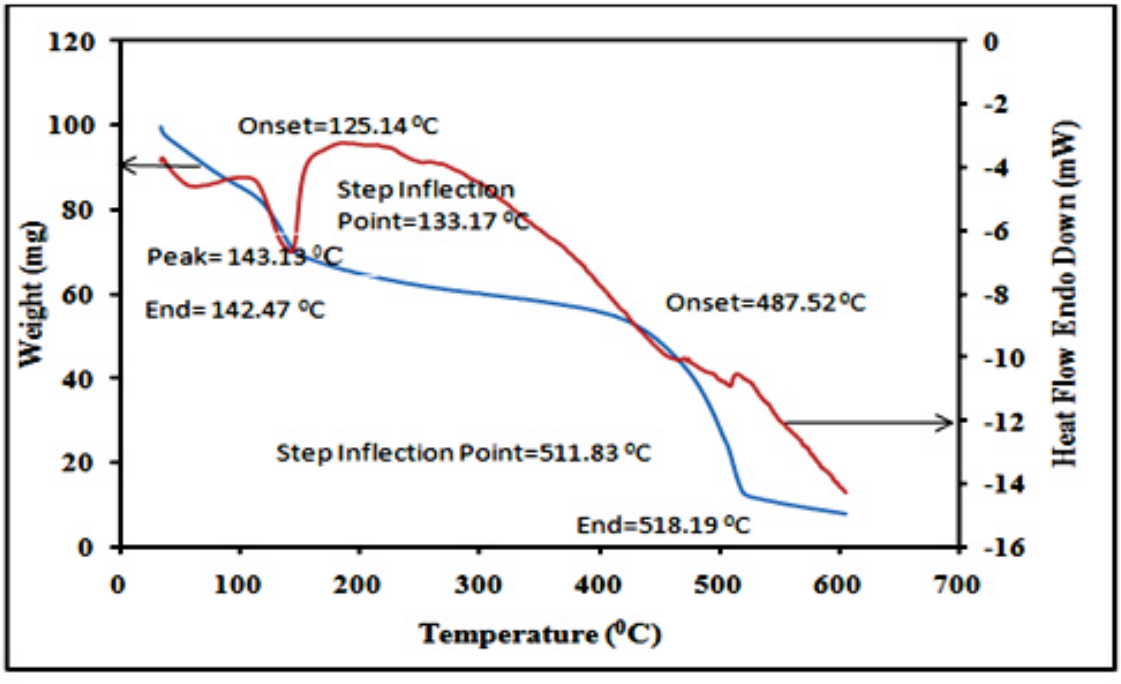

Fig. 16 : TGA and DTA of Mgq_2

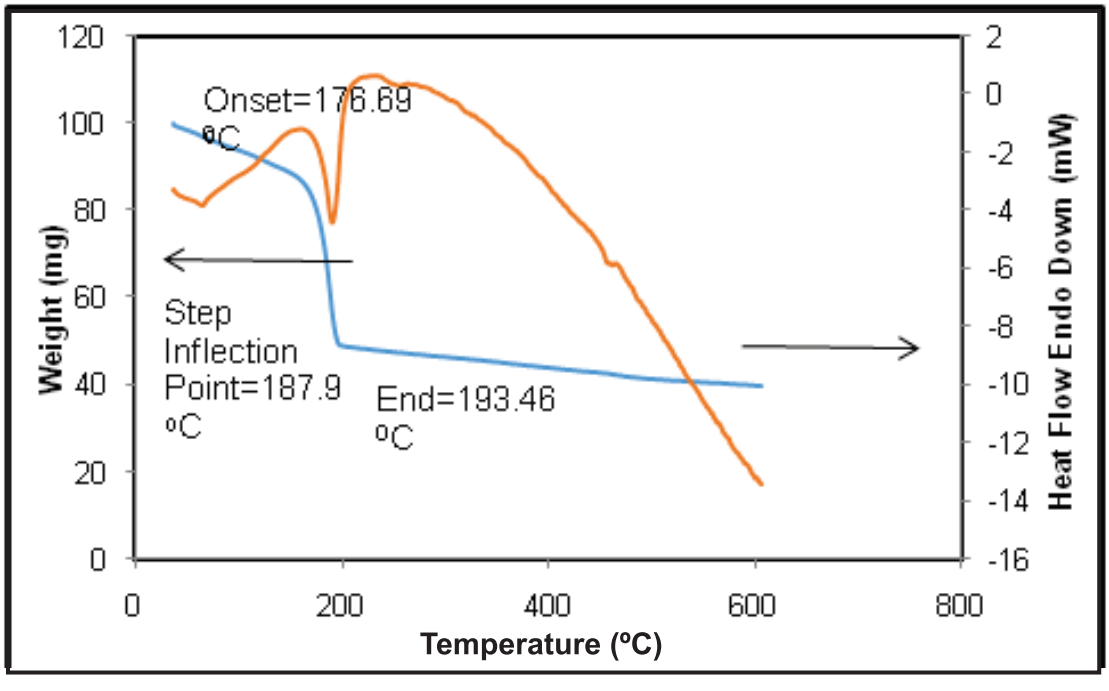

Fig. 17 : TGA and DTA of Baq_2

TGA was employed to assign the weight loss of the sample as a function of temperature. Fig.16-18 shows Differential thermal analysis (DTA) and Thermogravimetric analysisplots (TGA) of Mgq_2, $Baq_2$and $MgBaq_4$, respectively. These complexes were heated under argon atmosphere upto 600^{0}C with heating rate of 10° C/min so as to probe its thermal stability and glass transition temperature. From TGA traces of Mgq_2, Baq_2 and $MgBaq_4$, it has been observed that these materials show thermal stability around 125^{0}C, 176^{0}C and 151^{0}C, respectively.

Differential Thermal Analysis (DTA) determines the phase transition and chemical reactivity of material. Variations in heat content of material during phase transition was measured using DTA. The DTA traces of Mgq_2, Baq_2 and $MgBaq_4$, shows transition temperature around 143^{0}C 139^{0}C and 531^{0}C, respectively.

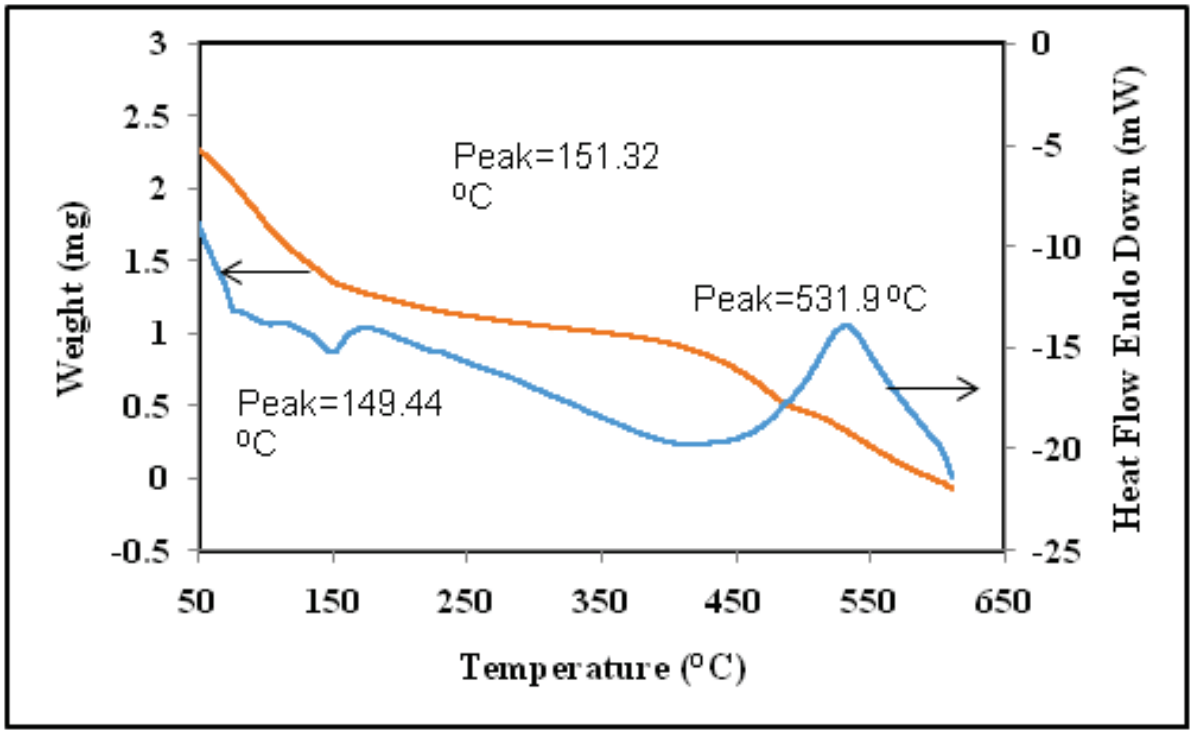

Fig. 18 : TGA and DTA of $MgBaq_4$.

4. Conclusion

Metal complex quinoline derivatives namely Mgq_2, Baq_2 and $MgBaq_4$have been synthesized by simple precipitation method at room temperature. FT-IR spectra of these complexes confirmed the molecular bonds in metal complexes. The pattern of FTIR spectra remained same with minor changes in the vibrational stretching. The absorption spectrum of all 8-hydroxyquinoline derivatives show characteristic wavelength in the range of 250 to 450 nm, attributed to the overlapping of the ^1L_a (385nm) and^1B_b (270 nm) transition bands. Two prominent peaks at 360 nm and 270 nm were observed in the absorption spectum of $MgBaq_4$, Baq_2, Mgq_2due to downward ltransitions among ^1L_a and ^1B_b.The energy band gaps of Baq_2 and $Mgq_2$and $MgBaq_4$was found to be 2.93eV and 3.17eV and 3.01eV, respectively. Mgq_2 and $Baq_2$when excited at 385 nm, blue light emission was harnessed from Mgq_2 andBaq_2 with emission peak registering at 490 nm and 469 nm respectively. $MgBaq_4$ when excitedat 380 nm, emission peak registered at 490 nm. full width at half maxima of the PL spectrum in organic material were found to be in-between 70–80 nm. The blended thin films of Baq_2 proffers better emission in green region at lower concentration.TGA/DTA show 8-hydroxyquinoline derivative complexes have better thermal stability which improve the operating lifetime and stability of the OLED.All these 8-hydroxyquinoline derivative shows color tunability in PL emission from blue to green (460-520 nm), an unique feature employed in lamps, watches, AMOLEDs and many more.

References

1. C. H. Chen, J. Shi, C. W. Tang, Macromolecular Symposia, 125 (1998) 1.
2. H. Tanaka, S. Tokito, Y. Taga, A. Okada, Journal of MaterialsChemistry, 8 (1998) 1999-2003.
3. Sheats, J. R.; Antoniadis, H.; Hueschen, M.; Leonard, W.; Miller, J.; Moon, R.; Roitman, D.; Stocking, A.; *Science 273(1996)* 884.
4. S. K. So, W. K. Choi, L. M. Leung, and K. Neyts, Interference effects in bier organic light-emitting diodes, Appl. Phys. Lett. 74(1999)1939-1941.
5. Fazia Batool, IJARCCE, Vol. 5, Issue 11, November 2016
6. Mr. Bhrijesh N. Patel, Mr. Mrugesh M. Prajapati, ijsrp, 4(6)(2014) 2250-3153
7. Pratik Shinde, Shekhar Pandharipande, **N. Thejokalyani,** S.J. Dhoble;Optik 162 (2018) 151–160
8. G. Yu, D. Shen, Y. Liu and D. Zhu, Synth. Met.,121 (2001) 1433.10.A
9. Zawadzka, P. P³ociennik, J. Strzelecki, Z.£ukasiak and B. Sahraoui, Opt. Mater.,36(2014) 91.
10. Kumar *et al.*[1]Kumar, S.; Shukia, V. K.; Tripathi, A.; *Thin Solid Films, 477(2005)* 240
11. K. Sanderson, "Quantum dots go large," Nature 459(7248), (2009) 760–761
12. S. A. Vanslyke, C. H. Chen, and C. W. Tang : Appl. Phys. Lett. 69 (1996) 2160.
13. T. Nakayama, Y. Itoh, A. Kakuta, Appl. Phys. Lett. 63 (1993) 595.
14. M. Hiramoto, J. Tani, M. Yokoyama, Appl. Phys. Lett. 62 (1993) 666
15. Y. Ohmori, A. Fujii, M. Uchida, C. Morishima, K. Yoshino, Appl. Phys. Lett. 63 (1993) 1871.
16. C. Hosokawa, H. Higashi, T. Kusumoto, Appl. Phys. Lett. 62 (1993) 3238
17. A. Curioni, W. Andreoni, J. Am. Chem. Soc. 121 (36) (1999) 8216.
18. A. Curioni, W. Andreoni, J. Am. Chem. Soc. 121 (36) (1999) 8216.
19. Dipti Chitnis,**N. Thejo Kalyani**, S.J. Dhoble; Results in Physics 13 (2019) 102302.
20. AadSempel, Michael B€uchel Organic Electronics 3 (2002) 89
21. C.W. Tang, S.A. VanSlyke, Appl. Phys. Lett. 51 (1987) 913
22. D.G.J. Sutherland, J.A. Carlisle, P. Elliker, G. Fox, T.W. Hagler, I. Jimenez, H.W. Lee, K. Pakbaz, L.J. Terminello, S.C. Williams, Appl. Phys. Lett. 68 (1996) 2046
23. H. Li etal material Science and Engineering 100 (2003) 40
24. Zidan H M, J. Appl. Polymer Sci;88 (2003) 104.
25. V Bernard, Molecular Fluorescence: Principles and Applications, Wiley-2001
26. Belay, Food Chem. 121 (2010) 585–590
27. G. Herzberg., Molecular Spectra and Molecular Structure. III Electronic Spectra and Electronic Structure of Polyatomic Molecules, Van Nostrand Reinhold Company, New York, 196
28. J.B. Birks, Photo Physics of aromatic Molecules, Wiley-Interscience, London; New York, 1970
29. H.H. Jaffe, M.Orchin, Theory and Applications of Ultrviolet Spectroscopy, John Wiley and Sons, New York, 1962

30. S. Morita, T. Akashi, A. Fujii, M. Yoshida, Y. Ohmori, K. Yoshimoto, T. Kawai, A. A. Zakhidrov, S. B. Lee, K. Yoshino, Synth. Met. 69 (1995) 433

31. Dr. César Pérez Bolívar, Dr. Shin ya Takizawa, Dr. Go Nishimura, Dr. Victor A. Montes, Prof. Dr. Pavel Anzenbacher Jr, 17(33)(2011) 9076-9082

32. G. Baldacchini, M. Bottomei, P. Cardoni, M. R. Montereali and L. C. Scavarda do carmo, , Vuoro, 19(1989)113

33. Tao X T, Watanabe T, Kono k, Deguchi T, Nakayama M, Miyata S, Chem. Mater; 8(1996)1326

34. W.Stampor, J. Kalinowski, G. Marconi, P. Di Marco, V. Fattori, G. Giro, Chem. Phys. Lett. 283 (1998) 373

35. A. curioni, M. Boero, W. Andreoni, Chem. Phys. Lett. 294 (1998) 263

Peer Reviewed and Refereed Journal 2022 **(ISSN : 09726330)**

Rashtrasant Tukadoji Maharaj Nagpur University

SCIENCE JOURNAL 2022

Vol. : XV

Thermoluminescence and photoluminescence study of Eu and Dy activated $KSrSO_4Cl$ phosphor

Archana Deshpande[1*], S. C. Gedam, N. S. Dhoble[2] and S. J. Dhoble[1]

[1] Department of Physics, R.T.M. Nagpur University, Nagpur- 440033, India.

[2] Department of Chemistry, Sevadal Mahila Mahavidhyalaya, Nagpur-440009, India

Corresponding author email:
asd.223@rediffmail.com

ABSTRACT

In the process of luminescence when radiation is incident on a material some of its energy may be absorbed and re-emitted as a light of longer wavelength. It is an interesting and initially mysterious phenomenon. Luminescent materials, also called phosphors, are mostly solid inorganic materials consisting of a host lattice, usually intentionally doped with impurities. Host material plays an important role while preparing the phosphor for particular application. Rare earth doped Chlorosulphates have been proved to be outstanding host materials. Present paper deals with the synthesis of Europium (Eu) and Dysprosium (Dy) activated $KSrSO_4Cl$. Present phosphors are synthesized by acid distillation as described by Yamashita et al and Azorin et al.Dopants are added as per concentration 0.05mol% to 1mol%. Prepared phosphors are characterized by Thermoluminescence (TL) and Photoluminescence (PL). Kinetic parameters are calculated by using Peak Shape Method. The thermoluminescence glow peak for $KSrSO_4Cl$:Dy has the highest intensity at 169°C and it follows the second order kinetics while $KSrSO_4Cl$:Eu has the highest peak at 185°C it follows the general order kinetic.

Photoluminescence studies of present phosphors shows that $KSrSO_4Cl$: Dy has six excitation peaks in the range of 290nm-400nm. In the visible range Dy^{3+} emit two principal PL bands at 483nm and 572nm due to transition of Dy^{3+} ion.When excited at 396nmphotoluminescence emission of $KSrSO_4Cl$:Eu shows two peaks at 595nm and 615nm which is the emission of Eu^{3+} ion. CIE chromaticity coordinates for $KSrSO_4Cl$:Eu and $KSrSO_4Cl$:Dy are also studied using Commission International del Eclairage (CIE) system.The aim of this study is to report rare earth doped Chlorosulphates under the investigation of Thermoluminescence (TL) and Photoluminescence (PL).

Keywords :
Thermoluminescence,
Photoluminescence,
Chlorosulphate

1. INTRODUCTION

Preparing the phosphors for various applications such as making lamps [1–3], CR tubes, TV screens [4], electroluminescent lamp display panels, LEDs, detectors for X-ray imaging [5–8], scintillation detectors [9], laser crystals [10], paints [11], solar concentrators [12] and both individual and environmental radiation monitoring[13] one has to take care of choosing the host material. Host material plays an important role while preparing the phosphor for particular application. Some factors which affect the efficiency of phosphor are the effects of the sizes, dimensionality, and co-dopants on luminescence of rare earth doped phosphors. These factors depend on the host material. Rare earth doped Chlorosulphates have been proved to be outstanding host materials [14].

TL dosimeters can be synthesized by using different host materials like borates, fluorides, silicates and sulphates. Among these host materials Sulphates are commonly used

host materials for TLD. As they are easily available, preparation method to synthesize phosphors using sulphates is comparatively easy, low cost. Keeping the aim, new phosphors have been studied in present paper. $KSrSO_4Cl$:Eu and $KSrSO_4Cl$:Dy is synthesized by acid distillation method. Prepared phosphors studied for Thermoluminescence (TL) and Photoluminescence(PL).

2. Experimental

$KSrSO_4Cl$ prepared by acid distillation method as described by Yamashita et al [15] and Azorin et al [16]. For the preparation of the mentioned phosphors the starting material $SrSO_4$, KCl and sulphate salts of rare earth are taken in AR grade. All the starting materials were dissolved in hot sulphuric acid and heated at temperature 300^0C for 24 hours. During acid evaporation the acid vapours kept for condensation. After cooling the prepared sample, washed it several times by double distilled water to remove the extra traces of acid. The filtered sample is kept at 50^0C for 24 hours in hot air oven. The prepared phosphors were taken for the further characterization.TL glow curves were recorded for 5mg of sample each time at a heating rate of 5°C s^{-1}. The TL glow curves were recorded with the usual set-up consisting of a small metal plate heated directly using a temperature programmer, photomultiplier (931B), dc amplifier and a millivolt recorder, Nucleonix 1009 TL reader. The Photoluminescence excitation and emission measurements were recorded on the Shimadzu RF5301PC Spectrofluorophotometer. The emission and excitation spectra were recorded using a spectral slit width of 1.5 nm.

3. Result and Discussion

3.1 XRD of $KSrSO_4Cl$ prepared by acid distillation method

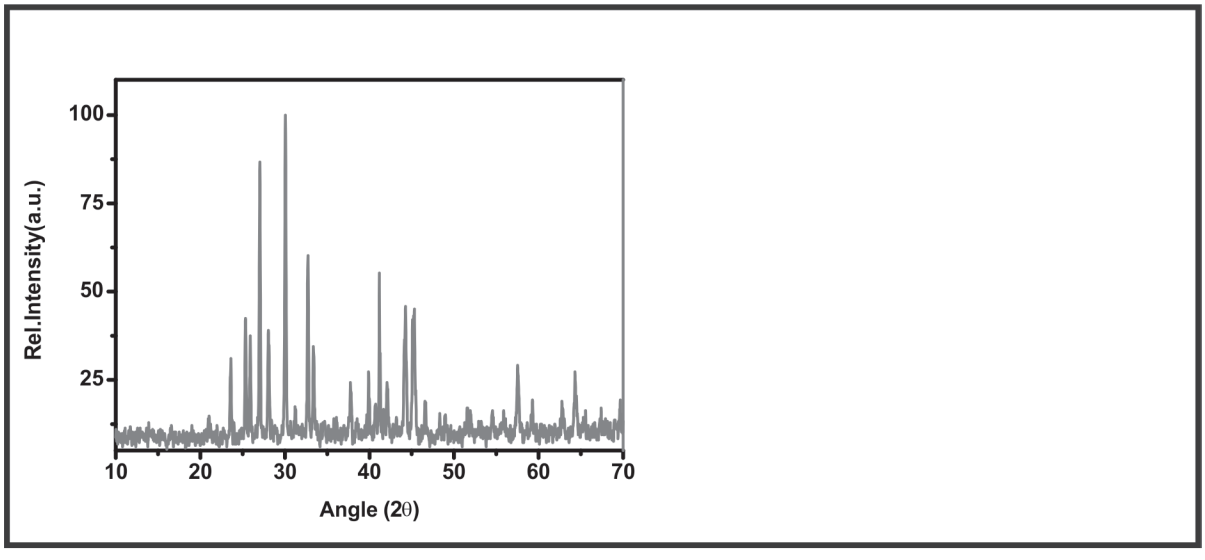

Fig. 1 XRD of $KSrSO_4Cl$

The XRD pattern did not indicate presence of the constituents $SrSO_4$ or KCl and other likely phases which are an indirect evidence for the formation of the desired compound. These results indicate that the final product was formed in homogeneous form.

3.2 Thermoluminescence characteristics and trapping parameters of $KSrSO_4Cl$: Eu

Fig. 2 shows the thermoluminescence characteristics of $KSrSO_4Cl$ doped Eu. The glow curve has been recorded at a heating rate of 5^0Cs^{-1} and irradiation of gamma rays at a dose rate of 0.995 $kGyh^{-1}$ for 5 Gy. From Fig. 2 it is clear that the TL intensity of prepared sample is very low for low concentration of dopant; however it has been suddenly increased for the further concentration (1m%). The evaluation of trapping parameters has been carried out by using Chen's method. The value of $ě_{mg}$ has been found 0.75 which shows that the above peak follows the general order. By taking the values of

T_M, T_1 and T_2 where T_M is maximum temperature and T_1 and T_2 are temperature on either side; the activation energy, order of kinetics and frequency factor has been calculated as 0.74eV, 0.8 and 1.59×10^8 s^{-1} respectively.

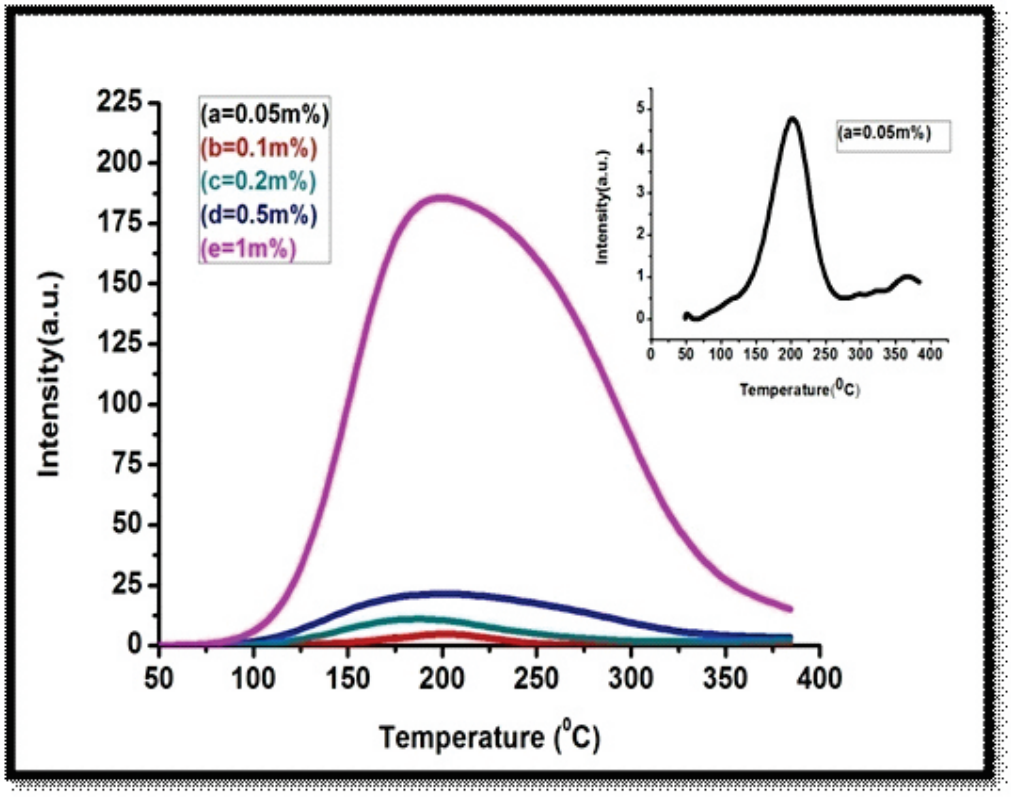

Fig. 2 Thermoluminescence characteristics of $KSrSO_4Cl$ doped Eu.

3.3 Thermoluminescence characteristics and trapping parameters of $KSrSO_4Cl$: Dy

To estimate the doses of high energy ionizing radiation absorbed by materials one can use the simple technique as TL. Though there are many techniques such as Secondary Ion Mass Spectroscopy, Focused Ion Beam, Rutherford Back Scattering and Elastic Recoid Detection (ERD) analysis the dose of energetic ions needs to be measured with great precision and accuracy, TL is most promising technique.

Fig. 3 shows the TL characteristics of $KSrSO_4Cl$ at different concentrations of Dy^{3+} recorded. TL properties were studied on a NUCLEONIX-TL1009I consisting of a small metal plate heated directly using a temperature programmer, a photomultiplier tube,a DC amplifier and a mill-voltmeter. The glow curve has been recorded at a heating rate of 5^0Cs^{-1} and irradiation of gamma rays at a dose rate of 0.995 $kGyh^{-1}$ for 5 Gy. The intensity first increased and further decreased for increasing the concentration. Further addition of dopant leads to the quenching of TL properties of $KSrSO_4Cl$. (Fig. 3 inset graph)

The main goal of measuring and analyzing TL glow curves is the extraction of several parameters that can be used to describe the TL process in the material. The dosimetric characteristic of any TL phosphor mainly depends on its trapping parameters which describe the defect centers responsible for the TL emission.

The computerized curve fitting method is commonly used to analyze multipeak glow curves and became popular with the development of sophisticated glow curve deconvolution techniques [3]. In present study the glow curve has been first deconvoluted by CGCD based on the Gaussian function as shown in Fig.4. Further the trapping parameters are calculated by Chen's method for each curve. Fig. 5a, b, c and d show that TL glow peak has been resolved into four peaks to enhance the degree of fitting with fitted and experimental glow curve. The separated peaks (peak 1 to peak 4) appear at the peak temperatures of 169, 227, 279 and 350 ^{0}C respectively.

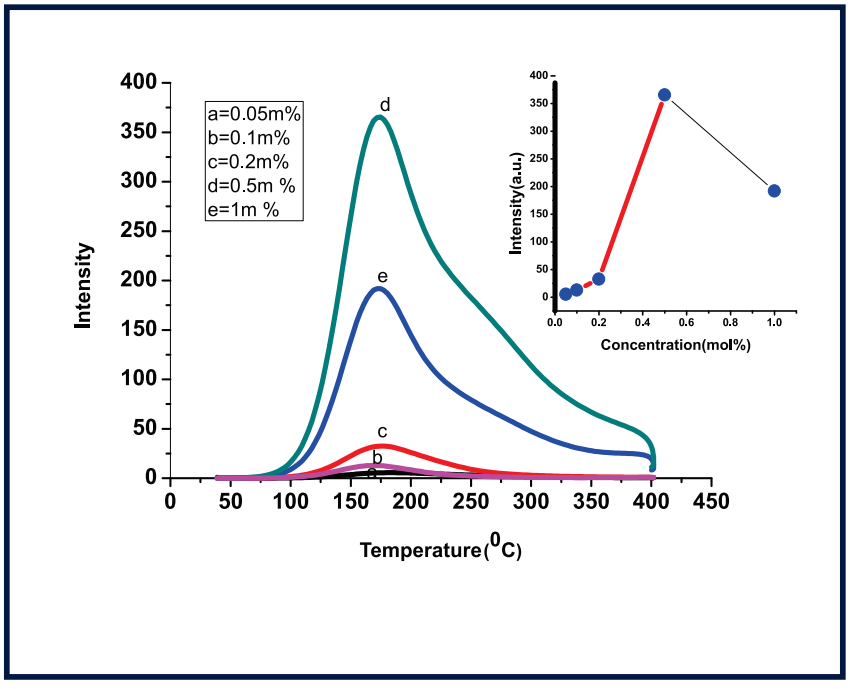

Fig. 3 Thermoluminescence characteristics of $KSrSO_4Cl$ doped Dy

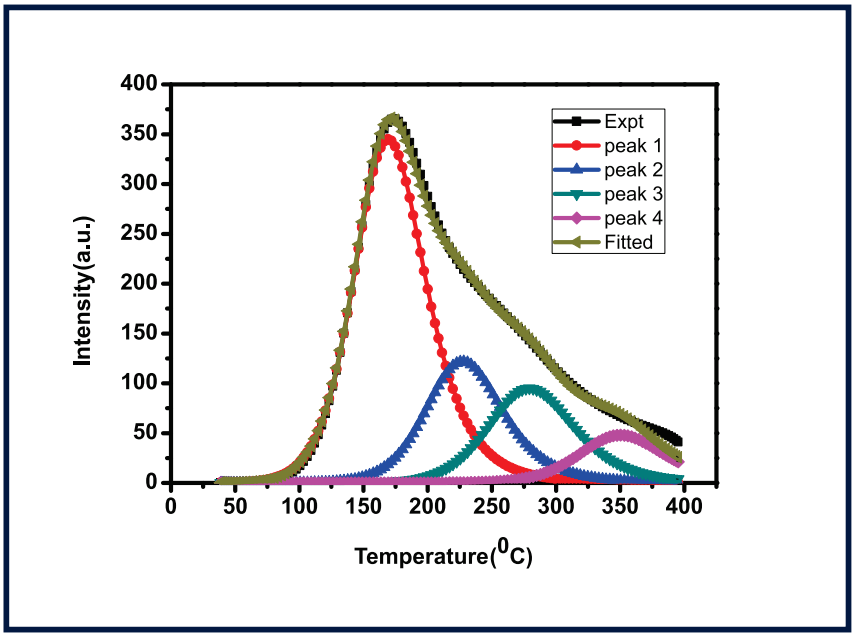

Fig. 4 Computerized Glow Curve Deconvolution of $KSrSO_4Cl$ doped Dy

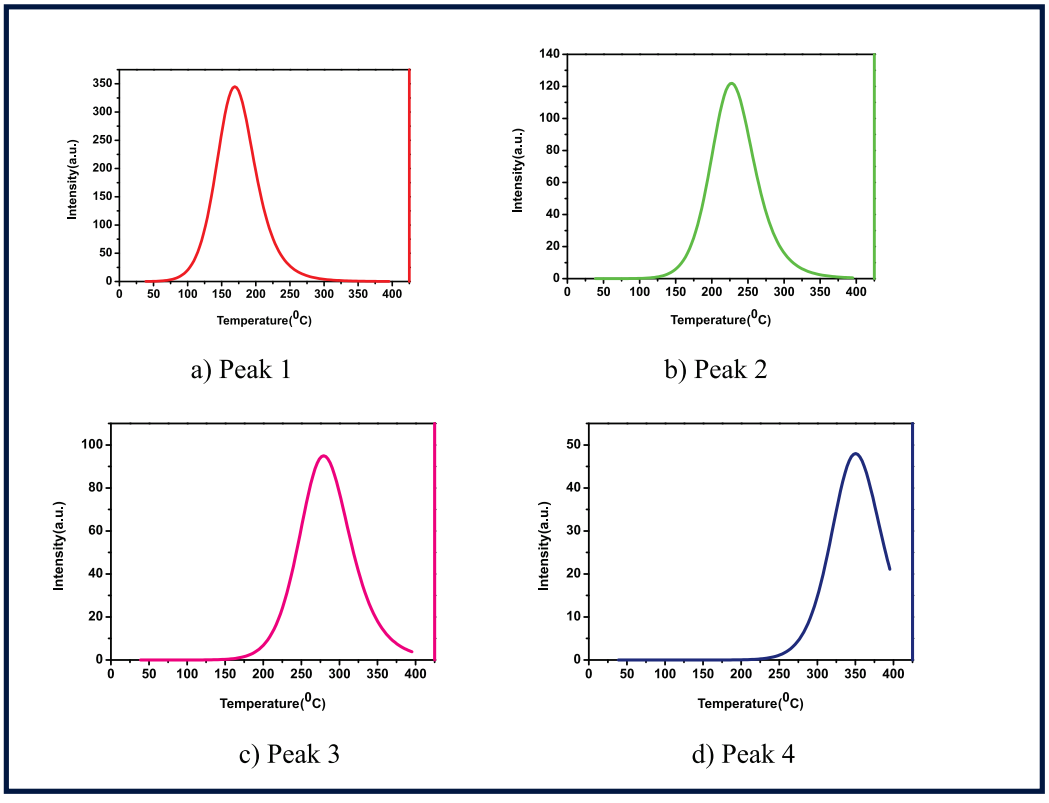

Fig. 5 a, b, c and d showing four glow peaks $KSrSO_4Cl$: Dy

In the present study using Chen's method the parameters have been calculated for all peaks. The total half intensity width ($w = T_2-T_1$), the high-temperature half width ($d = T_2 - T_M$), and the low-temperature half width ($t = T_M - T_1$), where T_M is the peak temperature and T_1 and T_2 are temperatures on either side of T_M corresponding to half peak intensity have been first determined and calculated values of activation energy (E), order of kinetics (b) and frequency factor (s) are reported as follows

Table 1 : Trapping Parameters of $KSrSO_4Cl$: Dy

Peak	CGCD				Chen's method			
	Tm	E(eV)	b	S	Tm	E(eV)	b	s
Peak 1	169	0.83	2	$6.67x10^8s^{-1}$	169.09	0.83	2	$6.63x10^8s^{-1}$
Peak 2	227	1	2	$2.56x10^9s^{-1}$	228.19	1.03	2	$4.99x10^9s^{-1}$
Peak 3	279	1.09	2	$1.69x10^9s^{-1}$	279.32	1.02	2	$3.59x10^9s^{-1}$
Peak 4	350	1.4	2	$4x10^{10}s^{-1}$	350.37	1.426	2	$6.50x10^{10}s^{-1}$

3.4 Study of Photoluminescence of $KSrSO_4Cl$: Eu

In the study of different phosphor by the addition of dopants the europium is considered as a special element. This is due to the fact that europium exhibits the property of valence fluctuation i.e. valence state is divalent or trivalent. Also it shows the different characteristics luminescence due to different valence. In our study the photoluminescence study of $KSrSO_4Cl$: Eu shows that at 396nm peak has the highest intensity than other peaks observed at 363nm, 382nm and 408nm(Fig. 6).Hence 396nm wavelength has been chosen as excitation wavelength, the emission has been carried out. The respective graph of the sample shows the Eu^{3+} emission of 595nm due to $^5D_0$-$^7F_1$ and 615nm due to $^5D_0$-$^7F_2$ which are

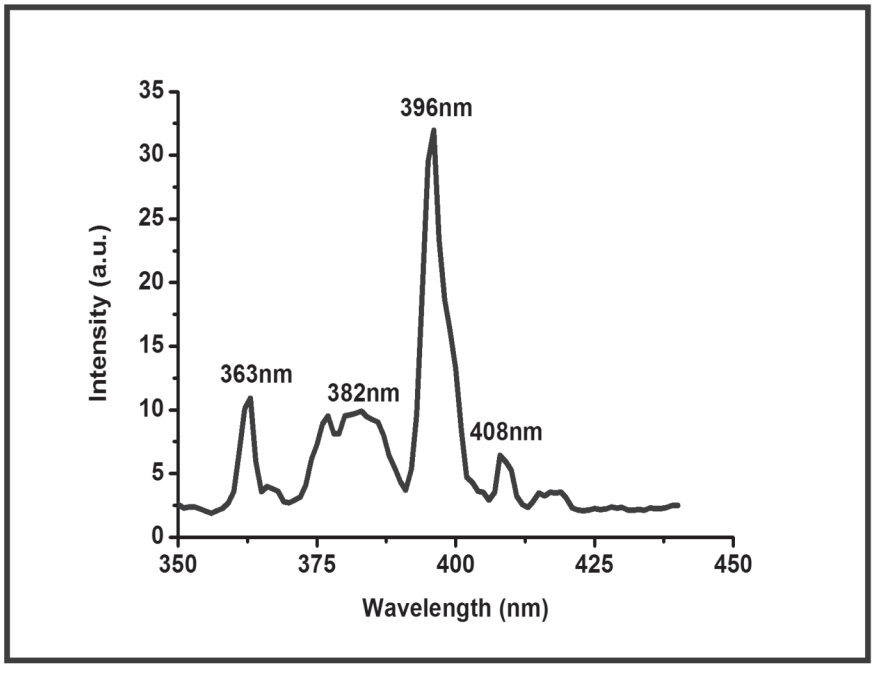

Fig. 6 Excitation of $KSrSO_4Cl$: Eu (λem=615nm)

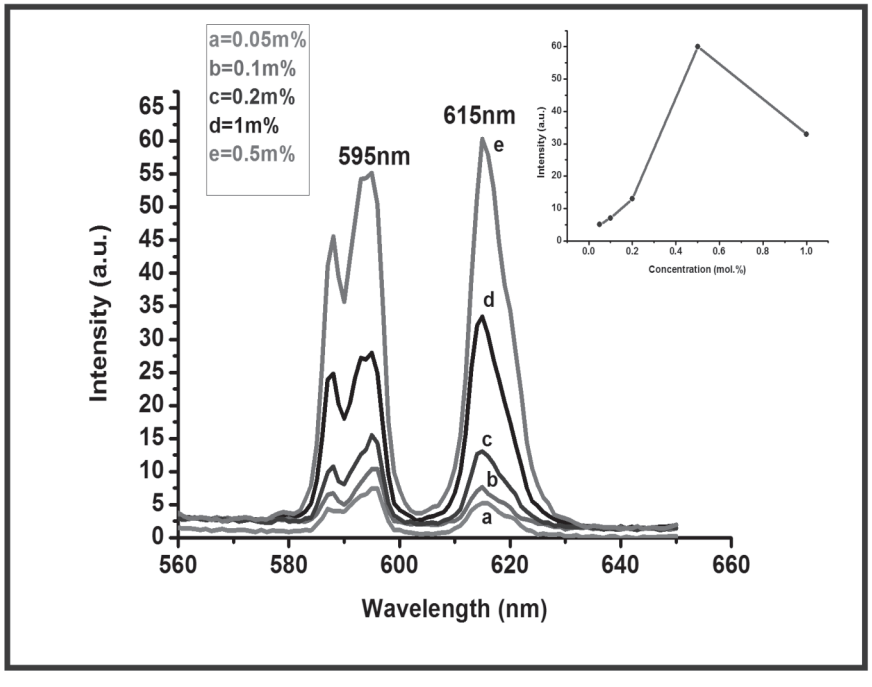

Fig. 7 Emission of $KSrSO_4Cl$: Eu(λex=396nm)

characteristic peaks of Eu^{3+}(Fig. 7).The red emission of $KSrSO_4Cl$: Eu^{3+} having the relatively high intensity at 615nm which corresponds to electric dipole transition while the intensity at 595nm corresponds to magnetic dipole transition has the weaker intensity.

When the rare earth (RE) ion is incorporated in a host material the energy level of the RE ion is generally splitted into number of sublevels due to the ligand field/crystal field. These sublevels are known as the Stark sublevels, and the maximum number of the f-f transition peaks due to RE ion can be given as 2J+1 (where J is the electronic angular momentum).It is also well known that the maximum numbers of Stark sublevels depend on the symmetry of the crystal field surrounding RE ion [17]. The $^5D_0$-$^7F_1$level has split into two peaks at 588nm and 595 nm which have the two peaks so the point symmetry is low at this site.

Phosphors (mol %)	Wavelength at Emission Peak (nm) [λex = 396 nm]	**Intensity (a.u.)**
$KSrSO_4Cl$: Eu 1%	595, 615	54, 60
$KSrSO_4Cl$: Eu 0.5%	595, 615	26, 33
$KSrSO_4Cl$:Eu0.2%	595, 615	15, 13
$KSrSO_4Cl$: Eu0.1%	595, 615	10, 7
$KSrSO_4Cl$: Eu0.05%	595, 615	7, 5

Table 2 : PL emission of $KSrSO_4Cl:Eu^{3+}$

3.5 Study of Photoluminescence of $KSrSO_4Cl$: Dy

Dy^{3+}has one interesting property that we can obtain white emission using Dy^{3+} when the ratio of blue to green emission is appropriate. Also while preparing the phosphors for the dosimetry of ionizing radiation using thermoluminescence Dy doped phosphors are useful candidates. Fig. 8 shows the excitation peak of Dy in the range of

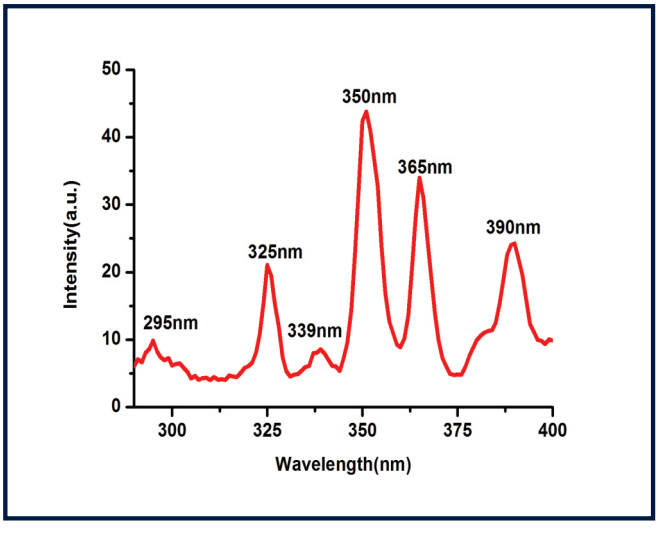

Fig. 8: Excitation of KSrSO4 Cl: Dy (λem=483nm)

290nm-400nm.The observed graph of Dy excitation shows that there are six peaks in the range of 290nm-400nm among which 350nm is chosen as excitation wavelength as it has the highest intensity.

Fig. 9 shows emission of Dy^{3+} doped in $KSrSO_4Cl$ at the excitation wavelength of 350nm.In the visible range Dy^{3+} emit two principal PL bands at 483nm and 572nm due to $^4F_{9/2}$-$^6H_{15/2}$ and $^4F_{9/2}$-$^6H_{13/2}$ transitions, in the blue and yellow region respectively. These are the principal emission bands of Dy^{3+}.The sharp line peaked at 483nm due to $^4F_{9/2}$-$^6H_{15/2}$ transition is corresponded to magnetic dipole transition while the peak at 572nm due to $^4F_{9/2}$-$^6H_{13/2}$ due to hypersensitive forced electric dipole transition. The magnetic dipole in Dy^{3+} hardly varies with crystal field transition around Dy^{3+} while the electric dipole transition is influenced by the outside surrounding.

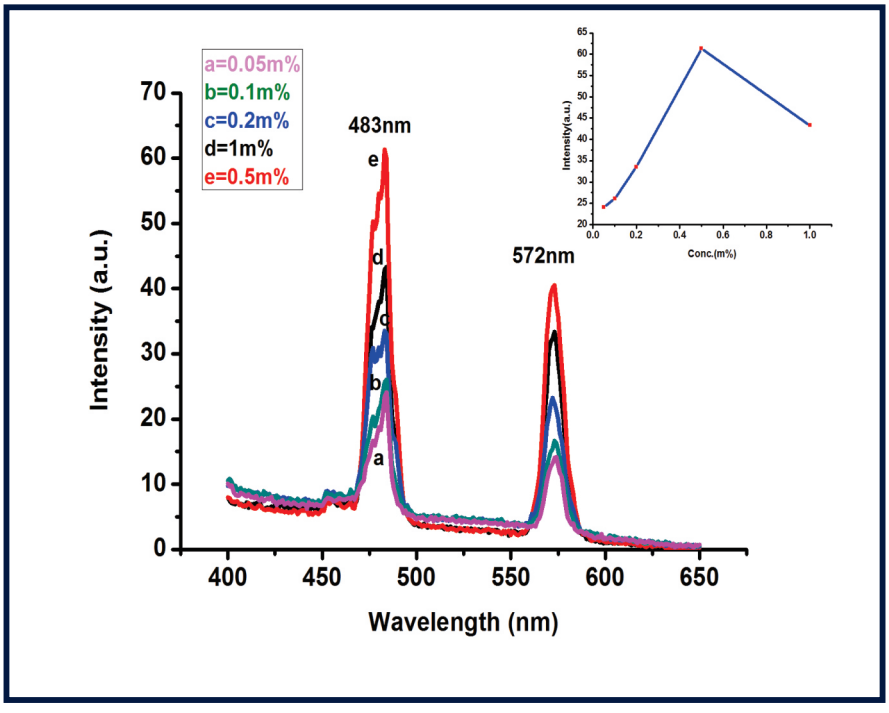

Fig. 9 Emission of $KSrSO_4Cl$: Dy (λex=350nm)

Table 3 : PL emission of $KSrSO_4Cl:Dy^{3+}$

Phosphors (mol %)	Wavelength at Emission Peak (nm) [λex= 350 nm]	Intensity (a.u.)
$KSrSO_4Cl$: Dy 0.5%	483, 572	61, 40
$KSrSO_4Cl$: Dy 1%	483, 572	43, 33
$KSrSO_4Cl$:Dy0.2%	483, 572	32, 23
$KSrSO_4Cl$: Dy0.1%	483, 572	26, 17
$KSrSO_4Cl$: Dy0.05%	483, 572	24, 14

3.5 CIE OF $KSrSO_4Cl:Eu^{3+}$ and $KSrSO_4Cl:Dy^{3+}$

In order to see how much promising the photoluminescence characteristics, the CIE chromaticity coordinates for $KSrSO_4Cl:Eu$ and $KSrSO_4Cl:Dy$ are investigated as shown in Fig. 10. The chromaticity co-ordinates x and y were computed for $KSrSO_4Cl:Eu$ (x = 0.627; y = 0.367) and $KSrSO_4Cl:Dy$(x = 0.3002; y = 0.382).

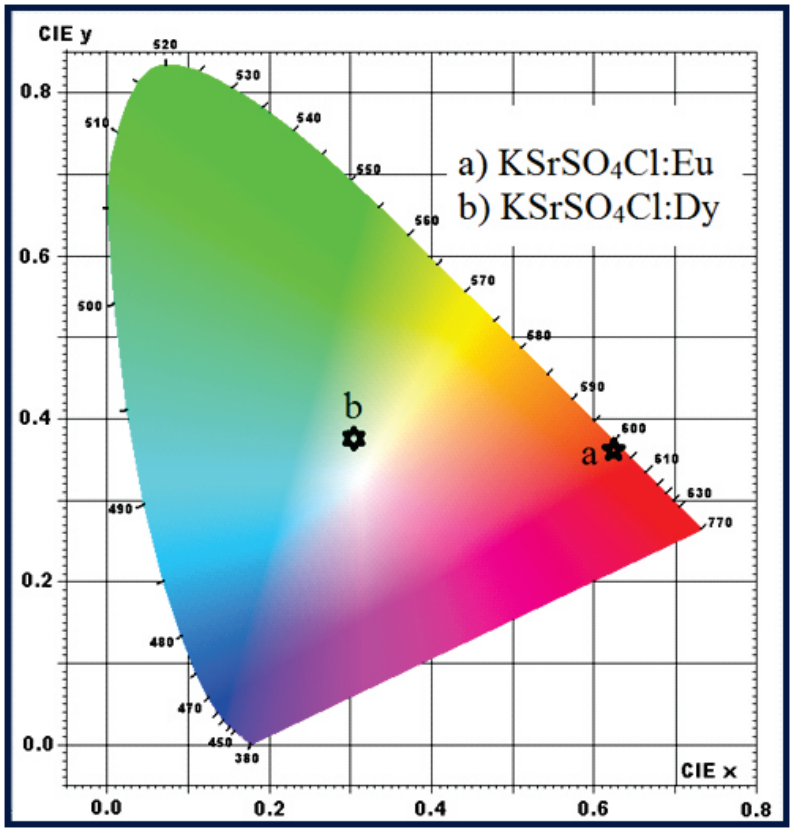

Fig. 10 CIE diagram for a) $KSrSO_4Cl:Eu$ and b) $KSrSO_4Cl:Dy$ phosphors depicted on the 1931 chart

Conclusion

The observed graph of $KSrSO_4Cl$: Dy excitation shows that there are six peaks in the range of 290nm-400nm among which 350nm is chosen as excitation wavelength. In the visible range Dy^{3+} emit two principal PL bands at 483nm and 572nm due to $^4F_{9/2}$-$^6H_{15/2}$ and $^4F_{9/2}$-$^6H_{13/2}$ transitions, in the blue and yellow region respectively. These are the principal emission bands of Dy^{3+}. The photoluminescence study of $KSrSO_4Cl$: Eu shows that at 396nm peak has the highest intensity than other peaks. Hence 396nm wavelength has been chosen as excitation wavelength, the $KSrSO_4Cl$: Eu shows the two peaks at 595nm and 615nm which is the emission of Eu^{3+}. The thermoluminescence glow peak for $KSrSO_4Cl$: Dy has the highest intensity at 169^0C and it follows the second order kinetics while $KSrSO_4Cl:Eu$ has the highest peak at 185^0C. The value of $ě_{mg}$ has been found 0.75 which shows that the peak of $KSrSO_4Cl:Eu$ follows the general order.

The aim of this study is to report a preliminary and qualitative result, related to PL and TL behavior of these materials. Therefore the new route opens for investigation of new TLD phosphors in Chlorosulphate materials.

References

[1] T. Welker, J. Lumin., 48 & 49 (1991) 49

[2] B.M.J. Smets, Mater. Chem. Phys., 16 (1987) 283

[3] B.M.J. Smets, in: DiBartolo (Ed.), Adv. Nonradiative Progress solids, Plenum Press, NY (1991)375.

[4] R. Raue, A.T. Vink, T. Welker, Phil. Tech. Rev., 44 (1989) 335

[5] M.K. Crawford, L.H. Brixner, J. Lumin., 48 & 49 (1991) 37

[6] H. Von Saggern, Cryst. Lattice Defects Amorph. Mater, 18 (1989) 399

[7] W. Rossner, B.C. Grabmainer, J. Lumin.,48 & 49 (1991) 29

[8] A. Miejerink, G. Blasse, J. Phys., D. 24 (1991) 626

[9] M. Ishi, M. Kobayashi, Prog. Cryst. Growth Charact. Mater., 23 (1991) 245

[10] Penzkoffer, Prog. Quantum Electron, 12 (1988) 291

[11] W.H. Byler, J.J. Maffis, in: T.C. Paton (Ed.), Pigment Handbook, Wiley, NY (1988) 881

[12] R. Reisfeld, C.K. Jorgenson, Handbook of Physics and Chemistry of RE, North-Holland, NY, 119(1982)1

[13] Y. Wang, N.Can , P.D.Townsend, J. Lumin., 131 (2011) 1864

[14] S. C. Gedam, S. J. Dhoble, S. V. Moharil, J. Lumin. 121(2006) 450

[15] T.Yamashita, N. Nada, H. Onishi andS. Kitamura, Proc. of Second Int. Conf. onLuminescence Dosimetry, Usaec-Conf.(1968)

[16] J. N. Azorin, G. M.Gonzalez , A.C. Guiterrez & Salvi R.P.C. Health Phys. 46(1984) 269

[17] Y. Kang, B. Thuy, Y. Shimokawa, T. Hayakawa, S. Sakaida, L. Miao, S. Tanemura, S. Honda,Y. Iwamoto,169(2016)78

Peer Reviewed and Refereed Journal 2022 **(ISSN : 09726330)**

Rashtrasant Tukadoji Maharaj Nagpur University

SCIENCE JOURNAL 2022

Vol. : XV

Graphene-SiO_2 Nanocomposite-Based Nanofluid : Ultrasonic-Assisted Synthesis, Characterization and Thermal Conductivity

Arihant M. Patil, Divya P. Barai, Bharat A. Bhanvase

Department of Chemical Engineering, Laxminarayan Institute of Technology, Rashtrasant Tukadoji Maharaj Nagpur University, Nagpur 440033, MS, India.

Corresponding author email: ba.bhanvase@nagpuruniversity.nic.in

ABSTRACT

Successful synthesis of graphene-SiO_2 nanocomposite particles was done using ultrasound-assisted process. FTIR and XRD analysis methods were used to confirm the decoration of graphene oxide with SiO_2nanoparticles. Furthermore, water-based nanofluids prepared using the synthesized graphene-SiO_2 nanocomposite particles showed enhanced thermal conductivity at different temperature and concentrations. Ultrasound-assisted process was found to be advantageous for the formation of the nanocomposite as well as for increasing thermal properties of the nanofluid.

Keywords : Nanofluid; graphene-SiO_2 nano-composite; ultrasound-assisted; thermal conductivity; Brownian motion

1. Introduction

Ever since the need to have efficient heat transfer systems to ensure full utilization of energy resources, innovations like surface modification of heat transfer equipment, attachment of external elements or vibration etc. have been employed [1]. However, increase in heat transfer area involves cost requirements. Therefore, there arose the need to have heat transfer fluids which are fluids that carry heat from one location to another, with high thermal properties. Back in history, Maxwell [2] recognized that when solids are dispersed in liquids, they can raise its thermal conductivity. However, there are several disadvantages of large solid particles dispersed in fluids as proposed by Das et al.[3]. In view of the heat transfer requirements and the disadvantages of large particles, the scientist Choi [4] came up with fluids, called as nanofluids, which contain solid particles having size smaller than 100 nm i.e. nanoparticles. Since then, nanofluids have been reported to have high thermal properties and superiorheat transfer performance compared to that of the corresponding base fluids [5–7]. Most commonly, water, ethylene glycol etc. are used as base fluids for nanoparticles dispersion. In view of the superior thermal transport properties, nanofluids have been used for various applications including electronic cooling systems [8,9], solar energy systems [10–12], as antibacterial agents [13,14] etc. Most commonly, nanoparticles of Al_2O_3[15–17], CuO [18,19], ZnO[20,21], and Fe_3O_4[22] have been used for nanofluids applications. CuO/water and CuO/ethylene glycol nanofluids exhibited 31.6% and 54% enhancement in thermal conductivity, respectively at concentration of 1 vol.% [23]. Similarly, thermal conductivity of 0.8 vol.% Al_2O_3 nanofluid was 9.8% to 17.89% more than that of base fluid (50:50 wt.%ethylene glycol-watermixture) at temperature ranging from 15°c to 50°c [24].

Further, with the development of carbonaceous nanosheet i.e. graphene, there has

been tremendous advancement in the field of energy conservation by its utilization[25–27]. Graphene (Gr), with the aid of surface functionalization can be associated with some other material thereby forming a nanocomposite. Nanofluids containing nanocomposites of graphene with Al_2O_3[28], Fe_3O_4[29], SnO_2[30], CuO [31], TiO_2[32], ZnO [33] etc. and have been explored. Decoration of graphene sheet with other nanoparticles prevents its restacking. However, decoration is only possible with graphene oxide (GO) sheet that provides surface oxygen functionalities as sites for attachment of foreign molecules [34]. Thus, attachment of other nanomaterials reduces graphene oxide to form reduced graphene oxide (rGO).

Kazemi et al. [35] prepared hybrid water-based nanofluid containing mixture of Gr and SiO_2 nanoparticles. They found a maximum thermal conductivity enhancement of 36.12% for the prepared nanofluid. However, the study involved simply mixing the two types of nanoparticles by magnetic stirring followed by ultrasonication. Also, to avoid aggregation of Gr sheets in the nanofluid, surfactant was utilized. On the other hand, graphene/SiO_2 nanocomposite material was synthesized by Li et al. [36] for preparation of water-based nanofluid. Coating of SiO_2 on Gr improved its hydrophilicity, stability and the thermal conductivity. Such technique can overcome the requirement of surfactant for preparation of water-based Gr nanofluid. However, a conventional method was used for synthesis of the nanocomposite particles. Moreover, SiO_2-graphene nanocomposite particles were synthesized by Qing et al. [37] by making use of ultrasonication for GO dispersion.Thermal conductivity of nanofluid containing the synthesized nanocomposite particles was found to enhance by 80%.This is because of the positive effects of ultrasonication in efficiently exfoliating the graphene oxide sheets thereby exposing their surface area for SiO_2 nanoparticles to cover them. Use of ultrasonication has many advantages during nanoparticle synthesis, including micro-convection effects, cavitation-induced turbulence,and localized high temperature-pressure conditions, as specified in different reports [38–40]. However, thermal conductivity of nanofluids containing graphene-SiO_2 nanocomposite prepared using fully ultrasonication-based method has not yet been investigated.

In this work, graphene-SiO_2 nanocomposite particles have been synthesized using the ultrasound-assisted process. The various characterization techniques confirm the synthesis of the nanocomposite particles. Further, water-based nanofluid was prepared by dispersing these particles. Thermal conductivity measurement of the prepared nanofluid was then performed to analyze its thermal transport ability.

2. Experimental

2.1 Materials

Reagents used for GO synthesis were same as those used by Barai et al. [29]. This included graphite powder (98%), $KMnO_4$ (99%), $NaNO_3$, $H_2SO_4^-$ (98%), H_2O_2 (30%), and HCl. Later, the synthesis of graphene-SiO_2 nanocomposite required tetraethyl orthosilicate (TEOS), ammonia solution (25%), and ethanol. All chemicals were used as purchased. Distilled water was utilised to prepare solutions.

2.2 Synthesis of graphene oxide-SiO_2 nanocomposite

Firstly, before proceeding towards synthesis of graphene-SiO_2 nanocomposite, GO was synthesized using same procedure as that followed by Barai et al. [29] i.e the modified Hummers' method in an ultrasonic horn type sonicator (PCI Analytics Pvt. Ltd., India) which has a fixed frequency of 20 KHz. The prepared graphene oxide powder was filtered and oven-dried.

Further, in order to synthesize graphene-SnO_2 nanocomposite, firstly, an ethanol-water mixture was prepared using 73.8 ml ethanol and 10.8 ml distilled water in a beaker. To this mixture, 0.5 g of the prepared GO powder was added. This mixture was ultrasonicated for 20 min to exfoliate GO. Then, 5.6 ml of TEOS was added to the same beaker and ultrasonication was continued for further 10 min. Further, 9.8 ml of ammonia solution (25%) was added to the existing solution which was then followed by ultrasonication for 1 hr. After ultrasonication, the obtained reaction mixture was filtered using a filter paper and washed with 100 ml of 3:1 v/v ethanol-water mixture. Then the obtained residue particles were dried in oven at 100°c for 4 hrs. It was then stored for further nanofluid preparation. Figure 1 graphically illustrates the steps followed for synthesis of graphene-SiO_2 nanocomposite particles.

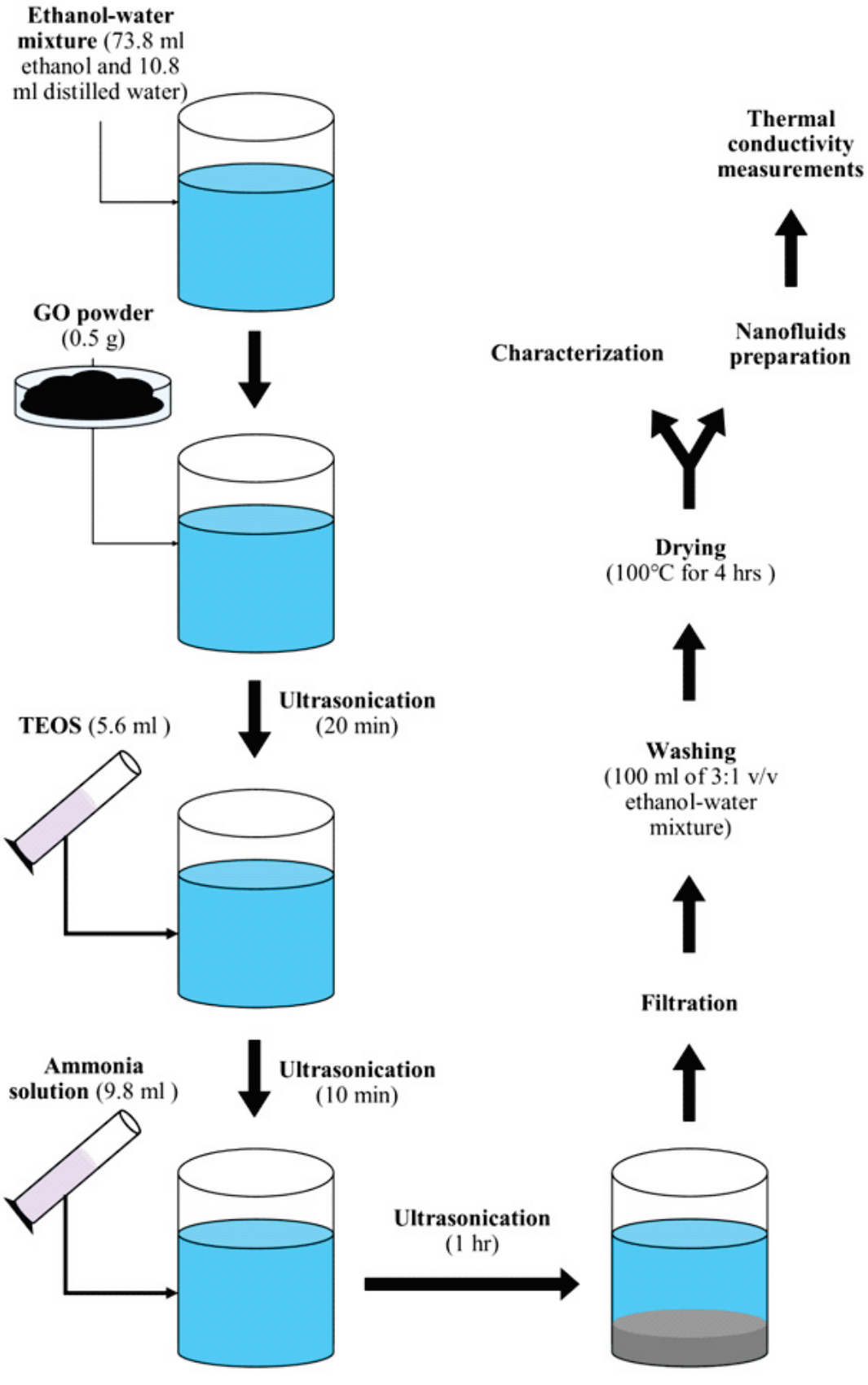

Fig.1. Ultrasound assisted synthesis process of graphene-SiO_2 nanocomposite particles

2.3 Characterization

FTIR of graphene-SiO_2 nanocomposite was acquired from FTIR Spectrometer (Bruker Alpha II) and XRD pattern of graphene-SiO_2 nanocomposite was acquired using X-ray diffractometer (Rigaku Mini-Flex).

2.4 Nanofluid preparation

Water-based nanofluids containing the ultrasonically synthesized graphene-SiO_2 nanocomposite particles were prepared by dispersing them in distilled water using ultrasonication. Two nanofluids (0.01 vol.% and 0.05 vol.%)for thermal conductivity measurement at different temperatures were prepared.

2.5 Thermal conductivity measurement

Thermal conductivities of graphene-SiO_2 nanofluids (0.01 vol.% and 0.05 vol.%) were measured using KD2 Pro thermal property analyser (Decagon Devices, Inc., USA) at temperature ranging from 30 to 37ºC. Moreover, thermal conductivity enhancement was also calculated (Equation 1), where k_{nf} and k_{bf} are thermal conductivities of nanofluid and base fluid, respectively.

$$\frac{(k_{nf} - k_{bf})}{k_{bf}} \times 100 \quad \text{..... (1)}$$

3. Results and Discussion

3.1 Characterisation of graphene-SiO_2 nanocomposite particles

Figure 2 depicts FTIR spectrum of the synthesized graphene-SiO_2 nanocomposite particles. In this, the sharp band at 1077 cm^{-1} is credited to the asymmetric stretching of Si-O-C/Si-O-Si [41].The Si-O-C band is said to strengthen the GO-

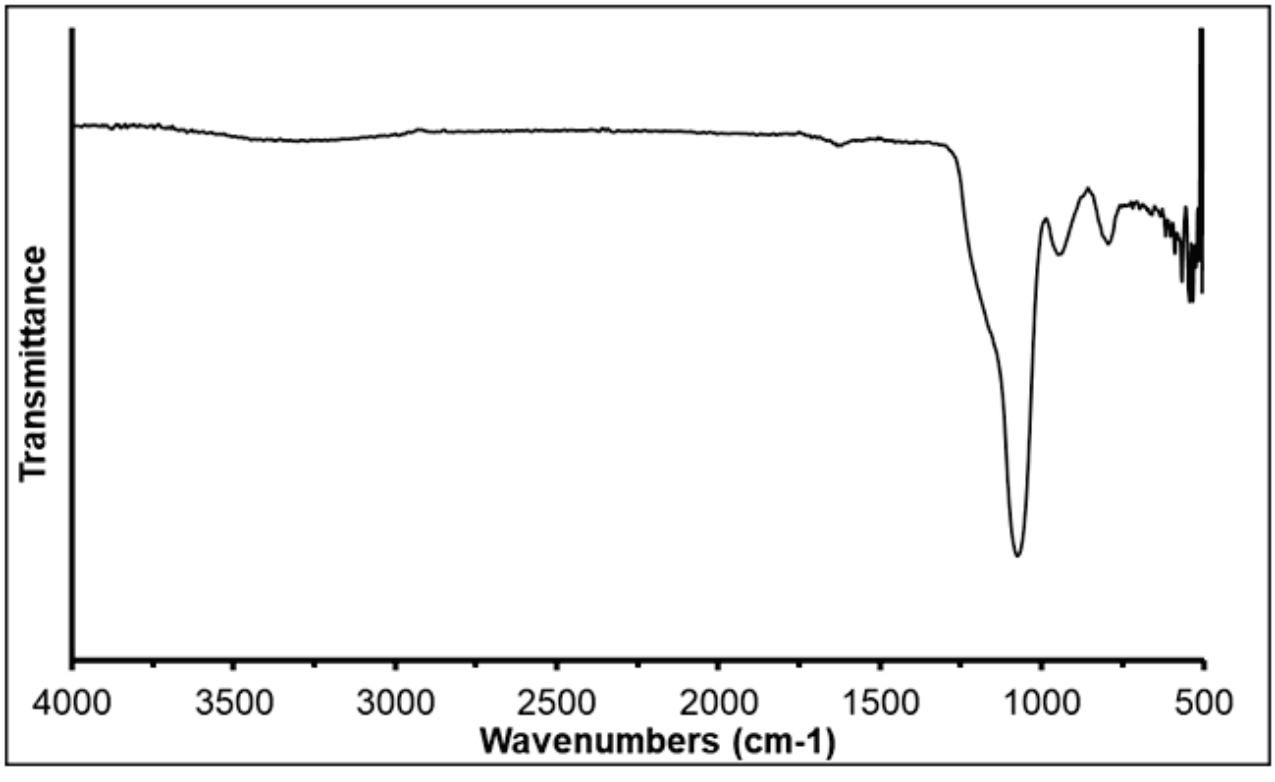

Fig.2. FTIR spectrum of the synthesized graphene-SiO_2 nanocomposite particles.

SiO_2 interaction [42]. Moreover, peaks at 797 cm^{-1} and 941 cm^{-1} are due to the Si-O-Si and Si-OH groups of SiO_2, respectively[41]. At the same time, the peaks of -OH and COOH stretching vibration of hydroxyl group and carboxylic group, respectively, present in GO, that commonly prevail at 3400 cm^{-1} and 1650 cm^{-1}, respectively are only slightly appearing in this spectrum [43]. This is because of the attachment of SiO_2 to the graphene surface with the aid of these functionalities thereby reducing it to graphene. This takes place more efficiently in presence of ultrasonic irradiations due to presence of intense environment of high temperature and pressure.

XRD pattern of synthesized graphene-SiO_2 nanocomposite particles is shown in Figure 3. The XRD pattern shows a broad peak between 15-25° which is scattered from the (100) plane of SiO_2 [44]. Further, the peaks at 11.6° and 42.7° appear to be very small. These peaks are attributed to the (001) plane and (400) plane, respectively belonging to graphene oxide [44,45]. However, their weakened intensity is due to the reduction of GO because of the attachment of SiO_2 nanoparticles which is in accordance with FTIR analysis. This is also an indication of prevention of restacking of GO nanosheets due to presence of SiO_2 nanoparticles [46]. Ultrasonication aids in complete exfoliation of GO sheet and thereby exposure for attachment of the SiO_2 nanoparticles.

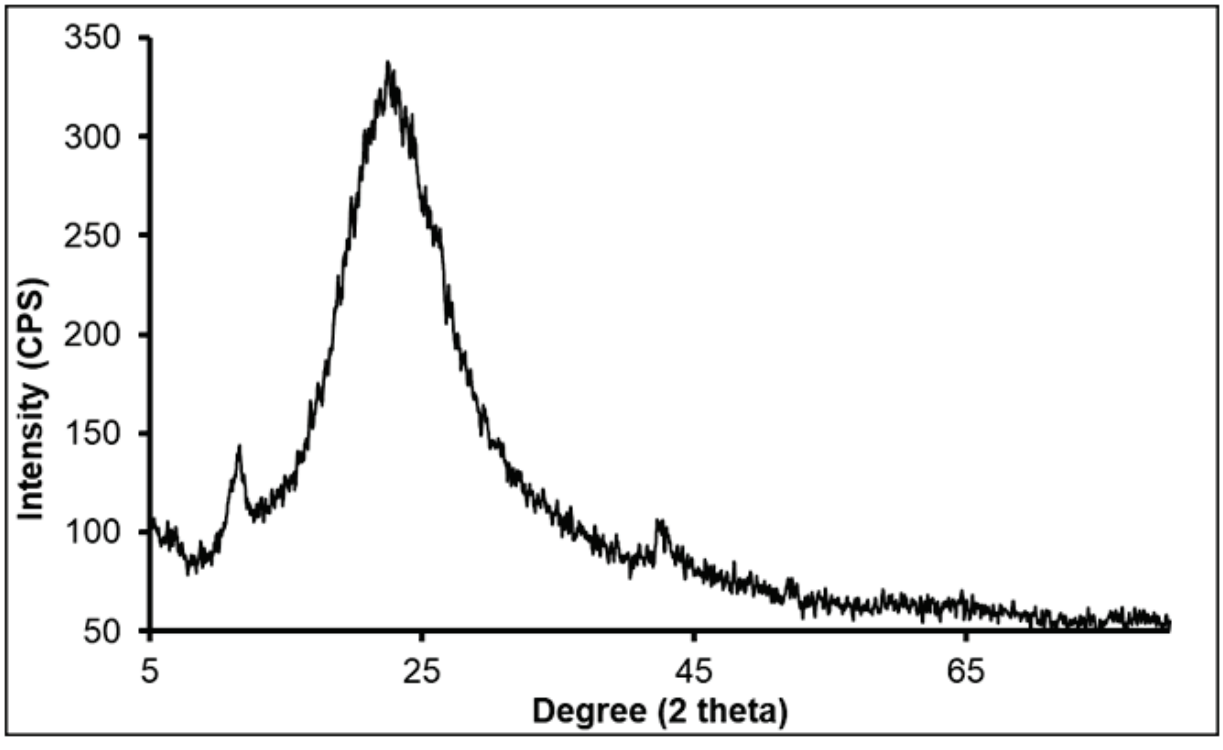

Fig.3. XRD pattern of the synthesized graphene-SiO_2 nanocomposite particles.

3.2 Thermal conductivity of graphene-SiO_2 nanocomposite particles-based nanofluid

Trend of thermal conductivity with temperature for graphene-SiO_2 nanofluid at concentrations of 0.01 vol.% and 0.05 vol.% is plotted in Figure 4. Firstly, thermal conductivity of nanofluids was greater than that of water at all temperatures and that it increased with rise in temperature. At 36.5ºC, thermal conductivity enhancement calculated for 0.01 vol.% and 0.05 vol.% graphene-SiO_2 nanofluid was 52.209% and 84.25%, respectively. For 0.05 vol.% graphene-SiO_2 nanofluid, the thermal conductivity increased to 1.15 W/mK from 0.62 W/mK with 5.5ºC increase in temperature from 31ºC. The reason for this is increased Brownian motion of nanoparticles dispersed within the fluid, specifically at elevated temperatures [47]. Brownian motion is a kind of natural random motion of nanoparticles which induces heat dissipation

due to micro-convection currents. Higher temperatures also reduce viscosity of the basefluid thereby easing the Brownian motion [29, 48]. High temperatures also aid in decrease of surface energy of graphene-SiO_2 nanocomposite particles which aids in reducing their aggregation [49].

Furthermore, thermal conductivity of the nanofluid increases when its concentration was increased. Thermal conductivity of 0.01 vol.% graphene-SiO_2 nanofluid was 0.95 W/mK at 36.5ºC which increased to 1.15 W/mK when the concentration was 0.05 vol.%. The most obvious reason for this is that the increase in the number of nanoparticles, which inherently have high thermal conductivity, raise the fluid thermal conductivity. However, the more specific reason is that the rise in number of nanoparticles raises the number of carriers of heat within the nanofluid. These heat carriers have an increased surface area that aids in heat absorption. Thus, there is more amount of heat energy being transported and thus dissipated throughout the nanofluid [29,50,51]. Also, the increased surface area is attributed to the positive effects of ultrasonication. Ultrasonication aids in complete exfoliation of the GO sheet thereby exposing it for the silica nanoparticles to get attached to. Moreover, this attachment prevents restacking of GO thereby allowing maximum area to be available for heat transfer. At the same time, the tiny size i.e., nano-size of the formed particles keep them dispersed in the nanofluids without settling down. This maintains the stability of the nanofluids and is the reason for the high thermal conductivity.

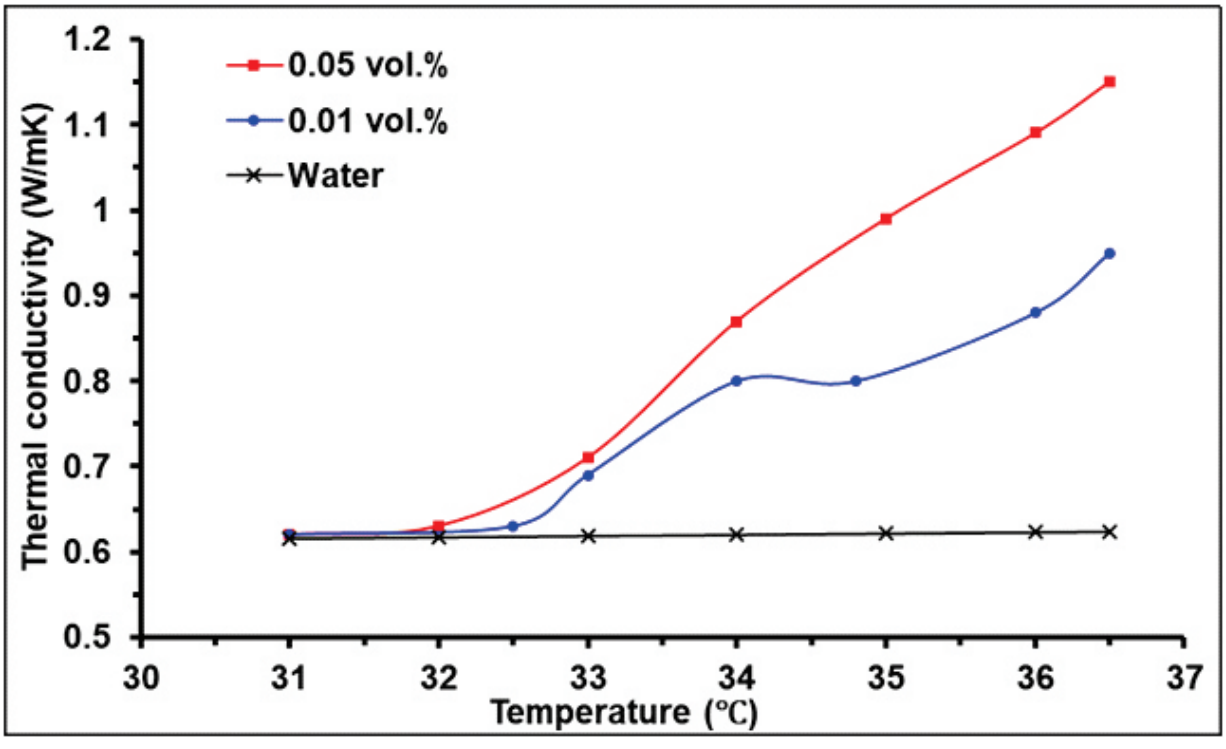

Fig.4. Thermal conductivity of graphene-SiO_2 nanofluid at concentration of 0.01 vol.% and 0.05 vol.% as a function of temperature.

4. Conclusions

Ultrasonic-assisted synthesis of graphene-SiO_2 nanocomposite particles was successfully done. FTIR and XRD analysis of synthesized product confirmed attachment of SiO_2 nanoparticles to the GO sheet. This attachment was assisted by the functional groups present on GO sheet and aided in reducing the restacking of the sheets. Furthermore, thermal conductivity of nanofluid prepared using the synthesized graphene-SiO_2 nanocomposite particles was found to be greater than that of water. Also, thermal conductivity measurements revealed enhancement with temperature and concentration. A maximum thermal conductivity enhancement of 84.25% was exhibited by graphene-SiO_2 nanocomposite-based nanofluids having concentration of 0.05 vol.%. The several mechanisms taking part for thermal conductivity enhancement include Brownian motion, micro-convection currents, viscosity reduction, surface energy

reduction, efficient heat dissipation, and high thermal conductivity and high surface area of graphene-SiO_2 nanocomposite particles. At the same time, positive effects of ultrasonication also play key role. Thus, nanofluid containing graphene-SiO_2 nanocomposite particles synthesized by ultrasound-assisted process can be successfully used for heat transfer applications.

References

[1] Bergles AE. Heat Transfer Augmentation. Two-Phase Flow Heat Exch., Dordrecht: Springer Netherlands; 1988, p. 343–73. https://doi.org/10.1007/978-94-009-2790-2_10.

[2] Maxwell JC. A Treatise on Electricity and Magnetism. vol. 1. 2nd Ed. Oxford: Clarendon Press; 1954.

[3] Das SK, Choi SUS, Patel HE. Heat transfer in nanofluids - A review. Heat Transf Eng 2006;27:3–19. https://doi.org 10.1080/01457630600904593.

[4] Choi SUS, Eastman JA. Enhancing thermal conductivity of fluids with nanoparticles. Am Soc Mech Eng Fluids Eng Div FED 1995;231:99–105. https://doi.org/10.1115/1.1532008.

[5] Senthilraja S, Vijayakumar K, Gangadevi R. A comparative study on thermal conductivity of Al2O3/water, CuO/water and Al2O3 – CuO/water nanofluids. Dig J Nanomater Biostructures 2015;10:1449–58.

[6] Chandrasekar M, Suresh S, Chandra Bose A. Experimental investigations and theoretical determination of thermal conductivity and viscosity of Al2O3/water nanofluid. Exp Therm Fluid Sci 2010;34:210–6. https://doi.org/10.1016/j.expthermflusci.2009.10.022.

[7] Suresh S, Venkitaraj KP, Selvakumar P, Chandrasekar M. Synthesis of Al2O3-Cu/water hybrid nanofluids using two step method and its thermo physical properties. Colloids Surfaces A Physicochem Eng Asp 2011;388:41–8. https://doi.org/10.1016/j.colsurfa.2011.08.005.

[8] Bahiraei M, Heshmatian S. Electronics cooling with nanofluids: A critical review. Energy Convers Manag 2018;172:438–56. https://doi.org/10.1016/j.enconman.2018.07.047.

[9] Ijam A, Saidur R. Nanofluid as a coolant for electronic devices (cooling of electronic devices). Appl Therm Eng 2012;32: 76–82. https://doi.org/10.1016/j.applthermaleng.2011.08.032.

[10] Sani E, Papi N, Mercatelli L, ¯y³a G. Graphite/diamond ethylene glycol-nanofluids for solar energy applications. Renew Energy 2018;126:692–8. https://doi.org/10.1016/j.renene.2018.03.078.

[11] Xuan Y, Duan H, Li Q. Enhancement of solar energy absorption using a plasmonic nanofluid based on TiO2/Ag composite nanoparticles. RSC Adv 2014;4:16206–13. https://doi.org/10.1039/c4ra00630e.

[12] Mahian O, Kianifar A, Kalogirou SA, Pop I, Wongwises S. A review of the applications of nanofluids in solar energy. Int J Heat Mass Transf 2013;57:582–94. https://doi.org/10.1016/j.ijheatmasstransfer.2012.10.037.

[13] Yadav N, Jaiswal AK, Dey KK, Yadav VB, Nath G, Srivastava AK, et al. Trimetallic Au/Pt/Ag based nanofluid for enhanced antibacterial response. Mater Chem Phys 2018;218:10–7. https://doi.org/10.1016/j.matchemphys.2018.07.016.

[14] Zhang L, Ding Y, Povey M, York D. ZnO nanofluids – A potential antibacterial agent. Prog Nat Sci 2008;18:939–44. https://doi.org/10.1016/j.pnsc.2008.01.026.

[15] Heyhat MM, Kowsary F, Rashidi AM, Momenpour MH, Amrollahi A. Experimental investigation of laminar convective heat transfer and pressure drop of water-based Al 2O 3 nanofluids in fully developed flow regime. Exp Therm Fluid Sci 2013;44:483–9. https://doi.org/10.1016/j.expthermflusci.2012.08.009.

[16] Syam Sundar L, Venkata Ramana E, Singh MK, Sousa ACM. Thermal conductivity and viscosity of stabilized ethylene glycol and water mixture Al2O3 nanofluids for heat transfer applications: An experimental study. Int Commun Heat Mass Transf 2014;56:86–95. https://doi.org/10.1016/j.icheatmasstransfer.2014.06.009.

[17] Subramani J, Nagarajan PK, Wongwises S, El-Agouz SA, Sathyamurthy R. Experimental study on the thermal performance and heat transfer characteristics of solar parabolic trough collector using Al2O3 nanofluids. Environ Prog Sustain Energy 2018;37:1149–59. https://doi.org/10.1002/ep.12767.

[18] Selvakumar P, Suresh S. Convective performance of CuO/water nanofluid in an electronic heat sink. Exp Therm Fluid Sci 2012;40:57–63. https://doi.org/10.1016/j.expthermflusci.2012.01.033.

[19] Khedkar RS, Sonawane SS, Wasewar KL. Influence of CuO nanoparticles in enhancing the thermal conductivity of water and monoethylene glycol based nanofluids. Int Commun Heat Mass Transf 2012;39:665–9. https://doi.org/10.1016/j.icheatmasstransfer.2012.03.012.

[20] Suganthi KS, Leela Vinodhan V, Rajan KS. Heat transfer performance and transport properties of ZnO-ethylene glycol and ZnO-ethylene glycol-water nanofluid coolants. Appl Energy 2014;135:548–59. https://doi.org/10.1016/j.apenergy.2014.09.023.

[21] Radkar RN, Bhanvase BA, Barai DP, Sonawane SH. Intensified convective heat transfer using ZnO nanofluids in heat exchanger with helical coiled geometry at constant wall temperature. Mater Sci Energy Technol 2019;2:161–70. https://doi.org/10.1016/j.mset.2019.01.007.

[22] Sundar LS, Singh MK, Sousa ACM. Thermal conductivity of ethylene glycol and water mixture based Fe3O4 nanofluid. Int Commun Heat Mass Transf 2013;49:17–24. https://doi.org/10.1016/j.icheatmasstransfer.2013.08.026.

[23] Karthikeyan NR, Philip J, Raj B. Effect of clustering on the thermal conductivity of nanofluids. Mater Chem Phys 2008;109:50–5. https://doi.org/10.1016/j.matchemphys.2007.10.029.

[24] Sundar LS, Farooky MH, Sarada SN, Singh MK. Experimental thermal conductivity of ethylene glycol and water mixture based low volume concentration of Al2O3 and CuO nanofluids. Int Commun Heat Mass Transf 2013;41:41–6. https://doi.org/10.1016/j.icheatmasstransfer.2012.11.004.

[25] Brownson DAC, Kampouris DK, Banks CE. An overview of graphene in energy production and storage applications. J Power Sources 2011;196:4873–85. https://doi.org/10.1016/j.jpowsour.2011.02.022.

[26] Sun Y, Wu Q, Shi G. Graphene based new energy materials. Energy Environ Sci 2011;4:1113–32. https://doi.org/10.1039/c0ee00683a.

[27] Liu J, Xue Y, Zhang M, Dai L. Graphene-based materials for energy applications. MRS Bull 2012;37:1265–72. https://doi.org/10.1557/mrs.2012.179.

[28] Singh K, Barai DP, Chawhan SS, Bhanvase BA, Saharan V. Synthesis, characterization and heat transfer study of reduced graphene oxide-Al2O3 nanocomposite based nanofluids: Investigation on thermal conductivity and rheology. Mater Today Commun 2020:101986. https://doi.org/10.1016/j.mtcomm.2020.101986.

[29] Barai DP, Bhanvase BA, Saharan VK. Reduced graphene oxide-Fe3O4 nanocomposite based nanofluids: Study on ultrasonic assisted synthesis, thermal conductivity, rheology and convective heat transfer. Ind Eng Chem Res 2019;58:8349–69. https://doi.org/10.1021/acs.iecr.8b05733.

[30] Chawhan SS, Barai DP, Bhanvase BA. Sonochemical preparation of rGO-SnO2 nanocomposite and its nanofluids: Characterization, thermal conductivity, rheological and convective heat transfer investigation. Mater Today Commun 2020;23. https://doi.org/10.1016/j.mtcomm.2020.101148.

[31] Sarode HA, Barai DP, Bhanvase BA, Ugwekar RP, Saharan V. Investigation on preparation of graphene oxide-CuO nanocomposite based nanofluids with the aid of ultrasound assisted method for intensified heat transfer properties. Mater Chem Phys 2020;251:123102. https://doi.org/10.1016/j.matchemphys.2020.123102.

[32] Koshta NR, Bhanvase BA, Chawhan SS, Barai DP, Sonawane SH. Investigation on the thermal conductivity and convective heat transfer enhancement in helical coiled heat exchanger using ultrasonically prepared rGO–TiO2 nanocomposite-based nanofluids. Indian Chem Eng 2019:1–14. https://doi.org/10.1080/00194506.2019.1658545.

[33] Mandhare H, P. Barai D, A. Bhanvase B, Saharan VKVK. Preparation and thermal conductivity investigation of reduced graphene oxide-ZnO nanocomposite-based nanofluid synthesised by ultrasound-assisted method. Mater Res Innov 2020;24:433–41. https://doi.org/10.1080/14328917.2020.1721809.

[34] Lin Z, Liu Y, Li Z, Wong CP. Novel preparation of functionalized graphene oxide for large scale, low cost, and self-cleaning coatings of electronic devices. Proc - Electron Components Technol Conf 2011:358–62. https://doi.org/10.1109/ECTC.2011.5898538.

[35] Kazemi I, Sefid M, Afrand M. Improving the thermal conductivity of water by adding mono & hybrid nano-additives containing graphene and silica: A comparative experimental study. Int Commun Heat Mass Transf 2020;116. https://doi.org/10.1016/j.icheatmasstransfer.2020.104648.

[36] Li X, Chen Y, Mo S, Jia L, Shao X. Effect of surface modification on the stability and thermal conductivity of water-based SiO2-coated graphene nanofluid. Thermochim Acta 2014;595:6–10. https://doi.org/10.1016/j.tca.2014.09.006.

[37] Qing SH, Rashmi W, Khalid M, Gupta TCSM, Nabipoor M, Hajibeigy MT. Thermal conductivity and electrical properties of Hybrid SiO2-graphene naphthenic mineral oil nanofluid as potential transformer oil. Mater Res Express 2017;4. https://doi.org/10.1088/2053-1591/aa550e.

[38] Chawhan SS, Barai DP, Bhanvase BA. Investigation on thermophysical properties, convective heat transfer and performance evaluation of ultrasonically synthesized Ag-doped TiO2 hybrid nanoparticles based highly stable nanofluid in a minichannel. Therm Sci Eng Prog 2021:100928. https://doi.org/10.1016/j.tsep.2021.100928.

[39] Shende TPP, Bhanvase BAA, Rathod APP, Pinjari DV V., Sonawane SHH. Sonochemical synthesis of Graphene-Ce-TiO2 and Graphene-Fe-TiO2 ternary hybrid photocatalyst nanocomposite and its application in degradation of crystal violet dye. Ultrason Sonochem 2018;41:582–9. https://doi.org/10.1016/j.ultsonch.2017.10.024.

[40] Satdeve NS, Ugwekar RP, Bhanvase BA. Ultrasound assisted preparation and characterization of Ag supported on ZnO nanoparticles for visible light degradation of methylene blue dye. J Mol Liq 2019;291:111313. https://doi.org/10.1016/j.molliq.2019.111313.

[41] Yan H, Jiang L, Xu X, Li Y, Shen Y, Zhu S. Ultrastrong composite film of Chitosan and silica-coated graphene oxide sheets. Int J Biol Macromol 2017;104:936–43. https://doi.org/10.1016/j.ijbiomac.2017.07.003.

[42] Zhang WL, Choi HJ. Silica-graphene oxide hybrid composite particles and their electroresponsive characteristics. Langmuir 2012;28:7055–62. https://doi.org/10.1021/la3009283.

[43] Khalili D. Graphene oxide: A promising carbocatalyst for the regioselective thiocyanation of aromatic amines, phenols, anisols and enolizable ketones by hydrogen peroxide/KSCN in water. New J Chem 2016;40:2547–53. https://doi.org/10.1039/c5nj02314a.

[44] In†situ polymerization of graphene/SiO2 hybrids modified phenolic resin for improved thermal stability at an ultralow filler loading n.d.

[45] Archana S, Kumar KY, Olivera S, Jayanna BK, Muralidhara HB, Ananda A, et al. Development of Multipurpose CuO–GO Nanocomposites for Heavy Metals Adsorption and Super Capacitor Applications. Energy Environ Focus 2017;5:305–15. https://doi.org/10.1166/eef.2016.1225.

[46] Peng L, Zhang J, Yang S, Han B, Sang X, Liu C, et al. Ultra-small gold nanoparticles immobilized on mesoporous silica/graphene oxide as highly active and stable heterogeneous catalysts. Chem Commun 2015;51:4398–401. https://doi.org/10.1039/c4cc09131k.

[47] Jang SP, Choi SUSS. Role of Brownian motion in the enhanced thermal conductivity of nanofluids. Appl Phys Lett 2004;84:4316–8. https://doi.org/10.1063/1.1756684.

[48] Mahian O, Kolsi L, Amani M, Estellé P, Ahmadi G, Kleinstreuer C, et al. Recent advances in modeling and simulation of nanofluid flows-Part I: Fundamentals and theory. Phys Rep 2019;790:1–48. https://doi.org/10.1016/j.physrep.2018.11.004.

[49] Vollath D, Fischer FD, Holec D. Surface energy of nanoparticles - influence of particle size and structure. Beilstein J Nanotechnol 2018;9:2265–76. https://doi.org/10.3762/bjnano.9.211.

[50] Issa RJ. Effect of Nanoparticles Size and Concentration on Thermal and Rheological Properties of AL2O3-Water Nanofluids. Proc. World Congr. Momentum, Heat Mass Transf., Prague: 2016. https://doi.org/10.11159/enfht16.101.

[51] Chamsa-ard W, Brundavanam S, Fung CC, Fawcett D, Poinern G. Nanofluid types, their synthesis, properties and incorporation in direct solar thermal collectors: A review. Nanomaterials 2017;7:131. https://doi.org/10.3390/nano7060131.

Peer Reviewed and Refereed Journal 2022 **(ISSN : 09726330)**

Rashtrasant Tukadoji Maharaj Nagpur University

SCIENCE JOURNAL 2022

Vol. : XV

Tourmaline Dumortierite and Borosilicates of India - A Review

Sneha Dandekar[1*], Kavita Pande[2], Dilip Peshwe[1] and Kirtikumar Randive[3]

[1]Metallurgical and Materials Engineering Department, VNIT, Nagpur

[2]Matverse Vision Pvt. Ltd.

[3]Department of Geology, Rashtrasant Tukadoji Maharaj Nagpur University, India

*Corresponding author email : snehandandekar@gmail.com

ABSTRACT

Borosilicates are boron containing, oxygen rich minerals which has SiO_4 tetrahedra forming the main structural constituent. Amongst the borosilicates, tourmaline is the widest spread mineral, followed by dumortierite. The empirical formula of tourmaline is XY_3Z_6 (T_6O_{18}) $(BO3)_3V_3W$; where X: Na^{1+}, Ca^{2+}, , K^{1+}, Pb^{2+}, Y: Mg^{2+}, Fe^{2+}, Al^{3+}, Li^{1+}, Ti^{4+}, Mn^{2+}, Fe^{3+}, Zn^{2+}, Z: Al^{3+}, Cr^{3+}, Fe^{3+}, Mg^{2+}, Fe^{2+}, T: Si^{4+}, B^{3+}, Al^{3+}, B: B^{3+}, V: OH^{1-}, O^{2-}, W: OH^{1-}, F^{1-}, O^{2-}. The mineral generally occurs as hydrothermal deposits or by the hydrothermal water vapors which carries boron element from the source. The mineral crystallizes in the open space that is in the form of pockets, voids, veins and fractures in the host rocks. They are commonly associated with igneous and metamorphic rock. The gem quality of tourmaline is mostly found in Southern California, Maine and Connecticut of United State, Brazil, Elba, Madagascar and the Ural Mountains. Taking into consideration the recent data, this paper deals with an overview of tourmaline and other borosilicates mineral occurring in India. The localities from India, discussed in detail covers a time range from Meso-Archean to Oligocene and of Chitradurg, Greenstone belt (CGB) and Hutti-Maski Greenstone Belt of Karnataka; Eastern Ghat Mobile Belt at Vizianagaram, and Bastipadu at Kurnool, Andhra Pradesh; Garhwal Higher Himalaya, Uttarakhand; Mashak Pahad, South Purulia Shear Zone, West Bengal; Simdega area of Chhotanagpur, Jharkhand and Girolla Hill of Bhandara, Maharashtra region.

Keywords : Borosilicates, CGB, Hutti-Maski Greenstone Belt, Eastern Ghat Mobile Belt, Bastipadu, Garhwal Higher Himalaya, MashakPahad, Simdega, Girolla Hill.

1. INTRODUCTION

Borosilicates are boron rich oxygen-bearing minerals in which SiO_4 tetrahedra make an important essential component. They signify extensive-elements of rocks emanating in the Earth's crust and commonly reveals the rock-forming processes. Predominant borosilicates include tourmaline, dumortierite, axinite, howlite, werdingite, grandidierite, holtite and boralsilite. Tourmaline [XY_3Z_6 (T_6O_{18}) $(BO3)_3V_3W$] is an utmost extensive borosilicate variety and it can be used to determine a wide diversity of geological processes based on its high compositional variance. Dumortierite [$(Al, \square) Al_6$ (BO_3) Si_6O_{13} $(O, OH)_2$], occurs second after the tourmaline as the most abundant borosilicate variety, but remains moderately understudied as compared to the tourmaline (Hawthorne and Henry, 1999). Presence of boron in a geochemical system has strong effects on the solubility in the system. Its presence partially disrupts the aluminosilicate network of melts in a haplogranite system resulting in, (i) increase in H_2O solubility, (ii) reducing the melt viscosity, and (iii) reducing the liquidus and solidus temperatures in such melts (Pichavant, 1981; 1987). Because of the melt depolymerization by dissolved boron, important strategic elements such as Sn, W, U, Y, Nb, and Be becomes more soluble in the melt, which results into formation of precious mineral deposits in their host rocks, mainly pegmatites (Hemingway et al., 1990). London (1986) and London et al. (1989) have concluded that pegmatite formation is the result of crystallization

from a volatile-rich, vapour-undersaturated melt. The B_2O_3 is strongly partitioned into the vapor phase of their host magma. Therefore, understanding of boron geochemistry in peraluminous systems and that of borosilicates would provide important information on the genesis of their host rocks.

The borosilicates are also known to form by the regional metamorphism of boron-bearing aluminosilicate rocks, as well as acid granulites and hydrothermally altered tuffs. The borosilicates usually appear after crystallization of kyanite, andalucite and sillimanite in the order suggested by Vrana (1979): grandidierite → kornerupine → dumortierite → tourmaline. Presence of borosilicates has been considered to be the indicator of aluminosilicate-rich alteration zone, which is a result of hydrothermal alteration and consequent metamorphism and deformation of the Al- and Si-rich trickled protoliths. In many cases development of borosilcates such as dumortierite is considered to be the mineralogical manifestation of the association of precious metal and base-metal mineralization with acid-metamorphism (Taner and martin, 1993).

The present paper attempts to review the tourmaline and other borosilicates of India reported in Chitradurg, Greenstone belt (CGB) and Hutti-Maski Greenstone Belt of Karnataka; Eastern Ghat Mobile Belt at Vizianagaram, and Bastipadu at Kurnool, Andhra Pradesh; Garhwal Higher Himalaya, Uttarakhand; MashakPahad, South Purulia Shear Zone, West Bengal; Simdega area of Chhotanagpur, Jharkhand and Girolla Hill of Bhandara, Maharashtra. Grew et.al (2003) worked on the consequence involving a tourmaline augmented lateritic predecessor precious by dehydration melting at Eastern Ghat Mobile Belt at Venugopalpuram, Vizianagaram; whereas, Mishra et.al (2018) studied the geology and tectonic implications of tourmaline bearing leucogranite of Bastipadu, Kurnool, Andhra Pradesh. Kumar et.al (2019), using Electron Probe Microanalysis, worked on the Boron measurement in tourmaline from pegmatite veins, Simdega area, Chhotanagpur Gneissic Complex of Eastern India. Gupta et.al. (2014) reported that tourmaline, though in small quantity but plays a vital role in the alteration zone of the Archean orogenic Gold Deposits of of Guddadarangavanahalli (G.R.Halli) in the Chitradurga greenstone belt of the western Dharwar craton. Hazarika et.al. (2015) discussed the varied tourmaline compositions from orogenic gold deposits in the Hutti-Maski greenstone belt, and its implications for sources of ore-forming fluids. Chemistry of tourmaline from Garhwal Higher Himalayas were studied by Jowhar (2010) and reported the changes in physical condition of leucogranitic magma of the area. Acharjee et.al. (2016) studied tourmaline chemistry of MashakPahar of West Bengal and stated that compositional deviations across zonal boundaries inside tourmaline crystal was controlled by changing metamorphic environment in the terrane. Whereas, Meshram and Ingle in 2012 reported dumortirite at Girolla Hills of Bhandara district, Maharashtra, studying the origin of the mineral, its composition and crystallographic nature (Table 1).

2. Tourmaline Study through times-

Tourmaline as a gemstone have an interestingly notable history. According to King, 2002; in early 18th century, the mixed packages of gemstones from Sri Lanka (Ceylon; that time) was reported by Amsterdam lapidaries, some low-density gems were categorized and were named as turamalin.

These were supposed to be new variety of gemstone and till 1717 they were stated as pierre de Ceylon, meaning Stone of Ceylon. The spelling of turamalin was changes to tourmalin in second half of 18th century. Till this period there were very less amount of Ceylonese tourmaline gem available. In the late part of 18thcentury, significant quantities of gem tourmaline were produced. It was by the discovery of pink to red variety of tourmaline that is rubellite deposits near Nerchinsk, Siberia, and the Brazilian tourmalines (smaragdusbrasilicus). Referring rubellite the term tourmaline garnet was coined in 1771 (Pezzotta, 2011).

By several hundred years,preceding the coining of the word tourmaline, before tourmaline was noted as gemstone, some splendid red colored tourmaline had been stradded as jewels for European monarchs. A large (39.5 × 36.5 × 14 mm), bright red ruby fashioned between 1346 and 1387, in the great Czech crown of Saint Wenceslas, was actually tourmaline. Whereas, the oldest-known tourmaline gemstone is noted in the Wenceslas crown is (Hyršl and Neumanova 1999). In 1925, a chicken's egg–sized, vivid pink gem was identified from the Kremlin's Treasure Room by Alexander Fersman (Russian mineralogist) as Burmese tourmaline. It was outlined to the sovereignty of Emperor Rudolph II (1575–1612), until Fersman's work was measured an oriental ruby (Glas 2002). Fisher, 2008 reported that the ruler of

China from 1860 to 1908, namely, Dowager Empress Tz'uHsi, her passion for carved pink tourmaline accordingly gave rise to its interest among the Chinese sovereigns, made the rise in the demand of tourmaline.

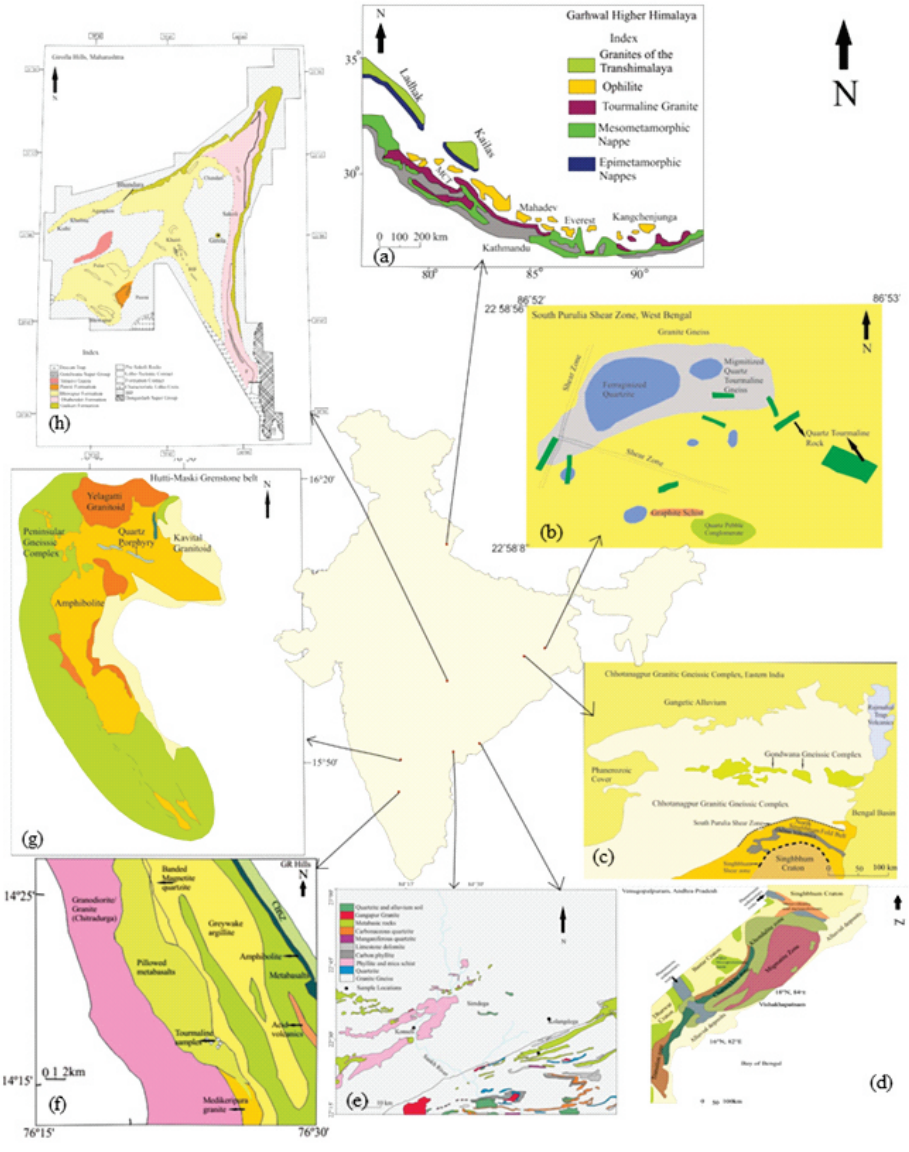

Fig. 1 : Showing Occurrence of Tourmaline in Indian Sub-continent; (a) Garhwal Higher Himalaya. (b) South Purulia Shear Zone, West Bengal. (c) Chhotanagpur Granitic Gneissic Complex, India. (d)Venugopalpuram, AndhraPradesh. (e) Chitradurg Greenstone belt, Karnataka. (f) GR Hills. (g) Hatti-Maski Greenstone Belt. (h) Girola Hills, Maharashtra.

Tourmaline studies appeared a significant part of research in technical world for periods and remains in study till date. In the 19th century scientist worked on the tourmaline grand amalgamation to the theories of heat, electricity and magmatism and were curious for piezoelectric and pyroelectric properties of the mineral (Dietrich1985). General occurrence of tourmaline was known to be granites and granitic pegmatites. At the end of 19th century tourmaline was reported in wide range of rock types like igneous, sedimentary and metamorphic and in various ore deposits. The complexity in the chemistry of the mineral became recognized and valued (Henry and Dutrow, 2018). Till the mid of 20th century, there was a great extent in the study of the aspects; exploration of tourmaline in wider geological settings (Moron and London, 1989), equipment improvement to distinguish physical and chemical properties of minerals and their application which were resulted from these studies (Henry and Dutrow, 2018). In clastic sedimentary rocks tourmaline as

a heavy mineral, plays very important role to approximate maturity of the clastic sediments, to regulate the source and assist in stratigraphic correlation (Krynine 1946). In 1960-1970's the crystallographic structure, general structure and general formula of tourmaline was completely understood.

The piezometric property of the mineral became more important in the 20th century. Depending on these properties one implementation was recognized after World War I, was the revealing and measurement of atomic and conventional explosion pressures (Keys, 1921; Henry and Dutrow, 2018). Tourmaline studies flourishes more since 1977 as the spectroscopic/crystallographic and micro-analytical techniques became extensively available (Henry and Dutrow, 2012b). As the mineral occurs in diverse rock type it became an important petrogenetic indicator of its host rock and sediments (Henry and Dutrow, 1996), its stability in high P-T range, from near surface to the deepest levels of the crust (van Hinsberg et al.2011a), its capability to hold the chemical imprints and to provide the history of its host rock (van Hinsbergand Schumacher 2011). Increase in research in its internal structure have resulted in the increase in quantity of tourmaline types from 4 to 33 (Hawthorne and Henry, 1999, Henry and Dutrow, 2018).

The long-range stability of tourmaline, in range of pressure and temperature assist for its long-range existence (Fig 2). The minimum limit of the stability is not well defined. It can be studied from the occurrence in sedimentary basin and surficial hydrothermal deposits which suggest the immovability of the mineral is less than 100 MPa and 150°C (Moore etal. 2004, Henry etal. 1999). With the experimentation and depending upon the pressure and composition, the upper thermal stability of the tourmaline was stated to be 750 and 950 °C (Robbins & Yoder 1969, Morgan & London 1989, Holtz & Johannes 1991, Krosse 1995, Wolf and London 1997, van Hinsberg 2011, von Goerne et al. 1999, Ota et al. 2008a, Spicer et al. 2004, London 2011,). The rescued boron through the breakdown of tourmaline does not essentially combines in the melt but formulates secondary tourmaline (van Hinsberg 2011), dumortierite, grandidierite, prismatine(Grew 1996).

Although, significant borosilicate mineralization has been scantily recorded from various parts of the world. According to VanHinsberg 2011, most of the previous research reported the chemical, crystallographic nature and structure of the minerals belonging to tourmaline super-group. Whereas, recent studies deal with the quantitative re-establishment of the environmental settings considering the parent rock using amalgamation of compositional,structural and crystallographic parameters of the mineral. This thematic matter followed a distinct conference at the 2009 GAC–MAC–AGU meeting in Toronto, highlighting these exhilarating advances.The occurrence of tourmaline is rare in India.

3. Host Rock of the mineral -

Tourmaline is reported to form in diverse geologically settings. It is included as gangue mineral in ore deposits, is also crystallizes in fractionated igneous bodies, in buried sedimentary basins, in metasomatism and is associated with contact, subduction and regional metamorphism (Morgan and London 1989, Slack 1996, Henry and Dutrow 1996, Henry et al. 1999, London et al. 1996, Roda-Robles et al. 2011, Nakano & Nakamura 2001, Van Hinsberg V, 2011). In such settings, tourmaline occurs in diverse host-rock of compositions, like silica saturated intrusive rocks and sediments, under-saturated mafic rocks, pelites, impure limestones and evaporates and their metamorphic equivalents (Van Hinsberg V, 2011). Generally, tourmaline occurs in the rocks exposed to the metasomatism by boron rich fluids is another evidence for accommodation of tourmaline in diverse rock composition (Morgan and London 1989, Marschall et al. 2006, Dutrow et al. 1999, Marocchi et al. 2011).

In the Chitradurga Greenstone belt (CGB), Dharwar craton, tourmaline is reported in the altered metabasalts aged 2.9-2.55 Ga that is Meso-Archean and is associated with unaltered metabasalts, less altered metabasalts, greywacke

Table 1 Representing summary of tourmaline deposits in India

	Chitradurg, Greenstone belt (CGB), Karnataka, India.	Hutti-Maski Greenstone Belt, Karnataka, India.	Bastipadu, Kurnool, Andhra Pradesh, India	Mashak Pahad, South Purulia Shear Zone, West Bengal, India.	Girolla Hill, Bhandara, Maharashtra, India.	Simdega area, Chhotanagpur, Jharkhand, India.	Eastern Ghat Mobile Belt at Venugopalpuram, Vizianagaram, Andhra Pradesh, India.	Garhwal Higher Himalaya, Uttarakhand, India.
Age	2900-2550 Ma (Meso-Archean)	~2600 Ma (Neo-Archean)	2500 Ma to 541 ± 1.0 Ma (Proterozoic)	1500-1600 Ma (MesoProteriozoic - Calymmian)	1200-1300 Ma (MesoProteriozoic -Ectasian)	~1200 Ma (MesoProteriozoic -Ectasian)	950-930 Ma (Neo Proteriozoic-Tonian)	23 + 0.2 Ma (Oligocene-Chattian)
Latitude/Longitude; spatial extent and subdivisions	14°17'00" N, 76°24'00"E ; Vein varies in thickness in between 0.5 to 2 cm. Occurs in altered meta-basalt veins.	16°12' 00" N, 76°43' 00" E Hutti- 1 km long, Hira-Buddini- ~2 m Uti- 50-700 m	15° 49' 48" N, 78° 03' 0"E; occurs as small plugs within the older litho units.	22°58'56"– 22°58'8.3"N 86°52'33.8"– 86°53'35.8"E; vein-like, tourmalines parallel to the foliation plane of migmatite	79°56'N; 21°03' E; The general strike of the rock is NNE-SSW with steep dip of 58° to 68° due east.	22°36'54.36"N 84°29'45.6"E	18° 09' 30" N, 83° 26' 40" E	30°43'22"-30°55'49"N, 79°04'41"-79°16'34"E; Numerous veins of tourmaline-muscovite leucogranite and garnet-beryl-tourmaline pegmatite intruded the biotite granite and the metamorphics.
Form	Vein of Albite-tourmaline-Carbonate-quartz; massive or fibrous.	Hutti- along the biotite-chlorite–defined mylonitic foliation and as tourmaline-calcite microveins. Hira-Buddini- tourmaline veins that replace amphiboles and tourmalines that replace hydrothermal biotite. Uti- grew along biotite-muscovite-defined foliation	The tourmaline veins display honeycomb structures indicating tourmalinisation along microfractures	Foliation planes in Migmatite and in quartz tourmaline veins.	Lensoids, veinlets.	Tourmaline occurs in the form of Veins	Lens form	Veins of tourmaline-muscovite leucogranite and garnet-beryl-tourmaline pegmatite intruded the biotite granite and the metamorphic rocks.
Intrusive/Extrusive	Intrusive (veins form)	Intrusive (veins and along with the foliation)	Intrusive	Intrusive	Intrusive	Intrusive	Intrusive	Intrusive (Veins form)
Host Rock	Altered Metabasalts	Hutti-biotite-chlorite defined mylonitic foliation and calcite microveins within rocks of the proximal alteration zone. Hira-Buddini- quartz-albite-tourmaline veins. Uti- metamorphosed volcaniclastic rocks.	Leucogranite	metapelitic schists, leucocratic granitoids and pegmatoids.	kyanitic rocks and chloritemuscovite-schist and chlorite-muscovite-schist	quartz–tourmaline pegmatitic veins at the contact region of granite-gneiss and metapelites	Pegmatites	biotite granite gneiss and porphyritic granite (Bhaironghati granite) and meta-sedimentary host rocks.
Associated rocks	Metabasalts (unaltered/less altered), , Greywacke and meta-phyllite,Carbonated metabasic dykes	Hutti- polymictic conglomerate, metabasites and garnetbiotite Schists. Hira-Buddini- amphibolite and metamorphosed felsic volcanic rocks. Uti- amphibolite (typically garnetiferous), metamorphosed felsic volcanic rocks and minor metapelite.	pegmatites (both K-feldspar rich and albite rich), gabbro/dolerite dyke and quartz reefs along the large-scale faults	granite gneiss, migmatized quartz tourmaline gneiss, quartz pebble conglomerate, quartz tourmaline veins and graphite schists.	Phyllite and slate with quartzpyrophyllite veins exposed at a few places in NE part of the area.	Metabasics, metapelites and metapsammites41 . Several basic to metabasic dykes cross-cut the country rock. Phylite and mica schist dominantly occur in the southern part having veins and patches of quartzite and limestone of varied composition.	quartz-sillimanite-hypersthene - cordierite gneiss.	Gangotri Granite.
Boro-silicate varieties	Schrol tourmaline, Dravite Tourmaline	Hutti and Hira-Buddini- Oxydravite. Uti- Tourmaline	Dravite, Schorl	Dravite, Schorl.	Dumortierite, Dravite.	Dravite, Schorl.	Prismatine, Tourmaline.	Alkali Group tourmaline and Schorl.

Petrology	Tourmaline occurs as pleochroic grain and constitute minor mineral of the fine grained matrix of the host rock.	Not known	The rock is fine to coarse grained and shows hypidiomorphic texture. Both orthoclase and microcline are observed. K-feldspars alter to sericite and appear cloudy (figure 3a and c). Graphic intergrowth of quartz in K-feldspar host is also recorded. Plagioclase occurs as clouded subhedral to anhedral crystals.	Quartz- tourmaline gneiss are mesocratic, medium- to coarse-grained with moderate specific gravity. Microscopically, the rock shows xenomorphic granular texture; quartz inclusions within tourmaline grains have also been recorded.	It shows pleochroism from colourless to light pink and pale blue to violet (azure blue) in the form of aggregates of needle-like or fibrous crystals.	Two types of tourmaline occus- Tur I: euhedral prismatic brown schorl tourmaline with no apparent optical zoning collected from the Konskeli, Kolangdega and Kodopani villages, and Tur II – oval to prismatic, green dravite tourmaline cluster showing optical zoning collected from the Bongera	In hand specimen the rock is black and appears to be opaque, but in thin section it has a cellular structure consisting of subparallel prisms up to several mm long of prismatine partly enclosed in oxides. Prismatine is transparent and is pleochroic	Tourmaline occurs as black euhedral-subhedral crystals up to 1cm in size, scattered throughout the granite or concentrated along layers by magmatic banding and can reach up to 5 modal%.
							from very pale yellow to pale grey-blue.	
Tectonic setting	The regional structure of the CGB has been described as second generation central anticline flanked by first generation synclines on either side.These structures are refolded along E-W trending warps formed during D3 deformation.	The Hutti-Maski greenstone belt has been interpreted as a convergent margin related to basaltic magmatism.	Gadwal schist belt of the Eastern Dharwar Craton (EDC), lying adjacent to the Proterozoic Cuddapah basin	The area had suffered poly-phased deformation, which is evident from three different phases of folding.	Sakoli Fold Belt.	The east-west trending Chhotanagpur Gneissic Complex (CGC) is a sub-arcuate belt of the east Indian Shield	Eastern Ghats rift system	The Himalayan orogenic belt is characterized by the presence of basement rocks. These rocks got involved in the evolution of the mountain belt and, as such, have played a great role in the structural architecture and tectonic framework of the orogeny.
Mineralization	Fe-rich chlorite with subordinate albite, ankerite, micaceous minerals (sericite, muscovite and paragonite) and sulphides (mainly pyrite and arsenopyrite).	Hutti- biotite, K-feldspar, chlorite, quartz, calcite, pyrite, arsenopyrite, tourmaline, and albitic plagioclase, with minor titanite. Hira-Buddini- actinolite, biotite, calcite. Uti- garnet, quartz, plagioclase, biotite, muscovite, minor chlorite, and accessory monazite.	Quartz, albite, perthite and K-feldspar, muscovite and tourmaline two-mica granite, composed of quartz, perthite, microcline, albite, tourmaline and muscovite.	tourmaline, biotite, muscovite, plagioclase and K-feldspar	mixture of kyanite or sillimanite, tourmaline, dumortierite, rutile, quartz.	Not Mentioned	Hercynite, hematite, Imenite, magnitite,muscovite.	Quartz, K-feldspar, plagioclase, tourmaline, muscovite , biotite, garnet, beryl
Associated (accessory) minerals	chlorite, albite, ankerite ,sericite, muscovite and chloritoid.	Titanite,zircon, pyrite, arsenopyrite, xenotime, monazite, and allanite.	biotite titanite hematite.	Perthite, Garnet	muscovite or sericite, dravite (tourmaline), gobbinsite, diaspore and microcline	Not mentioned	Sapphirine, sillimanite, Biotite,rutile and corundum and zircon.	Apatite, zircon and monazite

Formation of Tourmaline/ Genesis	Tourmaline formed from boron bearing hydrothermal fluids with available Fe and Mg content of the host rock. The required alumina for the formation of the tourmaline might have	Magmatic fluid origin.	Partial melting of boron-enriched source rocks is linked with the development of tourmalines in the leucogranite	Occurrence of tourmaline at the margin of biotite indicates that tourmaline has formed on consumption of biotite.Tourmaline grains, in migmatized quartz tourmaline gneiss typically follow overall foliation	Dumortierite is formed due to external agency i.e. intrusion of hydrothermal solution in schist which is considered to have been rich in boric acid and titanium dioxide, with accessory fluorine, titanium fluorite,	Not Known	B was intruded metasomatic ally in the country rock.	Tourmaline was formed during the crystallizati on of leucograniti c magma.
	been leached from the metasediment ary litho-units interlayered with the metabasalt in the area.			plane present in this rock (~syntectonic); while tourmaline grains that are found in quartz tourmaline veins appear to be post-tectonic, controlled by boron infiltration.	sodium fluoride, hydroxides and vanadium.			

meta-phyllite and carbonated meta-basic dykes (Gupta et.al. 2014). Neo-Archean aged Hutti-Maski greenstone belt tourmaline veins are hosted by biotite-chlorite defined mylonitic foliation and calcite micro-veins within rocks of the proximal alteration zone and is associated with polymictic conglomerate, metabasites and garnet biotite Schists in Hutti, quartz-albite riched rocks associated with Buddini- amphibolite and metamorphosed felsic volcanic rocks in Hira-Buddini and in Uti area it is reported in metamorphosed volcanoclastic rocks associated with amphibolite (typically garnetiferous), metamorphosed felsic volcanic rocks and minor metapelite (Hazarika, 2014). In Bastipadu area, Kurnool district, Andhra Pradesh dated as 2500 Ma to 541 ± 1.0 Ma that is Proterozoic tourmaline veins are found in the leucogranites and is associated with the K- feldspar and even albite enriched pegmatites, gabbro/dolerite dyke and quartz reefs along the large-scale faults (Mishra et.al. 2018). In MashakPahad-South Purulia Shear Zone of West Bengal aged 1500-1600 Ma that is Meso Proterozoic era and Calymmian period tourmaline crystals is hosted by metapelitic schists, pegmatoids and leucocratic granitoids which are associated with granite gneiss, quartz pebble conglomerate,migmatized quartz tourmaline gneiss, graphite schists and quartz tourmaline veins (Acharjee, 2016).

Ectasian-Meso Proterozoic dated rocks of the Girolla hills, comes under the part of Sakoli fold belt in Bhandara district, Maharashtra. Here,boro-silicates mineralization was reported by Meshram and Ingle in 2012. The boro-silicate minerals are hosted in the kyanitic rocks and chlorite-muscovite-schist whereas the rocks are associated with phyllite and slate with quartz-pyrophyllite veins exposed at a limited places in north-east part of the area. In the Simdega area, Chhotanagpur, Jharkhand (1200 Ma). The Chhotanagpur Gneissic Complex (CGC) is the E-W trending, sub arcuate belt of the East-Indian Shield (Acharyya 2003, Mahadevan 2002, and Sharma, 2009). Study area has two dominant rock types that is granite-gneiss and phyllite mica-schist. Tourmaline veins are found to be hosted in the contact region of granite-gneiss and metapelites. The granite-gneiss has an enclave of metabasics, metapelites and metapsammites supracrustals. These enclaves are older and of ENE-WSW trend (Singh et.al 2004). Several dykes of basic to metabasic nature cut across the country rock. The southern part of the area dominantly consists of phyllite and mica schist with veins of quartzite and limestone of different compositions (Kumar et.al. 2019).

In the Eastern Ghat Mobile Belt at Venugopalpuram of Andhra Pradesh (950-930 Ma) has reported the tourmaline mineralization in the pegmatite veins while the associated rock type is quartz-sillimanite-hypersthene-cordierite gneiss (Grew et.al 2003). Whereas in the Grahwal Higher Himalayas (23 +2 Ma) also has tourmaline mineralization. Here the tourmaline veins are hosted by biotite granite gneiss and porphyritic granite (Bhaironghati granite) and meta-sedimentary rocks whereas they are hosted with Gangotri Granite (Jowhar, 2010).

4. Type of Magmatism -

In igneous and metamorphic rocks, tourmaline generally occurs as an accessory mineral. Being hard and persistent it gets transported with beach and stream flow, as robust grains in the sediments and sedimentary rocks. Most remarkable tourmaline is formed by the hydrothermal activity. The minerals formed by the hydrothermal water and vapors carrying the element to form the mineral intruded in the cavities and fractures. The mineral crystallizes in the open spaces that is in the pockets, voids, veins and fractures in the host rocks.

The tourmaline mineralization formed in the CGB of Dharwar craton is intruded in the fractures of Albite-tourmaline-Carbonate-quartz and is massive and/or fibrous in nature, veins differs in width from 0.5 to 2 cm (Gupta et.al. 2014). Whereas, in the Hutti-Maski greenstone belt, Dharwar craton, the mineralization at Hutti is 1 km long, along the biotite-chlorite–defined mylonitic foliation and in calcite microveins. In Hira-Buddini the mineralization is reported in two forms, first- tourmaline veins that replaces amphiboles and another-tourmalines that replaced hydrothermal biotite and is ~2 m long. In Uti tourmaline crystals grew along biotite-muscovite defined foliation for 50-700 m (Hazarika, 2014). In Bastipadu region of Kurnool district the tourmaline veins display honeycomb structures signifying tourmaline mineralization along microfractures in the leucogranites, it occurs as a small plug in the older litho-units (Mishra et.al. 2018). The Mashak-Pahar of West Bengal mineralization is parallel to the foliation planes in migmatite and in quartz tourmaline veins (Acharjee, 2016).

In the Girolla hills of Bhandara district, the tourmaline minerals are found to be intruded in the lensoid and veinlet form. They are well developed needle shaped and perfect euhedral in nature (Meshram and Ingle, 2012). While in the Simdega area of Chhotanagpur district, tourmaline mineralized in the form of veins, where two types of mineralization is reported that is-Tur I: euhedral prismatic brown schorl tourmaline with no apparent optical zoning collected from the Konskeli, Kolangdega and Kodopani villages and Tur II – oval to prismatic, green dravite tourmaline cluster showing optical zoning collected from the Bongera (Kumar, 2019). The tourmaline reported in the Eastern Ghat Mobile Belt at Venugopalpuram area of Andhra Pradesh, is reported to be intruded in the form of veins in the pegmetites (Grew et.al 2003). Whereas, at Grahwal Higher Himalayas veins of tourmaline-muscovite leucogranite and garnet-beryl-tourmaline pegmatite intruded the biotite granite and the metamorphic rocks (Jowhar, 2010).

5. Minerology -

For the tourmaline-group minerals, an organized classification was proposed by Hawthorne and Henry in 1999, where, general proposed formula is $X\,Y_3\,Z_6\,(T_6O_{18})\,(BO_3)_3\,V_3W$. It is established on the basis of ordering at the different crystallographic sites of the tourmaline structure and chemical composition. Where,

$^{IX}X: Na^{1+}, Ca^{2+}, \square, K^{1+}, Pb^{2+}$

$^{VI}Y: Mg^{2+}, Fe^{2+}, Al^{3+}, Li^{1+}, Ti^{4+}, Mn^{2+}, Fe^{3+}, Zn^{2+}$

$^{VI}Z: Al^{3+}, Cr^{3+}, Fe^{3+}, Mg^{2+}, Fe^{2+}$

$^{IV}T: Si^{4+}, B^{3+}, Al^{3+}$

$^{III}B: B^{3+}$

$^{IV}V: OH^{1-}, O^{2-}$

$^{III}W: OH^{1-}, F^{1-}, O^{2-}$

Tourmaline belongs to ring-silicate structure, with its unit cell consisting of a six-fold ring of tetrahedra (T sites) on top of a concentric arrangement of three Y-site and six Z-site octahedra (van Hinsberg, et.al. 2011).The Z-site octahedra are slightly smaller than the Y-site octahedra, however the latter are more distorted (Bosi & Lucchesi 2007).

As stated by Hawthorne and Henry 1999, tourmaline formulae in table 2 obeys the IMA rules for recognition as distinct mineral species. In regard to the specific names, it is mentioned that the same principle to be used for tourmaline

as was used for amphibole.

6. Varieties of Tourmaline-

Depending upon the host rock composition and the crystallographic arrangement of the mineral, different varieties of borosilicates are formed. In India, there are very few varieties of tourmaline reported. Most of the tourmaline are from schorl-dravite series. In Chitradurg Greenstone belt schorl and dravite is found with Ferich chlorite with secondary albite, micaceous minerals (sericite,muscovite and paragonite) ankerite, and sulphides (mainly pyrite and arsenopyrite) and associated minerals are chlorite, albite, ankerite, sericite,muscovite and chloritoid (Gupta et.al. 2014). In Hatti-Maski Greenstone belt the Hutti and Hira-Buddini area has oxy-dravite species along with quartz, biotite,chlorite, K-feldspar, calcite, albitic plagioclase, pyrite, arsenopyrite, actinolite, biotite with negligible amount of titanite whereas the Uti region has tourmaline along with garnet, quartz, plagioclase, biotite, muscovite, minor chlorite and accessory monazite, titanite, zircon, pyrite, arsenopyrite, xenotime and allanite (Hazarika, et.al. 2014). Similar tourmaline variety is reported in Bastipadu region and associated mineralization is quartz, albite, perthite, K-feldspar, muscovite, microcline, biotite, titanite and hematite (Mishra et.al. 2018).

In Mashak-Pahar region schorl and dravite are reported along with biotite, muscovite, plagioclase and K-feldspar and perthite and garnet in accessory amount (Acharjee, 2016). Dravite and dumortierite is reported within the Girolla hills-Bhandara along with mixture of kyanite or sillimanite, quartz, rutile, muscovite or sericite, gobbinsite, diaspore and microcline (Meshram and Ingle, 2012). The Venugopalpuram region of Eastern Ghat Mobile Belt has reported Prismatine variety of tourmaline along with hercynite, hematite, ilmenite, magnetite, muscovite, sapphirine, sillimanite, biotite, rutile, corundum and zircon (Grew et.al 2003). In Garhwal Higher Himalaya region alkali group tourmaline and schorl is reported associated with quartz, K-feldspar, plagioclase, tourmaline, muscovite, biotite, garnet, beryl, apatite, zircon and monazite (Jowhar, 2010).

Table 2: Showing elements in X, Y, Z,T6O18, (BO3)3, V3, W positions (Rumyantseva (1983); Sokolov et.al. (1986); Donnay et al. (1966); Grice et.al. (1993); Dunn et al. (1977b); Grice & Robinson (1989); Dunn et al. (1977a); Selway et.al. (1998); MacDonald et.al (1993); modified Hawthorne and Henry, 1999).

Sr.No	Name of the mineral	X	Y_3	Z_6	T_6O_{18}	$(BO_3)_3$	V_3	W
	Alkali tourmaline							
1	Elbaite	Na	$Li_{1.5}Al_{1.5}$	Al_6	Si_6O_{18}	$(BO_3)_3$	$(OH)_3$	(OH)
2	Dravite	Na	Mg_3	Al_6	Si_6O_{18}	$(BO_3)_3$	$(OH)_3$	(OH)
3	Chromdravite	Na	Mg_3	Al_6	Si_6O_{18}	$(BO_3)_3$	$(OH)_3$	(OH)
4	Schorl	Na	$Fe^{2+}{}_3$	Al_6	Si_6O_{18}	$(BO_3)_3$	$(OH)_3$	(OH)
5	Olenite	Na	Al_3	Al_6	Si_6O_{18}	$(BO_3)_3$	O_3	(OH)
6	Buergerite	Na	$Fe^{3+}{}_3$	Al_6	Si_6O_{18}	$(BO_3)_3$	O_3	F
7	Povondraite	Na	$Fe^{3+}{}_3$	$Fe^{3+}{}_4Mg_2$	Si_6O_{18}	$(BO_3)_3$	$(OH)_3$	O
8	Hydroxy-buergerite	Na	$Fe^{3+}{}_3$	Al_6	Si_6O_{18}	$(BO_3)_3$	O_3	(OH)
9	Fluor-elbalite	Na	$Li_{1.5}Al_{1.5}$	Al_6	Si_6O_{18}	$(BO_3)_3$	$(OH)_3$	F

Sr.No	Name of the mineral	X	Y_3	Z_6	T_6O_{18}	$(BO_3)_3$	V_3	W
			Alkali tourmaline					
10	Fluor-dravite	Na	Mg_3	Al_6	Si_6O_{18}	$(BO_3)_3$	$(OH)_3$	F
11	Fluor-chromdravite	Na	Mg_3	Cr_6	Si_6O_{18}	$(BO_3)_3$	$(OH)_3$	F
12	Fluor-schorl	Na	$Fe^{2+}{}_3$	Al_6	Si_6O_{18}	$(BO_3)_3$	$(OH)_3$	F
13	Fluor-olenite	Na	Al_3	Al_6	Si_6O_{18}	$(BO_3)_3$	O_3	F
14	Oxy-elbaite	Na	$LiAl_2$	Al_6	Si_6O_{18}	$(BO_3)_3$	$(OH)_3$	O
15	Oxy-dravite	Na	$MgAl_2$	Al_5Mg	Si_6O_{18}	$(BO_3)_3$	$(OH)_3$	O
16	Oxy-schorl	Na	$Fe^{2+}Al_2$	$Fe^{2+}Al_5$	Si_6O_{18}	$(BO_3)_3$	$(OH)_3$	O
17	Oxy-chromdravite	Na	$MgCr_2$	$MgCr_5$	Si_6O_{18}	$(BO_3)_3$	$(OH)_3$	O
			Calcic Tourmaline					
18	Uvite	Ca	Mg_3	Al_5Mg	Si_6O_{18}	$(BO_3)_3$	$(OH)_3$	F
19	Hydroxy-feruvite	Ca	$Fe^{2+}{}_3$	Al_5Mg	Si_6O_{18}	$(BO_3)_3$	$(OH)_3$	(OH)
20	Liddicoatite	Ca	Li_2Al	Al_6	Si_6O_{18}	$(BO_3)_3$	$(OH)_3$	F
21	Hydroxyliddicoatite	Ca	Li_2Al	Al_6	Si_6O_{18}	$(BO_3)_3$	$(OH)_3$	(OH)
22	Feruvite	Ca	$Fe^{2+}{}_3$	Al_5Mg	Si_6O_{18}	$(BO_3)_3$	$(OH)_3$	F
23	Hydroxy-uvite	Ca	Mg_3	Al_5Mg	Si_6O_{18}	$(BO_3)_3$	$(OH)_3$	(OH)
24	Oxy-liddicoatite	Ca	$Li_{1.5}Al_{1.5}$	Al_6	Si_6O_{18}	$(BO_3)_3$	$(OH)_3$	O
25	Oxy-uvite	Ca	$MgAl_2$	Al_4Mg_2	Si_6O_{18}	$(BO_3)_3$	$(OH)_3$	O
26	Ferri-uvite	Ca	$MgFe^{3+}{}_2$	$Mg_2Fe^{3+}{}_4$	Si_6O_{18}	$(BO_3)_3$	$(OH)_3$	O
27	Oxy-Feruvite	Ca	$Fe^{2+}Al_2$	Al_4Mg_2	Si_6O_{18}	$(BO_3)_3$	$(OH)_3$	O
28	Ferri-feruvite	Ca	$Fe^{2+}Fe^{+3}{}_2$	$Mg_2Fe^{3+}{}_4$	Si_6O_{18}	$(BO_3)_3$	$(OH)_3$	O
			X-site vacant tourmaline					
29	Rossmanite	□	$LiAl_2$	Al_6	Si_6O_{18}	$(BO_3)_3$	$(OH)_3$	(OH)
30	Foitite	□	$Fe^{2+}{}_2Al$	Al_6	Si_6O_{18}	$(BO_3)_3$	$(OH)_3$	(OH)
31	Magnesiofoitite	□	Mg_2Al	Al_6	Si_6O_{18}	$(BO_3)_3$	$(OH)_3$	(OH)
32	Fluor-rossmanite	□	$LiAl_2$	Al_6	Si_6O_{18}	$(BO_3)_3$	$(OH)_3$	F
33	Fluor-Mg-foitite	□	Mg_2Al	Al_6	Si_6O_{18}	$(BO_3)_3$	$(OH)_3$	F
34	Fluor-foitite	□	$Fe^{2+}{}_2Al$	Al_6	Si_6O_{18}	$(BO_3)_3$	$(OH)_3$	F
35	Oxy-rossmanite	□	$Li_{0.5}Al_{2.5}$	Al_6	Si_6O_{18}	$(BO_3)_3$	$(OH)_3$	O
36	Oxy-Mg-foitite	□	$MgAl_2$	Al_6	Si_6O_{18}	$(BO_3)_3$	$(OH)_3$	O
37	Oxy-MgFerrifoitite	□	$MgFe^{3+}{}_2$	$Fe^{3+}{}_6$	Si_6O_{18}	$(BO_3)_3$	$(OH)_3$	O
38	Oxy-foitite	□	$Fe^{2+}{}_2Al_2$	Al_6	Si_6O_{18}	$(BO_3)_3$	$(OH)_3$	O
39	Oxy-ferri-foitite	□	$Fe^{2+}Fe^{+3}{}_2$	$Fe^{3+}{}_6$	Si_6O_{18}	$(BO_3)_3$	$(OH)_3$	O

7. Genesis of Tourmaline -

The growth and chemical variation in tourmaline depend upon number of interactive aspects, such as; availability of boron, major-element bulk rock composition (most favorably the Al_2O_3 content),composition of fluid phase and P-T conditions and native mineral assemblages. The crystallographic limits, surface-vitality collaboration, positively affects the growth and elemental zonation (Marocchi et al. 2011). With the great increase in research and information of the crystallographic arrangement and composition of the mineral, it is likely conceivable to make the tough petrological and tectonic analyses using the mineral (Nakano and Nakamura 2001, Bebout and Nakamura 2003). Generally, it is noted that the tourmaline mineralization resemblances to the breakdown of the boron bearing minerals (like clay, muscovite, etc) or the invasion of boron containing fluids (Henry and Dutrow 1996, Marocchi et al. 2011, Marschall et al. 2009b). In several subduction and exhumed high-pressure regions, the arrival of boron enriched fluids or melts is due to the past decompression of the rocks and there is metasomatic formation of tourmaline (Marschall et al. 2006a, 2009b,Altherr et al. 2004,Ota et al. 2008b,Kadarusman et al. 2007,). Basically, it is a late stage mineral available in the parting of vapor phases from magma, henceforth elements like fluorine, boron are available in the magma. Deposition of tourmaline may be frequent throughout the magmatic-hydrothermal cycle, therefore conveyance of metals like tungsten and tin is possible with it (King, 2000).

In India, the tourmaline deposition are reported to be of hydrothermal in origin. As stated in Table 1, tourmaline formed from in CGB is due to the injection of boron containing hydrothermal solutions with available Fe and Mg content of the parent rock. Essential alumina for the formation of the mineral might have been trickled from the metasedimentary litho-units interlayered with the metabasalt in the area(Gupta et.al. 2014). In Bastipadu region, formation of tourmalines in the leucogranite is associated with the fractional melting of boron-rich source rocks (Mishra et.al. 2018). The occurrence of the mineral at the periphery of biotite indicates that it has formed on ingesting of biotite. Tourmaline grains in Mashak Pahar region, in migmatized quartz tourmaline gneiss typically follow overall syntectonic association with the rock; while the crystals found in quartz, here tourmaline veins controlled by boron infiltration and seem to be post-tectonic (Acharjee, 2016). In the Girolla hills Meshram and Ingle in 2012 reported that formation dumortierite is a result of external intervention that is,intrusion of hydrothermal solution in schist which is considered to have been enrich in boric acid and titanium dioxide with accessory fluorine, sodium fluoride, titanium fluorite, vanadium and hydroxides. Whereas, in Garhwal Higher Himalaya the tourmaline was formed during the crystallization of leucogranitic magma (Jowhar, 2010).

8. Importance of tourmaline -

1. Tourmaline as Gemstone -

Tourmaline since long time is used as a gemstone. Its varieties due to variable mineralogical composition makes the mineral colorful and attractive in appearance. According to the studies of Feng Shui crystals-schorl-foundation stone that delivers an association between the Earth and the human spirit. It is supposed to help people find a sense of assurance, see the world visibly, and feel empowered during problematic situations. Rubellite-is thought to encourage compassion, gentleness, link love and spirituality. Siberite is all about peaceful energy, it is noted to ground and protect you, as well as help you intensely relax. Indicolite is meant to represent strong, authentic messages and the capability to express from the temperament. It is also supposed to inspire an open thoughts and hold of truth and morals. Dravite is supposed to transfer negative energy into positive. Verdilite is meant to enhance courage, stamina, strength and energy. Since 20th century, tourmaline was used as a precious stone and was used to decorate the queen's crown. It was also the symbol of royalty.

2. Due to the robust nature of the mineral that its capability to sustain high pressure, high temperature, extreme low rate of volume dispersal for major and trace elements in its structure tourmaline is a best indicator of its host rock environment (vanHinsberg et.al. 2011b).

3. The piezoelectric property of the mineral is utilized for various purposes, including the making of pressure devices to measure abrupt change in pressure, particularly hydrostatic and nuclear explosions. It was heavily used in World War II.

4. The pyroelectric characteristic has made the use of mineral in the radioactivity detection as it helps in the detection of radium or neutron it is also used for radiometric dating and even as a large range temperature detector.

References -

1. Hawthorne, F.C., Henry, D. J.,1999. Classification of the minerals of the tourmaline group. European Journal of Mineralogy; V. 11, 201–215.

2. Hemingway, B. S., Anovitz, L. M., Robie, R. A., McGee, J. J.,1990. The thermodynamic properties of dumortierite Si3B [Al6.75¡%0.25 (OH)3.75]. American Mineralogist; V. 75, 1370-1375.

3. London, D., 1986. Magmatic-hydrothermal transition in the Tancorareelement pegmatite: Evidence from fluid inclusions and phase-equilibrium experiments. American Mineralogist; V. 71, 376-395.

4. London, D., Morgan, G. B, VI, Hervig, R.L, 1989. Vapor-undersaturated experiments with macusanite glass + H2O at 200 MPa, and the internal differentiation of rare-element pegmatites. Contributions to Mineralogy and Petrology; V. 102, I-17.

5. Pichavant, M., 1981. An experimental study ofthe effect ofboron on a water saturated haplogranite at 1 kbar vapour pressure. Contributions to Mineralogy and Petrology; V. 76, 430-439.

6. Pichavant, M.,1987. Effects of B and H2O on liquidus phase relations in the haplogranite system at 1 kbar. American Mineralogist; V. 72, 1056-1070.

7. Taner, M. F. and Martin, R. F., 1993. Significance dumortierite in an aluminosilicate-rich alteration zone Louvicourt Quebec. Canadian Mineralogist; V. 31, 137-146.

8. Vrana, S., 1979. A polymetarnorphic assemblage of grandidierite, kornerupine, Ti-rich dumortierite, tourmaline, sillimanite and garnet. NeuesJahrbuchfiirMineralogieMonatshefte; V. H-1, 22-33.

9. Hyršl J, Neumanova P, 1999. Eine neueGemmologischeUntersuchung derSankt Wenzelskrone in Prag. Zeitschriftder DeutschenGemmologischenGesellschaft 48, 29-36

10. Fisher J., 2008. Gem pegmatites, southernCalifornia. In: Staebler GA, Wilson WW(eds) American Mineral Treasures.Lithographie LLC, East Hampton,Connecticut, pp. 186-195.

11. Glas M (2002) The Kremlin's carbuncle.extra Lapis English 3, 62-63

12. PezzottaF., Laurs B., 2011.Tourmaline: The Kaleidoscopic Gemstone, Elements, Vol. 7, pp. 333–338.

13. Van Hinsberg V., Henry D., Marschall H., 2011.Tourmaline: An Ideal Indicator of Its Host Environment, The Canadian Mineralogist, Vol. 49, 1-16

14. Grew E.S., Rao A.T., Raju K.K.V.S., Hejny C., Moore D. J., Yates M.G, Shearer C.K. 2003.Prismatine and ferroh² gbomite-2N2S in granulite-faciesFe-oxide lenses in the Eastern Ghats Belt at Venugopalapuram,Vizianagaram district, Andhra Pradesh, India: do such lenses havea tourmaline-enriched lateritic precursor?Mineralogical Magazine, Vol. 67(5), 1081–1098.

15. Mishra K.J., Bhattacharjee S., Reddy M.S., Praveen M.N., Bhimte A. D. and Mahanta N., 2018. J. Earth Syst. Sci;pp 127-145.

16. Kumar D., Pandit D., Sharma A. amdChalapati Rao N.V., 2019.Boron measurement in tourmalinefrom pegmatite veins, Simdega area,Chhotanagpur Gneissic Complex,Eastern India using Electron ProbeMicroanalysis, Current Science, Vol. 117, No. 5, 858-865.

17. Gupta S., Jayananda M., Fareeduddin, 2014.Tourmaline from the Archean G.R.Halli gold deposit, Chitradurga greenstone belt, Dharwar craton (India): Implications for the goldmetallogeny, Geoscience Frontiers, Vol. 5, 877-892.

18. Hazarika P., Mishra B. and Pruseth K.L., 2015.Diverse Tourmaline Compositions from Orogenic Gold Deposits in the Hutti-Maski Greenstone Belt, India: Implications for Sources of Ore-Forming Fluids,Society of Economic Geologists, Inc. Economic Geology, Vol. 110, 337–353.

19. Jowhar T. N., 2010, Chemistry of Tourmalines from the Gangotri Granite,Garhwal Higher Himalaya, Earth Science India, Vol. 3 (III), 181-194.

20. Acharjee S., Ray J., Dey P., Bhattacharyya D., Banerjee M., Chattopadhyay B., Sengupta S., Bhatt A.K., Chowdhury D., Dwivedi A. K., Mahato S, Jana A R, Maithani P.B and Ramesh Babu P.V., 2016.Mineral chemistry of tourmaline from MashakPahar,South Purulia Shear Zone (SPSZ), eastern Indian Shield, J. Earth Syst. Sci., Vol 125, No. 8, 1681–1696.

21. Meshram, R. R. and Ingle, K. B., 2012. Mineralogy and Origin of Dumortierite from Girola Area, Bhandara District, Eastern Maharashtra. Journal of the Geological Society of India; Vol. 79, 181 – 188.

22. Morgan, G.B.& London, D., 1989. Experimental reactions of amphibolite with boron-bearing aqueous fluids at 200 MPa: implications for tourmaline stability and partial melting in mafic rocks. Contrib. Mineral. Petrol. Vol. 102, 281-297.

23. Nakano, T. & Nakamura, E., 2001. Boron isotope geochemistry of metasedimentary rocks and tourmalines in a subduction zone metamorphic suite. Phys. Earth Planet. Int.,Vol. 127, 233-252.

24. London, D., 2011. Experimental synthesis and stability of tourmaline: a historical perspective. Can. Mineral. Vol. 49, 117-136.

25. HenryRY, D.J. &Dutrow, B.L., 1996. Metamorphic tourmaline and its petrologic applications. In Boron: Mineralogy, Petrology and Geochemistry (E.S. Grew & L.M. Anovitz, eds.). Rev. Mineral. Vol. 33, 503-557.

26. HenryR. Y, D.J., Kirkland, B.L. & Kirkland, D.W., 1999. Sector-zoned tourmaline from the cap rock of a salt dome. Eur. J. Mineral. 11, 263-280.

27. Roda-Robles, E., Pesquera, A., Gil-Cresp o, P.P.Torr es-Ruiz, J., 2011. Occurrence, paragenesis and compositional evolution of tourmaline from the Tormes Dome area, Central Iberian Zone, Spain. Can. Mineral. Vol. 49, 207-224.

28. Marsrschall, H.R., Ludwig, T., Altherr, R., Kalt, A. Tonarini, S., 2006. Syros metasomatic tourmaline: evidence for very high-d11B fluids in subduction zones. J. Petrol. Vol. 47, 1915-1942.

29. Marocchi, M., Mars chall, H.R., Konzett, J., Tropp er, P., Ludwig, T., Mair, V. &Bargossi, G.M., 2011. Metasomatic tourmaline in hybrid contact-bands between gneiss and peridotite in the Ulten Zone of the Eastern Italian Alps: chemistry and boron isotopic composition. Can. Mineral. Vol. 49, 245-261.

30. Dutrow, B.L., Foster, C.T., Jr. and HenryRY, D.J., 1999. Tourmaline-rich pseudomorphs in sillimanite zone metapelites: demarcation of an infiltration front. Am. Mineral. Vol. 84, 794-805.

31. Mahadevan, T. M., 2002. Geology of Bihar and Jharkhand, Geological Society of India, Bengaluru, 563.

32. Acharyya, S. K., 2003.The nature of Mesoproterozoic central Indiantectonic zone with exhumed and reworked older granulites.Gondwana Res., Vol.6 (2), 197–214.

33. Sharma, R. S., 2009. Cratons and Fold Belts of India, Springer, Berlin,Germany, pp. 304.

34. Singh, U. P., Venkatesh, N. S., Godhavari, K. S., Gopalkrishnan, R., Fareeduddin and Rao, M. S. (2004),Lamprophyre dykes in Chotanagpurgneissic complex, near Simdega, Gumla district,Jharkhand. J. Geol. Soc. India, Vol. 63, 655–658.

35. Dietrich RV, 1985. The Tourmaline Group. Van NostrandReinhold Company, New York; pp 1–300.

36. Krynine PD, 1946. The tourmaline group in sediments.J Geol, Vol 54, 65–87.

37. Keys DA, 1921. A piezoelectric method of measuring explosionpressures. Phil Mag Vol 42, 473–488.

38. Henry DJ, Dutrow BL, 2012b. The tourmaline diaries:an eye-catching mineral and its many facets. Natur Hist, Vol.120, 16–27.

39. van Hinsberg VJ, Henry DJ, Marschall HR, 2011a. Tourmaline: an ideal indicator of its host environment.Canad Mineral Vol 49, 1–16.

40. van Hinsberg VJ Schumacher JC, 2011. Tourmaline as apetrogenetic indicator mineral in the Haut-Allier MetamorphicSuite, Massif Central, France. Canad Mineral, Vol. 49, 177–194.

41. Bosi, F. &Lucchesi, S., 2007. Crystal chemical relationships in the tourmaline group: structural constraints on chemical variability. Am. Mineral. Vol, 92, 1054-1063.

42. Rumyantseva, E.V., 1983. Chrome-dravite - a new mineralfrom Karelia. Zap. Vses. Mineral Obsh., Vol 112, 222-225.

43. Sokolov, P.B., Gorskaya, M.G., Gordienko, V.V.,Petrova, M.G., Kretser, Yu. L., Frank-Kamenetsky,V.A.,1986.Olenite, Na, xAl3Al6B3Si6O27 (O, OH) 4- a new high-alumina mineral of the tourmalinegroup. Zap. Vses. Mineral Obsh. CXV; pp 119-123.

44. Donnay, G., Ingamells, CO., Mason, B., 1966.Buergerite, a new species of tourmaline. Am.Mineral, Vol 51, 198-199.

45. Grice, J.D. &Ercit, T.S., 1993. Ordering ofFe and Mgin the tourmaline crystal structure: the correct formula.NeuesJahrb. Mineral Abh, Vol 165, 245-266.

46. Grice, J.D. & Robinson, G.W., 1989. Feruvite, a newmember of the tourmaline group, and its crystalstructure. Can. Mineral, Vol 27, 199-203.

47. Dunn, P.J., Appleman, D.E., Nelen, J.E., 1977a. Liddicoatite, a new calcium end-member of thetourmaline group. Am. Mineral., Vol 62, 1121-1124.

48. Selway, J.B., Hawthorne, F.C., Cerny, P., Ottolini, L.,Novak, M., Kyser, T.K., 1998. Rossmanite, [LiAl2] Al6Si6O18 (BO3)3(OH) 4, a new alkali-deficienttourmaline: Description and crystal structure.Am. Mineral, Vol 83, 896-900.

49. MacDonald, D.J., Hawthorne, F.C., Grice, J.D., 1993.Foitite, [Fe^{2+}_2Al, Fe^{3+})] $Al^{6}Si^{6}O^{18}(BO^{3})^{3}(OH)^{4}$, anew alkali-deficient tourmaline: description andcrystal structure. Am. Mineral, Vol 7, 1299-1303.

50. Leake, B.E., Woolley, A.R., Arps, C.E.S, Birch, W.D.,Gilbert, M.C., Grice, J.D., Hawthorne, F.C, Kato,A., Kisch, H.J., Krivovichev, V.G., Linthout, K.,Laird, J., Mandarino, J.A., Maresch, W.V., Nickel,E.H., Rock, N.M.S., Schumacher, J.C, Smith, D.C,Stephenson, N.C.N., Ungaretti, L., Whittaker,E.J.W., Youshi, G. (1997): Nomenclature ofAmphiboles: Report of the Subcommittee onAmphiboles of the International MineralogicalAssociation, Commission on New Minerals andMineral Names. Eur. J. Mineral, 9, 623-651.

51. Bebout G.E. & Nakamura, E., 2003. Record in metamorphic tourmaline of subduction-zone devolatilization and boron cycling. Geology 31, 407-410.

52. Marschchall, H.R., Korsakov, A.V., Luvizotto, G.L., Nasdala, L. &Ludwiwig, T., 2009b. On the occurrence and boron isotopic composition of tourmaline in (ultra)high-pressure metamorphic rocks. J. Geol. Soc. London 166, 811-823.

53. Altherr, R., Topuz, G., Marschall, H., Zack, T. &Ludwi g, T., 2004. Evolution of a tourmaline-bearing lawsonite eclogite from Elekdag area (Central Pontides, N Turkey): evidence for infiltration of slab-derived B-rich fluids during exhumation. Contrib. Mineral. Petrol. 148, 409-425.

54. Kadarusman, A., Massonne, H.-J., van Roermund, H., Permana, H. &Munasri, 2007. P–T evolution of eclogites and blueschists from the Luk Ulo Complex of central Java, Indonesia. Int. Geol. Rev. 4, 329-356.

55. Marschall, H.R., Altherr, R., Ludwi g, T., Kalt, A., Gméliling, K. &Kasztovszky, Z., 2006b. Partitioning and budget of Li, Be and B in high-pressure metamorphic rocks. Geochim. Cosmochim. Acta 70, 4750-4769.

56. Ota, T., Kobobayashi, K., Kunihiro, T. & Nakamura, E., 2008b. Boron cycling by subducted lithosphere; insights from diamondiferous tourmaline from the Kokchetav ultrahigh-pressure metamorphic belt. Geochim. Cosmochim. Acta 72, 3531-3541.

57. King R.J., 2000.The tourmaline group (Part 1),Geology Today, Blackwell Science Ltd.

58. Robbins, C.R. & Yoder, H.S., Jr., 1962. Stability relations of dravite, a tourmaline. Carnegie Inst. Wash. Yearbook 61, 106-108.

59. Holtz, F. & Johannes, W., 1991. Effect of tourmaline on melt fraction and composition of first melts in quartzofeldspathic gneiss. Eur. J. Mineral. 3, 527-536.

60. Krosse, S., 1995. Hochdrucksynthese, Stabilität und Eigenschaften der BorsilikateDravit und Kornerupin, sowie Darstellung und Stabilitätsverhalteneinesneuen Mg–Al-borates. Thesis, Ruhr-Universität Bochum, Germany.

61. Wolf, M.B. & London, D.,1997. Boron in granitic magmas: stability of tourmaline in equilibrium with biotite and cordierite. Contrib. Mineral. Petrol. 130, 12-30.

62. von Goerne, G., Franz, G. & Heinrich, W., 2001. Synthesis of tourmaline solid solutions in the system Na2O–MgO–Al2O3–SiO2–B2O3–H2O–HCl and the distribution of Na between tourmaline and fluid at 300 to 700°C and 100 MPa. Contrib. Mineral. Petrol. 141, 160-173.

63. Spicer, E.M., Stevens, G. & Buick, I.S., 2004. The low-pressure partial-melting behavior of natural boron-bearing metapelites from the Mt. Stafford area, central Australia. Contrib. Mineral. Petrol. 148, 160-179.

64. Grew, E.S., 1996. Borosilicates (exclusive of tourmaline) and boron in rock-forming minerals in metamorphic environments. In Boron: Mineralogy, Petrology and Geochemistry (E.S. Grew & L.M. Anovitz, eds.). Rev. Mineral. 33, 387-502.

65. Robbins, C.R. & Yoder, H.S., Jr., 1962. Stability relations of dravite, a tourmaline. Carnegie Inst. Wash. Yearbook 61, 106-108.

66. Holtz, F. & Johannes, W., 1991. Effect of tourmaline on melt fraction and composition of first melts in quartzofeldspathic gneiss. Eur. J. Mineral. 3, 527-536.

67. von Goerne, G., Franz, G. & Wirth, R., 1999. Hydrothermal synthesis of large dravite crystals by the chamber method. Eur. J. Mineral. 11, 1061-1078.

68. Kawakami, T., 2004. Tourmaline and boron as indicators of the presence, segregation and extraction of melt in pelitic migmatites: examples from the Ryoke metamorphic belt, SW Japan. Trans. R. Soc. Edinburgh: Earth Sci. 95, 111-123.

69. Spicer, E.M., Stevens, G. & Buick, I.S., 2004. The low-pressure partial-melting behaviour of natural boron-bearing metapelites from the Mt. Stafford area, central Australia. Contrib. Mineral. Petrol. 148, 160-179.

70. Ota, T., Kobayashshi, K., Katsura, T. & Nakamura, E., 2008a. Tourmaline breakdown in a pelitic system: implications for boron cycling through subduction zones. Contrib. Mineral. Petrol. 155, 19-32Table Caption-

Peer Reviewed and Refereed Journal 2022 **(ISSN : 09726330)**

Rashtrasant Tukadoji Maharaj Nagpur University

SCIENCE JOURNAL 2022

Vol. : XV

Chlorite Geothermometry from a Quartz Xenocryst-laden Basaltic Dyke at Rorda, Chhota Udaipur Alkaline–Carbonatite sub-province, Deccan Large Igneous Province, India

Sanjeevani Jawadand[1] * and Kirtikumar Randive[1]

[1]Department of Geology, Rashtrasant Tukadoji Maharaj Nagpur University, Nagpur (MH) – 440 001, India.

*Correspondence :
sanju08@yahoo.com

ABSTRACT

The basaltic dyke exposed in Rorda area of Chhota Udaipur alkaline–carbonatite sub-province comprises quartz xenocryst set in a groundmass consisting of plagioclase, chlorite, barite ilmenite, rutile, magnetite, apatite, and hydrated Fe-oxides. The temperature estimates based on mineral thermometers provide a better understanding of the formation conditions of this composite dyke. During the present study, the mineral chemistry of quartz xenocrysts-laden basaltic dykes (QXLBD) was carried out using electron probe microanalyzer. The chemical analysis showed the chamosite and clinochlore variety of chlorites in QXLBD. The basaltic magma mixed with carbonated-hydrothermal (carbothermal) fluids have induced alteration of clinopyroxenes of the basalts and converted them to chlorites. The chlorite thermometry yields an average temperature of ~269°C. The micro-thermometric data from fluid inclusions within quartz xenocrysts are consistent with the estimates based on the chlorite thermometry, indicating similar formation conditions for quartz and chlorite and thus, the chlorites formed in the QXLBD are probably of hydrothermal origin.

Key-words : Quartz xenocrysts, basaltic dyke, alkaline-carbonatite province, geothermometry

1. INTRODUCTION

The dyke swarms are widespread in the Chhota Udaipur (CU) alkaline–carbonatitic sub-province of the Deccan Igneous Province. A diverse variety of rocks, especially intrusive dykes are known to occur in this area (e.g., Sukheswala and Avasia, 1972; Gwalani et al., 1993; Viladkar, 1996; Srivastava, 1997; Hari et al., 1998; Randive, 2005; 2015). The rare occurrence of quartz xenocrysts-laden basaltic dykes (QXLBD) near Rorda and Samalavat in the Sub-Province was previously reported by Randive (2015) and Randive and Hurai (2015). The xenocryst-laden basaltic dyke near Rorda shows a mineral assemblage comprising plagioclase, chlorite, barite, ilmenite, rutile, magnetite, apatite, and hydrated Fe-oxides. However, quartz is the main xenocrystic mineral occurring in varying sizes and shapes hosted in the basaltic groundmass (Randive, 2015). The presence of quartz xenocrysts in the basaltic magma is very intriguing, although previous studies (Randive, 2015; Randive and Hurai, 2015) indicated that the quartz xenocrysts could have been derived from the quartzite xenoliths, which were selectively trapped by the mafic magma mixed with the carbonate-rich hydrothermal (carbo-thermal) fluids.

The probability of retaining quartz xenocrysts in rocks depends on temperature and composition of mafic magmas as well as the original size of quartz grains and the relative

volume of xenocrysts embedded in the magma (Holub, 2003). In order to assess the temperature-pressure conditions during crystallization, the mineral chemistry can be very useful (Mercier 1980; Gasparik 1984; Berman 1988). The fluid inclusion study of quartz xenocryst by Randive and Hurai (2015) estimated the possible trapping temperature around 300-330°C, or even lower. However, this temperature range represents the formation conditions of quartz outside the magma system. Therefore, we employed mineral thermometry approach to estimate formation conditions of minerals inside the magma system. The study encompasses the range in temperature calculated on the basis of chlorite thermometers using WinCcac program (Yavuz et al., 2015).

2. GEOLOGY

The Chhota Udaipur area of Deccan Large Igneous Province (DLIP) has been studied in great details by a number of workers (e.g., Gwalani et al., 1993; Randive and Meshram, 2020, and references therein). A brief outline of geology of the study area is described here. The CU alkaline-carbonatite province mainly comprises of two igneous complexes, the Ambadungar alkaline igneous complex in the southeastern part of DLIP and the Phenai Mata igneous complex, in the western part (Randive et al., 2017). The study area is in close proximity to the Amba Dongar carbonatite breccia diatreme (Sukeshwala, 1972, Deans and Powell, 1972; Gwalani et al., 1993; Srivastava, 1997; Randive 2011; Randive and Hurai, 2015). The mafic-alkaline-carbonatite-lamprophyre dykes/sills have intruded the country rocks consisting mainly of Upper Cretaceous to Eocene Deccan Trap basaltic lava flows, Cretaceous Bagh sediments and the Archaean–Proterozoic Aravalli granites and metasediments. The study area is exposed near Rorda at N22°7'52.79" and E74° 4'14.57" (Fig.1).

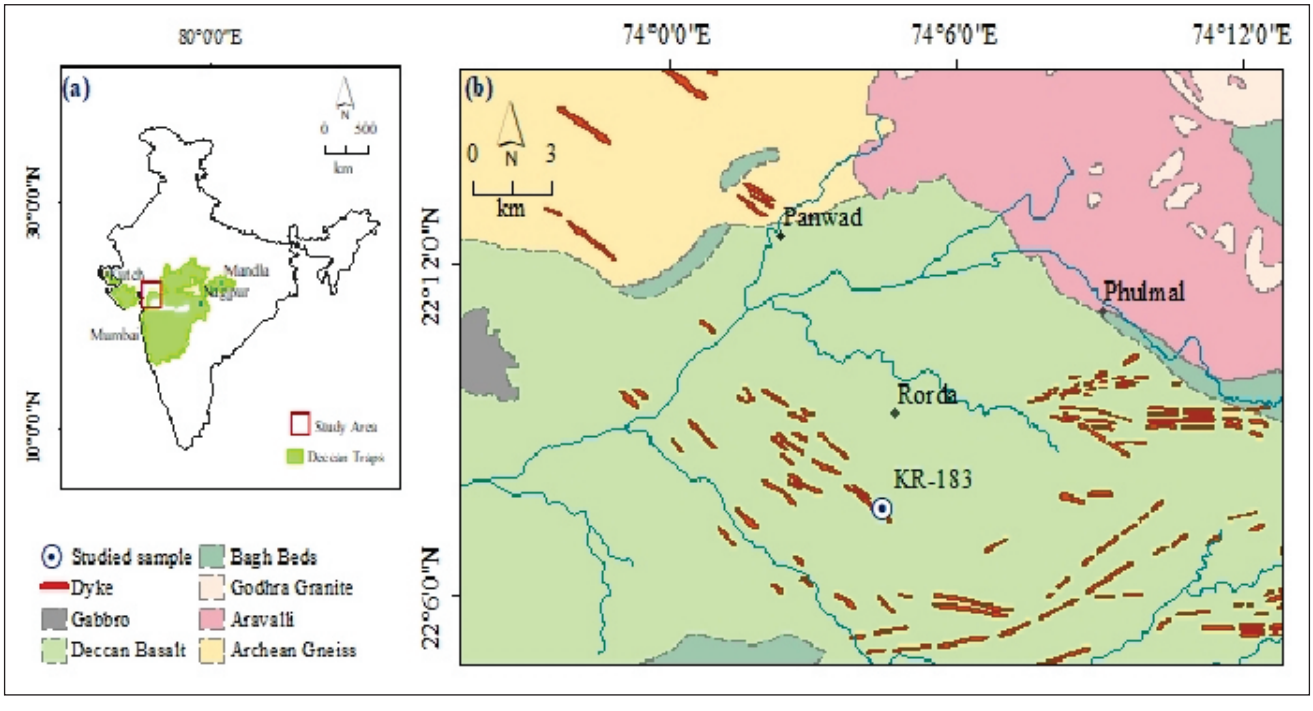

Fig. 1 : Geological map of study area (modified after Randive, 2015)

3. FIELD AND PETROGRAPHIC OBSERVATIONS

QXLBD in outcrop is a fine grained, porphyritic rock containing phenocrysts of quartz enveloped in the groundmass composed of plagioclase feldspars, chlorite, relict pyroxenes, barite, rutile, Fe-Ti oxides, and silicate glass. Megascopically, the quartz xenocrysts display a wide range of morphologies, including euhedral (equilibrium crystals), rounded (resorbed crystals), angular (crystal fragments), and glomerophyric shapes (intergrown crystals) (Figs. 2 and 3), but microscopically, they have irregular edges (Fig. 4a).

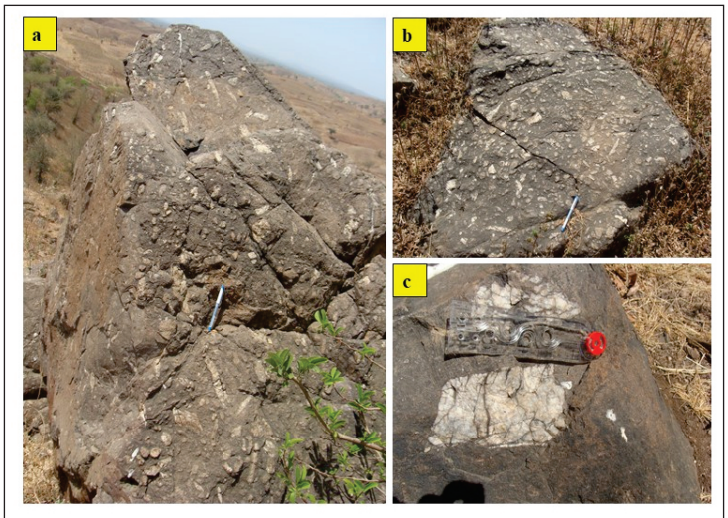

Fig. 2 Field photographs of an exposed block of the NW-SE trending dyke. a, b) Exposed blocks showing dense population of quartz xenocrysts. c) Closer view of a xenocryst showing the fragmental morphology.

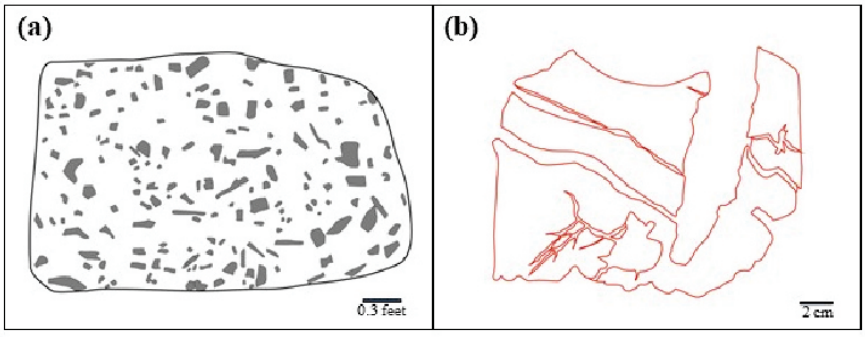

Fig. 3 a) Sketch of quartz xenocryst-laden dyke. b) Disintegrated quartz fragment with sharp edges.

Carbonate-rich fluids that invaded quartz xenocrysts resulted in the development of an intricate intergrowth pattern between quartz and carbonate. Quartz xenocrysts set in a fine-grained matrix rich in Fe-Ti oxides were magmatically corroded along contacts with the basaltic melt (Fig. 4a). The complex zoning, sieve texture as well as resorption are observed in the dyke (Figs. 4b and c).

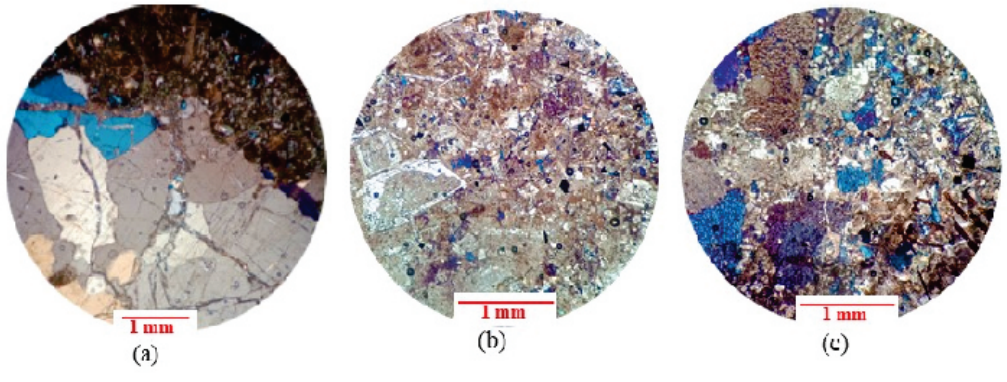

Fig. 4 Photomicrographs of dyke showing quartz xenocrysts in a fine-grained matrix rich in Fe-Ti oxides. a) Xenocryst of quartz with a fractured and partly resorbed rim in the basaltic groundmass. b, c) Sieve textures and resorption features.

The Backscattered electron (BSE) images of QXLBD shows the exsolved laths, fine streaks, and patches of ulvospinel in ilmenite. The exsolution of Fe-Ti bearing phases is observed as fine interleaving ilmenite and ulvospinel lamella (Fig. 5a and b). Also, the ulvospinel occurs as small individual anhedral grains between coarse ilmenite lamellae as well as coexisting with small, elongated ilmenite crystals. The symplectite of titanomagnetite / magnetite + rutile is myrmekite-like, and occurs within the ilmenite (Fig. 5b). The symplectite is composed of vermicular rutile and interstitial titanomagnetite where rutile is rimmed by titanomagnetite. Relics of ilmenite occasionally occur within or along the boundary of the symplectite.

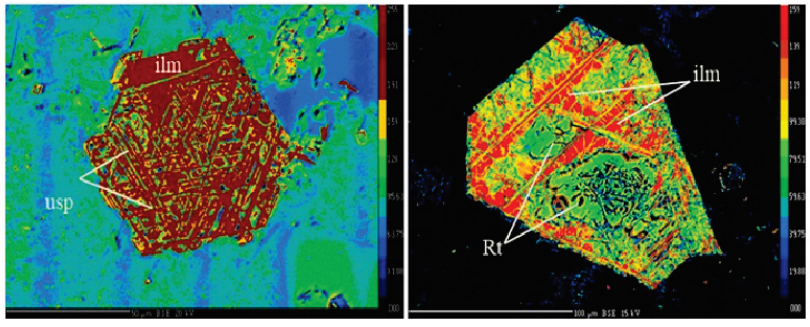

Fig. 5 BSE images showing a) interleaving of ilmenite (ilm) and ulvospinel (usp) lamellae b) rutile relics (Rt) in the symplectite and rest Fe-Ti phases (titanomagnetite, ilmenite).

4. ANALYTICAL TECHNIQUES

The petrographic study was carried out using a Nikon 50i POL microscope at the Post Graduate Department of Geology, RTM Nagpur University. The chemical analysis of chlorite ilmenite, rutile, carbonates, quartz, barite and feldspar were performed using a CAMECA SX-100 electron probe micro analyzer (EPMA) hosted at National Centre of Excellence in Geoscience Research (NCEGR), Geological Survey of India, Bangalore; operated at 15keV 15nA and a 1 µm beam diameter as analytical conditions and with synthetic oxides as well as natural silicate minerals (Jadeite (NaKa), wollastonite (SiKa CaKa), corundum (AlKa), apatite (PKa), orthoclase (KKa), rutile (TiKa), Cr_2O_3 (CrKa), rhodonite (MnKa), Fe_2O_3 (FeKa), Ni (Ka), celestine (SrLa), barite (BaLa), olivine (MgKa)) as standards. The average chemical composition on the basis of EPMA data of all the minerals occurring within QXLBD and the micro-area analysis of chlorites in QXLBD are given in table 1 and 2 respectively.

Table 1 : Average chemical composition using EPMA data of the minerals in QXLBD (Randive, 2015)

	Quartz n=8	Rutile n=2	Ilmenite n=12	Ulvospinel n=2	Apatite n=3	Barite n=3	Calcite n=9	Dolomite n=11	Siderite n=17	Feldspar n=2	Chlorite n=7
Na_2O	0.031	0.055	0.085	0.07	0.453	0.15	0.006	0.002	0.005	4.93	0.409
K_2O	0.024	0	0.094	0.055	0.647	0.027	0	0	0.001	0.375	0.501
MgO	0.034	0.105	1.308	0.415	2.1	0.083	1.142	18.631	14.688	0.12	10.856
CaO	0.215	0.225	0.273	0.095	40.5	0.067	52.621	31.094	3.965	11.385	2.993
MnO	0	0.05	0.038	0.015	0.033	0.043	0.799	0.169	1.04	0	0.036
FeO	0.321	2.945	23.55	59.915	2.97	0.567	3.849	6.135	36.361	0.8	23.411
NiO	0	0.04	0	0	0	0.06	0.017	0	0.034	0.03	0.033
SrO	0	0	0.022	0	0	1.6	0.083	0	0	0	0
BaO	0	1.485	0.781	0.395	0	62.647	0	0	0	0.015	0
Al_2O_3	0.204	0.37	1.594	0.86	2.607	0.363	0.081	0.014	0.005	27.79	15.016
Cr_2O_3	0.003	0.05	0.04	0.065	0	0	0	0	0.004	0.005	0.007
SiO_2	97.793	1.535	16.628	2.175	6.41	2.607	0.321	0.015	0.858	54.51	28.557
TiO_2	0.01	91.6	49.308	25.145	0.477	0	0	0.005	0	0.055	0.071
P_2O_5	0	0	0.006	0	28.72	0	0.07	0.043	0.002	0	0

Table 2 : Mean values from microprobe analyses of chlorites from QXLBD. Atoms per formula unit (apfu) calculated on the basis of 14 oxygens, which is an equivalent of 18 anions, i.e., $O_{10}(OH)_8$.

Sample No	18 / 1	28 / 1	69 / 1	71 / 1	72 / 1	73 / 1	74 / 1
(%)[SiO_2	31.88	26.09	26.84	34.85	23.81	28.52	27.91
TiO_2	0.04	0.03	0.10	0.20	0.05	0.00	0.08
Al_2O_3	14.69	14.76	14.73	14.63	13.18	15.75	17.37
Cr_2O_3	0.04	0.00	0.00	0.01	0.02	0.00	0.01
Fe_2O_3	2.38	0.58	1.31	6.94	0.00	1.02	1.60
FeO	25.43	28.74	8.22	9.32	24.47	27.34	27.97
MnO	0.08	0.00	0.06	0.05	0.02	0.04	0.05
NiO	0.05	0.00	0.02	0.08	0.07	0.00	0.08
MgO	14.60	11.56	6.04	9.50	8.50	13.80	11.99
CaO	0.52	0.16	13.17	0.28	6.46	0.23	0.13
BaO	0.00	0.00	0.00	0.07	0.00	0.01	0.02
Na_2O	0.07	0.02	1.28	1.38	0.03	0.04	0.04
K_2O	0.07	0.01	1.63	1.74	0.01	0.03	0.02
[H_2O(c)	11.6792	10.3176	9.7391	11.0123	9.5248	11.1207	11.1398
Total	101.53	92.27	83.14	90.06	86.14	97.90	98.41
Structural formulae on the basis of 14 oxygens							
(apfu)[Si	3.2737	3.0327	3.3052	3.7955	2.9981	3.0758	3.0049
Ti	0.0031	0.0026	0.0093	0.0164	0.0047	0.0000	0.0065
$Al^{(IV)}$	0.7263	0.9673	0.6948	0.2045	1.0019	0.9242	0.9951
$Al^{(VI)}$	1.0516	1.0549	1.4431	1.6733	0.9540	1.0777	1.2089
Cr	0.0032	0.0000	0.0000	0.0009	0.0020	0.0000	0.0009
$Fe^{(3+)}$	0.1839	0.0507	0.1214	0.5688	0.0000	0.0828	0.1296
$Fe^{(2+)}$	2.1839	2.7939	0.8465	0.8489	2.5768	2.4658	2.5183
Mn	0.0070	0.0000	0.0063	0.0046	0.0021	0.0037	0.0046
Ni	0.0041	0.0000	0.0020	0.0070	0.0071	0.0000	0.0069
Mg	2.2350	2.0032	1.1088	1.5424	1.5955	2.2187	1.9244
Ca	0.0572	0.0199	1.7377	0.0327	0.8715	0.0266	0.0150
Ba	0.0000	0.0000	0.0000	0.0030	0.0000	0.0004	0.0008
Na	0.0139	0.0045	0.3056	0.2914	0.0073	0.0084	0.0083
K	0.0092	0.0015	0.2561	0.2418	0.0016	0.0041	0.0027
Total]Tetrahedral	***4.0000***	***4.0000***	***4.0000***	***4.0000***	***4.0000***	***4.0000***	***4.0000***
Total]Octahedral	5.6719	5.9053	3.5374	4.6622	5.1423	5.8486	5.8000
Fe/(Fe + Mg)	0.5144	0.5868	0.4661	0.4789	0.6176	0.5346	0.5791
[Species(Zane and Weiss, 1998)]	Fe chlorite	Fe chlorite	Al chlorite	Al chlorite	Fe chlorite	Fe chlorite	Fe chlorite
[Species(Wiewiora and Weiss, 1990)]	Chamosite	Chamosite	Donbassite	Sudoite	Chamosite	Chamosite	Chamosite

5. RESULTS AND DISCUSSION

The EPMA data of QXLBD indicates presence of calcite, dolomite, as well as siderite, and also, the intermediate compositions. The feldspar is typically plagioclase, composition ranging between An_{50-60}. Chlorites range in composition between chamosite and sudoite, and the Fe-Ti oxide show wide variation between titanomagnetite, ulvospinel (Fe_2TiO_4), ilmenite ($FeTiO_3$) and rutile (TiO_2), with possible solid solution between titanomagnetite-ilmenite and ilmenite-rutile respectively. Ulvospinel commonly occurs as an exsolution product in titanomagnetite and forms under conditions of slow cooling and low oxygen partial pressure (Haggerty, 1968). Out of various geothermometers recommended by different workers, the empirical methods proposed by Cathelineau and Nieva (1985), Kranidiotis and MacLean (1987), Cathelineau (1988), Kavalieris et al. (1990), Jowett (1991), Hilliere and Velde (1991), De Caritat et al. (1993), Zang and Fyfe (1995), Xie et al. (1997), El-Sharkawy (2000) based on chlorite composition have been adopted in the present study based on available microprobe data.

5.1 Crystal chemistry of the chlorite minerals

Chlorite is found in metamorphic, diagenetic, and hydrothermal environments, and it has a wide range of stability and a chemical composition that is partially dependent on temperature (T) and pressure (P). Chlorite, a 2:1:1 phyllosilicate consists of two tetrahedral sheets surround an octahedral sheet, associated with an interlayer octahedral sheet (Bourdelle, 2021). There are several ways of chlorite classification. As per the AIPEA (Association Internationale Pour l'Étude des Argiles) Committee for nomenclature of clay minerals, the QXLBD chlorites can be classified as chamosite, donbassite and sudoite (Table 1), which is in-line with the classification schemes of Bayliss (1975), Wiewióra and Weiss (1990), and Bailey (1980). According to two-level classification scheme of Zane and Weiss (1998), the chlorites from the study area plot in type-I field (i.e., X_{Mg}+e"X_{Al}+$X_{Vacancy}$) 'Fe-chlorite' and Type-II (i.e., X_{Mg}+X_{Fe}<X_{Al}+$X_{Vacancy}$) 'Al-chlorite' field (Fig. 6c).

Table 2 and Fig. 6a show the distribution of various cations in the QXLBD chlorite, showing the dominant Fe-Al without significant Mg substitution. The chlorites in quartz-laden dyke fall in 'trioctahedral' subgroup (Fig. 6b). In the classification of Foster (1962), the QXLD chlorites plot in brunsvigite and diabantite fields (Fig. 6d). Using the compositional variations of chlorite (Al-free trioctahedral chlorite, chamosite and sudoite) (Fig. 6e), more convenient geothermometer applicable to chlorites are used. The relationships between chlorite composition and temperature of formation have been represented by isotherms in a R^{2+}–Si diagram (Wiewióra and Weiss, 1990). Several end-members and the compositional spaces defined by the models of Walshe (1986), Vidal et al. (2001, 2005, 2006), Inoue et al. (2009), and Bourdelle et al (2013) are outlined in Fig. 6f. This graphical representation in a R^{2+}–Si diagram (Wiewióra and Weiss, 1990) displays R^{2+}-Si-Al-vacancies relationships and thereby the relationship between chlorite composition and temperature of formation.

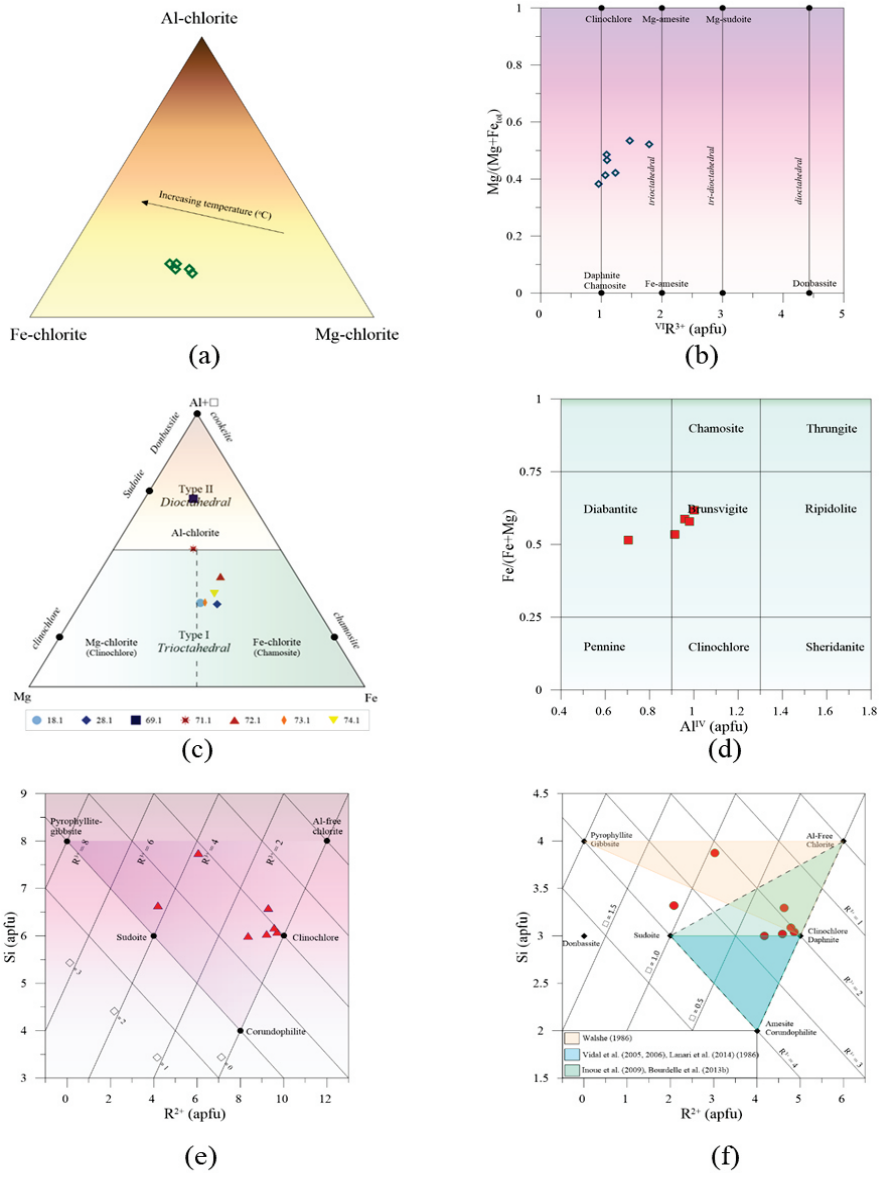

Fig. 6 a) Triangular plot correlating Al-Fe-Mg (Caritat et al., 1993), showing the dominant Fe-Mg substitution. b) Classification of chlorites in the Mg/(Mg+Fe_{tot}) vs. $^{VI}R^{3+}$ (apfu) diagram (Plissart et al., 2009) showing chlorites from quartz-laden dyke falling in the tri-octahedral field. c) Diagram after Zane and Weiss (1998) showing chlorites of the study area as dominantly the type-1 d) Al^{IV} versus Fe/(Fe+Mg) diagram after Foster (1962) showing chlorites to plot in brunsvigite and diabantite fields. (e) R^{2+} vs. Si diagram after Hillier and Velde (1991)) showing chlorite to project prominently in the clinochlore-chamosite field and the octahedral site occupied by R^{2+}. f) R^{2+}–Si diagram for chlorite compositions after Bourdelle and Cathelineau (2015) outlining compositional spaces defined by the models of Walshe (1986); Vidal et al. (2001, 2005, 2006), Inoue et al. (2009) and Bourdelle et al. (2013b). Chlorites from the study area project in the clinochlore-daphnite– sudoite–Al-free chlorite space.

5.2 Temperature estimation using chlorite thermometers

Due to the large compositional variation of chlorite and their susceptibility to the conditions of formation i.e., P–T conditions, bulk composition, and physicochemical properties of the environment; chlorites are the significant indicator of rock history (Inoue et al., 2009; Bourdelle and Cathelineau, 2015). Chlorite show three main types of substitutions, viz., FM [$Fe^{2+} \leftrightarrow Mg^{2+}$], Tschermak [$Al^{IV}Al^{VI} \leftrightarrow Si$ (Mg, Fe^{2+})], and di-trioctahedral [3(Mg, $Fe^{2+} \leftrightarrow \square + 2AL^{VI}$], where $\square$ octahedral vacancy). These substitutions are sensitive to the P–T conditions, bulk composition, and physicochemical properties of the environment (Inoue et al., 2009; Bourdelle et al., 2013 and references therein).

In this study, twelve empirical methods (Cathelineau and Nieva, 1985; Kranidiotis and MacLean, 1987; Cathelineau, 1988; Kavalieris et al., 1990; Jowett, 1991; Hilliere and Velde, 1991; De Caritat et al., 1993; Zang and Fyfe, 1995; Xie et al., 1997; El-Sharkawy, 2000) yielding the distinguishing temperatures were used for estimation of formation temperature of the QXLBD chlorites, discussed as follows.

[I] Cathelineau and Nieva (1985) Equation 1:

A systemic decline in the proportion of octahedral vacancies, an increase in the overall content of Mg and Fe, and a weak decrease in tetrahedral Al (Al^{IV}) resulting in an increase in the chlorite-based formation temperature (MacDowell and Elders, 1980). On the basis of this work Cathelineau and Nieva (1985) have proposed an equation for estimation temperatures which is given below:

$$T = (0.0826 + Al^{IV}) / 0.00471$$

According to this geothermometer, average temperature of study area chlorites is 218°C (Table 3).

[II] Cathelineau and Nieva (1985) Equation 2 : The same authors developed another chlorite geothermometer using following equation :

$$T = – (VACÿ – 2.41) / 0.00857$$

According to this geothermometer, average temperature of study area chlorites is 247°C (Table 3).

[III] Kranidiotis and MacLean (1987) : There is a linear relationship between Al^{IV} and Fe/(Fe+Mg) in chlorites. The chlorites having higher Fe/(Fe+Mg) tend to have higher formation temperatures. Therefore, Kranidiotis and MacLean (1987) modified the equation of Cathelineau and Nieva (1985) geothermometer using Al^{IV} content. The equation is given below:

$$T\,(°C) = 106Al^{IV}_{c} + 18$$

$$\text{Where, } Al_{c}^{IV} = Al^{IV} + 0.7 \times [Fe/(Fe+Mg)]$$

According to this geothermometer, average temperature of study area chlorites is 265°C (Table 3).

[IV] Cathelineau (1988) : A simple geothermometer proposed by Cahtelineau (1988) is based on the principle that Al^{IV} in chlorites is a function of temperature, which can be expressed in the following equation:

$$T\,(°C) = -61.92 + 321.98 \times (Al^{IV})$$

According to this geothermometer, average temperature of study area chlorites is 248°C (Table 3), which is higher than the averages of previous thermometers.

[V] Kavalieris et al. (1990): The approach adopted by Kavalieris et al. (1990) for estimation of temperatures from chlorite chemistry is based on the actual analysis of fluid inclusions and variation observed in tetrahedral silica. He proposed following quadratic equation:

$$T\,(°C) = 4833.946 – 2817.776 \times (Si^{IV}) + 419.858 \times (Si^{IV})^2$$

According to this geothermometer, average temperature of study area chlorites is 149°C (Table 3), which is lower than the previous thermometers

[VI] Jowett (1991): Jowett (1991) proposed a chlorite geothermometer based on variation in Fe/(Fe+Mg) correction factor. This geothermometer shows similar result to that of Cahtelineau (1988) method for the Fe/(Fe+Mg) ration less than 0.6. It yields reasonably accurate results for temperatures between 170°C and 270°C. The proposed equation is

given below:

$$T\,(°C) = 319Al_C^{IV} - 69$$

$$\text{Where, } Al_C^{IV} = A1^{IV} + 0.1(Fe / [Fe + Mg])$$

According to this geothermometer, average temperature of study area chlorites is 256°C (Table 3), which is slightly higher but similar to Cathelineau (1988).

[VII] Hilliere and Velde (1991) : These authors proposed a geothermometer based on regression line with a correlation coefficient of 0.84. This is especially applicable for the low-temperature (diagenetic) chlorites. The equation is given below :

$$T\,(°C) = (Al^{IV} - 1.303546) / 0.004007$$

According to this geothermometer, average temperature of study area chlorites is 155°C which is lower than the previous thermometers (Table 3).

[VIII] De Caritat et al. (1993) [Octahedral Occupancy] : This geothermometer is based on the octahedral site occupancy in the chlorite structure. In the octahedral occupancy vs temperature diagram, a regression line with good correlation coefficient (i.e., 0.89) is used for estimating temperature of formation of chlorites. The equation is as follows :

$$T\,(°C) = (\text{Octahedral Occupancy} - 5.550) / 0.001359$$

According to this geothermometer, average temperature of QXLD chlorites is 222°C (Table 3), which mimics that of Cathelineau (1988).

[IX] De Caritat et al. (1993) [Tetrahedral Occupancy]: These authors also proposed a geothermometer based on tetrahedral occupancy. The tetrahedral Si^{IV} (apfu) correlates with the formation temperature of chlorite based on '*Al-chlorite*' end-member composition. However, this '*Al-chlorite*' end-member has a drastic effect on temperature, therefore, divided into 3 categories, viz., '*Al-chlorite*' < 0.20, '*Al-chlorite*' between 0.20 – 0.24, and '*Al-chlorite*' > 0.24. following three equations were proposed :

$T\,(°C) = (Si^{IV} - 3.610) / -0.001327$ if *Al-chlorite* < 0.20

$T\,(°C) = (Si^{IV} - 3.233) / -0.001327$ if *Al-chlorite* between 0.20 & 0.24

$T\,(°C) = (Si^{IV} - 2.792) / -0.000486$ if *Al-chlorite* > 0.24

According to this geothermometer, average temperature of study area chlorites is 432°C (Table 3), which is slightly high. Apparently, this thermometer is not suitable for estimation of formation temperature of the QXLBD chlorites.

[X] Zang and Fyfe (1995): The approach adopted by Zang and Fyfe (1995) is based on the observation that the Mg / (Mg + Fe) ratio in hydrothermally altered bedrock increases from mineralized zone towards the distal end. Therefore, they proposed a different correction factor for Fe / (Fe + Mg). Following equation was proposed :

$$T\,(°C) = 106.2\,Al_C^{IV} + 17.5$$

$$\text{Where, } Al_C^{IV} = A1^{IV} - 0.88 \times [(Fe / (Fe + Mg) - 34]$$

According to this geothermometer, average temperature of study area chlorites is 201! (Table 3), which is similar to some of the above thermometers.

[XI] Xie et al. (1997): These authors proposed a new geothermometer with 0.31 limiting value modification in Fe / (Fe + Mg) ratio. The equation is as follows:

$T\,(°C) = 160.99 \times [(Al^{IV}) + 1.33 \times (0.31 - (Fe / (Fe + Mg)] - 61.92,$ if $(Fe / (Fe + Mg) < 0.31$

$T\,(°C) = 160.99 \times [(Al^{IV}) + 1.33 \times ((Fe / (Fe + Mg) - 0.31] - 61.92,$ if $(Fe / (Fe + Mg) > 0.31$

According to this geothermometer, average temperature of study area chlorites is 138°C (Table 3), which is much lower than the previous thermometers. Apparently, this thermometer is not suitable for study area chlorites.

[XII] El-Sharkawy (2000): This geothermometer is modified from Cathelineau and Nieva (1985) with a new Fe / (Fe + Mg) ratio to estimate the temperature of formation. The equation is given below:

$$T\,(°C) = 106.2 \times [(Al^{IV}) - 0.48 \times ((Fe / (Fe + Mg) - 0.163] + 17.5$$

According to this geothermometer, average temperature of study area chlorites is 181°C which is lower than the previous thermometers (Table 3).

5.3 Chlorite geothermometry

A total of twelve empirical thermometers (Cathelineau and Nieva, 1985; Kranidiotis and MacLean, 1987; Cathelineau, 1988; Kavalieris et al., 1990; Jowett, 1991; Hilliere and Velde, 1991; De Caritat et al., 1993; Zang and Fyfe, 1995; Xie et al., 1997; El-Sharkawy, 2000), were used to calculate the chlorite-forming temperatures. Five geothermometers that show unreasonably low values (Kavalieris et al., 1990; Hilliere and Velde, 1991; Zang and Fyfe, 1995; Xie et al., 1997; El-Sharkawy, 2000) were not considered. Moreover, the criteria of w(Na2O + K2O + CaO) < 0.5 percent proposed by Foster (1962), Hillier and Velde (1991), and Zang and Fyfe (1995) implies four of the chlorites analysed in QXLBD are contaminated (for w < 0.5 percent, chlorite is not contaminated while for w > 0.5 percent, chlorite is contaminated). Accordingly, the average temperature range is considered for non-contaminated chlorites (marked in grey shade in table 3). Thus, the most reliable temperature estimates lie in the range of 218 – 432°C.

The crystal-chemical data summarized in Table 2 show a systematic decline in the proportion of octahedral vacancies, an increase in the overall content of Mg and Fe, and a limited decrease in tetrahedral Al (Al^{IV}) resulting in an increase in the temperature of formation of chlorites in QXLBD (Fig. 7a). Isotherms in the R^{2+}–Si diagram (Bourdelle and Cathelineau, 2015) have been used to describe the relationships between chlorite structure and formation temperature (Fig. 7b). All the compositions in equilibrium at a given temperature project on the same graphic isotherm using this representation. The QXLBD chlorites plots below the low-temperature chlorite field in R^{2+}–Si diagram (Fig. 7c), corresponding to anchizonal conditions (Fig. 7d).

Table 3 : Various empirical geothermometers used and the estimated temperatures of formation of chlorites (Yavuz et al., 2015)

Geothermometers	18 / 1	28 / 1	69 / 1	71 / 1	72 / 1	73 / 1	74 / 1	Average	Best
Cathelineau and Nieva (1985) Equation 1	167	219	219	219	226	210	225	218	218
Cathelineau and Nieva (1985) Equation 2	205	259	259	259	81	246	235	247	247
Kranidiotis and MacLean (1987)	210	267	267	267	276	254	272	265	265
Cathelineau (1988)	172	249	249	249	261	236	258	248	248
Kavalieris et al. (1990)	109	150	150	150	160	139	158	149	
Jowett (1991)	179	258	258	258	270	243	267	256	256
Hilliere and Velde (1991)	n.c.	157	157	157	175	136	171	155	
De Caritat et al. (1993) [Octahedral Occupancy]	89	261	261	261	n.c.	219	184	222	222
De Caritat et al. (1993) [Tetrahedral Occupancy]	254	435	n.c.	n.c.	462	403	456	432	432
Zang and Fyfe (1995)	155	200	200	200	204	196	207	201	
Xie et al. (1997)	84	131	131	131	129	139	143	138	
El-Sharkawy (2000)	136	180	180	180	184	176	186	181	
								Average	269

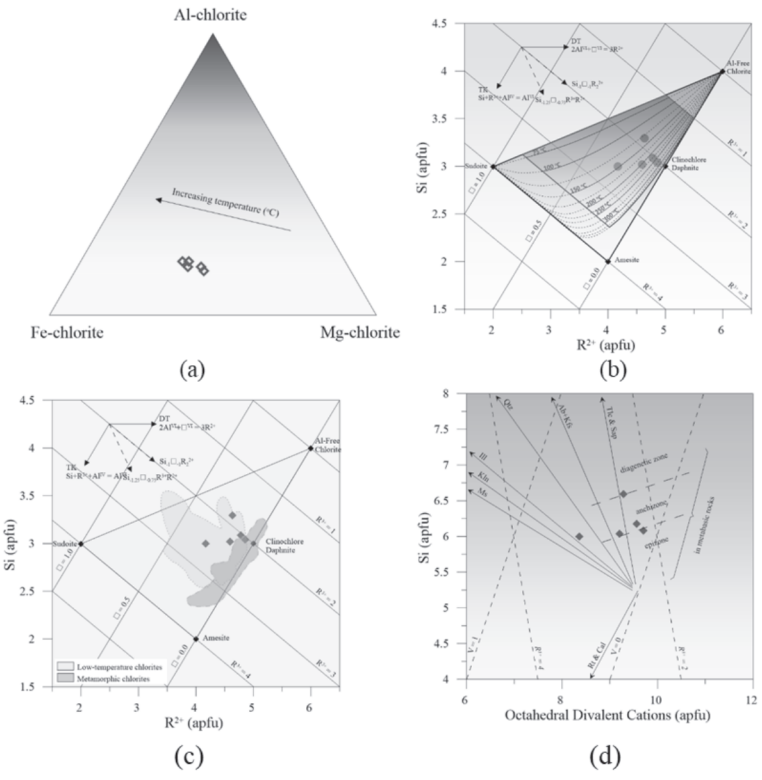

Fig. 7 a) Al-Fe-Mg (Caritat et al.,1993) plot depicting an increase in formation temperature of chlorites. b) Plot of R^{2+} versus Si (Bourdelle and Cathelineau, 2015) showing chlorite formation temperatures between 120 and 400°C. c) R^{2+}–Si plot (Bourdelle and Cathelineau, 2015) showing fields of low-temperature and metamorphic chlorites from several geological settings. Data points from the study area correspond to low-temperature chlorites. d) Si versus octahedral divalent cation diagram showing chlorites studied to plot in the anchizone (Árkai and Ghabrial, 1997).

6. DISCUSSION AND CONCLUSION

On the basis of combined studies mentioned in this paper, two types of chlorites are identified namely chamosite and clinochlore. It is known that the chamosite is formed at the beginning of hydrothermal alteration, and occurs mainly in a mineralized breccia type stock-work filling open spaces, and replaces the host rock through fissures (Rivas Sanchez et al., 2006). The clinochlore is commonly formed due to hydrothermal alteration of clinopyroxenes of the mafic and ultramafic igneous rocks. In case of QXLD, basaltic magma mixed with carbonated-hydrothermal (carbothermal) fluids have induced alteration of clinopyroxenes of the basalts and converted them to chlorites. The chlorite thermometry yielded the formation temperatures of 218°C – 432°C, average of which is 269°C. Therefore, it is apparent that not only the quartz xenocrysts, but the associated chlorites were also formed in the approximately similar temperature range. Therefore, the chlorites formed in the QXLBD are probably of hydrothermal origin.

Acknowledgements

KRR acknowledges the generous research grant by Science and Engineering Research Board, New Delhi, No. SERB/EMR/2017/003099 for facilitating research on geology and mineralization of Phenai Mata and surrounding areas in the Chhota Udaipur Province of DLIP. We are also thankful to our respective organizations for necessary permissions.

REFERENCES

Anderson, A.T., 1968. Oxidation of the La Blanche Lake titaniferous magnetite deposit, Quebec: Jour. Geology, v 76, no. 4, 528-547.

Anderson, A.T., Lindsley, D.H., 1985. New (and Final?) model for the Ti-magnetite/ilmenite geothermometers and oxygen barometers (abst.): Trans. Geophysical Union, v. 66, no. 18, 416.

Árkai, P., Sadek Ghabrial, D., 1997. Chlorite crystallinity as an indicator of metamorphic grade of low-temperature meta-igneous rocks: A case study from the Bükk Mountains, northeast Hungary. Clay Minerals, 32, 205–222.

Bailey, S.W., 1988. Introduction; Polytypism of 1:1-layer silicates. In: Bailey SW (ed) Hydrous phyllosilicates (Exclusive of Micas), review in mineralogy, vol 19. Mineralogical Society of America, Washington, DC, 1–27

Bayliss, P., 1975. Nomenclature Of the trioctahedral chlorites; Canadian Mineral, 178-180.

Berman, R.G., 1988. Internally-consistent thermodynamic data for minerals in the system Na2O–K2O-CaO-MgO-FeO-Fe2O3-Al2O3-SiO2-TiO2–H2O-CO2. J Petrol 29, 445–522

Bourdelle, F., Cathelineau, M., 2015. Low-temperature chlorite geothermometry: a graphical representation based on a T–R2+ –Si diagram. European Journal of Mineralogy, 27(5), 617–626. doi:10.1127/ejm/2015/0027-2467723–735.

Bourdelle, F., Parra, T., Chopin, C., Beyssac, O., 2013. A new chlorite geothermometer for diagenetic to low-grade metamorphic conditions. Contrib. Mineral. Petrol. 165.

Bourdelle, F., 2021. Low-Temperature Chlorite Geothermometry and Related Recent Analytical Advances: A Review. Minerals 11, 130. https:// doi.org/10.3390/min11020130

Carmichael, I. S. E., 1967. The iron-titanium oxides of salic volcanic rocks and their associated ferromagnesian silicates: Contrib. Mineral. Petrol., v. 14, no. l, 36-64.

Cathelineau, M., Nieva, D., 1985. A chlorite solid solution geothermometer. The Los Azufres (Mexico) geothermal system. Contrib. Mineral. Petrol. 91, 235–244.

De Caritat, P.D., Hutcheon, I. and Walshe, J.L., 1993. Chlorite geothermometry: a review. Clay Miner. 412, 219–239.

El-Sharkawy, M.F., 2000. Talc mineralization of ultramafic affinity in the Eastern Desert of Egypt. Mineral. Depos.35, 346–363.

Foster, M.D., 1962. Interpretation of the composition and classification of chlorites US Geological Survey Professional Paper 414A, 27.

Gasparik T., 1984. Experimental study of subsolidus phase relations and mixing properties of pyroxene in the system CaO-Al2O3-SiO2. Geochim Cosmochim Acta 48, 2537–2545.

Gwalani, L.G., Rock, N.M.S., Chang, W.J., Fernandez, S., Allegre, C.J., Prinzhofer, A., 1993. Alkaline rocks and carbonatites of Amba Dongar and adjacent areas, Deccan igneous province, Gujarat, India. 1. Geology, petrography and petrochemistry. Mineral. Petrol., 47, 219–253.

Haggerty, 1968. The Fe-Ti minerals of Icelandic basic rocks and their significance in rock magnetism. Ph.D. thesis. Department of Geology Imperial College of Science and Technology London, 22-56.
https://spiral.imperial.ac.uk/bitstream/10044/1/22317/2/Haggerty-SE-1968-PhD-Thesis.pdf

Hari, K.R., Satish Kumar, M., Santosh, M., Rai, S. K., 1998. Petrology, geochemistry, stable isotope studies of carbonate-rich dyke like bodies, Chhaktalao area, Madhya Pradesh. J. Geol. Soc. India, 52, 591–595.

Hillier, S., Velde, B., 1991. Octahedral occupancy and the chemical composition of diagenetic (low-temperature) chlorites. Clay Miner, 26, 149–168.

Holub F.V., 2003. Two genetic types of ocelli in some mafic rocks from the Central Bohemian Plutonic Complex: No room for transformistic speculations, Geolines, 16, 43.

Inoue, A., Meunier, A., Patier-Mas, P., Rigault, C., Beaufort, D., Vieillard, P., 2009. Application of chemical geothermometry to low temperature trioctahedral chlorites. Clay mineral.573, 371-382.

Jollands, Michael C., Bloch, Elias, Müntener Othmar, 2020. New Ti-in-quartz diffusivities reconcile natural Ti zoning with time scales and temperatures of upper crustal magma reservoirs. Geology 2020; 48 (7), 654–657. doi: https://doi.org/10.1130/G47238.1

Jowett, E.C., 1991. Fitting iron and magnesium into the hydrothermal chlorite geothermometer. GAC/MAC/SEG Joint Annual Meeting (Toronto, May 27.29, 1991).

Kranidiotis, P., Maclean,W.H., 1987. Systematic of chlorite alteration at the Phelps Dodge massive sulfide deposit, Matagami, Quebec. Econ. Geol. 82, 1898–1911.

Lepage, L.D., 2003. ILMAT: An excel worksheet for ilmenite–magnetite geothermometry and geobarometry; Comput. Geosci. 29(5), 673–678.

Lindsley, D.H., Spencer, K.J., 1982. Fe—Ti oxide geothermometry: Reducing analyses of coexisting Ti-Magnetite (Mt) and Ilmenite (Ilm) (abst.): Trans. Am. Geophysical Union, v. 63, no. 18, 471.

Macdowell, S.D., Elders, W.A., 1980. Authigenic layer silicate minerals in borehole Elmore 1, Salton Sea geothermal field, California, USA. Contrib. Mineral. Petrol. 74, 293–310.

Mercier, J-CC, 1980. Single pyroxene thermobarometry. Tectonophys 70, 1–37.

Nachlas, W.O., Whitney, D.L., Teyssier, C., Bagley, B., Mulch, A., 2014. Titanium concentration in quartz as a record of multiple deformation mechanisms in an extensional shear zone, Geochem. Geophys. Geosyst., 15, 1374– 1397, doi:10.1002/2013GC005200.

Plissart, G., Féménias, O., Mãruntiu, M., Diot, H., Demaiffe, D., 2009. Mineralogy and geothermometry of gabbro-derived listvenites in the Tisovita-Iutiophiolite southwestern Romania. Can. Mineral, 47, 81–105.

Powell, M., Powell, R., 1977. Geothermometry and oxygen barometry using coexisting iron-titanium oxides: a reappraisal: Mineral. Mag., 41, no. 318, 257-263.

Powell, R., 1985. Geothermometry and geobarometry: a discussion. Journal of the Geological Society of London 142, 29-38.

Powell, R., Holland, J.B., 2008. On thermobarometry. Jour of Metamorphic Geol 26, 155-179.

Randive, K.R., 2015. Occurrence of unusual quartz xenocryst-laden dykes in the Chhota Udaipur alkaline–carbonatite sub-province, Deccan Igneous Province, India. Current Science, Vol. 108, No. 12, 25, 2261- 2266.

Randive, K.R., Hurai V., 2015. Fluid Inclusion Study of Quartz Xenocrysts in Mafic Dykes from Kawant Area, Chhota Udaipur District, Gujarat, India. Open Geosci.; 7, 244–251.

Randive, Kirtikumar, Meshram, Tushar, 2020. An overview of the Carrbonatites from the Indian Subcontinent. Open Geoscience, 12, 85-116.

Ray, J. S., Ramesh, R., Pande, K., Trivedi, J. R., Shukla, P. N., Patel, P.P., 2000. Isotope and rare earth element chemistry of carbonatite–alkaline complexes of Deccan volcanic province: implications to magmatic and alteration processes. J. Asian Earth Sci., 18, 177–194.

Rivas-Sanchez, M.L., Alva-Valdivia, L.M., Arenas-Alatorre, J. Urrutia-Fucugauchi, J., Ruiz-Sandoval M. and Ramos-Molina M.A., 2006. Berthierine and chamosite hydrothermal: Genatic guides in the Peña Colorada magnetite-ore bearing deposit (PDF). Earth Planets Space. 58, 1389–1400. doi:10.1186/BF03352635

Srivastava, R.K., 1997 Petrology, geochemistry and genesis of rift related carbonatites of Ambadungar, India. Mineral. Petrol., 61, 47–66.

Stormer, J. C. Jr., 1983. The effects of recalculation on estimates of temperature and oxygen fugacity from analyses of multicomponent iron-titanium oxides: Am. Mineral., v. 68, no. 5/6, 586-594.

Sukheswala R.N., Avasia R.K., 1972. Carbonatite-alkaline complex of Panwad-Kawant, Gujarat and its bearing on the structural characteristics of the area, Bull. Volcanol., 35, 564–578

Vidal, O., de Andrade, V., Lewin, E., Munoz, M., Parra, T., Pascarelli, S., 2006. P-T-deformation-Fe3+/Fe2+ mapping at the thin section scale and comparison with XANES mapping: application to a garnet-bearing metapelite from the Sambagawa metamorphic belt (Japan). J. Metamorphic Geol., 24, 669–683.

Vidal, O., Parra, T., Trotet, F., 2001. A thermodynamic model for Fe-Mg aluminous chlorite using data from phase equilibrium experiments and natural pelitic assemblages in the 100 degrees to 600 C, 1 to 25 kb range. Am. J. Sci., 301, 557–592.

Vidal, O., Parra, T., Vieillard, P., 2005. Thermodynamic properties of the Tschermak solid solution in Fe-chlorite: Application to natural examples and possible role of oxidation. Am. Mineral., 90, 347–358.

Viladkar, S.G., 1996. Geology of the carbonatite–alkalic diatreme of Amba Dongar, Gujarat. GMDC Science and Research Centre, Ahmadabad.

Walshe, J.L., 1986. A six-component chlorite solid solution model and the conditions of chlorite formation in hydrothermal and geothermal systems. Econ. Geol., 81, 681–703.

Wark, D.A., Watson, E.B., 2004. The TitaniQ: a Ti-in-quartz thermometer. Geochim Cosmochim Acta Suppl 68, A543.

Wiewiora, A., Weiss, Z., 1990. Crystallochemical classifications of phyllosilicates based on the unifieled system of projection of chemical composition: II. The chlorite group. Clay Miner. 25, 83–92.

Xie, X., Byerly, G.R., Ferrell, R.E.J., 1997. IIb trioctahedral chlorite from the Barberton greenstonebelt: crystal structure and rock composition constraints with implications to geothermometry. Contrib. Mineral. Petrol. 126, 275–291.

Yauz, F., Kumral, M., Karakya, N., Karakaya, M.C., Yildrim D.K., 2015. A windows program for chlorite and classification. Elsevier Ltd., 102-103.

Zane A., Weiss Z., 1998. A procedure for classification of rock forming chlorites based on microprobe data; Rezd. Fis. Accad Lincei, 51-56.

Zang, W., Fyfe, W.S., 1995. Chloritisation of the hydrothermally altered bedrock at the Igarapé Bahia gold deposit, Carajás, Brazil. Miner. Depos. 30, 30–38.

Zhou, J.X., 2002. Quantitative Analysis of Silicate Minerals by Electron Probe Method; Standards Press of China: Beijing, China, 1–8. (In Chinese)

Peer Reviewed and Refereed Journal 2022 **(ISSN : 09726330)**

Rashtrasant Tukadoji Maharaj Nagpur University

SCIENCE JOURNAL 2022

Vol. : XV

Cryo-Electron Microscopy for Structural Analysis of Macromolecules

Mayuri S. Prasad and Pramod B. Khedekar

University Department of Pharmaceutical Sciences, Rashtrasant Tukadoji Maharaj Nagpur University, Nagpur – 440033 India.

Corresponding author email : jbrandhawa2@gmail.com
*pacific0701@gmail.com
Mob. No. 7776899668

ABSTRACT

An overview of cryo-electron microscopy is provided and modern studies are introduced to determine the structure and dynamics of biomolecules. Cryo-electron microscopy can be used to study the three dimensional structure of macro biomolecules and improve the techniques and equipment at near atomic resolution. The method has brought new development including single particle analysis and cryo-electron tomography for analyzing biological structures. For present creationin cryo-electron microscopy for dynamic studies of macromolecular structures, many changes have been acquired as direct electron detectors and image processing methods.

Keywords : Cryo-Electron Microscopy, Direct-Electron Detectors, Single-Particle Analysis, Sub-Tomogram Averaging.

1. INTRODUCTION

In 2017, Jacques Dubochet, Joachim Frank and Richard Henderson were awarded the Nobel prize for chemistry for developing Cryo-Electron Microscopy and for determining high resolution structure of biomolecules in solution[1]. Cryo-Electron Microscopy (cryo-EM) is a form of Transmission Electron Microscopy (TEM) used to establish the three dimensional structure of biological specimens that are in the hydrated state and having high resolution. It is an effective technique for the determination of studies of biological macromolecular structures that mainly includes assessment of their dynamics by making use of algorithms of advanced image processing. It is a dynamic tool to explain the structure of biomolecules at near-atomic resolution followed by X-ray crystallography and NMR spectroscopy. It requires no three dimensional crystals because organic macromolecules can be seen directly in many different conformations in their native environment. It is also used for determination of structure of isolated biomolecular complexes through a wide range of molecular mass from proteins with several tens kilo daltons to particles of virus with many megadaltons and to whole cells[2].

Many modelling approaches are presently used for translation of cryo-EM data into structural models including – rigid body fitting models (Chimera, COAN, Multifit, MODELLER, EM-fit, SITUS), flexible body fitting models (MDFF, MDFIT, EMFF, MODELLER, Flex-EM, SITUS), homology modelling (ROSETTA, FOLD-EM, MODELLER), de novo modelling (IMP, EM-fold, Pheonix, SITUS, RELION)[3]. All these approaches explore for single structural models reducing the deviation between observed and predicted cryo-EM density maps normally by integrating additional restraints into Molecular Dynamics (MD) stimulations. The thickness of the specimen that can be perforated

with beam of electron depending on mean free path limits the maximum observable object size to 500 nm in the case of 300 kV transmission with microscopes. It requires very small amount of sample and accepts a large variation of types of specimen including single molecules, large protein complexes of particles of virus, crystals of thin protein, bacteria, entire tissue section and complexes of helical fiber[4,5].

Generally, an intact structure in fully or partly hydrated form is build by biological molecules and represent their functions with surface having large areas subjected to aqueous environment. Cryo-EM procedure involves creation of specimens by quick freezing of macromolecules in solution and packed into the column of an electron microscope working at very high vacuum and at very low temperature so that the ice stays in its amorphous state and to decrease or reduce the effect of radiation damage. Ice exists in different temperature dependent alterations in cubic crystal form (-123ºC to -14ºC, 115K to 150K) and in hexagonal crystal form (-103ºC, 170K), during quick freezing, the development of these crystalline phases is neglected so that it can form amorphous ice but the sample should stay at a temperature that is below crystalline transition temperature[6]. Cryo-EM is a developing field surrounding two main areas of current research – cryopreservation for ultra-structural analysis and the usage of TEM cryo-stage for inspection of specimens at low temperature. Cryopreservation of many samples is enhanced by usage of cryoprotectants as glycerol or sugars that connects with water to restrict crystal information[7].

2. NEED FOR CRYO-EM

Biomolecules are not compatible in presence of intense electron beams and high vacuum conditions used in Transmission Electron Microscopy (TEM's) due to the presence of water surrounding the molecules gets evaporated and high energy electrons gets burn and molecules gets destroyed[8]. Cryo-EM uses frozen samples along with gentle electron beams and also sophisticated image processing. It results in overcoming of problems arise by other techniques[9].

X-ray diffraction produce very high resolution structure of biomolecules but was unable to crystallize the molecule because process of crystallization cause alteration in the structure. Cryo-EM needs no crystals and shows movement of biomolecules along with their interactions and leads to overcome the problems with other methods used[10].

Another way to obtain the best structural preservation for macromolecular EM was to let remain the aqueous macromolecules in their native environment or in buffer and speedly freeze them in a cryogen which is a very low temperature liquid[11]. Due to this, water molecules had no time to make regular arrays that are found in crystalline ice, but remained in reminiscent state of water at room temperature and imaging of molecules in this vitrified ice unfolded a new direction for macromolecular Electron Microscopes[12].

3. WORKFLOW OF CRYO-EM

Protein specimens or samples are kept in aqueous solution and are vitrified (glassy) in amorphous ice by a process called plunge freezing. Thick, large or bulky objects such as tissue samples or larger cells are required for high pressure freezing followed by cryo-milling. The images of such objects are captured as projections in electron microscopes at minimum temperature by using low electron dose method to neglect radiation damage[13].

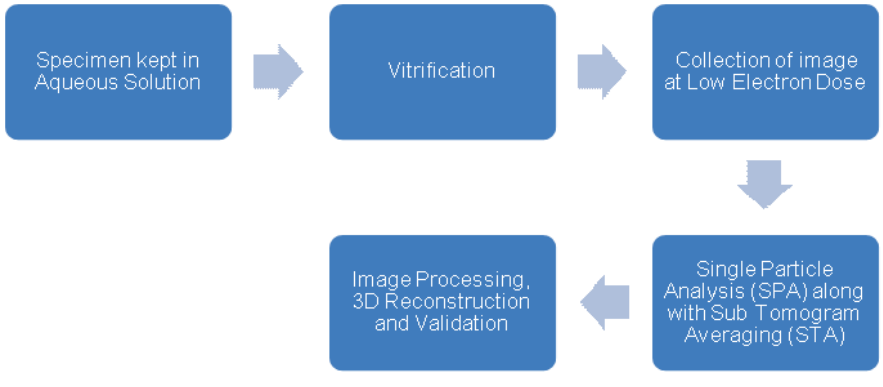

Fig. 1 – Workflow of Cryo-EM.

Steps involved in Cryo-electron microscopy includes –

§ Sample Preparation/Vitrification

§ Electron Microscopes Grid Preparation

§ Grid Screening

§ Data Collection

§ Image Processing

§ Model Building and Analysis

3.1. Sample Preparation/ Vitrification for cryo-EM

The sample under examination is in frozen hydrated state for preservation purposes. Solvents such as water or salt solution are used to make sure that sample remains stable. It is essential that the freezing process of the sample is very quick that prevents the frozen water around specimen sample to form cubic ice and absorbs electron beam that obscures the sample. The most important step of sample preparation is Fixation[14]. This technique involves the structure of sample (tissue, cells) to be remained close to natural form followed by dehydration using acetone/ethanol passing through another transition solvent (propylene oxide) and infiltrated and placed in liquid resins as epoxy or resins. This further leads to sectioning of sample through ultramicrotomy obtaining sections between 50 nm and 70 nm in thickness and once it is collected on metal mesh grid, staining of sample using electron dense stains is done. Macromolecules are observed in their native hydrated state by inserting the sample in vitrified water[15,16].

3.2. Electron Microscopes Grid Preparation

Macromolecules are placed on carbon or gold layer that are supported by a 3 mm metal grid made up of conductive material (gold, silicon oxide, silicon nitride, molybdenum). The most common method for EM grid preparation is negative staining method that use different stains as uranyl acetate or ammonium molybdate[17].

3.3. Grid Screening

To identify ideal blotting conditions, frozen grids are imaged on glaciosto and in order to achieve correct ice thickness, protein density and particle orientations, many vitrification and screening are necessary[18].

3.4. Data Collection

The higher end data collection microscopes that are equipped with latest generation of Direct Electron Detectors (DED) is very precious to observe a new sample on lower end instrument[19].

3.5. Image Processing

High resolution containing cryo-EM images of ice-embeded biomolecules on holey carbon EM grids are occupied to neglect irradiation damage that are recorded on digital detector or photographic films. Cryo transfer holder is equipped with liquid nitrogen is mounted by frozen grid. After loading the holder into column in a limit of 10 min, the stage gets established. Images of holes are captured using low dose method that decrease or reduce irradiation damage to the specimen/sample by travelling to the position of object at low magnification[20].

3.6. Model Building and Analysis

Atomic models are built into EM maps to interpret density and produce atom representation of model for final nucleic acid or protein structure[21].

4. DEVELOPMENT OF CRYO-EM

Recent development with automatic image recording have elevated the amount of information of image to be processed. These large data sets can be managed by software using Graphics Processing Unit (GPU) or running on high end Control Processing Unit (CPU) based workstations[22]. The development of cryo-EM assures to maximize the extent and speed of automation and also to enhance the resolution which can be attained making technology convenient to determine different variety of biological structures. Recent developments of cryo-EM includes Cryo Electron Tomography or Sub-Tomogram Averaging (STA) and single particle analysis (SPA) that are used to analyse biological structures[23].

4.1. Sub-Tomogram Averaging (STA)/ Cryo-Electron Tomography

Sub-Tomogram Averaging also called as Cryo-Electron Tomography is concerned with the novel structures that are having no known symmetry resulting in accurate set of three dimensional conformations[24]. It starts from tomograms of same three dimensional structure that are chilled in vitreous ice along with its data collection by tilt series accompanied by tomographic reconstruction. It takes record of multiple views of sample and therefore collects the full dose of electron of complete tomographic tilt series on to the protein sample that are radiation sensitive. One of the disadvantages depending upon the tilt series is referred as missing wedge effect. Drawback of this method is the lower through put occurring due to tilt series acquisition[25,26].

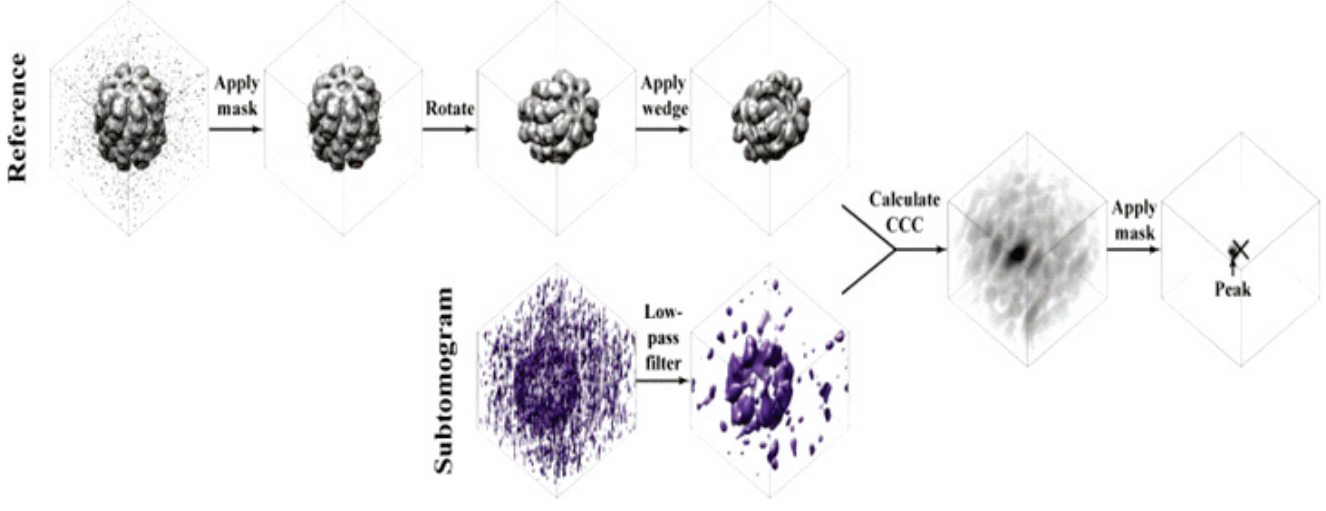

Fig. 2 – Sub Tomogram Averaging

4.2. Single Particle Analysis (SPA)

The principle of single particle analysis is based on averaging multiple views of several copies of same molecule. Therefore, SPA is also known as Single Particle Averaging. SPA data collection stratergy spreads the electron dose between several copies of identical biomolecules[27]. Due to freezing of individual sample in a random orientation, it is not necessary to tilt the specimen stage for complete sampling. SPA data sets comprises of 1000 of images, each of which consist of thousands of projections of biological molecule in various different orientations[25]

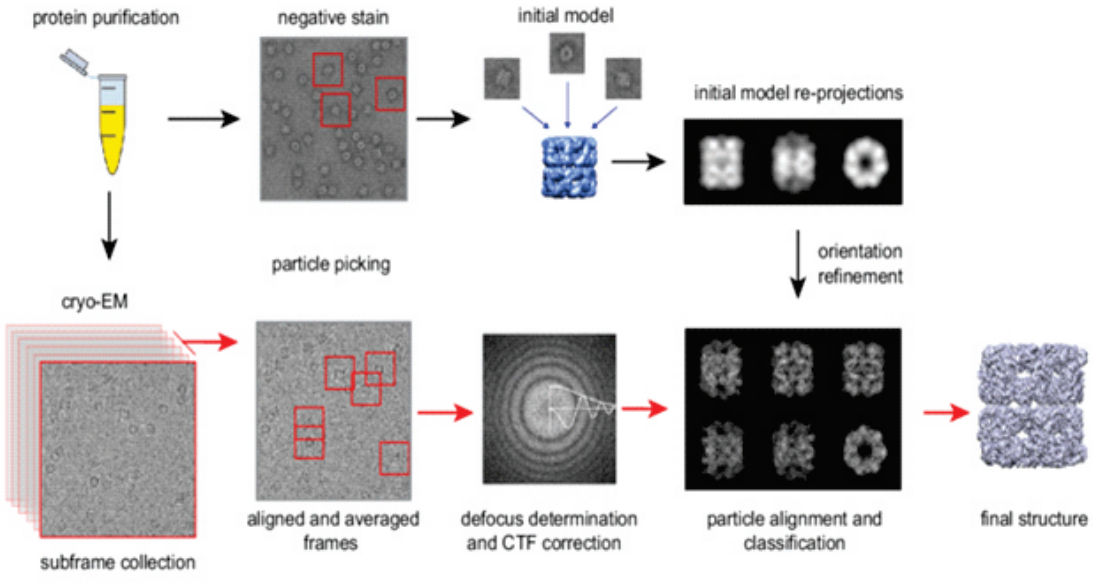

Fig. 3 – Single Particle Analysis

5. ADVANCED TECHNIQUES

For present advancement of cryo-EM for dynamic studies of biomolecular structures, many changes have been acquired.

5.1. Direct Electron Detectors (DED) –

High energy electrons in cryo-EM imaging are recoded using a detector including photographic film, Charged Coupled Device (CCD) cameras or Direct Electron Detectors (DED). Modern DED have activated the preservation of high resolution information in single movie frames. The combination of DED with high end electron microscopes improved their stability, optical quality and automation along with advances in software and computational power are moving a resolution revolution in a cryo-EM based structure determination[28]. All DED can operate at moderate frame rates (20-40 frames per second, example Direct Electron DE-20 and DE-64) to very high frame rates (400-800 frames per second, exampleGatan K2-IS) that makes possible to perform high resolution imaging. A good detector add no noise that can be expressed as Detective Quantum Efficiency (DQE)- the square of output signal to noise ratio (SNR') over input signal to noise ratio (SNRb")[29].

5.2. Image Processing Methods -

Due to constant improvement of software algorithms and utilization of computational hardware, image processing has been focusing on delivering high resolution three dimensional structure[30]. Techniques of image processing have make the best restoration of high resolution information from movie stack that results in output images that are used for further processing and image blurness can be decreased by alignment of single frames. Various algorithms and software packages have been advanced to calculate angular information from normal data set that are used for high resolution 3D reconstruction such as FREEALIGN, CRYOSPARC, e2 initial model module in EMAN2 and SIMPLE[31].

5.3. Phase Contrast and Phase Plates –

Contrast formation is the compilation of amplitude contrast due to inelastic interaction of beam with sample and phase contrast that is modulated by phase Contrast Transfer Function (CTF) of optical system of microscope. Amplitude

contrast fraction at energies (120-300keV) is only 5-10% and images are recorded as defocused condition to achieve phase contrast. The images in TEM was formed by interferences between the scattered waves whose phases were changed due to interaction with electric potential of object and unscattered waves that has never interacted with thin sample. Combination of scattered as well as unscattered waves in image plane causes rise in image with varying brightness and its features because of subtle phase differences and the CTF[32].

5.4. Energy Filters –

Energy Filters increase contrast by sieving out harmful contributions of out of phase inelasticity and multiply scattered electrons. An energy filter in cryo-EM acts like an optical prism. Two types of energy filters are commonly used as column type and bottom mount type. Column energy filter (omega and gamma type) has a symmetric optical design whereas bottom mount energy filters were more susceptible to image distortion due to its asymmetric design[32].

5.5. Advances in EM Automation and Data Handling –

The most remarkable improvements were mutispecimen auto ladders that permits cryo samples to stay for upto 5 days in autoladder with no contamination. Also, upgraded optics by attaching third condenser lens for easy parallel illumination, high coherence or cold field emission emitters (JEOL, Cryo-ARM)[33].

6. APPLICATIONS OF CRYO-EM

i. **In Drug Discovery** – Structural biology can be needful involving target identification, validation, hit generation, hit to lead and lead optimization, providing the mechanism of action and accessing drugability[34].

ii. **Gene Expression and Regulation** – Cryo-EM is used to determine the 3D structure of biomacromolecules in near native condition at close to atomic resolution and has ability to reveal conformations of dynamic molecular complexes.

iii. **Protein Synthesis and Degradation** – It is used to resolve high resolution structure of prokaryotic and eukaryotic cytoplasmic ribosomes[35].

iv. **Viruses and Protein Complexes** – The determination of their 3D structure helps to elucidate the mechanism of virus self assembly and infection but guide on drug design based on structure[36].

v. **Neurodegenerative disease related proteins** – Cryo-EM structure of human ” secretase recruited amyloid precursor provided important support for design of substrate specific inhibitors and pathogenesis of alzhiemer’s disease.

vi. It is an appropriate technique for visualization of radiation sensitive specimen[37].

7. ADVANTAGES OF CRYO-EM

- Very small samples are required for determination of its structure.
- The sample should be in solution form preventing contact with adhering surface.
- It is possible to view cells, cell organelles and macromolecules around 500kDa.
- It provides classification of large number of single molecular structures.
- It do not require crystallization of sample.
- It allows structural determination of large macromolecules in solution[38].

8. DISADVANTAGES OF CRYO-EM

- **Very low signal to noise ratio** – electron absorption of biological macromolecules including main building blocks as carbon, hydrogen, oxygen and nitrogen is very low and due to this there is low contrast of resulting images that make difficult to detect sample features[39].

- **Tilt imaging** – due to the cross section of frozen sample, it makes difficult to obtain images from a tilted specimen, because of this, it is essential that the specimen is not tilted to obtain better images[40].

9. LIMITATIONS OF CRYO-EM

- The lower molecular weight that is expected around 38kDa.
- The minimum detectable size of isolated biomolecules is constricted by the image contrast produced by the specimen tolerated electron dose.
- The permissible electron dose is constricted by damage to radiation of specimen depending on accelerating voltage estimated to be less than 20e/A2 at 200Kv for near atomic resolution.
- The low signal to noise ratio (SNR) on behalf of small mass cause electron scattering that eventually impairs identification and error free alignmnent of such particles in low dose images.
- There is a need of sample staining and dehydration so as to provide contrast and resist the vacuum inside the column of Em[41].

CONCLUSION

Cryo-EM is found to be a dynamic tool to explain the structure of biomolecules at near-atomic resolution followed by X-ray crystallography and NMR spectroscopy. Cryo-EM procedure involves creation of specimens by rapid freezing of biomolecules in solution and packed into the column of an electron microscope working at high vacuum and at low temperature so that the ice stays in amorphous state and to decrease the effect of radiation damage. The development of Cryo-EM assures to increase the extent and speed of automation and also to enhance the resolution which may be attained making technology convenient to determine different variety of biological structures.

LIST OF ABBREVIATIONS

CCD	Charged Coupled Devices
Cryo-EM	Cryo-Electron Microscope
CTF	Contrast Transfer Function
CPU	Control Processing Unit
DED	Direct Electron Detectors
DQE	Direct Quantum Efficiency
EM	Electron Microscope
GPU	Graphics Processing Unit
MD	Molecular Dynamics
NMR	Nuclear Magnetic Resonance
SPA	Single Particle Analysis
STA	Sub-Tomogram Averaging
SNR	Signal to Noise Ratio
TEM	Transmission Electron Microscope
3D	Three Dimensional

10. REFERENCES

1. Dubochet J, Adrian M, Chang JJ, et al. Cryo-electron microscopy of vitrified specimens. *Q Rev Biophys*. 1988;21(2): 129-228. doi:10.1017/s0033583500004297

2. Carroni M, Saibil HR. Cryo electron microscopy to determine the structure of macromolecular complexes. *Methods*. 2016;95:78-85. doi:10.1016/j.ymeth.2015.11.023

3. Mielanczyk L, Matysiak N, Michalski M, Buldak R, Wojnicz R. Closer to the native state. Critical evaluation of cryo-

techniques for Transmission Electron Microscopy: preparation of biological samples. *Folia Histochem Cytobiol*. 2014;52(1):1-17. doi:10.5603/FHC.2014.0001

4. Boland A, Chang L, Barford D. The potential of cryo-electron microscopy for structure-based drug design. *Essays Biochem*. 2017;61(5):543-560. doi:10.1042/EBC20170032

5. Czarnocki-Cieciura M, Nowotny M. Introduction to high-resolution cryo-electron microscopy. *Postepy Biochem*. 2016;62(3):383-394.

6. Hoenger A. High-resolution cryo-electron microscopy on macromolecular complexes and cell organelles. *Protoplasma*. 2014;251(2):417-427. doi:10.1007/s00709-013-0600-1

7. Lyumkis D. Challenges and opportunities in cryo-EM single-particle analysis. *J Biol Chem*. 2019;294(13):5181-5197. doi:10.1074/jbc.REV118.005602

8. Vénien-Bryan C, Li Z, Vuillard L, Boutin JA. Cryo-electron microscopy and X-ray crystallography: complementary approaches to structural biology and drug discovery. *Acta Crystallogr Sect F, Struct Biol Commun*. 2017;73(Pt 4):174-183. doi:10.1107/S2053230X17003740

9. Peplow M. Cryo-Electron Microscopy Reaches Resolution Milestone. *ACS Cent Sci*. 2020;6(8):1274-1277. doi:10.1021/acscentsci.0c01048

10. Milne JLS, Borgnia MJ, Bartesaghi A, et al. Cryo-electron microscopy—a primer for the non-microscopist. *FEBS J*. 2013;280(1):28-45. doi:10.1111/febs.12078

11. Shigematsu H. Electron cryo-microscopy for elucidating the dynamic nature of live-protein complexes. *Biochim Biophys acta Gen Subj*. 2020;1864(2):129436. doi:10.1016/j.bbagen.2019.129436

12. Serna M. Hands on Methods for High Resolution Cryo-Electron Microscopy Structures of Heterogeneous Macromolecular Complexes. *Front Mol Biosci*. 2019;6:33. doi:10.3389/fmolb.2019.00033

13. Murata K, Wolf M. Cryo-electron microscopy for structural analysis of dynamic biological macromolecules. *Biochim Biophys acta Gen Subj*. 2018;1862(2):324-334. doi:10.1016/j.bbagen.2017.07.020

14. Passmore LA, Russo CJ. Specimen Preparation for High-Resolution Cryo-EM. *Methods Enzymol*. 2016;579:51-86. doi:10.1016/bs.mie.2016.04.011

15. Cassidy CK, Himes BA, Luthey-Schulten Z, Zhang P. CryoEM-based hybrid modeling approaches for structure determination. *Curr Opin Microbiol*. 2018;43:14-23. doi:10.1016/j.mib.2017.10.002

16. Drulyte I, Johnson RM, Hesketh EL, et al. Approaches to altering particle distributions in cryo-electron microscopy sample preparation. *Acta Crystallogr Sect D, Struct Biol*. 2018;74(Pt 6):560-571. doi:10.1107/S2059798318006496

17. Danev R, Yanagisawa H, Kikkawa M. Cryo-Electron Microscopy Methodology: Current Aspects and Future Directions. *Trends Biochem Sci*. 2019;44(10):837-848. doi:10.1016/j.tibs.2019.04.008

18. Elbaum M. Quantitative Cryo-Scanning Transmission Electron Microscopy of Biological Materials. *Adv Mater*. 2018;30(41):e1706681. doi:10.1002/adma.201706681

19. Fujiyoshi Y. Low dose techniques and cryo-electron microscopy. *Methods Mol Biol*. 2013;955:103-118. doi:10.1007/978-1-62703-176-9_6

20. Vuloviæ M, Ravelli RBG, van Vliet LJ, et al. Image formation modeling in cryo-electron microscopy. *J Struct Biol*. 2013;183(1):19-32. doi:10.1016/j.jsb.2013.05.008

21. Binshtein E, Ohi MD. Cryo-electron microscopy and the amazing race to atomic resolution. *Biochemistry*. 2015;54(20):3133-3141. doi:10.1021/acs.biochem.5b00114

22. Merino F, Raunser S. Electron Cryo-microscopy as a Tool for Structure-Based Drug Development. *Angew Chem Int Ed Engl*. 2017;56(11):2846-2860. doi:10.1002/anie.201608432

23. Benjin X, Ling L. Developments, applications, and prospects of cryo-electron microscopy. *Protein Sci*. 2020;29(4) 872-882. doi:10.1002/pro.3805

24. Stewart PL. Cryo-electron microscopy and cryo-electron tomography of nanoparticles. *Wiley Interdiscip Rev Nanomed Nanobiotechnol*. 2017;9(2). doi:10.1002/wnan.1417

25. Taylor KA, Glaeser RM. Retrospective on the early development of cryoelectron microscopy of macromolecules and a prospective on opportunities for the future. *J Struct Biol*. 2008;163(3):214-223. doi:10.1016/j.jsb.2008.06.004

26. Wan W, Briggs JAG. Cryo-Electron Tomography and Subtomogram Averaging. *Methods Enzymol*. 2016;579:329-367. doi:10.1016/bs.mie.2016.04.014

27. Thonghin N, Kargas V, Clews J, Ford RC. Cryo-electron microscopy of membrane proteins. *Methods*. 2018;147: 176-186. doi:10.1016/j.ymeth.2018.04.018

28. Kühlbrandt W, Williams KA. Analysis of macromolecular structure and dynamics by electron cryo-microscopy. *Curr Opin Chem Biol*. 1999;3(5):537-543. doi:10.1016/s1367-5931(99)00005-8

29. Alnabati E, Kihara D. Advances in Structure Modeling Methods for Cryo-Electron Microscopy Maps. *Molecules*. 2019;25(1). doi:10.3390/molecules25010082

30. Frank J. Time-resolved cryo-electron microscopy: Recent progress. *J Struct Biol*. 2017;200(3):303-306. doi:10.1016/ j.jsb.2017.06.005

31. Mitra AK. Visualization of biological macromolecules at near-atomic resolution: cryo-electron microscopy comes of age. *Acta Crystallogr Sect F, Struct Biol Commun*. 2019;75(Pt 1):3-11. doi:10.1107/S2053230X18015133

32. Cheng Y, Grigorieff N, Penczek PA, Walz T. A primer to single-particle cryo-electron microscopy. *Cell*. 2015;161(3): 438-449. doi:10.1016/j.cell.2015.03.050

33. Auer M. Three-dimensional electron cryo-microscopy as a powerful structural tool in molecular medicine. *J Mol Med (Berl)*. 2000;78(4):191-202. doi:10.1007/s001090000101

34. Nwanochie E, Uversky VN. Structure Determination by Single-Particle Cryo-Electron Microscopy: Only the Sky (and Intrinsic Disorder) is the Limit. *Int J Mol Sci*. 2019;20(17). doi:10.3390/ijms20174186

35. Dillard RS, Hampton CM, Strauss JD, et al. Biological Applications at the Cutting Edge of Cryo-Electron Microscopy. *Microsc Microanal Off J Microsc Soc Am Microbeam Anal Soc Microsc Soc Canada*. 2018;24(4):406-419. doi:10.1017/ S1431927618012382

36. Luque D, Castón JR. Cryo-electron microscopy for the study of virus assembly. *Nat Chem Biol*. 2020;16(3):231-239. doi:10.1038/s41589-020-0477-1

37. Ognjenoviæ J, Grisshammer R, Subramaniam S. Frontiers in Cryo Electron Microscopy of Complex Macromolecular Assemblies. *Annu Rev Biomed Eng*. 2019;21:395-415. doi:10.1146/annurev-bioeng-060418-052453

38. Ruiz T, Erk I, Lepault J. Electron cryo-microscopy of vitrified biological specimens: towards high spatial and temporal resolution. *Biol cell*. 1994;80(2-3):203-210. doi:10.1111/j.1768-322x.1994.tb00931.x

39. Frank J. Advances in the field of single-particle cryo-electron microscopy over the last decade. *Nat Protoc*. 2017;12(2):209-212. doi:10.1038/nprot.2017.004

40. Yeates TO, Agdanowski MP, Liu Y. Development of imaging scaffolds for cryo-electron microscopy. *Curr Opin Struct Biol*. 2020;60:142-149. doi:10.1016/j.sbi.2020.01.012

41. Renaud J-P, Chari A, Ciferri C, et al. Cryo-EM in drug discovery: achievements, limitations and prospects. *Nat Rev Drug Discov*. 2018;17(7):471-492. doi:10.1038/nrd.2018.77

Peer Reviewed and Refereed Journal 2022 **(ISSN : 09726330)**

Rashtrasant Tukadoji Maharaj Nagpur University

SCIENCE JOURNAL 2022

Vol. : XV

REE carbonate- Galgenbergite [$CaREE_2(CO_3)_4.H_2O$] in Biotite Gneiss of Assam Meghalaya Gneissic Complex (AMGC), Chagligaon Area, Kamrup (Metro) District, Assam, North East India

M. Alam Siddiqui[1], Rajkumar R. Meshram[2*], Shatrughan Majhi[3], S. N. Bhagat[4], Hrushikesh Hari[5] and Niketan Khedkar[2#]

[1]Geological Survey of India, State Unit: Madhya Pradesh, Bhopal-462 016

[2]Regional Petrology Division, Geological Survey of India, Central Region, Nagpur-440 006.

[2#]Geological Survey of India, Central Region, Nagpur-440 006.

[3]Geological Survey of India, State Unit: Orissa, Bhuwaneshwar-751 012.

[4]Geological Survey of India, DGCO, New Delhi-110 062.

[5]Geological Survey of India, North Eastern Region, Guwahati-781 005.

Corresponding author :
rajkumar_meshram@rediffmail.com

ABSTRACT

REE carbonate Galgenbergite [$CaREE_2(CO_3)_4.H_2O$] or Ca (Ce, La, Nd)$_2$ $(CO_3)_4.H_2O$ have been reported from biotite gneiss of the Assam-Meghalaya Gneissic Complex (AMGC) of Chagligaon area of Kamrup (Metro) District, Assam and in the vicinity of Nongpo granitoids of Shillong Plateau.REE bearing carbonate phase occurs as individual small rounded to large anhedral mineral grains associated with plagioclase, sphene, biotite and quartz reflects their primary magmatic source. It is also present in the form of veinlets within deformed and fractured plagioclase indicating secondary hydrothermal activity. SEM and EPMA studies of seven mineral grain shows average REE composition of Ce_2O_3-29.06, La_2O_3-17.09, NdO_3-7.93 and Pr_2O_3-3.25 wt.%.The REE chondrite normalised diagram shows steeply inclined LREE enrichment pattern with negative Sm and positive Dy anomalies. Petrography and SEM/EPMA studies, REE carbonate minerals shows signatures of both primary magmatic (highly fractionated) and secondary hydrothermal processes. This REE carbonate Galgenbergite is being reported first time from the AMGC of North Eastern India.

Key-words : REE, LREE, Galgenbergite, Hydrothermal, Biotite gneiss, AMGC.

Introduction

Rare Earth Element (REE) occurs in a wide range of igneous, sedimentary and metamorphic rocks and their economic viability is strongly prejudiced by its REE minerals and their genesis. The rock forming minerals normally host (REEs), where they substitute for major ions. Higher concentrations of REE are required to form their own minerals (Moller, 1986). In nature, rare earth elements are primarily associated with silicate, carbonate, phosphate and halide.The significant geological concentration of rare earth mineral have been established in carbonatites, alkaline igneous complexes (Drew et al., 1990;Yuan et. al., 1992), pegmatite's or due to deposition by hydrothermal activity (Chao et. al., 1997), by weathering of the host mineral (Long and others, 2010), in beach placers and in clay minerals (Cheng Xu et. al., 2017).There are over 250 minerals which contain REE as important constituents in their chemical formula and crystal structure. These minerals typically comprise the bulk of the REE in a rock. REE are also hosted in minor amounts in the mafic rock-forming minerals such as amphiboles and biotite, where they substitute for major

cations of comparable radius and charge (Dostal, 2017). REE-bearing minerals tend to be dominated by either LREE or HREE, although each REE can be present.

The REE occurrences/deposits are known till date from diverse geological environments in India and are radioactive due to the presence of uranium and/or thorium in REE-bearing minerals. The suitable geological environment includes carbonatites, alkaline to sub-alkaline felsic rocks, pegmatite and hydrothermal deposits and inland stream placers. There are several other relatively minor natural sources also and possibilities of recoveries of REE from industrial wastes like phosphogypsum, coal fly ash, bauxite residue (red mud), waste electrical and electronic materials (Yamuna Singh, 2020). In north eastern India, four carbonatite complexes have been recognised in the Shillong Plateau, Karbi Anglong (erstwhile Mikir) -Hills area - e.g., Samchampi, Sung Valley, Jasra and Barpung, (Kumar et al., 1996; Nag et al., 1999). REE bearing minerals reported in Sung Valley carbonatites are bastnäsite-(Ce), ancylite-(Ce), belovite-(Ce), britholite-(Ce) and pyrochlore which are associated with calcite and apatite having an average total REE concentration of 0.103 wt% in bed rock (Sadiq et. al., 2014). The existence of REEs in the form of allanite, zircon, sphene, apatite etc. has been reported in parts of Nongpoh granite, Ri-Bhoi district, Meghalaya (Sadique et al., 2014). Rare earth element abundances reported in some A-type Pan-African granitoids in the Kathalguri (Dizu valley) and Panbari-Geleki (Kaziranga) granitoids of Karbi Hills, North East India (Mazumdar and Dutta, 2014). Borah et al., 2019 reported monazite and xenotime from metapelitic rocks and their U–Th–Pb total ages of both from central Shillong Meghalaya Gneissic Complex.

REE carbonates are important groups of compounds usually found in carbonatite deposits (e.g. Bayan Obo, China; Mountain Pass, USA; Castor and Hedrick, 2006). The REE-carbonates consist of bastnäsite, synchesite, parasite (with F and without H_2O), ancylite, galgenbergite and calcioancylite (without F and with H_2O), (Schoneveld et al., 2015; Huston et al., 2016), with the dominant REE in each of these being La, Ce, or Nd. Galgenbergite [$CaREE_2(CO_3)_4.H_2O$] or Ca (Ce, La, Nd)$_2(CO_3)_4.H_2O$ is a REE carbonate mineral, first reported by Hollerer (1997 and 1998).Walter et al., 2013 described crystal structure and composition in detailed where it is found within albite-chlorite schist as aggregates in association with siderite, ancylite-(Ce), pyrite and calcite. La-Nd-rich galgenbergite associated withcalcioancylite (Ca,Sr)(Ce,Nd)(CO3)2(OH)·H2O) and parisite (Ca(Ce,La)2(CO3)3F2) within fluorapatite vein deposit hosted by orthogneiss was reported from Nolans Bore REE deposit, Australia (Huston et al., 2016).Sr-rich galgenbergite (Sr(La,Ce)2(CO3)2·2(H2O) associated with bastnäsite (La,Ce)CO3F),roentgenite (Ca2(La,Ce)3(CO3)5F3 within secondary quartz, and are associated with sericite alteration of feldspar and chloritization of aegirine in trachyte is reported from Toongi rare metal deposit, NSW, Australia (Spandler and Morris, 2016). Another occurrence of Sr-rich galgenbergite is reported in a quartz–carbonate–chlorite matrix of sulphide layers & in core of pyrite nodules, Talgan Cu–Zn Massive Sulphide Deposit, Southern Urals (Ayupova et al., 2019). In the present study, REE bearing carbonate phase is identified through SEM and EPMA studies within biotite gneiss of AMGC.The main objective of this study is to report this REE carbonate phase and comment on its possible genesis.

Geological framework

The geological assemblages of Assam are considered as the northern extension of the Garo Hills of Shillong Plateau and is invariably called as Archaean Crystalline Inselbergs (Laskar, 1949) and northward drown of Shillong plateau (Gansser, 1964). The rocks of AMGC is the north and north eastern extension of the Proterozoic rocks of Meghalaya Plateau or Shillong plateau in Assam (G. S. I. 2009).The Assam Meghalaya Gneissic Complex (AMGC) occur as an E–W trending, oblong, uplifted horst-block and interpreted to be part of the north eastern extension of the Indian Peninsular Shield and is separated from the main mass of Peninsular India by Tertiary-Quaternary sediments of Ganga Brahmaputra valley and Cretaceous Rajmahal volcanics (Gupta and Sen, 1988). The Shillong plateau is considered as the detached portion of Eastern Ghats Mobile belt (Crawford, 1974) or Chotanagpur Gneissic Complex (Desikachar, 1974) (Fig.1A; after Mazumdar, 1976; Nandi, 2001; Srivastava and Sinha, 2004).The plateau comprises the Neoarchean-Proterozoic to Early Paleozoic (2.6"0.5 Ga) basement gneissic rocks (Bidyananda and Deomurari, 2007; Kumar et al., 2017; Chatterjee et al., 2007, 2011; Ghosh et al., 2005), the Paleo-Mesoproterozoic NE-SW trending intracratonic Shillong basin constituting metasedimentary supracrustal rocks of the Shillong Group (Mitra, 1998;

Bidyananda and Deomurari, 2007; Yin et al., 2010). Proterozoic-Early Paleozoic (881 to 479 Ma) equigranular to porphyritic coarse grained granite-granodiorites plutons (Mylliem, Kyrdem, Nongpoh, South Khasi, Rongjeng granitoids etc.) intruding the basement gneisses and the Shillong Group of rocks (Crawford, 1969; Mazumdar, 1976; Chimote et al., 1988; Van Breeman et al., 1989; Ghosh et al., 1991, 1994, 2005; Sadiq et al., 2014b). Basic volcanics of Sylhet /Mikir traps of Cretaceous age occurs as concordant to discordant bodies within the Shillong group of rocks.

The study area is the part of AMGC/Precambrian Gneissic Complex in the Kamrup (Metro) district, Assam and in the vicinity of known Nongpoh granitoids. The rocks of AMGC comprises of ortho and para gneiss, schist, migmatite, amphibolite intruded by felsic (granitoids) and mafic rocks (epidiortie, metadolerite). The area of investigation comprises of biotite gneiss, migmatite, non-porphyritic granite, epidiorite, porphyritic granite, pegmatite and quartz veins (Fig. 1B; after Majhi and Siddiqui, 2016).The tongue and apophyses of porphyritic granite and non-porphyritic granite is present in biotite gneiss which clearly shows their intrusive nature. The enclaves of biotite gneiss and non-porphyritic granite is also observed at several places in porphyritic granite which indicate younger intrusive phase (Majhi and Siddiqui, 2016).

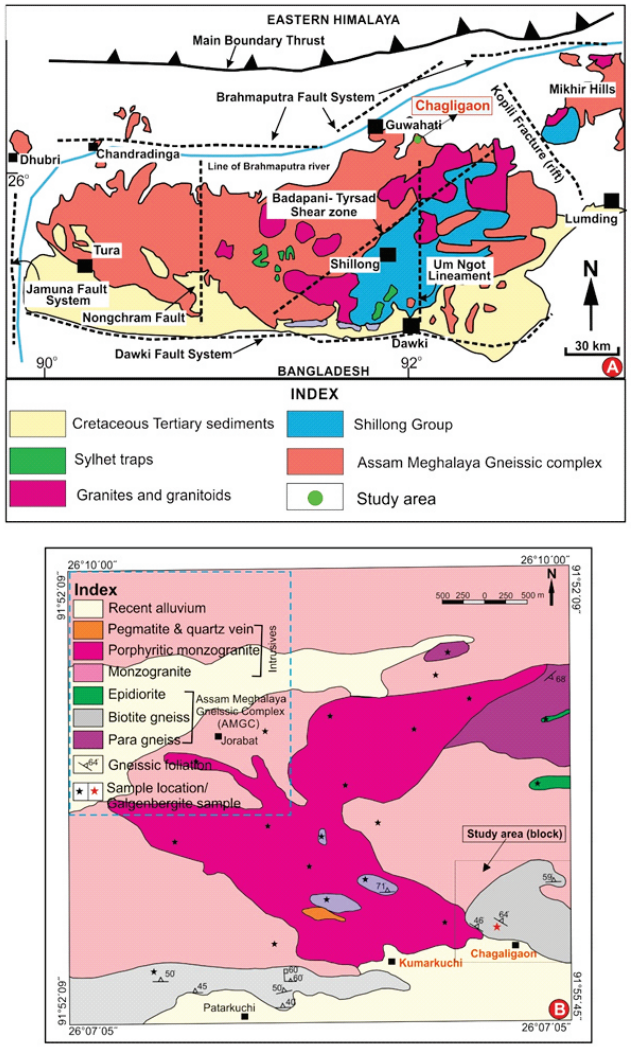

Fig.1 (A) Regional Geological and tectonic map of Assam Meghalaya Gneissic Complex (AMGC) showing location of Chagligaon area (after Mazumdar, 1976; Nandi, 2001; Srivastava and Sinha, 2004), and (B) Geological map of Kumarkuch-Chagligaon block, Kamrup (metro district), Assam (after Majhi and Siddiqui, 2016). Where red star is sample collection containing Galgenbergite.

Petrography of Biotite gneiss

Biotite gneiss from the study area is medium to coarse grained and composed of quartz, plagioclase, K-feldspar, biotite and/or amphibole with alternate felsic and mafic bands defining the gneissosity (Fig. 2A). The general strike of the foliation/gneissosity is E-W with dip amount varying from 40°to 60° towards north. It is intruded by quartzo-feldspathic veins, which show ptygmatic folds (Fig. 2B).In thin section study, the rock is medium to coarse grained and shows hypidiomorphic granular, myrmekitic and perthitic textures. Mineralogically, it consists of plagioclase, microcline, quartz, hornblende and biotite as major minerals. Whereas, titanite (sphene), zircon and magnetite occurs as accessory minerals. Plagioclase is subhedral to anhedral, exhibits polysynthetic twinning and sericitic alteration. Quartz occurs as small anhedral to rounded grains. Sphene is brown, anhedral and showing alteration to fine grained, earthy, yellow aggregate of leucoxene (Fig. 2C).Microcline is the dominant K-feldspar, which is displaying cross-hatch twinning, perthite texture with exsolved lamellae of plagioclase and bordered on either side by myrmekitic intergrowth of quartz in plagioclase (Fig. 2D). Biotite is tabular, pleochroric from yellow to yellow and showing perfect cleavage in one direction. Whereas, basal section of biotite is suhbedral to anhedral showing dark greasy yellow colour and without cleavage (Fig. 2 E). Quartz is in the form of anhedral crystals with diffuse margin along grain boundaries. Small grains of brownish hornblende as intercumulas phase along quartz and microcline are seen. The REE bearing mineral phase (galgenbergite) isanhedral with fractures and high relief and associated with leucoxene and biotite (Fig. 2Fand G). Apatite is accessory minerals and occurs profusely. Three forms of apatite are observed such as prismatic, tabular and acicular. Prismatic apatite is enclosed by quartz and tabular apatite is enclosed within alkali feldspar (Fig. 2 H), acicular apatite crystal and tabular apatite crystal are enclosed within alkali feldspar showing poikilitic texture (Fig. 2 I).

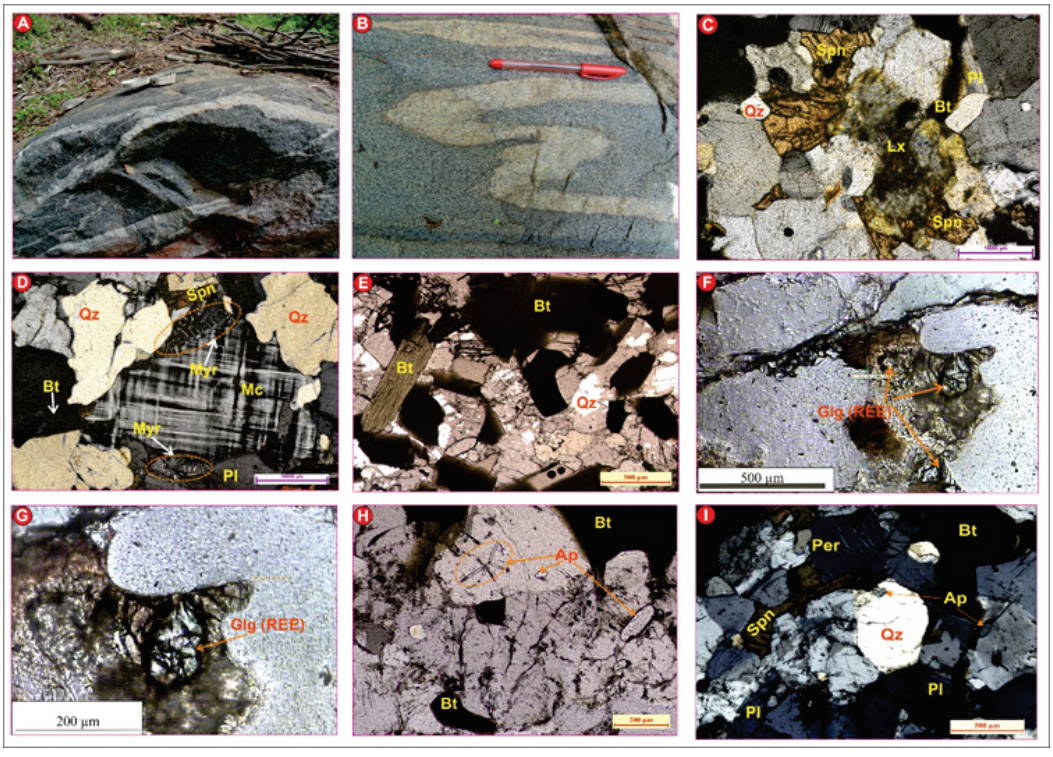

Fig. 2 (A) & (B) Field photographs of biotite gneiss with quartzo-feldspathic veins. Photomicrographs of biotite gneiss exhibits (C) Brown sphene (titanite) showing alteration into leucoxene (CPL), (D) Microcline exhibit cross hatch twinning and myrmekite intergrowth on either side (CPL), (E) Tabular crystal and dark yellow biotite (PPL), (F) and (G) Anhedral to rounded grains of Galgenbergite, (H) Cluster of apatite needles (PPL), and (I) Small apatite grain enclosed in large quartz crystal (CPL). **Abbreviation used are:** Pl-Plagioclase, Bt-Biotite, Spn-Sphene, Qz-Quartz, Lx-Leucoxene, Mc-Microcline, Myr-Myrmekite, Glg-Galgenbergite, REE-Rare Earth Element, Ap-Apatite, Per-Perthite (after Whitney and Evans, 2010).

Analytical Techniques

SEM study : Polished sections of the samples are studied under scanning electron microscope. Preliminary semi-quantitative data and BSE images of minerals has been carried out by Scanning Electron Microscope (SEM) using EVO-40 Series; Carl Zeiss coupled with energy dispersive spectrometry (EDS), oxford instrumentation at Palaeontology Division, Geological Survey of India, CHQ, Kolkata. During scanning bright mineral phase identified and semi-quantitative data with EDX extracted for the brighter mineral phase and associated mineral.

EPMA Study : Mineral compositions were determined using well-polished and carbon coated thin sections by CAMECA SX-100 electron microprobe at EPMA Lab., NCEGR, Geological Survey of India, CHQ, Kolkata, equipped with wavelength-dispersive spectrometers using 20 kV acceleration voltage and 30 nA current having beam size of 1 micron. REE glass (Synthetic) standards were used for REE analysis.

Mineral chemistry of Galgenbergite (REE carbonate)

Galgenbergite is anhedral and occurs as individual small rounded to large anhedral mineral grains associated with plagioclase, sphene, biotite and quartz reflects their primary magmatic source (Fig.3 A-C). It is also present in the form of veinlets within deformed and fractured plagioclase indicating secondary hydrothermal activity (Fig.3 D). The SEM graphs along with semi-quantitative data (LREE enriched such as La, Ce, Nd along with Ca) is given in Fig.3 E to H.

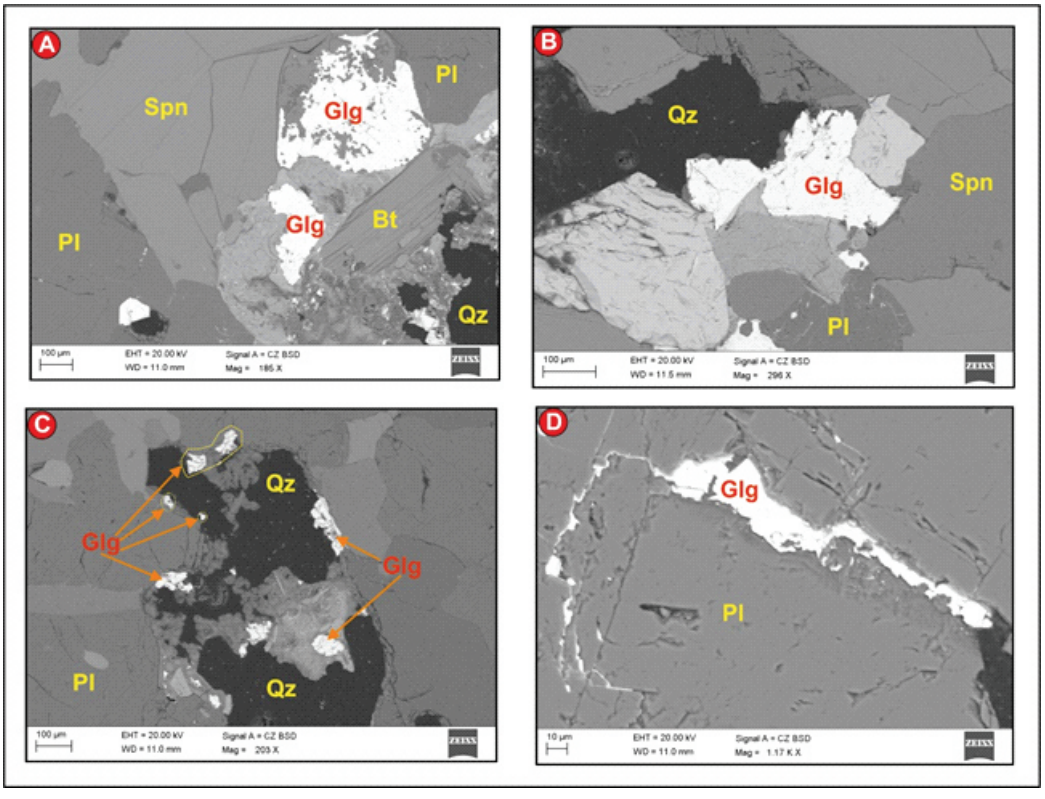

Fig. 3 BSE image showing (A) to (C) Small rounded to large anhedral mineral grains of Galgenbergite, and (D) Occurrence of galgenbergite along fracture in between plagioclase.

In EPMA, seven REE mineral grains from the sample has been analysed and their composition is given in (Table 1). The composition is indicating 5.95 to 7.11 wt.% of CaO, P_2O_5 varying from 0.21 to 0.39 wt.% and low amount of SiO_2 and Al_2O_3.The average composition of seven mineral grains shows 29.06 wt% Ce_2O_3, 17.09 wt% La_2O_3, 7.93 wt%NdO_3 and

3.25 wt%Pr_2O_3. EPMA data suggested that REE is not associated with oxide, silicate, phosphate and halide. Carbonate analysis could not be done due to carbon coating on the sample. Therefore, while carrying out stoichiometry calculation, CO_2 (26.776 wt. %) and H_2O (6.694 wt. %) has been taken into consideration. The empirical formula used (based on Ca + REE3.0) is $Ca_{0.76}(REE)_{2.41}$ (Si Al P & Pb)$_{0.04}$ $(CO_3)_4.H_2O$ (Walter et al., 2013).

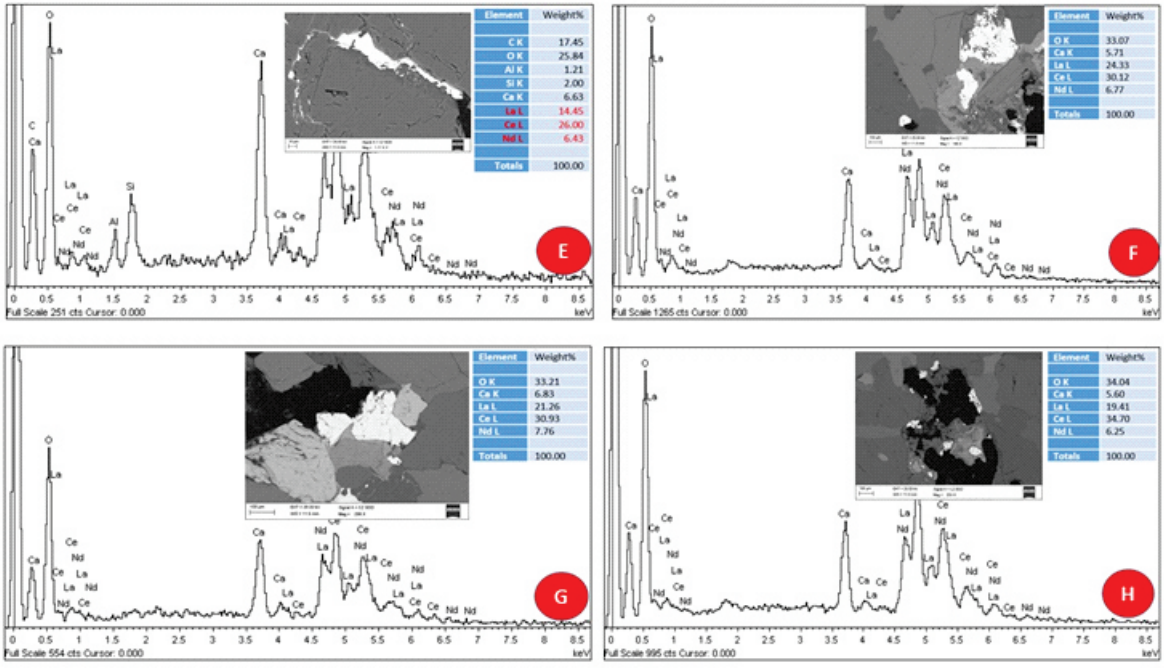

Fig. 3 (E) to (H) BSE micrograph with EDX analysis of REE carbonate phase.

The EPMA REE oxide data are converted into REE elements (Table 2). The EPMA data and EDX peak indicate presence of rare earth elements (La, Ce and Nd) along with Ca (Fig. 3 I) and REE elements plotted in chondrite normalised diagram of Sun and Mc Donough, 1989 (Fig. 3 J).The REE diagram shows steeply inclined LREE enrichment pattern with negative Sm and positiveDy anomalies. The LREE enrichment and negative Sm anomaly indicate fractionation of feldspar, apatite and carbonate minerals, whereas positive Dy anomaly indicate amphibole fractionation.

Table 1 : EPMA analysis of seven grains containing galgenbergite in biotite gneiss.

Analysis	1	2	3	4	5	6	7
SiO_2	0.09	0.07	0.28	0.22	0.24	0.57	0.17
Al_2O_3	0.01	0.01	0.03	0.02	0.01	0.24	0.08
P_2O_5	0.39	0.22	0.21	0.27	0.38	0.17	0.22
CaO	**5.95**	**6.4**	**6.78**	**7.11**	**6**	**6.17**	**6.18**
FeO	Nd	Nd	Nd	Nd	Nd	Nd	Nd
Y_2O_3	Nd	Nd	Nd	Nd	Nd	Nd	Nd
La_2O_3	**18.63**	**17.27**	**15.42**	**17.13**	**17.06**	**16.25**	**17.87**
Ce_2O_3	**28.42**	**27.97**	**28.65**	**31.29**	**30.09**	**28.59**	**28.41**
Pr_2O_3	**3.16**	**3.12**	**3.28**	**3.46**	**3.24**	**3.26**	**3.25**
Nd_2O_3	**7.14**	**7.9**	**8.53**	**8.62**	**7.66**	**7.84**	**7.79**
SmO	0.42	0.42	0.58	0.52	0.44	0.44	0.49
Dy_2O_3	0.07	0.06	0.02	0.06	0.02	0.07	0.09
Gd_2O_3	1.75	1.78	1.48	1.66	2.07	1.59	1.52
PbO	0.04	0	0.01	0	0.09	0.02	0.05
ThO_2	0.02	0	0.01	0.05	0.03	0.03	0
U_2O_3	0	0	0	0	0	0	0
CO_2	Nd	Nd	Nd	Nd	Nd	Nd	Nd
H_2O	Nd	Nd	Nd	Nd	Nd	Nd	Nd
Total	**66.07**	**65.23**	**65.3**	**70.42**	**67.33**	**65.25**	**66.11**

Nd-Not detected

Table 2 : REE element data obtained from REE Oxide determined in EPMA.

Elements	La	Ce	Pr	Nd	Sm	Dy	Gd
PS-8 (Biotite gneiss)	2.27	4.19	0.48	1.22	0.08	0.00	0.20
	2.52	4.58	0.50	1.23	0.07	0.01	0.22
	2.51	4.40	0.47	1.09	0.06	0.00	0.27
	2.39	4.18	0.47	1.12	0.06	0.01	0.21
	2.63	4.15	0.47	1.11	0.07	0.01	0.20
	2.74	4.16	0.46	1.02	0.06	0.01	0.23
	2.54	4.09	0.45	1.13	0.06	0.01	0.24

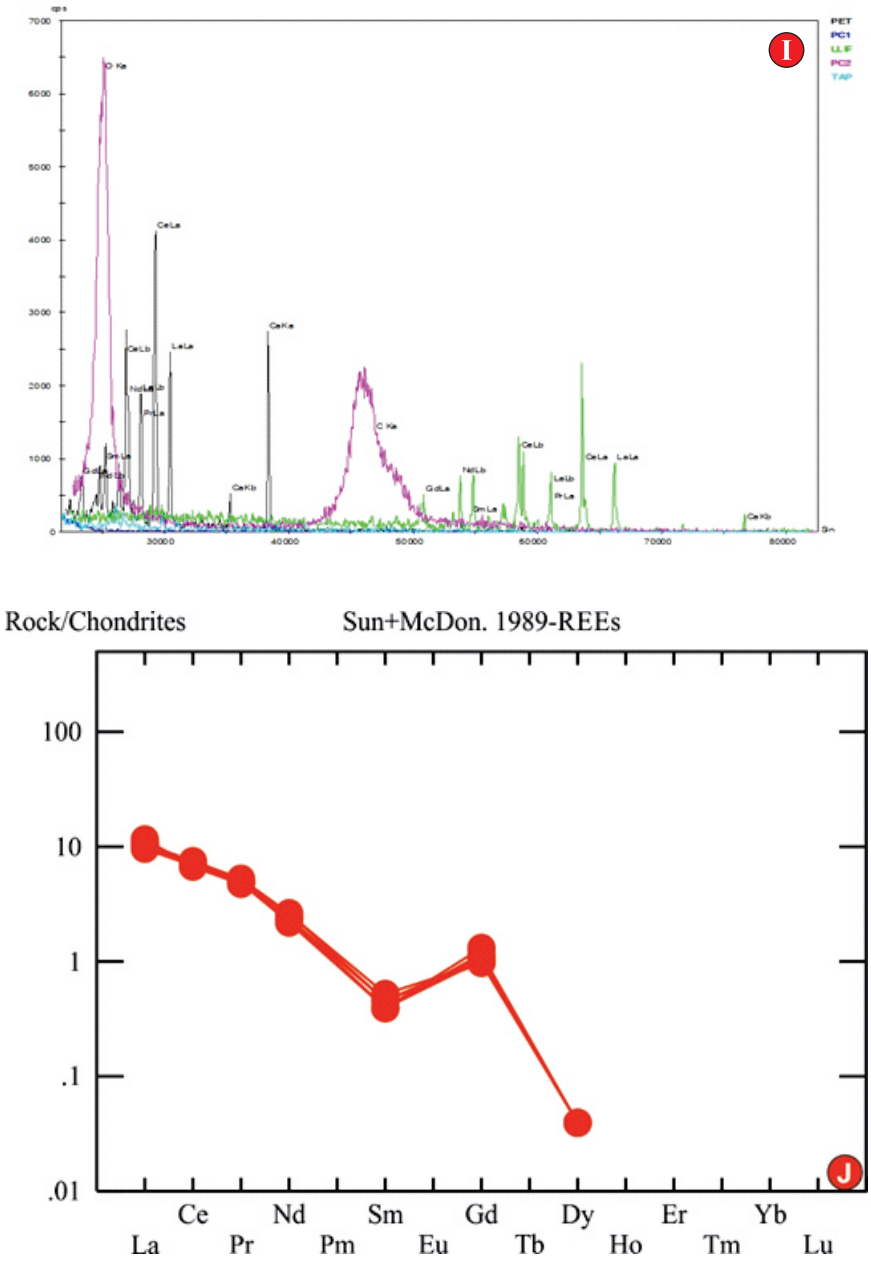

Fig. 3 (I) EDX peaks indicate presence of rare earth elements (La, Ce and Nd) In EPMA, and (J) REE chondrite normalised diagram indicate LREE enrichment (after Sun and Mc Donough, 1989).

Genesis of Galgenbergite

The geochemical behaviour and genesis of rare earth element (REE) ores are less understood in view of hydrothermal or magmatic fluids involvement in their genesis or combination of other factors or weathering of REE minerals and simultaneous enrichment in weathering crust (Anenburg et al., 2018). The formation of REE carbonates from hydrothermal systems related to carbonatites has been discussed by Hogarth et al. (1985), Andersen (1986), Zaitsev (1996), and Andrade et al.,1999. In hydrothermal systems, the REE can migrate as complexes; it has been demonstrated both empirically and experimentally (Balashov and Krigman, 1975; Flynn and Burnham, 1978; Bilal and Becker, 1979; Bulakh et al., 1998), that the anions F^{+}, Cl^{+}, OH^{+}, $CO3^{2+}$, $SO4^{2+}$ and $PO4^{3+}$ can be effective ligands for

complexing the REE. Additionally, the REE could be accumulating in a residual fluid, because in general, there is a low mineral/melt partition coefficient for the REE (Sokolov, 2005). The REE mineralization related to peralkaline igneous rock mainly formed by the fractional crystallization of REE rich magmatic fluid (Chakmouradin and Zaitsav, 2012; Dostal, 2017).

REE can be redistributed *in situ* into different minerals (commonly LREE; Andrade et al., 1999;Ruberti et al., 2008; Doroshkevich et al., 2009; Cooper et al., 2015; Moore et al. 2015; Trofanenko et al., 2016; Andersen et al., 2017). The REE are also considered hydrothermally mobile based on theoretical and experimental studies (e.g., Williams-Jones et al., 2012;Migdisov& Williams-Jones, 2014;Migdisov et al., 2016). Alteration of apatite releases crystal-bound REE into hydrothermal systems, making them available for transport by aqueous fluids. The mineral assemblage and composition of the secondary alteration can reveal whether the REE were redistributed or recrystallized in situ, leached and possibly deposited elsewhere, enriched or depleted by supergene processes, etc. Also, studies of secondary alteration chemistry can reveal differential mobilities of REE (e.g., LREE versus HREE) (Chakmouradian et al., 2017).

The processes responsible for many features observed in REE ore deposits are not easily determined. Significantly, the difference between igneous versus post-magmatic genesis, or the nature of the mineralizing and modifying fluids or melts, remains in argument (Anenburg et al., 2018). The granitoids of Kathalguri, Karbi hills, Assam contains good concentration of xenotime, allanite, monazite, sphene, bastansite, apatite and zircon as REE bearing mineral phases (Mazumdar and Dutta, 2014). This indicates evolved nature of the magma with high degree of differentiation leading to REE enrichment after parent magmas were generated due to anatexis of older crust (Mazumdar and Dutta, 2014). Similarly, the REE values and accessory mineral phases such as sphene, apatite, allanite, monazite and zircon in Nongpoh granites adjacent to study area indicate highly fractionated magmatic melt (Sadiq et al., 2014). In view of above aspects and in present study, sphene and apatite present as REE bearing minerals and alteration of sphene as observed in petrography study might be causative source for galgenbergite formation.In EPMA, galgenbergite occurred as individual, small rounded to large anhedral mineral grains and secondary veinlets which shows both primary and secondary signatures for their formation and might be derived from magmatic source and latter remobilisation or alteration trough hydrothermal fluids along fractures. The enrichment of LREE (La, Ce, Nd) and especially Ce_2O_3 and CaO in EPMA and SEM studies indicate that galgenbergite (REE carbonate mineral). This REE mineral grains are also devoid of radioactive minerals (U &Th) and fluorine in their EPMA composition, which indicate highly fractionated magmatic melt responsible for their genesis.

Conclusions

Among many carbonate bearing REE minerals discovered,galgenbergite do not possess fluorine in its composition and radioactive elements like U and Th which makes it more valuable and hazard free REE mineral. This REE carbonate is being first time reported in AMGC as per referred literatures in this MS. This carbonate bearing REE mineral might be formed from highly fractionated and differentiated primary magmatic melt and re-mobilised through secondary hydrothermal processes. The LREE enrichment, negative Sm anomaly indicate fractionation of feldspar, apatite and carbonate minerals, whereas positive Dy anomaly indicate amphibole fractionation in the source magma. This finding of REE carbonate bearing mineral opens a scope for search and evaluation of REE mineralization potential in different varieties of granitoids and gneisses in the area as formulating and taking new projects.

Acknowledgments

This work was the part of annual field season programme of GSI, SU: Assam, NER, Guwahati (FS 2015-16). The authors express their sincere gratitude to the then ADG &HOD, GSI, NER, Shillongfor providing logistics to carry out field work and analytical facility.The DDG, SU: Assam, NER, Guwahati is acknowledged for his constant encouragement during the fieldwork and laboratory studies. The authors are grateful to the anonymous reviewer for critical comments and suggestions which help in improving the quality of manuscript.

References

Andersen, A. K., Clark, J. G., Larson, P. B., Donovan, J. J., 2017. REE fractionation, mineral speciation, and supergene enrichment of the Bear Lodge carbonatites, Wyoming, USA. Ore Geol. Rev. 89, 780–807.

Andersen, T., 1986. Compositional variation of some rare earth minerals from the Fen complex (Telemark SE Norway): Implications for the mobility of rare earths in a carbonatite system. Mineral. Mag. 50, 503-509.

Andrade, F.R.D., Mo¨ller, P., Lu¨ders, V., Dulski, P., Gilg, H. A. 1999. Hydrothermal rare earth elements mineralization in the Barra do Itapirapua carbonatite, southern ˜Brazil: behaviour of selected trace elements and stable isotopes (C, O). Che. Geol. 155, 91–113.

Anenburg, M., Burnham, A. D., Mavrogenes, J.A., 2018. REE redistribution textures in altered fluorapatite: symplectites, veins, and phosphate-silicate-carbonate assemblages from the Nolans Bore p-ree-th deposit, Northern Territory, Australia. The Can. Mineral. 56, 331-354.

Ayupova, N. R., Maslennikova, V. V., Filippovaa, K. A., 2019. REE Geochemistry and Mineralogy in Ores of the Talgan Cu–Zn Massive Sulfide Deposit, Southern Urals. Doklady Ear. Sci. 487 (2), 973–975.

Balashov, Y. U. A., Krigman, L. D., 1975. The effects of alkalinity and volatiles on rare-earth separation in magmatic systems. Geochem. Int. 12 (6), 165–170.

Bidyanand, M., Deomurari, M. P., 2007 Geochronological constraints on the evolution of Meghalaya massif, northeastern India: an ion microprobe study. Curr. Sci. 93 (11),1620- 1623.

Bilal, B. A., Becker, P., 1979. Complex formation of trace elements in geochemical systems. II: Stability of rare earths Cuoro complexes in Cuorite bearing model system at various ionic strength. Jour. Inorg. Nucl. Chem. 41, 1607–1608.

Borah, P., Hazarika, P., Mazumdar, A. C., Rabha, M., 2019. Monazite and xenotime U–Th–Pb total ages from basement rocks of the (central) Shillong–Meghalaya Gneissic Complex, Northeast India. Jour. Earth Syst. Sci. 128 (68), 1-20.

Bulakh, A. G., Le Bas, M. J., Wall. F., Zaitsev, A. N. 1998.Ancylite-bearing carbonatites of the Seblyavr massif, Kola peninsula, Russia. NeuesJahrb. Mineral. Monatsh. 4,171–192.

Castor, S. B., Hedrick, J. B., 2006. Rare earth elements, in: J. ElzeaKogel, N.D. Trivedi and J.M. Barker (Eds.),Industrial Minerals and Rocks. Society for Mining, Metallurgy and Exploration, Littleton, Colorado, USA, pp. 769-792.

Chakmourdian, A. R.,Zaitsav, A. N., 2012. Rare earth mineralization in igneous rocks: Source and Processes. Elements 8, 347–353.

Chakmourdian, A.R., Reguir, E.P., Zaitsev, A.N., Coue¨slan, C., Xu, C., Kynicky´, J., Mumin, A. H., Yang, P., 2017. Apatite in carbonatitic rocks: Compositional variation, zoning, element partitioning and petrogenetic significance. Lithos. 274–275, 188–213.

Chao, E.C.T., Back, J. M., Minkin, J., Tatsumoto, M., Wang, J., Conrad, J. E., Makee, E. H., Hou, Z., Meng, Q. S., 1997. The sedimentary carbonate hosted giant Bayan Obo REE-Fe-Nb ore deposit of Inner Mongolia, China: a cornerstone example for giant polymetallic ore deposits of hydrothermal original. US Geol. Soc. Bul. 2143, 43-65.

Chatterjee, N., Bhattacharya, A., Duarah, B. P., Mazumdar, A. C., 2011. Late Cambrian Reworking of Paleo-Mesoproterozoic Granulites in Shillong-Meghalaya Gneissic Complex (Northeast India): Evidence from PT Pseudosection Analysis and Monazite Chronology and Implications for East Gondwana Assembly. The Journal of Geology. 119 (3), 311-330.

Chatterjee, N., Mazumdar, A. C., Bhattacharya, A., Saikia, R.R., 2007. Mesoproterozoic granulites of the Shillong-Meghalaya Plateau: Evidence of westward continuation of the Prydz Bay Pan-African suture into Northeastern India. Precamb. Res.152, 1-26.

Cheng Xu., Kynicky, J., Smith, M. P., Kopriva, A., Brtnicky, M., Urubek, T., Yang, Y., Zhao, Z., He, C., Song, W., 2017. Origin of heavy rare earth mineralization in South China, *Nat Commun.* 8.

Chimote, J.S., Pandey, B.K., Bagchi, A. K., Basu, A.N., Gupta, J. N., Sarsawat, A. C., 1988.Rb-Sr whole-rock isochron age for the Myllium granite, Khasi Hills, Meghalaya. Fourth Natl. Symp. Mass spectrometry, Bangalore, EPs- 9/1-9/4.

Cooper, A. F., Collins, A. K., Palin, J. M., Spratt, J., 2015. Mineralogical evolution and REE mobility during crystallisation of ancylite-bearing ferrocarbonatite, Haast River, New Zealand. Lithos. 216–217, 324–337.

Crawford, A. R., 1969. India, Ceylon and Pakistan: New age data and comparison with Australia. Nature. 223, 80-84.

Crawford, A. R., 1974. Indo-Antarctica, Gondwana Land and pattern of the distortion of a granulite belt. Tectonophysics. 22, 141-157.

Desikachar, S.V., 1974. A review of the tectonic and geological history of eastern India in terms of plate tectonic theory. Geol. Soc. India. 15, 137-149.

Doroshkevich, A. G., Viladkar, S.G., Ripp, G. S., Burtseva, M. V., 2009. Hydrothermal REE mineralization in the AmbaDongar carbonatite complex, Gujarat, India. Can. Mineral. 47, 1105–1116.

Dostal, J., 2017. Rare Earth Element Deposits of Alkaline Igneous Rocks.Resources. 6 (34), 1-12.

Drew, L. J., Qingrun, M., Weijun, S., 1990. The Bayan Obo iron-rare-earth-niobium deposits, Inner Mongolia, China.Lithos, 26 (1–2),43-65.

Flynn, R. T., Burnham, C. W. 1978. An experimental determination of rare earth partition coefficients between a chloride containing vapour phase and silicate melts. Geochim. Cosmochim. Acta. 42, 685–701.

Gansser, A., 1964.Geology of Himalaya. Wiley Interscience, 289p.

Ghosh, S., Bhalla, J. K., Paul, D. K., Sarkar, A., Bishui, P. K., Gupta, S. N., 1991. Geochronology and geochemistry of granite plutons from East Khasi Hills, Meghalaya. Geol. Soc. Ind. 37, 331-342.

Ghosh, S., Chakraborty, S., Paul, D.K., Bhalla, J.K., Bishui, P.K., Gupta, S. N., 1994. New Rb-Sr isotopic ages and geochemistry of granitoids from Meghalaya and their significance in middle to late Proterozoic crustal evolution. Indian Minerals. 48, 33-44.

Ghosh, S., Fallick, A. E., Paul, D. K., Potts, P. J., 2005. Geochemistry and origin of Neoproterozoic granitoids of Meghalaya, northeast India: implications for linkage with amalgamation of Gondwana Supercontinent. Gond. Res. 8, 421-432.

Geological Survey of India., 2009. Geology and Mineral resources of Assam. Misc. Publ. No.30 pt-IV. V. 2 (i), 7-9.

Gupta, R.P., Sen, A. K., 1988.Imprints of Ninety-East Ridge in the Shillong Plateau, Indian Shield. Tectonophysics. 154,335-341.

Hogarth, D. D., Hartree, R., Loop, J., Solberg, T. N., 1985 Rare-earth element minerals in four carbonatites near Gatineau, Quebec. Am. Mineral. 70, 1135-1142.

Hollerer, C. E., 1997. Ca(REE)2(CO3)4·H2O, einneues Mineral ausdemEisenbahntunnelGalgenbergbei St. Michael obLeoben, Steiermark, Österreich. Unpublished diploma thesis, Karl-Franzens-University of Graz, 160p.

Hollerer, C. E., 1998 Ca(REE)2(CO3)4·H2O, einneues Mineral aus der Steiermark. Mitt Österr Mineral Ges. 143, 200-201.

Huston, D. L., Maas, R. Cross, A., Hussey, K. J., Mernagh, T. P., Fraser, G., Champion, D.C., 2016. The Nolans Bore rare-earth element-phosphorus-uranium mineral system: geology, origin and post-depositional modifications. Miner Deposita, 1-26.

Kumar, D., Mamallan, R., Diwedy, K. K., 1996. Carbonatite magmatism in northeast India: Jour. Southeast Asian Ear. Sci. 13, 145–158.

Kumar, S., Rinob, V., Hayasakac, Y.,Kosuke Kimura.C., ShunmugamRajud, KentaroTeradae, Manjari Pathak., 2017. Contribution of Columbia and Gondwana Supercontinent assembly- and growth-related magmatism in the evolution of the Meghalaya Plateau and the Mikir Hills, Northeast India: Constraints from U-Pb SHRIMP zircon geochronology and geochemistry. Lithos. 277, 356-375.

Laskar, B., 1949. Notes on the mineral investigations in the Binji Raj Estate, Goalpara district, Assam. Unpub. GSI. Rep. FS 1948-49.

Long, K. R., Gosen, B. S., Foley, N. K., Cordier, D., 2010. The Principal Rare Earth Elements Deposits of the United States-A Summary of Domestic Deposits and A Global Perspective. U.S. Geol. Sur. Scientific Investigations Report. 96p.

Majhi, S., Siddiqui, M. A., 2016. Investigation for W, Sn and REE in Kumarkuchi and Chagaligaon, Kamrup (Metro) district, Assam. Geol. Surv. India. Unpubl. Rep. FS 2015-16.

Mazumdar, D., Dutta, P., 2014. Rare earth element abundances in some A-type Pan-African granitoids of Karbi Hills, North East India. Current Science. 107 (12), 2023-2029.

Mazumder, S. K., 1976. A summary of the Precambrian Geology of Khasi Hills, Meghalaya. Geol. Surv. India. Misc. Publ. 23 (2), 311-334.

Migdisov, A. A., Williams-Jones, A. E., 2014. Hydrothermal transport and deposition of the rare earth elements by fluorine-bearing aqueous liquids. MineraliumDeposita. 49, 987–997.

Migdisov, A. A., Williams-Jones, A. E., Brugger, J., Caporuscio, F.A., 2016. Hydrothermal transport, deposition, and fractionation of

the REE: Experimental data and thermodynamic calculations. Chemical Geology. 439, 13– 42.

Mitra, S. K., 1998. Structure, sulphide mineralization and age of the Shillong group of rocks, Meghalaya,in: M.S. Krishnan Commemorative Nat. Sem. 1 and 2 Nov., Kolkata, pp.118-119.

Moller, P., 1986. Rare earth mineral deposits and their industrial importance,*in:* Moller, P., Cerny, Saupe, F., (Eds.), Lanthanides, Tantalum and Niobium. Jour. Earth Syst. Sci. Proceedings of a workshop in Berlin, November 1986, Springer-Verlag.

Moore, M., Chakmourdian, A.R., Mariano, A. N., Sidhu, R., 2015. Evolution of rare-earth mineralization in the Bear Lodge carbonatite, Wyoming: Mineralogical and isotopic evidence. Ore Geol. Rev. 64, 499– 521.

Nag S., Sengupta, S. K., Gaur, R. K., Absar, A.1999.Alkaline rocks of Samchampi-Samteran, District Karbi-Anglong, Assam, India, *Proc. Indian Acad. Sci. (Earth Planet. Sci.),* 108, No. 1, 33-48.

Nandi, D. R., 2001. Geodynamics of the Northeastern India and the adjoining Region. ACB. Publ. 209p.

Ruberti, E., Enrich, G.E.R., Gomes, C. B.,Comin-Chiaramonti, P., 2008. Hydrothermal REE fluorocarbonate mineralization at Barra Do Itapirapua˜, a multiple stockwork carbonatite, Southern Brazil. Can. Mineral. 46, 901–914.

Sadiq, M., Ranjith, A.,Umrao, R. K., 2014. REE Mineralization in the Carbonatites of the Sung Valley Ultramafic-Alkaline-Carbonatite Complex, Meghalaya, India. Cent. European Jour. Geosci. 6 (4), 457- 475.

Sadiq, M., Umrao, R.K., Dutta, J, C., 2014b. Occurrence of rare earth elements in parts of Nongpoh granite, Ri-Bhoi district, Meghalaya. Current Science. 106 (2), 162-165.

Schoneveld, L., Spandler, C., Hussey, K., 2015. Genesis of the Central Zone of the Nolans Bore rare earth element deposit, Northern Territory, Australia. Contrib. Mineral. Petrol. 170 (11),1-23.

Singh, Y., 2020. Rare Earth Element Resources: Indian Context. Society of Earth Scientists Series, Springer. 395p.

Sokolov, S. V., 2005. Physical and chemical conditions for ore formation of carbonatites; Explor. Conser. Res. 4, 29–32 (in Russian).

Spandler, C., Morris, C., 2016. Geology and genesis of the Toongi rare metal (Zr, Hf, Nb, Ta, Y and REE) deposit, NSW, Australia, and implications for rare metal mineralization in peralkaline igneous rocks. Contrib. Mineral. Petrol. 171(104), 1-24.

Srivastava, R. K., Sinha, A. K., 2004. The Early Cretaceous Sung Valley ultramafic-mafic-alkaline-carbonatite complex, Shillong Plateau, Northeastern India: Petrological and genetic significance. Mineral. Petrol. 80, 241-263.

Van Breeman, O., Bowes, D. R., Bhattacharjee, C. C., Chowdhary, P. K., 1989. Late Proterozoic-Early Proterozoic Rb-Sr whole rock and mineral ages for granite and pegmatite, Goalpara, Assam, India. Geol. Soc. Ind. 34 (1), 89-92.

Walter, F., Bojar, H., Hollerer, C. E., 2013. The crystal structure of galgenbergite-(Ce), $CaCe_2(CO_3)_4'"H_2O$. Miner. Petrol. 107, 189–199.

Whitney, D. L., Evans, B. W., 2010. Abbreviations for names of rock-forming minerals. Amer. Mineral. 95, 185-187.

Xin, Y. Z., Ge, B., Chenyu, W., Zhongqin, Z., Xianjiang, Y., 1992. Geological features and genesis of the Bayan Obo REE ore deposit, Inner Mongolia, China. Applied Geochem.7 (5), 429-442.

Yin, A., Dubey, C.S., Webb, A. A. G., Kelty, T. K., Grove, M., Gehrels, G.E., Burgess, W. P., 2010. Geologic correlation of the Himalayan orogen and Indian craton: part1. Structural geology, U–Pb zircon geochronology, and tectonic evolution of the Shillong Plateau and its neighbouring regions in NE India. Geol. Soc. Am. Bull. 122,336-359.

Zaitsev, A. V., 1996. Rhombohedral carbonates from carbonatites of the Khibina Massif, Kola Peninsula, Russia. Can. Mineral. 34, 453–468.

Peer Reviewed and Refereed Journal 2022 **(ISSN : 09726330)**

Rashtrasant Tukadoji Maharaj Nagpur University

SCIENCE JOURNAL 2022

Vol. : XV

Design, Synthesis and Biological Screening of Novel 3-[2-(9*H*-carbazole-9-*yl*)-2-oxoethylamino]-2-arylthiazolidine-4-one as Antimicrobial Agent

Prafulla M. Sabale*, Lata C. Potey, Nusrat B. Sayyad, Vidya Sabale[1]

Department of Pharmaceutical Sciences, Rashtrasant Tukadoji Maharaj Nagpur University, Nagpur-440033 M.S.

[1]Dadasaheb Balpande College of Pharmacy, Besa, Nagpur-440034 M S.

Corresponding author email : prafullasable@yahoo.com

ABSTRACT :

In this study, design and synthesis of novel *3-[2-(9H-carbazole-9yl)-2-oxo-ethylamino]-2-arylthiazolidine*-4-one was started with carbazole as basic pharmacophore and evaluated for antimicrobial activity. Carbazole is an important scaffold known to be associated with several biological activities including antimicrobial activities. Incorporation 4-oxothiazolidine moiety in carbazole moiety may lead to a new series of antimicrobials compounds. After molecular docking, active compound were synthesized and screened for *in vitro* antimicrobial activity against *candida albicans* and gram-positive and Gram-negative bacterial strains such as *S. aureus, B. subtilis, E. coli.* All compounds were shown good antimicrobial activity at 25(µg/ml)–510 (µg/ml). The molecular docking studies demonstrated that compound **2e** shown ligand protein interaction with glide score **(-6.213, -8.1122)** followed by compound **2d (-5.120, -7.854)** against (1KZN, 1EA1).

Keywords : Molecular Docking, Carbazole, Oxothiazolidine, Antimicrobial activity, Antifungal activity.

INTRODUCTION

Carbazole is tricyclic heterocyclic aromatic organic compound.[1] It is consider as potential building block for the synthesis of bioactive compounds[2] and prominent pharmacophore which mostly found as essential in many plant origin compound like alkaloid.[3] Carbazole and it's derivatives have attributed promising biological activities such as anti-inflammatory,[4] anti-tumor, anti-diabetic,[5] anti-oxidant,[6] anti-tubercular, anti-bacterial,[7] anti-fungal,[8] and anti-histaminic activity.[9] According to Drissa new carbazole alkaloids named calothrixins from cell extracts of *Cyanobacterial Calothrix* species. They display a unique indolo [3, 2-j] phenanthridine ring system, it exerts *in vitro* growth inhibitory effects in antiplasmodial and anticancer assays at nanomolar concentrations.[11] Kucukguzel reported synthesis, characterization and screening of antimicrobial,[10] antituberculosis, antiviral and anticancer activity of novel 1,3-thiazolidine-4-ones derived from 1-[2-(benzoylamino)-4-(methylthio) butyryl]-4-alkyl/arylalkyl thiosemicarbazides.[11] Molecular docking leads an important tool for drug design and discovery.[12] S. Vasanthkumar and coworkers in their studies have shown synthesis of 1, 4-naphthoquinone derivatives containing carbazole-6, 11-dione moiety and the molecular docking of all the synthesized compounds were carried out by using (version 8.5, Schrodinger, LLC) and compounds were evaluated for *In vitro* antibacterial studies against different Gram-positive and Gram-negative bacteria.[13,14]

EXPERIMENTAL :

Molecular Docking Study

Molecular docking study was carried out by Schrödinger software (Maestro10.5) in order to develop selective antimicrobial agents. The molecule were docked on the *DNA gyrase* enzyme (PDB ID: 1KZN) for antimicrobial activity and *Lanosterol 14á-demethylase* enzyme for antifungal activity (PDB ID: 1EA1) retrieved from the Protein Data Bank (www.rscb.org).[15]

Ligand Preparation

Two dimensional structures were drawn in 2D Sketcher in Maestro workspace using build panel. Three dimensional ligand preparation was done by using LigPrep panel application and optimize the structure by minimizing its energy through OPLS-3 force field.

Protein Preparation and Minimization

In Protein preparation X ray crystalline structures of *DNA Gyrase* enzyme and *Lanosterol 14-á-Demethylase* enzyme (proteins) were imported from Protein Data Bank with PDB ID (1KZN &1EA1) respectively. Through protein preparation Wizard, protein structures were refined minimized and optimized.

Receptor Grid Generation

Grid generation required to be perform prior to running a virtual screen with glide. The shape and properties of the receptor has represented in a grid by field that provides progressively more accurate scoring of the ligand poses.

Validation of Protein

Validation of *DNA Gyrase* and *Lanosterol 14*-a-*Demethylase* protein to test the reliability and reproducibility of the docking protocols for the study was shown by Ramachandran Plot.

Molecular Docking

The ligand docking was done flexibly using Standard Precision (SP) mode of Glide module and further refinement was done by using extra precision (XP) mode. The ligand docking process helps to predict ligand conformation and orientation within a target binding site and thus results in an accurate structural modeling and correct prediction of activity of ligands.[16]

Chemical Work

Intermediate **1(a-f)** were obtained by reacting chloroacetyl chloride (10 ml, 0.09 moles) with carbazole (5.00 g, 0.02 mole) in dry acetone by refluxing for 4 hrs to get 1-(9H-carbazole-9-yl)-2-chloroethanone, further reacted with hydrazine hydrate (1.73 ml, 0.05 moles) in ethanol: dioxane 18:2 v/v (9:1 v/v) to get 1-(9*H*-Carbazole-9-*yl*)-2-hydrazinylethanone, further reacted with substituted benzaldehyde. Compound **2 (a-f)** were synthesized by cyclization of compound 1 with thioglycolic acid.[15]

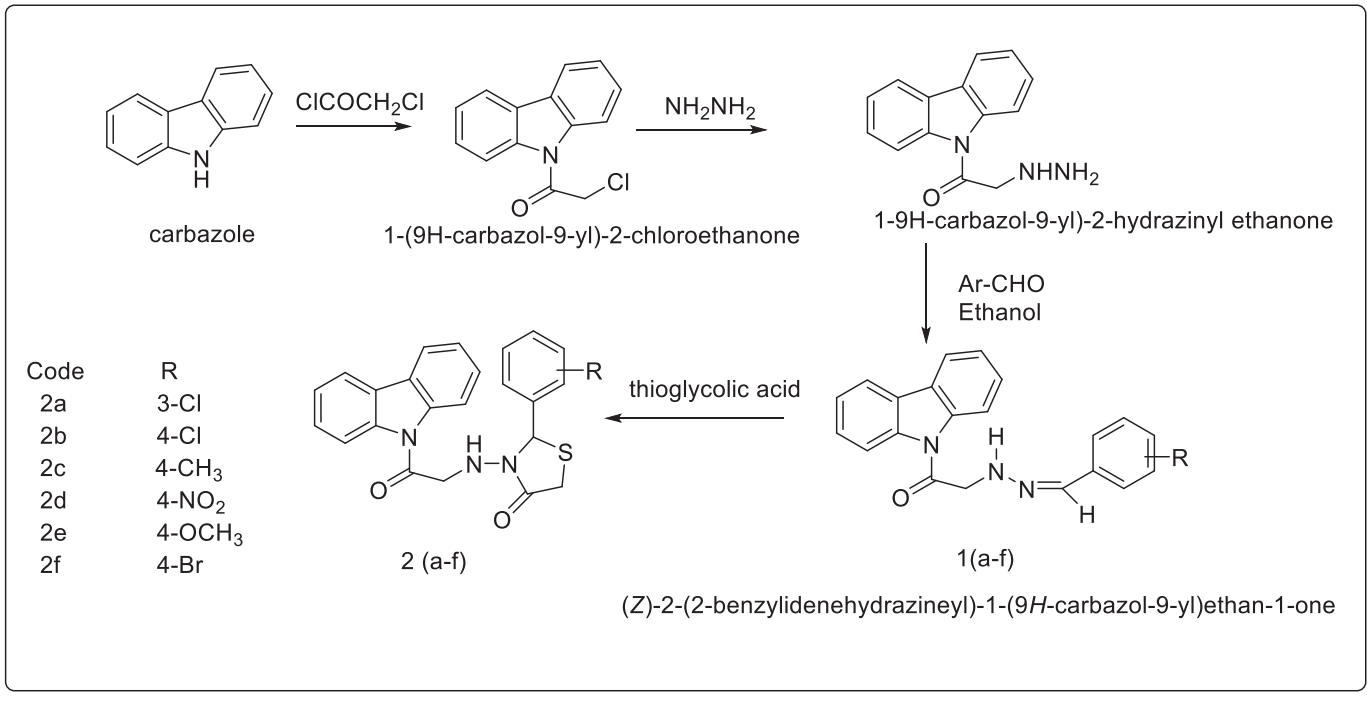

Fig. 1 : Sythetic scheme

Biological Work

The microbiological assay is based upon measurement of Minimum Inhibitory Concentration (MIC) to check the lowest concentration of the compound at which growth of microorganism was completely inhibited. The assay was tested against *S. aureus* (Gram positive), *B. Subtilis* (Gram positive), *E. Coli* (Gram Negative) bacteria's and *C. albicans* fungi including Streptomycin and Chloramphenicol as reference standard for antibacterial & antifungal activity respectively. Procedure for all over the assay was followed as per reported procedure.[17]

RESULTS and DISCUSSION :

Synthesis and Characterization

Naturally carbazole is an alkaloid, tricyclic scaffold with large number of pharmacological profile. The current work emphasized on the synthesis of novel carbazole derivatives as antibacterial and antifungal activities with molecular docking studies.[17,18] Our scheme was initiated with carbazole which was condensed with reactive chloroacetyl chloride with formation of 1-(9*H*-carbazol-9-yl)-2-chloroethanone, reactive towards hydrazine hydrates with formation of second intermediate (1-9*H*-carbazol-9-yl)-2-hydrazinyl ethanone) further second intermediate reacted with substituted benzaldehyde, with formation of compound **1(a-f)**, having benzylidenehydrazineyl moiety. Aldehyde is very reactive towards hydrazine and carbazole doesn't has any substitution from starting, so the formation of compound **1(a-f)** was confirmed by TLC, and was further confirmed by spectral analysis. After having compound **1 (a-f)**, a series of novel carbazole derivatives **(2a-2f)**, were synthesized and characterized. All carbazole derivatives **(2a-2f)** prepared by stirring compound **1(a-f)** with thioglycolic acid, ethylidine cyclized to thiazolidinone scaffold in final carbazole derivatives. Completion of reaction was confirmed by TLC, crystallized with suitable solvent and finally purified with silica gel (60-120 mesh) column chromatography.[19] Analysis of compounds were done by spectral analysis that is elemental analysis, IR, ^{1}HNMR, ^{13}C NMR, MS, was supporting successful analysis of **(2a-2f**).

IR spectra of compound **1 (a-f)** showed absorbance at 3345 cm^{-1} for secondary amine and peaks at 3356 cm^{-1}

(asymmetric stretching) and 3313 cm^{-1} (symmetric stretching) for primary amine were disappeared, C-N stretching observed at 1245 cm^{-1}, peak for carbonyl was observed at 1660 cm^{-1},in 1(a-f) additional peaks observed at 810 cm^{-1} for C-Cl, 1260 cm^{-1} for methyl, 1550 cm^{-1} for NO_2, 2810 cm^{-1} for methoxy, 660 cm^{-1} for C-Br. IR spectra of compounds 2 (a-f) showed absorbance at 3332 cm^{-1} for secondary amine, C-N stretching observed at 1240 cm^{-1}, Carbonyl peak observed at 1670 cm^{-1} in compound 2a additional peak observed at 840 cm^{-1} for C-Cl, in NMR signal shift at downfield region, H-5 and H-3 of phenyl ring appeared at same ppm at d 7.8 as three doublet due to substitution of 4-Cl. Three doublets at d 7.38 corresponds to H-2 and H-6 due to substitution of thiazolidinone moiety. In Mass spectrum base peak was appeared at 436 (MH^+). In compound 2d, absorbance at 1560 cm^{-1} observed in IR spectrum for C-NO_2, in NMR signal shifted towards downfield region, where H-5 and H-3 appeared at same ppm, at d 7.54 as three doublets, due to the substitution of C-NO_2 at C-4 of phenyl ring, Three doublets at d 8.20 corresponds to H-2 and H-6 due to substitution of thiazolidinedione moiety. In mass spectrum base peak appeared at 447 (MH^+). In compound 2e, absorbance at 2850 cm^{-1} observed in IR spectrum for C-OCH_3, in NMR, signal shifted towards downfield region, where H-5 and H-3 appeared at same ppm, at d 6.89 as three doublets, due to the substitution of C-OCH_3at C-4 of phenyl ring, Three doublets at 5R 7.83 corresponds to H-2 and H-6 due to substitution of thiazolidinedione moiety. In mass spectrum base peak appeared at 430 (MH^+). In compound 2f, absorbance at 680 cm^{-1} observed in IR spectrum for C-Br, in NMR, signal shifted towards downfield region, where H-5 and H-3 appeared at same ppm, at d 7.17 as three doublets, due to the substitution of C- Br at C-4 of phenyl ring, Three doublets at d 7.85 corresponds to H-2 and H-6 due to substitution of thiazolidinedione moiety. In mass spectrum base peak appeared at 481 (MH^+).

3-((2-(9H-carbazol-9-yl)-2-oxoethyl)amino)-4-(4-chlorophenyl)thiazolidin-2-one ($C_{23}H_{18}ClN_3O_2S$) (2b) **:** C,63.37; H, 4.16; Cl, 8.13; N,9.64; O,7.34; S,7.35; IR (KBr, cm^{-1}) 3132, 1621, 1400, 820, ^{1}H NMR (DMSO)5Ř˙Ţ:7.54(2H, phenyl proton, ddd, *J*=8.41, 1.52, .55 Hz), 7.56 (2H, Phenyl proton, ddd, *J*=8.41, 1.42, .55 Hz), 6.3 (1H, triazole proton, s), 3.85(2H, Methylene, s), 3.81(1H, triazole proton, s), 4.2 (s, NH), 7.8(2H, Phenyl proton, ddd, *J*=7.94, 1.94, .52 Hz), 7.38 (2H, Phenylproton, td, *J*=7.94, 2.57 Hz), 7.53 (2H, Phenylproton, ddd, *J*=7.98,7.72, 1.94 Hz), 7.98 (2H, Phenylproton, dddd, *J*=7.72, 2.57, .5, .55Hz), ^{13}CNMR (DMSO) 5Ř˙Ţ: 115.6, 124.3, 119.8, 121.4, 125.1, 138, 125.1, 138, 121.4, 119.8, 124.3, 115.6, 168.3, 50, 164.9, 32.7, 62.0, 141.6, 127.2, 127.2, 128.6, 128.6, 132.3, MS(m/z) 436 (MH^+), m.p.: 177-180^{0}C.

3-((2-(9H-carbazol-9-yl)-2-oxoethyl)amino)-2-(4-nitrophenyl)thiazolidin-4-one, ($C_{23}H_{18}O_4N_4S$)(2d) **:** C, 61.87; H, 4.06; N, 12.55; O, 14.33; S, 7.18 IR (KBr, cm^{-1}) 3133, 1601, 1400, ^{1}H NMR (DMSO)5Ř˙Ţ: 4.2 (s, NH), 5.92 (s CH Thiazole proton), 3.80, 3.70 (s, CH_2 Thiazole proton), 7.54, 8.20, (ddd, (*J*= 8.4,1.3,0.5 Hz) 4H Phenyl proton), 7.97(2H, Phenyl proton, ddd, (*J*= 7.94, 1.94, .52 Hz), 7.38(2H, phenyl proton, td, (*j*=7.94, 2.56 Hz), 7.53(2H, Phenyl proton, ddd, (*J*= 7.98, 7.72, 1.94 Hz), 7.9 (2H, phenyl proton, dddd, (*j*=7.72, 2.56, 0.52, 0.5 Hz), 3.85(s, 2H, CH_2), ^{13}CNMR (DMSO) 5Ř˙Ţ: 115.6, 124.3, 119.8, 121.4, 125.1, 138, 125.1, 138, 121.4, 119.8, 124.3, 115.6, 168.3, 49.3, 168.8, 35.9, 64.1, 145.3, 129.6, 123.8, 146.3, 123.8, 129.5 MS(m/z) 447 (MH^+), m.p.: 166-170^{0}C.

3-((2-(9H-carbazol-9-yl)-2-oxoethyl)amino)-2-(4-methoxyphenyl)thiazolidin-4-one ($C_{24}H_{21}N_3O_3S$) (2e) *:* C, 66.80; H, 4.91; N, 9.74; O, 11.12, S, 7.42, IR (KBr, cm^{-1}) 3112, 1619, 1404, 1215, , ^{1}H NMR (DMSO)5Ř˙Ţ:4.2 (s, NH), 5.92 (s CH Thiazole proton), 3.80, 3.70 (s, CH_2 Thiazole proton), 6.89, 7.83, (ddd, (*J*= 8.8,1.1,0.5 Hz) 4H Phenyl proton), 3.81 (s, OCH_3), 7.97(2H, Phenyl proton,ddd, (*J*= 7.94, 1.94, .52 Hz), 7.38(2H, phenyl proton, td, (*j*=7.94, 2.56 Hz), 7.53(2H, Phenyl proton, ddd, (*J*= 7.98, 7.72, 1.94, Hz), 7.9 (2H, phenyl proton, dddd, (*j*=7.72, 2.56, 0.52, 0.5 Hz), 3.85(s, 2H, Ch_2), ^{13}CNMR (DMSO) 5Ř˙Ţ:119.8,124.3, 115.6, 138.0, 121.4, 125.1, 125.1, 121.4, 119.8, 128.6, 124.3, 126.9, 139.2, 115.6, 138.0, 61.5, 168.3, 49.3, 168.8, 42.8, 126.9, 128.6, 127.1, 55.8, 159.5, 114.8, 114.8, 131.9, 131.9, 127.1 MS(m/z) 430 (MH^+), m.p.: 160-162^{0}C.

3-((2-(9H-carbazol-9-yl)-2-oxoethyl)amino)-2-(4-bromophenyl)thiazolidin-4-one ($C_{23}H_{18}BrN_3O_2S$)(2f) **:** C, 57.51; H, 3.78; Br, 16.63; N, 8.75; O, 6.66; S, 6.67,IR (KBr, cm^{-1}) 3133, 1601, 1400, 601,^{1}H NMR (DMSO)5Ř˙Ţ: 4.2 (s, NH), 5.92 (s CH Thiazole proton), 3.80, 3.70 (s, CH_2 Thiazole proton), 7.17, 7.85, (ddd, (*J*= 8.4,1.3,0.5 Hz) 4H Phenyl proton),

7.97(2H, Phenyl proton, ddd, (*J*= 7.94, 1.94, .52 Hz), 7.38(2H, phenyl proton, td, (*j*=7.94, 2.56 Hz), 7.53(2H, Phenyl proton, ddd, (*J*= 7.98, 7.72, 1.94 Hz), 7.9 (2H, phenyl proton, dddd, (*j*=7.72, 2.56, 0.52, 0.5 Hz), 3.85(s, 2H, CH_2), ^{13}CNMR (DMSO) 5Ř˙Ţ: 115.6, 124.3, 119.8, 121.4, 125.1, 138, 125.1, 138, 121.4, 119.8, 124.3, 115.6, 168.3, 49.3, 186.8, 35.9, 64.1, 138.2, 130.9, 131.5, 130.9, 131.5, 121.5 MS(m/z) 481 ($MH^{\cdot}$), m.p.: 169-172^{0}C.

Molecular Docking

In molecular Modelling, molecular docking is one of the tool which predict the possible orientation of one molecule to another molecule, after bound to each other to form the stable complex, where free binding energy is calculated in the form of Glide score. In this work molecular docking of total 13 compounds was done in Schrodinger software (Maestro 10.5v) against DNA Gyrase (PDB-1KZN) and Lanosterol 14-á-Demethylase proteins (PDB-1EA1) for antibacterial and antifungal activities respectively.[20] All compounds have shown good interaction with imported proteins against standard. Compound **2e with** C-OCH_3 substitution have shown highest G-Score (-6.213), (-8.112) on 1KZN and 1EA1 respectively, followed by compound 2d with C-NO_2 substitution. On the basis of G-Score top ranked compounds were selected for the synthesis

Table 1: Results of Molecular Docking Analysis (Glide score).

Compound Code	Substitution (R)	Glide Score (1KZN)	Glide Score (1EA1)
2a	3-Cl	-4.231	-5.435
2b	4-Cl	- 4.374	-4.786
2c	4-CH_3	- 4.890	-5.346
2d	**4-NO_2**	**-5.120**	**-7.854**
2e	**4-OCH_3**	**-6.213**	**-8.112**
2f	4-Br	- 3.325	-6.576
2g	4-OH	- 4.645	- 5.678
2h	4-CF_3	- 3.536	- 4.478
2i	3,4,5-OCH_3	- 4.345	-5.768
2j	2,4-Cl	- 5.108	-7.768
2k	3-NH_2	- 3.167	- 3.124
2l	4-NH_2	- 3.107	- 3.245
2m	4-F	- 4.243	- 5.345
Chloramphenicol	-	-5.110	-
Fluconazole	-	-	-7.789

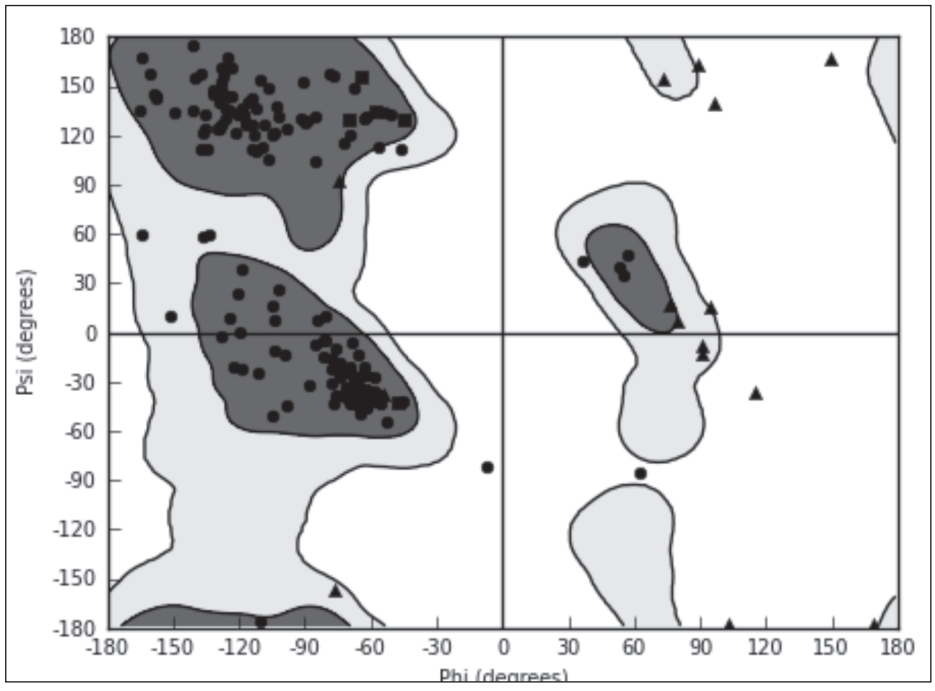

Fig. 2: Ramachandran Plot for DNA Gyrase Enzyme (PDB ID- 1KZN)

Antimicrobial study

All novel carbazole derivative were evaluated for their antibacterial and anti-fungal activity against *S-aureus, B. subtilis, E-coli* and *C. albicans* respectively. The minimum inhibitory concentration of every compound was determined by standard agar dilution method with streptomycin and Ketoconazole as reference.[21,22,23] Compound 2c (with CH_3 substitution at C-4)Shown excellent activity against *S-aureus*, remaining compound also shown good to moderate activity against *S-aureus*. Compound 2b (with Cl substitution at C-4) and 2c (with CH_3 substitution at C-4) were strongly active against B. subtilis. Compound 2d (with NO_2substitution at C-4) was strongly active against *E. coli* and *C. albicans*, remaining compound also shown good to moderate antifungal activity.[24,25,26,27,28,29,30]

Table 2: Activity profile of Carbazole derivatives.

Tested Compounds	S. aureus		B. subtilis		E. coli		C. albicans	
	MIC_{50}	MIC_{100}	MIC_{50}	MIC_{100}	MIC_{50}	MIC_{100}	MIC_{50}	MIC_{100}
2a	255	510	510	510	250	500	55	110
2b	75	150	125	250	250	500	25	50
2c	25	50	125	250	255	510	25	50
2d	255	510	510	510	25	50	25	25
2e	510	510	255	510	250	500	55	110
2f	255	255	255	510	75	150	55	55
Streptomycin	75	75	75	150	75	150	25	25
Ketoconazole	-	-	-	-	-	-	15	30

CONCLUSION :

The present work emphasized on design, synthesis and evaluation of novel carbazole derivative. The molecules with carbazole moiety already known to possess wide range of pharmacological activities. The research focused on synthesizing potential antimicrobial agents as new antimicrobial agent are urgently required and carbazole represent novel set of lead. In future structural modification of compound may allow development of pharmacologically acceptable compounds.

CONFLICT OF INTEREST:

Authors declared that we have no conflict of interest.

ACKNOWLEDGEMENT :

Authors are gratefully acknowledge to Department of Pharmaceutical Sciences, Rashtrasant Tukadoji Maharaj Nagpur University, Nagpur for providing research facilities.

REFERENCES :

1. Maryam Bashir, Afifa Bano, Abdul Subhan Ijaz, Bashir Ahmad Chaudhary, "Recent Developments and Biological Activities of N-Substituted Carbazole Derivatives. A Review" molecules, 2015; 20: 13496-13517.
2. Drissa S, Lucie M, Sylvain C,. "Concise and Efficient Synthesis of Calothrixin B." Journal of Organic Chemistry, 2006;71: 8384-8389.
3. Esra Tatar, Ýlkay Küçükgüzel,Erik De Clercq,Medine Güllüce. "Synthesis, characterization and screening of antimicrobial,antituberculosis, antiviral and anticancer activity of novel 1,3-thiazolidine-4-ones derived from 1-[2-(benzoylamino)-4-(methylthio)butyryl]-4-alkyl/arylalkyl thiosemicarbazides." ARKIVOC xiv, 2008: 191-210.
4. Feng-Ming Ho, Li-Jiau Huang, Tsun Cheng Kuo, Chien M. Chao, Wan-Wan Lin. "The anti-inflammatory carbazole, LCY-2-CHO, inhibit slipopolysaccharide-induced inflammatory mediator expression through inhibition of the p38 mitogen-activated protein kinase signaling pathway in macrophages." British Journal of Pharmacology, 2004;141: 1037-1047.
5. Ghazala Yaqub, Abdul Hannan, Erum Akbar, Muhammad Usman, Almas Hamid, Zubi Sadiq,and Mehwish Iqbal. "Synthesis, Antibacterial, and Antifungal Activities of Novel Pyridazino Carbazoles." Journal of Chemistry, 2013: 1-7.
6. Hall, J. H. Burckhalter Verlin C. Stephens Luther A. R. "Antihistaminics: The N Beta Dimethylaminoethyl derivatives of carbazole and diphenylamine." Journal of the American Pharmaceutical Association.,1950; 39 (5): 271-273.
7. Kanwal Raj, Namita Misra , Geetali Pachauri , Mithelesh Sharma , Akhilesh Kumar Tamrakar , Amar Bahadur Singh , Arvind Kumar Srivastava , K. Phani Kiran , C.V. Narasimha Rao & S.R. Prubhu. "Novel class of hybrid natural products as antidiabetic agents." Journa lNatural Product Research Formerly Natural Product Letters, 2009; 23 (1): 60-69.
8. Madiha Kazmi, Imtiaz Khan, Ajmal Khan, Sobia Ahsan Halim, Aamer Saeed, Saifullah Mehsud, AhmedAl-Harrasi, Aliya Ibrara. "Developing new hybrid scaffold for urease inhibition based on carbazole-chalcone conjugates: Synthesis, assessment of therapeutic potential and computational docking analysis." Bioorganic & Medicinal Chemistry, 2019; 22 (27): 115-123.
9. Nadia Salih, Jumat, Salimon, Emad Yousif. "Synthesis and antimicrobial activities of 9H-carbazole derivatives." Arabian Journal of Chemistry, 2016; 9 (1): S781-S786.
10. Swapnali Mohite, Rutuja Shah, Naziya Patel. "Antimicrobial activity of leaves extracts of Passiflora foetida. Asian J. Res. Pharm. Sci. 2018; 8(1):17-20.
11. Nakatani, Yukari TachibanaHiroe KikuzakiNordin Hj. LajisNobuji. "Antioxidative Activity of Carbazoles from Murraya koenigii Leaves." Journal of Agricultural and Food Chemistry, 2001; 49 (11): 5589-5594.
12. P. Ravichandiran, D. Premnath, and S. Vasanthkumar. "Synthesis, molecular docking and antibacterial evaluation of new 1,4-naphthoquinone derivatives contains carbazole-6,11-dione moiety." J Chem Biol,2014; 7 (3): 93-101.
13. Thevissen, Karin, Marchand, Arnaud, Chaltin, Patrick, Meert, Els M.K., Cammue, Bruno P.A. "Antifungal Carbazoles." Current Medicinal Chemistry,2009; 16 (17): 2205-2211.

14. G. Baskar, J. Chandhuru, K. Sheraz Fahad, A.S. Praveen. "Mycological Synthesis, Characterization and Antifungal Activity of Zinc Oxide Nanoparticles." Asian J. Pharm. Tech. 2013; 3(4):142-146.

15. Sudhakar P, Poorana Pushkalai S, Sabarinath C, Priyadharshini S, Haripriya S . "Molecular docking and synthesis of 1, 2, 4 - triazin analogue of diclofenac as potential ligand for parkinson's." Res. J. Pharmacology and Pharmacodynamics.2018; 10(1): 08-12.

16. E. Otuokere, F.J. Amaku, C.O. Alisa. In Silico Geometry Optimization, Excited – State Properties of (2E)-N-Hydroxy-3-[3-(Phenylsulfamoyl) Phenyl] prop-2-Enamide (Belinostat) and its Molecular Docking Studies with Ebola Virus Glycoprotein. Asian J. Pharm. Res. 5(3): July- Sept., 2015; Page 131-137.

17. Valmik P. Jejurkar, Suraj N. Mali, Rajpratap Kshatriya, Hemchandra K. Chaudhari, Satyajit Saha. "Synthesis, Antimicrobial Screening and In Silico Appraisal of Iminocarbazole Derivatives." Medicinal Chemistry & Drug Discovery, 2019; 04: 9470-9475.

18. Bhavana J. Deshmane. "Design, Synthesis and Biological Evaluation of some new Quinoline Derivatives."Res. J. Pharma. Dosage Forms and Tech. 2018; 10(3):163-168.

19. Xuan-Yu Meng, Hong-Xing Zhang, Mihaly Mezei, and Meng Cui. "Molecular Docking: A powerful approach for structure-based drug discovery." Current Computer Aided Drug Design, 2011; 7 (2): 146-157.

20. Zhang F.F., Gan L.L. and Zhou G.H. "Synthesis anti-bacterial and antifungal activites of some carbazole derivatives." Bioorganic and Medicinal Chemistry,2010; 22: 1881-1884.

21. Athar Jamal, Ayesha Maqsood. "Review of Synthesis of Silver Nanoparticles from different Medicinal Plants and their Pharmacological Activities." Asian J. Pharm. Tech. 2021; 11(1):88-93.

22. Rakesh Saini, Awani K Rai, AN Kesari, M Shahar Yar. "Synthesis and Biological Evaluation of 2, 5 Di-substituted 1, 3, 4 oxadiazoles." Asian J. Research Chem.2009; 2(1):34-36.

23. Swapna S Kulkarni, AP Mehere, Priyank A Shenoy. "Synthesis and In-Vitro Antimicrobial Activity of 4-(Piperazin-1-Ylcarbonyl) Aniline – An Amide Derivative of P-Aminobenzoic Acid." Asian J. Research Chem.2009; 2(3):300-303.

24. Karthik Dhananjayan, Arunachalam Sumathy, Sivanandy Palanisamy. "Molecular Docking Studies and in-vitro Acetylcholinesterase Inhibition by Terpenoids and Flavonoids." Asian J. Research Chem. 20133; 6(11):1011-1017.

25. Anarul Islam, Roksana Khatun, Monirul Islam, Md. Kudrat-E-Zahan. "Synthesis, Spectroscopic Monitoring and Biological Activities of N2O4 Schiff base Ligand containing Metal Complexes of Cd(II), Pd(II), Hg(II) and Zr(IV)." Asian J. Research Chem. 2014; 7(2): 163-165.

26. Vijayabaskaran M, Lakshmi G, Senthilraja M, Sivakumar P, Vaijayanthimala P, Perumal P. "Synthesis, Characterization and Anti-microbial Evaluation of Substituted Benzo[g]indol-2-one Derivatives."Research J. Science and Tech. 2011; 3(6): 313-317.

27. Jignesh P Raval, Hemul V Patel, Pradip S. Patel, Nilesh H Patel, Kishor R Desai. "A Rapid, Convenient Microwave assisted and Conventional Synthesis of novel azetidin-2-one derivatives as Potent Antimicrobial agents." Asian J. Research Chem. 2009; 2(2):171-177.

28. Ameya G Yadav, Vrushali Patil, AS Bobade, SV Athlekar, LS Patil, Abhay Chowdhary. "Synthesis and Antimicrobial Activity of Some Benzimidazolyl Pyrazolone Derivatives." Asian J. Research Chem. 2009; 2(4):516-518.

29. V. Murugan, Brijesh Joshi, Geetha K.M. "Synthesis of 2-Imino-3-(5-Aryl-1, 3, 4-Thiadiazol-2-Yl)-5-Arylidene-1, 3-Thiazol-4-One as Potent CNS Depressant and Antimicrobial Agents." Asian J. Research Chem. 2010; 3(3):698-702.

30. Balaji P. N., K. Prathusha, Chandu T. J., M. Sai Sreevani, P. Johnsi Rani, P. Harini. "Synthesis, Characterization and Antimicrobial Activity of Some Synthesized Isoxazole and Pyrazole Derivatives." Asian J. Research Chem. 2011; 4(2): 301-303.

Address for correspondence :

Dr. Prafulla M. Sabale, Professor in Pharmaceutical Chemistry, Department of Pharmaceutical Sciences, R.T.M Nagpur University,

Mahatma Jyotiba Fuley Shaikshanik Parisar, Amravati Road, Nagpur - 440033. (India)

E-mail: prafullasable@yahoo.com Contact: +919158537050

Peer Reviewed and Refereed Journal 2022 **(ISSN : 09726330)**

Rashtrasant Tukadoji Maharaj Nagpur University

SCIENCE JOURNAL 2022

Vol. : XV

Neutraceutical Value of Flavonoids : A Short review

Prafulla M. Sabale[1], Lata C. Potey,[1] Priya Rahangdale,[1] Vidya Sabale[2]

[1]Department of Pharmaceutical Sciences Rashtrasant Tukadoji Maharaj Nagpur University, Nagpur-440033 M.S.

[2]Dadasaheb Balpande College of Pharmacy, Besa, Nagpur-440034 M.S.

Corresponding author email : prafullasable@yahoo.com

Abstract :

Flavonoids, commonly known as polyphenolic compounds most abundantly found in plant originated foods, All naturally occurring flavonoids can be classified into flavanols, flavones, flavonols, flavanones, isoflavones and anthocyanidins. They have been demonstrated to possess various potential activities such as strong antioxidant, antiviral, antibacterial, anticancer and disease-preventing properties especially for various degenerative diseases such as cancers and cardiovascular diseases. This review has been focused on pharmacokinetic properties and various biological activities of flavonoids and flavones.

Keywords : Flavonoids; Flavone; antioxidant; anticancer; enzyme inhibition; Pharmacokinetic study.

INTRODUCTION

Flavonoids are plant based compounds, they belong to a class of low-molecular weight phenolic compounds that are widely distributed in the plant kingdom, (Cheynier, 2012) obtained from variety of leaves, fruits and flowers, shows enormous health benefits. Naturally occurring flavonoids are primary classified into six types, each of which have health promoting effects, like Flavonols, Flavones, Flavan-3-ols, Flavanones, Anthocyanin's, Isoflavones, catechin, chalcone etc.(Pandey, 2013) **(figure 1)**. These all six types of flavonoids can be obtained from variety of fruits, vegetables, grains, bark, roots, stems, flowers, tea and wine. (K.S. Sridevi Sangeetha, 2016) Flavonoids are present in different parts of plants, so they can be easily extracted from these. Many scientist have shown health benefits of these phytochemicals in their respective studies. Researchers have found that eating a diet rich in flavonoids reduces the risks of cardiovascular disease, (J. X. Li, 2005) diabetes, anti-oxidative, (E. H. Kelly, 2002) anti-inflammatory, (Middleton, 1998) Antiviral, (K. Hayashi, 1993) Alzheimer's disease (AD), atherosclerosis, anti-mutagenic and some cancers. They are also known to be potent enzyme inhibitors such as *xanthine oxidase* (XO), *cyclo-oxygenase* (COX), *aromatase, lipoxygenase* and *phosphoinositide 3-kinase*. In addition they play a very important role in plants, animals, and bacteria also. In plant flavonoids are naturally synthesized in specific sites and distributes aroma and colours to flowers, in fruit they are responsible for attraction of pollinators, and help in spore germination. (A. Gil-Izquierdo, 2001) Flavonoids protect plants from different biotic and abiotic stresses and act as unique UV filters. Recent advances in ruminant nutrition researches suggest that flavonoids helps on the productivity and health of animals. It was reported that the increase in milk yield and lactation performance in dairy cows were observed after administration of sylimarin in the feed (10 g/d) which mainly consist of flavonolignans. Flavonoids have been reported to have antibacterial activities. (Lamb, 2005)

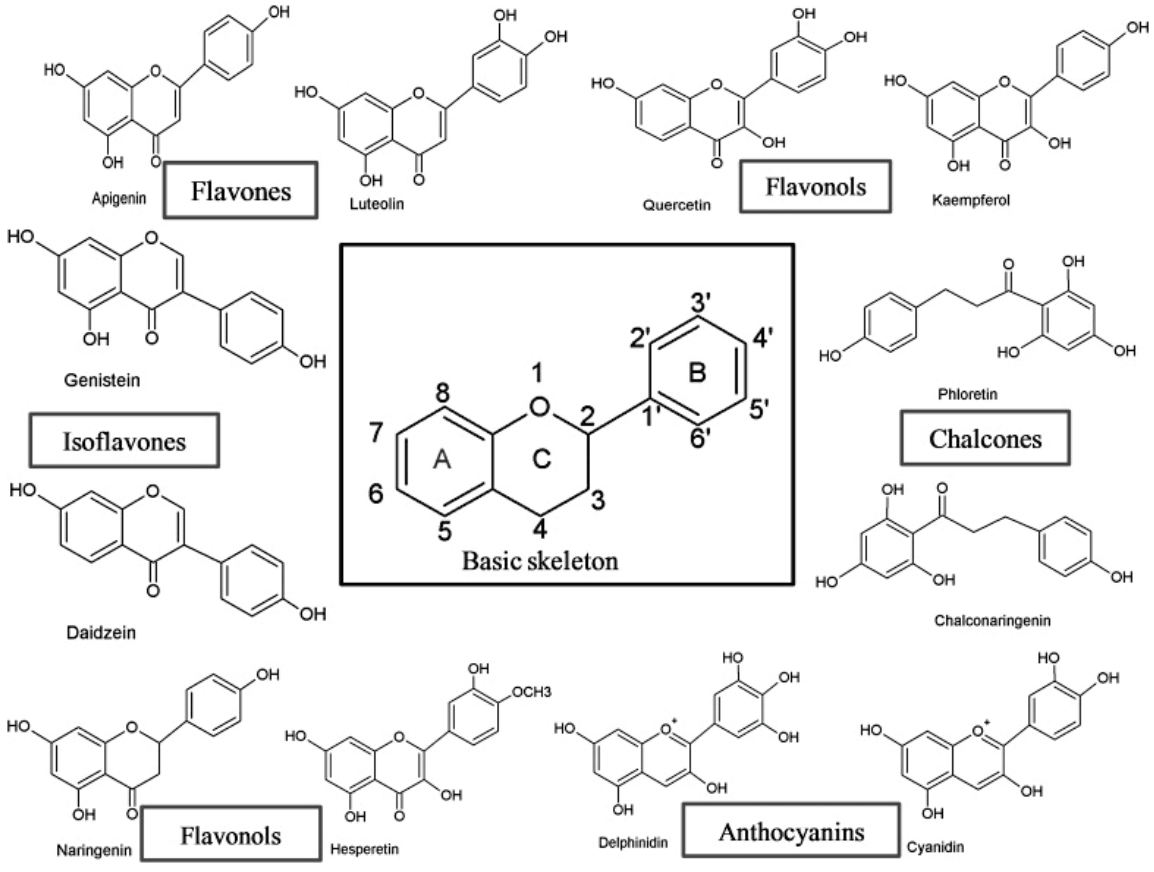

Fig. 1: Classification of naturally occurring flavonoids.

Pharmacokinetic of flavonoids

Average daily Intake :

Worldwide the mean intake of flavonoids ranges between 150 and 600mg/day, this range may get vary in negligible amount in the population with low/high black tea intake, such as UK (from 500-1000 mg/day). This intake may vary from country to country, quercetin is most important component estimated in the intake of flavonoids.(Ock Kyoung Chun, 2007) **(Table 1)**

Absorption :

In nature flavonoids present in both glycone and aglycone form, but most predominantly present in glycosylated form. Research shown that glycosylated form (quercetin) absorb more readily than the aglycone form, but this statement of research is remains in doubt as catechin, which is not glycosylated in nature, is absorbed relatively efficiently.

Table 1 : Average Intake of Flavonoids in different countries

Countries	Intake of Flavonoids (mg/day)	Source
Australia	696	Black tea
Spain	443	Fruit
France	436	Fruit, tea, red wine
Italy	364	Fruit
Finland	209	Berries, Fruit
Poland	898	Tea, Cocoa
Brazil	54.6	Citrus fruit, beans
China	225	Soy, Pome, Fruit
Korea	318	Fruit, tofu, onions

Metabolism :

After oral absorption flavonoids are extensively metabolized in small intestine and goes through liver as conjugates of O-methylation, sulfation and glucuronidation. Non absorbed flavonoids goes to colon where it is degrades by colonic micro flora and metabolized in liver. All the metabolites are eliminated through biliary or urinary routes.

Contraindications :

Researchers found that Lipo-flavonoid plus is contraindicated with following.

Allergies :

- Ascorbic Acid (Vitamin C)
- Niacin Preparations
- Nicotinamide Analogues
- Riboflavin (Vitamin B-2)
- Vitamin B
- Vitamin B6 Preparations - Pyridoxine
- Vitamin B1 Preparations - Thiamine
- Bioflavonoids

Toxicities :

Due to consumption of high dosage of flavonoids daily, potential safety issues may be persist to normal human being. Flavonoids with phenolic ring oxidized by peroxidase enzyme to form phenoxyl radicals which are cytotoxic in nature, Catechol containing flavonoids have been observed to bind with DNA, Protein, hepatotoxicity found by epigallo catechin gallate which is present in green tea.

Biological Activities :

Flavonoids and their derivatives exhibits enormous pharmacological activities, in literature they have found to be good Cardio protective, Anti-inflammatory, Antioxidants, Anticancer, Antiviral, Anti-HIV, along with it also found that they are good hormones suppressor and enzymes inhibitors, few of them are discussed below.

Cardio protective

Flavonoids are essential component of food so it is also called as 'Functional Food' due to their antioxidant activity they have good impact on vascular system (Agrawal, 2011). In cardiovascular system flavonoids shows Antihypertensive, Anti-atherosclerotic, Antiplatelet activities and potentially used in the treatment of Myocardial Ischemia. Vincenzo Calderone *et al.,* in his work demonstrated the cardio protective activity of different flavonoids on the heart of Langendorff-perfused rat having Ischemia. (Calderone, 2013)

Dina Maaliki *et al.,* discussed in his review that Luteolin is one of the flavone and decreases blood pressure in spontaneous hypertensive rats and helps in improvement of vascular relaxation in aortic ring. Luteolin causes relaxation by stimulation of NO dependent and independent mechanism in endothelium, in which Luteolin increases CAMP level by inhibiting phosphodiestrase enzyme so, accumulation of cAMP activates endothelial Nitric oxide synthetase and increases the level of nitric oxide in endothelial cells. (Maaliki, 2019)

Anti-inflammatory

Inflammation is biological response of our body which is common in various diseases like Asthma, Gout, Arthritis, Carcinoma, Diabetes, Multiple Sclerosis, Bacterial and Viral infection etc. It is caused by the releases of various inflammatory mediators like prostaglandins, leukotrienes, histamines, serotonins, etc. These mediators are releases due to stimulation of signalling pathways which involves cyclooxygenase, caspases and kinases.

Ran Wen *et al,* isolated 52 flavonoids and chalcones from the root of Pongamia pinnata (L) Pierre, anti-inflammatory activity of isolated compounds were assessed through the inhibition of nitric oxide formation, ten compounds were shown significant effect than the standard drug Dexamethasone. (RanWen, 2018)

Ji-Young An *et al,* synthesized different flavone derivatives and evaluated them against the production of nitric oxide and prostaglandins E_2, in which few compounds were more potent against both the mediators. (Ji-YoungAn, 2017)

Antioxidant

Antioxidants are able to prevent the damage of the living tissues by preventing the oxidation of bio-molecules which are taking place by high level of free radicals in living system. This oxidation can leads to tissue damage, death of cells and cause of various diseases like cancer, cardiovascular diseases, skin diseases, and inflammation etc. (Gulcin, 2009)

Antioxidants acts by two ways : prevention of oxidation and chain breaking antioxidants. Various natural and synthetic derivatives flavones and flavonoids are potentially act as antioxidants by both the mechanism. (Halliwell, 1995)

H.Venkatachalam *et al,.* reported the synthesis and antioxidant activity of flavones and chalcones. Compounds were tested for radical scavenging activity by four models, 1,1-Diphenyl-2-picrylhydrazyl radical assay, *2,2-azinobis (3-ethylbenzothiazoline-6-sulphonic acid)*, Nitric oxide and Lipid per oxidation scavenging assays. (H.Venkatachalam, 2012)

Anticancer

Cancer is one of the death causing health hazard. Incidence and mortality of Cancer are consistently rising universal. As per the survey of International Agency on Cancer Research, There may be chances of 18.1 million new cancer cases and 9.6 million deaths in 2018. (Bray, 2018) . In literature it comes to know that flavonoids can inhibit carcinogenesis *in vitro* and some evidences prove that flavonoids also can do so *in vivo* also. (Kamei H, 1996)

Hirano and co-workers have evaluated anticancer activity of 28 different derivatives of flavonoids on human acute

myeloid leukaemia cell line HL-60, and activity was compared against known anticancer agents. Eight compounds were shown inhibition of growth of HL-60 cell line with IC_{50} value 10-940ng/ml. The flavonoid genistein was shown the highest activity which was almost equivalent to known anticancer agents. (Hirano T, 1994)

Literature also shows that fermented soya milk contain larger amount of genistein and daidzein as compared to the unfermented milk, when the mixture of this fermented milk and isoflavone given to rat at seven week of age it helps to inhibit the mammary carcinogenesis which was induced by 2-amino-1-methyl-6-phenylimidazo [4,5-b] pyridine.

Enzyme Inhibition

Flavonoids are found to be active at inhibition of certain enzymes like topoisomerase, acetychloliestrase, xanthine oxidase, cyclooxygenase, aldehyde oxidase and aromatase enzyme.

Topoisomerase is an enzyme which can inhibit DNA metabolism, the agents which will be act through the inhibition of this enzyme will be potentially act as anti-cancer agents. There are so many compounds which are found to be topoisomerase inhibitors, Quinoline derivatives, flavonoids derivatives, metal complexes, fatty acid etc. (Liang, 2019)

Angiotensin Converting enzyme inhibitors play their vital role in regulation of blood pressure. Ligia Guerrero and co-workers evaluated different flavonoids for *in vitro* ACE inhibitor activity by fluorimetric method for which two concentrations were taken 100 µm and 500 µm. Luteoline was found highly active ACE inhibitors with IC_{50} value 23 µm. (Ligia Guerrero, 2012) . Recently flavonoids are reported to have aromatase enzyme inhibitory activity. Aromatase enzyme is responsible for the development of hormone dependent breast tumor. Due to the over expression of aromatase enzyme in breast tissues, increases the level of estrogen though the conversion of androgen, Cancerous cell depend on estrogen for the growth and progression which leads to development of estrogen dependent breast tumor. Flavonoids have structural similarity with natural substrate of aromatase enzyme so it is easily recognized by the enzyme to bind with active amino acid residues in the binding pocket of enzymes. (Fengjuan Li, 2011), Nga Ta and Thomas Walee in their study reported the synthesis of methylated flavones and evaluated the compound against aromatase enzyme, in which 7-methoxy flavones and 2,4-dihydroxy flavones were potent with IC_{50}value of 2-9 µm. (ThomasWalle, 2007)

Conflict of Interest

Authors have no conflict of interest.

Acknowledgement

Authors are grateful to University Department of Pharmaceutical Sciences, Rashtrasant Tukadoji Maharaj Nagpur University, Nagpur, for providing research facilities for the completion of this research.

References :

1. A. Gil-Izquierdo, M. I.-B. (2001). n vitro availability of flavonoids and other phenolics in orange juice,. *Journal of Agricultural and Food Chemistry, 49*(2), 1035–1041.

2. Agrawal, A. D. (2011). Pharmacological Activities of Flavonoids: A Review. *Journal of Pharmacy and Pharmacology, 4*(2), 1395-1398.

3. Bray, F. (2018). Global Cancer Satistics 2018: GLOBOCAN estimate of incidence and mortality.

4. Calderone, V. (2013). Cardioprotective effects of different flavonoids againstmyocardial ischaemia/reperfusion injury inLangendorff-perfused rat hearts. *Journal of Pharmacy and Pharmacology, 65*, 750-756.

5. Cheynier, V. (2012). Phenolic compounds: from plants to foods. *Phytochemistry Reviews, 11*, 153-177.

6. E. H. Kelly, R. T. (2002). Flavonoid antioxidants: chemistry, metabolism and structure-activity relationships. *Journal of Nutritional Biochemistry, 13*(10), 572–584,.

7. Fengjuan Li, L. Y. (2011). Dietary flavones and flavonones display differential effects on aromatase (CYP19) transcription

in the breast cancer cells MCF-7. *Molecular and Cellular Endocrinology, 344*(1-2), 51-58.

8. Gulcin, I. (2009). Antioxidant activity of L-Adrenaline: An activity-structure insight. *Chem. Biol. Interact., 179*, 71-80.

9. H.Venkatachalam. (2012). Synthesis, Characterization and Antioxidant Activities of Synthetic Chalcones and Flavones. *APCBEE Procedia, 3*, 209-213.

10. Halliwell, B. (1995). The characterization of antioxidants. *Food Chem. Toxicol, 33*, 601-617.

11. Hirano T, G. M. (1994). Natural flavonoids and lignans are potent cytostatic agents human leukemic HL-60 cells. *Life Sci, 55*, 1061-1069.

12. J. X. Li, B. X. (2005). Antihypertensive effect of total flavonoid fraction of Astragalus complanatus in hypertensive rats,. *The Chinese Journal of Physiology, 48*(2), 101–106.

13. Ji-YoungAn. (2017). Identification and structure activity relationship of novel flavone derivatives that inhibit the production of nitric oxide and PGE2 in LPS-induced RAW 264.7 cells. *27*(11), 2613-2616.

14. K. Hayashi, T. H. (1993). n vitro inhibition of viral disease by flavonoids. *Antiviral Chemistry and Chemotherapy, 4*(1), 49–53.

15. K.S. Sridevi Sangeetha, S. U. (2016). FLAVONOIDS: THERAPEUTIC POTENTIAL OF NATURAL PHARMACOLOGICAL AGENTS. *International Journal Of Pharmaceutical Sciences And Research*, 3924-30. doi:10.13040/IJPSR.0 75-8232.7(10).3924-30

16. Kamei H, K. T. (1996). Flavonoids-mediated tumor growth suppression demonstrated by in vivo study. *Cancer Biother Radiopharm , 61*(11), 193-196.

17. Lamb, T. P. (2005). Antimicrobial activity of flavonoids. *International Journal of Antimicrobial Agents, 26*(5), 343–356.

18. Liang, X. (2019). A comprehensive review of topoisomerase inhibitors as anticancer agents in the past decade. *European Journal of Medicinal Chemistry, 171*, 129-168.

19. Ligia Guerrero, J. C.-V. (2012). Inhibition of Angiotensin-Converting Enzyme Activity by Flavonoids: Structure-Activity Relationship Studies. *Plos One, 7*(11), 1-11.

20. Maaliki, D. (2019). Flavonoids in Hypertension: A Brief Review and Under Lying Mechanism. *Current Opinian in Pharmacology, 45*, 54-65.

21. Middleton, E. J. (1998). Effect of plant flavonoids on immune and inflammatory cell function. *Advances in Experimental Medicine and Biology, 439*, 175–182.

22. Pandey, S. K. (2013). Chemistry and Biological Activities of Flavonoids: An Overview. *The Scientific World Journal*. doi:https://doi.org/10.1155/2013/162750

23. RanWen. (2018). Anti-inflammatory flavones and chalcones from root of Pongamia Pinnata(L) Pierre. *Phytochemistry, 145*, 56-63.

24. ThomasWalle, N. (2007). Aromatase inhibition by bioavailable methylated flavones. *The Journal of Steroid Biochemistry and Molecular Biology, 107*(1-2), 127-129.

Peer Reviewed and Refereed Journal 2022 **(ISSN : 09726330)**

Rashtrasant Tukadoji Maharaj Nagpur University

SCIENCE JOURNAL 2022

Vol. : XV

In Silico Designing of Biologically Active 3-acetyl-2-oxo-2H-Chromen-7-yl Benzoate Derivatives

Prafulla Sabale*, Nusrat Sayyad, Vaibhav Sawale, Vidya Sabale[1]

Department of Pharmaceutical Sciences Rashtrasant Tukadoji Maharaj Nagpur University, Nagpur-440033 M.S.

[1]Dadasaheb Balpande College of Pharmacy, Besa, Nagpur-440034 M S.

Corresponding author email : prafullasable@yahoo.com

ABSTRACT :

Inflammation is the body's immediate response to damage to its tissues and cells by pathogens, noxious stimuli such as chemicals, or physical injury. The main objective of molecular docking is to predict the biological activity of given ligand. To overcome the challenges of inflammatory disorders, several classes of anti-inflammatory drugs have been used. Coumarin ring composed of Benzene ring fused with pyrone ring, 2*H*-chromen-2-one (1,2-benzopyrone, or 2*H*-1-benzopyran-2-one) oxa-heterocycle can be synthesised by methods such as Claisen rearrangement, Perkin reaction, Pechmann reaction, Knoevenagel condensation. Coumarin have been considered for a variety of biological activities such as anticoagulant, anti-inflammatory, antimicrobial, anticancer, antiviral and antioxidant activities. The Molecular Docking study was done by using (Maestro 11.5) Schrodinger software to find the interaction between active Coumarin derivatives with *COX-2 enzyme* **(PDB ID: 1*CX2*).** Molecular docking studies showed that novel Coumarin derivatives have shown formation of hydrogen bond and good binding affinity with some amino acid residues. Coumarin derivatives may inhibit the activity of enzyme *COX-2* binding at its active site. The compounds (**3a 3c 3g**) were showed potent against the *COX-2* compared with standard celecoxib. On the basis of docking result Coumarin may be good Anti-inflammatory agents.

Keywords : Coumarin, COX-2, Molecular docking, Anti-inflammatory. Celecoxib.

INTRODUCTION

Inflammation is the body's immediate response to damage to its tissues and cells by pathogens, noxious stimuli such as chemicals, or physical injury. [1] Acute inflammation is a short-term response that usually results in healing : leukocytes infiltrate the damaged region, removing the stimulus and repairing the tissue. Such persistent inflammation is associated with many chronic human conditions and diseases, including allergy, atherosclerosis, cancer, arthritis and autoimmune diseases. To overcome the challenges of inflammatory disorders, several classes of anti-inflammatory drugs have been used. [2] Coumarins are broadly distributed in the plant kingdom.Coumarin ring composed of benzene ring fused with pyrone ring. 2*H*-chromen-2-*one (1,2-benzopyrone, or 2H-1-benzopyran-2-one)* oxa-heterocycle [3,4] can be synthesised by methods such as Claisen rearrangement, Perkin reaction, Pechmann reaction, Knoevenagel condensation [5] Coumarin have been considered for a variety of biological activities such as anticoagulant [6], antimicrobial [7], antioxidant andanti-inflammatory [8], anticancer [9] activities. Coumarin derivatives may inhibit the activity of enzyme *COX-2* binding at its active site [10] the interaction between active Coumarin derivatives with *COX-2 enzyme* **(PDB ID: 1*CX2*)**. Molecular docking studies showed that

novel Coumarin derivatives has shown formation of hydrogen bond and good binding affinity with some amino acid residues. [11] There are several possible conformations in which a ligand may bind to an active site, called the binding modes. Molecular docking involves a computational process of searching a conformation of the ligand that is able to fit both geometrically and energetically into the binding site of a protein. Docking calculations are required to predict the binding mode of new hypothetical compounds. Depending on the docking score the results obtained were compared with standard drug or potent drug.

MATERIALS& METHODS

Docking protocol

Molecular docking study on coumarin derivatives was carry out by software Maestro11.5 from Schrödinger in order to develop selective anti-inflammatory agents. The docking study of Eleven substituted Coumarin Derivatives was carried out using GLIDE (Grid Based Ligand Docking and Energetics) module of Maestro 11.5 Schrodinger software. The molecules were docked on the COX-2 enzyme (PDB ID: 1*CX2*) retrieved from the Protein Data Bank (www.rscb.org).

The steps are involved in molecular docking studies : -

Ligand Preparation:

The 3D Ligand structures of Thirteen Substituted Coumarin derivatives were drawn in MAESTRO workspace using build panel. The Schrödinger ligand preparation was done by using LigPrep panel application and optimized the structure by minimizing its energy through OPLS-3 force field.

Protein Preparation and its Minimization :

Protein for ligand docking was prepared by using protein preparation Wizard which was used to import, refine and minimize the energy of the *COX-2*. Early to that removing of water, side chain and charges were added. The protein preparation prior to docking is necessary as the protein retrieved from the Protein Data Bank, Vendors, and other sources often have missing hydrogen, partial charges, side chain, and completely loop regions.

Receptor Grid Generation :

Grid generation required to be performing prior to running a virtual screen with glide. The shape and properties of the receptor has represented in a grid by field that provides progressively more accurate scoring of the ligand poses.

Protein-Ligand Docking :

The ligand docking was done flexibly using Standard Precision (SP) mode of GLIDE module and further refinement was done by using extra precision (XP) mode. The ligand docking process helps to predict ligand conformation and orientation within a targeted binding site and thus results in an accurate structural modelling and correct prediction of activity of ligands.

RESULTS

Coumarins include a very large class of compound found throughout the plant kingdom. Coumarin derivatives have been shown to possess a notably broad spectrum of biological activity. All the compounds were docked into the binding site of the receptor (PDB ID- 1*CX*2), docking result shows (figure 1) that binding of ligand to protein was done independently as per applied constrains with interaction in preferred manner as shown in (table 1). Best docking score of the compound were compared using docking score and glide docking energy. Compound 3c showing the best docking score for which is comparable with the standard (Celecoxib) as shown in table 1. Docking is an automated computer algorithm that determines how a compound will bind in the active site of a protein. Ramchandran plot shows that the ligand and protein is suitable for docking (figure 2).

Code	2D Images	3D Images
3 a	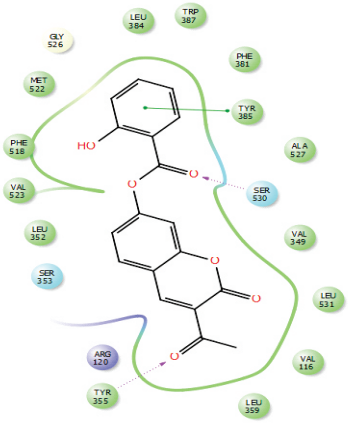	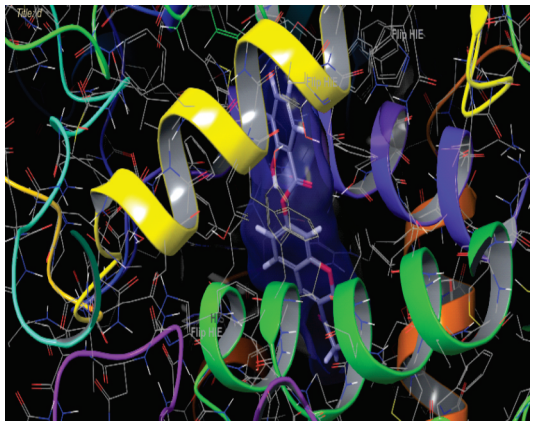
3 b	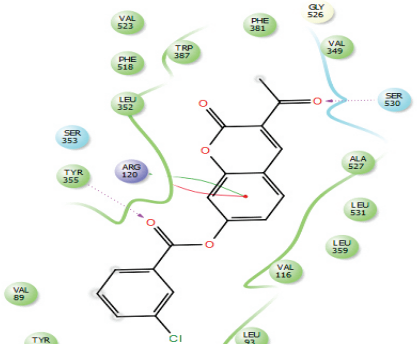	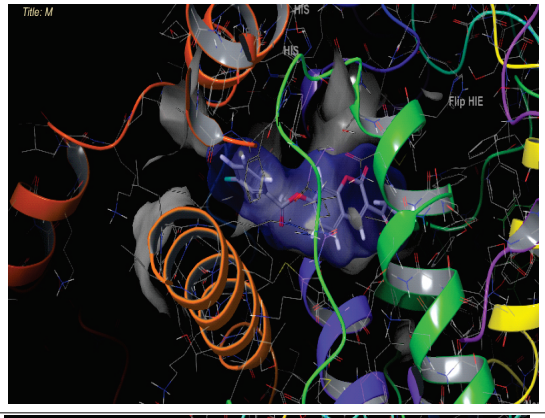
3 c	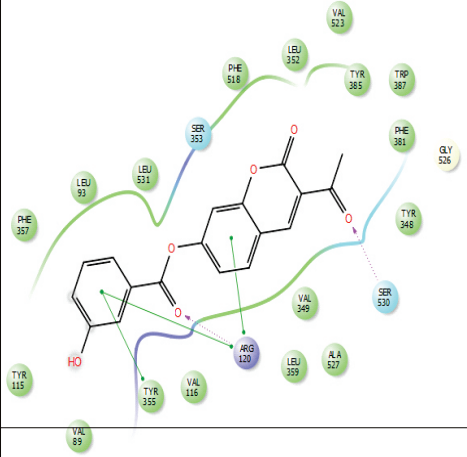	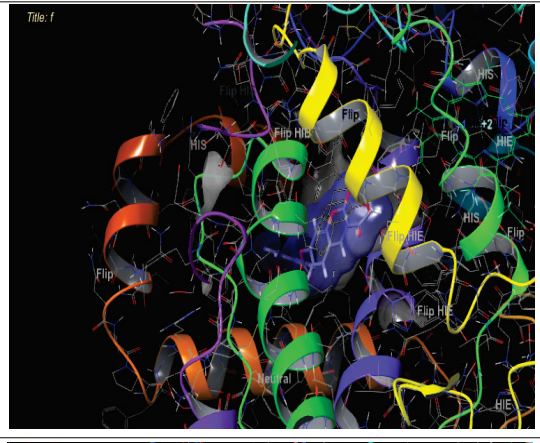
3 d	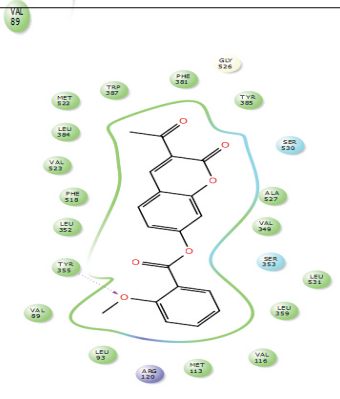	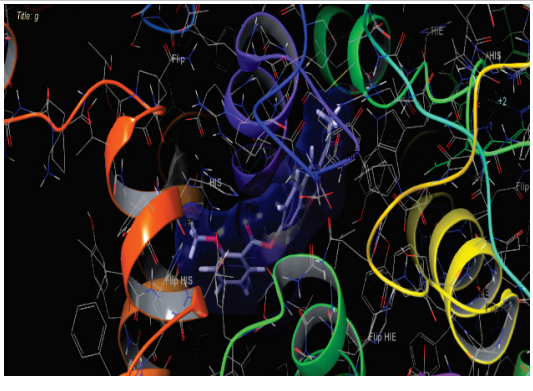

Code	2D Images	3D Images
3 e	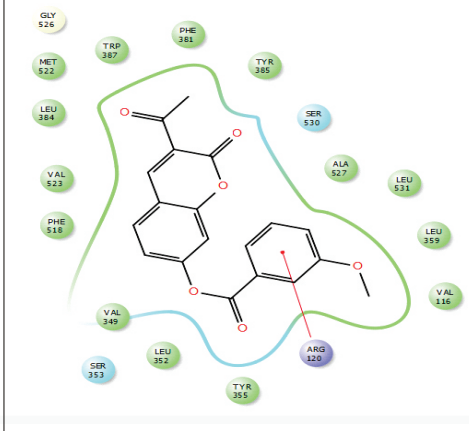	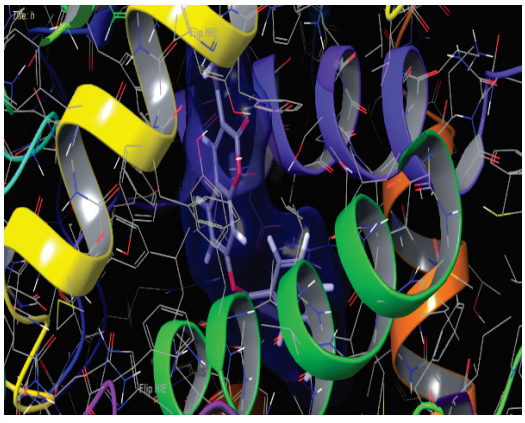
3 f	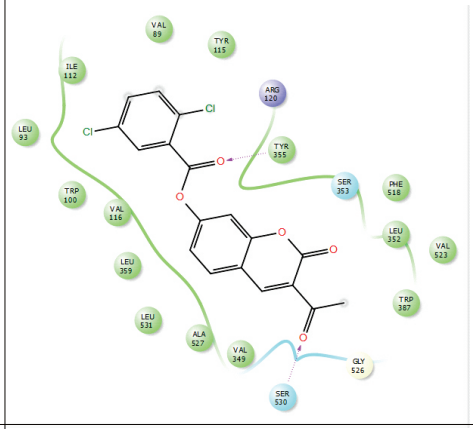	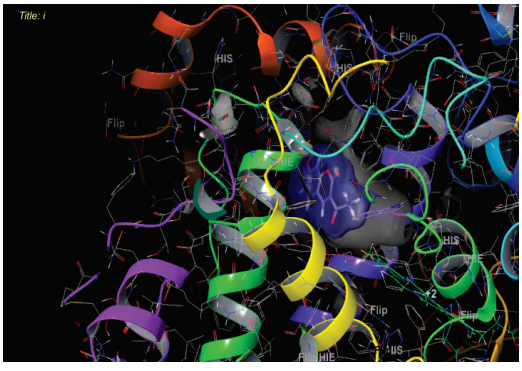
3 g	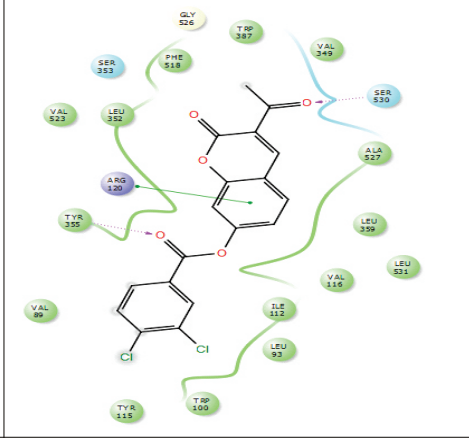	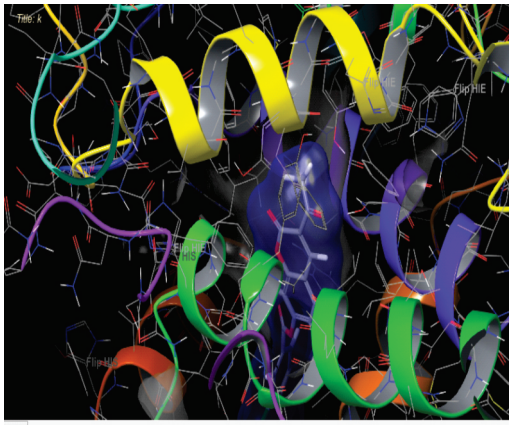
3 h	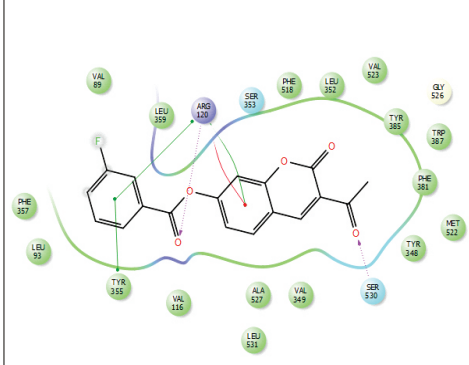	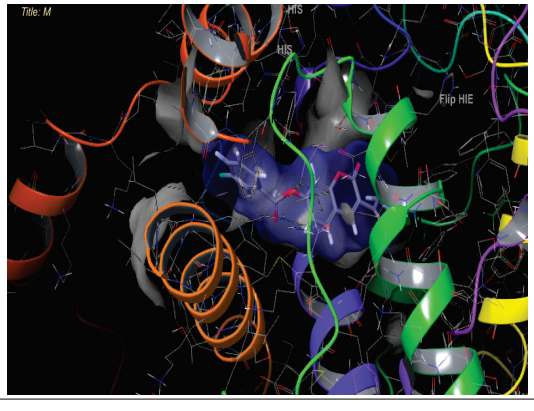

Code	2D Images	3D Images
3 i	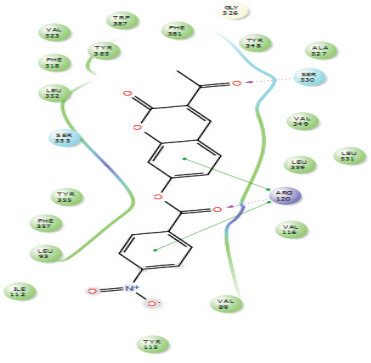	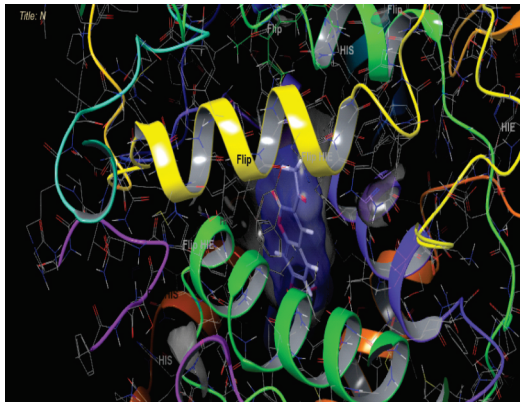
3 j	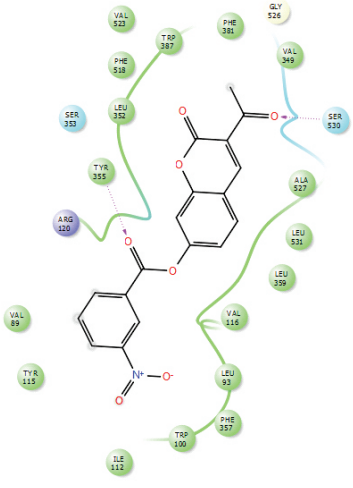	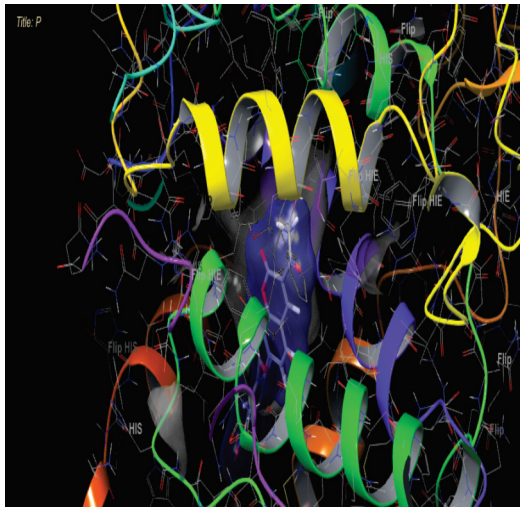
3 k	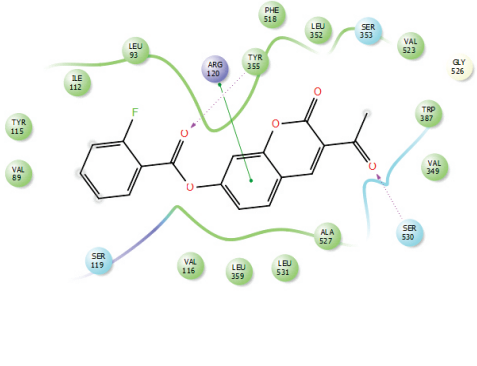	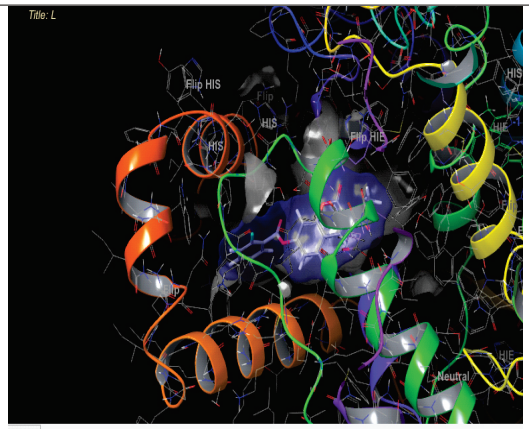

Fig 1. 2D and 3D interaction of ligands and protein

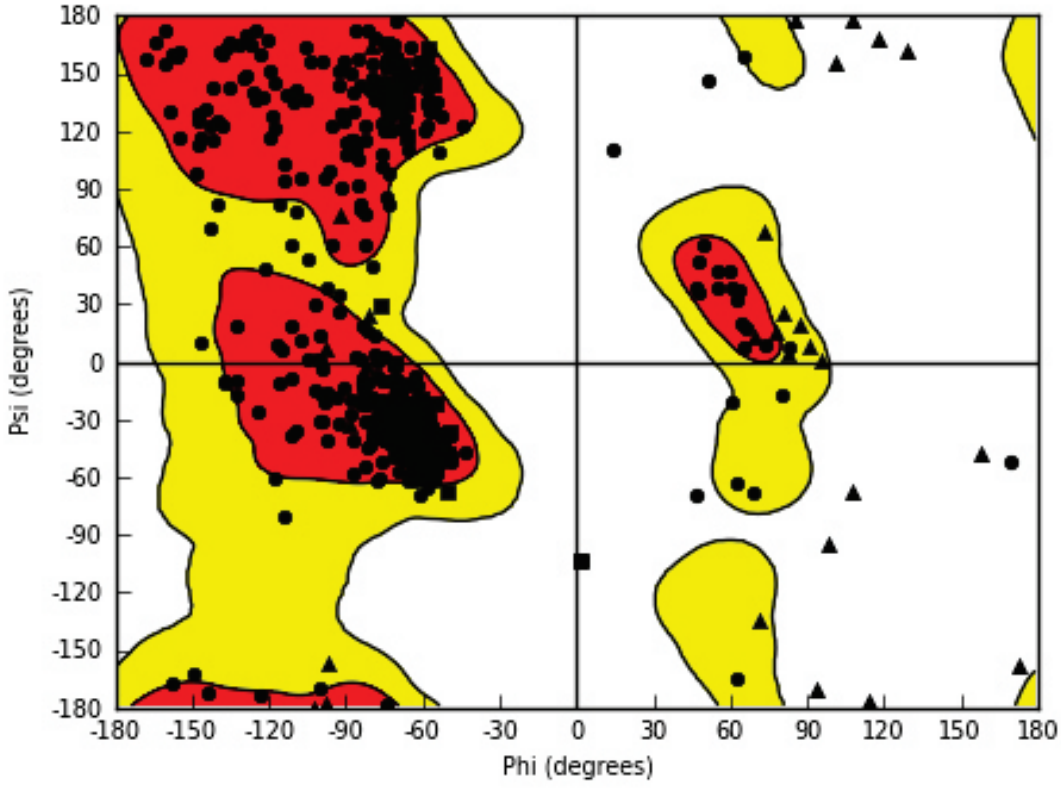

Fig. 2 - Ramachandran Plot

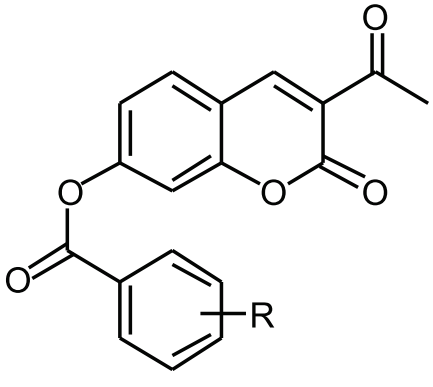

Fig. 3 - Structure of substituted Coumarin

Table 1. Showing various substituted Coumarin derivatives and Docking results for Anti-inflammatory study

Sr.No.	Compound Code	Derivative of Benzoyl Chloride	Glide Docking Score	Glide Docking Energy	No. of Hydrogen Bonds
1	3a	2-Hydroxy	**-7.209**	54.32	1
2	3b	3-Chloro	-5.914	53.96	0
3	3c	3-Hydroxy	**-8.274**	60.53	2
4	3d	2-Methoxy	-5.274	52.30	0
5	3e	3-Methoxy	-4.596	57.58	0
6	3f	2,5-Dichloro	-3.951	53.45	0
7	3g	3,4-Dichloro	**-6.892**	54.65	2
8	3h	3-Fluro	-4.354	62.66	0
9	3i	4-Nitro	-4.487	58.32	1
10	3j	3-Nitro	-3.234	56.27	0
11	3k	2-Fluro	-4.896	57.45	1
12		**Standard**	**-6.067**	53.45	1

Molecular docking study

Molecular docking studies femonstrated that compounds (**3a, 3c, 3g**) possessed higher G-score and have shown good hydrogen bond interaction with COX-2 enzyme as shown in table 1. compared to standard Celecoxib (**-6.067**) which are most active for anti-inflammatory activity. Therefore, it was decided to synthesis above three derivatives. On the basis of result of molecular docking, these three compounds are were selected as a lead compounds for further development of anti-inflammatory agents.

ADME-Toxicity Investigation

For determining pharmacokinetic properties, the ADME (Absorption, Distribution, Excretion, and Metabolism) properties of compounds are predicted using Pre-ADMET server. The results are showed in table 2 illustrated potent pharmacokinetic activity and all contents satisfies parameter to be taken as potential for generation as drug.

Table 2. ADME values of ligands

Sr. No	Compound Code	BBB	HIA	PPB	Skin Permeability
1	3a	0.012823	96.7030	88.0733	-2.98465
2	3b	0.015446	98.5812	95.1986	-2.98810
3	3c	0.021354	96.4141	91.8067	-2.96540
4	3d	0.039490	98.1910	92.2809	-2.51623
5	3e	0.018306	98.7903	91.1936	-2.87364
6	3f	0.020706	97.8828	93.4762	-2.91443
7	3g	0.032365	97.8815	93.5665	-2.92407
8	3h	0.013775	98.7414	91.4305	-3.23875
9	3i	0.034508	93.0377	90.2152	-3.00041
10	3j	0.036738	96.3772	93.5654	-3.00036
11	3k	0.031624	98.3214	91.2146	-3.05461
	Celecoxib	0.030365	98.8815	93.8665	-2.82407

DISCUSSION

There are several possible conformations in which a ligand may bind to an active site, called the binding modes. Molecular docking involves a computational process of searching for a conformation of the ligand that is able to fit both geometrically and energetically into the binding site of a protein. Docking calculations are required to predict the binding mode of new hypothetical compounds. The docking procedure consists of three interrelated components - identification of the binding site, a search algorithm to effectively sample the search space (the set of possible ligand positions and conformations on the protein surface), and a scoring function. The scoring function used by the docking algorithm gives a ranking to the set of final solutions generated by the search. Different forces that are involved in binding are electrostatic, electrodynamic, and steric forces and solvent related force. The 2D and 3D interaction of ligand and protein shown in fig 1. The free energy of a particular conformation is equal to the solvated free energy at the minimum with a small entropy correction. All energy calculations are based on the assumption that the small molecule adopts a binding mode of lowest free energy within the binding site. Docking is an automated computer algorithm that determines how a compound will bind in the active site of a protein. This includes determining the orientation of the compound, its conformational geometry, and the scoring. In some way, every docking algorithm automatically tries to put the compound in many different orientations and conformations in the active site, and then computes a score for each. Some programs store the data for all of the tested orientations, but most only keep a number of those with the best scores. In general, there are two key components of molecular docking, as follows

a. Accurate pose prediction or binding conformation of the ligand inside the binding site of the target protein.
b. Accurate binding free energy prediction, which later is used to rank the order of the docking poses.

The interaction between protein and ligands found to be potent in glide docking. compounds (**3a, 3c, 3g**) possessed higher G-score with satisfactory hydrogen bonding and show that compounds have self-association with protein.

CONFLICTS OF INTERESTS

The authors have no conflicts of interest.

ACKNOWLEDGEMENT

Authors are gratefully acknowledged to University Department of Pharmaceutical Sciences, Rashtrasant Tukadoji Maharaj Nagpur University, Nagpur for all necessary facilities to conduct the research work.

REFERENCES

[1] El-Haggar, R. and Al-Wabli, R.I. (2015) Anti-inflammatory screening and molecular modeling of some novel coumarin derivatives. *Molecules*, **20**, 5374–91. https://doi.org/10.3390/molecules20045374

[2] Srivastava, P., Vyas, V., Variya, B., Patel, P., ... G.Q.-B. and 2016, undefined. Synthesis, anti-inflammatory, analgesic, 5-lipoxygenase (5-LOX) inhibition activities, and molecular docking study of 7-substituted coumarin derivatives. *Elsevier*,

[3] Stefanachi, A., Leonetti, F., Pisani, L., Catto, M. and Carotti, A. (2018) Coumarin: A natural, privileged and versatile scaffold for bioactive compounds. Molecules. https://doi.org/10.3390/molecules23020250

[4] Jain, P.K. and Joshi, H. (2012) Coumarin: Chemical and pharmacological profile. *Journal of Applied Pharmaceutical Science*, **2**, 236–40. https://doi.org/10.7324/JAPS.2012.2643

[5] Bogdal, D. (1998) Coumarins: Fast Synthesis by Knoevenagel Condensation under Microwave Irradiation. *Journal of Chemical Research - Part S*, 468–9. https://doi.org/10.1039/a801724g

[6] Duric, K., Kovac-Besovic, E.E., Niksic, H., Muratovic, S. and Sofic, E. (2015) Anticoagulant activity of some artemisia dracunculus leaf extracts. *Bosnian Journal of Basic Medical Sciences*, **15**, 9–14. https://doi.org/10.17305/bjbms.2015.384

[7] Sandhya, B., Giles, D., Mathew, V., Basavarajaswamy, G. and Abraham, R. (2011) Synthesis, pharmacological evaluation and docking studies of coumarin derivatives. *European Journal of Medicinal Chemistry*, Elsevier Masson SAS. **46**, 4696–701. https://doi.org/10.1016/j.ejmech.2011.07.013

[8] Witaicenis, A., Seito, L.N., Da Silveira Chagas, A., De Almeida, L.D., Luchini, A.C., Rodrigues-Orsi, P. et al. (2014) Antioxidant and intestinal anti-inflammatory effects of plant-derived coumarin derivatives. *Phytomedicine*, Elsevier GmbH. **21**, 240–6. https://doi.org/10.1016/j.phymed.2013.09.001

[9] Mohareb, R.M., Fleita, D.H. and Sakka, O.K. (2011) Novel synthesis of hydrazide-hydrazone derivatives and their utilization in the synthesis of coumarin, pyridine, thiazole and thiophene derivatives with antitumor activity. *Molecules*, **16**, 16–27. https://doi.org/10.3390/molecules16010016

[10] Ibrar, A., Shehzadi, S.A., Saeed, F. and Khan, I. (2018) Developing hybrid molecule therapeutics for diverse enzyme inhibitory action: Active role of coumarin-based structural leads in drug discovery. *Bioorganic and Medicinal Chemistry*, Elsevier. **26**, 3731–62. https://doi.org/10.1016/j.bmc.2018.05.042

[11] Shoichet, B.K., McGovern, S.L., Wei, B. and Irwin, J.J. (2002) Lead discovery using molecular docking. *Current Opinion in Chemical Biology*, **6**, 439–46. https://doi.org/10.1016/S1367-5931(02)00339-3.

Peer Reviewed and Refereed Journal 2022 **(ISSN : 09726330)**

Rashtrasant Tukadoji Maharaj Nagpur University

SCIENCE JOURNAL 2022

Vol. : XV

Enhancement of Solubility of Lurasidone Hydrochloride by Pastillation Method

Rohit Mudliar[1]*, Nilesh Mahajan[1], Purushottam Gangane[1], Amol Warokar[2]

1. Department of Pharmaceutics, Dadasaheb Balpande College of Pharmacy, Nagpur, MS, India 440037
2. Department of Pharmaceutical Quality Assurance, Dadasaheb Balpande College of Pharmacy, Nagpur, MS, India 440037

Corresponding author email : 1*rohitmudliar321@gmail.com

Abstract

The Lurasidone HCl (LSH) is a BCS class II drug which comes under the anti-psychotic class, and has a wide range of uses. But, due to its low solubility it has slow dissolution rate and hence lower bioavailability. Pastillation is a method that can produce solidified discrete units, acquired directly from the molter mass called as pastilles. Pastillation is an effective and easiest method for the enhancement of solubility and dissolution rate. Initial saturation solubility of LSH and dissolution rate was determined and found to be 7.84 mg/ml which is quite low. The selection of polymer was done on the basis of solubility studies of physical mixture of drug with different polymers like Poloxamer 188, Kolliphor HS 15, PVP 10000 and PEG 400 in 1:1 ratio. Highest solubility of LSH was found to be 15.10 mg/ml with Kolliphor HS 15 and hence it was used to make pastilles. Formation of pastilles were confirmed by FT-IR and further evaluated for % practical yield, drug contents, solubility study and dissolution rate. Practical yield and drug contents were found to be 90% w/w and 85% w/w respectively. From the results, it was concluded that, solubility of LSH was increased by pastillation to 17.89 mg/ml which is almost 2.5 fold as compared to pure drug. Dissolution rate of LSH pastilles was also enhanced by double than that of the pure drug. Thus, pastillation can be an effective and easiest method to enhance the solubility, dissolution rate and bioavailability of poorly water-soluble drugs having good permeability.

Keywords : Lurasidone HCl, Pastillation, Kolliphor HS 15, Solubility enhancement, Dissolution rate

INTRODUCTION

Oral administration is the most convenient and commonly employed route of drug delivery due to ease of administration, high patient compliance, cost effectiveness and flexibility of design of dosage form. Solubility is one of the important parameters to achieve desired concentration of drug in systemic circulation for achieving pharmacological response. Poorly water-soluble drug often requires high doses in order to reach therapeutic plasma concentration[(1)]. The poor solubility and low dissolution rate in an aqueous gastrointestinal fluid often cause insufficient bioavailablity. Especially for BCS class II drug substance like LSH which is having poor aqueous solubility and poor oral bioavailability of 9-19%[(2)]. The bioavailability can be enhanced by increasing the solubility and dissolution rate of the drug in gastrointestinal fluid. As for BCS class II drug rate limiting step is drug release and not the absorption, so increasing the solubility in turn increase the bioavailablity for BCS class II drugs[(3)].

Pastillation is the process in which the solid dispersion using the drug and the polymer is made. Then this dispersion is placed in the glass syringe and then as the heat is applied and hot molten mass is allowed to fall drop by drop on the metallic plate with cooling

system. Then over cooling plate the hot droplets solidifies and forms the pastilles[4].

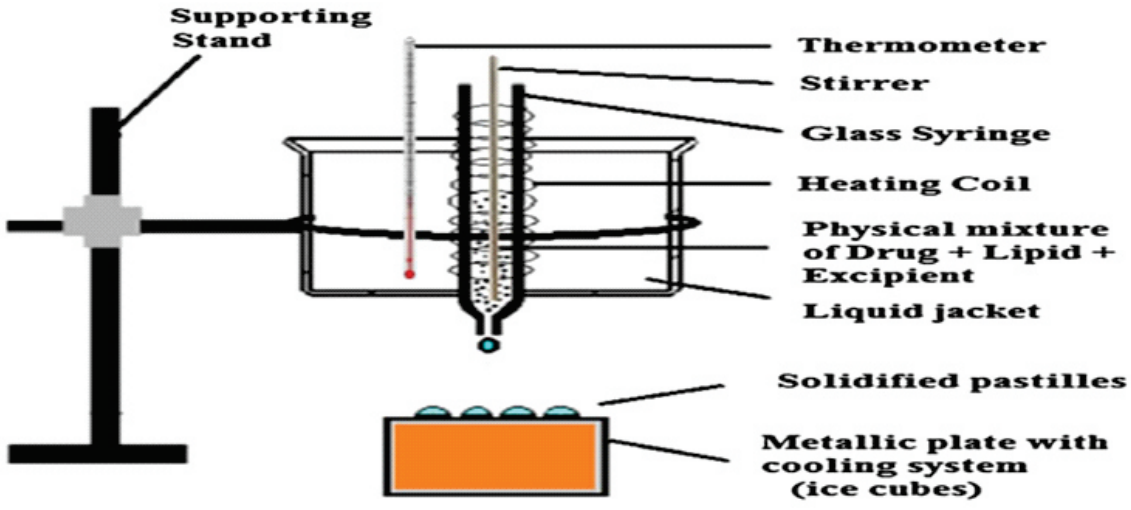

Fig. no. 1.1 : - Schematic diagram of pastillation assembly. [4]

Pastilles are lipid-based formulation used to increase the solubility, dissolution rate and bioavailability of BCS class-II drug. Lipid which melt and resolidifies are of good choice in pastillation process. These are the solid descrete unit made by pastillation process.Drug delivery using lipid-based formulation is emerging dosage form due to versatile structural appearance of lipid excipient this are considered as valuable alternative. The apparatus used for the pastillation is also known as droplet solidification apparatus.[5]

Materials

Lurasidone HCl was gifted by Emcure Ltd., Pune, Kolliphor HS 15 was gifted by BASF India, Poloxamer P188, Polyvinyl pyrrolidone 10000, Polyethylene glycol 400, Aerosil, Potassium Chloride, Methanol was purchased from LobaChemie, Mumbai.

Methods

Saturation solubility study

Lurasidone Hcl

Saturation solubility was conducted to determine the saturation concentration of LS4 in water. This study was conducted by the method proposed by Higuchi and Conors[6]. The drug was taken in excess quantity and then it was added in the 10 ml distilled water. It was kept for 48hrs on orbital shaker for equilibrium. After 48 hrs, the solution was filtered and absorbance was recorded at 240 nm for the determination of drug contents in the solution.

Physical mixture

Saturation solubility of drug with polymer mixture was done to select the polymer for pastillation. Mixture of drug and polymer showing highest solubility was selected for the preparation of pastilles. The drug and polymer were taken in 1:1 ratio. Then it was added in 10 ml distilled water. It was kept on orbital shaker for 48 hrs to equilibrate. Absorbance was taken at 240 nm for the determination of drug contents in the solution.

Dissolution study of drug : -

900 ml of phosphate buffer pH 6.8 was poured in the dissolution apparatus flask.Then the single dose of drug, LS4

was tied in muslin cloth on the paddle of Type-II of USP apparatus.Then the 1ml solution was pipetted out of the vessel and it was diluted to 10 ml with the solvent.The fresh solvent was replaced.This is done after every 15 min for 90 min.Then % cumulative drug release was calculated.

Preparation of pastilles :-

Pastillation is the process in which the solid dispersion using the drug and the polymer was made. LSH and Kolliphore HS 15 were mixed in 1:1 ratio by adding 500mg each. Then this dispersion was placed in the glass syringe and then as the heat is applied by the heating coil then this hot molten mass is allowed to fall drop by drop on the metallic plate with cooling system. Hot droplets were solidifies and forms the pastilles[4].

Evaluation of pastilles : -

Practical Yield : -

Total quantity of LSH and Kolliphor HS 15 was considered as theoretical yield. Final quantity of pastilles after the completion of pastillation process was considered as practical yield. By using following formula and comparing the practical yield with theoretical yield the % practical yield was calculated. This was calculated to know the suitability of method.

$$\% \text{ Practical yield} = \frac{\text{Practical yield} \times 100.}{\text{Theoretical yield}}$$

Drug content : -

The pure drug solution of concentration 10 µg/ml was prepared. The solution of pastilles of concentration 10 µg/ml was made.The absorbance of both was taken at 240 nm.The absorbance was noted and the drug content was calculated by using formula : -

$$\% \text{ Drug content} = \frac{\text{Abs of test} \times 100.}{\text{Abs of std.}}$$

Fourier- transform infrared spectroscopy (FT-IR) : -

The FT-IR spectrum was used to determine the interaction of the drug with the polymer used. Samples were mixed with potassium bromide and scanning from 4000-400 cm^{-1}. Spectrum of pure drug, polymer and pastilles were interpreted and compared to know any chemical interaction between them.

Solubility study of pastilles : -

Saturation solubility was conducted to determine the saturation concentration of LSH pastilles in distilled water. This study was conducted by the method proposed by Higuchi and Conors[6]. The pastilles was taken in excess quantity and then it was added in the 10 ml water. It was kept for 48hrs on orbital shaker. The solution was filtered and absorbance was recorded at 240 nm.

Dissolution test : -

Dissolution test of pastilles was carried out to know any changes in the dissolution rate of drug following the pastillation.900 ml of phosphate buffer was poured in the dissolution apparatus vessel.Then the pastilles having weight equivalent to single dose was tied in muslin cloth on the paddle of Type-II of USP apparatus.Then the 1ml solution was pipette out of the vessel and it was diluted to 10 ml with the solvent. The fresh solvent was replaced. This is done after every 15 min for 1.5 hr. Then % cumulative drug release was recorded.

Results and Discussions :

Saturation solubility study :

Lunosidone Hydrochloride :

Saturation concentration of Lurasidone HCl in distilled water was found to be 7.84µg/ml. This value is an indication of low solubility of the drug.

Dissolution study of Lunosidone Hydrochloride : - In 90 min. only 45% of drug has been released. This indicates the need for enhancement of dissoultion rate.

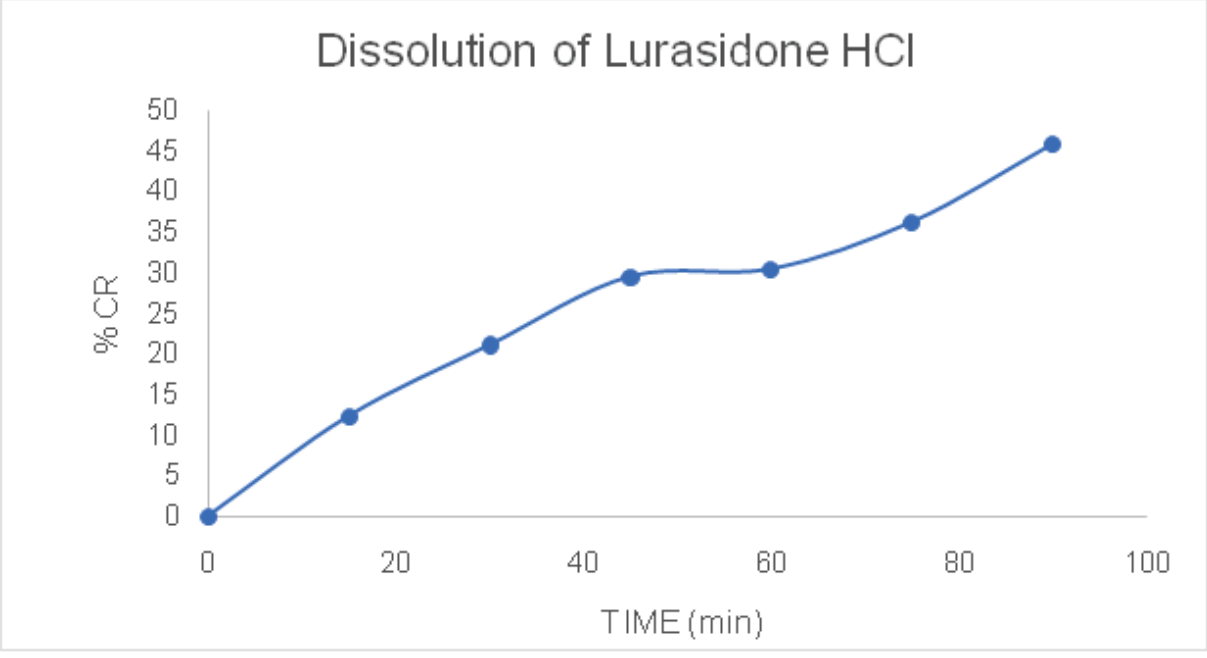

Fig 4.8 : - Dissolution profile of LSH

Selection of Carrier for Pastillation : -

Table no. 4.7:- Saturation solubility of Physical mixture of drug and polymer

Sr. No.	Drug	Polymer	Concentration (µg/ml)
1	Lurasidone HCl	Poloxamer P188	9.47
2	Lurasidone HCl	Kolliphor HS 15	15.10
3	Lurasidone HCl	Polyvinyl pyrrolidone 10000	8.51
4	Lurasidone HCl	Polyethylene glycol 400	8.96

It was found that, combination of Kolliphor HS 15 showed maximum saturation concentration of drug 15.01 µg/ml and hence selected for the preparation of pastilles.

Evaluation of pastilles: -

% yield : -

% practical yield was found to be 90% which suggests the suitability of this method for industrial or large scale.

Drug content :-

Drug content was found to be 85.02% which was quite satisfactory.

FT-IR of LSH :-

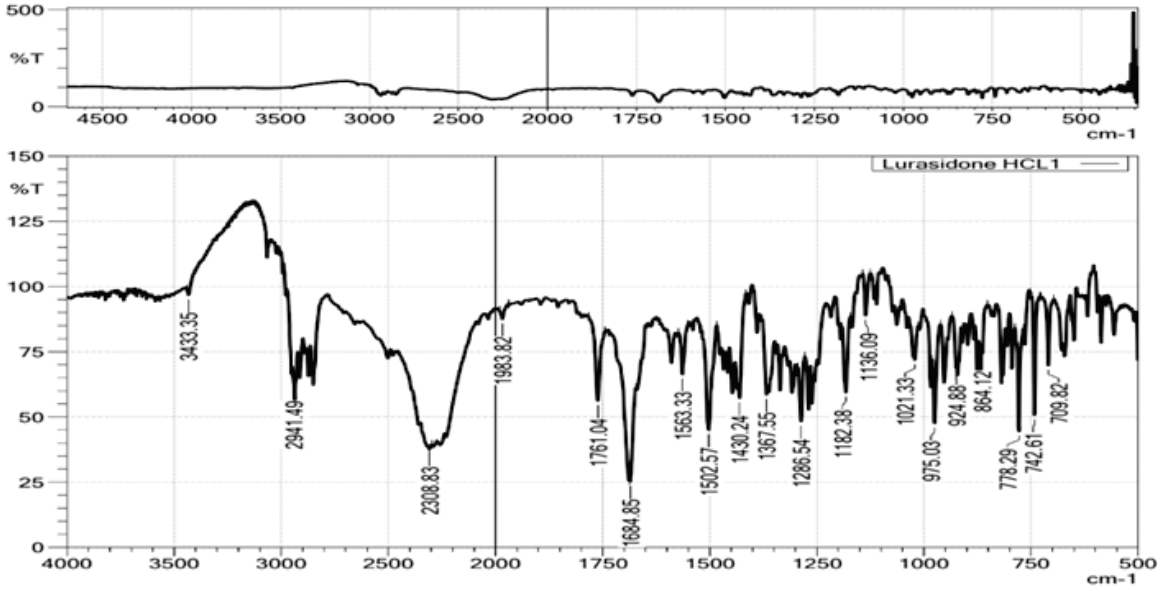

Fig. 4.4 : - FT-IR spectrum of Lurasidone HCl

After interpretation of FT-IR spectrum of drug, it was concluded that all the characteristic peaks corresponding to the functional group present in molecular structure of Lurasidone HCL were found within the reference range, confirming its identity.

FT-IR of Kolliphor HS 15 :-

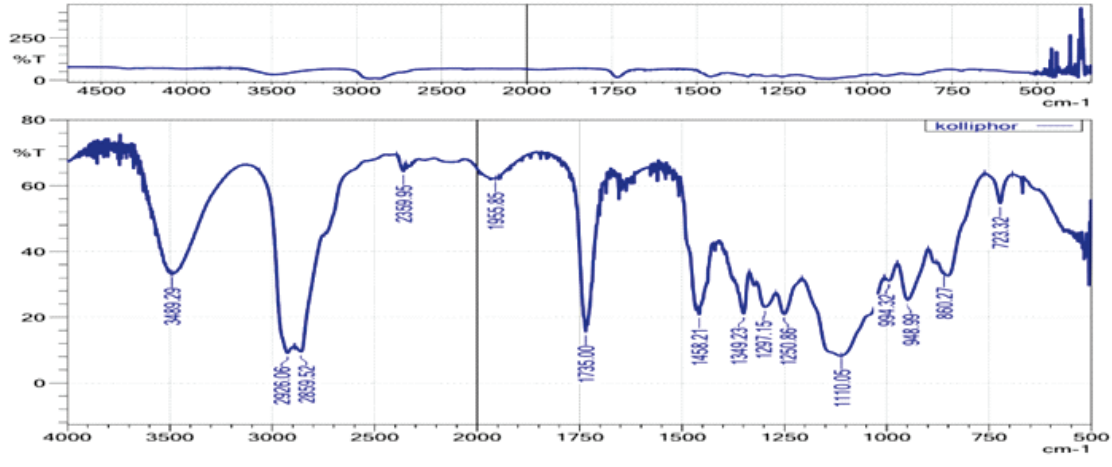

Fig. 4.6: - FT-IR spectrum of Kolliphor HS 15

After interpretation of FT-IR Spectrum of polymer, it was concluded that all the characteristic peaks corresponding to the functional group present in molecular structure of Kolliphor HS 15 were found within the reference range, confirming its identity.

FT-IR of LSH + Kolliphor HS 15 physical mixture: -

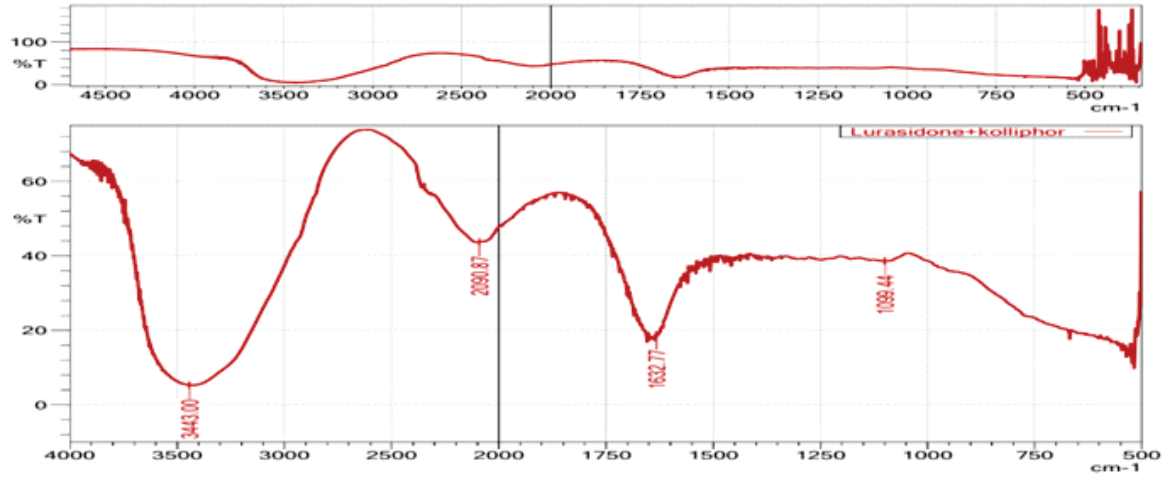

Fig 4.7: -FT-IR spectrum of physical mixture of Lurasidone HCl and Kolliphor HS 15

After interpretation of FT-IR spectrum of Kolliphore HS 15 and its physical mixture with drug, it was concluded that all the characteristic peaks corresponding to the functional group present in molecular structure of LSH were not found intact within the reference range, confirming its reactivity with Kolliphore HS 15. This interaction further supports the selection of polymer.

FT-IR spectrum of LSH pastilles

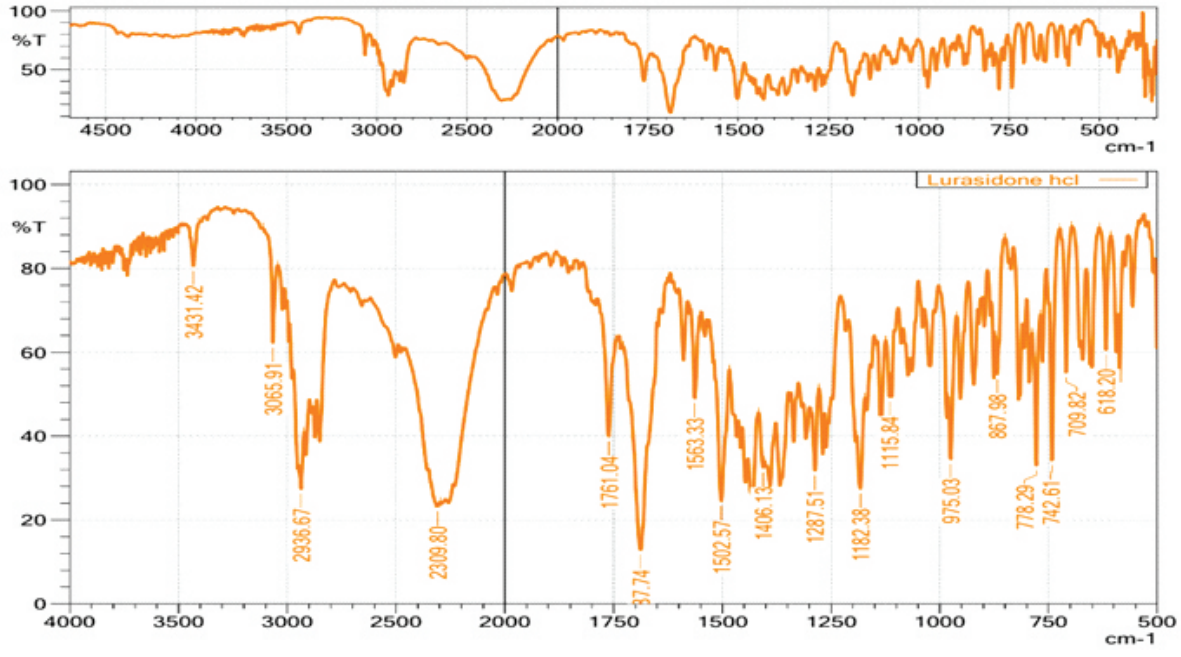

Fig 4.9: - FT-IR of Pastilles of LS4

After interpreting FT-IR Spectrum of LSH pastilles with Kolliphor HS 15, new peak of C-H stretching at 3065.91 $cm^{-1}$was observed confirming the formation of complex with Kolliphor HS 15. Most of the peak of the drug were retained at their position revels the structural integrity of drug.

Solubility study of pastilles : -

Formation of pastilles further increased the drug solubility as indictive from saturation concentration of drug which was found to be 17.89 µg/ml. This was almost 52.93 % increment of solubility.

Dissolution study of LSH pastilles

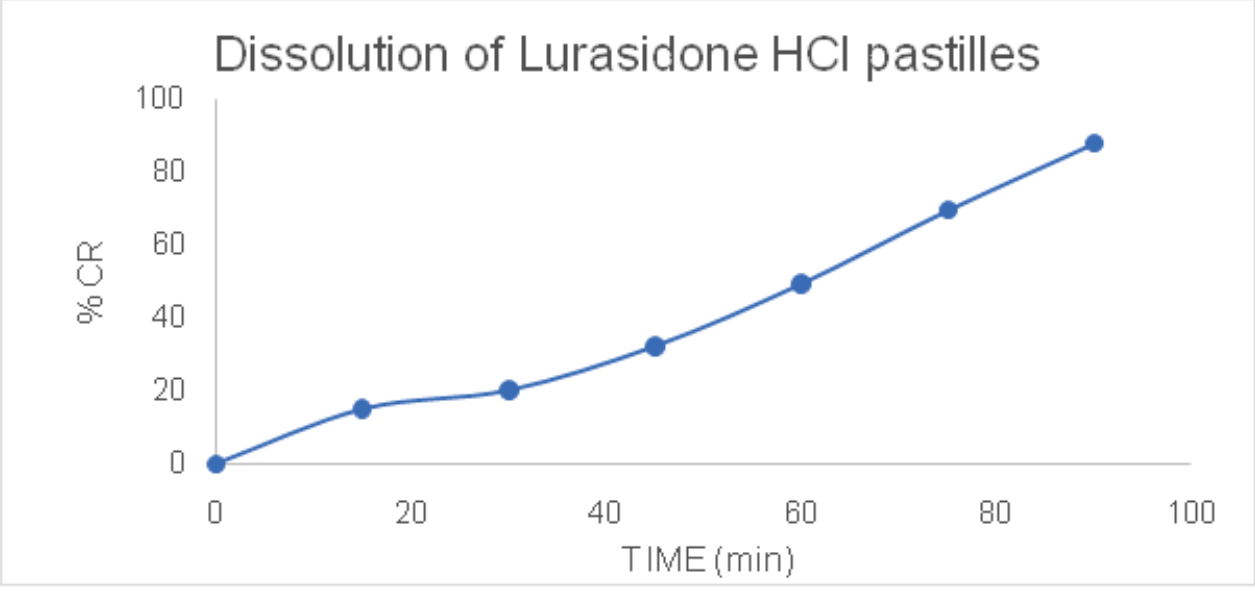

Fig 4.10 : - Dissolution of pastilles of Lurasidone HCl.

Comparative dissolution profile of Lurasidone HCl and its pastilles:-

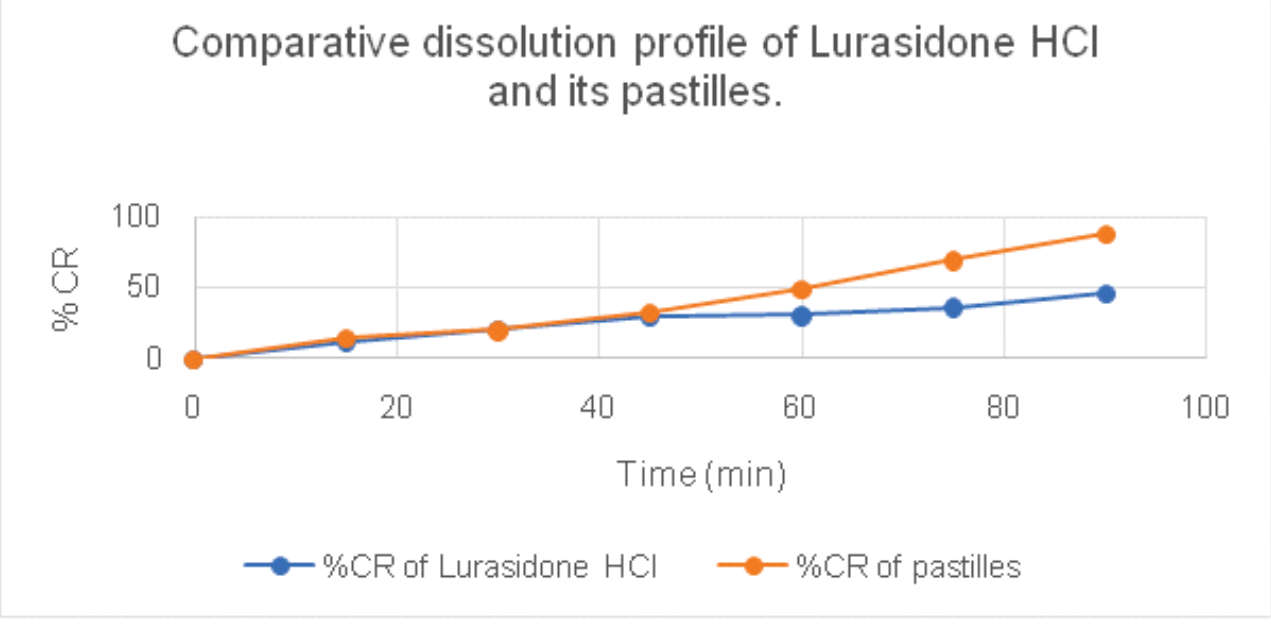

Fig 4.11 :- Comparative dissolution profile of Lurasidone HCl and its pastilles.

Almost 90% of drug has been released in 90 min. from the prepared pastilles. This is much higher release as compared to pure drug LSH, indicating that the pastillation can be suitable method for the enhancement of drug release.

Conclusion

Pastillation can be the most suitable, easiest, reliable and reproducible method for the enhancement of drug solubility and dissolution rate. More importantly, it also leads to the higher drug absorption as pastilles were predominantly prepared by using polymers that can be melted when dispersed with the drug. Increased solubility and dissolution rate may be attributed to the interaction of drug with the hydrophilic polymers.

Reference

1. S. R. K. Yellela, "Pharmaceutical technologies for enhancing oral bioavailability of poorly soluble drugs," Journal of Bioequivalence & Bioavailability, vol. 2, no. 2, pp. 28–36, 2010.

2. D. Sharma, M. Soni, S. Kumar, and G. D. Gupta, "Solubility enhancement—eminent role in poorly soluble drugs, Research Journal of Pharmacy and Technology, vol. 2, no. 2,pp.220–224, 2009.

3. A. Kumar, S. K. Sahoo, K. Padhee, P. S. Kochar, A. Sathapathy, and N. Pathak, "Review on solubility enhancement techniques for hydrophobic drugs," PharmacieGlobale, vol. 3, no. 3, pp.001–007, 2011.

4. Pandit .P. Ashlesha,Chavan .T. Tushar,Khandelwal .R. Kishanchandra,Oral lipid based multipurticulatepastilles:design and effect of pore former; Journal of pharmaceutical investigation, 2015.

5. Rajiv Bajrachaiya, Sang Hoon Lee et al, Development of a Ternary solid dispersion formulation of LW6 to improve the invitro activity as BCRP inhibitor: prepration and in vitro/ in vivo characterization, 1-5,2019.

6. Higuchi T., Conors KA., Phase solubility technique advance . Anal. Chem.Instr.,4,117-112.

Peer Reviewed and Refereed Journal 2022 **(ISSN : 09726330)**

Rashtrasant Tukadoji Maharaj Nagpur University

SCIENCE JOURNAL 2022

Vol. : XV

Corona Pandemic

Akash G. Jadhav and Pramod B. Khedekar

University Department of Pharmaceutical Sciences, Rashtrasant Tukadoji Maharaj Nagpur University, Nagpur - 440033 India.

Corresponding author email :

Abstract

With the origination and extending of the new coronavirus in 2019, a newly public health crisis is threatening to the world (2019-nCoV) or Severe Acute Respiratory Syndrome Coronavirus 2. This virus is developed in bats and started to spread quickly to humans in Wuhan, Hubei Province, China in December 2019. Transmitted by an unidentified intermediary animal. Disease started to spread via through the inhalation or contact with infected droplets, and it includes the incubation period of 2 to14 days. Mainly it includes symptoms like fever, cough, sore throat, difficulty of breathing, tiredness, and malaise. This disease causes mild symptoms not leading to severe conditions. In some people (generally the elderly and patients with the comorbidities), it may engross into the pneumonia, acute respiratory syndrome (ARDS) and also leads to the multiple organ dysfunction. The case fatality rate is found to be 2% to 3%. The diagnosis of this virus is mainly confirmed by an special molecular test in the respiratory secretions of the virus. Common findings about this virus in the laboratory are normal/low white blood cell count and elevated C-reactive protein (CRP). Treatment is supportive in nature, the effect of antiviral drugs is not yet established. Prevention needs the isolation of suspicious cases at home and those having the mild illness and severe infection should be treat in hospital control measures. The virus transmits quickly than its both ancestors which are SARS-CoV and Middle East respiratory syndrome coronavirus (MERS-CoV), but having the low mortality rate.

Keywords : SARS-CoV-2. COVID-19. Pneumonia. MERS-CoV.

Introduction

Corona virus on its outer surface reflects like coronal spike viral because of this, it was named as Coronavirus. Coronaviruses exists in the Coronaviridae family in the Nidovirales order. The size of the coronavirus is small (65-125nm) in diameter, and it contains a single-stranded RNA as a nucleic acid material, size range length from 26 to 32kbs. Corona viruses 'family's subgroups are alpha (α), beta (β) gamma (γ) and delta (δ) corona virus.These viruses were assumed to spread among the animals until the world observe a severe acute respiratory syndrome (SARS) outbreak caused by SARS-CoV, 2002 in Guangdong, China. Just ten years later, other pathogenic Coronavirus named Middle East Respiratory Syndrome Coronavirus (MERS-CoV) caused epidemics in Middle Eastern countries.[1] In humans corona viruses causes the respiratory infections, which generally are mild, which normally have the common cold; but are rare SARS, MERS and new other coronavirus and forms. The current outbreak can be fatal.[2]

History

There are four coronaviruses which are HKU1, NL63, 229E and OC43 which has been circulated in the human body and generally spreads mild respiratory disease to the peoples.

There has been two incidents in the past last two decades in which there is exchange of animal beta corona viruses to humans is reported and showing the severe illness. Such type of first example was in 2002 -2003, a new beta coronavirus was originated in Bats and were passed to humans by the intermediate hosts Palm civet cat in Guangdong Province, China. This virus was known as the severe acute respiratory syndrome coronavirus, because of that virus 8422 people were affected and this incident took place in China and Hong Kong that leads to 916 deaths (11% mortality).[3] After that incident about ten years later, in 2012, the Middle East Respiratory Syndrome Coronavirus also the origin of bats, was noted in Saudi Arabia alongside with the dromedaries serving as an intermediate host to the virus because of which 2494 people were affected, and 858 deaths took place (34% death rate) in that incident.[4]

Origin and spread of covid19

China's major transportation hubs were beginning to appear to the local hospital showing the severe pneumonia symptoms unaware of the reason. Many firstly cases have the common opportunities. To the South China Seafood Wholesale Market which buys and trades the live animals surveillance system (put into use after SARS Outburst) and the patient's respiratory sample were activated and sent to a reference laboratory for the further etiological investigation. On December 31, 2019, China notified the outbreak of this pandemic to WHO and Huanan. On January 1st Seafood market was closed because of the outburst of pandemic condition. On January 7 the virus was recognized as a corona virus having a >95% similar to the corresponding bat corona virus. The similarity of bat corona virus to SARSCoV is > 70%. Environmental samples of the Huanan Seafood market also tested positive, revealing that the spreading of the virus was from there.[5] This infection started to expand aggressively in short span of time because of this the number of cases started to increase aggressively, in that some cases which didn't have the contact to the animal market place were also showing positive symptoms of the virus. From this point it was conclude that the spreading of the infection occurs by the humans.[6] This infection case was firstly reported on January 11, 2020. Mass migration of china's people sat the time of Lunar New Year has engrossed this epidemic. Another cases in the Chinese provinces, other countries/regions (Thailand, Japan in short span of time people quickly reported in South Korea) who came back from Wuhan. Spreading of this virus to the healthcare workers and the staff who were taking care of the patients carrying this disease was notified on Jan 20 2020. As of January 23, entire population of Wuhan which is approximately 11 Million restricted access restriction from that area. Soon this lockdown had been extended to other Hubei Provinces city. Cases of COVID-19 in another countries outside territories of the china were reputed which states that the transmission of COVID-19 cases are transmitted locally by humans in their respected countries only without having any travel history to china.[7]Airports of various countries including India have established screening mechanisms to detect people showing the symptoms of (Covid19) returned from China and to isolate them and afterwards test them for COVID-19. Quickly it was observed that the infection can spread from the asymptomatic people before the onset of symptoms. Therefore, most of the countries including India evacuated their citizens and contingent passengers from the contaminated regions of Wuhan via through special flights return from China, so that all the people having the symptoms or another symptoms had been isolated for next 14 days and examined for the corona virus symptoms.[8] In fact, on February 12 china changes its clarity on confirmed cases to incorporate patients with negative/pending molecular tests, but with clinical, radiology and epidemiology reports. Because of the covid-19 infection that has led to an increase in cases 15,000 a day.[9]

Pathogenesis

Patients suffering with COVID-19 showed higher white blood cell counts, abnormal breathing, elevated plasma pro-inflammatory levels such as cytokines. A COVID-19 case report says that patients having fever for 5 days cough, and difficulty in breathingas well the body temperature was upto 39.0°C are the usually symptoms of the infection.The patient's sputum showed positive to the real-time polymerase chain reaction results that confirmed COVID-19 infection. Laboratory reports says that leukopenia with leukocyte counts of 2.91 × 10 ^ 9 cells / L of which 70.0% were neutrophils. In addition, a value of 16.16 mg / L of blood C-reactive protein was observed to be above the normal range (0-10 mg / L). Elevated erythrocyte sedimentation rate and D-dimer were also observed in the reports.[10] The main pathogenesis of COVID-19 infection is that the virus targeting towards the respiratory system and that leads to the disease like severe pneumonia, RNAaemia, combined along the incidence of ground glass opacities and acute heart disease injury.

Remarkable high blood levels of cytokines and chemokines were reported in patients showing COVID-19 infection that comprises IL1-â, IL1RA, IL7, IL8, IL9, IL10, Basic FGF2, GCSF, GMCSF, IFNă, IP10, MCP1, MIP1á, MIP1â, PDGFB, TNFá, and VEGFA. Some of the serious cases admitted to the intensive care unit showed high levels of pro-inflammatory cytokines comprising IL2, IL7, IL10, GCSF, IP10, MCP1, MIP1á, and TNFá that leads to the disease severity.[11] Studies have reveal that there is greater viral loads in the nasal cavity comparatively to the throat without any difference in viral load between symptomatic and asymptomatic people.[12] Such infected droplets might spread from 1–2 m and settles on surfaces. Virus can stay viable on the surfaces for days in favorable weather conditions, but are destroyed in less than a minute by some common disinfectants such as the sodium hypochlorite, hydrogen peroxide, etc.[13]

Clinical Features

The clinical characteristics of COVID-19 are diverse, ranging from asymptomatic state to the acute respiratory distress syndrome and multi-organ dysfunction. Common clinical reports states that fever (not for everyone), cough, sore throat, headache, fatigue, headache, myalgia, and shortness of breath are the common symptoms. Conjunctivitis has also been observed in some cases. Because of this they are indistinguishable from other respiratory infections. In a subset of patients, at the end of the the first week the disease may progress to pneumonia, respiratory failure and cause death. This progression leads with an extremes increased inflammatory cytokines comprising IL2, IL7, IL10, GCSF, IP10, MCP1, MIP1A and TNFá.[14] The average time for the start of symptoms to dyspnea was 5 days, hospitalization 7 d and for acute respiratory distress syndrome (ARDS) 8 days. The need for admission to intensive care was in 25-30% of affected patients in published series. Witnessed obstacle comprises acute lung injury, ARDS, shock, and acute kidney injury. Recovery started in the second or third week. The average time span of hospital stays in those who recovered was 10 d. Unfavorable outcomes and death are more common in the elderly and those with underlying comorbidities (50-75% of fatal cases cases). The mortality rate in hospitalized adult patients varies from 4 to 11%. The overall fatality rate is approximate to vary between 2 and 3%.[15] Studies indicates that the main manifestations of COVID-19 are fever (90% or more), cough (about 75%) and dyspnea (up to 50%). A mild but significant subset has gastrointestinal symptoms. Preliminary estimates fatality, probably decrease as better early diagnosis efforts come into play, it is around 2%, mainly due to ARDS, AKI and myocardial injury.[16] The disease in newborns, infants, and children has also been reported to be noted softer than their adult counterparts. In a series of 34 children admitted to a hospital in Shenzhen, China between January 19 and February 7, there were 14 men and 20 women. Average age was 8 year and 11 months taken and in 28 children the infection was related to a family member and 26 children had travel /residency history to Hubei Province in China. All patients were asymptomatic (9%) or having a mild illness. No severe and censorious were observed. The most common symptoms were fever (50%) and cough (38%). All patients recovered with symptoms therapy and there were no mortalities. A case of severe pneumonia and multi-organ dysfunction in a child has also been reported.[17]

Diagnosis

Diagnosing new SARS-CoV-2 infection and related diseases, that is, COVID19 utilize two important method; a diagnostic use of RNA bases Quantitative Reverse Transcriptase Polymerase Chain Reaction (RT-PCR) and the second serological test, namely plasma antibody.[18] The complete genome of the new SARS-CoV-2 is available on NCBI, other biological databases provide simplified quantitative RT-PCR.[19] Based on the genomic information from WHO and CDC provided guidelines; universal primers and methods for RT-PCR testing of new SARS-Co-2. The RT-PCR test is mainly observed on throat and the nasal swab sample contains SARS-CoV-2 as its genetic material i.e. Ss RNA. Viral RNA is used as a template here for the reverse transcription and conversion to the DNA. Converted DNA enables PCR amplification of genes of the using suggested materials (identical to viral load) primer. The RT-PCR-based diagnostic test for SARS-CoV-2 is the most useful and reliable method currently and widely used and recognized around the globe. Advantages of RT-PCR-based diagnosis SARS-CoV-2 detection is an early detection of the virus infection. This technology (RT-PCR) is systematic and capable of diagnosing whether there are some copies of the new SARSCoV 2 gene transcripts (ssRNA). Recently discoveries reveals that there is a slight genetic variation in the new SARS-CoV-2 in various parts of the world; but it doesn't have that much impact on RT-PCR is the primer conserved regions in the viral genome.[20] Suspected cases are defined as those who having fever, sore throat and cough alongwith travel history to the

China or other regions which normally have continuous local transmission or contact with the following patients having the similar travel experience or travel history with confirmed COVID-19 infection. However, the situation may have no symptoms or even no fever but the confirmed case has positive molecular test. Other laboratory examinations are not that much specific. The white blood cell count is usually normal or low. It might have lymphocyte decrease in count; lymphocyte count <1000 suffering from a serious illness. Platelet count is gradually normal or mildly low. CRP and ESR are gradually increased, but procalciton in levels are generally constant. High procalcitonin levels it might indicate that the bacterial co-infection. ALT / AST, Prothrombin time, creatinine, D-dimer,CPK and LDH might elevated and high levels are associated with the serious illness.Chest X-ray (CXR) normally shows the bilateral invasion but it may be normal in the early disease and the CT is more sensitive and specific. CT imaging generally shows infiltration, the ground glass is cloudy and subdivided into the segments. Abnormal in asymptomatic patients with regardless clinical evidence of lower respiratory tract participate. In fact, abnormal CT scans are being normally used for diagnosing COVID-19 in suspected cases with negative molecules diagnosis; many of these patients are molecule positive after the repeating testing.[21]

Differential Diagnosis

Differential diagnosis includes all types of breathing viral infection [influenza, parainfluenza, respiratory syncytial Virus (RSV), adenovirus, human metapneumovirus, non-COVID-19 coronavirus], atypical organisms (mycoplasma, chlamydia) and bacterial infections. It is nearly impossible to distinguish COVID-19 from other infections clinically, or Pass routine laboratory tests. So, travel history becomes an important aspect for diagnosing. However, as the epidemic spread, travel history will become irrelevant.[22]

Treatment

The first step in the treatment is having assurance of adequate isolation to prevent the circulation of the virus to other contacts, patients and medical staff. Mild disease should be managed and consult about its hazard signs at home. Generally the main principle to avoid this infection is to maintain moisture and nutrition and also to control fever and cough. Routinely use of antibiotics and also avoid using the antiviral drugs such as the oseltamivir in the confirmed cases. Hypoxic patients need to provide oxygen through the nasal prongs, masks, high-flow nasal catheters (HFNC) or non-invasive ventilation. Mechanical ventilation, and also the extra membrane may need for the oxygen support. Kidney replacement therapy might be required in some severe cases. Antibiotics and antifungals should be taken if co-infection is suspected or proven, it is required. The role of corticosteroids has not been proven; and the current international Consensus, WHO opposed for using the corticosteroid treatment. The Chinese guidelines do recommend short-term treatment and low dose corticosteroids in COVID-19 ARDS.[23][24] Detailed guidelines for intensive care management by WHO has released on documents of COVID-19.[25] Severe acute respiratory infection, respiratory distress, Hypoxemia or shock requires immediate treatment of Oxygen therapy. This should reach the SpO_2 target at a rate of 5 L/min in non-pregnant adults and in children e”90%, pregnant e”92-95% females.[26] If there is no shock, intravenous fluids should be given carefully.[27] National Health Commission of the People’s Republic of China, it is recommended to use IFN-á and lopinavir/ritonavir. This suggestion is according to previous studies, these drugs can reduce mortality rate in patients with severe acute respiratory syndrome (SARS).[28] Neuraminidase inhibitor Oseltamivir is currentlyunder the development although lacking, it is still used by Chinese medical staff for suspected infection without any conclusive evidence of its effectiveness against COVID-19. Glucocorticoids can also be used in severely immune patient’s reaction. For children, methylprednisolone should set up a limited to 1-2 mg/kg/day, up to 5 days.[29]

Prevention

As there is currently no approved treatment for the infection, prevention is essential to stop or inhibiting this infection. Some of the characteristics of corona virus make prevention difficult that is the non-specific characteristics of preventive measures disease, contagious even before the onset of symptoms. The incubation time, the spreading of the virus through the asymptomatic people, long incubation period, tropism on mucosal surface conjunctiva, disease and

prolonged transmission time even after clinical recovery. Isolate confirmed or suspected cases of mild illness it is recommended to stay at home. Home ventilation is good because in the sunlight the virus can be destroy. Patient should wear a simple surgical mask and should maintain cough hygiene. Nursing staff should perform surgery by wearing a mask and maintain hand hygiene when in the same room as the patient is there after every 15-20 minutes. The biggest risk of COVID-19 is to transmission to medical personnel. In the SARS outbreak in 2002, Medical staff were affected mostly. [30] At the community level, people should be asked to avoid crowded places and postpone unnecessary travel to the continuous spreading of the virus. People should follow to practice cough by coughing sleeves/tissues instead of hands and practice hand hygiene every 15-20 minutes. Patients with respiratory symptoms should be use or wear surgical mask. Healthy people use masks in public no place shown to prevent respiratory virus infection not currently recommended by WHO. [31]

Recommendations for Patients, Their Families and Caregivers

General Recommendations

- Being isolate at home is the best way to save yourself from covid-19 infection. Keep minimal contact with people having the suspicious symptoms. (E.g. Handshake, hug or kiss).
- Pay special attention towards the fever, cough, shortness of breath, chills, headache, diarrhea, nausea, vomiting and runny nose, especially in two weeks in contact with anyone having such kind of symptoms.
- If your throat is sore, dry cough, with or without a cold fever or shortness of breath, please contact your consultant Doctor, the center where you are being treated or Centers that provide COVID-19 care.
- Wash your hands mainly with the soap and water for at least 20 seconds, or use disinfectants containing at least 70% alcohol.
- Cover your mouth when you sneeze or cough, and immediately throw the tissues in the trash can.
- Minimize touching to the eyes or face.
- In areas such as tonic public places or medical centers, sneezing or coughing symptoms are observedthen take care for patients with fever and cough should wear mask.
- Ensure the regular consumption of fresh fruits and vegetables with properly cleaned and sterilized.

In Medical Centers

- Ask your therapist to delay or minimize the diagnostic procedure which should not harm your treatment, and health.
- If it is necessary to be in a medical center be there, if not then reduce your presence time and avoid crowding waiting area.
- Keep at least one-meter distance from each another while people are waiting for visit in hospital or office lounge.
- Wear a mask and it is best to wear gloves to avoid touching the mouth and nose or eyes while attending the medical centers.

In Public Places

- Minimize outdoor activities as much as possible. Avoid going to public areas or crowded areas and keep Minimum distance of one meter.
- If you must go to public places, please wear a mask.
- Avoid touching public transportation surfaces. Therefore, wash and disinfect your hands immediately and regularly.
- To press elevator button in a public place, use the object Such as napkins, cotton swabs or toothpicks, then throw them into the nearest trash can immediately.
- In the elevator, don't face the door, and avoid chatting with peoples.
- Do not go to the restaurant, you can use if it is needed, and use disposable tableware and glasses in the restaurant to avoid spreading of this infection.
- Wash your hands with soap and water or disinfectant solution immediately after touching the keyboard, Computer mouse, telephone, elevator button, ATM, Light switches, doorbells in public places or houses, personal fingerprint device.

At Home

- If you have been to a hospital, clinic or medical office, put the clothes in the washing machine immediately take a shower and put on clean clothes after returning.
- Should appoint a person as care of cancer patient: This person should pay more attention to hygiene advice and minimal contact with other family members outdoor environment.
- Nursing staff should wear masks at all times caring for cancer patients should wash their hands immediately after and before treatment regularly.
- Do not let people with any symptoms like common cold, even mild runny nose or sneezing, to enter the patient's place of residence.
- Plan a balanced weekly diet for the patient and follow all the hygiene recommendations mentioned, especially wash your hands regularly when preparing meals.[32]

Conclusions

The recent COVID-19 outbreak is considered as the global health emergency situations. It is obvious, that isolation may not be enough to stop the spreading of COVID-19 and the impact of this virus infection is one of the growing concerns. Further undoubtedly it needs to do research to help and also to define how exactly the virus is transmitting from human-to-human and animal-to-human. For the promotion of development of virus-specific vaccines. Obviously, the possibility of a pandemic COVID-19 requirements are strictly monitoring and ongoing monitoring is to accurately track and possibly predict its future host adaptability, evolution, transmissibility and pathogenicity. These factors ultimately it will affect the mortality and prognosis. However, the rapidly evolving nature of the COVID-2019 epidemic is changing with each passing day statistics, and constantly revealing new research results represent the major limitation of this review.

References

1. Zhong N, Zheng B, Li Y, Poon L, Xie Z, Chan K, et al. Epidemiology and cause of severe acute respiratory syndrome (SARS) in Guangdong, People's Republic of China, in February, 2003. The Lancet 2003;362(9393):1353–8..

2. International Committee on Taxonomy of Viruses. "ICTV Master Species List 2009 – v10". Available from: https://en.wikipedia.org/wiki/Coronavirus.

3. Chan-Yeung M, Xu RH. SARS: epidemiology. Respirology. 2003;8:S9–14.

4. Middle East Respiratory Syndrome Coronavirus. Available at: https://www.who.int/emergencies/mers-cov/en/. Accessed 16 Feb 2020.

5. Xinhua. China's CDC detects a large number of new coronaviruses in the South China seafood market in Wuhan. Available at: https:// www.xinhuanet.com/2020-01/27/c_1125504355.htm. Accessed 20 Feb 2020.

6. Huang C, Wang Y, Li X, et al. Clinical features of patients infected with 2019 novel coronavirus in Wuhan, China. Lancet. 2020;395: 497–506.

7. Rothe C, Schunk M, Sothmann P, et al. Transmission of 2019- nCoV infection from an asymptomatic contact in Germany. N Engl J Med. 2020. https://doi.org/10.1056/NEJMc2001468.

8. Li Q, Guan X,Wu P, et al. Early transmission dynamics in Wuhan, China, of novel coronavirus-infected pneumonia. N Engl J Med. 2020. https://doi.org/10.1056/NEJMoa2001316.

9. World Health Organization. Situation reports. Available at: https:// www.who.int/emergencies/diseases/novel-coronavirus-2019/ situation-reports/. Accessed 22 Feb 2020.

10. J. Lei, J. Li, X. Li, X. Qi, CT imaging of the 2019 novel coronavirus (2019-nCoV) pneumonia, Radiology(2020) 200236, https://doi.org/10.1148/radiol. 2020200236.

11. C. Huang, Y. Wang, X. Li, L. Ren, J. Zhao, Y. Hu, et al., Clinical features of patients infected with 2019 novel coronavirus in Wuhan, China, Lancet 395 (10223) (2020)497–506, https://doi.org/10.1016/S0140-6736(20)30183-5

12. Zou L, Ruan F, Huang M, et al. SARS-CoV-2 viral load in upper respiratory specimens of infected patients. N Engl J Med. 2020 https://doi.org/10.1056/NEJMc2001737.

13. Kampf G, Todt D, Pfaender S, Steinmann E. Persistence of coronaviruses on inanimate surfaces and its inactivation with biocidal agents. J Hosp Infect. 2020 Feb 6. pii: S0195–6701(20)30046–3.

14. Chen N, Zhou M, Dong X, et al. Epidemiological and clinical characteristics of 99 cases of 2019 novel coronavirus pneumonia in Wuhan, China: a descriptive study. Lancet. 2020;395:50713.

15. Coronavirus Outbreak. Available at: https://www.worldometers.info/coronavirus/. Accessed 23 Feb 2020.

16. Review of the Clinical Characteristics of Coronavirus Disease 2019 (COVID-19) Fang Jiang1, Liehua Deng2, Liangqing Zhang3, YinCai1, Chi Wai Cheung1, and Zhengyuan Xia1,3.

17. Chen F, Liu ZS, Zhang FR, et al. First case of severe childhood novel coronavirus pneumonia in China. ZhonghuaErKeZaZhi. 2020;58:E005.

18. Fang Y, Zhang H, Xie J, Lin M, Ying L, Pang P. Sensitivity of chest CT for COVID-19: comparison to RT-PCR. Radiology. 2020: 200432. https://doi.org/10.1148/radiol.2020200432

19. Tian X, Li C, Huang A, Xia S, Lu S, Shi Z. Potent binding of 2019 novel coronavirus spike protein by a SARS coronavirus-specific human monoclonal antibody. EmergMicrob Infect. 2020;9: 382e385.

20. Corman VM, Landt O, Kaiser M, Molenkamp R, Meijer A, Chu DKW. Detection of 2019 novel coronavirus (2019-nCoV) by real-time RT-PCR. Euro Surveill. 2020;25(3):2000045. https: //doi.org/10.2807/1560 7917.ES.2020.25.3.2000045.

21. Huang P, Liu T,Huang L, et al.Use of chest CTin combination with negative RT-PCR assay for the 2019 novel coronavirus but high clinical suspicion. Radiology. 2020. https://doi.org/10.1148/radiol. 2020200330.

22. A Review of Coronavirus Disease-2019 (COVID-19) Tanu Singhal1 The Indian Journal of Pediatrics (April 2020) 87(4) : 281–286 https://doi.org/10.1007/s12098-020-03263-6.

23. Chen Z-M, Fu J-F, Shu Q, et al. Diagnosis and treatment recommendations for pediatric respiratory infection caused by the 2019 novel coronavirus. World J Pediatr. 2020:1–7. https://doi.org/10. 1007/s12519-020-00345-5.

24. Russell CD, Millar JE, Baillie JK. Clinical evidence does not support corticosteroid treatment for 2019-nCoV lung injury. Lancet. 2020;395:473–5.

25. Zhao JP, Hu Y, Du RH, et al. Expert consensus on the use of corticosteroid in patients with 2019-nCoV pneumonia. ZhonghuaJie He He Hu Xi ZaZhi. 2020;43:E007.

26. World Health Organization. Coronavirus disease [COVID-19] Technical Guidance: Infection Prevention and Control. Available at: https://www.who.int/emergencies/diseases/novel-coronavirus-2019/technical-guidance/infection-prevention-and-control. Accessed 20 Feb 2020

27. M.J. Schultz, M.W. Dunser, A.M. Dondorp, et al., Current challenges in the management of sepsis in ICUs in resource-poor settings and suggestions for the future, Intensive Care Med. 43 (2017) 612–624.

28. C.M. Chu, Role of lopinavir/ritonavir in the treatment of SARS: initial virological and clinical findings, Thorax 59(2004) 252–256.

29. D. Wang, B. Hu, C. Hu, et al., Clinical characteristics of 138 hospitalized patients with 2019 novel coronavirus–infected pneumonia in wuhan, China, J. Am. Med.

30. Chang D, Xu H, Rebaza A, Sharma L, Dela Cruz CS. Protecting health-care workers from subclinical coronavirus infection. Lancet Respir Med. 2020. https://doi.org/10.1016/S2213-2600(20)30066- 7.

31. Li J, Li J, Xie X, et al. Game consumption and the 2019 novel coronavirus. Lancet Infect Dis. 2020. https://doi.org/10.1016/ S1473-3099(20)30063-3.

32. COVID19 Prevention & Care; A Cancer Specific Guideline. Ali Motlagh, MD, MPH1,2; MaisaYamrali, MD3*; Samira Azghandi, MD4; PayamAzadeh, MD2; Mohammad Vaezi, MD4; FarzanehAshrafi, MD5; KazemZendehdel, MD, PhD6; HamidrezaMirzaei, MD2; Ali Basi, MD7; AfshinRakhsha, MD2; ShararehSeifi, MD8; MortezaTabatabaeefar, MD2; Ahmad Elahi, MD9; PounehPirjani, MD10; Leila MoadabShoar, MD3; FaranakNadarkhani, MS11; MostafaKhoshabi, MS12; MassihBahar, PhD13; FatemehEsfahani, MD8,14; HosseinFudazi, MD15; FarhadSamiei, MD16,17; BornaFarazmand, MD18; AzinAhmari, MD19; MojtabaVandRajabpour, MD6; GhasemJanbabaei, MD4,20; AlirezaRaisi, MD21,22; AfshinOstovar, MD, PhD1,23; Reza Malekzadeh MD1,24,25 doi10.34172/aim.2020.07.

Peer Reviewed and Refereed Journal 2022 **(ISSN : 09726330)**

Rashtrasant Tukadoji Maharaj Nagpur University
SCIENCE JOURNAL 2022
Vol. : XV

A Review on Carbon Nanotubes

Mangesh A. Mapari[a], Pramod B. Khedekar.[b]

Department of Pharmaceutical Sciences, RTM Nagpur University, Nagpur, Maharashtra, India, 440033

Corresponding author email :
jbrandhawa2@gmail.com
*pacific0701@gmail.com
Mob. No. 7776899668

Abstract

Carbon nanotubes show special tubular shape of nanometer diameter. The carbon atom of the shells is carefully connected to form honeycomb like structure in the graphite sheets. The nanotubes can be steel or semiconducting relying on their structural parameters. Different types of carbon nanotubes can be produced in a number of ways. The most accepted strategies used at existing are: arc discharge, laser ablation and chemical vapour deposition. Purification of the tubes can be divided into a couple of fundamental techniques: oxidation, acid treatment, annealing sonication, filtering and functionalisation techniques. The principal goal of this paper is to spotlight synthesis, properties and utility of carbon nanotube.

Keywords : Carbon nanotubes, Synthesis, Drug discovery,Functionalisation chemistry.

INTRODUCTION

Nanoparticle is a microscopic particle with at least small size less than 100 nm. A nanotube is a tube like structure having size in nanometer. Carbon nanotubes are tubes consist graphine sheet and carbon atom. Carbon containing sp^2 hybridisation having extraordinary structures. Graphite is properly regarded instance of it however now beside graphite carbon can structure closed and open cages with honeycomb arrangement[1]. Graphene is regarded as 2D single layer of graphite in the listing of carbon nanomaterials. Graphene is more desirable fabric than diamond due to the fact it comprise sp^2 hybridisation which is better than the sp^3 hybridisation in diamond. In latest a long time carbon nanotubes are the most thrilling areas of research. Carbon nanotubes are made up of carbon and it is a tube formed material. Its diameter is too small and is measured by using nanoscale. CNH are tube like in structure made up of single layer graphene sheets two to three nanometer in diameter that cluster into aggregates with a diameter round eight nanometer[2].

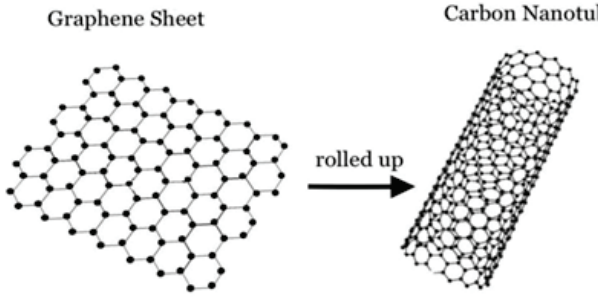

Fig.1. Formation of Carbon Nanotube from Graphene Sheet.[3]

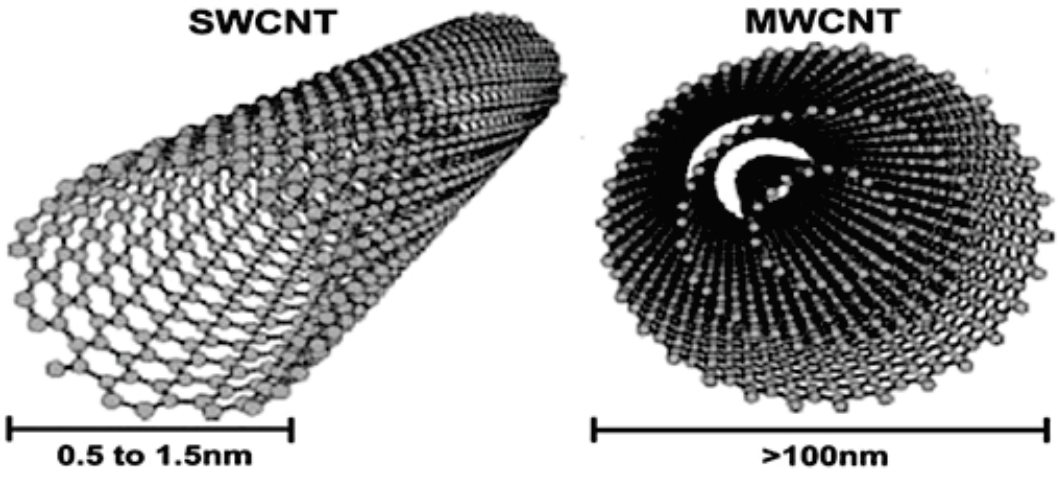

Fig.2. Type of Carbon Nanotube.[3]

2. Method of Preparation Carbon Nanotubes

I. Arc discharge method

Plasma based totally synthesis approach : For high-quality satisfactory of nanotubes plasma primarily based methods or arc discharge method can be used.

It entails two graphite electrode in presence of helium and a contemporary of 50 ampere is surpassed through two graphite electrodes. It motives vapourization of graphite some phase of it condense on response vessel and some of it condense on cathode. The phase which is savings on cathode carbon nanotube. If we desire single walled carbon nanotubes then Co, Ni metals can be added in anode[5].

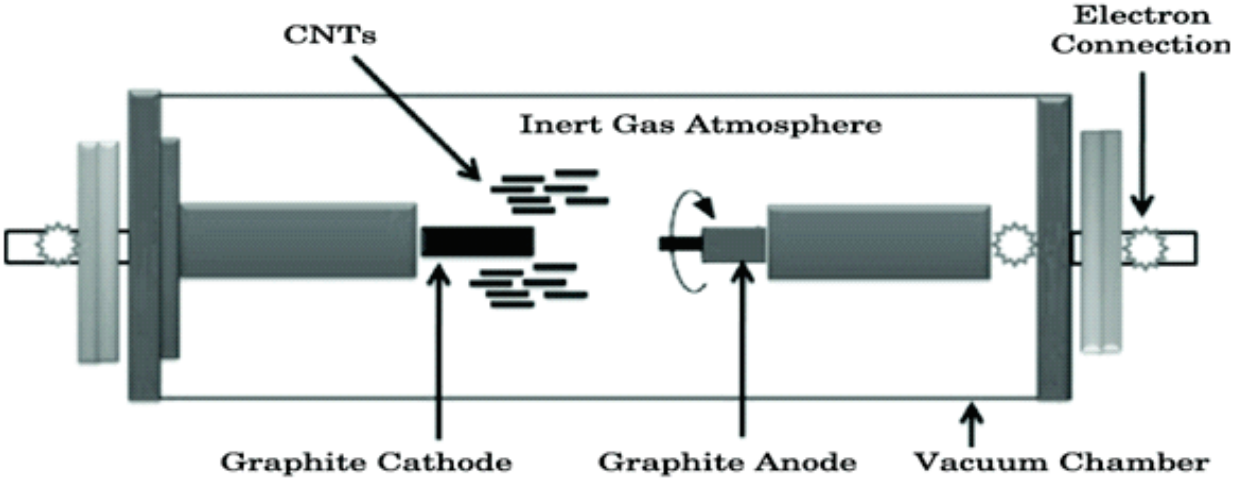

Fig.3. Arc discharge method for CNT.[7]

II. Laser Ableation Method

In 1996 Laser was once used for manufacturing of carbon nanotubes with 70% purity. Presently this technique is used for production of carbon nanotubes. This procedure consist of graphite rods and it comprise 50:50 catalyst combination of Co and Ni at 12000 C and argon is flowing via it for pattern instruction [7].

In this approach metallic catalyze the increase of single walled carbon nanotubes and additionally many aspect

merchandise are formed. We can get nanotubes by using cooling vaporized species.[8]

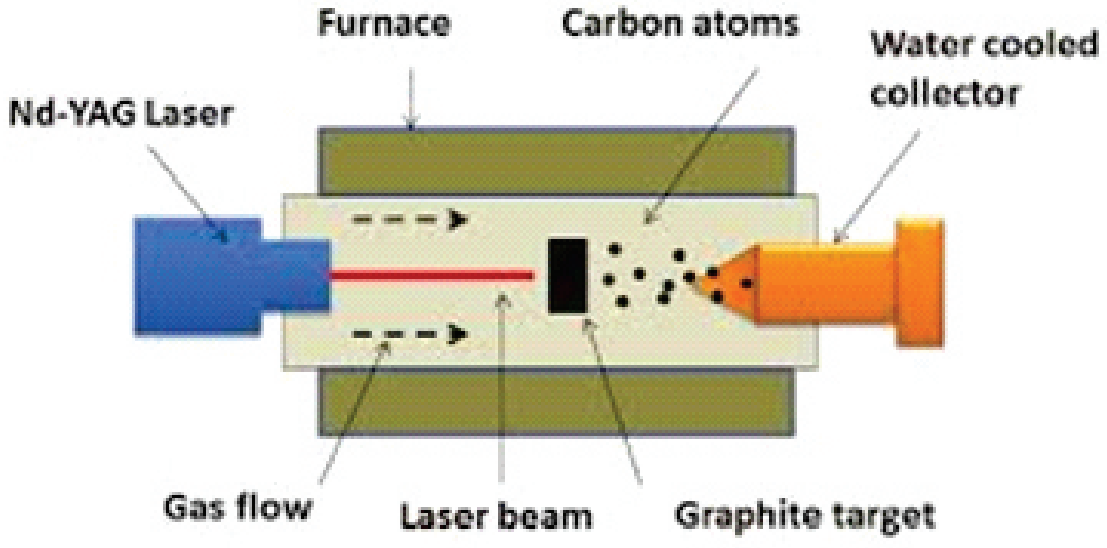

Fig.4. Leaser Ableation Method for CNT.[8]

III. Chemical vapour deposition

It is carried out in two steps :

A. Catalyst is accumulat on substrate and then nucleation of catalyst is carried via chemical linocutor. Reaction catalysts used are Ni, Fe or Co.

B. Then Carbon is supplied in reaction chember. Plasma heated coli used to transfer carbon to atomic level. This carbon then move towards the starting matterial and cover the catalyst to form nanotube. The yield of product may vary.[7-8]

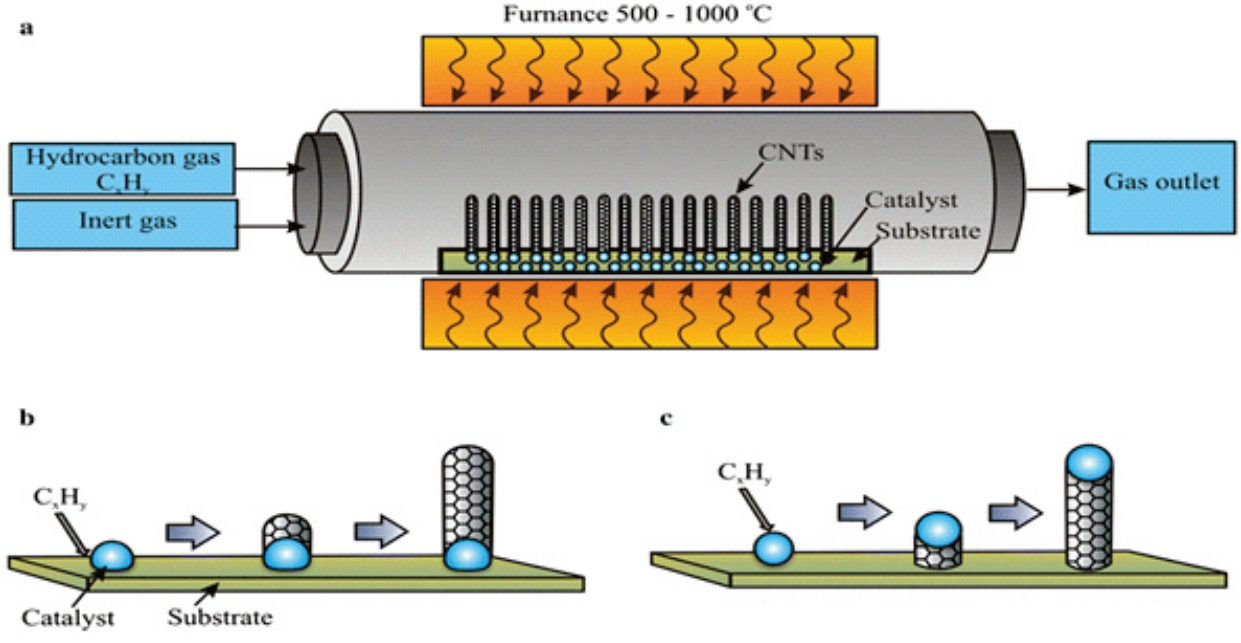

Fig.5. Chemical Vapour deposition method for CNT.[8]

3. Purification of Carbon nanotube [12-14]

Nanotubes which are prepared contain some amount of impurity. That is not acceptable. So that, tube need to be purify using any suitable method given below.

I. Air Oxidation

Air oxidation is one of the easiest and common method used for carbon nanotube purification. This method useful for washing amorphous carbon and reaction catalyst.[12]

II. Acid Refluxing

Refluxing using acid is one of the vigrous method used for purification of nanatube. If air oxidation is not efficient then acid refluxing method is used. Commonly used acid in acid refluxing method are hydrochloric acid, nitric acid, sulphuric acid.

III. Surfactant aided sonication filtration

After air oxidation or acid refluxing the CNT free from amorphous impurity but contain some amount of trapped rection mixture including carbon partical and rection catalyst. This impurity difficult to remove by acid refluxing or air oxidation so that it removed by surfactant aided sonication and filtration. Sodium dodecyl benzene sulphonate (SDBS) used as surfactant for purification using methanol as solvent for sonication.[14]

4. Properties[15]

I. Mechanical

Sp^2 hybridization between carbon atom provide mechanical strength to the CNT. The strength of carbon tube is enough to bear littel stress. Due to its good mechanical strength CNT are used as drug carrier.

II. Electrical

CNT are semiconducting unlike graphene which is a two-dimensional semimetal carbon nanotubes.

III. Optical

Some therotical studies prove that optical activity of CNT are dependent upon its size. This properties are vanished if size of tube become exceptnally larger.

5. Carbon Nanotube in drug discovery

Carbon nanotubes generally and actively explored as progressive carriers for drug shipping and diagnostic applications.Their versatile physicochemical features allow the covalent and noncovalent introduction of numerous pharmaceutically applicable entities and permit for rational format of novel candidate nanoscale constructs for drug development. CNT can functionalized with exceptional useful agencies to lift concurrently quite a few moieties for targeting, imaging and therapy.[16] The bioaccumulation and invivo toxicity of some drugs having low molecular weight affect so much on their activity and efficacy. Because low molecular weight compound posses surface charge which is problematic in drug development and delivary this problem can be solve easily using carbon nanotube carrier. CNT are commen drug carrier in drug discovery. Now a days Functionalized carbon nanotube used as drug conjugate. Some resercher look at CNT as vector for gene encoding and gene transfer in gene therapy.[17-18]

6. Carbon Nanotube functionalised chemistry

CNT are pipe like material in the nanoscale size. They are of two type based on their shape into two fundamental types single-walled carbon nanotubes (SWNT) made up of single layer of graphene sheet rolled into joint less cylindrical

tube and multiwalled carbon nanotubes (MWNT) which consist of double layers of graphene sheet .The distance between two layer is about 0.3 nm. Chemical reactivity of CNT is lies in its tip and sidewall. The tips having same shape as of fullerene hemisphere and it is reactive. The sidewalls are curved and from a tube like structure. Sidewall of CNT are less reactive compair to its tip. So that the most reactions are take place at the tips first and then at sidewalls. This diffrence in reactivity of CNTs tip and sidewall useful in selective oxidation at carbon nanotube tip.[19-20]

7. Functionalisation of CNT

CNT are materials insolvable or hardly distribute in any type of solvent. As CNT are used as carrier in drug delivery system. It solubility is one of the important factor as per biological point of view. To solve this problem functionalisation of CNT is important method. Various methods of solubilization and dispersion used to improve solubility of CNT. Use of surfactants, ploymers and peptides are some common for functionali-zation. Benefit of this technique is that the structure of tube remain intact. Other methodology used for functionalization is covalent modification in this techinque carbon nanotube are reduced and oxidised then functionalized with various functional group .[21]

8. Applications

Ø Carrier for drug delivery

- Ø Amphotericin B and Cisplatin incarporated into carban nanotube to achive sustain drug release. Using carbon nano tube as drug carrier this can achive easily.

  The released Cisplatin form tube is good to achive better activity.
- Ø Some Anticancer drug shows poor permiability as well as distribution this can be solved by using CNT. Polyphosphazene platinum anticancer drug with nanotubes show better distribution and bioavalibility.
- Ø Doxorubicin given with nanotubes showed more intracellular penetration. The gelatin CNT combination has been used as workable carrier machine for biomedicals. [21-23]

Ø Genetic Engineering

Gene transfer and defective gene manupulation is one of the challenging task in the field of genetic engineering. CNT are used as vector carrier for gene delivery in target cell. It also useful for genetic manupulation.[21]

Ø Artificial Implant

Human boadydeany most of implants due to its incompatilbility with body tissue.

Implants also causes post administration pain in body this problem solved upto certain level using carbon nanotube.[21]

Ø As Catalyst

CNT used as catalyst due to its large surface area. It is non rective with many of chemical this properties of CNT make it better catalyst.[21]

- Ø Preservative Carbon nanotubes and nanohorns are antioxidant in nature. Hence, they are used to keep pills formulations susceptible to oxidation. Their antioxidant property in antiaging cosmetics and with zinc oxide as sunscreen dermatological to stop oxidation of essential pores and skin factors .[21]
- Ø Carbon nanotubes technology are used for tissue preparation. In latest years carbon nanotubes are first-class for tissue era due to the fact these are biocompatible, resistant to biodegradation and bettering the organ generation. [24]
- Ø Carbon nanotubes are used for Gene remedy with the aid of DNA delivery. Gene therapy is a therapy used to introducing DNA into cells. [25-26]

9. Disadvantages of CNT

- Ø It is challenging to preserve high quality and lower impurities.[27]
- Ø Cost of nanotechnology is very high.[28]
- Ø In arc discharge and leaser technique big quantity of electricity is required to whole the process. [29]
- Ø It is hard to target massive quantity of graphite in industrial process.[29]
- Ø Poor solubility in most solvents compatible with the biological system.[21]

10. Conclusion

This article on carbon nanotubes displays the overview on structure, preparation their function in drug discovery, functionalization chemistry and purification strategies of carbon nanotubes alongside with their properties hindrance and applications.

The distinct structural properties of carbon nanoparticles make them useful as carrier vectors for pharmaceutical nanodelivery. Carbon nanotubes have the added benefit of being potential nanodevices for managed drug delivery. In this we learn about that chemical vapour deposition is nice strategies for manufacturing of carbon nanotubes due to the fact it offers excessive purity carbon nanotubes.

11. Acknowledgement

I take this oppounity to express my deep sence of gratitude to my guide Dr. P. B. Khedekar, M. Pharm., Ph.D., D.B.M. Professor, University Department of Pharmacutical Sciences Nagpur, for their guidance and valuable suggestions.

It is my previlege and honor to special Thanks for Dr. R.V. Chikhale, M.Pharm., Ph.D., School of Pharmacy, University of East Anglia, Norwich, UK for his valuable suggestion, guidance and liberal encouragment to complete this article.

References :

1. Valentin N. Popove "Carbon nanotubes: properties and application" Materials Science and Engineering R 43 (2004) 61–102.
2. B.K. Kaushik and M.K. Majumder, Carbon Nanotube Based VLSI Interconnects, Springer Briefs in Applied Sciences and Technology, DOI 10.1007/978-81- 322-2047-32.
3. Peter J.F. Harris"Carbon nanotubes science:Synthesis, properties and applications" www.cambridge.org/9780521828956.
4. Kalpna Varshney "Carbon Nanotubes: A Review on Synthesis, Properties and Applications" International Journal of Engineering Research and General Science Volume 2, Issue 4, June-July, 2014 ISSN 2091-2730.
5. Dresselhaus MS, Dresselhaus G, Charlier JC, Hernandez E. Electronic, Thermal and mechanical properties of carbon nanotubes.362(2004);2065- 2098.
6. Brenner D. Empirical potential for hydrocarbons for use in simulating the chemical vapor deposition of diamond films. Physical Review B 42(15): 9458- 9471, 1990.
7. Kaushik B.K, Majumder M.K. "Carbon Nanotube: Properties and Applications" 2015,XI, 86 P 57 illus., softcover. ISBN : 978-81-322-2046-6.
8. Sinnott S.B.; Andrews R. Carbon Nanotubes: Synthesis, properties and applications. Critical Reviews in Solid State Mat. Sci. 26, 145–249, 2001.
9. Mamalis AG, Vogtländer LOG, Markopoulos A. Nanotechnology and nanostructured materials: trends in carbon nanotubes. Precis Eng, 28, 16 (2004). http://dx.doi.org/10.1016/j.precisioneng. 2002.11.002
10. Li WZ, Xie SS, Qian LX, Chang BH, Zou BS, Zhou WY, Zhao RA, Wang G. Large-scale synthesis of aligned carbon nanotubes. Science, 274, 1701 (1996). http://dx.doi.org/10.1126/science.274.5293.1701.
11. Xie S, Li W, Pan Z, Chang B, Sun L. Carbon nanotube arrays. Mater Sci Eng A 286, 11 (2000). http://dx.doi.org/10.1016/S09215093(00)00657-2.

12. Ibrahim Khan "Carbon nanotubes- Properties and Applications: A Review" Article Carbon letters. July 2013 DOI: 10.5714/CL.2013.14.3.131.

13. Vaisman L, Wagner HD, Marom G, The role of surfactants in dispersion of carbon nanotubes, adv Colloid Interface Sci;(2006);128-130.

14. Fernando Ka, Lin Y, Sun YP, High aqueous solubility of functionalized single-walled carbon nanotubes, Langmuir 20;(2004);4777-4778.

15. Peng H, Alemany LB, Margrave JL, Sidewall carboxylic acid functionalization of single-walled carbon nanotubes, J Am Chem Soc 125; (2003);15174-15182.

16. Duncan, R. Polymer conjugates as anticancer nano medicines. Nat. Rev. Cancer 2006, 6, 688–701.

17. Bianco A., Kostarelos K., Partidos C. D., Prato M. Biomedical applications of functionalised carbon nanotubes. Chem. Commun. 2005, 571–577.

18. Iijim S. Helical microtubules of graphitic carbon. Nature (London) 1991, 354 56 58.

19. Niyogi S., Hamon M. A., Zhao, B. Bhowmik, Chemistry of single-walled carbon nanotubes. Acc. Chem. Res. 2002, 35, 1105–1113.

20. Foldvari.M., Bagonluri.M., Carbon nanotubes as functional excipients for nanomedicines: I. Pharmaceutical properties, Nanomedicine: NBM 4, 2008 173-182.

21. Hirlekar R., Yamagar. M., Garse.H., Vij. M., Kadam.V., Carbon nanotubes and its applications, Asian Journal of Pharmaceutical and Clinical Research, Vol 2,Issue 4,2009,24-26.

22. Hou PX, Bai S, Yang GH, Liu C, Cheng HM. Multi-step purification of carbon nanotubes. Carbon 2002; 40: 81-85.

23. Vander Wal, Randall L. and Ticich, Thomas M. Flame and Furnace Synthesis of SingleWalled and Multi-Walled Carbon Nanotubes and Nanofibers. Journal of Physical Chemistry B 2001;105: 10249–10256.

24. Hua He, L.Ai Pham-Huy, P.Dramou, D.Xiao, PengliZuo, and C.Pham-Huy" Carbon Nanotubes: Applications in Pharmacy and Medicine" Hindawi Publishing Corporation BioMed Research International Volume 2013, Article ID 578290.

25. E. Bekyarova, Y. Ni, E. B. Malarkey., "Applications of carbon nanotubes in biotechnology and biomedicine," Journal of Biomedical Nanotechnology, vol. 1 no. 1pp. 3–17, 2005.

26. H. Liao, B. Paratala, B. Sitharaman, and Y. Wang, "Applications of carbon nanotubes in biomedical studies," Methods in Molecular Biology, vol. 726, pp. 223– 241, 2011.

27. R.Chavan, U.Desai, P.Mhatre, R.Chinchole "A REVIEW : CARBON NANOTUBES"Volume 13, Issue 1, March – April 2012; Article-022

28. N. Saifuddin, A. Z. Raziah, and A. R. Junizah "Carbon Nanotubes: A Review on Structure and Their Interaction with Proteins" Hindawi Publishing Corporation Journal of Chemistry Volume 2013, Article ID 676815, 18.

Peer Reviewed and Refereed Journal 2022 **(ISSN : 09726330)**

Rashtrasant Tukadoji Maharaj Nagpur University

SCIENCE JOURNAL 2022

Vol. : XV

Antidiabetic Potential of Isolated Compound from the Stem Bark of *Bauhinia Purpurea* Linn.

Meshram Satish*[1], Itankar Prakash[2]

*[1]Department of Pharmacognosy, Kamla Nehru College of Pharmacy, Butibori, Nagpur -441108, Nagpur (M.S) India

[1]Department of Pharmaceutical Sciences, Rashtrsant Tukadoji Maharaj Nagpur University, Nagpur

Corresponding author email : satish.meshram@gmail.com

ABSTRACT

Bauhinia purpurea Linn. widely known as Purple Orchid-Tree is cultivated throughout India. The Literature survey revealed that the bark of *Bauhinia purpurea* Linn. is traditionally used as an astringent in diarrhea. Flowers are laxative. The bark, root, and flower assorted with rice water are used as suppuration for boils and abscesses[2]. Medicinal uses of bark can be largely attributed to the presence of these tannins and Flavonoids which are a common feature of Bauhinia. It is taken internally as a febrifugal, antidiarrhoeal, and antidysenteric remedy and also as an astringent. In India, the bark is extensively applied in glandular diseases. The present study was undertaken to evaluate the antidiabetic activity of a compound isolated from methanolic extract from the stem bark of *Bauhinia purpurea* using mice i.e. alloxan induced diabetes in mice by glucometer method, with 10 mg/kg of the compound showed significant value.

Keywords : Bauhinia purpurea Linn, Flavenoids Antidiabetic activity, Alloxan, Mice

INTRODUCTION :

Bauhinia purpurea is a small to medium-sized deciduous fast-growing shrub or tree with a round, symmetrical, moderate dense crown to 10 m tall, young branches becoming glabrous or nearly so (glabrescent). In dry forests, the size is much smaller. The bark is pale grey brown, fairly smooth to slightly fissured, and scaly. The twigs are slender, light green, slightly hairy, and angled, becoming brownish grey. The heart wood is brown, hard, and durable. Leaves simple, alternate, base rounded to shallow-cordate, up to 12 cm x 12 cm, deeply 2-lobed at apex up to 1/3-1/2, ca. 7-12 cm long, and equally wide, margin entire and the surfaces smooth and glabrous, and 9- or 11- nerved at the base, the apex lobes rounded or obtuse to subacute, minute stipules 1-2 mm long, petioles puberulous to glabrous, 2.5-3.5 cm long; leaf blades 4.5-11 cm long. Inflorescence a 6-10-flowered raceme in terminal panicles; flowers numerous, hypanthium, turbinate, purple to nearly white or at least purple marked, the flower buds clavate (club-shaped), velvety, ca 3-4 cm long prior to anthesis; fertile stamens 3 or 4, the anthers ca 6 mm long, versatile; ovary superior; corolla of 5 narrow petals and constricted at base, oblanceolate, 3-5cm long, claws 5-10mm long, the banner purplestriate, ca 7 mm wide; calyx tubular, erupted by corolla along one side when flower fully expanding; calyx split into 2 valves with 5 teeth. The young leaves and flowers of various Bauhinia species are eaten as a side dish with rice, or used to flavour meat and fish. Sometimes the seeds are edible. Fodder: In an experiment in Nepal, *Bauhinia purpurea* was found to increase milk production in lactating buffaloes. Leaves with protein content make

good fodder and are greedily eaten by sheep, goats and cattle Fibre : The bark of bauhinia is used to make rope and stems of smaller lianescent species are used for binding. Some Bauhinia species are used for binding. Some Bauhinia species are reputed for their fiber application are used medicinally as well. Tannin or dyestuff. The bark of various Bauhinia species contains considerable amounts of tannin widely used in the leather industry in India.

Diabetes Mellitus is a metabolic disorder; that promote microvascular changes like Neurotoxic, Nephrotoxic and Cardiovascular complication to cause morbidity and mortality. Oral hypoglycemic drugs (OHD's) are the frontline treatment. However, more individual variation in response to OHD's results in treatment failure.

Thus, based on the phytochemical study, quantitative estimation, and antidiabetic activity, the methanolic extract was subjected to the column chromatography for separation and isolation of the constituents present in it. The constituents were collected in fractions and tested. One component was isolated (oil) in 1 to 9 elutes (sample1) and two components were obtained in 10 to 20 elutes (samples 2&3) The Phytochemical screening of the constituent was performed which confirmed the presence of steroids (sample 1) and flavonoid and carbohydrates (sample 2 & 3). The antidiabetic activity of the isolated compound (sample 2) was performed at (10 mg/kg) which showed potent antidiabetic activity due to the presence of flavenoid. [28] The Physico-chemical studies of the isolated constituent were carried out. The melting point of the separated constituent was recorded by using the Melting point apparatus. The UV Spectra and IR Spectra of the constituents were recorded. The isolated constituent may be an isoquercetin.[5,6,7]

MATERIAL AND METHODS :

Plant Material : The stem bark extract of plant *Bauhinia purpurea* Linn[1]. were collected locally, from Bharatnagar opposite L.I.T Nagpur. It was authenticated by Prof. (Mrs.) Alka Chaturvedi, Department of Botany, Nagpur University, Nagpur. Its herbarium is deposited in the Department. (Voucher specimen no.9132) The stem bark of *Bauhinia purpurea* was dried in shade under normal environmental conditions and subjected to size reduction with the help of a Labortory Grinder. The coarsely powdered drug was charged into Soxhlet apparatus and extraction was carried out with Petroleum ether, Chloroform, Ethyl Acetate, Acetone, Methanol, and Hydro-alcoholic extract successively.

Animals : Swiss albino mice (25-30 g) of either sex were used. They were subjected to water and diet (ad libitum Gulmohar rat feed, supplied by Hindustan lever, Hyderabad.) and kept in the animal house with control temperature and the 12h light : 12h dark cycle[14,15,16].

Isolation of active constituent by column chromatography[17]

1) Selection of mobile phase

The solvent system nonpolar to polar was used. The Petroleum ether (60-80ºC), chloroform, ethyl acetate, acetone, methanol were used for isolation with column chromatography. Altering in the composition of the eluting solvent was achieved by adding the second solvent gradually to a reservoir of the first with efficient mixing. This technique is known as gradient elution, wherein proper choice of adsorbent and gradient reduced the tailing of the compound on the column.

2) Preparation of column

The free flowing slurry of adsorbent (silica gel G 60-120 mesh) was prepared by mixing the adsorbent with the mobile solvent (pet. ether). The solvent was poured into the column before adding the slurry. After that, the slurry it was poured gradually and allowed to settle .The air entrapment was removed by vibrating the column with the help of an air bulb inserted in a glass rod, adding an excess amount of solvent, and running off until all the air bubbles were removed. Then place the solvent 1cm above the adsorbent layer and was kept for 30 min. for the full saturation of adsorbent with solvent.

3) Preparation and application of sample

A saturated solution was prepared by suspending the extract (2.5 g) in a particular solvent (methanol), then it was

mixed with silica gel G, the solvent was evaporated and the free flowing sample was loaded over the column, a cotton plug was placed on the sample for preventing the disturbance of sample when the solvent gets added on it.

4) Collection of fraction

The flow rate of the eluent was maintained at 5 ml. per min. Fractions of 25 ml. each were collected.

RESULT AND DISCUSSION

Analysis of fraction

The column was eluted by following the gradient elution technique and analysis of the fraction was done in the following manner.

Table 1 : Gradient elution technique

Sr. no.	Solvent	Proportion (%)	No. of fraction	Analysis
1	Pet. ether	100	10	UV
2	Pet.ether:chloroform	75:25	5	UV
3	Pet.ether:chloroform	50:50	5	UV
4	Pet.ether:chloroform	25:75	5	UV
5	Chloroform	100	15	UV
6	Chloroform: ethyl acetate	75:25	10	UV
7	Chloroform: ethyl acetate	50:50	10	UV
8	Chloroform: ethyl acetate	25:75	10	UV
9	Ethyl acetate	100	10	UV
10	Ethyl acetate: acetone	75:25	10	TLC
11	Ethyl acetate: acetone	50:50	10	TLC
12	Ethyl acetate: acetone	25:75	10	TLC
13	Acetone	100	15	TLC
14	Acetone: methanol	95:5	5	TLC
15	Acetone: methanol	90:10	5	TLC
16	Acetone: methanol	80:20	5	TLC
17	Acetone: methanol	75:25	5	TLC
18	Acetone: methanol	50:50	5	TLC
19	Acetone: methanol	25:75	5	TLC
20	Methanol	100	10	TLC

In all 165 fractions, of 25 ml. each were collected and fractions were pooled on the basis of UV and TLC patterns. **1 to 9** elutes were analyzed by UV spectrum and the elute having the same spectrum were mixed together and elute **10 to 20** were analyzed by TLC pattern using ethyl acetate: methanol : glacial acetic acid : formic acid: water (5:2:1:1:1) as developing solvent, and the spots were visualized by spraying the plate with 5% methanolic sulphuric acid reagent followed by heating in an oven at 110° c for 5 min.

One component was isolated (oil) in 1 to 9 elutes (compound1) and two components were obtained in 10 to 20 elutes (compound 2 & 3), components were studied for Phytochemical study, physicochemical study, antidiabetic study, UV & IR studies.

5.1 - Phytochemical Study [6, 7, 8]

Constituents	Constituents category	Test/reagent	Result
1	Steroids	Salkowaski Libermann Burchard	+ + +
2	Flavonoid Carbohydrate	Shinoda Molisch	+ +
3	Flavonoid Carbohydrate	Shinoda Molisch	+ +

Table 2 : Phytochemical study of isolated compound (1, 2 & 3) :

Physicochemical studies of isolated compounds

A) Colour

Sr.no	Constituent	Colour
1	Compound 1	Yellow
2	Compound 2	Blackish
3	Compound 3	Brown

Table 3 : Colour of isolated compound (1, 2 & 3) :-

B) Solubility

Sr.no	Constituent	Solubility
1	Compound 1	Petroleum ether, chloroform.
2	Compound 2	Methanol, ethanol, water
3	Compound 3	Methanol, ethanol, water, DMSO

Table 4:- Solubility of the isolated compound

C) Melting point (m.p)

Compound 1

The melting point of all the isolated constituents was determined by the open end capillary method.

Sr.no	Constituent	Melting point(°c)
1	Compound 1	-
2	Compound 2	258-260
3	Compound 3	88-90

Table 5-:Melting point of the isolated compound

D) Electron Absorption studies (UV)

UV absorption spectrums of pure constituents were determined by using the spectrophotometer (Shimadzu UV -1601) over the scanning range of 200-400 nm.

Sr.no	Constituent	Absorbance maximas(nm)
1	Compound 1	212
2	Compound 2	274, 267, 258, 251, 225
3	Compound 3	279, 258, 250, 219

1) UV Absorption Spectrums of Compound 1

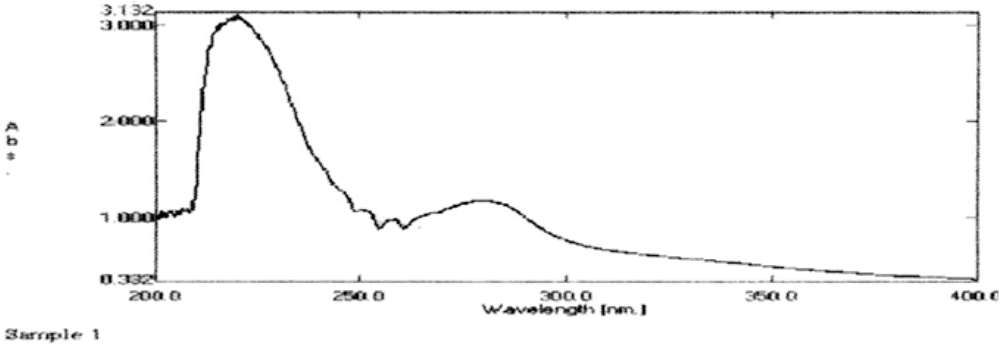

Fig. 1 - UV Absorption Spectrum of Compound 1

2) UV Absorption Spectrum of Compound 2

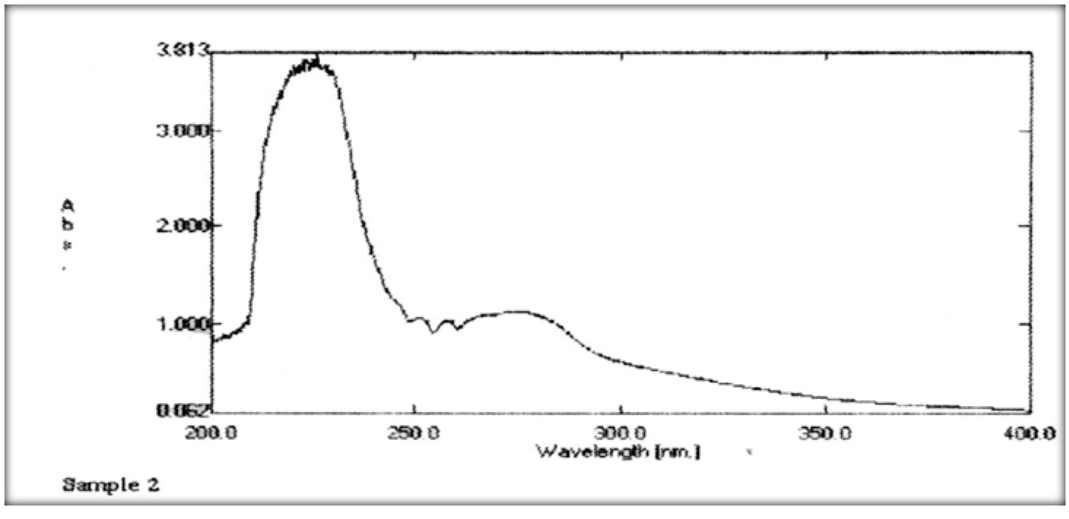

Fig. 2 : UV Absorption Spectrums of Compound 2

3) UV Absorption Spectrum of Compound 3

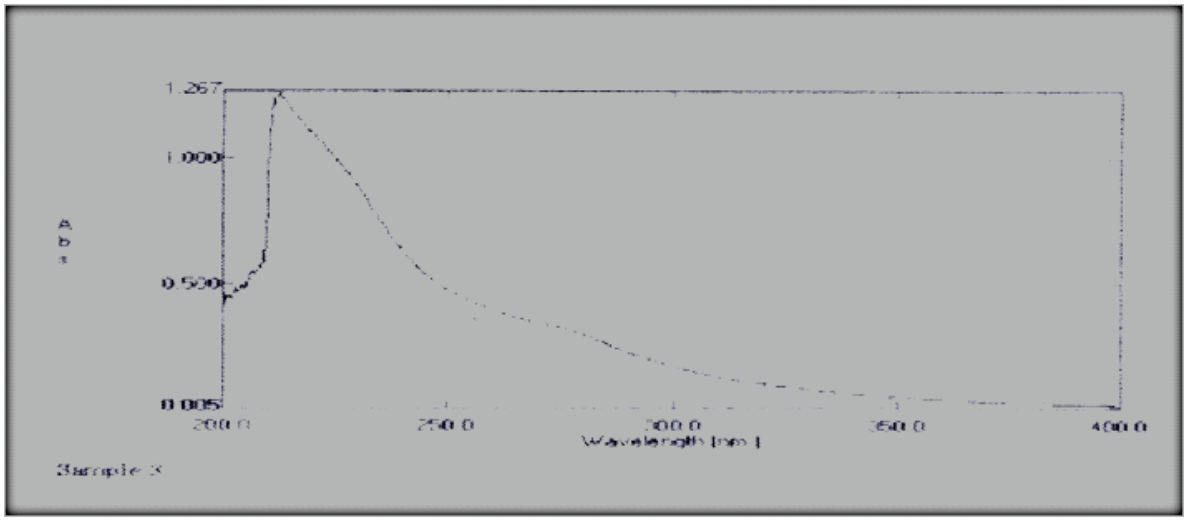

Fig. 3: UV Absorption Spectrum of Compound 3

E) Rotational and Vibrational Absorption studies (IR)

Infrared absorption spectra of a pure constituent in potassium bromide were recorded using FTIR-8010R Spectrophotometer, Shimadzu.

1) IR spectrums of Compound 1

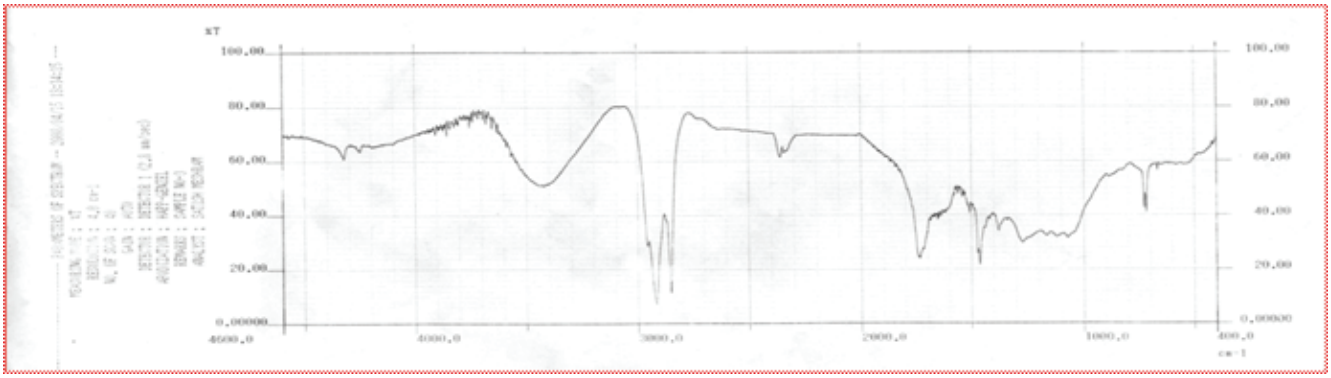

Fig. 4: IR spectrum of Compound 1

Sr.no	Frequency	Type of compound
1.	3400	Alcohol/Phenol , O-H&C-O stretching
2.	2957	Carboxylic acid C=O &O-H stretching
3.	1655	Aromatic C=C bending
4.	1379.3	CH3-X
5	1271.2	Ester unconjugated,C=O&C-O stretching

Table 7 - IR spectrum of Compound

2) IR spectrum of Compound 2

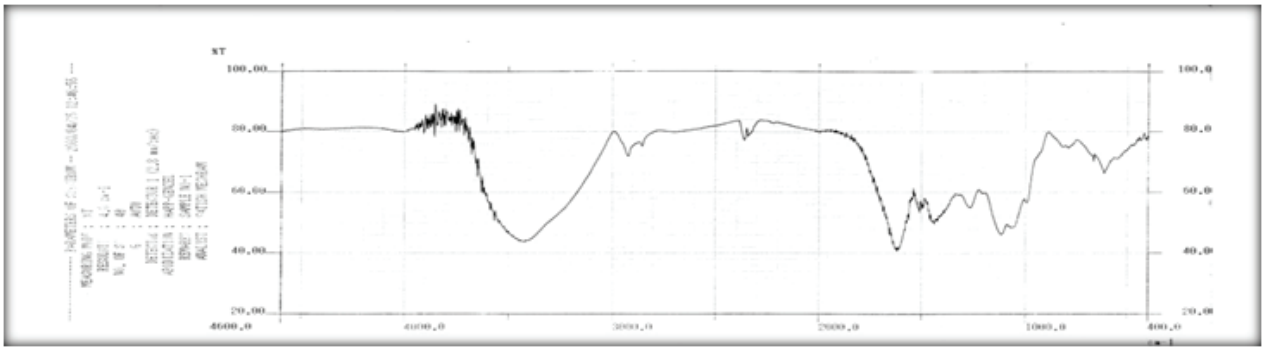

Fig. 5 : IR spectrum of Compound 2

Sr.no	frequency	Type of compound
1.	3300	Alcohol/Phenol, O - H&C-O stretching
2.	2920	Carboxylic acid C=O &O - H stretching
3.	1736	Aldehyde C=O, unconjugated stretching
4.	1458	CH3 - X
5.	1265	Ester unconjugated,C=O&C - O stretching

Table 8 : IR spectrums of Compound 2

3) IR spectrum of Compound 3

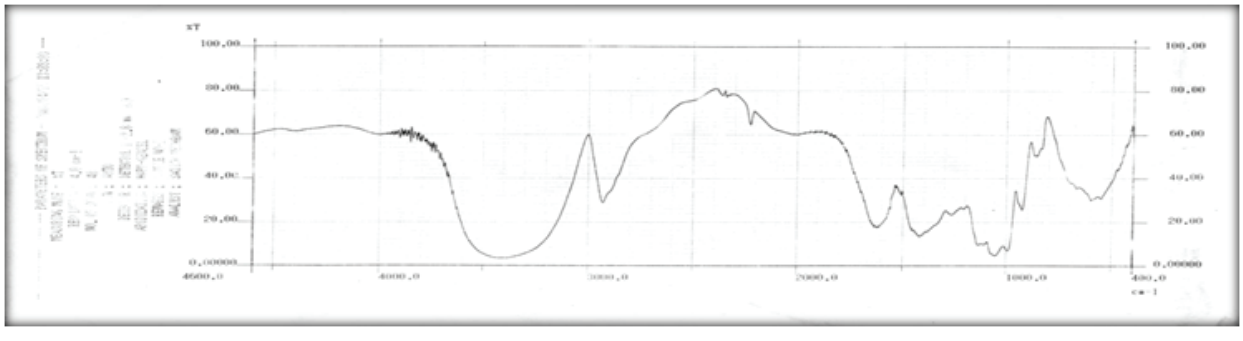

Fig. 6: IR spectrum of Compound 3

Sr.no	frequency	Type of compound
1.	3300	Alcohol/Phenol , O-H&C-O stretching
2.	2928	Carboxylic acid C=O &O - H stretching
3.	2226	Nitrile R-C=N (Aromatic)
4.	1650	Aromatic C=C
5.	1265	Ester unconjugated,C=O&C - O stretching
6.	833	Aromatic C - H bending

Table 9 : IR spectrum of Compound 3

Antidiabetic activity of isolated compound no. 2[11, 12, 13]

Table 10 Antidiabetic activity of isolated compound (compound no.2)

Treatment	0 hr	1 hr	3 hr	5 hr
Control (saline)	271.75 ±1.652	269.25 ±0.8529	264.25 ± 0.8539	262.75 ± 0.4784
Standard (Metform in 50mg/kg)	264.75 ±1.931	241.25 ±1.315	208.75 ±1.315	167.75 ± 0.7500
Isolated compound no. 2 (10mg/kg)	276.25±2.327	253 ±1.080	234.75 ±0.6292	212.25 ±0.8660

Antidiabetic activity of isolated compound no. 2 at 10 mg/kg dose

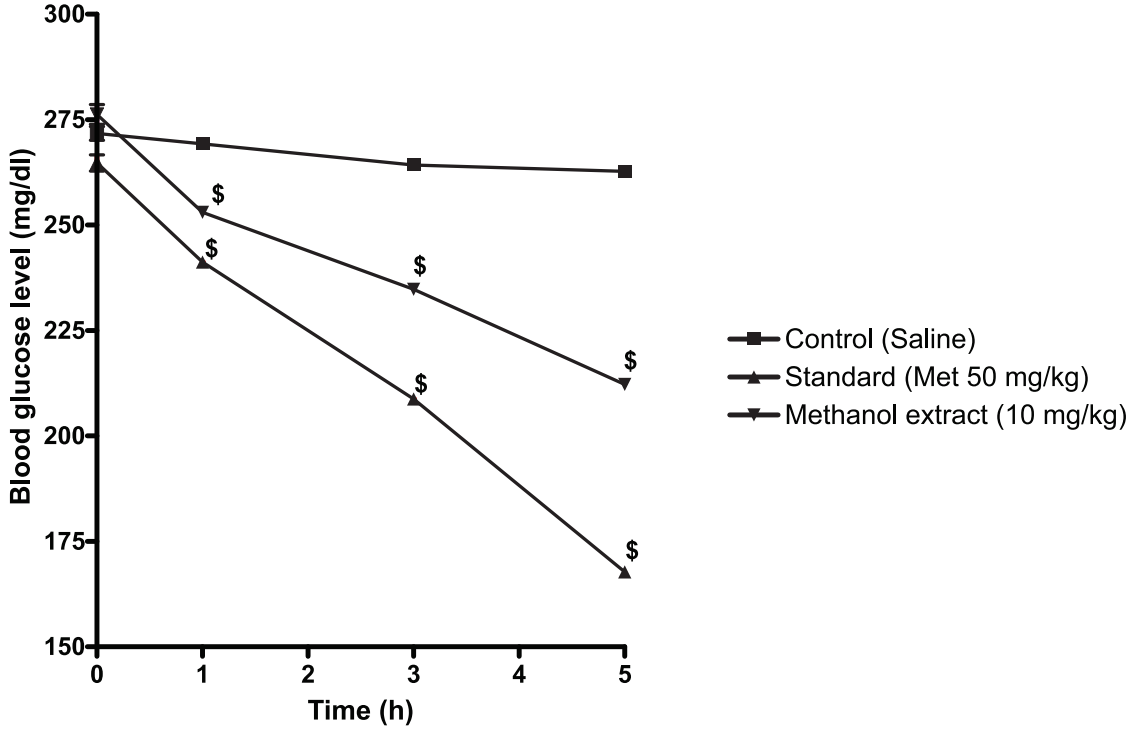

Fig. 7: - Antidiabetic activity charts at 10mg/kg (compound no.2)

*$P < 0.05$, #$P < 0.01$, \$$P < 0.001$ when compared with control.

(Mean ± SEM, n = 4) (Two-way ANOVA followed by Bonferroni test)

According to some researchers, polyphenolic compounds (flavonoids) in plants are responsible for the antidiabetic activity and follows the possible mechanism of flavonoids which shows significant reduction in plasma glucose levels[28]. The methanolic extracts showed the presence of polyphenolic compounds (flavonoids) thus, isolated compound no. 2 showed significant antidiabetic activity. Based on Phytochemical study, quantitative estimation, methanolic extract was subjected to column chromatography for separation and isolation of the constituents present in it. The constituents were collected in fractions and tested. One component was isolated (oil) in 1 to 9 elutes (compound 1) and two components were obtained in 10 to 20 elutes (compounds 2 & 3)The phytochemical screening of the constituent was performed which confirmed the presence of steroids (compound 1) and flavonoid and carbohydrates (compounds 2 & 3). The antidiabetic activity of the isolated compound (compound 2) was performed at (10 mg/kg) and showed potent antidiabetic activity due to the presence of flavanoid.[28]

The physicochemical studies of the isolated constituent were carried out. The melting point of the separated compound no. 2 was found to be 258 - 260°C. The UV Spectra and IR Spectra of the constituents were recorded and on the basis of above study, the compound is likely to be the Flavonoid (Isoquercetin).

ACKNOWLEDGEMENT :

I would like to express my special thanks to AICTE for the grant of Fellowship.

CONFLICT OF INTEREST :

No conflict of interest.

REFERENCES :

1. Kirtikar K .R and Basu B.D, "Indian medicinal plant" vol-1, second edition, pg 897-898.
2. Yadav R. N.and Tripathi P., "A novel flavones Glycosides from the stem of *Bauhinia purpurea".*, Natural Product Laboratory, feb.2000, Sagar.
3. Menezes F.D. "Hypoglycemic activity of two Brazilian Bauhinia species, *Bauhinia forficata,* and *Bauhinia monandra* Kurz." School of pharmacy and pharmaceutical sciences, vol17Jan/Mar Ireland.
4. Russo E.M and Chacra A.R "Clinical trial of *Myrcia Uniflora* and *Bauhinia* leaf extract in normal and diabetic patients" Brazilian Journal of Medical Biological Research, 23 Jan,1990 ,pg 11-20.
5. Saranabasapa .G K "Phytochemical studies on *Bauhinia racemosa* Lam, Bauhinia *purpurea* Linn and *Hardwickia binata* Roxb", E-Journal of chemistry vol.4 no.1, Jan 2007 pg 21-31.
6. Edward F. Gillman and Dennis G. Watson "*Bauhinia purpurea* purple orchid tree".
7. Khandelwal K. R,Practical Pharmacognosy, Nirali publication, 2nd Ed., August 2000, pg. 100-110.
8. Quality Control Methods for Medicinal Plant Materials. World Health Organization, Geneva, 1998, pg. 28-30.
9. Mukherjee P.K., "Quality control of herbal drugs- an approach to the evaluation of botanicals" 1st Ed.
10. Brain K.R., Turner T.D., "The practical evaluation of Phytopharmaceuticals", 1975, pg-83.
11. Farnsworth N. R. "Biological and Phytochemical Screening of Plants", *J. Pharmaceutical Sciences*. 1966; 55 (3): pg 225-286.
12. Maksimovic Z., Malencic D., (2005). "Polyphenol contents antioxidant activity of *Maydis stigma* extracts" *Bioresource Technology* 96: pg 873-877.
13. Turner R."Screening methods in pharmacology" Academic press, London, 1965, pg -99

14. Nagappa A.N., Thakurdesai P.A., Venkat Rao N., Singh j., "antidiabetic activity of *termanalia catappa* lion fruits" journal of ethnopharmacology 88(2003) pg 45-50.

15. Aderogba M. A., ogundaini A.O, and Eloff J.N "Isolation of two flavonoids from *Bauhinia monandra* kurz leaves and their antioxidative effects" African Journal of Traditional ,complementary and Alternative Medicines,Vol.3, No.4,2006, pg.59-65.

16. Cleide de Sousa Lino,*a* João Paulo Luz Diogenes,*a* Bruno Azevedo Pereira, "Antidiabetic Activity of *Bauhinia forficata* Extracts in Alloxan-Diabetic Rats" *Biol. Pharm. Bull.* **27**(1) 125,127 (2004).

17. Gondane P "Isolation and identification of active constituents from *Tinospora cordifolia* and Evaluation of preliminary antidiabetic activity"

Peer Reviewed and Refereed Journal 2022 **(ISSN : 09726330)**

Rashtrasant Tukadoji Maharaj Nagpur University

SCIENCE JOURNAL 2022

Vol. : XV

An Overview on 3D Printing Technology and Biomedical Application

Ranjana S. Kumbhalkar and Pramod B. Khedekar

Department of Pharmaceutical Sciences, Rashtrasant Tukadoji Maharaj Nagpur University, Nagpur - 440033 India.

Corresponding author email : jbrandhawa2@gmail.com *pacific0701@gmail.com Mob. No. 7776899668

ABSTRACT

3D printing is an increasingly powerful tool for researchers, engineers and clinicians, and it holds a huge potential as an accelerator to translate tissue engineering concepts into rapid, cheap and promising clinical implementations. 3D printing can be done by various method like elective leaser sintering, fused deposition melting, laminated object manufacturing. This technique have an great advantages in biomedical sciences. In this review we are going to discuss some of its biomedical application along with the advantages and limitations.

Keywords : Fused deposition, laser sintering, 3D printing technique, Tissue engineering.

INTRODUCTION :

3D printing is additionally described as additive manufacturing process. Additive manufacturing introduced to the manufacturing with the help of layer-by-layer method, by joining with each other. This technology changes the whole scenario of manufacturing in world. Right now, any product is often made with simply making its 3D model or by scanning with the 3D scanner (1). We use a CAD file to form objects on software then this file is uploaded to the 3D printer and it's made by printer. It's a tool less manufacturing method, it is often utilized where there is mass production with high accuracy is mandatory. It doesn't that much energy for its functioning. Rapid prototyping features are there having various wide types of selected of applications in various fields of human activity: which includes research, engineering, medical industry, military, construction, architecture, fashion, education, the computer industry and lots of others (2).

3D PRINTING TECHNIQUES :

Many different 3D printing processes and technologies are invented from late 1970. The printers originally were very large and expensive. Now a days a large number of Additive manufacturing processes are now available. Some of the techniques melt or soften material to produce the layers, e.g. selective laser melting (SLM), selective laser sintering (SLS), fused deposition modeling (FDM), while others cure liquid materials using different other technologies, e.g. stereolithography (SLA) and with laminated object manufacturing (LOM) (4).

A. Selective Laser Sintering

Selective laser sintering (SLS) was innovated the technique and patented by Dr. Carl

Deckard and academic adviser, Dr. Joe Beaman at the University of Texas at the mid-1980, under the sponsorship of DARPA. Selective laser sintering can also be a 3D-printing technique that utilizes a laser because the facility that provides to sinter powdered material (mostly metal), aiming the laser at points in space defined by a 3D model, binding to the material to form a solid structure. Selective laser melting uses a comparable concept, but in SLM the material is fully melted and then sintered, enabling the different properties (crystal structure, porosity). SLS might also be a comparatively new technology that has been used for the additive manufacturing and for low-volume production of parts. Production roles are increasing because of the commercialization of additive manufacturing technology improving.

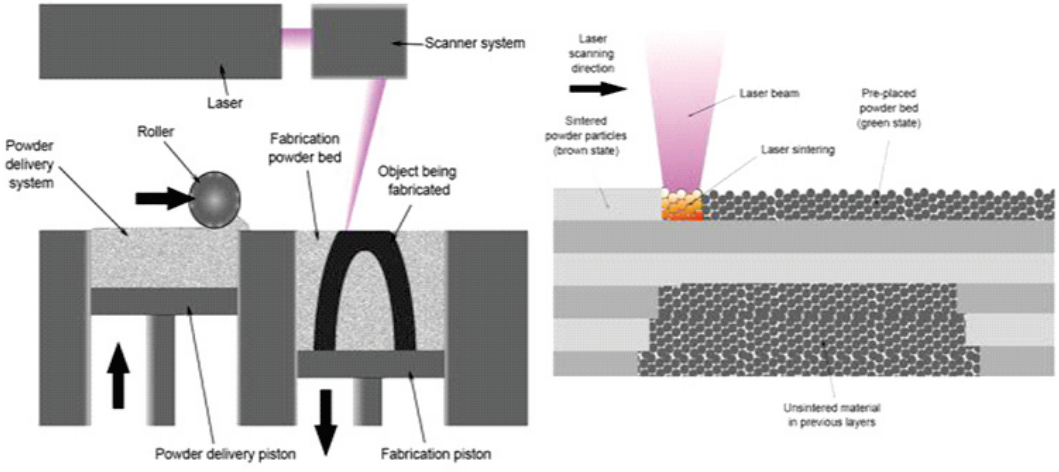

Fig.1. Selective Laser Sintering

B. Fused Deposition Modeling

Fused deposition modeling (FDM) method was invented by S. Scott Crump within the late 1980s and after that it was designed in 1990 by Stratasys. As the patent on this technology gets expired, a lot of open-source development community developed and commercial variants started utilizing this sort of 3D printer were observed. As a result, the cost of FDM technology has dropped by two orders of magnitude since it was developed. In this technique, the model is formed by extruding small beads of fabric which are harden to make the layers. A thermoplastic filament or wire that's wound into a coil is unwinding to support the material to an extrusion nozzle head. The nozzle head gets warms as the fabric up to the certain temperature and turns it flows towards on and off. Typically, the stepper motors are employed to move the extrusion head within the z-direction and adjust the flow consistent with the wants. This head can be shifted in both horizontal and vertical directions, and control of the mechanism is donned by a computer-aided manufacturing (CAM) software package running on a micro controlled.

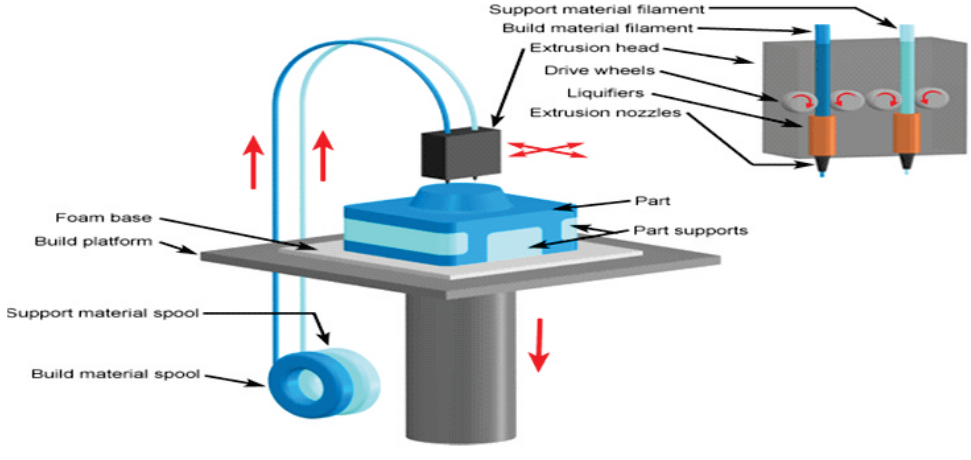

Fig.2. Fused Deposition Modeling

C. Stereolithography

Stereolithography is mainly and broadly used in 3D printing technology. 3D printing was designed with the intention of allowing engineers to develop the prototypes of their own designs in little time and in an effective manner. This technology first developed as early in the 1970. Dr. Hideo Kodama Japanese researcher firstly discovered the modern layered approach towards the stereolithography by utilizing the UV light to cure photosensitive polymers. Stereolithography is a form of 3D printing technology used for creating the models, prototypes, patterns in a layer-by-layer fashion using the photopolymerization, a method in which the light induces chains of molecules to link together for formation of the polymers. Those polymers then form the body of a three-dimensional solid. Research in this particular area had been regularly conducted during the 1970s, but the term was coined by Charles (Chuck) W. Hull in 1986 firstly when he patented the process after then he set up the 3D Systems Inc. to commercialize his patent.

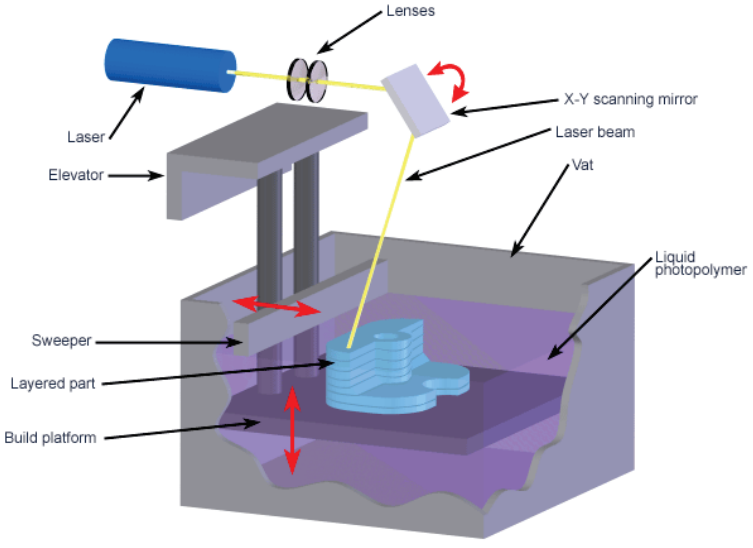

Fig. 3. Stereolithography

D. Laminated Object Manufacturing

It is a 3D-printing technology discovered by the Helisys Inc. (now Cubic Technologies). In this technology it is used as layers of adhesive-coated paper, plastic, or metal laminates are successively joined together and cut into a proper shape with a laser cutter. Objects printed with the help of this technique can be additionally modified by machining after the printing process. This type of typical layer resolution process is defined by the material feedstock and it generally ranges within thickness from one to a many sheet of paper of a copy.

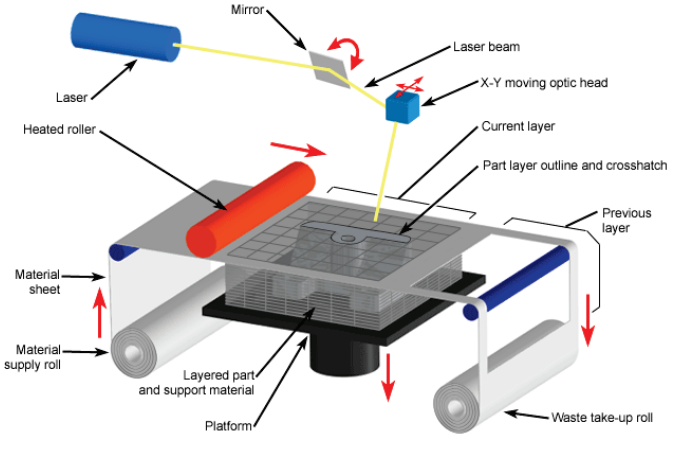

Fig.4 Laminated Object Manufacturing

Biomedical applications :

Tissue engineering and regenerative medicine

Tissue engineering can utilize in the biology and engineering principles to develop functional substitutes for replacing, repairing and regenerating (3R) the lost, damaged or diseased tissues and other organs.This field has been rapidly expanding to tackle the donor tissue limitations and transplant rejections. Scaffold designs should be capable of creating complex 3D constructs with hierarchical porous architectures and arbitrary anatomical shapes to obtained the desired mass transport and mechanical properties, thereby coupling mechanical functionality with tissue/organ regeneration. However, traditional fabrication methods e.g., solvent casting, phase separation, gas foaming, fiber bonding, freeze-drying and porogen leaching/particulate leaching there are some limitations for scaffold designs with complex topology structures and adequate mechanical properties. As of an advanced manufacturing technology having distinct advantages e.g. customizability and precision, 3D printing is an promising powerful tool for the various purposes like researchers, engineers and clinicians, and it also hold a huge potential as an accelerator to mimic tissue engineering concepts into rapid, cheap and promising clinical implementations.(5)

Bone regeneration

Bone damages caused by some disease like (e.g., osteoporosis), trauma (e.g., bone fracture), surgical resection (e.g., bone tumor therapy) and congenital bone condition should need for regeneration and reconstruction by the customized substitutes (grafts) to repair the lost bone structure and physiological function. Right now, generally there are many ways to regenerate bone defects (particularly large bone defects) including autografts and allografts. Therefore, novel hypothesis and schemes for bone tissue engineering are desperately needed, among which the 3D bioprinting is expected to model bone-biomimetic complex constructs having the anatomical characteristics of natural bone tissues; therefore, it increases the bone regenerative ability. Overall, this study states a bone biomodelling approach enabling localized control of osteogenic and angiogenic niches and forming of biophysical and/or biochemical gradients within the bio printed bone constructs. Developed a proof-of-concept design of dual 3D bioprinting platform for modelling the vascularized bone biphasic constructs consisting hard mineral structures encompassed by cell-laden GelMA hydrogels to simulate native bone, such an integrated scheme can combine the advantages of multiple 3D bioprinting platforms with regional immobilization of bioactive factors to allow hierarchical bone biomimetic reconstruction and regeneration, and is expected to produce an innovative approach for the complicated multicellular tissue regeneration.(6)

Cartilage regeneration

Cartilage is a smooth elastic connective tissue which is prominently found as the structural and functional component of many specific body parts such as ear, nose, trachea, meniscus, osteochondral, articular cartilage, intervertebral disc and costal cartilage. The cartilage matrices contain proteoglycans, collagen fibers, glycosaminoglycans having high water content; they are gelatinous, tough and rigid, thereby playing the character of holding and supporting in the body. Cartilage tissue mainly contains one type of cells, i.e., chondrocytes, which can be distinguished into three types having hyaline cartilage (e.g., trachea, articular cartilage), elastic cartilage (e.g., ear, nose) and fibrocartilage (e.g., meniscus, intervertebral disc), having different relative content of collagens and proteoglycans. Cartilage seems as a comparatively simple tissue: it doesn't have any blood vessels (avascular) or nerves (aneural). Nutrients are regulated as through the diffusion to chondrocytes. Cartilage tissue don't have any self-repair capacity and once cartilage defect appears, it will finally originates the degenerative and osteoarthritic changes.(7)

Spinal cord regeneration

The spinal cord tissues are not structurally homogeneous, but composed of different cell types in high degree of spatial distribution. Traumatic spinal cord injury (SCI) can cause immediate loss of motor or sensory function below the site of injury, with poor prognosis. In the context of engineering functional spinal cord tissues, it is important to take into consideration the spatial distribution of different cell components to mimic the spinal cord structure within the engineered tissue-like bioconstructs. To this point, the 3D bioprinting enables directly printing cells into scaffold for predefined

localization, which is very advantageous compared with other fabrication methods involving printing scaffolds first and then seeding cells onto them after printing. The recently reported using microscale continuous projection printing (aCPP) to fabricate complex CNS constructs for tissue regeneration applications in SCI repair. The injured axons are able to regenerate into the biomimetic 3D printed scaffolds and the implanted NPCs can extend axons out of scaffold and into spinal cord below injury to significantly repair synaptic transmission and functions. Therefore, the biomimetic 3D scaffold fabrication by aCPP may offer an effective way for improving SCI regeneration.(8)

Skeletal muscle regeneration

The skeletal muscle tissues are extremely organized cable-like architectures and meanwhile have hierarchical structure units at a variable size. Skeletal muscle tissue engineering points towards the regenerate and the skeletal muscle defects. The application of the 3D bioprinting is anticipated to give an encouraging strategy and tool for skeletal muscle tissue regeneration. It adopted the 3D integrated organ printing (IOP) system to print four various ink components, which allows the fabricating single integrated muscle tendon unit. The 3D printed bio constructs were able to mature into functional muscle in vivo and the implanted muscle grafts could respond to electrical stimulation to a degree accordant with the developing immature muscles. It demonstrated a novel 3D bioprinting scheme to fabricate skeletal muscle tissues of functional morphologies. The microfluidic printing head was coupled with a co-axial needle extruder, thus enabling the 3D bioprinting of myoblast-laden PEG-fibrinogen hydrogel fibers at high resolution the fabrication of 3D multicellular constructs with accurate location of encapsulated cells. Histological analysis showed that the muscle-like tissue formation within the 3D bio printed implants with significant parallel organization and orientation. This scheme is robust and promising for the 3D bioprinting of skeletal muscle tissues for regenerative applications.(9)(10)

Skin regeneration

The human skin (average thickness <“2.5 mm) has a unique anatomy consisting of three various layers i.e., epidermis, dermis and hypodermis. Differing types of skin cells are positioned at high degree of region specificity including keratinocytes and melanocytes in epidermis, fibroblasts in dermis and fat at hypodermis base meanwhile, collagen are normally found altogether in the three layers. Tissue-engineered skin substitutes are believed to get control of the limitations of conventional skin therapy methods. 3D bioprinting is an encouraging scheme to allow rapid, reliable and scalable production of biomimetic skin substitutes to catch up the clinical requirements for the human skin regeneration.Demonstrated the 3D spatial arrangement of fibroblasts and keratinocytes in collagen hydrogel by laser cell printing to model multicellular 3D skin grafts. This study reveals the future of laser cell printing for engineering functional skin substitutes. Recently reported that the novel 3D cell printing platform is going to increase the complexity of the printed skin anatomy, which can engineer the perfusable vascularized 3D human skin equivalent. The full-thickness skin model consists of epidermis, dermis and hypodermis demonstrated tissue maturation and better recapitulation of native human skin (11).

Vasculature regeneration

Nearly all the tissues in the human body have complicated branched internal vascular system to fulfill oxygen and nutrient supply. To encourage the performances and functions of the engineered tissues, advancing 3D vascular networks interconnected within the tissue-engineered constructs can play an important role. However, imitating the natural vascular networks for blood transport, mass exchange and long-term tissue survival remains a major problem for tissue engineering. Up to this point, 3D bioprinting has been evolving as an encouraging advancement towards the manufacturing functional 3D vascular networks via predefined deposition of cell and material components. It demonstrated a versatile 3D printing scheme to fabricate biomimetic vasculature for tissue regeneration applications. The vasculature modelling was based on 3D printed caramel construct as sacrificial template and polymer coating with phase separation. The patterned microchannel networks have biomimetic three-level vascular architectures i.e., 3D framework, interconnected microchannels and the permeable walls. This 3D modelling method can be implied to varied polymers and integrated with various matrices e.g., hydrogels. The perfused vascular channels may maintain a

metabolic functions of rat primary hepatocytes in tissue-engineered bio constructs. A coaxial 3D bioprinting approach was developed to produce the GelMA microfibers encapsulated in alginate and generates mini tissues containing human umbilical vein endothelial cells; these cells can moderately migrate and connect to cre lumen-like blood vessels (12), (13).

Ovary regeneration

Patients which are going under treatments of cancers and autoimmune diseases can suffer from weakened ovary function and the cause of puberty loss, infertility and early menopause. Current artificial reproduction and hormone restoration approaches e.g., ovary transplant and assisted fertilization are not able to give long-term solution and can leave metastatic diseases like to the pediatric patients. Thus, while developing whole organ replacement scheme is important for the oncofertility field in order to maintain the long-term fertility and the hormone functions for all cancer patients. In this context, tissue engineered hydrogel scaffolds e.g., alginate, fibrin, matrigel, PEG based play an increasingly pivotal asset for ovarian tissue regeneration and function restoration. Because of its unique advantages, 3D printing technology has high potential to model human ovary bio prostheses for ovarian tissue replacement. It uses the 3D printed porous hydrogel scaffolds to examine the influence of varied scaffold pore geometry on the survival and function of ovarian follicles. They presented that the 30° and 60° scaffolds can generate the corners surrounding follicles on various sides and promote the interactions of follicles with scaffolds. After implantation in sterilized mice, the follicle-seeded 3D scaffolds became highly vascularized and their ovarian function was completely maintained. This study says that 3D printing can be used for modelling the bioprosthetic ovarian implants with predefined scaffold designs to attain the whole ovary replacement and restore ovary functions (14), (15).

Islet transplantation

Type 1 diabetes (T1D), also termed juvenile-onset diabetes, is an autoimmune disease where immune system will attack and damage the insulin-producing islet cells in pancreas. Over the last decades, pancreatic islet transplantation has become a promising therapy for the Type 1 diabetes to give sustained extrinsic insulin supply. However, after transplantation, factors like the lack of vasculature and autoimmune attack will cause the substantial loss of islet mass and function. To tackle these problems, encapsulating islets in hydrogel matrix can protect them from immune system and 3D printing can be used for favorable hydrogel scaffold designs, therefore, the combination of islet encapsulation and 3D printing of hydrogel scaffolds is a promising strategy to enhance the islet viability and functions. Formulated the alginate/gelatin bio ink for islet and islet-related cell encapsulation and 3D printing. The designed coaxial printer allowed for 3D printing of the multicellular islet-containing bio constructs with a precise control of distribution. After 3D printing, the viability of pancreatic islets was well maintained, showing the potential for islet transplantation. Adopted the 3D bio plotting to fabricate 3D alginate-based porous hydrogel scaffolds as the islet delivery system. They demonstrated that the INS1E a-cells, mouse and human islets can be successfully encapsulated into the 3D plotted hydrogel constructs without influence on their viability and morphology. These islets can be confined at one site in the 3D plotted hydrogel scaffolds and blood vessels can grow into the scaffold pores and come in closer contact with the encapsulated islet tissue. In a recent work, 3D bio printed the pancreatic islets in alginate/methylcellulose hydrogel constructs. With the maintained viability, morphology and function within scaffolds, these embedded islets can continuously generate insulin and glucagon during observation (16), (17), (18).

Heart regeneration

Cardiovascular diseases are the major for the reason of mortality rate and morbidity rate in the world. Cardiovascular tissues e.g., heart valves, arteries and myocardium are highly evolved and continually loadbearing. At least right now, heart transplantation is the main therapy choice for patients having heart failure at the end stage. However, having the fact that the number of presently cardiac donors is quite narrowed, it is of large request to develop novel strategies to regenerate infarcted hearts, thereby decreasing the too much reliability on cardiac donors. To concur this problems, cardiac tissue engineering plays a pivotal role by the integration of cardiac cells within 3D hydrogel

scaffolds. Getting expanding attentions have been paid to 3D bioprinting, a very encouraging method to develope customized cardiac valves, patches or even whole heart. Although there is still a long way to achieve 3D bioprinting of totally functional organs, this work shows the potential of 3D bioprinting to rebuild tissue engineere bioconstructs that can begin to recapitulate the complex architectures, mechanics and biological properties of natural tissues/organs (19).

Advantages

1. **Time-to-Market :** 3D printing enables the ideas to develop at a fast speed. Having the ability to print a hypothesis on the same day it was designed shrinks a development process from what might have been months to a number of days, giving benefits to the companies stay one step ahead of the other.
2. **Save Money :** Prototyping injection mould tools and production runs in a costly investment. The 3D printing process enables the modelling of parts and/or tools through additive manufacturing at rates much lower than traditional machining.
3. **Mitigate Risk :** It allows to examine a design before investing in an expensive moulding tool is worth its weight in 3D printed plastic, and then some. It is too economical to 3D print a test prototype than to redesign or modified an existing mould.
4. **Feedback :** Having a prototype, you can examine the market by displaying it at a tradeshow, showing it to buyers or increasing capital by pre-selling on Indigo or Kick-starter. Getting buyer's attention to the product before it actually goes into production is a valuable way to verify the product has market potential or not.
5. **Get the Feel :** One thing you can't get a picture or virtual prototype on the computer screen is the way something feels in your hand. If you want to ensure the ergonomics and fit of a product are just right, you must actually hold it, use it and examine it.
6. **Personalize It :** With standard mass-production, all parts come off the assembly line or out of the mould the same. With 3D printing, now a days one can personalize, customize a part to uniquely fit their needs, which enables for custom fits in the medical industries and helps set people to explain their idea in new world.
7. **Build your Imagination :** In the modern era of digital art and design, the chances are not only speed up but are limitless. One can now a day's 3D prints almost everything they imagine after drawing it up virtually or by other. In a short span time, an idea, hypothesis, dream or invention can go from a simple thought to a produced part.

Disadvantages

1. **Intellectual property issues :** The ease with which copies can be generated using 3D technology rises problems over the intellectual property rights. The availability of blueprints online free of cost may change with for-profit organizations wanting to generate profits from this new technology.
2. **Limitations of size :** 3D printing technology now a days limited by size constraints. Very large objects are still cannot be feasible when built using 3D printers.
3. **Limitations of raw material :** At present, 3D printers can work with precisely 100 different raw materials. This is insignificant when compared with the wide range of raw materials used in traditional manufacturing. More research is required to devise methods to allows 3D printed products to be more long lasting and robust.
4. **Cost of printers :** Price of buying a 3D printer is still not affordable to the average householder feasible. Also, various 3D printers are needed in order to print various types of objects. Also, those printers which can manufacture in colorsare costlier than those printers manufacturing monochrome objects.
5. **Fewer Manufacturing Jobs :** As having all these new technologies, manufacturing jobs will be declined. This disadvantage can produce a huge impact to the economies of third world countries especially China, that relies on a huge number of low skill jobs.

6. **Unchecked production of danger items :** Liberator, the world's first 3D printed functional gun, showed how simple it was to generate its one's own weapons, gives one had access to the design and a 3D printer. Governments should have a kneen observations on such activities which are harmful to the societies and should be prevented.

Conclusion :

This review summarizes recent progress related to the 3D Printing and biomedical application discuss. 3D printing can be done by various method like elective laser sintering, fused deposition modeling, laminated object manufacturing. This technique haves an great advantages in biomedical sciences. From our studies it is concluded that Fused deposition study found best method for 3D printing.

References :

1. Chandwani L, Sharma H, Kumar P. A Review on 3D Printing Technology. 2020;3072–4.
2. Nale SB, Kalbande PAG. A Review on 3D Printing Technology. 2015;2(9):33–6.
3. Jovic TH, Kungwengwe G, Mills A, Whitaker IS. i v o r l a n o i v o l. 2019;
4. Gokhare VG. A Review paper on 3D-Printing Aspects and Various Processes Used in the 3D-Printing. 2017;6(06): 953–8.
5. Hollister SJ. Porous scaffold design for tissue engineering. Nat Mater. 2005;4(7):518–24.
6. Cui H, Zhu W, Holmes B, Zhang LG. Biologically Inspired Smart Release System Based on 3D Bioprinted Perfused Scaffold for Vascularized Tissue Regeneration. Adv Sci. 2016;3(8).
7. Li J, Wu C, Chu PK, Gelinsky M. Materials Science & Engineering R 3D printing of hydrogels/ : Rational design strategies and emerging biomedical applications. 2020;140(January).
8. Joung D, Truong V, Neitzke CC, Guo SZ, Walsh PJ, Monat JR, et al. 3D Printed Stem-Cell Derived Neural Progenitors Generate Spinal Cord Scaffolds. Adv Funct Mater. 2018;28(39):1–10.
9. Ostrovidov S, Salehi S, Costantini M, Suthiwanich K, Ebrahimi M, Sadeghian RB, et al. 3D Bioprinting in Skeletal Muscle Tissue Engineering. Small. 2019;15(24):1–14.
10. Kang HW, Lee SJ, Ko IK, Kengla C, Yoo JJ, Atala A. A 3D bioprinting system to produce human-scale tissue constructs with structural integrity. Nat Biotechnol [Internet]. 2016;34(3):312–9. Available from: http://dx.doi.org/10.1038/nbt.3413
11. Koch L, Deiwick A, Schlie S, Michael S, Gruene M, Coger V, et al. Skin tissue generation by laser cell printing. Biotechnol Bioeng. 2012;109(7):1855–63.
12. Kolesky DB, Truby RL, Gladman AS, Busbee TA, Homan KA, Lewis JA. 3D bioprinting of vascularized, heterogeneous cell-laden tissue constructs. Adv Mater. 2014;26(19):3124–30.
13. Lei D, Yang Y, Liu Z, Yang B, Gong W, Chen S, et al. 3D printing of biomimetic vasculature for tissue regeneration. Mater Horizons. 2019;6(6):1197–206.
14. Laronda MM, Jakus AE, Whelan KA, Wertheim JA, Shah RN, Woodruff TK. Initiation of puberty in mice following decellularized ovary transplant. Biomaterials [Internet]. 2015;50(1):20–9. Available from: http://dx.doi.org/10.1016/j.biomaterials.2015.01.051
15. Laronda MM, Rutz AL, Xiao S, Whelan KA, Duncan FE, Roth EW, et al. A bioprosthetic ovary created using 3D printed microporous scaffolds restores ovarian function in sterilized mice. Nat Commun [Internet]. 2017;8(May):1–10. Available from: http://dx.doi.org/10.1038/ncomms15261
16. Sneddon JB, Tang Q, Stock P, Bluestone JA, Roy S, Desai T, et al. Stem Cell Therapies for Treating Diabetes: Progress and Remaining Challenges. Cell Stem Cell [Internet]. 2018;22(6):810–23. Available from: https://doi.org/10.1016/

j.stem.2018.05.016

17. Fomby P, Cherlin AJ, Hadjizadeh A, Doillon CJ, Sueblinvong V, Weiss DJ, et al. Stem cells and cell therapies in lung biology and diseases: Conference report. Ann Am Thorac Soc [Internet]. 2010;12(3):181–204. Available from: http://dx.doi.org/10.1016/j.trsl.2010.06.007

18. Marchioli G, Van Gurp L, Van Krieken PP, Stamatialis D, Engelse M, Van Blitterswijk CA, et al. Fabrication of three-dimensional bioplotted hydrogel scaffolds for islets of Langerhans transplantation. Biofabrication [Internet]. 2015;7(2):25009. Available from: http://dx.doi.org/10.1088/1758-5090/7/2/025009

19. Vunjak-Novakovic G, Tandon N, Godier A, Maidhof R, Marsano A, Martens TP, et al. Challenges in cardiac tissue engineering. Tissue Eng Part B Rev. 2010;16(2):169–87.

Peer Reviewed and Refereed Journal 2022 **(ISSN : 09726330)**

Rashtrasant Tukadoji Maharaj Nagpur University

SCIENCE JOURNAL 2022

Vol. : XV

PHYSICOCHEMICAL EVALUATION AND FORMULATION OF MICROEMULGEL OF GAULTHERIA

Kamlesh Machewar, Rajendra Kakde, Prafulla Sabale, Manish Kamble, Roshni Kunte.

Department of Pharmaceutical Sciences, Rashtrasant Tukadoji Maharaj Nagpur University, Nagpur, Maharashtra, India.

Corresponding author email : machewar31@gmail.com

ABSTRACT

The aim of the present study was to evaluate physicochemical properties of gaultheria oil and to investigate the potential of a micro-emulgel formulation for topical delivery of *Gaultheria oil*. Various Parts of *Gaultheria* are used for the treatment of wind-damp, as well as relieving pain. Modern research has demonstrated that these plants exhibit anti-inűammatory, anti-oxidative, antibacterial and analgesic activities. Essential oils were distilled using a dean-stark steam apparatus for 4 hrs, until the milky distillate became clear. Essential oil were extracted from the distillate by treatment with an equal volume of diethyl ether. Micro-emulgel of *Gaultheria* oil was prepared by screening of oils, emulsifier, and co-emulsifier on bases of solubility of an API in it. An API has high solubility and oil may also have more or less pharmacological property, so it may assist the therapeutic action of API. Due to presence of oil portion, it leads to more penetration of API in the skin. Prepared micro-emulgel was evaluated for pH, particle size, spreadability and viscosity.

Keywords :
Microemulgel, Topical delivery, Micro-emulsion, Gaultheria oil

1. INTRODUCTION

Inflammation is part of the complex biological response of body tissues to harmful stimuli, such as pathogens, damaged cells, or irritants, and is a protective response involving immune cells, blood vessels, and molecular mediators. The function of inflammation is to eliminate the initial cause of cell injury, clear out necrotic cells and tissues damaged from the original insult and the inflammatory process, and initiate tissue repair. (Dworkin *et al.,*2016)

Inflammation is a natural part of the healing process. But when it becomes chronic, it's important to get it under control to reduce your risk of long-term damage. (Vane*et al.,* 1998)

The genus Gaultheria is widely distributed all over the World, and many species have been used as traditional herbal medicines. So far, phytochemical research on the genus has revealed the extensive presence of methyl salicylate derivatives, C_6-C_3 constituents, terpenoids, and other compound types, together with prolific essential oils. The pharmacological activities of pure compounds and crude extract from this genus were mainly focused on anti-inflammatory and analgesic properties. A salicylate derivative fraction (SDF), which is rich in gaultheria reported from *G. yunnanensis*, exhibited a significant inhibition of pain and inflammatory processes.(Liu W *et al.,* 2013)

Emulgels with advantage of both gels & emulsion act as a controlled drug delivery system for topically applied drugs. They are emulsion of either oil in water type or water in oil

type which are gelled by mixing with a gelling agent. Gels have extended the contact period of medication over the skin due to muco adhesive property. In a order to increase emulsion ability & stability to penetrate stratum corneum it is jellified in a gel base & the resulting preparation is called Emulgels. Gels in dermatological preparation have advantage of ease of application & offer better stability as compare to cream & ointment. Emulgels may serve as better choice for topical delivery of poorly water-soluble drugs (Singla *et al.,* 2012, Khullar R *et al.,* 2012) S. For hydrophobic or poorly water-soluble drugs emulsified gel has proven a stable and better vehicle.(Boyd B J*et al.,* 2019)The aim of present work was to develop an emulgel for the topical delivery of combinations of herbal drugs which is useful in the treatment of Inflammation and Pain.

2. MATERIALS AND METHODS

2.1 COLLECTION, IDENTIFICATION AND AUTHENTICATION OF PLANTS

The leaves of the plant Gaultheria collected from forest region. The plant was identified and confirmed by standard literature.

2.2 ESSENTIAL OIL EXTRACTION

Mature green leaves (100g) were collected, Fresh leaves were cut into fine pieces and macerated using a blender in a round-bottom flask with 200 ml sterile distilled water at 49 for 18 h in a water bath (Goodarzi, F*et al.,* 2018). Essential oils were distilled using a dean-stark steam apparatus for 4 h, until the milky distillate became clear. Essential oil was extracted from the distillate by treatment with an equal volume of diethyl ether. The essential oil dissolved in the diethyl ether. While the separate aqueous layer was removed using a separating funnel. The upper layer of solvent (diethyl ether) was evaporated at 40 under vacuum (13.33 kPa) using a rotary evaporator, extraction was carried out three times and the yield quoted represents average value.

2.3 PHYSICOCHEMICAL PARAMETERS

2.3.1 PERCENTAGE YIELD OF OIL

Percentage yield of oil was calculated using this formula

$$\% \text{ Yield} = \frac{\text{weight of oil} \times 100}{\text{weight of sample}}$$

2.3.2 COLOUR DETRMINATION

Determination of colour of the oil is to be determined by using ultraviolet radiation of 254 and 366 nm by physical observation in day light (Desai S A *et al.,* 2015).

2.3.3 DETERMINATION OF SOLUBILITY OF ESSENTIAL OIL

The solubility of the essential oil was determined by taking two liquids (solvent and oil in the ratio 3:1). Approximately 3ml of water was taken in a test tube containing 1 ml of essential oil and then stirred thoroughly; the same was followed using chloroform, diethyl ether, methanol separately (Sawant A, Mohite S *et al.,* 2015).

2.3.4 DETERMINATION OF REFRACTIVE INDEX

The refractive index of the oil samples was determined by using Abbe's refractometer model A 80151(BS). First the prism is cleaned by using cotton and acetone, then the apparatus was left aside for 5 min for the purpose of drying the prism, then two drops of particular oil sample was placed on prism and the prism

was firmly closed, after that reading was recorded from the display screen.(Khullar R *et al.,* 2012).

2.3.5 DETERMINATION OF SPECIFIC GRAVITY

Determination of specific gravity of the oil was done using a 50 ml specific gravity bottle, a clean 50 ml specific gravity bottle was weighted (W_0). Then the bottle (W_0) was filled with the brim with water and stopper and bottle were carefully wiped off and reweighed (W_1). In the same manner, the oil sample were used instead of water it was weighed (W_2). The specific gravity of essential oil was calculated by using the following formula given below :

$$\text{Specific gravity} = \frac{W_2 - W_0}{W_1 - W_0}$$

W_0= Weight of empty specific gravity bottle 0

W_1= Weight of water + weight of specific gravity bottle 1

W_2= Weight of test sample + specific gravity bottle

2.3.6 DETERMINATION OF pH OF ESSENTIAL OIL

pH meter was used to record the pH value of the oil sample. This was repeated for three times and then the average was recorded.

2.3.7 DETERMINATION OF BOILING POINT OF THE OIL

Determination of boiling point of the oil sample was done by using Thiele's apparatus which has the liquid paraffin bath inside it, which was heated slowly and stirring was done gently keeping an eye on the liquid and the fusion tube and also on the thread of the mercury in the thermometer. At first a bubble or two will be seen escaping at the end of the capillary dipping in the liquid, but soon a rapid and continuous stream of air bubble escape from it. This is the stage when the vapour pressure of the liquid in the sealed capillary just exceeds the atmospheric pressure. The temperature when continuous stream of bubbles starts coming out was noted when the evolution of bubbles from the end of capillary tube stops.

2.4 STANDARD CALIBRATION CURVE OF GAULTHERIA BY UV SPECTROSCOPY

Solution of Gaultheria in methanol (20µg/ml) was scanned within the range of 200-400nm to determine the wavelength of maximum absorption by using UV-visible spectrophotometer. Standard calibration curve of Gaultheria was developed in methanol. Dilutions were made in the range of 4 to 20 µg/ml with methanol. The absorbance of resulting solutions was measured at 366 nm using double beam UV-visible spectrophotometer against methanol as blank.

2.5 CONSTRUCTION OF PSUDO TERNARY PHASE DIAGRAM

Pseudo-ternary phase diagrams were c on to determine the concentration range of components for microemulsion and to identify region by water titration method with different weight ratios of Tween 20 : Tween 80 (Smix) as 1:1, 1:2, and 2:1. The coordinates of the ternary phase diagram represent three components of microemulsion system i.e., oil phase (Sunflower oil), Smix and water.Oil and Smix were mixed thoroughly in various weight ratios (1:9, 2:8, 3:7, 4:6, 5:5, 6:4, 7:3, 8:2, 9:1). Water was added drop wise under moderate agitation to each oil-Smix mixtures to identify the phase boundary of the emulsion. Percentage of oil, Smix and water at end point was calculated and the values were used to construct ternary phase diagram using CHEMIX School Ver. 4.01 software (MN, USA).

2.6 METHOD OF PREPARATION OF EMULGEL

The Gel in formulations were prepared by dispersing Sodium Alginate (5%) in purified water with constant stirring at a moderate speed and then the pH is adjusted. Microemulsion were prepared by incorporating gaultheria into oil and mixture of accurately weighed quantity of Smix (Tween 20: Tween 80) mix in a beaker. Components were mixed using a mechanical stirrer and further heated 50°C using water bath to form a homogenous mixture. Then the oily phase was added to the aqueous phase with continuous stirring. And then add this microemulsion to gel base in 1:1 ratio to obtain a Emulgel.

2.7 MESUREMENT OF pH

Glass electrode pH meter (VHS Electronics, Pune) was used to measure the pH of Emulgel formulation.

2.8 PARTICLE SIZE ANALYSIS

Microemulgels were diluted with distilled water to produce a suitable concentration for particle size analysis. The globule diameter analysis of the prepared Emulgel dispersion were performed using zetasizer ZS 90 (Malvern Instruments, Worcestershire, UK), utilizing laser diffraction with length 2.40 mm, range lens of 300 RF mm, and at 14.4% obscuration

2.9 SPREDABILITY OF EMULGEL

The spreadability of Emulgel was examined by using Texture Analyser (Make: Brookfield, Model: CT 100). Optimised Emulgel was taken in the cup of the texture analyser, previously aligned with the probe (TA3/100). The trigger load was 0.5 g and test speed were 1 mm/sec. The hardness value obtained was recorded.

2.10 DETERMINATION OF VISCOCITY

Brookfield digital viscometer (Make: Brookfield, Model: DV II + Pro viscometer) was used for the viscosity determination. The quantity of 100 g of optimized Emulgel was taken in a beaker, spindle S 07 was dipped into it and the viscosity in centipoise (cp) was measured at 20 rpm after 30 sec at ambient temperature and in triplicate. The % torque (}) was in the range of 10-100 %.

3. RESULTS AND DISCUSSION

3.1 Physicochemical parameters

The leaves of Gaultheria were subjected to extraction by using steam distillation and subjected to physicochemical analysis. In this study we have analysed the various physicochemical parameters such as % yield, colour, solubility, iodine test, pH, refractive index, boiling point, specific gravity. The results are presented in a below table.

Table 1: Physicochemical parameters

Physicochemical parameters	Results
Yield	0.6%
Colour of extracted oil	Colourless at visible light
Solubility	Soluble in methanol, diethyl ether and chloroform. Insoluble in water
pH at 22^{0}C	8.808 ± 0.05
Specific gravity	0.633 ± 0.04
Boiling point	220 - 224^{0}C
Refractive Index	0.472 ± 0.002

The extraction was done by steam distillation using a dean stark steam apparatus continuously for 6 hrs. The oil was collected, wherein 100gm of leaves gives a yield of 1 ml of oil in an average. Oil was found to be colourless at visible light at 366 nm using UV spectrophotometer. The pH was found to be 8.808 ± 0.05 at 22 which show that oil is basic in nature. The specific gravity was found to be 0.633 ± 0.04 at room temperature which indicate that the oil is lighter than water. The refractive index was found to be 0.472 ± 0.002 and this shows how light propagates when it passes through the oil. Boiling point was found to be 220 which proves that methyl salicylate is an active ingredient of the essential oil as the boiling point of methyl salicylate is also 220.

3.2 STANDARD CALIBRATION CURVE OF GULTHERIA

Calibration of Gaultheria was performed at T_{max} 366 nm in methanol. Beer's law was obeyed between concentration range of 4- 20 µg/ml. (Figure 1). The line equation and r^2 was found to be y = 0.094x + 0.126 and 0.988 respectively.

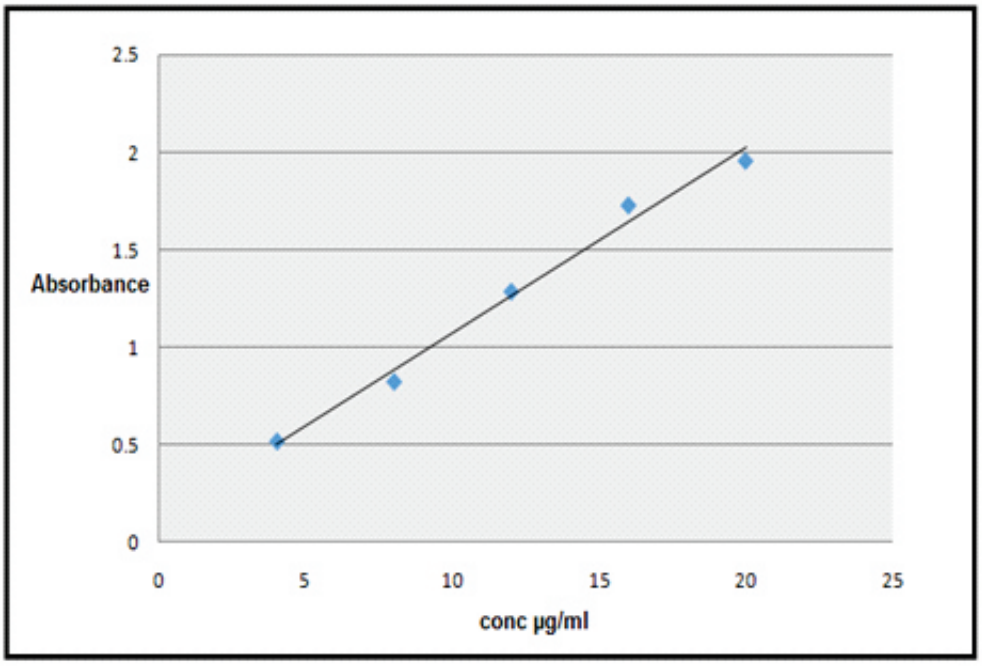

Fig. 1 : Caliberation curve of Gultheria in methanol

3.3 CONSTRUCTION OF PSEUDO TERNARY PHASE DIAGRAM

Pseudo ternary phase diagrams (Fig 2) were constructed to identify micro emulsifying regions. Selection of oil (methyl salicylate), Smix, and oil to Smix ratio, play an important role in the formation of the micro-emulsion. Amongst three ternary phase diagram (1:1,1:2 and 2:1) micro-emulsion region for Smix 2:1 was found to be larger than other Smix ratios (1:1 and 1:2). However, the dispersions were highly viscous which could have prevented ease of emulsification. Among the other Smix ratios 2:1 combination displayed greater emulsification region than other two ratios. The Smix forms a tightly packed oil-water interfacial film resulting in reduced droplet size and better stability(Corbo M*et al.,* 1995). Thus,in the phase diagrams, the free energy of micro-emulsion formation due to change in entropy can be considered to depend on the extent to which the surfactant lowers the surface tension of the o/w interface and the change in dispersion entropy. So, a negative free energy formation is achieved when a large reduction in surface tension is accompanied by significant favourable entropic changes.In such cases,micro emulsion formation is spontaneous and the resulting dispersions are thermodynamically stable (Zhang Y *et al.,* 2014).

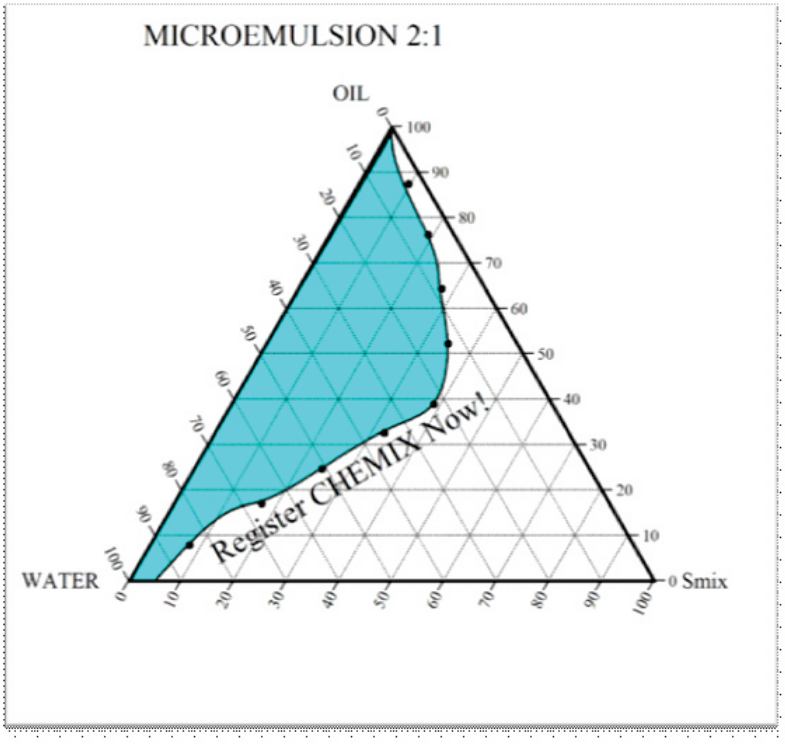

Fig. 2 : Pseudo ternary phase diagram of ratio 2:1

3.4 MESUREMENT OF (pH)

The pH of emulgel formulation was in the range of 5.6 to 6.8, which lies in the normal pH range of the skin & would not produce any skin irritation.

3.5 DETRMINATION OF PARTICLE SIZE

The mean diameter of optimized batch was found to be 337 nm and zeta potential –41 mV.

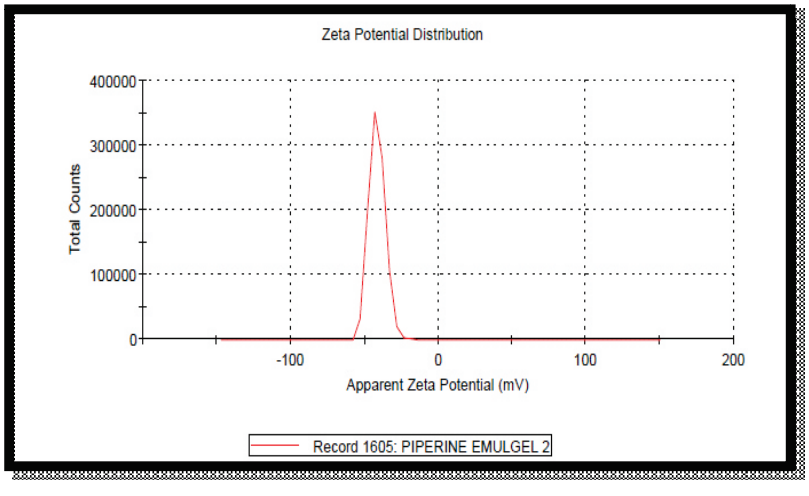

Fig 3 : Particle size distribution and Apparent zeta potential of prepared microemulsion

3.6 SPREDABILITY

The spreadability of optimised Emulgel was determined by texture analyser with trigger load of 0.5 g and test speed of 1 mm/sec by measuring force required to spread the formulation. This property depends on hardness of Emulgel, as hardness increases spreadability of Emulgel decreases. The hardness value of the optimised Emulgel was found to be 53.40 g which indicate good spreadability of the formulation. The spreadability of the formulation is inversely proportional to the viscosity. Hence it could be concluded that the formulation is having good spreadability and will evenly distribute on skin surface covering larger skin surface area.(Patel H*et al.*, 2013)

3.7 VISCOSITY

Viscosity of the optimized Emulgel was determined by Brookfield digital viscometer at ambient temperature and at fixed rpm (20). The viscosity of the optimised formulation was found to be 45000-46000 cp. This indicated that incorporation of microemulsion into the Sodium CMC gel increases the viscosity of the formulation. This might be due to microemulsion being incorporated into the gel matrix. The results indicate that the optimised Emulgel has adequate viscosity and hence will have good residence time on skin as well as good spreadability.

4. CONCLUSION

The study is first attempt to evaluate and investigate the physicochemical parameters of the oil from the leaves of Gaultheria. Microemulgels can serve as the better alternative of the present available marketed topical formulation for delivery of hydrophobic drugs. Microemulgels also shows good spreadability, ease of application and a good patient compliance. Microemulgels provide property of both gels and emulsion and thus it can be used for controlling rate of release of drugs with short half-life. By providing it a gel base they provide stability to the emulsion.

5. REFERENCES

Boyd, B.J., Bergström, C.A., Vinarov, Z., Kuentz, M., Brouwers, J., Augustijns, P., Brandl, M., Bernkop-Schnürch, A., Shrestha, N., Préat, V. and Müllertz, A., 2019. Successful oral delivery of poorly water-soluble drugs both depends on the intraluminal behavior of drugs and of appropriate advanced drug delivery systems. Eur J of Pharm Sci; 137, p.104967.

Corbo, M., 1995. Techniques for conducting in vitro release studies on semisolid formulations. Dissolution Technol, 2, pp.3-6.

Desai, S.A., Mohite, A. and Hajare, A.A., 2015. Screening of safflower oil microemulsion for enhancing bioavailability of lovastatin. Inter J Pharm Sci and Res, 6(1), pp.29-49.

Dworkin, R.H., Bruehl, S., Fillingim, R.B., Loeser, J.D., Terman, G.W. and Turk, D.C., 2016. Multidimensional diagnostic criteria for chronic pain: introduction to the ACTTION–American Pain Society Pain Taxonomy (AAPT). J of Pain, 17(9), pp.T1-T9.

Goodarzi, F. and Zendehboudi, S., 2019. A comprehensive review on emulsions and emulsion stability in chemical and energy industries. Can J Chem Engg, 97(1), pp.281-309.

Khullar, R., Kumar, D., Seth, N. and Saini, S., 2012. Formulation and evaluation of mefenamic acid emulgel for topical delivery. Saudi pharmaceutical journal, 20(1), pp.63-67.

Khullar, R., Kumar, D., Seth, N. and Saini, S., 2012. Formulation and evaluation of mefenamic acid emulgel for topical delivery. Saudi pharm J; 20(1), pp.63-67.

Liu, W.R., Qiao, W.L., Liu, Z.Z., Wang, X.H., Jiang, R., Li, S.Y., Shi, R.B. and She, G.M., 2013. Gaultheria: Phytochemical and pharmacological characteristics. Molecules, 18(10), pp.12071-12108.

Patel, H.K., Barot, B.S., Parejiya, P.B., Shelat, P.K. and Shukla, A., 2013. Topical delivery of clobetasol propionate loaded microemulsion based gel for effective treatment of vitiligo: ex vivo permeation and skin irritation studies. Colloids and Surfaces B: Biointerfaces, 102, pp.86-94.

Singla, V., Saini, S., Joshi, B. and Rana, A.C., 2012. Emulgel: A new platform for topical drugdelivery. Int J Pharma Bio Sci; 3(1), pp.485-498.

Sawant, A.A. and Mohite, S.K., 2015. Formulation and evaluation of itraconazole emulgel for topical drug delivery. In Vitro, 90(F9), pp.84-86.

Vane, J.R. and Botting, R.M., 1998. Anti-inflammatory drugs and their mechanism of action. Inflammation Research, 47(2), pp.78-87.

Zhang, Y.T., Shen, L.N., Zhao, J.H. and Feng, N.P., 2014. Evaluation of psoralen ethosomes for topical delivery in rats by using in vivo microdialysis. Int J nanome; 9, p.669.

Peer Reviewed and Refereed Journal 2022 **(ISSN : 09726330)**

Rashtrasant Tukadoji Maharaj Nagpur University

SCIENCE JOURNAL 2022

Vol. : XV

An Overview on Synthetic Study and Biological Screening of Benzimidazole Derivatives

Kawade D.P., Bhadke M.Y., Asnani A.J., Chaple D.R.

Department of Pharmaceutical Chemistry, Priyadarshini J.L. College of Pharmacy, Electronic zone, MIDC, Hingna road, Nagpur-440016, Maharashtra, India.

Corresponding author email : drdinesh03@gmail.com
Mobile No : 9545383111

ABSTRACT

Benzimidazole is a heterocyclic sweet-smelling natural compound. It is a significant pharmacophore and advantaged structure in restorative science. It assumes a vital part with a lot of valuable restorative exercises, for example, antiulcers, antihypertensives, pain relieving, mitigating, hostile to virals, antifungals, anticancers, and antihistaminics. The survey of the writing shows that the benzimidazole subordinates are exceptionally compelling compound and number of audits accessible for biochemical and pharmacological investigations adjusted that their particles are valuable against a wide assortment of miniature organic entities. Due to their significance, the techniques for their amalgamation have become a focal point of synthetic organic chemists. Thusly in the current survey we attempted to accumulate the science of various subordinate of subbed benzimidazole just as different pharmacological exercises and a portion of the significant procedures utilized for the combination. In this audit, endeavors have been taken to reveal insight into the most recent informations accessible on the combinations and uses of various benzimidazole subordinates.

Keywords :
Benzimidazole, analgesic, anti-inflammatory, biochemical pharmacological activities, synthetic study.

INTRODUCTION

N-containing heteroaromatic compounds are important structural motifs found in many natural and synthetic compounds. Among them, benzimidazole and its derivatives are decisive core structures utilized in drugs and materials. In early sixties, benzimidazole nucleus was originally developed as plant fungicides and later as veterinary anthelmintics. In 1962, first benzimidazole, thiabendazole was discovered and approved for its anthelmintic property. Further, a number of veterinary anthelmintics were developed and marketed, including parbendazole, fenbendazole, oxfendazole and cambendazole.

Benzimidazole consists of an imidazole ring fused with benzene and is also called as 1,3-diazaindene. N-ribosyl-dimethylbenzimidazole is regarded as a prominent benzimidazole derivative in nature which serves as an axial ligand for cobalt in vitamin B12 [1]. In this heterocyclic scaffold, the formic acid carbon between the two nitrogen atoms is the most reactive site for probable substitution(s). The structure-activity relationship studies suggest that substitution at C-2 position of this heterocyclic system highly influences the biological activity. The benzimidazole is a fundamental pharmacophore in the molecular drug discovery and most important fragment in medicinal chemistry because of its broad variety of biological activities. Benzimidazole and its derivatives are reported to possess a number of interesting biological activities such as antitumor/antiproliferative/anticancer [2-3], antimicrobial [4], DNA binding activity [5], antibacterial [6], antiangiogenic [7], anthelmintic [8], antimalarial [9], anti-psychotic [10], potassium-competitive acid blockers [11], antifungal

[12], against serotoninergic 5-HT3 and 5-HT4 receptors [13], antiviral [14], protein tyrosine phosphatase 1B inhibitors [15], anti-trypanosomatid agent [16], protein kinase inhibitors [17], JAK1-selective inhibitors [18], cytotoxic activity [19] and anti-estrogen breast cancer agents [20-21].Thus, benzimidazole is considered as the important bicyclic ring systems and due to its significant pharmaceutical applications, the synthesis of various derivatives of this heterocycle has become noticeably attractive.

These are confirmed by the presence of benzimidazole nucleus in many traded drugs such as albendazole (A) as an anthelmintics, omeprazole (B) as proton pump inhibitors, astemizole (C) as an antihistaminic, and telmisartan (D) as an antihypertensive drugs. Thus, because of its growing medicinal importance, efforts have done from time to time to expand the methodologies for the synthesis of these new derivatives, in a hope to obtain a potent pharmacophore for the future.

Structure of Benzotriazole with their properties :

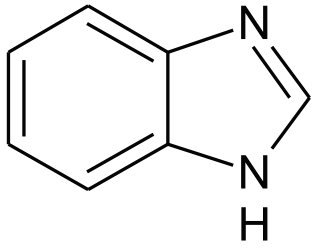

Fig. 1 : Stucture of Benzimidazole

Molecular Formula	=	$C_7H_6N_2$
Formula Weight	=	118.13594
Composition	=	C(71.17%) H(5.12%) N(23.71%)
Molar Refractivity	=	36.61 ± 0.3 cm^3
Molar Volume	=	95.0 ± 3.0 cm^3
Index of Refraction	=	1.696 ± 0.02
Surface Tension	=	60.1 ± 3.0 dyne/cm
Density	=	1.242 ± 0.06 g/cm^3
Polarizability	=	14.51 ± 0.5 10-24 cm^3

2. Study on Structural modifications and their pharmacological actions:

2.1. Anti-microbial Activity :

2.1.1. Anti-bacterial activity :- Literature survey shows that among the benzimidazole derivatives, 2-substituted ones are found to be pharmacologically more potent and hence the design and synthesis of 2-substituted benzimidazoles are the potential area of research [22-23].

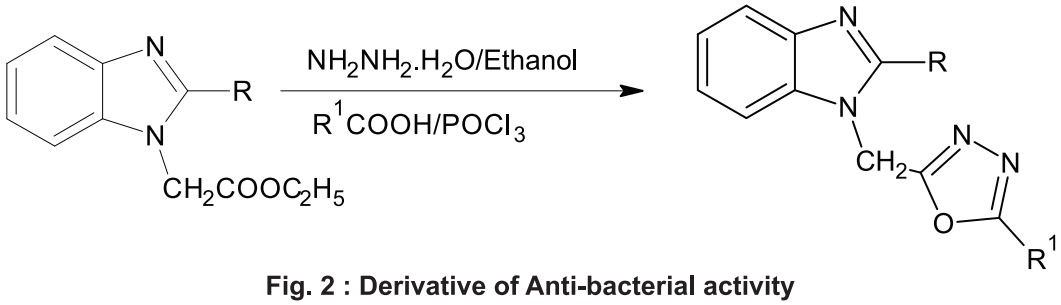

Fig. 2 : Derivative of Anti-bacterial activity

Some oxadiazol-1H-benzimidazole has been reported to possess antimicrobial activities. The compounds also showed moderate activity against tested fungi. Extensive biochemical and pharmacological studies have confirmed that its derivatives are effective against various strains of microorganisms [24]. In a study it was reported that by modifying the amide group to the anilide on the 2-phenyl benzimidazole produces antimicrobial activity [25]. Hydrazone is another considerable pharmacophore group for antimicrobial activity.

Some widely used antibacterial drugs such as furacilin, furazolidone and ftivazide are known to contain this group [26]. In past decades, hydrazones have received much attention and many studies [27] have been reported due to their chemotherapeutic value in the development of novel anti- microbial agents. A series of 1, 2-disubstituted-1Hbenzimidazole-N alkylated- 5-carboxamidine derivatives are very potent antibacterial activities against S. aureus and methicillin resistant S. aureus [28]. The study revealed the best activity, with MIC values of 0.78 - 0.39 µg/mL against these species. Various Chloro and dichloro substituted benzimidazole also possess antibacterial activities[29].

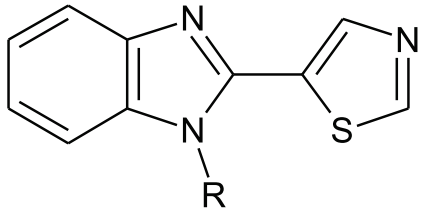

Fig. 3 : N-alkyl and N-acyl derivatives of 2-(4thiazolyl)-1H-benzimidazole [3]

2.1.2. Anti-fungal activity : Isoxazolyl substituted compounds were screened for activity against Gram Negative species like E. coli and Proteus vulgaris,Gram positive like Bacillus mycoides and staphylococcus aureus [30]. Some Benzimidazole compounds possessing hydrazone moiety were studied in order to investigate their possible antibacterial and antifungal activity. Most of the test compounds found to be significantly effective against Proteus vulgaris, Staphylococcus typhimurium, Klebsiella pneumoniae and Pseudomonas aeruginosa gram-negative bacterial strains. Some fluroquinolones substituted Benzimidazole derivatives have been reported by microwave assisted method. The synthesized compounds are reported to be the derivatives of Ciprofloxacine [31].

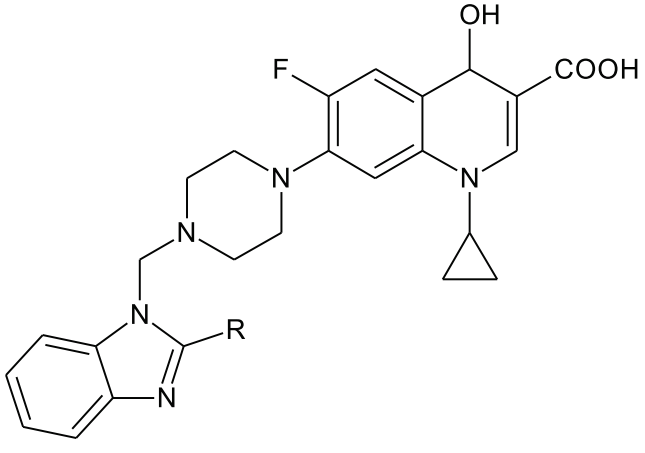

Fig. 4 : Ciprofloxacin derivatives(Anti-fungal activity)

Compounds which have no substitution of N1 position displayed better antibacterial activities, the trihalogen benzimidazole analogues exhibited the most potent antibacterial activity with MIC 3.12 µg/ml against S. aureus. In a study it was reported that by modifying the amide group to the anilide on the 2-phenyl benzimidazole produces antimicrobial activity [32].

A series of 2 alkylsulphanylbenzimidazoles was synthesised and the compounds were evaluated for their in vitro antimycobacterial activity. The structures of the compounds were confirmed by instrumental methods. Antimycobacterial activities against Mycobacterium tuberculosis and nontuberculous mycobacteria as well as antifungal activities against *Candida albicans, Candida tropicalis, Candida krusei, Candida glabrata, Trichosporonbeigelii, Trichophytonmentagrophytes and Aspergillusfumigatus* were expressed as the corresponding MIC values. The substances exhibited appreciable antimycobacterial activity, in particular, against non-tuberculosis mycobacteria. The activity of the most active compound in the set, 3, 5-dinitro derivative has also been reported. Another approach to synthesize antimicrobial agents is by synthesis of N-alkyl2. Phenyl-1H Benzimidazole-5-carboximidines. These compounds have been reported to be active against S. aureus and methicillin resistant S.aureus. The reported MIC is 0.780.39 µg/mL[33]. Some new compounds have been synthesised bearing azetidin-2-one and 1, 3, 4 thiadiazole moieties [34].

2.2. Anti-parasitic Activity :- 2-(Trifluoromethyl)-1H benzimidazole derivatives showed the most desirable in vitro antiparasitic profile against Giardia intestinalis, Entamoeba histolytica, Trichomonas vaginalis and Trichinella spiralis [35].The anthelmintic drugs derived from benzimidazole 2-carbamates, such as albendazole (ABZ) and mebendazole (MBZ), are used mainly to treat endoparasitic diseases in domestic animals and humans. These types of compounds are characterized by a high therapeutic index and low toxicity; however, they find little use in tissue-dwelling parasites mainly due to poor solubility and absorption problems [36].

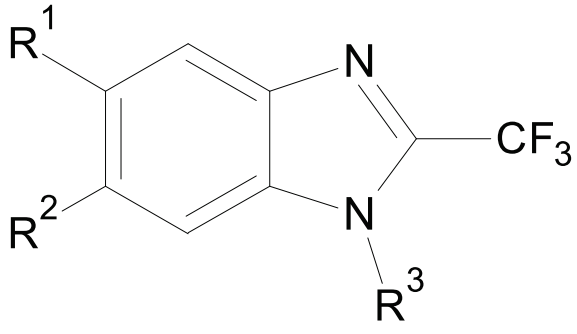

Fig. 5 : 2- (Trifluoromethyl) -1 H benzimidazole derivatives

1b : R_1 = 2,3-$C_{l2}C_6H_3O$. R_2=H, R_3=CH_3

1c : R_1 = H ,R_2=2,3-$C_{l2}C_6H_3O$, R_3=CH_{31} : R_1=H ,R_2=2,3-$C_{l2}C_6H_3O$, R_3=CH_3

1e : R_1 = $C_{10}H_7O$,R_2=Cl , R_3=H

2.3. Anti-hypertensive Agents: The biphenyl benzimidazoles have potent antihypertensive action as compared to the previous related drugs due to better availability upon the oral administration, 2- position of biphenyl is essential for the activity [37]. The 5 substituted aryl or alkyl caboxamido derivatives have reported to possess Angiotensin-II AT1 receptor antagonistic activity so are good antihypertensives agents [38].

2.4. Anti-convulsant Activity : - Some potential anticonvulsant compounds have been synthesized, a series of 1, 2, 5-trisubstituted benzimidazoles derivatives has been reported [39]. The results of QSAR investigation and the study of various physicochemical properties indicates that the change in linker at position one (R_1) does not change the activity of the synthesized compounds and optimum chain length at position two (R_2) is responsible for the anti- convulsant activity. The results also showed that the synthesized compounds with electron withdrawing group such as nitro at position five (R_3) have been reported to possess better anti-convulsant activity as predicted by QSAR studies.

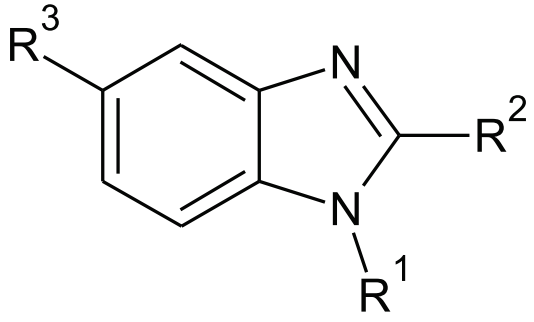

Fig no. 6 :- 1, 2, 5-trisubstituted benzimidazole ([11]
R$_1$= picoline, R_2= varying alkyl chain, R_3=NO_2

2.5. Anti-protozoal activity: - Another benzimidazole derivatives reported are 5, 6 dinitro and thioalkyl or thioaryl substituted compounds .These active compounds reported to possess activity against Stenotrophomonasmalthophilia. These compounds have activity related to metronidazole against gram positive and gram negative bacteria. Substituted 2trifluorobenzimidazoles have been reported [40]. Earlier it have reported anti-giardial activity [41],[42].

One of another research involves the synthesis of series of 2-(trifluoromethyl)1H- Benzimidazole derivatives by using Phillips cyclocondensation of a substituted 1, 2-phenylenediamine and trifluoroaceticacid.The compounds were evaluated in vitro against various protozoan parasitesnaming Giardia intestinalis, Entamoeba histolytica, Trichomonasvaginalis and sLeishmaniamexicana, and they showed nanomolar activities against some of the above mentioned protozoa. The compounds were also tested in vitro and in vivo against the nematode Trichinellaspiralis.[42]

3. Methods for synthesis of benzimidazole derivatives :

3.1.Kuldeep Kumar and D. P. Pathak [43] have reported the synthesis of some new 2-substituted benzimidazole derivatives from microwave irradiation method by condensation of 2-nitroaniline with different carboxylic acids (aliphatic, aromatic and hetrocyclic).

3.2. Davood Azarifar et al [44] have reported for the green synthesis of various 2-aryl-1-(arylmethyl)-1Hbenzimidazoles in high yields by acetic acid-promoted condensation of o-phenylenediamine with aldehydes in air under microwave irradiation.

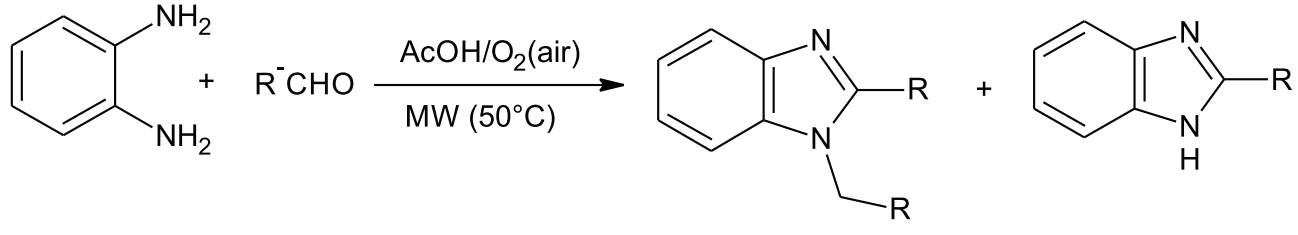

3.3. Komal P et al [45] have reported the synthesis of 2-chloromethyl-1H-benzimidazole by condensing 2 chloromethyl-1H-benzimidazole with different aromatic amines and heterocycle.

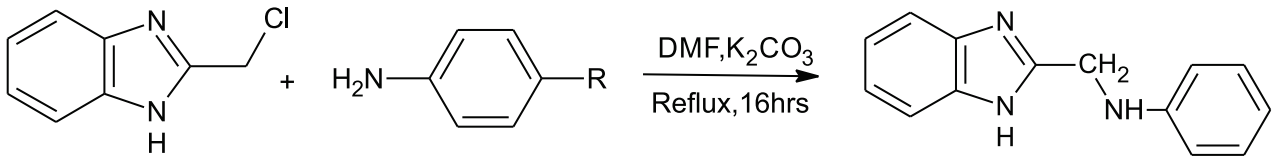

3.4. Marriappan G et al [46] have reported the synthesis of [1-(N-subistituted amino)methyl]-2-ethyl benzimidazole derivative(1-10) by the condensation of 2-ethyl benzimidazole with primary/secondary amines.

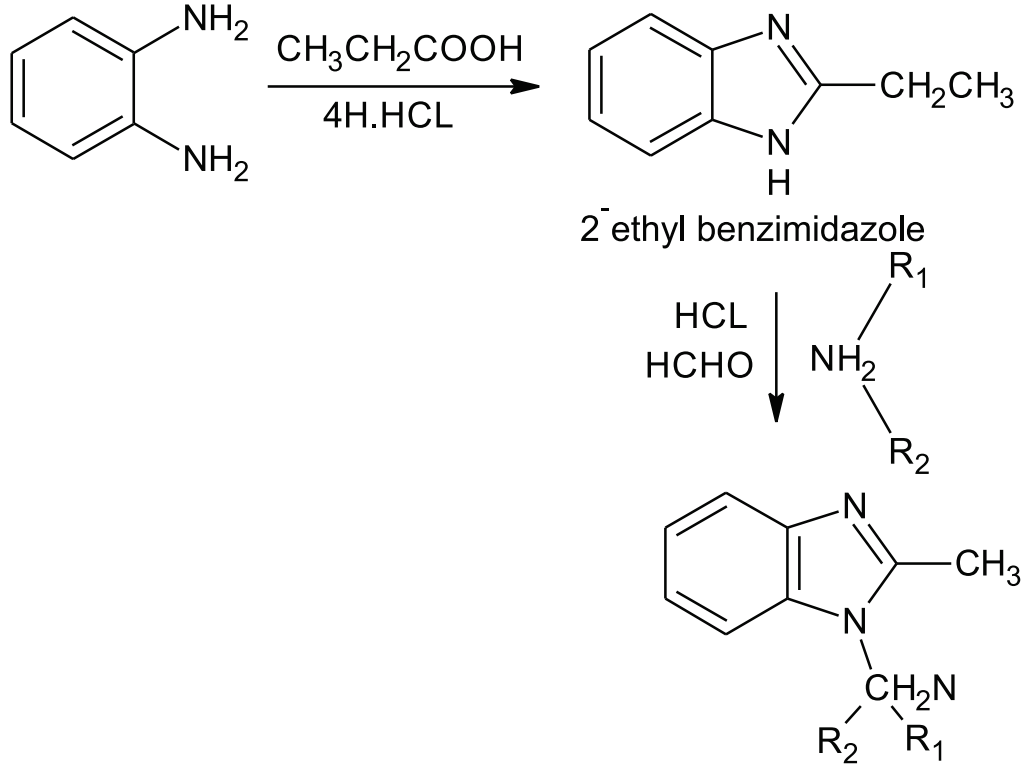

4. Pharmacological activity of benzimidazole derivatives :

4.1. Analgesic and anti inflammatory

Sr.no	Compounds structure	Derivatives	References
a.	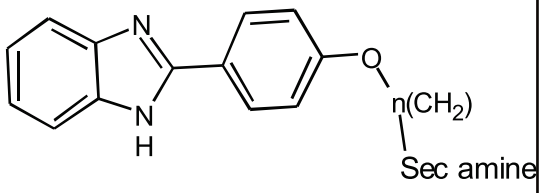 2-(4-Ethoxy-phenyl)-1H- benzimid- azole: compound with secondary amine.	Secondary amine replaced by: 1. Piperidine. 2. N-methylcyclo-hexyl amine. 3. Di-propyleamine . 4. N-methyl cyclohexyl amine 5. 1 phenyl piperazine 6. N ethyl piperazine	Shukla, , Synthesis and Biological Screening of benzimidazole derivatives, IJPSR; 2012; Vol. 3(3): 922-927 [47]
Analgesic activity- Out of all compound studied only 3, 4, 5 and 6 showed significant analgesic activities. Other compound did not produce significant analgesic activity.			
b.	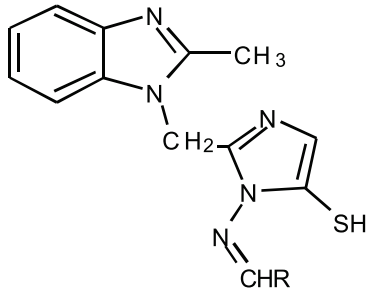 Schiff s bases of 2-methyl benzimidaz-ole derivative.	R a.-2-nitro benzaldeyde b.-3-nitro benzaldehy -de c.-4-chloro benzal-dehyde d.-4-hydroxy benzaldehyde e.-4-hydroxy3-methoxy benzaldehyde	Sanahanbi N.* and T. Sivakumar: AJBPAD, Issue 2 (Vol. 4) 2013.[48]
The compound a, b, c, d and e showed significant analgesic activity. The compound e showed mild to moderately significant analgesic activity. The compound a, d and e showed significant antiinflammatory activity. The compound b and c showed non-significant anti-inflammatory activity.			
c.	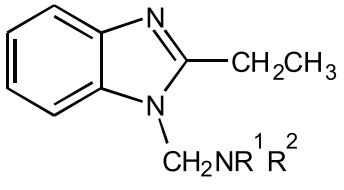 [1-(N-Substituted amino) methyl] -2-ethyl benzimidazole derivatives.	$-NR_1R_2$ -Diethylamine -Piperidino -Morpholino -Diethanol 2-Chloroanilino 3-Chloroanilino 2,3-dichloroanilino 3,4-dichloroanilino 4-fluroanilino -4-bromanilino	Marriappan G et al. Synthesis and evaluation of Mannich bases of benzimidazole derivatives, Indian Journal of Chemistry, vol.50B, Septem-ber2011; vol.5:4.1216-1219.[49]

The compounds synthesized were screened for anti inflammatory and analgesic activity among which derivative 1,2,8,9 and 10 are found to have anti inflammatory response and 2,4,6,8,10 have potent analgesic

4.2. Anti-bacterial and antifungal activity.

a. 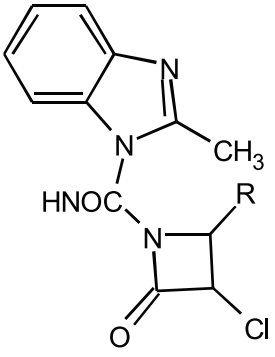 N-[3-cholro-2-(substituted) alkyl/aryl -4-oxoazetidin-1-yl]-1-Carboxamido-2-methyl-1H-benzimidazoles.	R CH_3 CH_2CH_3 $CH_2CH_2CH_3$ C_6H_5 2 $CH_3C_6H_4$ 3 $CH_3C_6H_4$ 2 $C_lC_6H_4$ 4 $C_lC_6H_4$ 2 OHC_6H_4 3 OHC_6H_4 4 OHC_6H_4 2 $OCH_3C_6H_4$ 4 $OCH_3C_6H_4$	K. F. Ansari and Synthesis and biological activity of some heterocyclic comp- ounds containing benzimidazole and betalactam moiety ,J. Chem. Sci., 2009;Vol.121: No. 6, November 2009, pp. 1017 1025. [50]
Among the synthesized benzimidazoles, compounds with alkyl, phenyl and hydroxyphenyl at 4-position of azetidin- 2-one were found to increase the antibacterial activity and compounds with phenyl and hydroxyphenyl substituents at azetidin-2-one sub-unit showed good antibacterial and antifungal activities		
b. 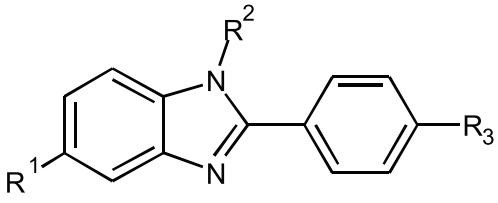	R_1 R_2 R_3 1.NO_2 C_2H_5 H 2.NO_2 C_2H_5Br 3.NO_2cycloH pentane 4.NH_2 C_2H_5H 5.NH_2 C_2H_5 Br 6.NH_2cycloH pentane	Hamdan s. Al-ebaisat. Synth- esis and Biolo- gical Activities of Some Benzimidazoles Derivatives, Sept, 2011; Vol.15: 3, 451 454. [51]
Compounds 2,3,4 and 5 possessed comparable activity to fluconazole against C. albicans.		

4.3. Anthelmintic activity

a.	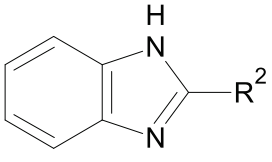	R_2 ---CH_3 ---C_6H_5 --- $CH_3C_6H_5$ --- $CH_3C_6H_5NH_2$	K Sreena et al .Synthesis and biolo- gical activity of novel 1H,3H-thiazolo[3,4-a]benzimidazoles:1991;10:211–217. [52]
All the synthesized compounds showed significant anthelmintic activity among these 2phenylbenzimidazole showed potential anthelminitic activity.			

4.4. Anti viral activity

a.	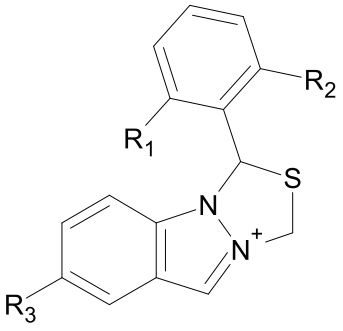 1H, 3H-thiazole [3,4-a] benzimidazole derivatives.	R_1 R_2R_3 1.-- F F 2.-- ClCl 3.-- F F 4.-- ClF 5.-OCH_3 F F 6.-OCH_3 ClF 7.-OCH_3ClF 8.-F F F 9.-F ClF 10.-F ClCl 11.CF_3F F 12.CF_3ClF 13.CF_3ClCl 14.COPh F F 15.COPh ClF 16.COPh ClCl	Chimirri A et al Synthesis and Anthelmintic Activity of Benzimidazole Derivatives HYGEIA / March-Aug 09; 1.[53].
The antiviral activities of compounds 1 –16 were evaluated in MT-4 cells acutely infected with HIV-1 (IIIB) or HIV-2 (ROD). Derivatives 3, 4, 8, and 9 were found to inhibit HIV-1 (IIIB). None of the compounds inhibited the replication of HIV-2 (ROD) in MT-4 cells.			

4.5. Anti convulsant activity

a.	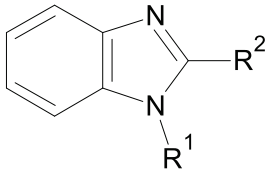 1,2-disubstituted benzimidazole	R_1=Picoline R_2= Varing alkyl chain R_3= NO_3	Ramanpreet Walia et al. Benzimidazole derivatives An over-view, IJRPC 2011; 1(3). [54]
The study of various physicochemical properties indicates that the change in linker at position one (R_1) does not change the activity of the synthesized compounds and optimum chain length at position two (R_2) is responsible for the anticonvulsant activity. The results also showed that the synthesized compounds with electron withdrawing group such as nitro at position five (R_3) have been reported to possess better anticonvulsant activity as predicted by QSAR studies.			

4.6. Antihypertensive activity

a.	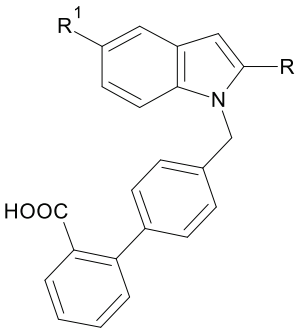	R R_1 -Phenyl - NH_2 -Ethyl $-NO_2$	Jatrakeshkumar, synthesis of benzim-idazole derivatives: as anti-hypertensive agents., e-journal of chemistry october 2006; 3: no.4, PP 278-285. [55]
From the study it was found that compounds that contain ethyl at position –2 gave better result than 2-phenyl. In the biphenyl ring carboxylic group at ortho position is necessary for pharmacological activity. At 2' position tetrazolyl moiety had the best pharmacological activity was found in the literature. At position 5 of benzimidazole NH_2 group gives good activity			

5. Conclusion :

The benzimidazole ring is an important pharmacophore in modern drug discovery. Attention has been increasingly given to the synthesis of benzimidazole derivatives as a source of new antimicrobial agents. The Benzimidazole derivatives are a resource for medicinal research. The knowledge gained by various researches has suggested that substituted benzimidazoles and heterocycles, which are the structural isosteres of nucleotides allow them to interact easily with the biopolymers, possess pharmacological activity with lower toxicities. Since now, researchers have been attracted toward designing more potent Benzimidazole derivatives having wide diverse of biological activity.

Compliance with ethical standards :

Acknowledgments

We would thank and express our gratitude to Principal of Priyadarshini J. L. College of Pharmacy, Nagpur.

Disclosure of conflict of interest

The authors declare that there are no conflicts of interest.

References :

[1] Barker HA, Smyth ,RDWeissbach, H Toohey, JI Ladd, JN Volcani, BE. Isolation and properties of crystalline cobamide coenzymes containing benzimidazole or 5,6-Dimethylbenzimidazole. J. Biol. Chem., 1960; 235(2): 480-488

[2] Rashedy AE. Benzimidazole derivatives as potential anticancer agents. Mini. Rev. Med. Chem,2013;13(3): 399-407

[3] Velagapudi, SP Steven J. Seedhouse, SJ French, J Disney, MD Defining the RNA Internal Loops Preferred by Benzimidazole Derivatives via 2D Combinatorial Screening and Computational Analysis. J. Am. Chem. Soc, 2011;133(26) : 10111-10118

[4] Alasmary, FAS Snelling, AM Zain, ME Ahmed M. Alafeefy, AM Awaad, AS Karodia, N Synthesis and evaluation of selected benzimidazole derivatives as potential antimicrobial agents. Molecules 2015; 20: 15206-15223

[5] Gao, C Li, B Zhang, B Sun, Q Li, X Chen, C Tan, C Liu, H Jiang. Synthesis and biological evaluation of benzimidazole acridine derivatives as potential DNA-binding and apoptosis-inducing agents. Bioorg. Med. Chem, 2015; 23(8) : 1800-1807

[6] Mohammed, NNA Alias, Y Abdullah, Z Shakir, RM Taha, EM Hamid. Synthesis and antibacterial evaluation of some novel imidazole and benzimidazole sulphonamides Molecules,2013;18: 11978-11995

[7] Yellol, JG Perez, SABuceta, A Yellol, GS Donaire, A Szumlas, P Bednarski, PJ Makhloufi, G Janiak, C Ferao, AE Ruiz. J Novel C,Ncyclometalated benzimidazole ruthenium(II) and iridium(III) complexes as antitumor and antiangiogenic agents: a structure-sctivity relationship study. J Med. Chem,2015;58(18): 7310-7327

[8] Sawant, R. Kawade, D. Synthesis and biological evaluation of some novel 2-phenyl benzimidazole-1-acetamide derivatives as potential anthelmintic agents. Acta Pharm,2011;61: 353-361

[9] Camacho, JBarazarte, AGamboa, N Rodrigues, J Rojas, R Vaisberg, A Gilman, R Charris. Synthesis and biological evaluation of benzimidazole-5-carbohydrazide derivatives as antimalarial, cytotoxic and antitubercular agents. Bioorg. Med. Chem, 2011;19(6): 3523-3530

[10] Norman, MH Navas, F Thompson, JB Greg, C Rigdon. Synthesis and Evaluation of Heterocyclic Carboxamides as Potential Antipsychotic Agents. J. Med. Chem,1996;39: 4692-4703

[11] Webel, M Palmer, AM Scheufler, C Haag, D Muller, B Development of an efficient process towards the benzimidazole BYK308944. A key intermediate in the synthesis of a potassium-competitive acid blocker. Org. Proc. Res. Dev, 2010;14(1): 142-145

[12] Bai, YB Zhang, AL Tang, JJ Gao, JM. Synthesis and antifungal activity of 2-chloromethyl-1H-benzimidaole derivatives againstphytopathogenic fungi in vitro J Agric. Food Chem,2013;61: 2789-2795

[13] Rodriguez, MLL Benhamu, B Morcillo, MJ Tejada, ID Orensanz, L Alfaro, MJMartin, MI Benzimidazole derivatives. 2. Synthesis and structure-activity relationships of new azabicyclic benzimidazole-4-carboxylic acid derivatives with affinity for serotoninergic 5-HT3 Receptors. J. Med. Chem, 1999; 42: 5020-5028

[14] Zou, R Ayres, KR Drach, JC Townsend, LB. Synthesis and antiviral evaluation of certain disubstituted benzimidazole ribonucleosides. J. Med. Chem, 1996; 39: 3477-3482

[15] Combs, AP. Zhu, W Crawley, ML Glass, B et al, B Potent Benzimidazole Sulfonamide Protein Tyrosine Phosphatase 1B Inhibitors Containing the Heterocyclic (S)IsothiazolidinonePhosphotyrosine Mimetic. J. Med. Chem, 2006; 49: 3774-3789

[16] Boiani, M Boiani, LDenicola, A de Ortiz, ST Serna. González, M 2HBenzimidazole 1,3-Dioxide Derivatives:A New Family of Water-Soluble Anti-Trypanosomatid Agents. J. Med. Chem, 2006; 49: 3215-3224

[17] Singla, P Luxami, V Paul, K Benzimidazole-biologically attractive scaffold for protein kinase inhibitors. RSC Adv,2014;4: 12422 -12440

[18] Kim, MK Shin, H Park, KS Kim, H Park, J Kim, K Nam, JChoo, H Chong, Y Benzimidazole derivatives as potent JAK1-selective inhibitors. J. Med. Chem,2015;58: 7596-7602

[19] Buia, HTB Ha, QTK Oh, WK Vo, DDChau. Microwave assisted synthesis and cytotoxic activity evaluations of new benzimidazole derivatives. Tetrahedron Lett,2016;57(8): 887-891

[20] Yde, CW Frogne, T Lykkesfeldt, AEFichtner, I Issinger, OG Stenvang, J .Induction of cell death in antiestrogen resistant human breast cancer cells by the protein kinase CK2 inhibitor DMAT. Cancer Lett,2007; 256(2): 229-237

[21] Chu, B. Liu F. Li, L. Ding, C. Chen, K. Sun, Q.Shen, ZY. A benzimidazole derivative exhibiting antitumor activity blocks EGFR and HER2 activity and upregulates DR5 in breast cancer cells. Cell Death and Disease,2015;6: 1686-1696

[22] Preston PN.Benzimidazoles and Congeneric Tricyclic Compounds Part 2.Wiley Interscience New York, 1980:531

[23] Foks H, Ksepko DP, Kuzmierkiewicz W, Zwolska Z, Augustynowicz EK, and Janowiec M. Synthesis and tuberculostatic activity of new benzimidazole derivatives.Chem Het Comp. 2006;42:611-614

[24] Ansari KF and Lal C. Synthesis, physicochemical properties and antimicrobial activity of some new Benzimidazole derivatives. European Journal of Medicinal Chemistry. 2009;44:4028–4033

[25] Göker H, Kus C, Boykin DW, Yildiz S and Altanlar N. Synthesis of some new 2-substitutedphenyl-1Hbenzimidazole-5-carbonitriles and their potent activity against Candida species. Bioorg Med Chem. 2002;10: 2589-2596

[26] Sharma D, Narasimhan B, Kumar P and Jalbout A. Synthesis and QSAR evaluation of 2-(substituted phenyl)1H-

benzimidazoles and [2(substituted phenyl)-benzimidazol-1yl]-pyridin-3-yl-methanones. Eur J Med Chem. 2009;44:1119-1127.

[27] Chornous VA, Bratenko MK, Vovk MV and Sidorchuk II. Synthesis and Antimicrobial Activity of Pyrazole-4carboxylic Acid Hydrazides and N-(4Pyrazoyl)hydrazones of Aromatic and Heteroaromatic Aldehydes. Pharmaceutical Chemistry Journal. 2001;35(4):203-205.

[28] Rollas S, Gulerman N and Erdeniz H. Synthesis and antimicrobial activity of some new hydrazones of 4fluorobenzoic acid hydrazide and 3acetyl-2,5-disubstituted-1,3,4oxadiazolines. Farmaco. 2002;57:171-174.

[29] Göker H, Ozden S, Yildiz S and Boykin DW. Synthesis and potent antibacterial activity against MRSA of some novel 1,2-Disubstituted-1HBenzimidazole-N-alkylated-5carboxamidine. Eur J Med Chem. 2005;40:1062 -1069.

[30] Rajanarendar E, Ramu K, Reddy ASR and Shaik FP. Synthesis and in vitro study of novel isoxazolylbenzoimidazolylbenzamides, acrylamides and propionamides as antimicrobial agents. Ind J Chem. 2008;47: 12-84.

[31] Jubie S, Rajeshkumar R, Yellareddy B, Siddhartha G, Sandeep M, Surendrareddy K, Dushyatha HS And Elango K. Microwave assisted synthesis of some novel Benzimidazole submitted fluoroquinolones and their antimicrobial evaluation. J Pharm Sci and Res. 2010;2(2):69-76.

[32] Klimesova V, Kocý J, Waisser K and Kaustova J. New Benzimidazole derivatives as antimycobacterial agents. IL Farmaco. 2002;57:259–265.

[33] Göker H, Alp M and Yildiz S. Synthesis and potent Antimicrobial activity of some novel N-(alkyl)-2Phenyl-1H-benzimidazole-5carboxamidines. Molecules. 2005;10:1377-1386.

[34] Ansari KF and Lal C. Synthesis and evaluation of some new Benzimidazole derivatives as potent antimicrobial agents. European Journal of Medicinal Chemistry. 2009;44:2294–2299.

[35] Hernández-Luis F, HernándezCampos A, Castillo R, NavarreteVázquez G, Soria-Arteche O, Hernández-Hernández M and YépezMulia L. European Journal of Medicinal Chemistry. 2010;45(7):31-35.

[36] Cook GC. Use of benzimidazole chemotherapy in human helminthiases: indication and efficacy, Parasitol. Today. 1990;(6):133–136.

[37] Shah DI, Sharma M, Bansal Y, Bansal G and Singh M. Angiotensin II—AT1 receptor antagonists: design, synthesis and evaluation of substituted carboxamido benzimidazole derivatives. Eur J Med Chem. 2007;20:1-5.

[38] Jat RK, Jat JL and Pathak DP. Synthesis of benzimidazole derivatives: As Anti-hypertensive agents. E- Journal of Chem. 2006;3:278.

[39] Kazimierczuk Z, Upcroft JA, Upcroft P, Gorska A, StarosciakB andAgnieszka L. ActaBiochimicapolonica. 2002;49 : 185- 195.

[40] Navarrete-Vázquez G, Cedillo R, Hernández-Campos A, Yepez L, Hernández-Luis FJ, Valdéz R, Morales R, Cortés M, and Castillo R. Synthesis and antiparasitic activity of 2-(trifluoromethyl) benzimidazole derivatives. Bioorg Med ChemLett. 2001;11:187–190.

[41] Xiao L, Saeed K and Herd RP. Efficacy of albendazole and fenbendazole against Giardia Infection in cattle Vet. Parasitol. 1996;61:165- 170.

[42] Hernández-Luis F, HernándezCampos A, Castillo R, NavarreteVázquez G, Soria-Arteche O, Hernandez Hernandez M and YépezMulia L. Synthesis and biological activity of 2-(trifluoromethyl)-1Hbenzimidazole derivatives against some protozoa and Trichinellaspiralis. European Journal of Medicinal Chemistry. 2010;45(7):3135-3141.

[43] KuldeepKumar , Prof.(Dr). D. P. Pathak., Synthesis, Characterization and Evaluation For Antimicrobial Activity Of 2 Substituted Benzimidazole Derivatives.,THE PHARMA INNOVATION., 2012;Vol.1 No. 9.

[44] DavoodAzarifar et al., Acetic acid-promoted condensation of o-phenylenediamine with aldehydes into 2-aryl-1-(arylmethyl)1H-benzimidazoles under microwave irradiation., J. Serb. Chem. Soc.2010;75 (9): 1181–1189.

[45] KomalPetkar *, Pranav Parkh,Preeeti Mehta , Abha Kumar, AnjanaBaro, Synthesis and evaluation of 2-chloromethyl-1Hbenzimidazole derivatives as antifungal agents Int J Pharm PharmSci, Vol 5, Issue 2; 115-119.

[46] Marriappan G et al, Synthesis and evaluation of Mannich bases of benzimidazole derivatives, Indian Journal of Chemistry,

September 2011; vol.50B:1216-1219.

[47] Shukla, Synthesis and Biological Screening of benzimidazole derivatives,IJPSR; 2012; Vol. 3(3): 922-927

[48] Sanahanbi N.* and T. Sivakumar, Synthesis of Some Schiff's Bases of 2-Methyl Benzimidazole Derivatives and Screening of Analgesic and Anti-Inflammatory Activities, CODEN(USA) : AJBPAD, Issue 2 (Vol. 4) 2013.

[49] Marriappan G et al, Synthesis and evaluation of Mannich bases of benzimidazole derivatives, Indian Journal of Chemistry, vol.50B, September 2011; vol.5:4.1216-1219.

[50] K F Ansari and C Lal, Synthesis and biological activity of some heterocyclic compounds containing benzimidazole and betalactam moiety ,J. Chem. Sci., 2009;Vol.121: No. 6, November 2009, pp. 1017–1025.

[51] Hamdan S. Al-Ebaisat., Synthesis and Biological Activities of Some Benzimidazoles Derivatives, J Appl. Sci. Environ. Manage. Sept, 2011; Vol.15: 3, 451 – 454.

[52] Chimirri A et al., Synthesis and biological activity of novel 1H,3H-thiazolo[3,4-a]benzimidazoles: non-nucleoside human immunodeficiency virus type 1 reverse transcriptase inhibitors, Antiviral Chemistry & Chemotherapy 1991;10 : 211–217.

[53] K Sreena et al, Synthesis and Anthelmintic Activity of Benzimidazole Derivatives HYGEIA / March-Aug 09; Vol.1: No.1.

[54] Ramanpreet et al. Benzimidazole derivatives-An overview, IJRPC 2011; 1(3).

[55] JatRakesh Kumar, JatJawahar I and D. P. Pathak., Synthesis of Benzimidazole Derivatives: As Anti-hypertensive Agents., E-Journal of Chemistry October 2006;Vol. 3: No.4, pp 278-285.

Peer Reviewed and Refereed Journal 2022 **(ISSN : 09726330)**

Rashtrasant Tukadoji Maharaj Nagpur University

SCIENCE JOURNAL 2022

Vol. : XV

Combination Therapy against Breast Cancer (Overview of effective combination therapies for breast cancer)

Monu Shahu*, Pramod B. Khedekar

Department of Pharmaceutical Sciences,
Rashtrasant Tukadoji Maharaj Nagpur University, Amravati Road, Nagpur 440033,
Maharashtra, India.

Corresponding author email :
*monushahu009@gmail.com
Mobile No. 9175080025

Abstract :

After skin cancer, most women die of breast cancer. Breast cancer mainly occurs in women, and its development occurs due to abnormal breast tissue. There are a variety of monotherapy that can be used to suppress breast cancer, but it shows some side effects. Instead of monotherapy, combinations of different combination therapies and therapeutic agents for breast cancer show synergistic effects and anticancer activity against breast cancer. A variety of combinations, such as the combination of tetrandrine and cisplatin, the combination of lapatinib and luteolin, the combination of nutritional supplements and chemotherapy, the combination of Pertuzumab and Trastuzumab, etc. Therapeutic agents act on receptors present on the cell surface, such as estrogen (ER), progesterone (PR) and (HER2) human epidermal growth factor 2, and show anticancer activity and synergy.

Keywords : Composite; Cancer, combination therapy, breast cancer, apoptosis.

INTRODUCTION

In the current treatment, compared with monotherapy, combination therapy plays an important role, because complementary chemotherapeutic drugs can obtain synergistic effects and reduce the incidence of tumor recurrence and treatment failure. The recommended method is to prevent the development of drug resistance, increase the treatment effect and reduce the treatment time [1]. The leading cause of death among women in the world is breast cancer [2]. Breast cancer is a type of cancer that develops from breast tissue and can treat the most expensive malignant tumors [3,4]. Breast cancer is the most common auxiliary cancer in women, followed by skin cancer. It can be detected earlier by mammography, or it can be detected before it spreads. First, classify breast cancer based on clinical variables such as tumor size, lymph node status, and histological grade. The cells of the terminal duct lobular unit (TDLU) start from epithelial cells, and most breast cancer cells are cancers. Sarcoma is a smaller part of cancer that develops in other tissues of the breast. Diagnosis of life-threatening and more aggressive cell receptors present on the cell surface, such as oestrogen (ER), progesterone (PR) and human epidermal growth factor 2 (HER2) form triple-negative breast cancer [5]. Breast cancer is divided into the following subgroups: 1. A and B-ER positive luminescent tumors with expression of epithelial markers; 2. HER2 positive, HER2 gene overexpression; 3. A normal-like expression profile similar to non-cancerous breast tissue; 4. Normal breast muscle epithelium-specific basal-like/triple-negative breast cancer (TNBC) expression markers; 5. Claudin low epithelial to mesenchymal transition (EMT) function. There are varieties of combined treatments,

showing synergy and anticancer activity against breast cancer as follows :

1. Combination of Tetrandrine and Cisplatin:

The effect of chemotherapeutics will induce cell apoptosis in different molecular pathways, including cell cycle, autophagy, reactive oxygen species-mediated pathways, angiogenesis, etc [6,7]. Various chemotherapeutic drugs may induce nausea, gastrointestinal lesions, bone marrow suppression, hair loss and the development of drug resistance [8]. Cisplatin (Cis) is most commonly used in the treatment of different types of cancer [9,10]. Cis has the ability to induce apoptosis through the purine cross-linking base of DNA, and interfere with DNA repair, and then interfere with the cell cycle. It also induces ROS-mediated or intracellular calcium-mediated elevation or death receptor-mediated apoptosis of cancer cells [10]. Cis exhibits various side effects in patients, such as vomiting, nausea, nephrotoxicity, neurotoxicity, immunosuppression, etc., which limits the use of very low-dose platinum drugs. By combining with other anti-tumor drugs, Cis can reduce side effects [10,11,12].

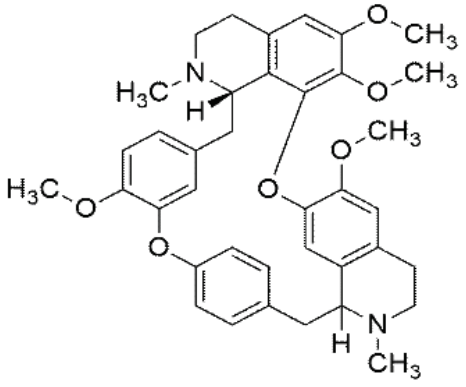

Figure 1. Tetrandrine

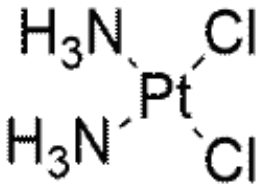

Figure 2. Cisplatin

Tetrandrine (Tet) is an effective biologically active compound [13], obtained from Stephania tetrandra, which belongs to the bisbenzylisoquinoline group of alkaloids, and has been shown strong anti-cancer activity to be effective against different types of cancer by acting on protein molecules in different signal pathways [7]. Tet is used in combination with arsenic trioxide [14], doxorubicin/vincristine [15,16], fluorouracil, oxaliplatin, docetaxel [17], sodium arsenite [6], etc., which can prevent the drug resistance of many cancer cells by reversing the expression of P-glycoprotein on the cell surface and enhance the cytotoxicity of other chemotherapeutic drugs. When Tet is used in combination with Cis, Cis-resistant lung cancer cells and Cis-sensitive cells show apoptosis [18]. When other tumor drugs are used in combination with Tet, anti-proliferative effects can be obtained through multiple signal pathways. When used together with arsenite, Tet exhibits synergistic cytotoxicity in human breast cancer cells (MCF-7) by inducing cell cycle arrest and autophagy-mediated pathways as well as the regulation of multiple efflux transporters [6]. Because of their effect on more than one pathway, when two or more drugs are used in combination therapy [12], it reduces the toxicity of the drugs. Therefore, instead of monotherapy, combination therapy is most commonly used for cancer treatment.

2. Combination of Lapatinib and luteolin :

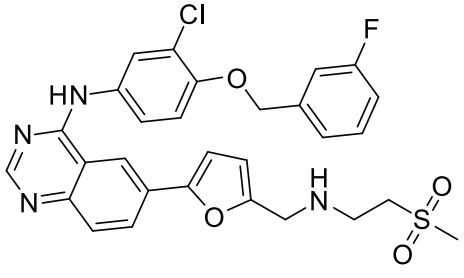

Figure 3. Lapatinib

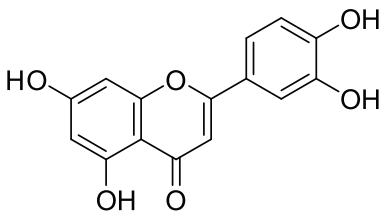

Figure 4. Luteolin

Lapatinib is a 4-aminoquinazoline derivative [19]. Lapatinib is a tyrosine kinase inhibitor that can block the activation of HER1 and HER2 tyrosine kinases by inhibiting the activation of downstream signaling pathways, thereby inhibiting tumor survival and proliferation [20]. Luteolin is formed by yellow needle-like crystals and is easily soluble in organic solvents [21]. The results of many pharmacological tests and clinical trials prove that luteolin can actually inhibit breast cancer in different ways before, and it can also have multiple effects, such as antiviral, antitumor, analgesic, antibacterial and anti-inflammatory effects [22]. Studies have shown that NQO1 can stably express p53, so it is closely related to tumor and has the effect of quinone detoxification [23]. In some studies, there is no NQO1 protein in normal breast epithelial cells, but it has a strong positive expression in about 20% of breast tumors [24]. It was studied that the combination of lapatinib and luteolin on human breast cancer cells showed anticancer activity in human breast cancer.

3. Nutritional Supplements in combination with Chemotherapy :

Triple negative breast cancer (TNBC) is an aggressive and complex subtype of breast cancer that is deficient in oestrogen receptor (ER), progesterone receptor (PR) and human epidermal growth factor receptor 2 (HER-2). This subtype accounts for approximately 10-15% of new breast cancer diagnoses each year [25]. Compared with non-TNBC and TNBC, the prognosis of patients is poor, early recurrence, and overall survival rate is significantly shortened [26]. At present, chemotherapy is still the main standard treatment for TNBC, and anti-vascular endothelial growth factor (anti-VEGF) targeted therapy has also been used for the treatment of metastatic TNBC [27]. TNBC initially had a clinical response to chemotherapeutic drugs including paclitaxel and anthracyclines, although apoptosis caused by chemotherapy resistance may lead to its rapid progression to metastasis and cancer recurrence, leading to a poor prognosis [28].

There are various mechanisms have been studied, such as inhibition of hypoxia and pro-angiogenesis signaling pathways, indicating cytotoxic oxidative stress, targeting and eradicating breast cancer stem cells (CSC), blocking invasion and metastasis potential, and selective chelation of transition metal ions androle of fusion in the development of potential anti-TNBC therapeutic agents [29,30]. In addition, the expression of AXL receptor tyrosine kinase and targeted immune checkpoints and selective down-regulation of heat shock protein (HSP) are also potential therapeutic strategies for TNBC [31]. The currently available therapeutic agents are associated with frequent and unpredictable side effects of resistance to treatment [25]. Therefore, complementary therapeutic interventions for TNBC will be crucial to extend life expectancy and reduce the progress of metastasis.

The super-nutritive dose of certain nutritional supplements in fish meal, whey protein, vitamins and essential minerals (calcium, selenium) (such as docosahexaenoic acid (DHA, 22: 6 n3) and eicosapentaenoic Acid (EPA, 20:5 n3) has anticancer effects [Se] and zinc [Zn] have been fully proven, and have been reported to be related to the ability of cancer animal models and the ability to target multiple molecular pathways in cell culture. These pathways include induction of pro-oxidative cell death in vitro and in vivo, inhibition of angiogenesis and tumor metastasis, and immunomodulation [32,33]. Previous studies have shown that even in the non-TNBC mode of tumor-bearing, selenium supplementation has anti-cancer effects on the induction of tumor tissue apoptosis and oxidative stress [34]. In addition, when combined with Se or EPA/DHA, compared with Se or EPA/DHA, it has a greater anti-tumor effect on lung adenocarcinoma cells [35]. Therefore, for TNBC patients receiving anti-cancer therapeutics at the same time, when the appropriate combination of supplements can provide active nutrients, the anti-tumor response can be improved.

4. Combination of Pertuzumab and Trastuzumab :

The human epidermal growth factor receptor 2 (HER2) gene hide the HER2 receptor tyrosine kinase, which can amplify about 20% of breast cancer [36] and aggressive phenotypes, and is associated with poor prognosis [37]. When trastuzumab (Herceptin)-based therapy is used to treat early and metastatic HER2-positive breast cancer, the patient's prognosis has been substantially improved. The various mechanisms of trastuzumab inhibiting tumor growth include inhibiting downstream signal transduction by blocking the ligand- independent HER2/HER3 heterodimer [38] or HER2 homodimer [39]. Finally, trastuzumab can produce antibody-dependent cell-mediated toxicity [40]. Relying on the HER2 oncogene, tumor cells continue to acquire resistance to trastuzumab. For further introduction, protein/RNA overexpression and gene amplification still exist in trastuzumab-resistant HER2+ clones [41].

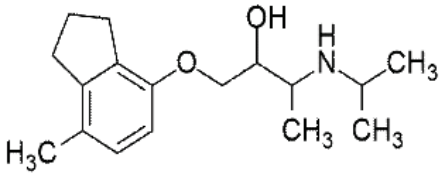

Figure 5. Pertuzumab

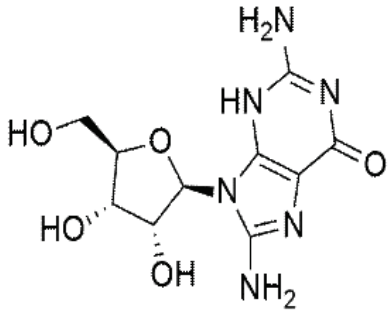

Figure 6. Trastuzumab

Pertuzumab is a monoclonal antibody that binds to the extracellular HER2 dimerization domain II (the region where trastuzumab binds, located on the opposite side of domain IV). Pertuzumab can inhibit the expression of HER2, HER4 [42,43,44] and IGF-1R (insulin-like growth factor-I receptor) [45] on the heterodimer HER2, although trastuzumab has prefentially active against on HER2 homodimer-driven tumors [46]. Pertuzumab can inhibit the growth of tumor cells after HER2 heterodimerization induced by heregulin (HRG).

The combination of Pertuzumab and Trastuzumab showed a synergistic effect when compared with the in vitro monotherapy of Pertuzumab on the BT474 breast cancer cell line overexpressing HER2. The combination of trastuzumab and pertuzumab can significantly enhance the anti-tumor effect of non-small cell lung cancer and HER2-positive breast cancer xenografts and induce tumor regression [47].

Conclusion:

Heterogeneous disease, namely breast cancer, is a secondary cause of death in women. Therefore, to understand the biological knowledge of breast cancer and realize that simple changes in the cellular microenvironment may be dangerous to the growth of tumors, it is necessary to increase the intensity of breast cancer. Researchers work hard to find biomarkers in order to recognize tumor development at the earliest stage and encounter new treatments. Conventional drugs show higher resistance to tumors. Therefore, the determination of key regulatory pathways makes it possible to target cancer cells more specifically, reduce drug resistance and minimize toxicity to normal cells. When drugs are used in combination with conventional treatments or between them, the enhanced activity against cancer cells can provide more prominent beneficial results and improve survival rates. In addition, monotherapy may provide beneficial anticancer activity, but exhibit more side effects. Therefore, various combination therapies for breast cancer have anticancer activity and synergistic effects.

References :

1. Z. Guo *et al.*, "pH-Responsive charge switchable PEGylated å -poly- L -lysine polymeric nano particles-assisted combination therapy for improving breast cancer treatment," *J. Control. Release*, vol. 326, no. April, pp. 350–364, 2020.

2. Benson JR, Jatoi I (2012) The global breast cancer burden. Future Oncol 8:697–702.

3. National Cancer Institute. (2014) Cancer topics: Breast cancer. http://www.cancer.gov/cancertopics/types/breast. Accessed 5 Jan 2015. 2015:1–1.

4. Sullivan R, Peppercorn J, Sikora K et al (2011) Delivering affordable cancer care in high-income countries. Lancet Oncol 12:933–980.

5. G. Bianchini, J.M. Balko, I.A. Mayer, M.E. Sanders, L. Gianni, Triple-negative breast cancer: challenges and opportunities of a heterogeneous disease, Nat. Rev. Clin. Oncol. 13 (2016) 674–690.

6. M. Yao, B. Yuan, X. Wang, A. Sato, K. Sakuma, K. Kaneko, H. Komuro, A. Okazaki, H. Hayashi, H. Toyoda, X. Pei, X. Hu, T. Hirano, N. Takagi, Synergistic cytotoxic effects of arsenite and tetrandrine in human breast cancer cell line MCF-7, Int. J. Oncol. 51 (2017) 587–598.

7. N. Bhagya, K.R. Chandrashekar, Tetrandrine and cancer – An overview on the molecular approach, Biomed. Pharmacother. 97 (2018) 624–632.

8. S. Nussbaumera, P. Bonnabrya, J.L. Veuthey, S.F.S. Talanta, Analysis of anticancer drugs: a review, Talanta 85 (2011) 2265–2289.

9. S. Dasari, P.B. Tchounwou, Cisplatin in cancer therapy: molecular mechanisms of action, Eur. J. Pharmacol. 5 (2014) 364–378.

10. A.-M. Florea, D. Busselberg, Cisplatin as an anti-tumor drug: cellular mechanisms of activity, drug resistance and induced side effects, Cancers 3 (2011) 1351–1371.

11. S. Rodriguez-Enriquez, A. Marin-Hernandez, J.C. Gallardo-Perez, L. CarrenoFuentes, R. Moreno-Sanchez, Targeting of cancer energy metabolism, Mol. Nutr. Food Res. 53 (2009) 29–48.

12. R.B. Mokhtari, T.S. Homayouni, N. Baluch, E. Morgatskaya, S. Kumar, B. Das, H. Yeger, Combination therapy in combating cancer, Oncotarget 23 (2017) 38022–38043.

13. N. Bhagya, K.R. Chandrashekar, Tetrandrine – a molecule of wide bioactivity, Phytochemistry 125 (2016) 5–13.

14. Y. Chen, P. Li, S. Yang, N. Tong, J. Zhang, X. Zhao, Tetrandrine enhances the anticancer effects of arsenic trioxide in vitro, Int. J. Clin. Pharmacol. Ther. 52 (2014) 416–424.

15. L.W. Fu, Y.M. Zhang, Y.J. Liang, X.P. Yang, Q.C. Pan, The multidrug resistance of tumour cells was reversed by tetrandrine in vitro and in xenografts derived from human breast adenocarcinoma MCF-7/adr cells, Eur. J. Cancer 38 (2002) 418–426.

16. A.X. Sun, Z.G. Ye, C.Y. Li, B.Y. Xue, L.F. Li, X.F. Cao, Q. Yang, B.Q. Dai, Synergistic anticancer effects of tetrandrine combined with doxorubicin or vincristine in vitro, Zhongguo Yao Li Xue Bao 20 (1999) 69–73.

17. J. Wei, B. Liu, L. Wang, X. Qian, Y. Ding, L. Yu, Synergistic interaction between tetrandrine and chemotherapeutic agents and influence of tetrandrine on chemotherapeutic agent-associated genes in human gastric cancer cell lines, Cancer Chemother. Pharmacol. 60 (2007) 703–711.

18. L.-Y. Ye, S. Hu, H.-E. Xu, R.-R. Xu, H. Kong, X.-N. Zeng, W.-P. Xie, H. Wang, The effect of tetrandrine combined with cisplatin on proliferation and apoptosis of A549/DDP cells and A549 cells, Cancer Cell Int. 17 (2017) 40.

19. P.J. Medina, S. Goodin, Lapatinib : a dual inhibitor of human epidermal growth factor receptor tyrosine kinases, Clin. Therapeut. 30 (2008) 1426e1447, https://doi.org/10.1016/j.clinthera.2008.08.008.

20. L. Garciaestevez, Biologic study of the effects of lapatinib in PI3K/akt- and ras/ raf/MAK-signaling pathways in HER2-positive ductal breast carcinoma in situ (DCIS), J. Clin. Oncol. 29 (2011) 135e142, https://doi.org/10.1200/jco.2011.29.15_suppl.e13581.

21. T. Matsuzaki, T. Ishinabe, H. Fujikake, Crystal Axis control of soluble organic semiconductors in nematic liquid crystal solvents based on electric field, IEICE Trans. Electron. 98 (2015) 1032e1034, https://doi.org/10.1587/transele.E98.C.1032.

22. S. Kapoor, Luteolin and its inhibitory effect on tumor growth in systemic malignancies, Exp. Cell Res. 319 (2013) 777e778, https://doi.org/10.1016/ j.yexcr.2013.01.006.

23. G. Tudor, M. Alley, C.M. Nelson, R. Huang, D.G. Covell, P.L. Gutierrez, E.A. Sausville, Cytotoxicity of RH1: NAD(P)H:quinone acceptor oxidoreductase (NQO1)-independent oxidative stress and apoptosis induction, Anti Canc. Drugs 16 (2005) 381e391, https://doi.org/10.1097/00001813-200504000- 00004.

24. Y. Yang, X. Zhou, M. Xu, J. Piao, Y. Zhang, Z. Lin, L. Chen, b-lapachone suppresses tumour progression by inhibiting epithelial-to-mesenchymal transition in NQO1-positive breast cancers, Sci. Rep. 7 (2017), https://doi.org/ 10.1038/s 41598-017-02937-0, 2681-2681.

25. Collignon J, Lousberg L, Schroeder H, Jerusalem G. Triple-negative breast cancer: treatment challenges and solutions. Breast Cancer (Dove Med Press). 2016; 8:93-107.

26. Mustacchi G, De Laurentiis M. The role of taxanes in triple-negative breast cancer: literature review. Drug Des DevelTher. 2015; 9:4303-18.

27. Marmé F, Schneeweiss A. Targeted therapies in triple-negative breast cancer. Breast Care. 2015; 10:159-66.

28. Mayer IA, Abramson VG, Lehmann BD, Pietenpol JA. New strategies for triple-negative breast cancer—deciphering the heterogeneity. Clin Cancer Res. 2014; 20:782-90.

29. Oualla K, El-Zawahry HM, Arun B, Reuben JM, Woodward WA, Gamal El-Din H, et al., Novel therapeutic strategies in the treatment of triple-negative breast cancer. Ther Adv Journal Pre-proof Journal Pre-proof 26 Med Oncol. 2017; 9:493-511.

30. Sun T, Zhang G, Guo Z, Chen Q, Zhang Y, Chu Y, et al. Co-delivery of Cu(I) chelator and chemotherapeutics as a new strategy for tumortheranostic. J Control Release. 2020; 321:483-96.

31. Schoumacher M, Burbridge M. Key Roles of AXL and MER receptor tyrosine kinases in resistance to multiple anticancer therapies. Curr Oncol Rep. 2017; 19:19.

32. Lopes CM, Dourado A, Oliveira R. Phytotherapy and nutritional supplements on breast cancer. BioMed Res Int. 2017; 2017:7207983.

33. Collery P. Strategies for the development of selenium-based anticancer drugs. J Trace Elem Med Biol. 2018; 50 : 498-507.

34. Guo CH, Hsia S, Hsiung DY, Chen PC. Supplementation with selenium yeast on the prooxidant-antioxidant activities and anti-tumor effects in breast tumor xenograft-bearing mice. J NutrBiochem. 2015; 26:1568-79.

35. Kao RH, Lai GM, Chow JM, Liao CH, Zheng YM, Tsai WL et al. Opposite regulation of CHOP and GRP78 and synergistic apoptosis induction by selenium yeast and fish oil via AMPK activation in lung adenocarcinoma cells. Nutrients. 2018; 10(10). pii: E1458.

36. Ross JS and Fletcher JA. 1998. The HER-2/neu oncogene in breast cancer: prognostic factor, predictive factor, and target for therapy. Stem Cells 16(6): 413-428.

37. Slamon DJ, Clark GM, Wong SG, Levin WJ, Ullrich A and McGuire WL. 1987. Human breast cancer: correlation of relapse and survival with amplification of the HER-2/neu oncogene. Science 235(4785): 177-182.

38. Junttila TT, Akita RW, Parsons K, Fields C, Lewis Phillips GD, Friedman LS, Sampath D and Sliwkowski MX. 2009. Ligand-independent HER2/ HER3/PI3K complex is disrupted by trastuzumab and is effectively inhibited by the PI3K inhibitor GDC-0941. Cancer Cell 15(5): 429-440.

39. Ghosh R et al. 2011. Trastuzumab has preferential activity against breast cancers driven by HER2 homodimers. Cancer Res 71(5): 1871-1882.

40. Hudis CA. 2007. Trastuzumab—mechanism of action and use in clinical practice. N Engl J Med 357(1): 39-51.

41. Ritter CA, Perez-Torres M, Rinehart C, Guix M, Dugger T, Engelman JA and Arteaga CL. 2007. Human breast cancer cells selected for resistance to trastuzumab in vivo overexpress epidermal growth factor receptor and ErbB ligands and remain dependent on the ErbB receptor network. Clin Cancer Res 13(16): 4909- 4919.

42. Nahta R, Hung MC and Esteva FJ. 2004. The HER-2- targeting antibodies trastuzumab and pertuzumab synergistically inhibit the survival of breast cancer cells. Cancer Res 64(7): 2343-2346.

43. Agus DB et al. 2002. Targeting ligand-activated ErbB2 signaling inhibits breast and prostate tumor growth. Cancer Cell 2(2): 127-137.

44. Metzger-Filho O, Winer EP and Krop I 2013. Pertuzumab: optimizing HER2 blockade. Clin Cancer Res 19(20): 5552-5556.

45. Nahta R, Yuan LX, Zhang B, Kobayashi R and Esteva FJ. 2005. Insulin-like growth factor-I receptor/human epidermal growth factor receptor 2 heterodimerization contributes to trastuzumab resistance of breast cancer cells. Cancer Res 65(23): 11118-11128.

46. Ghosh R et al. 2011. Trastuzumab has preferential activity against breast cancers driven by HER2 homodimers. Cancer Res 71(5): 1871-1882

47. Scheuer W, Friess T, Burtscher H, Bossenmaier B, Endl J and Hasmann M. 2009. Strongly enhanced antitumor activity of trastuzumab and pertuzumab combination treatment on HER2-positive human xenograft tumor models. 69(24) : 9330-9336.

Peer Reviewed and Refereed Journal 2022 **(ISSN : 09726330)**

Rashtrasant Tukadoji Maharaj Nagpur University

SCIENCE JOURNAL 2022

Vol. : XV

Design and Synthesis of Novel Chalcone Derivative from 5-Nitrosalicylaldehyde

Dhabarde Disha[1], Kamble Manish[2], Gupta Nandini[1], Baheti Jagdish[1], Sabale Prafulla[2]*

[1.] Kamla Nehru College of Pharmacy, Butibori, Nagpur. (M.S.) India. 441108.

[2.] Department of Pharmaceutical Sciences, Rashtrasant Tukadoji Maharaj Nagpur University, Nagpur (M.S.) India. 440033.

Corresponding author email : prafullasable@yahoo.com

ABSTRACT

Chalcones also known as benzyl acetophenone or benzylidene acetophenone are promising and privileged structures have been widely used in medicinal interest due to their numerous pharmacological as well as broad spectrum of biological activities. They recognized as antioxidant, antibacterial, anthelmintic, amoebicidal, anti-ulcers, antiviral, anticancer, immunosuppressive etc. Chalcones are precursors for flavonoids and isoflavonoids, are abundant in edible plants. Chemically they are open-chain flavonoids where the two aromatic rings are joined by a three-carbon α, β–unsaturated carbonyl system. Modifications in their structure have offered a high degree of diversity that has proven useful for the development of new medicinal agents. The present study focused on the design and synthesis of novel Chalcone derivatives from 5-Nitro Salicylaldehyde.

Keywords : Chalcone, Benzyl acetophenone, Benzylidene acetophenone, 5-Nitro Salicylaldehyde.

INTRODUCTION

Chalcone is a common simple scaffold found in many naturally occurring compounds. The word “chalcone” is derived from the Greek word “chalcos”, meaning “bronze”, which results from the colors of most natural chalcones.[1] Chalcones have a common chemical scaffold of 1,3- diaryl-2-propen-1-one, also known as chalconoid, that exists as *trans* and *cis* isomers. Chalcones have been designed, synthesized and investigated since long due to versatile usefulness and became an object of continued interest in both academia and industry.[2] Currently, chalcones derivatives have been widely used for the treatment of viral diseases, cardiovascular diseases, stomach cancer, food additives, cosmetics ingredients etc.[3] As chalcones are precursors for flavonoids and isoflavonoids, natural chalcones have been isolated and structurally elucidated. Similarly, Chalcones generally synthesized by condensation reactions via base or acid catalysis. Although chalcones are one type of easily synthesizable α, β–unsaturated ketone, a growing number of new techniques and procedures have recently been reported because of their interesting biological activities and the development of various catalysts or reaction conditions. Claisen[4]–Schmidt[5] Condensation reaction is deemed one of the most classical reactions in organic chemistry.[6] The main drawback of this reaction is the slow reaction rate; the reaction typically needs several days for completion. The reaction could also result in a complex mixture containing the desirable product, byproducts, and sometimes starting materials. The current research

work represents useful method for synthes is of novel Chalcone derivative from 5-Nitrosalicylaldehyde with several advantages such a simple operation, readily available materials and reagents.

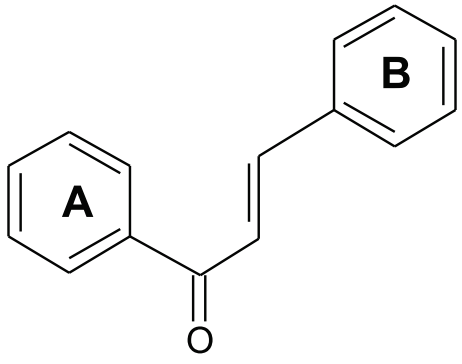

Fig. 1: Basic ring structure of Chalcone

Material and Method:

All the chemicals of analytical grade were purchased from LOBA chemicals. Chemicals and solvents were purified by general laboratory techniques before use. All moisture free operations were performed in oven-dried glassware.

5-Nitrosalicylaldehyde

Salicylic aldehyde (2-Hydroxybenzaldehyde) is the organic compound with the formula $C_6H_4CHO_2OH$. Along with 3-Hydroxybenzaldehyde and 4-Hydroxybenzaldehyde, it is one of the three isomers of hydroxybenzaldehyde. This colorless oily liquid has a bitter almond odor at higher concentration. Salicylaldehyde is a key precursor to a variety chelating agents, some of which are commercially important.

Chloroacetic acid

Chloroacetic acid, industrially known as monochloroacetic acid (MCA), is the organochlorine compound with the formula $ClCH_2CO_2H$. This carboxylic acid is a useful building-block in organic synthesis. It is a colorless solid. Related compounds are dichloroacetic acid and trichloroacetic acid.

2-(2-Formyl - 4 - *Nitrophenoxy*) acetic acid

Acetic acid systematically named ethanoic acid is a colorless liquid organic compound with the chemical formula CH_3COOH (also written as CH_3CO_2H, $C_2H_4O_2$, or $HC_2H_3O_2$). When undiluted, it is sometimes called glacial acetic acid. Vinegar is no less than 4% acetic acid by volume, making acetic acid the main component of vinegar apart from water. Acetic acid has a distinctive sour taste and pungent smell.

4- Amino acetophenone

Acetophenone is the organic compound with the formula $C_6H_5C(O)CH_3$ (also represented by the pseudo element symbols PhAc or BzMe). It is the simplest aromatic ketone. This colorless, viscous liquid is a precursor to useful resins and fragrances

2-(2-(3-Aminophenyl] acryloyl]-4- Nitrophenoxy] acetic acid.

(4-nitrophenyl) acetic acid is a member of the class of phenylacetic acids that is phenylacetic acid in which the phenyl group is substituted at the para-position by a nitro group. It is a C-nitro compound and a member of phenylacetic acids. It derives from a phenylacetic acid. It is a conjugate acid of a (4-nitrophenyl) acetate.

2-(2-(3-(4-Aminophenyl]acroloyl]-4- Nitrophenoxy] acetic acid

4-Aminophenylmercuric acetate ($CH_3CO_2HgC_6H_4NH_2$), also known as 4- (Acetoxymercurio)aniline or APMA), is an organomercurial compound and thiol-blocking reagent used in experimental biology and chemistry to activate matrix metalloproteinases and collagenase proteolyticenzymes.

Experimental and Methods :

Proposed Scheme :

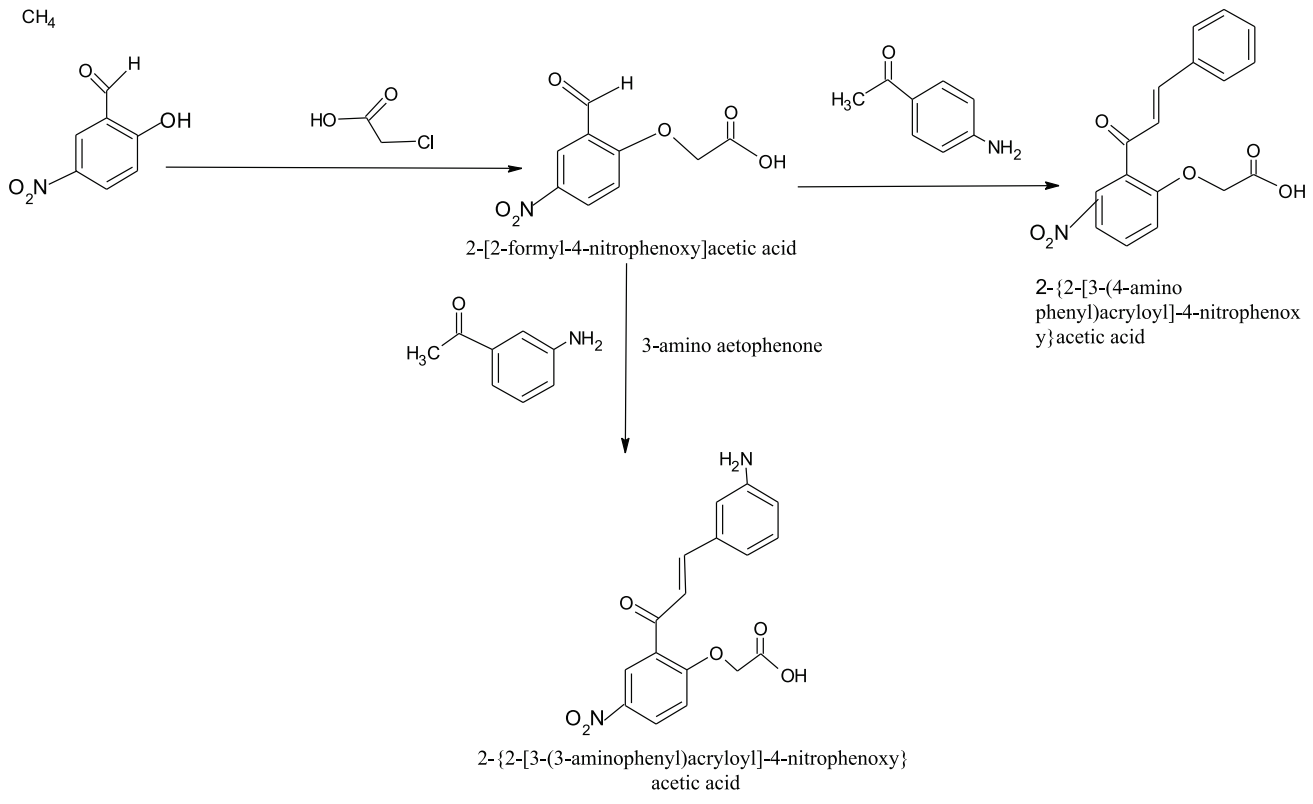

Method 1: Potassium hydroxide 1.5 g was dissolved in 3 ml of water and then mixed with 5-Nitrosalicylaldehyde 0.75 g in round bottom flask in fuming hood. Reaction mixture was stirred until a homogeneous solution was obtained and then refluxed for 30 minutes. In the reaction mixture 2.25 ml of a 50% aqueous solution of Chloroacetic acid was added drop-wise using a separating funnel placed in the side arm of round bottom flask, continued reflux for another 10 minutes. The completion of reaction was monitored by TLC, after completion of reaction, hot solution was transferred to small beaker in water. Cooled it at room temperature and acidified drop wise by adding 12 M HCl. It might be beneficial to ensure that it should not isolate the potassium salt to heat the acidified mixture with the solid until it all dissolved at a higher temperature. Then the mixture was cooled in an ice bath to attain maximum yield of solid product. Be sure the precipitate must be formed completely within 15 minutes before filtration. The precipitate was filtered and collected by using buchner funnel vacuum filtration setup. Re-crystallization can be done by adding the entire crude product to boiling water. More than 50 ml of water should not be used to ensure isolation of crystallized product using vacuum filtration. Re-crystallized [2-(2-Formyl-4-nitro-phenoxy) acetic acid] was collected using a vacuum filtration.

Method 2: The 0.108 ml solution of in 0.288 ml ethanol was stirred in the conical flask. To the reacting mixture, 0.104 g of 2-(2-Formyl-4-nitrophenoxy) acetic acid was added and then drop wise 0.144 ml of NaOH 30% was added into it. The mixture was stirred the in ice cold water bath till it becomes solidified. The mass of [2-(2-(3-(4-Aminophenyl] acryloyl]-4-nitrophenoxy] acetic acid] was solidified by keeping it in cold condition overnight. The final product was collected and dried at room temperature.

Results and Discussion:

The present study reveals a new methodology for synthesis of chalcone. Chalcone was synthesized by the reaction of 5-Nitro salicylaldehyde and chloroacetic acid to give 2-(2-Formyl-4-nitrophenoxy) acetic acid. This product undergoes reaction with 4-Aminoacetophenone and 3-Aminoacetophenone to form 2-(2-(3-(4- Aminophenyl] acryloyl]-4-Nitro phenoxy] acetic acid and 2-(2-(3-(3-Aminophenyl] acryloyl]-4-Nitrophenoxy] acetic acid. The product was purified by

crystallization. The physicochemical characterizations of synthesized compound was carried out by recording melting point and element detection. Final product formed shows significant antibacterial potential.

Table1 : Synthesis of 2-(2-(3-(4-Aminophenyl]acryloyl]-4-Nitrophenoxy] aceticacid (compound 1)

Molecular formula	$C_{17}H_{14}N_2O_6$
State	Solid
Molecular weight	342.11g/mol
TLC	0.42
Yield	89.24%
Melting point	110-120°C
Element	Nitrogen

Table 2: Synthesis of 2-(2-(3-(3-Aminophenyl]acryloyl]-4-Nitrophenoxy] aceticacid (Compound 2)

Molecular formula	$C_{17}H_{14}N_2O_6$
State	Solid
Molecular weight	342.11g/mol
TLC	0.40
Yield	87.53%
Melting point	105-115°C
Element	Nitrogen

Antibacterial activity of Novel Chalcones compound.

Nutrient agar plates using agar well diffusion method[7] with Ciprofloxacin disc (10µg/ml) at the center which served as a positive control. Zones of inhibition was measured for all the contents and activity was compared. Shown in Figure 2 and Table 3.

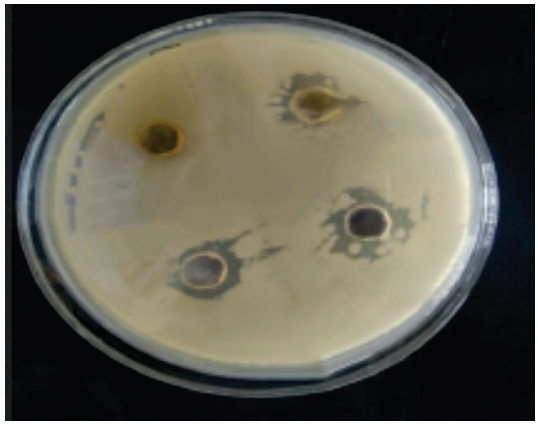

Fig. 2: Zone of Inhibition (antibacterial potential) of synthesized Novel Chalcones.

Table 3: Zone of inhibition of leaf extract, fruit extract, gel and standard drug.

Bacteria	**Diameter of zone of inhibition in mm**		
Escherichia-coli	Compound 1	Compound 2	Standard (Ciprofloxacin)
	17mm	15mm	22mm

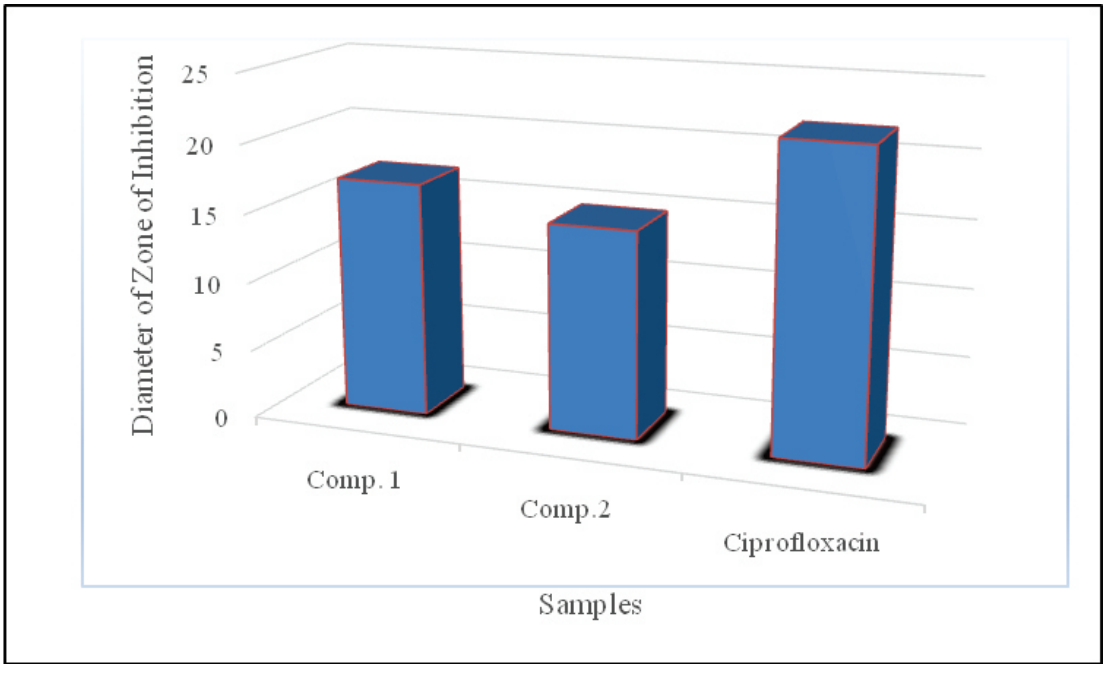

Fig. 3: Graphical representation of Zone of inhibition of Compound 1, Compound 2 and standard Ciprofloxacin

Conclusion : A practical approach was made for synthesis of chalcone. The present method provides a useful method for preparation of synthesis of Novel Chalcone Derivative from 5-Nitrosalicylaldehyde. This method has several advantages such a simple operation, and readily available material and reagents. The synthesized products are characterized by TLC, melting point and element detection. The results obtained from this study confirmed that the product has formed having antimicrobial potential.

Copyright Statement

This work has not been published in any journal, and Author is solely responsible for the plagiarism.

Reference :

1. Sahu NK; Balbhadra SS; Choudhary J; Kohli DV Exploring pharmacological significance of chalcone scaffold: a review. Current Medicinal Chemistry 2012, 19, 209–225. (doi: 10.2174/092986712803414132.)

2. Zhou B; Xing C, Diverse Molecular Targets for Chalcones with Varied Bioactivities. Med. Chem, 2015, 5, 388–404. (doi: 10.4172/2161-0444.1000291.)

3. Singh P; Anand A; Kumar V, Recent developments in biological activities of chalcones: a mini review. European Journal

of Medicinal Chemistry, 2014, 85, 758–777. (doi: 10.1016/j.ejmech.2014.08.033.)

4. Claisen L; Claparede A Condensationen von KetonenmitÌ Aldehyden. Ber. Dtsch. Chem. Ges 1881, 14, 2460–2468. (doi.org/10.1002/cber.188101402192)

5. Schmidt JG Ueber die Einwirkung von Aceton auf Furfurol und auf Bittermandelöl in Gegenwart von Alkalilauge. Ber. Dtsch. Chem. Ges 1881, 14, 1459–1461. (doi.org/10.1002/cber.188101401306)

6. Powers DG; Casebier DS; Fokas D; Ryan WJ; Troth JR; Coffen DL Automated parallel synthesis of chalcone-based screening libraries. Tetrahedron, 1998, 54, 4085–4096. (doi.org/10.1016/S0040-4020(98)00137-9)

7. Valgas C., De Souza S.M., Smania E.F.A. Screening methods to determine antibacterial activity of natural products. *Brazilian Journal of Microbiology,* 2007; 38, 369–380. (doi.org/10.1590/S1517-83822007000200034)

Peer Reviewed and Refereed Journal 2022 **(ISSN : 09726330)**

Rashtrasant Tukadoji Maharaj Nagpur University

SCIENCE JOURNAL 2020

Vol. : XV

Occurrence of Hydrothermal PGM in the Calcareosiliceous dyke of the Chhota Udaipur Carbonatite-Alkaline-Mafic Province, Deccan LIP, India

Tejashree Raut[1], Kirtikumar Randive[1], Sanjeevani Jawadand*[1], M. M. Korakoppa[2], M. L. Dora[3], Tushar Meshram[3], Rajkumar Meshram[3], Manoj Sahu[4] and J. Vijaya Kumar[5]

[1]Department of Geology, RTM Nagpur University, Nagpur-44001 (MH), India

[2]EPMA Lab, National Centre for Excellence in Geoscience Research, Bangalore, India

[3]Petrology Division, Geological Survey of India, Central Region, Nagpur-440006 (MH), India

[4]Lloyds Metals and Energy Ltd., Chandrapur-442405 (MH), India

[5]Ore Dressing Division, Indian Bureau of Mines, Bangalore-56022, India

Corresponding author email : randive101@yahoo.co.in

ABSTRACT

The hydrothermal Platinum Group Metals (PGM) mineralization is known to occur all over the world, and also considered an important source of economically important PGM deposits. We are reporting occurrence of hydrothermal PGM in calcareosiliceous dyke of the Chhota Udaipur Province (CUP). The PGM are hosted by colloform banded calcite-quartz-Fe-oxide matrix. The grains are irregular, often elongated, and less than 5 mm in size.The mineral phases include pure (native) platinum and Pt-Au (±Pt-Au-Cu-Fe) alloys. The chlorite thermometry yielded the formation temperatures of 122 °C to 208 °C. It is likely that the hydrothermal fluids have leached the metals from the preexisting mafic-alkaline igneous rocks belonging to the Deccan Large Igneous Province. Discovery of hydrothermal PGM in the CUP after the discovery of magmatic PGM in the cumulate gabbro at Phenai Mata, provides new window for the exploration of PGE mineralization in the CUP.

Keywords : Carbonatite, Hydrothermal PGM, Chhota Udaipur

INTRODUCTION

The Platinum Group Metals (PGM) are a diverse group of minerals that concentrate the platinum-group elements (PGE; Os, Ir, Ru, Rh, Pt, and Pd) and are formed naturally by three processes, namely, (1) direct crystallization from a sulfide melt in a sulfur saturated magma (e.g., Naldrett and Duke 1980; Mungall 2005), (2) subsolidus exsolution from base metal sulfides (e.g., Makovicky 2002; Peregoedova et al. 2004), and (3) mobilized and precipitated from the hydrothermal solutions. The hydrothermal PGM is obtained from the hydrothermal solutions either derived from magma by exsolution of volatiles or dissolution of PGM from the sulfides hosted in magmatic rocks (Li and Naldrett 1992, 1993; Wood 2002; Hanley 2005; Campos-Alvarez et al., 2021).

The PGM minerals, namely daomanite and michenerite, were recently reported from the Phenai Mata Igneous Complex by Randive et al., (2015) and a detailed study by Vijaya Kumar and Randive (2021) has been recently undertaken. A note on the occurrence of hydrothermal PGE was published by Randive (2017), in which it was postulated that the regional hydrothermal event at the Cretaceous-Paleogene (K-Pg) boundary might have leached and mobilized ("flushed") the sulfides (Co-Ni-Cu-PGE) from the early formed mafic rocks in the Chhota Udaipur Province of the Deccan Large Igneous Province (DLIP). In this paper, we present additional evidences of occurrence of hydrothermal PGE such as Native Platinum

(Pt), Pt-Au alloy and Pt-Au-Cu-Fe alloy in calcareosiliceous dyke of the Chhota Udaipur Province.

2. Geology of the Area

The Chhota Udaipur Province comprises world famous carbonatite ring dyke at Amba Dongar and a number of intrusive rocks forming dykes, sills, plugs and veins of variable sizes intruding the country rocks, which is mainly Upper Cretaceous to Eocene Deccan Trap basaltic lava flows, Cretaceous Bagh sediments and the Archaean – Proterozoic Aravalli granites and metasediments (Sukheswala and Udas, 1963; Sukheswala and Sethna, 1967; Gwalani et al., 1993; Viladkar, 1996; Srivastava, 1997; Hari et al., 2013; Randive, 2015). The intrusive rocks may be grouped into the following categories: (a) carbonatite and carbonatite breccia, (b) alkaline rocks including nephelinite, phonolite, ijolite, tinguiate, pseudoleucite tinguite and camptonite and monchiquite, (c) mafic rocks including gabbro, dolerite, and picrobasalt, (d) layered gabbro-anorthosite-granophyre comprising cumulate gabbro, anorthosite, granophyre with intrusive dolerite and lamprophyre dykes, and trachyte and trachytic rocks, and (e) calcareosiliceous dykes, quartz xenocrysts laden dykes (Randive, 2015; Randive and Hurai, 2015). Among above, the calcareosiliceous, quartz xenocrysts laden dykes and several minor veins and dykes in the area represent precipitated hydrothermal solutions in the area. The present study area where occurrence of hydrothermal PGE is reported in one of the calcareosiliceous dyke is exposed near Dungargam at 22°8 ‘54.20" north latitude and 74°7'53.11" east longitude (Fig.1).

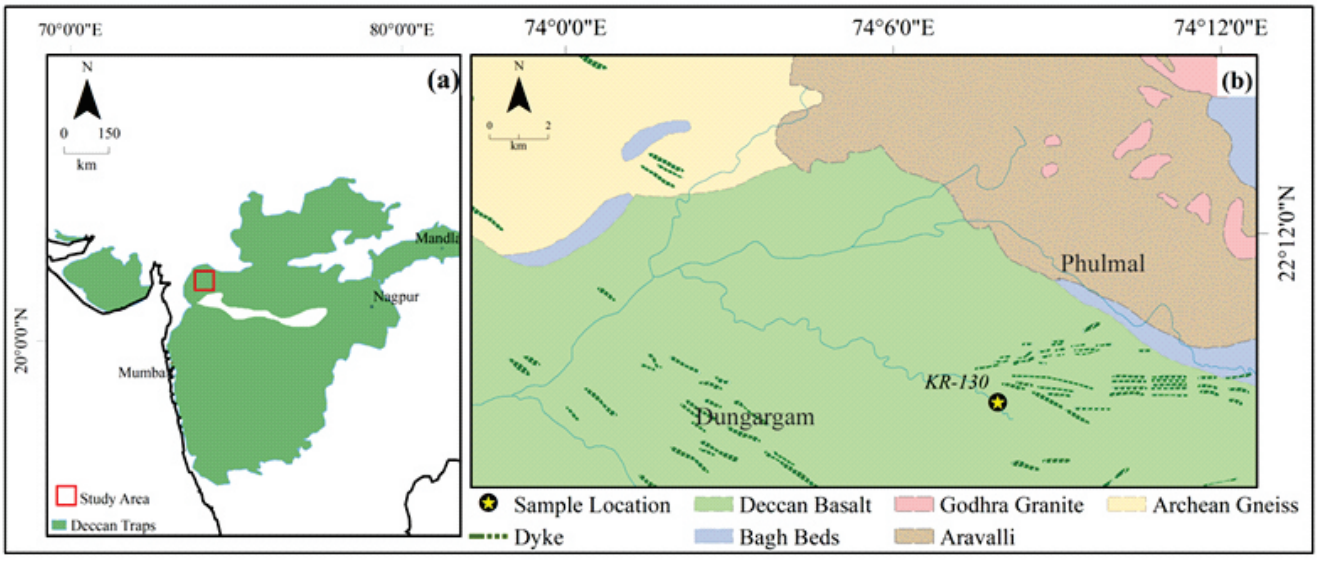

Fig. 1 Map showing location and geological setting of the calcareosiliceous dyke near Dungargam, Chhota Udaipur Province Gujarat (modified after Randive, 2015)

3. Petrography

This rock has dominantly two end-member components, namely, quartz and carbonates, however chlorite and opaque oxides (hematite) also occur. There are several layers of carbonates that surround irregular cavities filled with granular quartz. The grains are anhedral but often rounded. They are roughly coarser at the center of the cavity and finer towards margin. They form colloform banding. The carbonate layers are often brownish. Some of the cavities are filled with chert. Several bands of alternate carbonate and silicate are intricately mixed. They indicate pronounced low-temperature hydrothermal (rock melt – groundwater interaction) in the area.

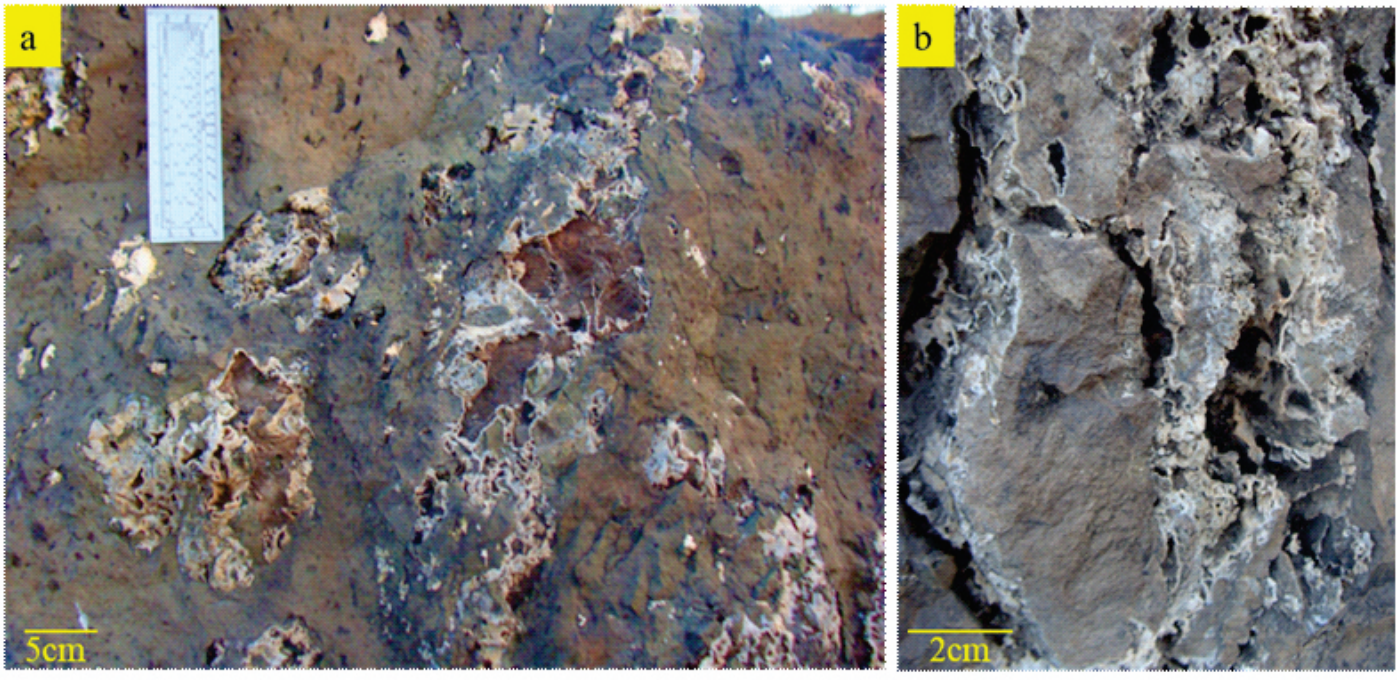

Fig. 2 a) Field Photographs showing cavities lined with silicate and carbonate b) quartz vein showing crustiform banding

4. Analytical Techniques

Sampling was carried out during several field seasons. One of the calcareosiliceous dykes near Dungargaum in the Kawant Tehsil of Chota Udaipur district (Fig. 2) was selected for study. A thin polished section of the rock slab was made and mineral investigation was carried out using electron probe micro analyzer (EPMA). The quantitative analysis of the major mineral phases was carried out using wavelength dispersive spectrometer (WDS), whereas, the small (typically < 5 micron) grains were detected by qualitative measurements using energy dispersive spectrometer (EDS). The EPMA analyses were conducted at the NCEGR Laboratory, Geological Survey of India, Bangalore, using CAMECA SX-100 instrument.For the identification of silicate and oxide mineral phases, accelerating current of 15 keV & 15nA with a beam size 1µm was used. The raw electron microprobe data were processed using peak sight GEOQUANTA software, which uses standard ZAF correction algorithms. Standards used for calibration were: Na on Jadeite, Si and Ca on Wollastonite, Mg on Diopside, Al on Corundum, K on Orthoclase, Ti on Rutile, Fe on Fe_2O_3, and Cr on Cr_2O_3. The PGM grains are less than 3 micron in size, therefore X-ray mapping was done with 20keV and 20 nA current with beam mode to quantify the PGM grains mineral chemistry. The signals used were Ru: La, Rh: La, Os: Lb, Pt: La, Pd: La, Ag: Lb, Ir: La, Au: La, Cu: Ka, Fe: Ka. Calibration was done with 100% metal standards for PGE, Au, Ag, Cu and Fe on Fe_2O_3. X-ray maps with quantification are presented in the fig 6 to 8. The EPMA data of the oxide and sulfide mineral phases are presented in tables 1 to 4, their mineral chemistry is discussed below.

Table 1 : EPMA point analyses of chert, quartz and hematite

Mineral	Chert				Quartz		Hematite
Point	5 / 1 .	6 / 1 .	8 / 1 .	10 / 1 .	15 / 1 .	18 / 1 .	26 / 1 .
Analyte				Weight %			
SiO_2	73.21	78.29	84.83	81.78	98.68	96.26	0.15
TiO_2	0.05	0.03	0	0.15	0	0.02	7.9
Al_2O_3	0.08	0.1	0.07	0.14	0.03	0	0.09
FeO Total	0.14	0.08	0	0.01	0.09	0	79.32
MnO	0.08	0.09	0.03	0.04	0.01	0.02	0.73
MgO	0.03	0.04	0	0	0	0.1	0.75
CaO	0.32	0.17	0.11	0.14	0.03	0.05	0.15
Na_2O	0.1	0.1	0.09	0.13	0	0.03	0
K_2O	0.02	0.02	0.02	0.04	0.01	0.02	0.02
P_20_5	0	0	0	0	0	0	0
Cl	0.1	0.08	0.08	0.05	0.01	0	0.01
Total	74.18	78.99	85.26	82.52	98.89	96.49	89.12
				Recalculated on the basis of 5 oxygens			
Coef.	2.039	1.91	1.767	1.828	1.521	1.558	3.728
Si	2.485	2.489	2.495	2.488	2.498	2.496	0.009
Ti	0.001	0.001	0	0.003	0	0	0.369
Al	0.003	0.004	0.002	0.005	0.001	0	0.007
Fe^{2+} all ferrous	0.004	0.002	0	0	0.002	0	4.116
Mn	0.002	0.002	0.001	0.001	0	0	0.038
Mg	0.002	0.002	0	0	0	0.004	0.069
Ca	0.012	0.006	0.003	0.005	0.001	0.001	0.01
Na	0.007	0.006	0.005	0.008	0	0.002	0
K	0.001	0.001	0.001	0.002	0	0.001	0.002
P	0	0	0	0	0	0	0
Cl	0.006	0.004	0.004	0.003	0	0	0.001
Total	2.522	2.517	2.511	2.514	2.502	2.504	4.621

Table 2: EPMA point analyses of calcite

Mineral	Calcite									
Point	1 / 1 .	2 / 1 .	3 / 1 .	7 / 1 .	9 / 1 .	12 / 1 .	13 / 1 .	14 / 1 .	16 / 1 .	25 / 1 .
Analyte						Weight %				
SiO_2	0.07	0	0.82	0.25	1.35	6.2	0	0.04	0	1.3
TiO_2	0	0	0	0	0.01	0.01	0	0	0.01	2.94
Al_2O_3	0	0	0	0	0	0	0.02	0	0	0.16
FeO Total	0.48	0.98	0.23	0.09	0.01	0.29	0.61	0.06	0.92	1.1
MnO	2.74	2.43	1.16	0	0.14	0.92	2.95	1.25	2.91	0.89
MgO	0.53	0.55	0.27	0.27	0.92	0.19	0.53	0.23	0.53	0.55
CaO	58.97	58.46	58.63	59.77	58.23	54.23	59.14	60.39	58.91	51.62
Na_2O	0.04	0.02	0	0.01	0	0.01	0	0	0	0.09
K_2O	0	0	0	0	0	0	0	0	0.01	0.01
P_20_5	0.12	0.03	0.01	0.05	0.05	-0.01	0.03	0.05	0.06	0.2
Cl	0	0	0.01	0	0	0.01	0.01	0.01	0	0.02
Total	62.95	62.47	61.13	60.44	60.71	61.85	63.29	62.03	63.35	58.88

					Recalculated on the basis of 5 oxygens					
Coef.	4.476	4.523	4.548	4.613	4.504	4.183	4.467	4.529	4.465	4.578
Si	0.005	0	0.062	0.019	0.101	0.432	0	0.003	0	0.099
Ti	0	0	0	0	0.001	0.001	0	0	0.001	0.168
Al	0	0	0	0	0	0	0.002	0	0	0.014
Fe2+ all ferrous	0.03	0.062	0.015	0.006	0.001	0.017	0.038	0.004	0.057	0.07
Mn	0.173	0.155	0.074	0	0.009	0.054	0.186	0.08	0.183	0.057
Mg	0.059	0.062	0.03	0.031	0.103	0.02	0.059	0.026	0.059	0.062
Ca	4.706	4.715	4.755	4.916	4.676	4.045	4.71	4.877	4.69	4.214
Na	0.006	0.003	0	0.001	0	0.001	0	0	0	0.013
K	0	0	0	0	0	0	0	0	0.001	0.001
P	0.008	0.002	0.001	0.003	0.003	-0.001	0.002	0.003	0.004	0.013
Cl	0	0	0.001	0	0	0.001	0.001	0.001	0	0.003
Total	4.986	4.999	4.938	4.977	4.893	4.57	4.998	4.993	4.994	4.716

Table 3 : EPMA point analyses of carbonated chert

Mineral	Carbonated Chert				
Point	4 / 1 .	11 / 1 .	17 / 1 .	19 / 1 .	20 / 1 .
Analyte			Weight %		
SiO_2	42.25	27.63	28.55	15.41	33.25
Al_2O_3	0.03	0	0	0	0
FeO Total	0	0.07	0.04	0	0.04
MnO	0.06	0.01	0.14	0.25	0.04
MgO	0.04	0.01	0	0.05	0
CaO	31.93	39.8	39.88	46.98	37.09
Na_2O	0.05	0.01	0.04	0.03	0.01
K_2O	0.01	0	0.03	0	0
P_20_5	0	0	0.06	0.03	0.03
Cl	0.02	0.01	0	0.02	0.01
Total	74.39	67.54	68.74	62.77	70.47
			Formulae on the basis of 5 oxygens		
Coef.	2.526	3.066	2.999	3.685	2.824
Si	1.776	1.41	1.425	0.945	1.563
Al	0.001	0	0	0	0
Fe2+ all ferrous	0	0.003	0.002	0	0.002
Mn	0.002	0	0.006	0.013	0.002
Mg	0.003	0.001	0	0.005	0
Ca	1.438	2.176	2.133	3.087	1.868
Na	0.004	0.001	0.004	0.004	0.001
K	0.001	0	0.002	0	0
P	0	0	0.003	0.002	0.001
Cl	0.001	0.001	0	0.002	0.001
Total	3.227	3.592	3.574	4.056	3.437

Table 4 : EPMA point analyses of chlorite (recalculated on the basis on 28 oxygens)

Mineral	Chlorite		
Point	21 / 1	22 / 1	23 / 1
Analyte		Weight %	
SiO_2	34	35.12	33.48
TiO_2	0.01	0	0.03
Al_2O_3	16.02	15.71	15.93
Fe_2O_3	4.108	4.629	3.779
FeO	13.624	12.785	12.979
MnO	0.36	0.33	0.37
MgO	19.17	19.7	19.64
CaO	0.31	0.4	0.32
BaO	0.05	0.01	0
Na_2O	0.15	0.12	0.18
K_2O	0.21	0.17	0.23
Cl	0.03	0.07	0.04
O=Cl	0.0068	0.0158	0.009
Total](%)	88.0352	89.0282	86.969
[H_2O(c)	12.1465	12.3375	12.0293
(apfu)[Si	3.3549	3.4089	3.3351
Ti	0.0007	0	0.0022
Al	1.863	1.7972	1.8702
Fe(3+)	0.305	0.3381	0.2833
Fe(2+)	1.1243	1.0378	1.0812
Mn	0.0301	0.0271	0.0312
Mg	2.8199	2.8506	2.9165
Ca	0.0328	0.0416	0.0342
Ba	0.0019	0.0004	0
Na	0.0287	0.0226	0.0348
K	0.0264	0.0211	0.0292
Cl	0.0052	0.0121	0.007
OH](apfu)	7.9948	7.9879	7.993
[Si	3.3549	3.4089	3.3351
Al(IV)	0.6451	0.5911	0.6649
Total]Tetrahedral	4	4	4
[Al(VI)	1.218	1.2061	1.2053
Ti	0.0007	0	0.0022
Fe3+	0.305	0.3381	0.2833
Fe2+	1.1243	1.0378	1.0812
Mn	0.0301	0.0271	0.0312
Mg	2.8199	2.8506	2.9165
Total]Octahedral	5.498	5.4597	5.5198
[Octahedral vacant]	0.502	0.5403	0.4802
[Ca	0.0328	0.0416	0.0342
Ba	0.0019	0.0004	0
Na	0.0287	0.0226	0.0348
K	0.0264	0.0211	0.0292
Total]	0.0898	0.0856	0.0981
[OH	7.9948	7.9879	7.993
Cl	0.0052	0.0121	0.007
Total	8	8	8

5. Results and Discussion

The EPMA data indicates presence of calcite as the major carbonate phase present, which forms an intricate immiscibility with the silicate fractions represented by quartz and chert (Fig. 3). The ferric phase is represented by hematite. Table 1-3 give representative analyses of each of these minerals. Another mineral that occurs in this rock is chlorite. The chlorite analyses (Table 4) were recalculated on the basis of 28 oxygen assuming ideal site occupancy. The empirical calculations indicate that chlorite variety is diabantite (Fig. 4a). The temperature estimations of the chlorite using various thermometers are given in Table 5; the overall temperature range for formation of chlorites is represented using isotherms in an R^{2+}–Si diagram (Fig. 4b).

Table 5 : Various empirical geothermometers used and the estimated temperatures of formation of chlorites (Yavuz et al., 2015 and references therein)

Geothermometerter	Equations	21 / 1	22 / 1	23 / 1	Average
Cathelineau and Nieva (1985) Equation 1	T = (0.0826+ Al^{IV}) / 0.00471	150	139	154	148
Cathelineau and Nieva (1985) Equation 2	T = – (VAC? – 2.41) / 0.00857	164	155	169	163
Kranidiotis and MacLean (1987)	T (°C) = 106Al^{IV}_C + 18 where, Al_C^{IV} = Al^{IV} + 0. 7 x [Fe/(Fe+Mg)]	180	167	183	177
Cathelineau (1988)	T (°C) = -61.92 + 321.98 x (Al^{IV})	146	128	152	142
Jowett (1991)	T (°C) = 319Al_C^{IV} – 69 where, Al_C^{IV} = $A1^{IV}$ + 0.1(Fe / [Fe+ Mg])	148	130	153	144
De Caritat et al. (1993) [Tetrahedral Occupancy]	T (°C) = (Si^{IV} – 3.610) / -0.001327 if *Al-chlorite* < 0.20 T (°C) = (Si^{IV} – 3.233) / -0.001327 if *Al-chlorite* between 0.20 & 0.24 T (°C) = (Si^{IV} – 2.792) / -0.000486 if *Al-chlorite* > 0.24	193	152	208	184
Zang and Fyfe (1995)	T (°C) = 106.2 Al_C^{IV} + 17.5 where, Al_C^{IV} = $A1^{IV}$ – 0.88 x [(Fe / (Fe+ Mg) – 34]	155	144	161	153
Xie et al. (1997)	T (°C) = 160.99 x [(Al^{IV}) + 1.33 x (0.31 - (Fe/(Fe+ Mg)] – 61.92, if (Fe/(Fe+ Mg)<0.31 T (°C) = 160.99 x [(Al^{IV}) + 1.33 x ((Fe/(Fe+ Mg) - 0.31] – 61.92, if (Fe/(Fe+ Mg)>0.31	134	122	148	135
El-Sharkawy (2000)	T (°C) = 106.2 x [(Al^{IV}) – 0.48 x ((Fe / (Fe+ Mg) – 0.163] + 17.5	137	126	143	135
		Average			159

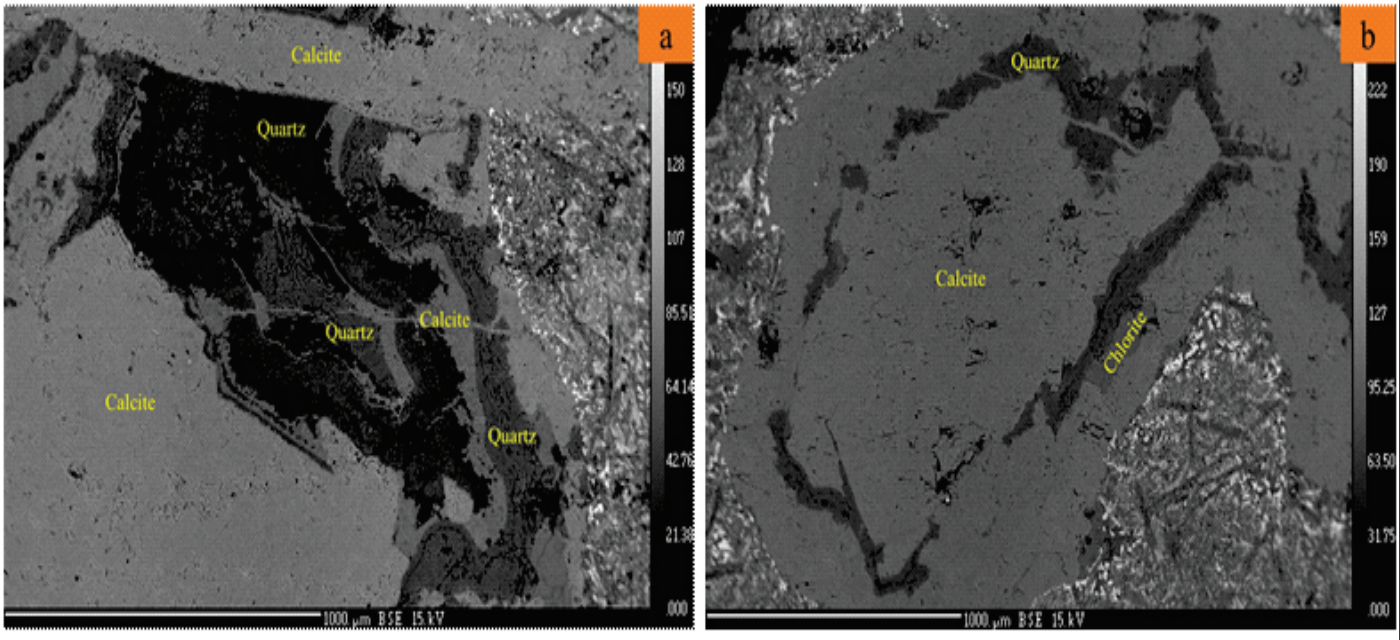

Fig. 3 The back scattered electron images showing various mineral phases present in the rock. (a) quartz and carbonate in intricate association forming colloform banding and (b) presence of chlorite along with calcite and quartz.

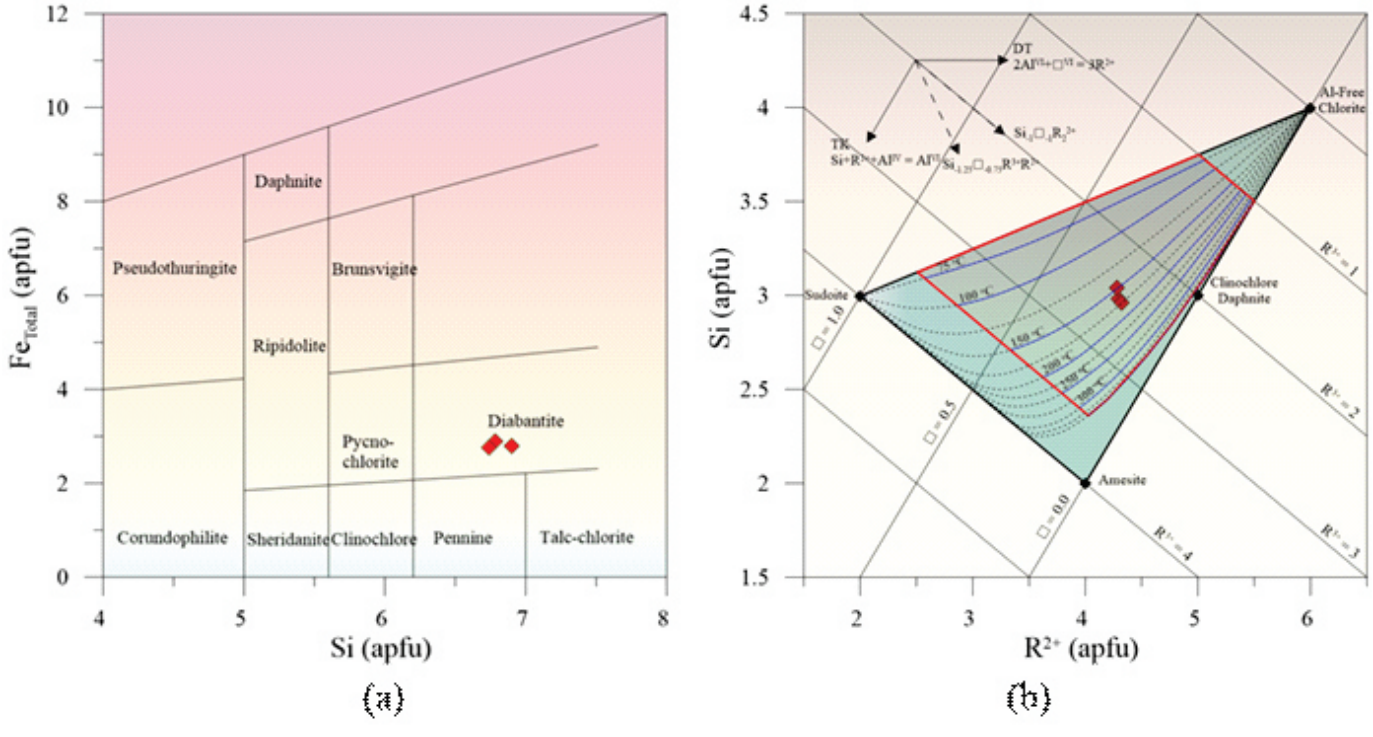

Fig. 4 a) Fe_{total} versus Si (after Deer et al., 1962) shows study area chlorites plot in diabantite field b) Plot of R^{2+} versus Si (after Bourdelle and Cathelineau, 2015) showing chlorite formation range between 130°C and 200°C.

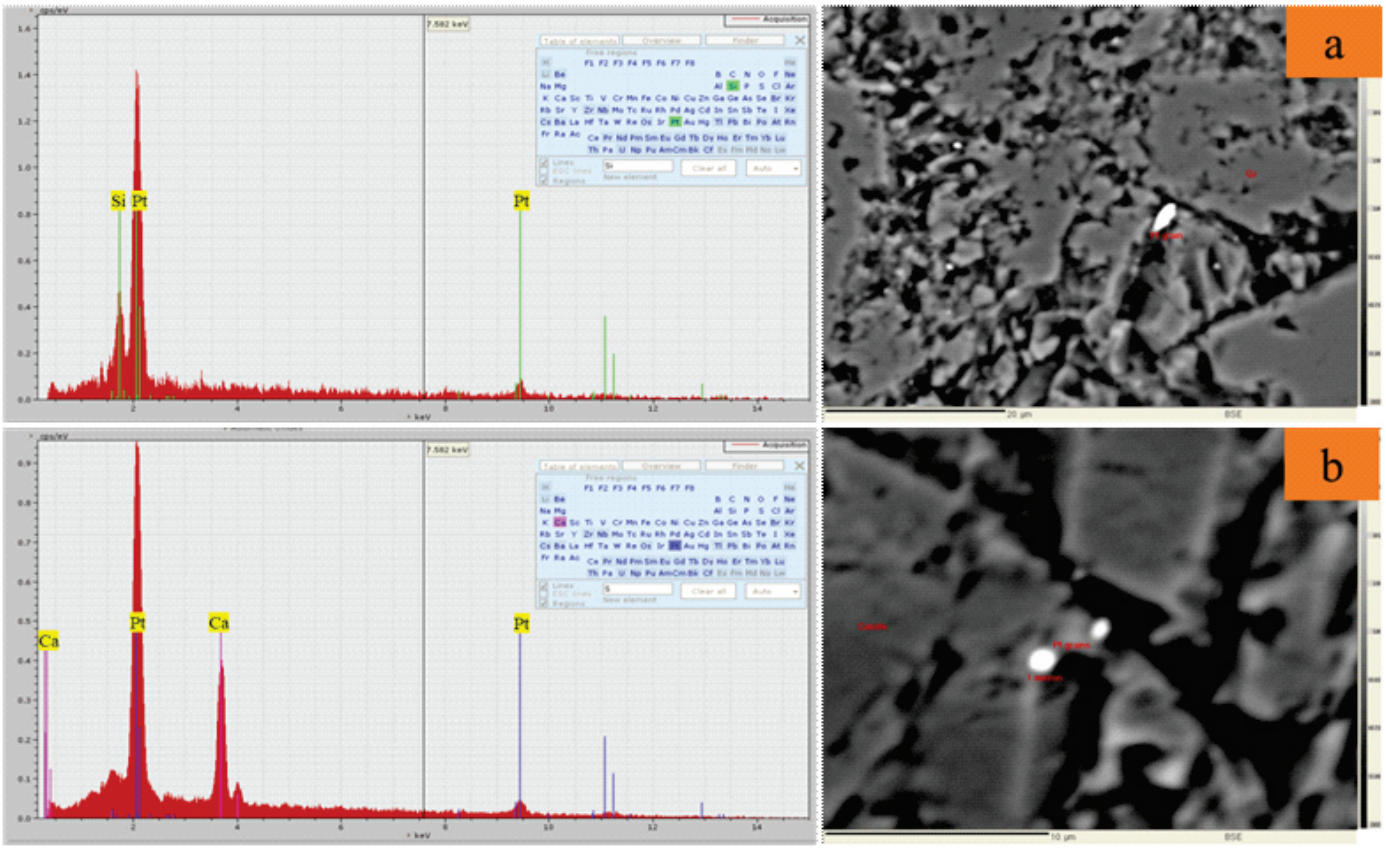

Fig. 5 The EDS Spectra and SE image indicating presence of platinum grains in (a) and (b). Both grains are less than 2 mm and represents pure platinum metal. The peaks for Si and Ca are due to matrix effect of host mineral.

The PGM grains were detected in the EDS spectra as well Secondary Electron images (Fig. 5). These grains are typically less than 2 mm, and elongated or bulb-shaped. Such shapes are typical of hydrothermal PGM (Oberthur et al., 2018). The X-ray mapping of the PGM grains was carried out on three grains. Grain one (Pt-1; Fig. 6) is prismatic shaped and measures ~2.5 mm along the longer axis. The X-ray mapping shows about 90% Pt and 7% Au, indicating that it could be an alloy of Pt-Au. The second grain (Pt-2; Fig. 7) is elliptical, measuring ~2.0 mm along the longer axis. It is composed of about 85% Pt, 7% Au, 4% Cu, and ~2% Fe; indicating a complex alloy of these metals. The third grain (Pt-3; Fig. 8) is a small bulbous grain of about 1 mm size. It is entirely composed of native platinum.

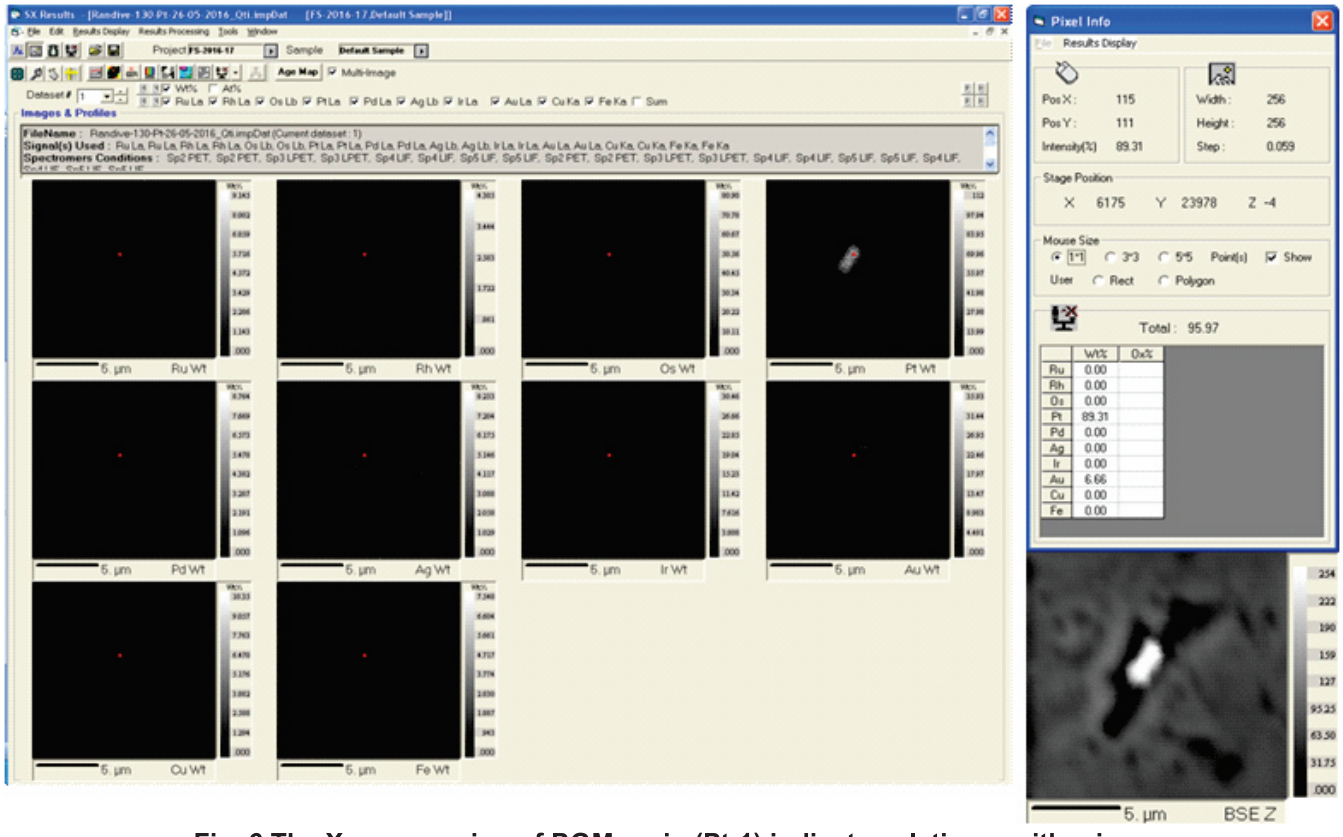

Fig. 6 The X-ray mapping of PGM grain (Pt-1) indicates platinum with minor concentration of gold, indicating possible Pt-Au alloy.

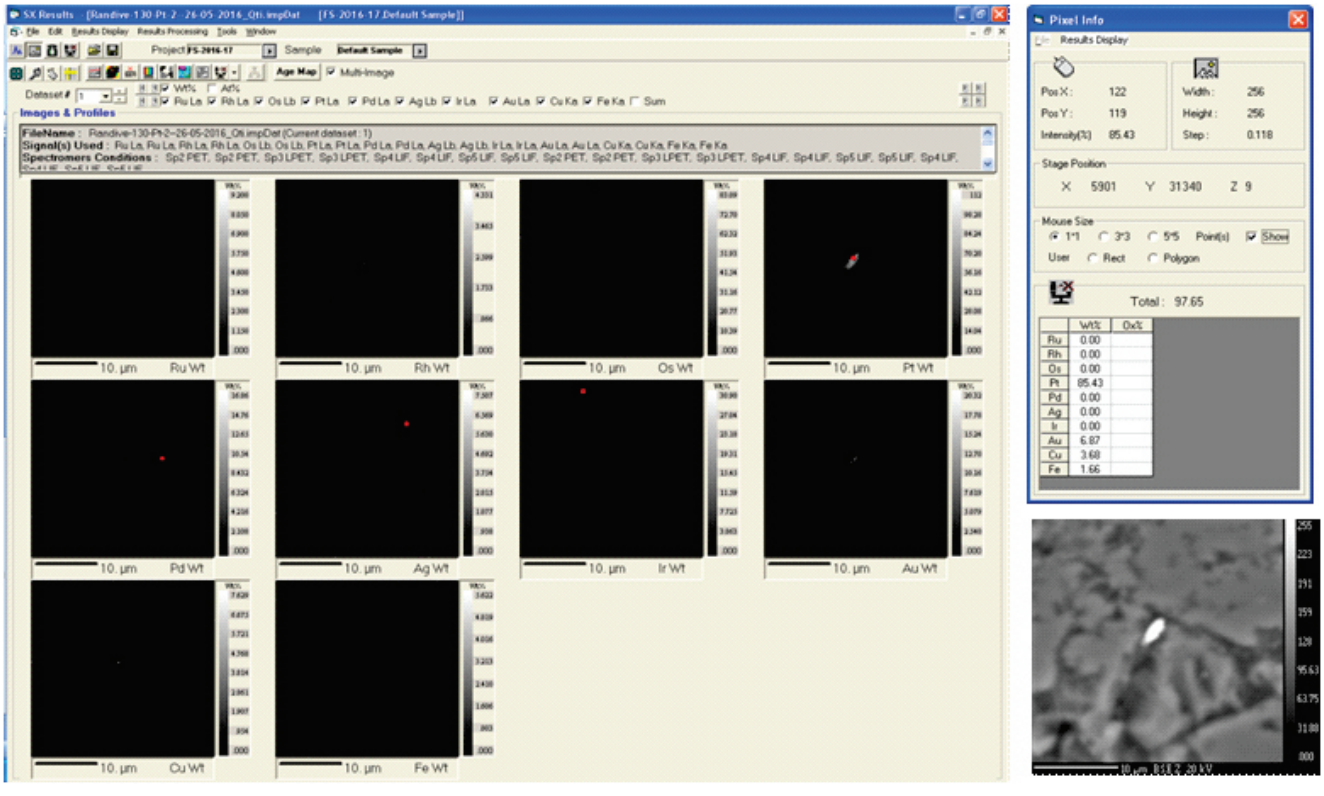

Fig. 7The X-ray mapping of PGM grain (Pt-2) indicates platinum with minor concentration of gold, copper, and iron indicating possible Pt-Au-Cu-Fe alloy.

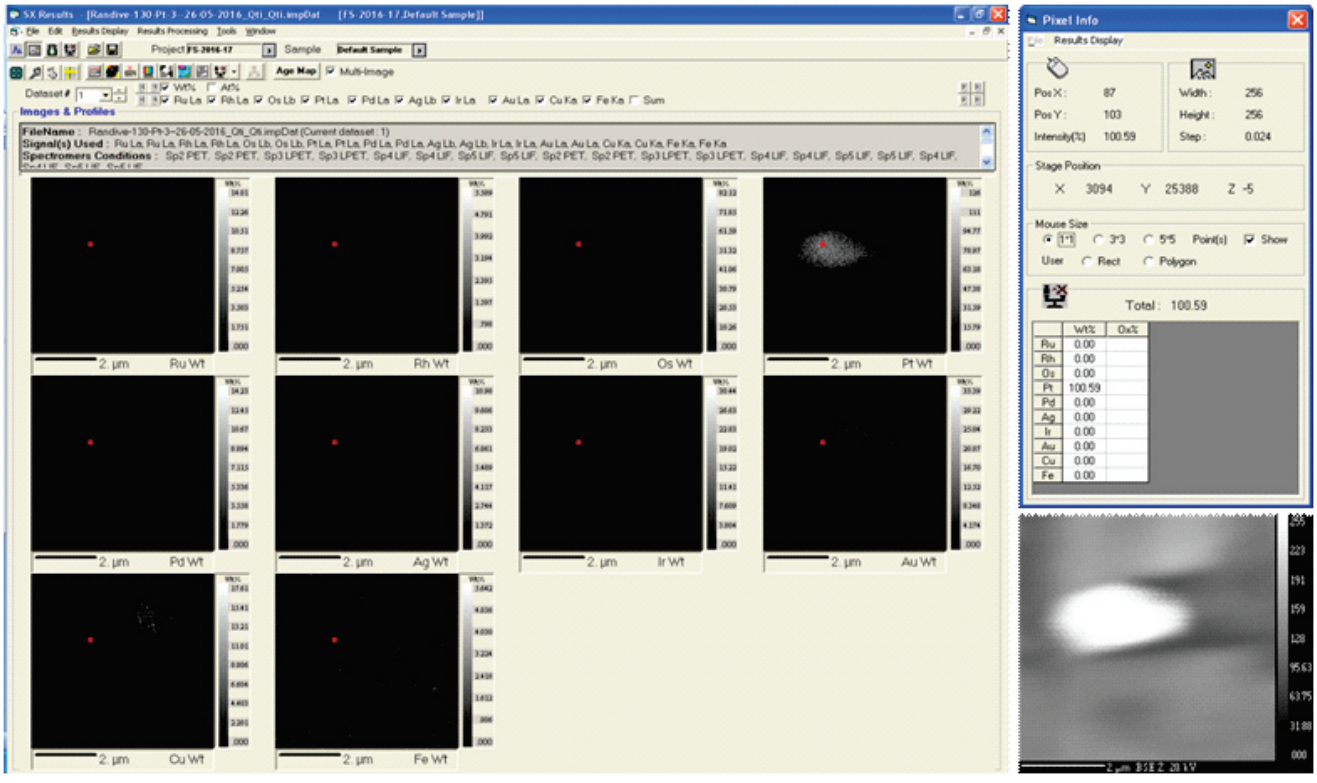

Fig. 8 The X-ray mapping of PGM grain (Pt-3) indicates pure platinum grain. The elongates bulb like shape of grain, which is approximately ~1 mm, is commonly seen in hydrothermally mobilized PGM.

6. Discussion and Conclusion

The occurrence of hydrothermal PGM is known worldwide, and being increasingly considered as an important source of PGM mineralization. Some of the world class hydrothermal PGM deposits include Serra Pelada in Brazil (e.g., Cabral, 2006), Jabiluka, Coronation Hill, Gold Ridge; Australia (e.g., Wilde, 2005), the Bled'da Far West deposit in Morocco (Barakat et al., 2002; El Ghorfi et al., 2006), South Devon, UK (e.g., Shepherd et al., 2005). New Rambler mine, Wyoming (McCallum et al., 1976); the Bucko Lake intrusion, Thompson Belt, Manitoba (Good et al., 1993); the Sudbury area (Farrow et al., 1992), and Eastern Desert, Egypt (Helmy, 2005). The common factors involved in precipitation of hydrothermal PGM are: (1) accumulation of PGE-enriched fluids, (2) regional scale fractures that may act as the conduits for fluid flow, and (3) host rock composition having suitable Eh-pH conditions (chemical traps) to facilitate the precipitation of metals. The environments having above characteristics are known to occur in the Sudbury footwall as well as mafic–ultramafic intrusions associated with primary magmatic PGE from several locations around the world (Compos-Alvarez et al., 2012).

It is commonly noticed that the sulfides are lacking in the hydrothermal PGM deposits. The reason being that the sulfides are readily dissolved (leached out) by the hydrothermal solutions and the hydrothermal solutions have high oxygen fugacity and low sulfur fugacity. In this case presence of mineral hematite is of particular importance (Oberthur et al., 2018). The textures of hydrothermal PGM are well constrained. The grains never show idiomorphic crystal shapes; instead, they occur as warts or bulges (verruciform), irregular shaped veins, as garlands, ribbons, cockades, sometimes showing internal growth zoning. Smaller grains sometimes form immiscible emulsion-like textures. These ore textures indicate that the 'platinum' was deposited as a gel, corroborating the early suggestion of Wagner (1929). Similar textures were observed in the hydrothermal PGM of the CUP, in which PGM are hosted by colloform banded calcite-quartz-Fe-oxide matrix. Presence of chert also indicate significant water activity. The chlorite thermometry has indicated a temperature range of 122 °C to 208 °C.

The hydrothermal PGM are usually associated with gold, so much so, in the order Au>Pd>Pt (Kucha, 1982; Oszczepalski et al.,1999). Although, the genesis of hydrothermal PGM is not fully understood, the Cl-rich aqueous fluids or even the higher salinity brines seem to have involved in segregating PGM (Wilde, 2005). Shepherd et al., (2005) also suggested that the precious metals could be transported in oxidizing, slightly acidic, chloride brines in the Lubin district of Poland. However, there are exceptions such as Waterberg platinum mineralization in Mookgophong area in the Waterberg District, Limpopo Province, South Africa (Oberthur et al., 2018). In this deposit, the metal proportion is in the order Pt>Pd>Au. So far, Pd grains were not recorded during the present study, however, presence of Au and Cu is noticed. Therefore, the style of PGM mineralization in CUP looks similar to Waterberg mineralization. Presence of tiny grains of platinum in the hydrothermally precipitated rocks, opens up new exploration targets for the searching PGM in the Deccan large igneous province.

References :

Barakat, A., Marignac, C., Boiron, M-C, Bouabdelli, M., 2002. Caractérisation des paragenèses et des paléocirculations fluids dans l'indice d'or de Bleïda (Anti-Atlas, Maroc). ComptesRendu Geosciences 334, 35–41.

Bourdelle, F., Cathelineau, M., 2015. Low-temperature chlorite geothermometry: a graphical representation based on a T–R2+ –Si diagram. European Journal of Mineralogy, 27(5), 617–626. doi:10.1127/ejm/2015/0027-2467723–735.

Cabral, A.R., 2006. Palladian gold mineralization (OuroPreto) in Brazil: Gongo Soco, Itabira and Serra Pelada.Geologisches Jahrbuch, Reihe D, Sonderheft, SD 8,115.

Campos-Alvarez Nelson O., Samson, Iain M., Fryer, Brian J., 2012. The roles of magmatic and hydrothermal processes in PGE mineralization,Ferguson Lake deposit, Nunavut, Canada, Miner Deposita 47, 441–465. doi: 10.1007/s00126-011-0385-0

Cathelineau, M., 1988. Cation Site Occupancy in Chlorites and Illites as a Function of Temperature. Clay Minerals - CLAY MINER. 23, 471-485. 10.1180/claymin.1988.023.4.13.

Cathelineau, M., Nieva, D., 1985. A chlorite solid solution geothermometer. The Los Azufres (Mexico) geothermal system. Contrib. Mineral. Petrol. 91, 235–244.

De Caritat, P.D., Hutcheon, I. and Walshe, J.L., 1993. Chlorite geothermometry: a review. Clay, Miner. 412, 219–239.

Deer, W.A., Howie, R.A., and Zussman, J., 1962. Rock-forming minerals, 3. Longmans, London, 270.

El-Sharkawy M.F., 2000. Talc mineralization of ultramafic affinity in the Eastern Desert of Egypt. Mineralium Deposita, 35(4), 346-363.

Farrow C.F.G., Watkinson D.H., 1992. Alteration and the roleoffluids in Ni, Cu, and platinum-group element deposition,Sudbury Igneous Complex Contact, Onaping-Levack area, Ontario, Mineralogy and Petrology,46, 67–83.

Ghorfi, M. El, Oberthür, T., Melcher, F., Lüders, V., Boukhari, A. El, Maacha, L., Ziadi, R., Baoutoul, H., 2006.Gold–palladium mineralization at Bleïda Far West,Bou Azzer–El Graara Inlier, Anti-Atlas, MoroccoMiner Deposita, 41, 549–564. doi: 10.1007/s00126-006-0077-3

Good D.J., Naldrett A.J., 1993. Geology and distribution ofPGE, Bucko Lake Intrusion, Thomsen belt, Manitoba,Canadian Mineralogist, 31, 45–60.

Gwalani, L.G., Rock, N.M.S., Chang, W.J., Fernandez, S., Allegre, C.J., Prinzhofer, A., 1993. Alkaline rocks and carbonatites of Amba Dongar and adjacent areas, Deccan igneous province, Gujarat, India. 1. Geology,

petrography and petrochemistry. Mineral. Petrol., 47, 219–253.

Hanley, J.J., 2005.The aqueous geochemistry of the platinum-groupelements (PGE) in surficial, low T hydrothermal and high-Tmagmatic hydrothermal environments. In: Mungall JE (ed)Exploration for platinum-group element deposits. MineralogicalAssociation of Canada short course 35. Mineralogical Associationof Canada, Québec, 35–56.

Hari, K.R., Chalapathy Rao, N.V.C., Swarnakar, V., Hou, G., 2013. Alkali feldspar syenites with shoshonitic affinities from Chhotaudepur area: implication for mantle metasomatism in the Deccan large igneous province. GeoSci. Front. doi:org/10.1016/ j.gsf.2013.06.007.

Helmy H.M., 2005. Melonite group minerals and othertelluride from three Cu-Ni-PGE prospect, EasternDesert, Egypt, Ore Geology Review. 26, 305–324.

Jowett, E.C., 1991. Fitting iron and magnesium into the hydrothermal chlorite geothermometer. GAC/MAC/SEG Joint Annual Meeting (Toronto, May 27.29, 1991).

Kranidiotis, P., Maclean,W.H., 1987. Systematic of chlorite alteration at the Phelps Dodge massive sulfide deposit, Matagami, Quebec. Econ. Geol. 82, 1898–1911.

Kucha, H., 1982. Platinum-group metals in the Zechsteincopper deposits, Poland. Economic Geology, 77,1578–1591.

Li, C., Naldrett, A.J., 1992. PGE studies in the footwall at Sudbury,Ontario. Geoscience research grant program, grant no. 326;Ontario Geological Survey, Open-File Report 5830, 118 p

Li, C., Naldrett, A.J., 1993. Platinum-group minerals from the deepcopper zone of the Strathcona deposit, Sudbury. Ontario Can Min31, 31–44.

Makovicky, E., 2002. Ternary and quaternary phase systems with PGE.In: Cabri LJ (ed) The geology, geochemistry, mineralogy andmineral beneficiation of platinum-group elements. CanadianInstitute of Mining, Metallurgy and Petroleum, special volume54. Canadian Institute of Mining, Metallurgy and Petroleum,Westmount, 131–175.

McCallum M.E., Loucks R.R., Carson R.R., 1976. Platinumore associated with hydrothermal copper ore Newrambler mines, Wyming, Economic Geology, 71,1429–1450.

Mungall, J.E., 2005. Magmatic geochemistry of the platinum-group elements. In: Mungall JE (ed) Exploration for platinum-group element deposits. Mineralogical Association of Canada, short course 35. Mineralogical Association of Canada, Québec, 1–34.

Naldrett, J.A., Duke, J.M., 1980. Platinum metals in magmatic sulfideores. Science, New Series 208(4451), 1417–1424.

Oberthür, Thomas, Melcher, Frank, Fusswinkel, Tobias, Van den Kerkhof, Alfons M., Sosa Graciela M., 2018. The hydrothermal Waterberg platinum deposit, Mookgophong (Naboomspruit), South Africa. Part 1: Geochemistry and ore Mineralogy. Mineralogical Magazine, Vol. 82(3), 725–749.

Oszczepalski, S., Rydzewski, A. and Speczik, S., 1999. Rote Fäule-related Au-Pt-Pdmineralization in SWPoland: new data. In: MineralDeposits: Processes to Processing (Stanley, editors).Balkema, Rotterdam, 1423–1425

Peregoedova A, Barnes SJ, Baker DR (2004) The formation of Pt–Iralloys and Cu–Pd-rich sulfide melts by partial desulfurization ofFe–Ni–Cu sulfides: results of experiments and implications fornatural systems. Chem Geol 208, 247–264.

Randive, K.R., 2015. Occurrence of unusual quartz xenocryst-laden dykes in the Chhota Udaipur

alkaline–carbonatite sub-province, Deccan Igneous Province, India. Current Science, Vol. 108, No. 12, 25, 2261-2266.

Randive, K.R., 2017. Is? And Why is? Deccan LIP Barren with Respect to Ni-Cu-PGE Mineralization? DOI: 10.13140/RG.2.2.16514.07363

Randive, K.R., Hurai V., 2015. Fluid Inclusion Study of Quartz Xenocrysts in Mafic Dykes from Kawant Area, Chhota Udaipur District, Gujarat, India. Open Geosci.; 7, 244–251.

Randive, K.R., Vijaya Kumar, J. and Korakoppa, M., 2015. Platinum-group elements mineralization in the cumulate gabbro of Phenai Mata Complex, Deccan Large Igneous Province, India. Curr. Sci. 108, 1796 – 1798.

Shepherd, T.J., Bouch, J.E., Gunn, A.G., McKervey, J.A.,Naden, J., Scrivener, R.C., Styles, M.T. and Large, D.E., 2005. Permo-Triassic unconformity-related Au-Pdmineralization, South Devon, UK: new insights and theEuropean perspective. Mineralium Deposita, 40, 24–44.

Srivastava, R.K., 1997 Petrology, geochemistry and genesis of rift related carbonatites of Ambadungar, India. Mineral. Petrol., 61, 47–66.

Sukheswala R.N.,Viladkar, S.G., 1996. Geology of the carbonatite–alkalic diatreme of Amba Dongar, Gujarat. GMDC Science and Research Centre, Ahmadabad.

Sukheswala, R.N., Sethna, S.F., 1967. Giant pseudoleucites of Ghori, Chhota Udaipur. Am. Miner., 52, 1904–1910.

Wagner, P.A. 1929. The Platinum Deposits and Mines of South Africa. Oliver & Boyd, Edinburgh, 257–263.

Wilde, A.R., 2005. Descriptive ore deposit models:Hydrothermal and supergene Pt & Pd deposits. In: Exploration for Platinum-Group Element Deposits (J. Mungall, editor).Mineralogical Association of Canada Short Course,35, 145–161.

Wood, S.A., 2002. The aqueous geochemistry of the platinum-groupelements with applications to ore deposits. In: Cabri LJ (ed) Thegeology, geochemistry, mineralogy and mineral beneficiation ofplatinum-group elements. Canadian Institute of Mining, Metallurgyand Petroleum, special volume 54. Canadian Institute ofMining, Metallurgy and Petroleum, Westmount, 211–249.

Xie X.G., Byerly G.R., Ferrell R.E., 1997. IIb trioctahedral chlorite from the Barberton greenstone belt: crystal structure and rock composition constraints with implications to geothermometry. Contrib Mineral Petrol., 126(3), 275–291.

Yauz, F., Kumral, M., Karakya, N., Karakaya, M.C. and Yildrim D.K., 2015. A windows program for chlorite and classification. Elsevier Ltd. 102-103.

Zang, W., Fyfe, W.S., 1995. Chloritisation of the hydrothermally altered bedrock at the Igarapé Bahia gold deposit, Carajás, Brazil. Miner. Depos. 30, 30–38.

Rashtrasant Tukadoji Maharaj Nagpur University

Sarthak Creations : : 9822221748